THE GENESIS AND TECTONIC SIGNIFICANCE OF CHROMITITE-BEARING SERPENTINITES IN SOUTHERN NSW

Thesis submitted as a requirement of the Doctor of Philosophy degree,
University of Technology, Sydney
New South Wales, Australia

Ian.T.Graham

1998

"I declare that the work presented in this thesis is the result of original research by the author"

Production Note:
Signature removed prior to publication.

Ian.T.Graham

ACKNOWLEDGEMENTS

Many people have provided help during the duration of this project and this is hereby acknowledged.

I would like to thank my co-supervisors, Adjunct Professors Brenda J. Franklin and Brian Marshall for the initiation of this project, their enthusiastic encouragement and support throughout its duration, and their numerous comments on the manuscript. They are also thanked for receiving the various grants, which were necessary to fund this research, and also, for undertaking all of the administrative work associated with these grants.

Professor Evan Leitch of the Geology Department is thanked for his comments on the manuscript, and especially, for his advice and comments on tectonics. Leighonie Hunt of the Geology Department is much appreciated for her help with the drafting of figures and tables, and most useful advice on working with Microsoft Word and Microsoft Excel.

Alan Giles of the Geology Department is thanked for his help with the production of thin-sections and polished mounts, advice on fluid inclusions, and for being a good mate. Rod Hungerford of the Geology Department is thanked for his help with the collection of samples for geochronological investigations, advice on beer, and particularly for being a good mate. Alan Buttenshaw of the Geology Department helped with computer problems and is also thanked for letting me use his laser printer. Dr Edgar Frankel of the Geology Department is very much thanked for his support and encouragement throughout the duration of this project. Dr Graziella Caprarelli of the Geology Department is thanked for her advice and comments on the Nd-Sm isotope results.

David Colchester is thanked for sharing his great practical knowledge on XRD analysis and mineralogy. Maree Anast is thanked for her advice and help with XRD analysis. Mathew Phillips and Ric Wuhrer of the Microanalysis Unit of the Faculty of Science are thanked for their advice and guidance on Scanning Electron Microscopy.

Jeff Davis from the CSIRO Division of Exploration and Mining, North Ryde is thanked for his advice and help with sample preparation and zircon grain separation. Dr John McAndrew is thanked for his advice on the mineralogy, chemistry and analysis of chromitites. Helen Waldron and Brian Garnett of Becquerel Laboratories, Lucas Heights, are thanked for their advice on Neutron Activation Analysis. Mark Fanning of the RSES, ANU, is thanked for his advice on the age-dating of the plagiogranites. Helena Basden from the Geological Survey of NSW is very much thanked for sharing her vast knowledge of the Tumut region.

Paul Jones, Dieter Bruggermann, Somaly Srey, Piers Reynolds, James Wilson, Robert Parker, Paul Cheadle and Jane Giddey, all former undergraduate students within the Geology Department of UTS, are very much thanked for their help and companionship in the field.

My sister, Tina Graham, is thanked for her help with photocopying and advice on Microsoft Word and Microsoft Excel, while my brother Paul is thanked for lending me the money when it was needed.

My friends, Andrew, Julie, Paul, Barbara, Dion, Doug, Ross, Tony, Terry and David are thanked for providing distractions when I needed a break. Scott and Martin are thanked for the distracting and competitive golf. My niece, Breannan, and nephew, Conor are also thanked for distracting me during their visits.

Funding was provided by an Australian Postgraduate Research Award. Work on the podiform chromitites was funded by a joint CSIRO/UTS co-operative research grant. The neutron activation analyses were funded by grants from ANSTO while, funding for the geochronological investigations was provided by an internal UTS research grant. Financial support for attending conferences in Australia and overseas was provided by grants from the UTS Vice-Chancellors postgraduate student conference fund, the Geology Department at UTS, and the NSW Division of the Geological Society of Australia.

Finally, most of all I would like to thank my parents, Paul and Hilary Graham, for their continual support and encouragement throughout my life, especially in times of hardship.

ABSTRACT

The Tumut Serpentinite Province consists of four major serpentinite belts and numerous small serpentinite bodies, that occupy a long narrow tract within the Lachlan Fold Belt of southern NSW. The tectonic setting of one belt, the Coolac Serpentinite Belt, has been contentious. Much of the uncertainty results from lack of a combined study on the major belts and inadequate age constraints. Resolving the uncertainty will benefit construction of a tectonic model for the evolution of the Lachlan Fold Belt.

The belts mainly comprise massive serpentinite or harzburgite, with internal shear zones of schistose serpentinite, and intrusions of plagiogranite, gabbro, basalt, pyroxenite, dunite and chromitite. The main foliation has a consistent NNW-SSE trend and is similar in the adjacent rock units. The various rock types of the serpentinite belts are geochemically akin to similar rocks from ophiolite sequences.

Podiform chromitites are geochemically, mineralogically and geometrically akin to those in the mantle sequence of most ophiolites. The different chromitite types are interpreted in terms of the degree of evolution of the MORB-type magma and hence the extent of fractionation of the source. Serpentinisation and rodingitisation occurred during progressive cooling of the chromitites and host rocks and were accompanied by systematic fracturing and remobilisation of chemical components.

Radioisotope dating gives an age of crystallisation of 412-400 Ma for the plagiogranites and leucogabbros, whilst an inherited zircon age of 430 Ma appears to be derived from Early Silurian felsic volcanic rocks of the region. As the plagiogranites, leucogabbros and other rock types within the serpentinite belts have common deformational and metamorphic histories, their crystallisation age constrains the ages of deformation and metamorphism.

The serpentinite belts are interpreted as ophiolites of the 'embryonic' type that formed within a back-arc basin setting in the Late Silurian-Early Devonian. Crystallisation of the MORB sequence and emplacement onto continental crust, together with metamorphism and deformation may have only spanned 20 Ma. In the Late Silurian to Early Devonian, the Tumut Serpentinite Province

differed from basins elsewhere within the Lachlan Fold Belt in that a volcanic arc was ruptured by mantle-derived MORB magmas which ascended to the surface. Their extrusion was short-lived and after the Early Devonian, the development of the Tumut region differed little from that in the rest of the Lachlan Fold Belt.

The development of oceanic crust within the Tumut Serpentinite Province and the generation of granitic magmas within the central and eastern parts of the Lachlan Fold Belt are symptomatic of the same Late Silurian to Early Devonian tectonothermal event. An important aspect of this is that oceanic and crustal rocks need not form from different events or in substantially different tectonic settings.

TABLE OF CONTENTS

LIST OF PLATES

LIST OF FIGURES

LIST OF TABLES

LIST OF APPENDICES

CHAPTER 1: INTRODUCTION

1.1 GENERAL STATEMENT

A series of linear serpentinite belts and smaller serpentinite bodies occupy a north-south tract of the Lachlan Fold Belt, in southern NSW, southeastern Australia. They are herein collectively named the Tumut Serpentinite Province. Ultramafic rocks also occur in several other broad associations within the Lachlan Fold Belt (Figure 1.1):

(a) Some eleven Alaskan-type intrusive complexes occur in a northerly trending belt 180km long and 80km wide in the central portion of the Lachlan Fold Belt (Figure 1.1). The tract has been termed the Fifield Platinum Province by Barron *et al.* (1991) and several of the intrusions have been described by Elliott *et al.* (1991). The complexes were emplaced, dominantly within metasedimentary rocks of the Girilambone Group, during the Devonian (Johan *et al.* 1989). They are spatially associated with Devonian potassic granitoids (Elliott *et al.* 1991).

(b) Ultramafic rocks, all partially serpentinised and intimately associated with ultramafic cumulates and ultramafic lavas (limburgites), occur at more than thirty localities within the Lucknow Fault Zone (Figure 1.1) in the eastern half of the Lachlan Fold Belt in central NSW. They tend to be small (approx. $100m^2$) fault-bounded blocks (Barron 1994).

(c) The Cambrian greenstone belts of Victoria (Crawford *et al.* 1984) possibly form the basement to the Lachlan Fold Belt and outcrop in three north-south trending sub-parallel tracts termed the Heathcote, Mount Wellington and Stavely greenstone belts. The belts comprise fault-bounded blocks consisting of variable proportions of metamorphosed tholeiitic dolerite, low-Ti boninite, low Ti-andesite, calc-alkaline and high-K orogenic andesites, serpentinised ultramafic cumulates, dacite and ferrodiorite (Crawford *et al.* 1984). Similar rocks form a small ($0.05km^2$) isolated body on Phillip Island (Henry & Birch 1992), while Gray (1997) suggested that similar rocks on the South Coast of NSW might be of Cambrian age, and a similar interpretation was tentatively assigned to the Tumut Serpentinite Province (Stuart-Smith 1990b, 1991b).

The serpentinite belts of the Tumut Serpentinite Province differ geometrically and petrographically from the foregoing associations. They consist of large (up to 110km in length) fault-bound linear bodies which dominantly consist of variably serpentinised harzburgite; volcanic rocks akin to those found in Victoria (item (c), above) are of minor occurrence. The Tumut Serpentinite Province rocks have been interpreted as oceanic crust (e.g. Scheibner 1985; Ashley *et al.* 1979), whereas some consider that the Lachlan Fold Belt in this part of NSW was floored by continental crust (e.g. Stuart-Smith 1990b). An understanding of the age, origin and emplacement of these ultramafic bodies is therefore vital to any tectonic reconstruction of the Tumut region and Lachlan Fold Belt.

Two of the serpentinite belts contain podiform chromitite bodies and associated platinum-group element mineralisation. The genesis of podiform chromitite deposits is contentious (e.g. Lago *et al.* 1982; Johan 1986; Leblanc & Ceuleneer 1992) to the extent that the same textures have been ascribed to primary magmatism (Leblanc 1980) and secondary tectonism (Gates 1991), and inclusions within chromite grains have been attributed to magmatic (Talkington *et al.* 1984) and secondary-recrystallisation (Christiansen 1986) processes. Thus, a study of the podiform chromitites may provide evidence of their origin and evolution, as well as contributing to an understanding of the serpentinite belts.

1.2 OBJECTIVES/AIMS

The principal objectives of this work are:

(a) to determine the origin of chromitite bodies and associated Ni-bearing and platinum-group element bearing mineralisation found within the Tumut Serpentinite Province; and,

(b) to determine and describe the geology, geochemistry, contacts and internal structure of the serpentinite belts, and then, using this information in conjunction with appropriate literature, develop a tectonic model for the portion of the Lachlan Fold Belt associated with the Tumut Serpentinite Province.

To achieve these objectives the following aims were set:

(a) to determine the mineralogy, petrology, geochemistry and structure of the serpentinite belts in the Tumut Serpentinite Province;

(b) to determine the field relationships, mineralogy, petrology, textures, whole rock geochemistry, chromite-grain geochemistry and structure of the podiform chromitite deposits;

(c) to establish the nature of the platinum-group element mineralisation within the podiform chromitite deposits and associated wallrocks;

(d) to determine the physical and chemical effects of alteration and regional metamorphism on the protoliths of the serpentinite belts; and,

(e) to obtain radiometric data in order to constrain the age of the ultramafic protolith.

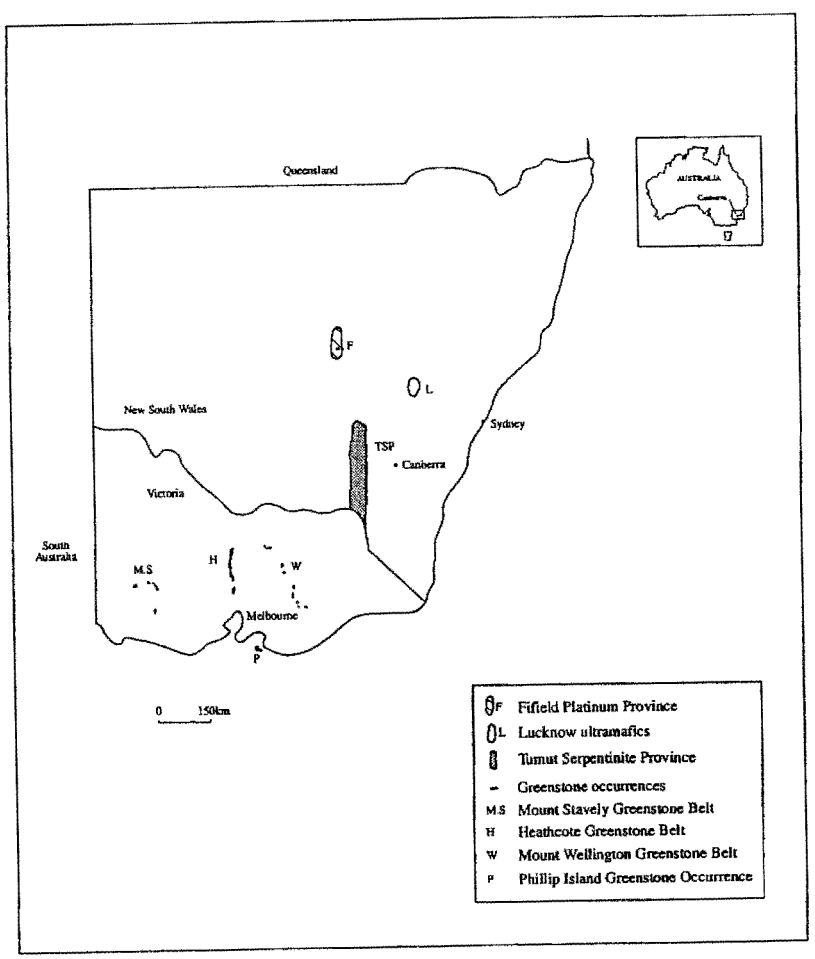

Figure 1.1 Location of the Tumut Serpentinite Province, Fifield Platinum Province, Lucknow ultramafic occurrences and Cambrian greenstone occurrences.

1.3 LOCATION AND ACCESS

The Tumut Serpentinite Province and adjacent rocks occupy a tract 240km long by 60km wide extending from the township of Young southward to the township of Cabramurra (Figure 1.2). Good access to the northern half of the Tumut Serpentinite Province is provided by the Hume Highway and many other sealed and unsealed roads. Access to the southern half of the region is relatively poor, largely due to the rugged topography and the fact that much of this area is situated within the Kosciusko National Park. Vehicular entry is confined to the Snowy Mountains Highway and fire trails within the National Park and adjacent state forests (Plate 1.1).

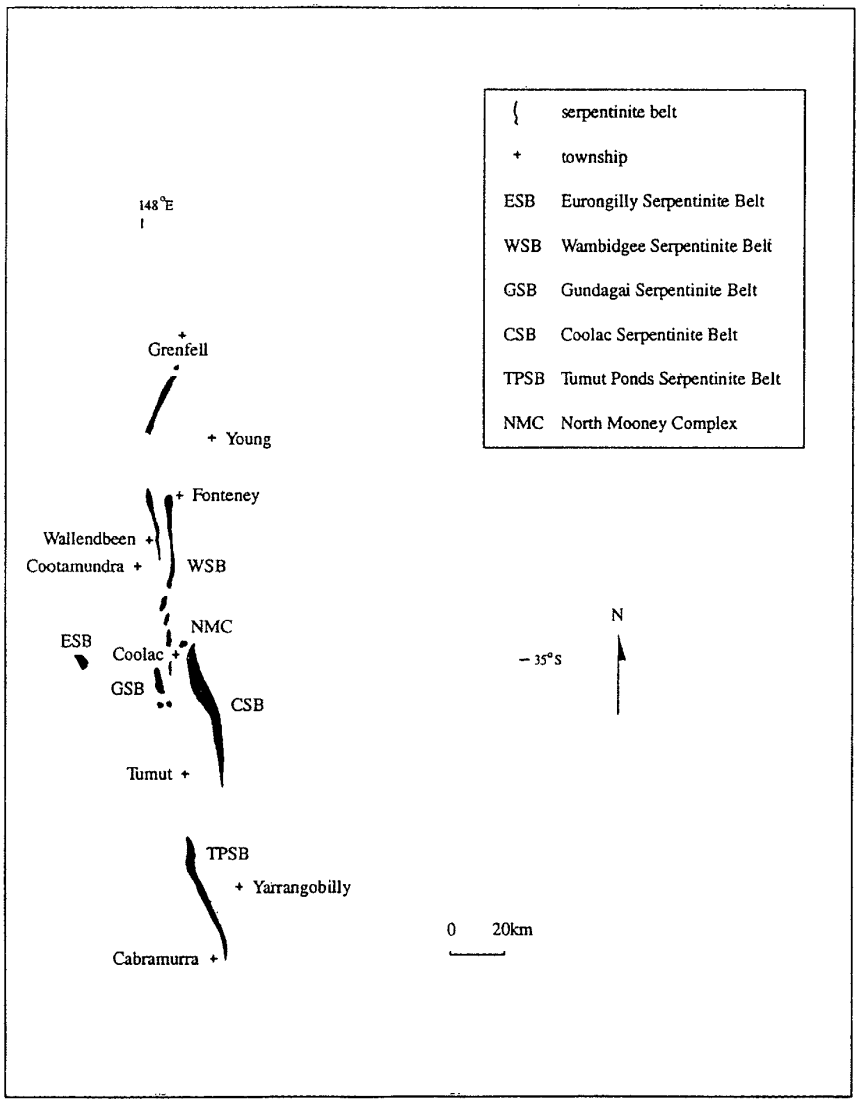

Figure 1.2 The Tumut Serpentinite Province.

Plate 1.1 View of the rugged topography within the southern half of the study region. The range of hills in the central portion of the photograph is occupied by the Tumut Ponds Serpentinite Belt.

1.4 PHYSIOGRAPHY, VEGETATION AND CLIMATE

In the northern half of the region (Figure 1.3), topography is subdued and consists largely of cultivated, relatively flat-lying fields separated by low ridges. Jacks Hill (393m asl) and Memagong Hill (464m asl) are two of the more prominent features. Outcrop is poor and largely confined to ridges and creek beds.

The central region (Figure 1.3) is more hilly with prominences including Muttama Hill (678m asl), Coolac Hill (452m asl) and the Honeysuckle Range (500-800m asl); outcrop is generally good. The central region is cut by the Murrumbidgee River, the principal focus for drainage throughout the region.

In the southern part of the region (Figure 1.4), the terrain is mountainous and local relief reaches almost 600m. Elevation ranges from 700m asl on the floor of the steep-sided valleys, to over 1300m asl on intervening plateaus. Prominent highs on the plateau regions include Mount Hovell (1388m

asl), Gurkeroo Ridge (approx. 700m asl), Jounama (1719m asl), Big Talbingo Mountain (1384m asl) and Mount Selwyn (1614m asl).

The northern half of the region has been extensively cleared for grazing and cultivation, but a few patches of eucalyptus woodland remain. A distinctive vegetation (Lyons *et al.* 1975) characterises the Coolac Serpentinite Belt and consists of *Xanthorrhoea glauca* (Grass Tree or Black Boy) (Plate 1.2), *Ricinocarpus bowmanii* (Pink Wedding Bush) and *Allocasuarina verticillata* (Drooping She Oak).

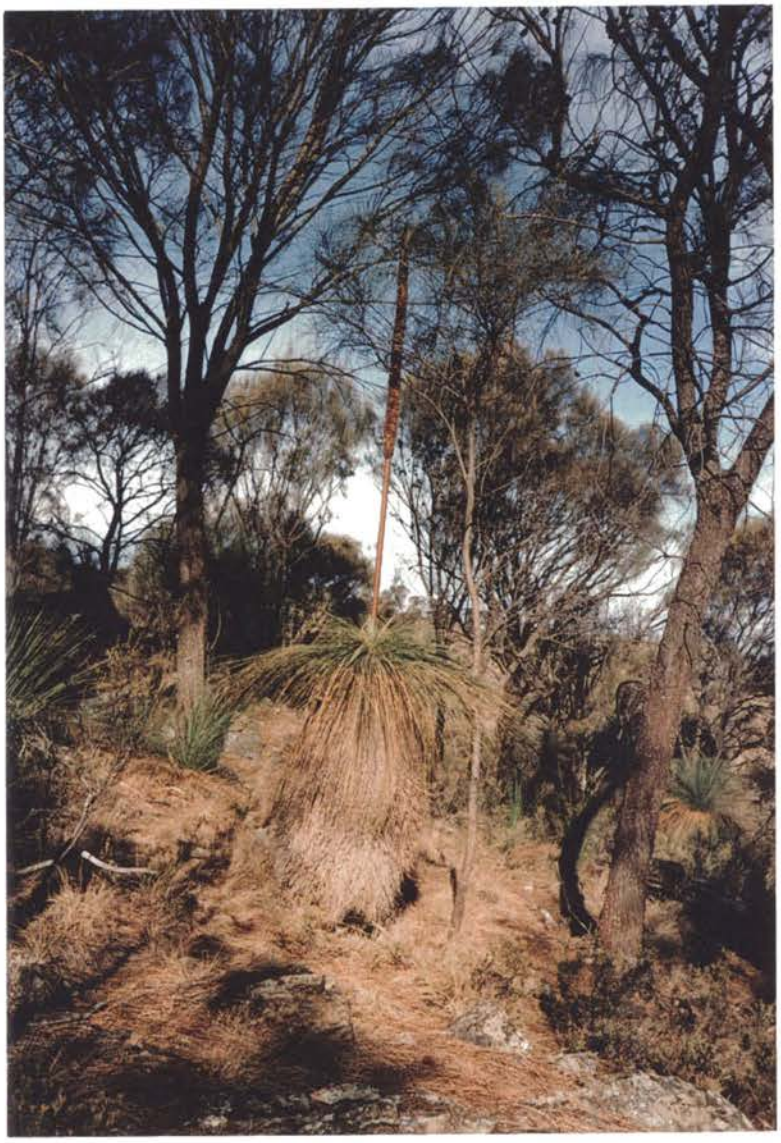

Plate 1.2 Distinctive vegetation, exemplified by *Xanthorrhoea glauca* (Grass Tree or Black Boy) on the Coolac Serpentinite Belt.

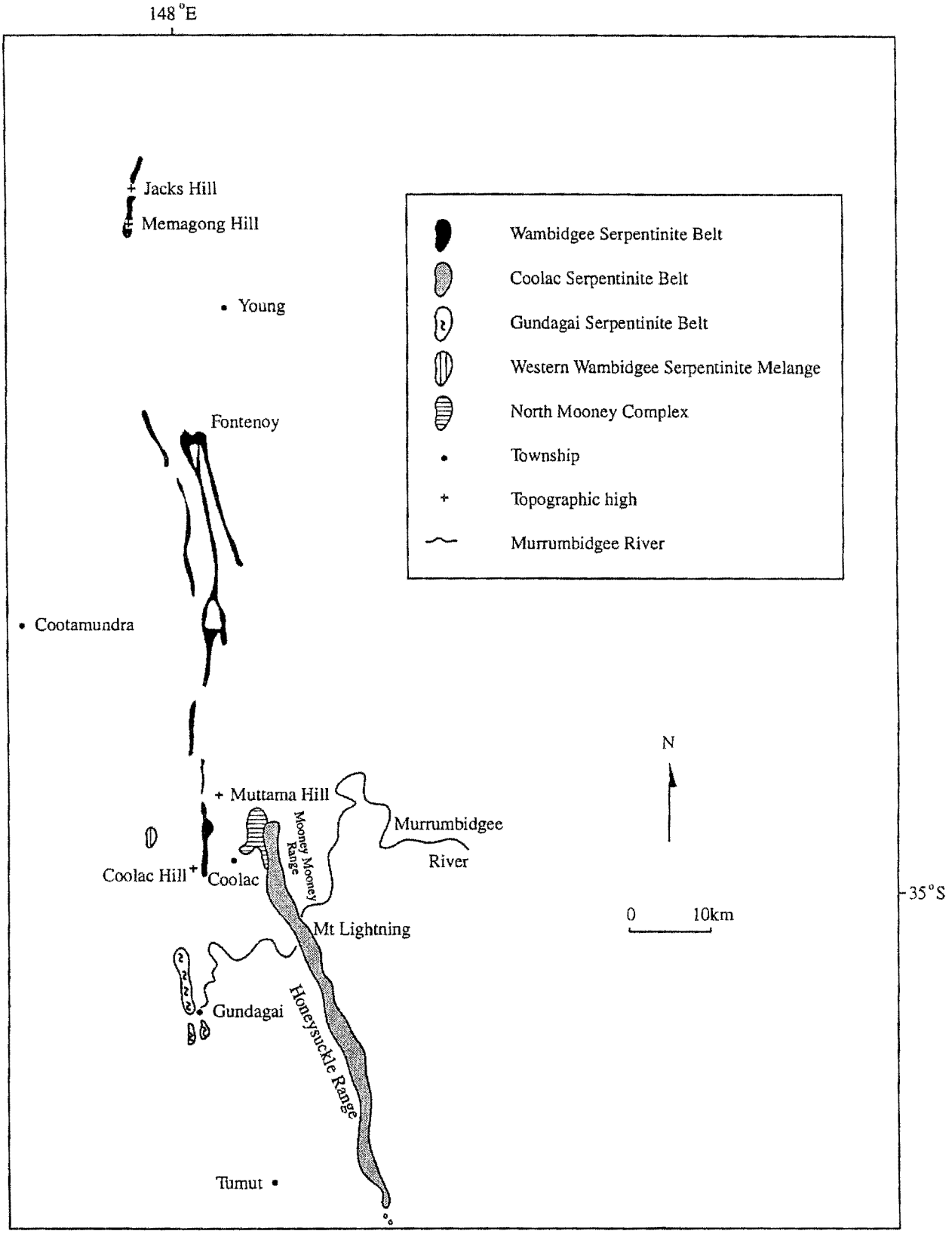

Figure 1.3 The northern and central portions of the study region.

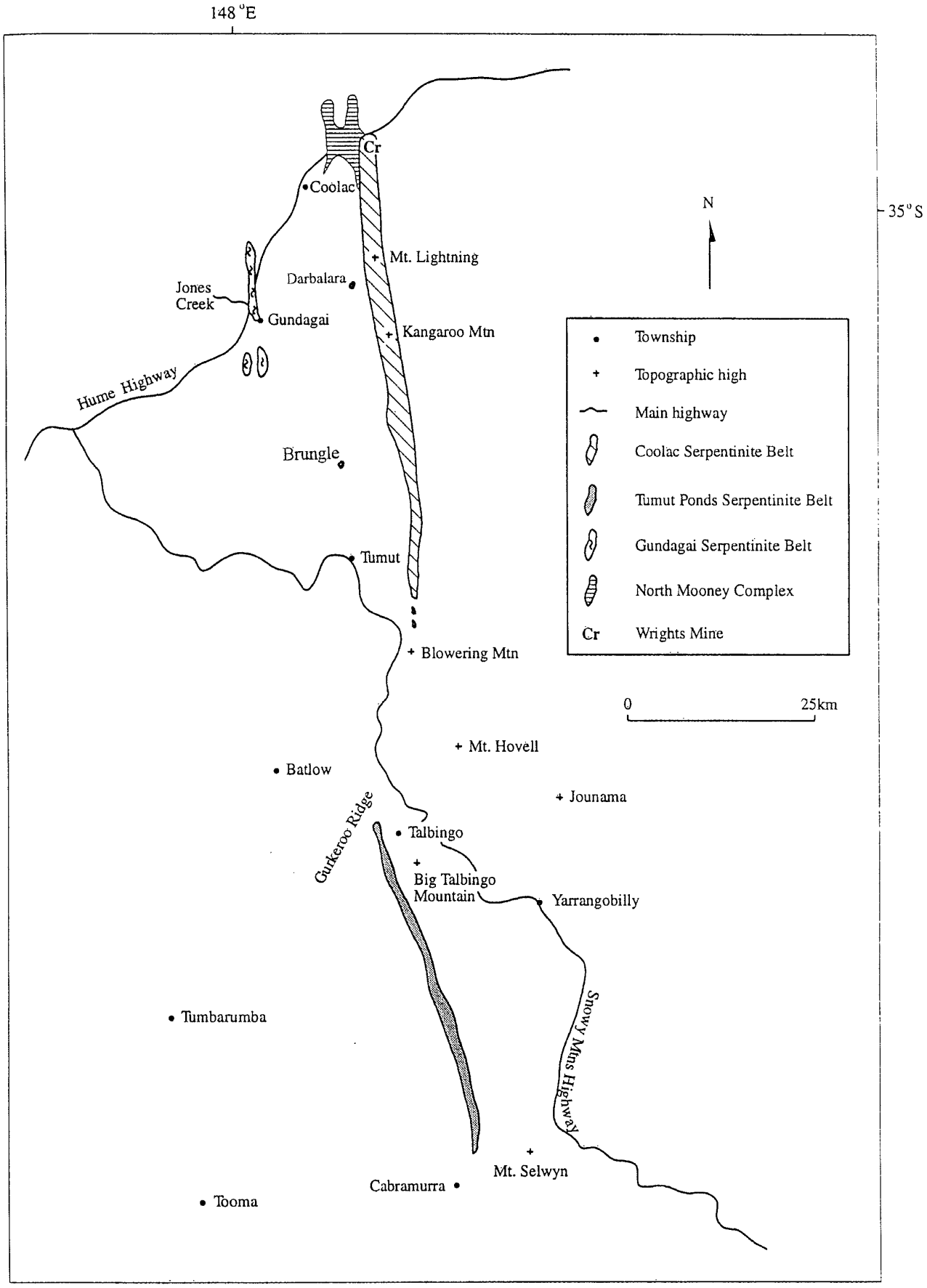

Figure 1.4 The southern portion of the study region.

1.5 PREVIOUS WORK

(Refer to Figures 1.2, 1.3 and 1.4 for locality information)

The first record of ultramafic rocks in the region was that of Pittman (1882) who noted the occurrence of serpentinite near Jones Creek from the Gundagai Serpentinite Belt. Carne (1893, 1896 and 1898) described podiform chromitite deposits from the Mooney Mooney Range east of Coolac, including that at Wrights Mine, which was the first chromite mining operation in NSW. Slee (1895) commented on podiform chromitite deposits from the Tumut region and Jacquet (1896a, 1896b) reported on gold and chromite deposits from the Fontenoy area. Card (1896) described a peridotite specimen from Gundagai, and the ultramafic rocks were briefly described by Benson (1926). Lloyd (1942) and Whitworth (1942) described aspects of the Fontenoy chromitite deposit. The Tumut Ponds Serpentinite Belt was first mapped by Adamson (1953). Gibbons (1963) reported on the economic potential of the Wallendbeen talc deposits centred on the township of Wallendbeen. Other work of this period includes that of Hall & Relph (1957) who described the geology of the Tumut-Talbingo region, and Adamson (1954, 1960) who described the geology and produced geological maps of the Tumut-Yarrangobilly region. Adamson & Louden (1966) and Rose (1967) published regional geological maps during this period.

The period from 1960 to 1980 saw extensive studies in the Tumut Serpentinite Province, centred almost exclusively on the Coolac Serpentinite Belt. The pioneer of this work was Golding (1961, 1962, 1963a, 1963b, 1966, 1967, 1969, 1971, 1975; Golding & Bayliss 1968; Lawrence & Golding 1970; Golding & Johnson 1971; Golding & Ray 1975a, 1975b) who studied the ultramafic and associated rocks, including the chromitite deposits. Another major contributor was Ashley (1967, 1968, 1969a, 1969b, 1970, 1973a, 1973b, 1974, 1975a, 1975b; Ashley *et al.* 1971; Ashley & Basden 1973; Ashley & Chenhall 1976; Ashley *et al.* 1979) who studied the petrology, geochemistry of the ophiolitic rocks and base metal mineralisation, metamorphism and tectonic setting. Franklin (1975) investigated the North Mooney Complex (Figure 1.3). Ray (1977) studied the rodingites of Mount Lightning, and Brown (1973, 1979, 1980) investigated a small sheeted dyke complex on the western margin of the Coolac Serpentinite Belt. During this period, regional geological maps of the region were produced by Brunker *et al.* (1970), Basden *et al.* (1975), Wyborn (1977) and Degeling (1977, 1982).

The overall structure and tectonic development of the Tumut region were reported by Basden (1974, 1978, 1980, 1982, 1986, 1990), Basden *et al.* (1978, 1985, 1987), Stuart-Smith (1988, 1989, 1990a, 1990b, 1991a, 1991b) and Warner *et al.* (1992). Also, Basden (1990) and Warren *et al.* (1995) produced regional geological maps during this period.

To date, a number of publications and conference abstracts have resulted from the work pertaining to this thesis. These publications involve work on the platinum-group element mineralisation of the chromitite deposits (Graham, Marshall & Franklin 1991a, 1991b; Franklin, Marshall, Graham & McAndrew 1992), the podiform chromitite deposits (Graham, Franklin & Marshall 1993, 1996; Graham, Marshall & Franklin 1993; Franklin, Graham & Marshall 1993), and the general geology of the Tumut Serpentinite Province and its tectonic setting (Franklin, Graham & Marshall 1992; Graham, Franklin & Marshall 1994; Graham, Franklin, Marshall, Leitch & Fanning 1996a, 1996b).

(Grid-references for localities mentioned throughout this thesis are presented in appendix LOC)

CHAPTER 2: THE LACHLAN FOLD BELT AND REGIONAL GEOLOGICAL FEATURES OF IMPORTANCE

2.1 THE LACHLAN FOLD BELT

2.1.1 Introduction

The Lachlan Fold Belt (Scheibner 1972) is part of the Tasman Fold Belt System (Scheibner 1993), a mainly Palaeozoic to Early Mesozoic fold mountain and thrust belt extending over the eastern third of Australia. It has a width of 750km across central and eastern Victoria and stretches 500km northwards into southeastern and central NSW (Figure 2.1; Scheibner 1985). The total exposed area of the belt is close to 300 000km^2 (Chappell *et al.* 1988).

Compared with other fold mountain belts (e.g. the Appalachians - Price & Hatcher 1983, Hatcher 1987, Horton *et al.* 1989; the New England Fold Belt - Korsch & Harrington 1981, Leitch 1982, Coney *et al.* 1990), the Lachlan Fold Belt is unusual in having an extremely consistent deformational style from west to east, dominated by a remarkably uniform sequence of turbidite-deposited sedimentary rocks, and having disproportionately large amounts (approximately one third of the belt) of granitic rocks (Coney *et al.* 1990). Chappell *et al.* (1988) identified the existence of eight 'basement' terranes, Coney *et al.* (1990) recognised a number of subterranes or structural belts, Gray (1990) delineated western, central and eastern macrotectonic units, and Scheibner (1993) divided the belt into 18 structural zones.

2.1.2 Lithology and structural/metamorphic evolution

[Except where otherwise acknowledged, this section is derived from Scheibner (1985), Coney *et al.* (1990) and Fergusson & Coney (1992).]

Cambrian rocks of the Lachlan Fold Belt primarily crop out in Victoria and consist of mafic to intermediate volcanics, chert, limestone and various ultramafic rocks, the latter comprising the greenstone belts of Victoria (Crawford 1988). Minor outcrops occur on the South Coast of NSW (Bischoff & Prendergast 1987).

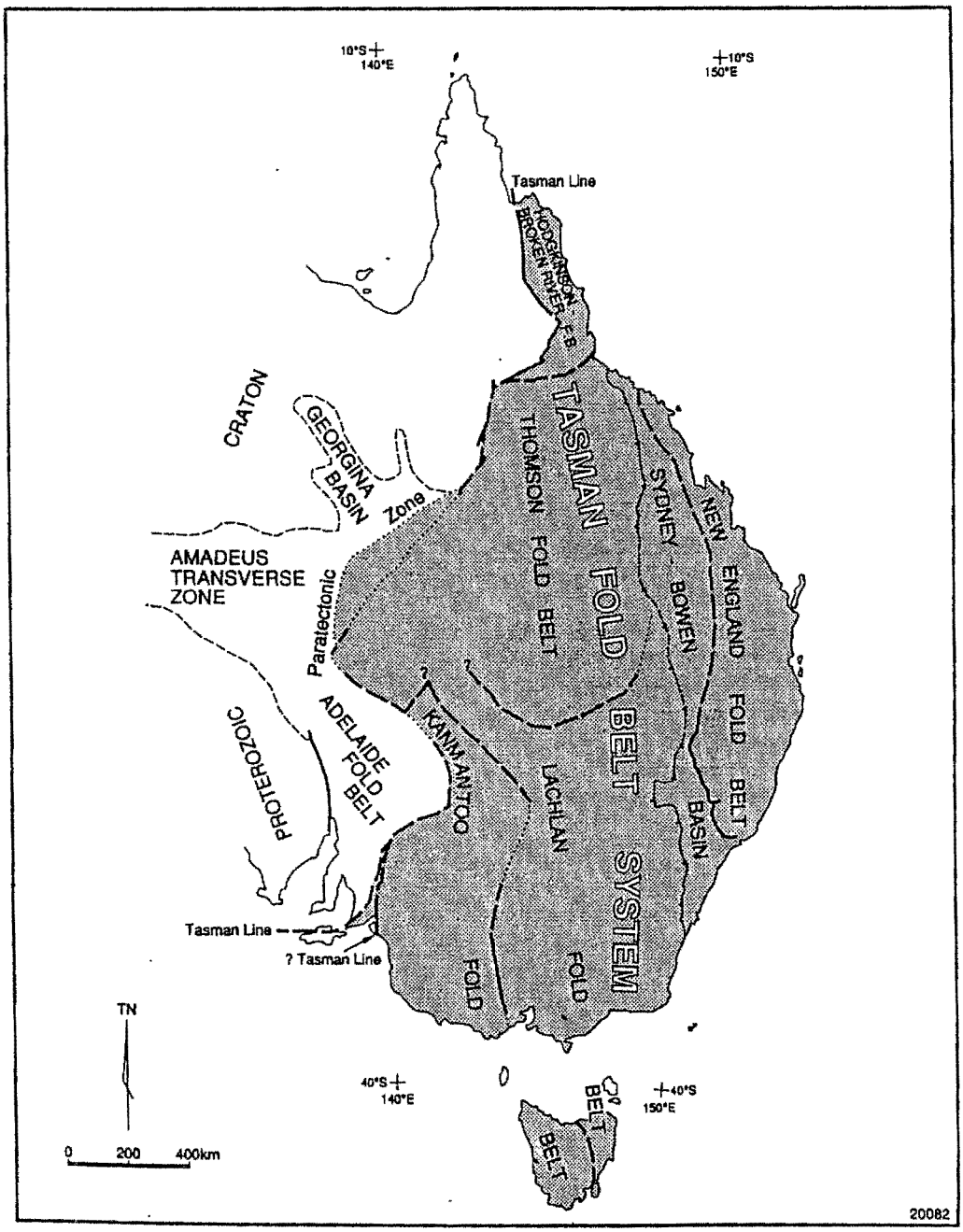

Figure 2.1 Location of the Lachlan Fold Belt (from Scheibner 1993).

Ordovician to Early Silurian successions dominate the Lachlan Fold Belt and largely consist of a widespread succession of quartz-rich turbidite and black shale (VandenBerg & Stewart 1992). Mafic volcanic rocks, with their associated epiclastic rocks and limestone, are largely restricted to the eastern part of the belt.

Middle Silurian to Middle Devonian successions predominantly consist of silicic volcanic rocks, siliciclastics, volcaniclastics and limestone. These successions are widespread throughout the eastern part of the belt but of limited occurrence in the west (Cas 1983; Powell 1984).

The Late Devonian and Early Carboniferous successions in the central and eastern parts of the belt, are characterised by basal silicic and mafic volcanics, grading up into shallow marine to fluviatile sedimentary rocks.

Most of the granites within the Lachlan Fold Belt are in the age range of 440 to 390 Ma (Chappell 1994), but a few plutons have been dated at 360 Ma and 312 Ma from the central and more easterly parts of the belt respectively. Both I- and S-type granites are present (Figure 2.2) and, in some cases, the granites are subvolcanic (e.g. the Young Batholith - Basden 1990) and invade penecontemporaneous and comagmatic volcanic sequences.

The Lachlan Fold belt has a variably developed, episodic deformational history. The oldest known deformational event in NSW is recorded by Late Ordovician ages from the Narooma Accretionary Complex (Offler *et al.* 1998a). The next deformational event (the Benambran Orogeny of Early to Middle Silurian age) is widespread within the central part of the belt where, within the Wagga-Omeo Metamorphic Belt it resulted in the formation of upright E-W trending folds and dextral strike-slip movements along major faults. In the Late Silurian to Early Devonian, the Bowning-Bindi Orogeny resulted in multiple deformation of the Ordovician basement and highly variable deformation of the Silurian to Devonian successions. With the exceptions of the Melbourne Zone, the eastern part of the Bendigo-Ballarat Zone, the western part of the Darling Basin, and the Hill End Trough, deformation was widespread and intense. Major faults underwent significant (up to 50km) dextral strike-slip displacement (Morand & Gray 1991), and bulk shortening as high as 76% (Fergusson & VandenBerg 1990) gave rise to intense folding, cleavage-development, and thrusting.

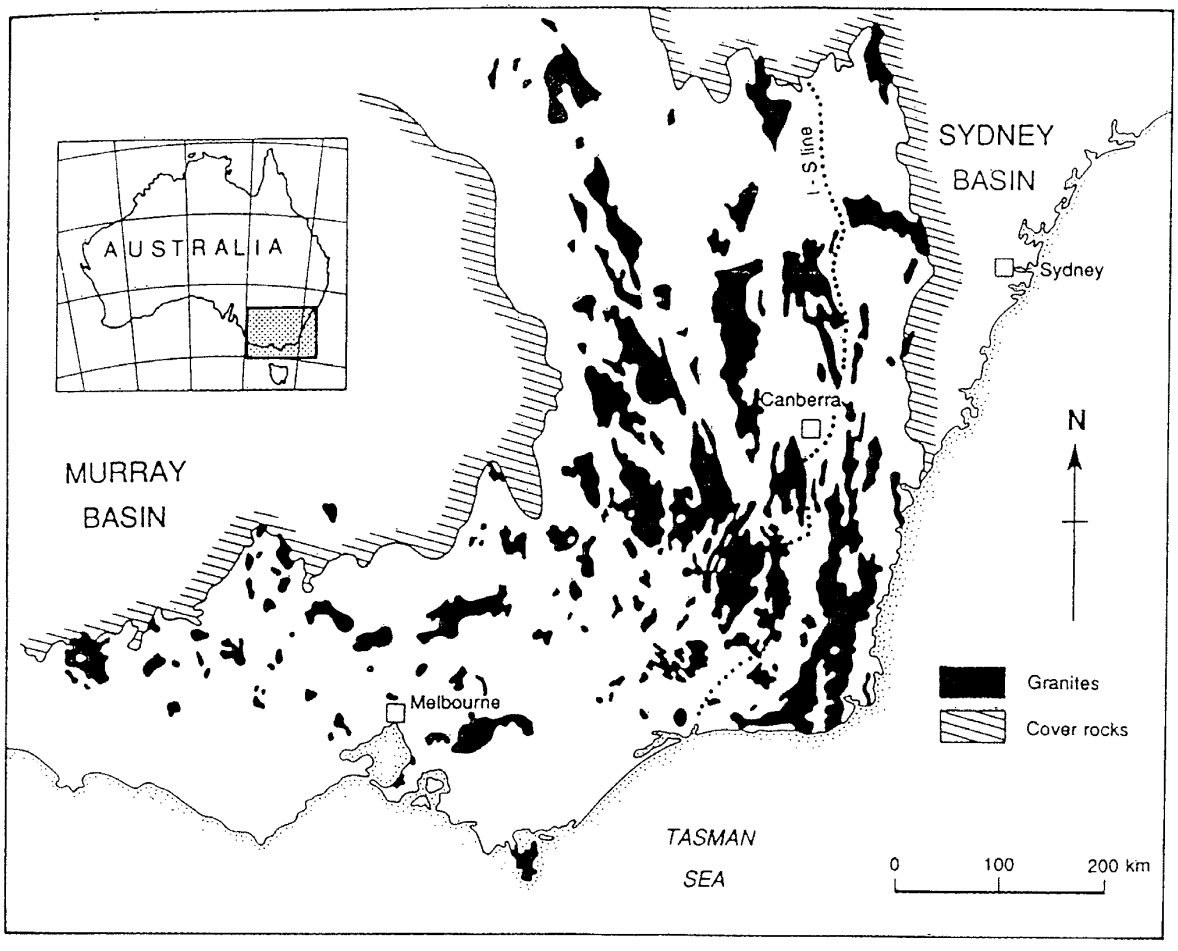

Figure 2.2 Distribution of granitic rocks within the Lachlan Fold Belt (from Johnson *et al.* 1994).

The Middle Devonian Tabberabberan Orogeny was the next orogenic episode. Its effects are most apparent in the Ordovician to Middle Devonian succession of the Melbourne Zone (Gray 1988). The resulting structures are mainly upright N-trending folds which, within the Bendigo-Ballarat Zone, were accompanied by bulk shortening of up to 70% (Gray & Willman 1991). In the eastern half of NSW and the Wagga-Omeo Metamorphic Belt, strike-slip faults were either formed or reactivated, while broad folding and uplift affected the Hill End Trough (Powell & Edgecombe 1978). After the Middle Devonian, although most of the Lachlan Fold Belt had been significantly deformed, the Early Carboniferous Kanimblan Orogeny took place. It was particularly widespread within the northeasterly part of the belt, where upright folds and pervasive cleavage developed. Elsewhere, close to gentle upright synclinal structures were formed, along with bounding faults.

Although metamorphic conditions throughout most of the Lachlan Fold Belt were believed to have been those of the lower greenschist facies (e.g. Cox *et al.* 1995; Wilson *et al.* 1992), subgreenschist facies conditions (i.e. prehnite-pumpellyite facies) have been reported from the western Lachlan Fold Belt by Offler *et al.* (1998b). In the Wagga-Omeo Metamorphic Belt, Morand (1990) found upper amphibolite facies conditions of 700°C at 350 MPa for gneissic cores surrounded by schists of the greenschist facies. Similar conditions have been recorded in parts of the Cooma and similar complexes (Johnson *et al.* 1994), and in parts of the Southern Serpentinite Belts (Franklin *et al.* 1992). Thus, although the Lachlan Fold Belt is dominated by low-grade metamorphism, there are localised higher-grade areas, commonly centred on granitic bodies.

2.1.3 Problems with tectonic models for the Lachlan Fold Belt

Any realistic model for the tectonic history of the Lachlan Fold Belt must satisfactorily explain:

(a) the consistent deformational style across the fold belt (Gray 1988; Gray *et al.* 1991; Coney 1992);

(b) the regionally extensive uniform sequence of turbidite-deposited sedimentary rocks (Coney *et al.* 1990; Vandenberg & Stewart 1992; Gray 1997);

(c) the large proportion and regional extent of granitic rocks (Chappell *et al.* 1988; Coney *et al.* 1990; Gray 1997); and

(d) the occurrence of Cambrian greenstone belts in Victoria (Crawford & Keays 1978; Crawford *et al.* 1984), the greenstones of the South Coast of NSW (Gray 1997), and supposedly Silurian ophiolitic rocks in the Tumut region (Crook & Felton 1975; Ashley *et al.* 1979; Scheibner 1985; Basden *et al.* 1987).

Many models (e.g. Crook 1980; Powell 1984; Scheibner 1985; Gray & Willman 1991; Glen *et al.* 1992; Fergusson & Coney 1992; Gray & Webb 1995; Gray 1997) have been constructed in order to explain the tectonic evolution of the Lachlan Fold Belt. These models, most of which involve accretion and a mixed ensimatic and ensialic basement, will be evaluated relative to items (a) to (d) above.

Crook (1980) and Scheibner (1985) advocated similar models for the development of the belt. Both invoked progressive accretion of island arc terranes and subduction of oceanic crustal elements as

crucial to the cratonisation of the eastern margin of Australia. The Cambrian greenstone belts of Victoria were interpreted as Cambrian oceanic crust, while ophiolitic rocks in eastern NSW were considered to have formed in Middle Silurian inter-arc basins (Figure 2.3). The widespread deformation was ascribed to collisions, reflecting terrane accretion throughout the Lachlan Fold Belt's history. These models explain the occurrence of the ophiolitic rocks and regionally extensive turbiditic sediments, but they inadequately account for the uniform deformational style and the large proportion and geographic distribution of granitic rocks.

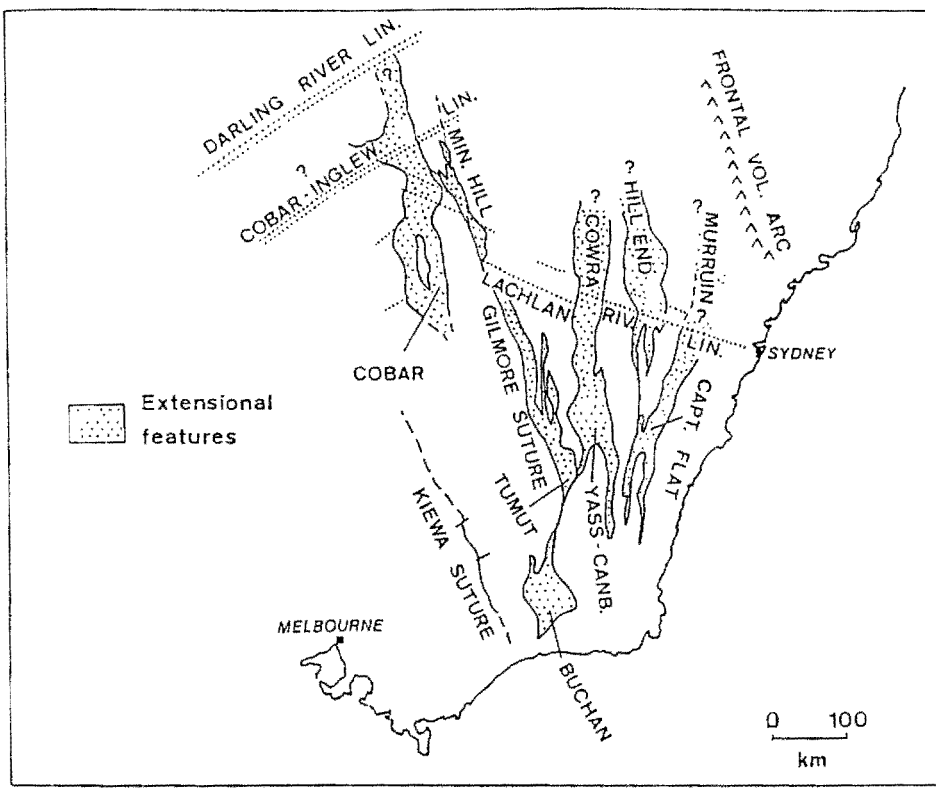

Figure 2.3 Middle Silurian basins (the extensional features) of the Lachlan Fold Belt (from Scheibner 1985).

Powell (1984) advocated the existence of Cambrian oceanic crust, but considered that, subsequent to this, the belt was floored solely by continental crust. He ascribed the regionally extensive Ordovician turbidite deposits to mixing of quartzose sediment derived from the craton to the west with juvenile detritus from a mafic volcanic arc to the east. He also associated the Wagga-Omeo Metamorphic Belt with burial of the high heat flow zone of the back-arc basin, possibly coupled with subduction of the ocean-floored portion. Erosion of the Wagga-Omeo Metamorphic Belt shed quartzose sediment eastwards into Silurian submarine fans on a slope and abyssal plain (Powell 1984). Deformation in the Late Silurian to Early Devonian was attributed (Powell 1984) to the

intrusion of the granitic bodies within a contractional regime. This model explains the development of the regionally extensive turbidite deposits, but has no explanation for the consistent deformational style across the belt, the large proportion and regional extent of granitic rocks and the occurrence of Cambrian greenstone belts in Victoria, greenstones of the South Coast of NSW, and supposedly Silurian ophiolitic rocks in the Tumut region.

Gray & Willman (1991), Gray *et al.* (1991), Gray & Webb (1995) and Gray (1997) concentrated on the structural development of the Lachlan Fold Belt and the formation of the extensive turbidite deposits. They believed that the Lachlan Fold Belt had a composite lower crust involving ensialic and ensimatic elements. They invoked the concept of a thin-skinned fold and thrust belt and envisaged eastward transport along detachment faults within the Cambrian greenstone and Early Ordovician sequences, together with chevron folding of the Ordovician upper plates. They advocated a major décollement at depths of 15-20km, overlain by stacked thrust sheets, which resulted in thick crust, older strata structurally overlying younger strata and apparently diachronous (younger from west to east) deformation. The various authors also advocated reactivation of major faults over the Cambrian to Carboniferous interval. Such a model, involving major fault-reactivation, crustal delamination, and imbrication and stacking of thrust sheets, adequately explains the consistent deformational style across the belt, the regionally extensive turbidite deposits and the occurrence of the Cambrian greenstone belts. The extensive turbidite deposits formed in a Cambrian-Ordovician oceanic setting by rapid uplift and erosion along the cratonic margin to the west. They were deposited within a deep water setting, leading to the formation of a continental margin sediment prism. However, it does not explain the occurrence of serpentinite belts within the Tumut region.

Fergusson & Coney (1992) ascribed the development of the Lachlan Fold Belt to three main tectonic phases. The Cambro-Ordovician phase involved an intraplate oceanic setting, the Silurian to Middle Devonian phase a convergent margin setting, with widespread and intense deformation and magmatism, and the Late Devonian to Early Carboniferous phase, a continental back-arc setting to the west of the continental margin arc of the New England Fold Belt in northeastern NSW. They argued that deformation was absent in the Cambro-Ordovician, and that crust was ensialic but much thinner than 'normal' continental crust. The Ordovician turbidite successions

developed as a huge submarine abyssal fan that, expressing plate convergence at a distant subduction zone, underwent extensive Silurian to Middle Devonian intraplate compressional deformation and granite emplacement. Thus, the Silurian to Middle Devonian tectonic setting of the Lachlan Fold Belt was a back- or intra-arc continental margin, and the granites were generated by westward underthrusting of the Late Proterozoic lower crust. Such a model adequately explains regionally extensive turbidite deposits, and the formation of large volumes of granitic rock; it fails to explain the consistent deformational style across the belt, the greenstone belts of Victoria that formed as oceanic crust in a suprasubduction zone setting (Crawford *et al.* 1984), and the serpentinite belts of the Tumut region.

Collins & Vernon (1992) suggested that deformation and silicic magmatism migrated synchronously across the Lachlan Fold Belt, during the Palaeozoic, due to the growth, deformation and migration of a volcanic arc above a west-dipping subduction zone. This produced discrete fold-thrust belts characterised by low-grade metamorphic assemblages. They advocated an Early Palaeozoic west-Pacific type plate margin, characterised by a continental margin-back-arc basin-volcanic arc system (e.g. Cas *et al.* 1980; Scheibner 1987, 1989), that finally stabilised as true continental crust in the Early Carboniferous. They ascribed the chemistry of the granitic magmatism to partial assimilation of remnant Cambrian arc material and the Ordovician turbidite sequence by subduction-generated mantle-derived magmas. The belt-wide deformation was attributed to mid-crustal thermal softening from numerous and protracted granitoid intrusion. This model adequately explains the occurrence of the greenstone belts of Victoria, the serpentinite belts of the Tumut region, the origin of the granitic rocks, the regionally extensive turbidite deposits, and the consistent deformational style across the fold belt. However, it does not fully explain the atypical tholeiitic geochemistry (Wyborn 1992) of the Early Silurian to Middle Devonian volcanic rocks of the eastern half of the Lachlan Fold Belt. Nor does it explain the absence of extensive melange units and molasse-type sediments, that typify subduction zone environments (Leitch 1984).

Chappell (1994) contended that there is no petrological evidence for a subduction component within the granitic and volcanic rocks of the Lachlan Fold Belt. He stated that the S-type granites were solely derived from sedimentary material within the crust and that the I-type granites were derived from the fractional melting of previously solidified mantle-derived material. He contended that

thickening of the crust within the belt would have resulted in significant uplift which cannot be seen. He therefore, advocated high heat flow through thinning of continental crust or lithosphere to explain the voluminous granitic bodies, but he did not explain why thinning occurred. He stated that there was no oceanic crust throughout the tectonic history of the belt and that the tectonic style of the belt was not one of accretion. This model accounts for the large volume and geographic distribution of the granitic rocks but not for the regionally extensive turbidite deposits, the consistent deformation style, the Cambrian oceanic crust, and the serpentinite belts of the Tumut region.

Gray (1997) proposed a 'new' model in which the Cambrian greenstone belts formed in an oceanic setting with a number of submarine arcs. In the Late Cambrian to Early Ordovician, subduction-related convergence formed an east-verging thrust belt, and associated metamorphism and plutonism, inboard of the cratonic margin. Turbidites of Delamerian provenance were concurrently deposited from the west and southwest. In the Early Silurian, a west-dipping subduction zone resulted in a continent-ocean convergent setting and east-verging thrusts within the western part of the fold belt (Figure 2.4), whilst the Late Silurian to Early Devonian period was marked by eastward thrusting throughout the belt.

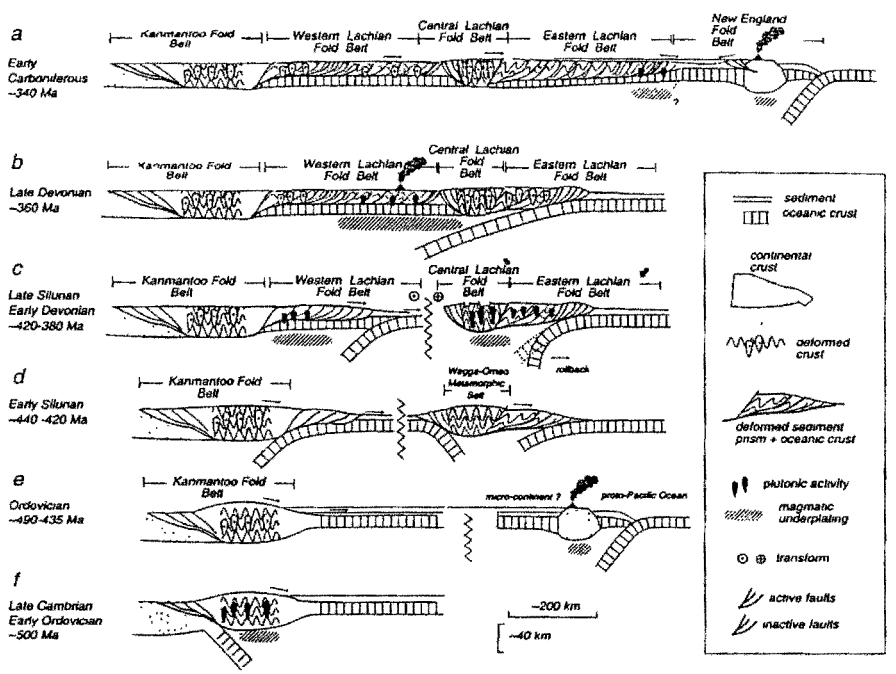

Figure 2.4 Early Silurian continent-ocean convergent setting of the Lachlan Fold Belt (from Gray 1997).

Following a change in plate motion, oblique convergence resulted in a change in the angle of subduction, magmatic underplating inboard of the continental margin, and development of the extensive silicic volcanism and plutonism. Although these few sentences only give a rudimentary summary of the model (Gray 1997), it is sufficient to emphasise that, whereas many features of the Lachlan Fold Belt are explained, the Tumut Trough remains unexplained.

2.2 REGIONAL GEOLOGICAL FEATURES OF IMPORTANCE

2.2.1 The Tumut Trough

Introduction

The name "Tumut Trough" was used to describe a sequence containing deformed and metamorphosed Silurian sedimentary and volcanic rocks that apparently formed within a deep basin floored by oceanic crust and mantle (as in the Coolac Serpentinite Belt) (Figure 2.5) (Basden 1986).

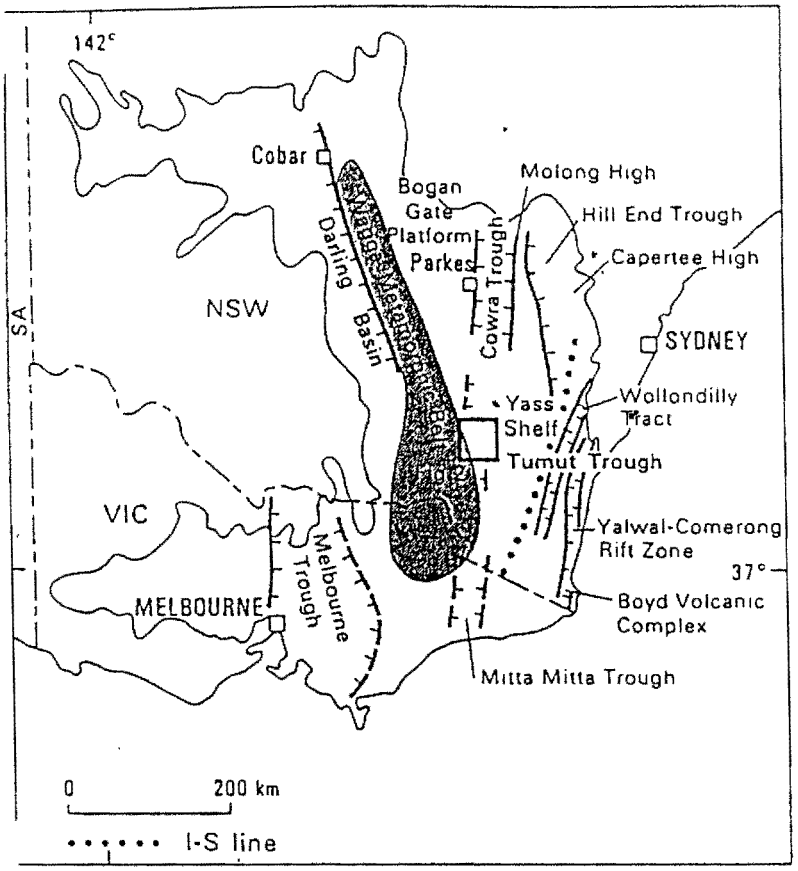

Figure 2.5 Location of the Tumut Trough (from Stuart-Smith 1990).

Ashley *et al.* (1979), Basden *et al.* (1987) and Basden (1990) interpreted the Coolac Serpentinite Belt (Golding 1966) as part of a Silurian ophiolitic suite associated with flysch, an association that is atypical of other Silurian sequences in the Lachlan Fold Belt (Stuart-Smith 1988; 1991). Powell (1984) referred to the Tumut Trough as the Tumut pull-apart basin, whilst Stuart-Smith (1991) contended that his restricted Tumut Trough sequence (Early to Late Silurian units comprising the Wyangle and Blowering Formations and the Honeysuckle Beds) was identical with other Silurian sequences in eastern Australia, and that the term "Tumut Trough" should be superseded by the term "Tumut Basin".

Much of the debate regarding the existence of the Tumut Trough depends upon the relationship between the Honeysuckle Beds and adjoining rock units. It therefore reflects the formational tectonics of the Honeysuckle Beds, the age relationships between the Honeysuckle Beds, Coolac Serpentinite Belt, Blowering Formation, North Mooney Complex and Young Granodiorite, and on whether the Honeysuckle Beds, gabbroic and plagiogranite intrusions, and Coolac Serpentinite Belt are part of an ophiolite.

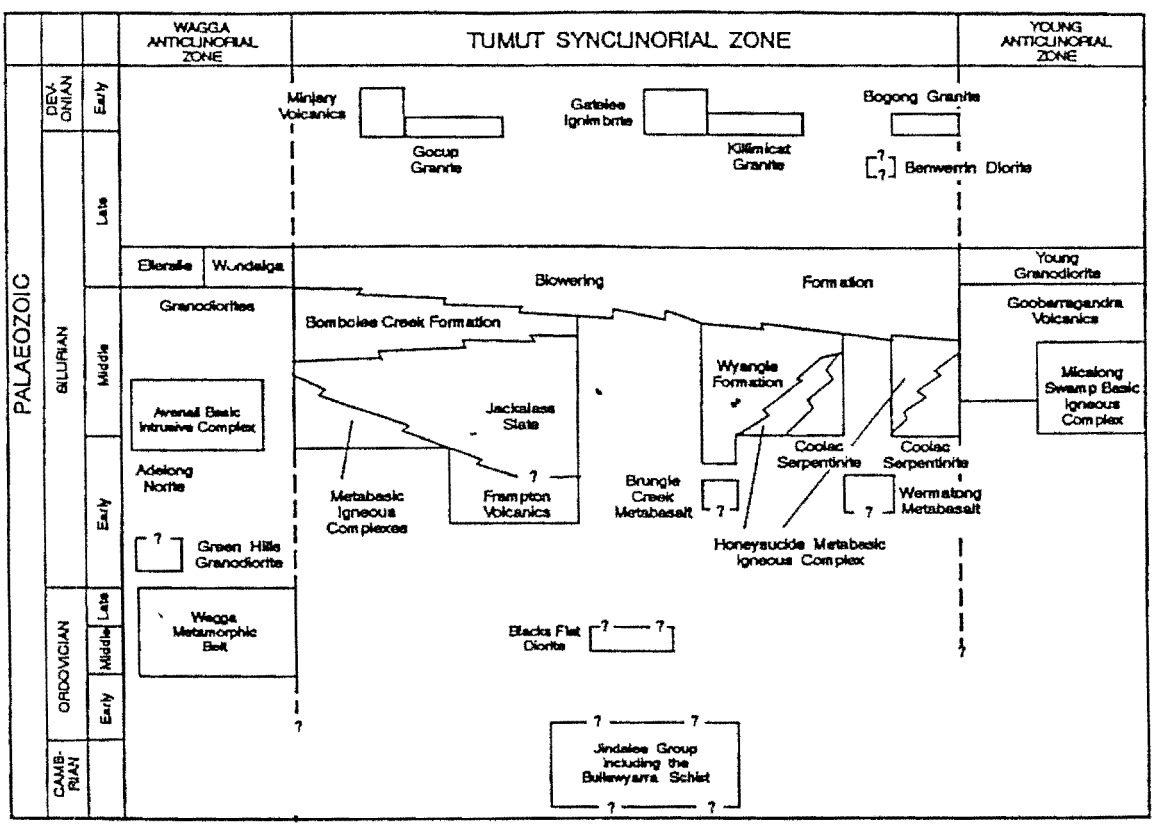

Figure 2.6 Tumut Trough stratigraphy of Basden (from Warner *et al.* 1992).

Tectonic evolution

The original stratigraphy of the Tumut Trough of Basden (1986, 1990) (Figure 2.6) has been questioned by Stuart-Smith (1988, 1990a, 1990b, 1991a, 1991b), Stuart-Smith *et al.* (1992) and Warner *et al.* (1992). The main problems contributing to the diverse interpretations of the geological development of this region are the dearth of reliable age data, inadequate exposure, and many faulted contacts. Metamorphism is a lesser problem as it is commonly accepted that the Tumut Trough sequence has only attained the lower greenschist facies of regional metamorphism (Basden 1990; Stuart-Smith *et al.* 1992).

Basden (1986, 1990) stated that the Tumut Trough was initiated in the Early Silurian as a rift in a super-terrane, comprising the Wagga Arch to the west, and the Yass-Canberra Rise to the east. During initial extension, the Brungle Creek and Wermatong Metabasalts were formed, but ongoing extension resulted in the development of the Honeysuckle, Long Tunnel, Snowball and Valley View Metabasic Igneous Complexes and the Coolac Serpentinite Belt. The evolving rift was bounded by major faults (the Mooney Mooney Fault Zone and Gilmore Fault Zone) and is subdivided into the Gundagai, Brungle and Bogong Basins, by the subsidiary Killimicat and Lacmalac faults (Basden 1986). The Gundagai Basin hosts the Jackalass Slate, Bumbolee Creek Formation and Blowering Formation, the Brungle Basin contains the Wyangle Formation and Blowering Formation, and the Bogong Basin solely consists of the Blowering Formation. The basement to the basins comprises the Jindalee Group, including the Wambidgee and Gundagai Serpentinite Belts.

Lightner (1977), Stuart-Smith (1988, 1990a, 1990b, 1991a, 1991b) and Warner *et al.* (1992) found that the sedimentary and basaltic rocks of the Honeysuckle Metabasic Igneous Complex (Basden 1986, 1990) were intercalated with and overlying the Blowering Formation, such that the latter could not be the youngest unit within the Tumut Trough sequence. For the same reason, the basaltic rocks could not conformably overlie the ultramafic rocks of the Honeysuckle Metabasic Igneous Complex and Coolac Serpentinite Belt.

Stuart-Smith *et al.* (1992) rejected the concept of the Tumut Trough and subdivided the region into the Tumut and Jindalee structural blocks, separated by the Killimicat Fault. They also rejected the existence of an Early Silurian oceanic substrate, and stated that the ultramafic rocks were

dismembered basement slices of a Cambro-Ordovician ophiolitic suite, based on: (a) distinct compositional differences between the sedimentary rocks of the Bumbolee Creek Formation and Blowering Formation; (b) differing geochemistry and interpreted tectonic environment of the Honeysuckle Beds compared to the mafic volcanics of the Long Tunnel and Snowball metabasic igneous complexes, and the Wermatong and Brungle Creek Metabasalts; and (c) the recognition of an earlier deformation within some of the units. Stuart-Smith *et al.* (1992) subdivided the rocks of the Tumut Trough into an Ordovician to Early Silurian package and an Early to Late Silurian package. The Ordovician to Early Silurian package consisted of the Gooandra Volcanics, Frampton Volcanics, Jackalass Slate, Bumbolee Creek Formation, Blacks Flat Diorite, Wermatong Metabasalt, Brungle Creek Metabasalt and Snowball Metabasic Igneous Complex. The Early to Late Silurian package, which consisted of the Wyangle Formation, Blowering Formation and Honeysuckle Beds, was separated from the Ordovician to Early Silurian package by an unconformity. They interpreted the intrusive mafic igneous rocks of the Honeysuckle Metabasic Igneous Complex of Basden (1986, 1990) as a separate Late Silurian complex and included the ultramafic igneous rocks of this complex with the Coolac Serpentinite Belt. Their stratigraphic relationships are shown in Figure 2.7.

The rock units throughout most of this region are dominated by N-NW trending folds, with a penetrative subvertical axial-plane cleavage (Basden 1986, 1990; Stuart-Smith *et al.* 1992), related to the Siluro-Devonian Bowning orogeny (Stuart-Smith 1988, 1990a, 1991b). However, Stuart-Smith *et al.* (1992) recognised an earlier deformation that is restricted to their Ordovician to Early Silurian package and is characterised by thrust faults, recumbent folds with east-west hingelines and, locally, later coaxial upright folds. The recumbent folds were interpreted by previous workers as either the result of granitoid emplacement (Crook 1980) or soft sediment slumping (e.g. Crook & Powell 1976). Stuart-Smith *et al.* (1992) suggested that Tumut Basin only during the deposition of the Early to Late Silurian sediments.

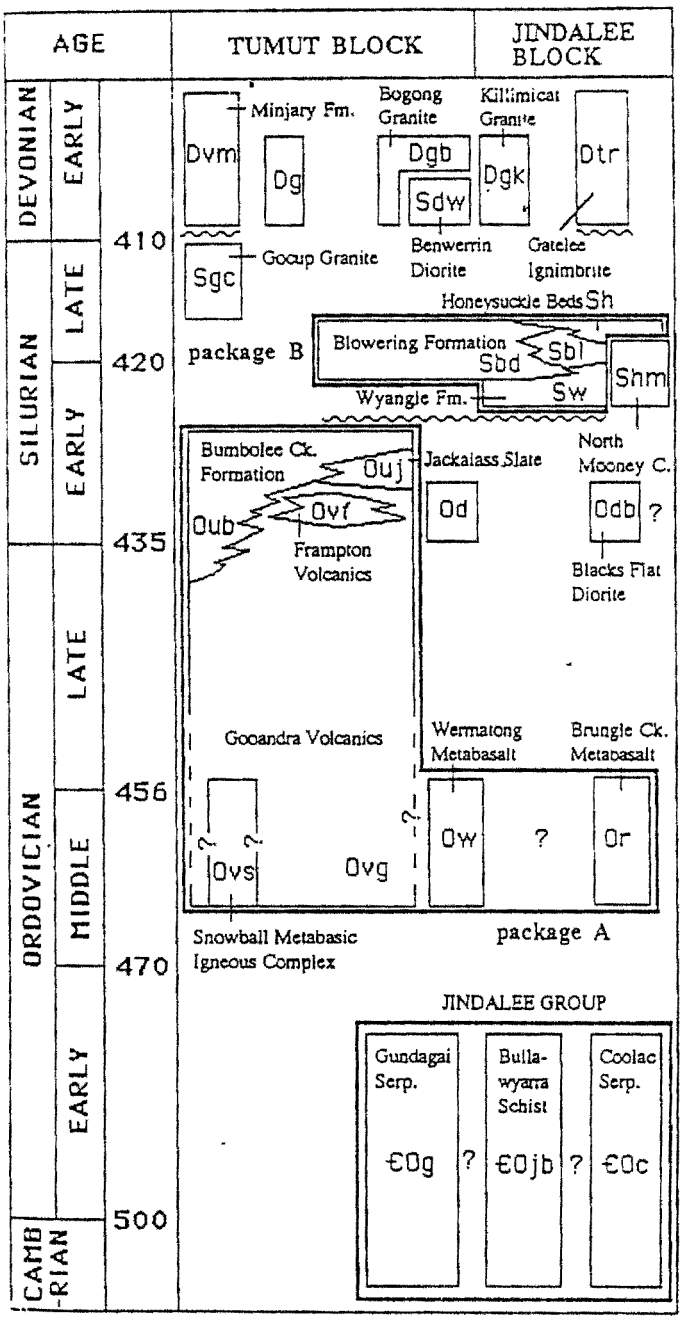

Figure 2.7 Tumut Trough stratigraphy of Stuart-Smith *et al.* (1992).

With the exception of the Honeysuckle Beds, which was recognised as the youngest Late Silurian unit, Warner *et al.* (1992) largely retained the stratigraphy of Basden (1986, 1990). However, they rejected the notion that the Coolac Ophiolite Suite (Ashley *et al.* 1979) was the substrate to the Tumut Trough. Instead, they stated that late in the Middle Silurian, the mafic rocks of the Honeysuckle Metabasic Igneous Complex of Basden (1986, 1990) were emplaced at various levels. Early in the Late Silurian, during tectonic inversion of the Tumut Trough sequences, upthrusting of some of the ultramafic rocks occurred (i.e. the Coolac Serpentinite and ultramafic rocks of the

Honeysuckle Metabasic Igneous Complex) resulting in components of the Coolac Ophiolite Suite became spatially associated with the basaltic and sedimentary rocks of the Honeysuckle Beds. They termed this an embryonic ophiolite, suggesting that the relationships were characteristic of early rifting before separation allowed creation of true ocean-floor stratigraphy. The revised stratigraphy of the Tumut Trough, based on the work of Warner *et al.* (1992), is shown in Figure 2.8.

There are, in essence, three tectonic models for the Tumut Trough, one based on the existence of typical oceanic crust during the Mid to Late Silurian, one on the existence of embryonic oceanic crust during the Late Silurian, and the remaining one on the serpentinite belts of the Tumut region representing Cambro-Ordovician basement to the region.

The Silurian "ophiolite model" (Ashley *et al.* 1979; Crook 1980; Scheibner 1985; and Basden 1990) was based on the spatial association of the Coolac Serpentinite Belt and Honeysuckle Metabasic Igneous Complex as a function of their association in Silurian oceanic crust.

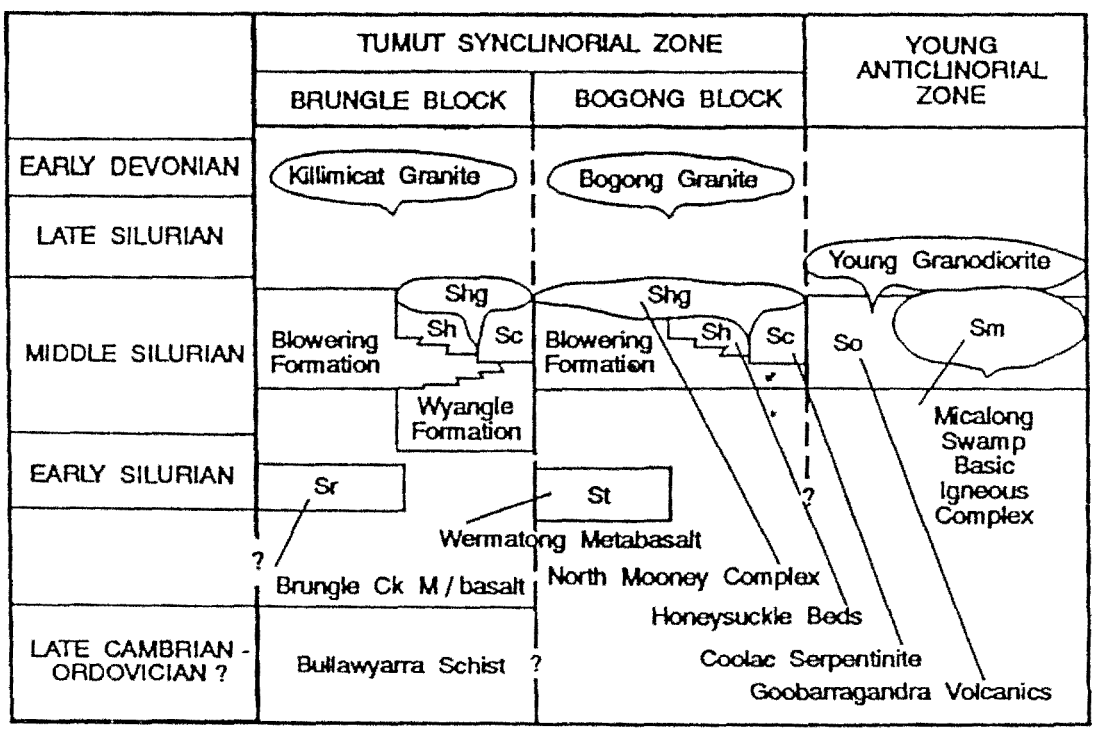

Figure 2.8 Tumut Trough stratigraphy of Warner *et al.* (1992).

In effect, they believed that the rock units represented a dismembered ophiolite suite (Figure 2.9), upthrust from an Early Palaeozoic marginal sea, because:

(a) the mineralogy and chemistry of the primary tectonised harzburgite and associated podiform chromitites are typical of ophiolites;

(b) the whole-rock geochemistry of the basaltic rocks is compatible with either a marginal sea or back-arc basin tectonic setting;

(c) the juxtaposition of the Honeysuckle Metabasic Igneous Complex and the Coolac Serpentinite Belt, although tectonically disrupted in places, is similar to that found in ophiolites elsewhere; and,

(d) sulphide occurrences within the basaltic rocks have many similarities to ophiolitic pyritic massive sulfide deposits.

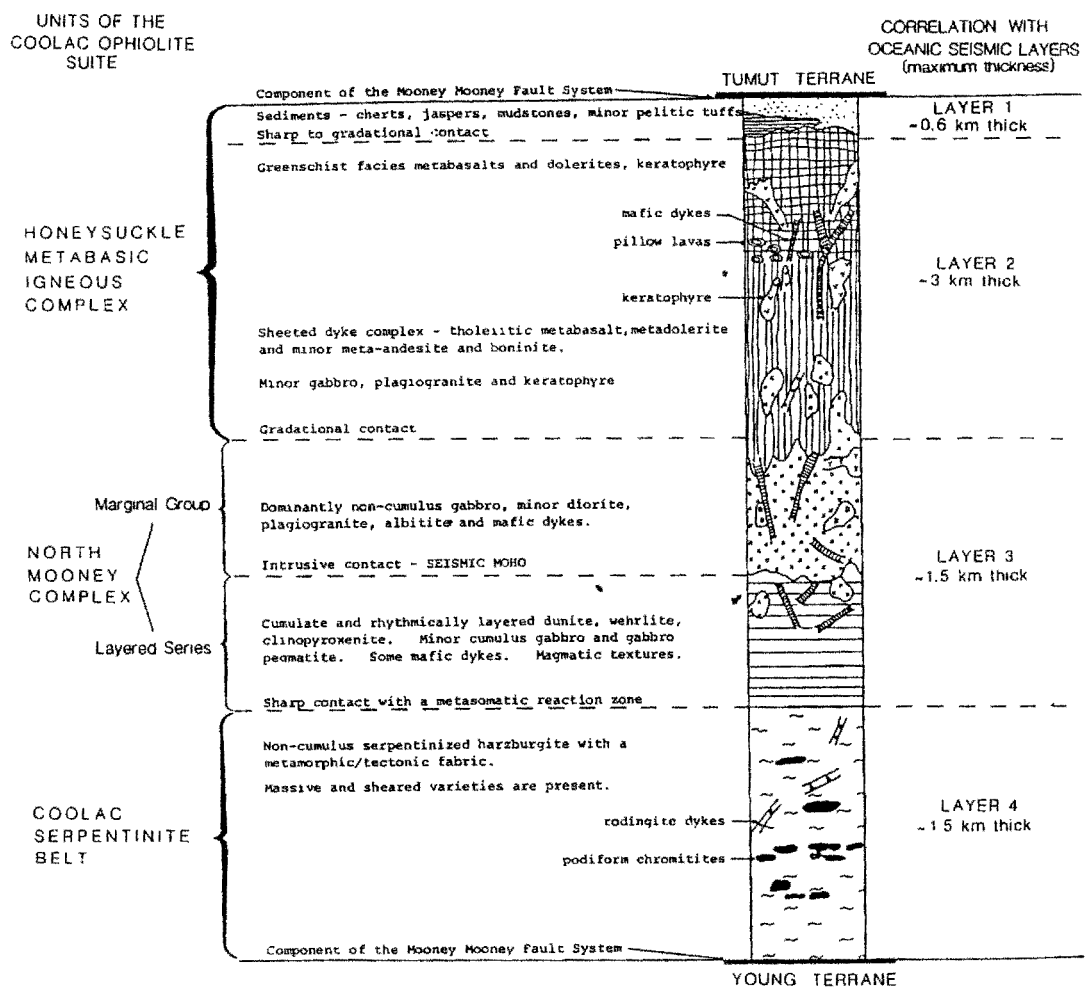

Figure 2.9 The Coolac Ophiolite Suite of Ashley *et al.* 1979 (from Basden *et al.* 1987).

Pre-existing faults influenced the development of the Tumut Trough. During the Late Silurian to Early Devonian Bowning-Bindi Orogeny, the Tumut Trough sequence was deformed and the Coolac Ophiolite Suite obducted along the eastern margin.

Warner *et al.* (1992) proposed that the development of Tumut Trough began in the Early Silurian by rifting of an Ordovician volcanic arc. Early fissure basalt and turbidite sedimentation was followed by voluminous silicic magmatism in the Middle Silurian. Subsequently, late in the Middle Silurian, through-going fractures developed in the lower crust and allowed the emplacement of little-modified mantle-derived magmas at high crustal levels (the mafic volcanic rocks of the Honeysuckle Metabasic Igneous Complex). Mafic intrusive rocks of the Honeysuckle Metabasic Igneous Complex were then emplaced within the mafic volcanic rocks resulting in the loose spatial association of the various phases of the Coolac Ophiolite Suite. Early in the Late Silurian, inversion of the Tumut Trough occurred and resulted in upright folding of the trough sequence and upthrusting of parts of the mafic intrusive rocks of the Honeysuckle Metabasic Igneous Complex and Coolac Serpentinite Belt to form the 'embryonic' ophiolite. The Young Granodiorite was then emplaced at its final crustal level alongside and locally intruding the Coolac Ophiolite Suite.

Stuart-Smith (1990a, 1990b, 1991b) interpreted the Coolac Serpentinite Belt as a tectonic slice that was derived from the underlying Cambro-Ordovician Jindalee Group and emplaced within the Mooney Mooney Fault System during Early Silurian extension. He based this upon the following:

(a) a conformable contact between the mafic volcanic rocks of the Honeysuckle Metabasic Igneous Complex and Blowering Formation;

(b) the intrusive mafic rocks of the Honeysuckle Metabasic Igneous Complex forming a dyke complex within the Coolac Serpentinite Belt, the mafic volcanic rocks of the Honeysuckle Metabasic Igneous Complex and the Blowering Formation, and being intruded by the Young Granodiorite - that is, the mafic rocks of the Honeysuckle Metabasic Igneous Complex were intruded ensialically;

(c) the Silurian cover rocks of the Tumut Trough record only one major deformation whereas the rocks of the Coolac Serpentinite Belt and Jindalee Group record at least two older periods of deformation.

Stuart-Smith (1990b) interpreted the development of the region in terms of a metamorphic core complex, but his use is not in accord with Lister (1998) who stated that metamorphic core complex

should be restricted to where gneissic domes are present as an integral part of the complex, and should not be used to describe metamorphic rocks surrounded by less metamorphosed or less deformed rock packages. Stuart-Smith believed that a major subhorizontal detachment fault (associated with the extension and development of the Tumut Trough) exists in the Brungle-Darbalara area (see Figure 1.4). During extension, and following the intrusion of the Blacks Flat Diorite, mafic and ultramafic rocks were emplaced into high strain zones. Major movement on this fault took place prior to the deposition of the Early Silurian Wyangle Formation which unconformably overlies both the basement and Brungle Creek Metabasalt, which he interpreted as forming steep-sided fault blocks resting on the detachment surface (see Figure 2.7). Felsic volcanic rocks of the Blowering Formation later filled the troughs. Stuart-Smith (1991b) stated that the Early to Late Silurian rocks formed a pull-apart basinal sequence, little different from other Silurian basins throughout the Lachlan Fold Belt.

Based on field relationships and detailed geochemistry, Dadd (1998) interpreted the development of the Honeysuckle Beds to the initial stages of back-arc spreading within an intracontinental rift setting. She stated that spreading was short-lived so that a basin floored by oceanic crust never developed, and a modern analogue for the Tumut Trough was the early stages of the western Lau Basin. Dadd also suggested that the juxtaposition of the Honeysuckle Beds, Coolac Serpentinite Belt and North Mooney Complex was fortuitous, and simply due to the utilisation of the same deep crustal fracture system over a protracted time period. She concluded that the Honeysuckle Beds, Coolac Serpentinite Belt and North Mooney Complex were unrelated, and therefore could not have formed part of a single Silurian ophiolite.

2.2.2 The Mooney Mooney Fault System

Introduction

The Mooney Mooney Fault System is a complex faulted shear zone (Basden *et al.* 1987) which separates the Tumut Synclinorial Zone in the west from the Young Anticlinorial Zone in the east and encloses the Coolac Ophiolite Suite of Ashley *et al.* (1979) and Basden (1990) (Figure 2.10). An understanding of the initiation and movement history of this fault system is vital to any interpretation of the tectonic history of this region and the entire Lachlan Fold Belt.

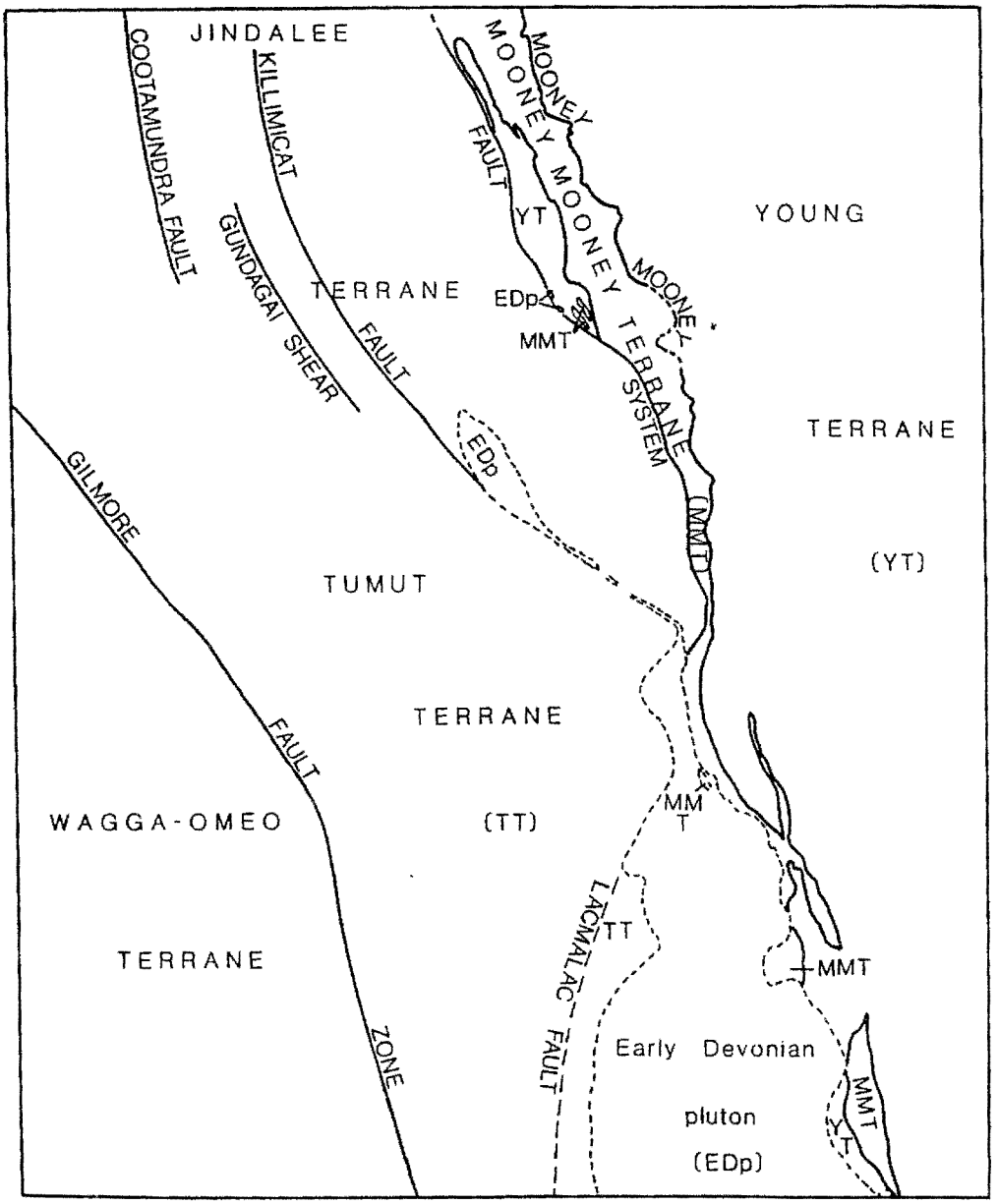

Figure 2.10 Location of the Mooney Mooney Fault System (from Stuart-Smith *et al.* 1992).

Extent and Nature

The Mooney Mooney Fault System extends from at least the southern extremity of the Coolac Serpentinite Belt (and perhaps from as far south as Cabramurra, Basden 1990) to Berthong in the north, a distance of 130km (see Figure 1.4). It comprises two major faults between which are many minor faults. Basden (1990), described the Mooney Mooney Fault System and the Jugiong Shear Zone (which can be traced from east of Brungle in the south, north to Cootamundra, a distance of

70km) as two separate fault systems whereas Warner *et al.* (1992) suggested that they are intimately related and thus should be treated as the one complex oblique thrust and strike slip fault system.

The eastern fault of the Mooney Mooney Fault System is marked by the intermittent development of mylonites within the Young Granodiorite and its associated volcanics (Ashley & Chenhall 1976; Basden 1990; Stuart-Smith 1990; Warner *et al.* 1992). The mylonites extend for up to 2km into the massive Young Granodiorite. Zonation of the mylonites from the contact outwards into the granodiorite generally consists of 10m of ultramylonite, 100m of orthomylonite and 1000m of protomylonite (Warner 1988). However, both the ultramylonites and orthomylonites are discontinuously developed and the most intense mylonitisation is not always at the fault contact (Warner 1988). Further, in places, mylonitisation is absent and the contact is intrusive to the adjacent serpentinite. Overall, there is a complex faulted/intrusive contact between the Young Granodiorite to the east and the rocks comprising the Coolac Ophiolite Suite of Ashley *et al.* (1979) to the west (Harris 1987; Stuart-Smith 1990; Marshall & Franklin 1992). The amount of deformation within the serpentinites seems minor compared to that in the granodiorite. The Young Granodiorite is intensely mylonitised along or close to this contact, whereas the S-C fabric within the serpentinites is not always developed. In fact, in some places, relatively massive harzburgite occurs at or close to the contact.

In the north of the Coolac Serpentinite Belt on the eastern side of Mount Lightning, relatively massive aplitic dykes of the Young Granodiorite have intruded schistose S-C fabric serpentinite, suggesting that the development of the S-C fabric within the serpentinite occurred prior to intrusion of the Young Granodiorite.

Structural and tectonic interpretations

The debate on the tectonic interpretation of the Mooney Mooney Fault System arises from contradictory structural evidence on the nature of the S-C relationships observed in the Young Granodiorite and adjoining Coolac Serpentinite Belt. Much of the argument stems from the identification and interpretation of the extension lineation within both units, since this is used to construct the structural history of this fault zone. Stuart-Smith (1988) stated that S-C fabrics within

both the Coolac Serpentinite Belt and Young Granodiorite support sinistral strike-slip displacement but Warner *et al.* (1992) noted that, mesoscopically, a stretching lineation is generally absent and therefore the S-C relationships are inconclusive. Stuart-Smith (1988) recognised different structural histories within the Young Granodiorite and Coolac Serpentinite Belt. He proposed a major Early Silurian sinistral strike-slip movement within the serpentinite, that pre-dated all structures within the Mooney Mooney Fault System, followed by a major Mid Devonian (375 Ma) sinistral strike-slip movement on the Mooney Mooney Fault System. However, Warner *et al.* (1992) stated that, depending upon the local strike of the fault relative to the Devonian east-northeast/west-southwest shortening direction, both sinistral and dextral movement components are possible. Stuart-Smith (1990) invoked a three-stage movement history for the fault zone; Late Silurian vertical movement preceded Mid Devonian sinistral strike-slip displacement, which was followed, in turn, by Mid Devonian NE-trending dextral strike-slip movement (Figure 2.11). In contrast, Warner *et al.* (1992) stated that there is good agreement between the movement senses within both the Young Granodiorite and Coolac Serpentinite Belt and therefore invoked a more simple movement history for the fault zone (Figure 2.11).

(a) Stuart-Smith (1990)

STAGE 1
Late Silurian reverse movement

STAGE 2
Mid Devonian sinistral strike-slip movement

STAG
Mid Devonian dextral strike-slip movement

b) Warner *et al.* (1992)

STAGE 1
Late Silurian east side-up movement with a minor dextral component south of the Mooney Mooney Fault System - Jugiong Shear Zone divergence. Mainly sinistral strike-slip movement north of the divergence.

STAGE 2
Early Devonian sinistral strike-slip movement

Figure 2.11 Movement histories for the Mooney Mooney Fault System.
a) Stuart-Smith (1990) b) Warner *et al.* (1992)

They stated that the easterly fault of the E-NE-dipping Mooney Mooney Fault System is a high angle reverse fault and that, where the extension lineation plunges to the north, there is a dextral component, whereas, where it plunges to the SE, there is a sinistral component. This change in movement direction is said to coincide with the convergence of the east branch of the Mooney Mooney Fault System with the Jugiong Shear Zone, which, away from the Mooney Mooney Fault System, displays dominantly dextral strike-slip movement. Both Stuart-Smith (1988, 1990) and Warner *et al.* (1992) agreed that the Mooney Mooney Fault System was reactivated in the Middle Devonian. Stuart-Smith (1990) also ascribed the development of the western schistose margin of the Coolac Serpentinite Belt to this reactivation event.

The differing structural interpretations have major tectonic implications. If the Coolac Serpentinite Belt has pre-Mooney Mooney Fault System structures, it proves that the Coolac Serpentinite Belt has recorded an event prior to emplacement of the Young Granodiorite; the age of this event and its significance to the proto Mooney Mooney Fault System needs to be resolved. If the interpretation of Stuart-Smith (1990) is correct, the Coolac Serpentinite Belt must have been emplaced into the upper continental crust by at least the Early Silurian and he stated that it most likely represented a basement slice emplaced during the strike-slip faulting associated with Early Silurian extension; that is prior to the intrusion of the North Mooney Complex gabbros. However, if Warner *et al.* (1992) are correct, the Tumut Trough and Coolac Serpentinite Belt would not have pre-dated structures within the Mooney Mooney Fault System, producing similar senses of movement within the Coolac Serpentinite Belt and Young Granodiorite would have been synchronous. They considered this deformation to be associated with the Late Silurian closure of the Tumut Trough sequence when the obduction of the Coolac Ophiolite Suite occurred prior to emplacement of the Young Granodiorite. This obductive movement of the Coolac Serpentinite Belt would have imparted an S-C fabric that was overprinted during the emplacement of the Young Granodiorite. As the granodiorite was progressively emplaced and cooled, deformation partitioned into the serpentinite thereby producing the same movement sense.

2.2.3 The Gilmore Fault Zone

Introduction

The Gilmore Fault Zone (Crook & Powell 1976; Basden 1990) or Gilmore Suture (Scheibner 1985) is a major structure throughout the western Lachlan Fold Belt in NSW (Stuart-Smith 1991). In the study area, it forms the boundary between the Wagga-Omeo Terrane and the Tumut Terrane (Scheibner 1985; Basden 1990) (Figure 2.12). The Gilmore Fault Zone supposedly separates the higher-grade metamorphic rocks of the Wagga-Omeo Terrane from the lower grade metasedimentary rocks to the east (Bradley 1968; Basden 1990). None of the serpentinite belts occur west of the fault zone, which partly coincides with the Tumut Ponds Serpentinite Belt.

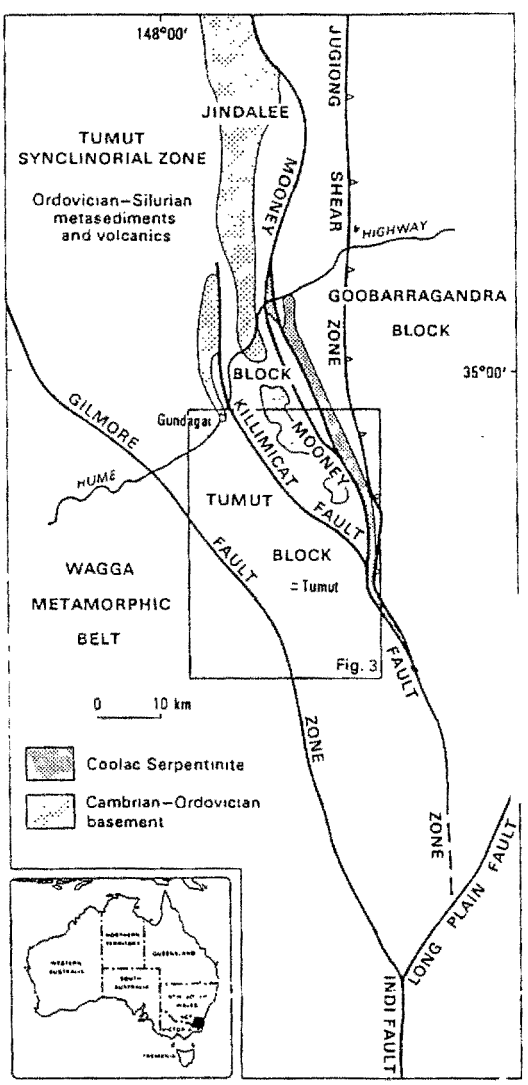

Figure 2.12 Location of the Gilmore Fault Zone (from Basden *et al.* 1987).

Extent and nature

The Gilmore Fault Zone trends north-northwest and extends for several hundred kilometres from the southeastern to the central western region of NSW (Stuart-Smith 1991). In the Tumut Serpentinite Province, it extends from near Cabramurra in the south (where it joins the Long Plains-Indi Fault Zone - Wyborn 1977), past the north-western limit of the study area (Figure 2.12). The Gilmore Fault Zone is well-defined by both aeromagnetic and gravity data (Wyatt *et al.* 1980; Suppel *et al.* 1986), is up to 6km in width (Stuart-Smith 1991) and is composed of a number of braided fault and mylonite zones (Basden *et al.* 1987; Stuart-Smith 1991). It is generally thought to be steeply west-dipping throughout most of its length with the exception from Condobolin to Cobar where it is east-dipping (Warren *et al.* 1995). According to Basden *et al.* (1987), the surface expression of the Gilmore Fault Zone is that of a weakly emergent or eroded, tip-stick thrust front, as defined by Morley (1986).

Structural and tectonic interpretations

The Gilmore Fault Zone has been interpreted (Basden *et al. 1985,* 1987; Scheibner 1985) as the boundary between the Ordovician to Early Silurian rocks of the Wagga-Omeo Terrane to the west, and the Middle to Late Silurian rocks of the Tumut Terrane to the east; that is, it forms a terrane boundary. Basden *et al.* (1987) believed that the proto-Gilmore fault zone marked the western boundary of the Tumut Trough. However, Stuart-Smith (1991a) and Stuart-Smith *et al.* (1992) considered that the Gilmore Fault Zone was not a terrane boundary in the Late Ordovician or Early Silurian but instead was a reactivated basement fault, corresponding in part to an older terrane boundary. The difference between these two models largely arises from differing interpretations of the structural and metamorphic histories of rock units across the fault zone. Scheibner (1985) and Basden *et al.* (1985, 1987) believed that rocks of the Wagga-Omeo Terrane had undergone more intense deformation and attained a higher grade of metamorphism than those to the east of the Gilmore Fault Zone, whereas Stuart-Smith (1991b) and Stuart-Smith *et al.* (1992) advocated common structural and metamorphic histories for the rock units across the fault zone. Precise age dates of the rock units on both sides of the Gilmore Fault Zone, and a clear definition of the fault zone itself are needed to resolve this dispute, but beyond looking at the Tumut Ponds Serpentinite Belt, the nature of the Gilmore Fault Zone was not investigated during the course of this study.

CHAPTER 3: THE COOLAC SERPENTINITE BELT

3.1 INTRODUCTION

The Coolac Serpentinite Belt is steeply-dipping and of alpine-type (Golding 1966; Graham *et al.* 1992). It forms a well-defined ridge (Plate 3.1), and mostly consists of partially serpentinised and massive harzburgite along with a diverse assemblage of variably altered ultramafic, mafic and felsic rocks. It is divisible into an eastern zone of massive harzburgite and a western zone of schistose harzburgite/serpentinite, and contains the largest recorded concentration of podiform chromitites in Australia. The chromitites are hosted by massive harzburgite or schistose serpentinite and occur as small dyke-like bodies and lenses, usually rimmed by a thin dunite shell. The belt has been interpreted as the basal section of a Silurian ophiolite complex, (the "Coolac Ophiolite" of Ashley *et al.* 1979), or as Cambro-Ordovician basement (Stuart-Smith 1990b, 1991b).

Plate 3.1 Typical topography of the Coolac Serpentinite Belt, forming the Honeysuckle Range. View from the southern slope of Mount Lightning, looking south.

3.2 THE WESTERN CONTACT AND ABUTTING ROCKS

The stratigraphy west of the Coolac Serpentinite Belt is generally consistent and, from east to west, consists of the North Mooney Complex/Honeysuckle Beds, Goobarragandra Volcanics/Blowering Formation and Jindalee Group.

3.2.1 The Honeysuckle Beds

The Honeysuckle Beds, a group of basaltic, metavolcanic rocks with subordinate basic intrusions and metasedimentary rocks, occur immediately to the west of the Coolac Serpentinite Belt (Figure 3.1). The name was suggested by Ashley *et al.* (1971) and Ashley (1973a) who restricted the term to the basaltic volcanic and associated metasedimentary rocks and placed the intrusive basic and ultrabasic rocks (that now comprise the North Mooney Complex) within the Coolac Serpentinite Belt. In contrast, Basden *et al.* (1975; 1978) included the North Mooney Complex rocks and termed the collective unit the Honeysuckle Metabasic Igneous Complex (Basden 1982, 1990). Dadd (1998) restricted the use of the term "Honeysuckle Beds" to include only the volcanic and sedimentary rocks. She suggested that the intrusive rocks are part of a younger sequence. The Honeysuckle Beds, as used in this thesis, largely follows Ashley *et al.* (1971) and Ashley (1973a), but gabbroic intrusions, other than in the North Mooney Complex, are also included (see below).

Basden *et al. 's* (1975) type section for the Honeysuckle Beds, from G.R. 084 364 to G.R. 112 365 on the Cootamundra 1:100 000 sheet, includes rocks of the North Mooney Complex. The type section for this thesis is on the western side of Mount Lightning (G.R. 113 260 to G.R. 135 260), where thin lenses of siltstone, phyllite and chert are interbedded with spilitic metabasalt over an approximate thickness of 2km. Basden (1990) placed the Honeysuckle Metabasic Igneous Complex within the Late Silurian, Stuart-Smith (1990b) assigned the Honeysuckle Beds (as defined by Ashley *et al.* 1972) to the Late Silurian, and Warner *et al.* (1990) considered the Honeysuckle Beds (again as defined by Ashley *et al.* 1972) to be Middle Silurian.

Contact relationships with the Coolac Serpentinite Belt

The Coolac Serpentinite Belt abuts the Honeysuckle Beds across a fault striking 310-355° and dipping steeply (75° to 90°) eastward. At the contact, the Coolac Serpentinite Belt largely consists

of schistose serpentinite, which acts as a matrix to infaulted blocks of Honeysuckle Beds metabasalt, dyke-like bodies of plagiogranite and albitite, and irregular masses of rodingite. In the terminology of Raymond (1984), the contact is a tectonic mélange with a serpentinite matrix, or a polygenetic melange with a serpentinite matrix, infaulted blocks and dyke-like intrusions including fragments of the Honeysuckle Beds.

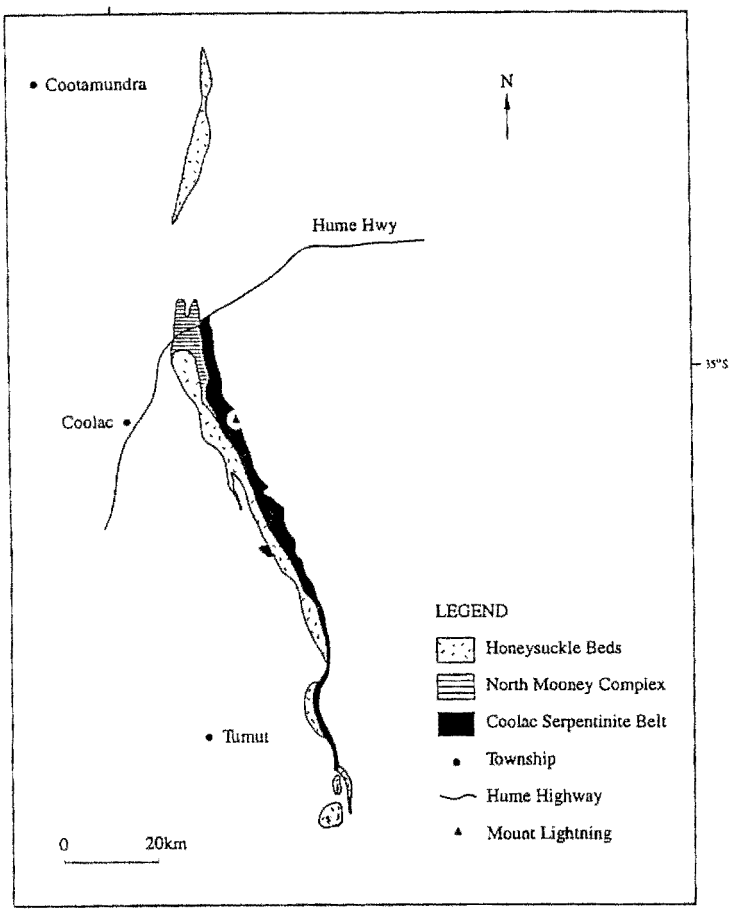

Figure 3.1 Location and extent of the Honeysuckle Beds along the western contact of the Coolac Serpentinite Belt (adapted from Basden 1990).

Lithology

(For detailed petrographic descriptions, see Appendix 3PD)

The principal metasedimentary components of the Honeysuckle Beds comprise phyllite, chert and well-laminated siltstone, while minor components include intermediate tuffs and quartzite (Ray 1977). The metasediments are rare near the contact with the Coolac Serpentinite Belt, but they become increasingly common westward, where they pass transitionally into sandstone and siltstone of the Blowering Formation (Ashley *et al.* 1971). They typically occur overlying or interbedded

with mafic pillow lavas (Dadd 1998). Most of the metavolcanic rocks are spilitised basalts. Variolitic varieties (with the variolites defined by slender quenched plagioclase and augite) are of minor occurrence, whereas pillow basalts are common. Rare basaltic breccias occur interbedded with the pillow lavas.

The volcanic rocks were originally composed of plagioclase, augite, glass and magnetite and metamorphism/alteration has led to the replacement of plagioclase by albite/zoisite/calcite and augite by actinolite, and development of chlorite, epidote and quartz (Dadd 1998).

3.2.2 The North Mooney Complex

The North Mooney Complex was recognised by Golding (1969) and defined by Franklin (1975) as a series of layered, cumulus mafic to ultramafic rocks, having most of the characteristics of a relatively undisrupted ophiolite sequence (albeit somewhat thinned). Generally, the rocks are massive and range in composition from dunite, wehrlite and clinopyroxenite, through olivine-, hornblende- and quartz-gabbros, to minor diorite and plagiogranite. Basden (1990) assigned this group of rocks to the Honeysuckle Metabasic Igneous Complex, whereas Stuart-Smith (1990) placed the layered portion of the North Mooney Complex within the Coolac Serpentinite Belt and redefined the North Mooney Complex as the intrusive massive hornblende gabbros. In this thesis, the original definition of the North Mooney Complex of Franklin (1975) is retained. The complex occupies an area of approximately 15 km^2 and dips steeply (>75°) to the east (Figure 3.2). Franklin (1975) divided the North Mooney Complex into an ultramafic cumulate zone termed 'the layered series' and a massive gabbroic zone termed 'the marginal series'. The layering is of magmatic origin striking 350° to 005° and dipping between 75°E and vertical (Franklin 1975). Webb (1980) obtained K-Ar ages of 426 ± 6Ma and 425 ± 6Ma on hornblende from the North Mooney Complex; Basden (1990) interpreted this as the magmatic crystallisation age. Further south, small isolated, fault-bound bodies of wehrlite, gabbro, diorite and pyroxenite up to 1-2km in length and considered to be equivalents of the North Mooney Complex (Ashley 1973a), occur within the Coolac Serpentinite Belt.

Contact relationships with the Coolac Serpentinite Belt and North Mooney Complex

Franklin (1975) stated that portions of the North Mooney Complex intrude the Coolac Serpentinite Belt. She based this on:

(a) the existence at several localities, of metasomatic reaction zones (up to 5m wide), that comprise intensely altered wehrlite, a mixed rock and intensely altered harzburgite, between fresh wehrlite (North Mooney Complex) and massive harzburgite (Coolac Serpentinite Belt). However, these have alternatively been ascribed to serpentinisation by Ashley (1973) and Ray (1977).

(b) serpentinised harzburgite containing abundant antigorite where it abuts the North Mooney Complex; antigorite is rare and confined to contacts with intrusive granitoids elsewhere in the belt (Franklin 1975, 1997 pers. comm.).

(c) the ultramafic rocks being massive rather than schistose at the contact.

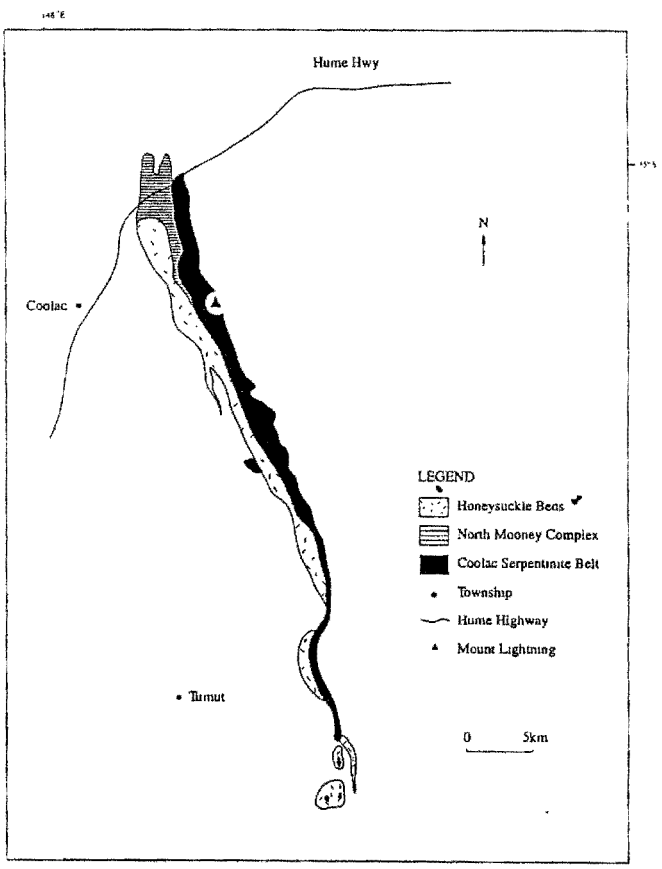

Figure 3.2 Location and extent of the North Mooney Complex (adapted from Basden 1990).

The above interpretation (Franklin 1975) is supported by Stuart-Smith (1990), who described the North Mooney Complex as a gabbroic dyke complex intruding the Coolac Serpentinite Belt. Similarly, the present study has shown that abundant rodingitised gabbroic dykes (equated with the North Mooney Complex) intrude the western contact of the Coolac Serpentinite Belt. Thus, although the metasomatic zone between the Coolac Serpentinite Belt and North Mooney Complex might have resulted from serpentinisation, the development of antigorite and intrusion of dykes are consistent with the North Mooney Complex intruding and therefore being younger than the Coolac Serpentinite Belt.

At its southern end, the North Mooney Complex intertongues with (Franklin 1975) and intrudes (Stuart-Smith 1990a; Warner *et al.* 1992) mafic volcanic rocks of the Honeysuckle Beds. Since the Honeysuckle Beds are intercalated with, but grossly overlie the Blowering Formation (Lightner 1977; Stuart-Smith 1988; Warner *et al.* 1992), the North Mooney Complex must be younger than both the Honeysuckle Beds and Blowering Formation.

Petrology

(For detailed petrographic descriptions, see Appendix 3PD)

The layered series: Franklin (1975) subdivided the 'layered series' into a main series consisting of well-layered dominantly massive and fresh rocks, and a western series consisting of poorly-layered, intensely altered and sheared rocks, though both series contain the same lithologies. Wehrlite is the dominant ultramafic rock and forms mappable layers (some 30-100m thick and up to 2km in length) within the main layered series and thin (some 5m thick) lenses in the western series (Franklin 1975). Dunite occurs as discontinuous lenses and pods (2-20m wide and up to 60m long) in the lower portion of the main series and pods in shear zones (3m by 150m) in the western series. Clinopyroxenite is less common and occurs as discontinuous irregular layers (up to 100m thick). Gabbro occurs as rare pods either between two different ultramafic units or within the clinopyroxenite unit (Franklin 1975). Pegmatitic gabbro forms rare intrusive patches (up to 5m across) or dykes (up to 0.3m across), particularly within the clinopyroxenite units in both series.

The marginal series: This is composed of gabbro, with subordinate amounts of hornblende-gabbro pegmatite and diorite, and rare albitite and plagiogranite. Dykes and angular xenoliths of metabasalt occur in all the other rock types. Although the gabbros vary in texture and grainsize, they are mineralogically and chemically similar. The diorites, albitites and plagiogranites are mainly found close to the western contact of the marginal series, where it abuts the Honeysuckle Beds (Franklin 1975).

3.3 THE EASTERN CONTACT – YOUNG GRANODIORITE

The eastern contact is principally with the Young Granodiorite (after Ashley & Basden 1973), which was first described as the "Young Granite" by (Adamson 1960) and is the main component of the Young Batholith (Basden 1990) which extends over 210km from north to south (Ashley & Basden 1973) and is generally less than 30km in width (Basden *et al.* 1974) (Figure 3.3). Parts of the Young Batholith have been termed the "Cowra Granodiorite" (Stevens 1952) and "Burrinjuck Granite Complex" (Adamson & Loudon 1966).

Contact relationships

Ashley *et al.* (1971), stated that the contact between the Young Granodiorite and Coolac Serpentinite Belt is faulted and marked by the development of a zone of brecciated and mylonitised Young Granodiorite. Franklin (1975) indicated that, in the vicinity of the North Mooney Complex, the Coolac Serpentinite Belt is separated from the Young Granodiorite by the easternmost fault of the Mooney Mooney Thrust System. Conversely, Harris (1987), Warner (1988), Marshall & Franklin (1992) and Warner *et al.* (1992) have shown that along certain parts of the contact, the Young Granodiorite has intruded the Coolac Serpentinite Belt.

Although stating that the Young Granodiorite is faulted against the Coolac Serpentinite Belt, Stuart-Smith (1990b) indicated that granodioritic dykes and irregularly-shaped bodies intrude the Coolac Serpentinite Belt in the vicinity of the North Mooney Complex. He stated that these minor bodies, although separated from the main mass of the Young Granodiorite by a 5m wide zone of mylonite, have fine-grained chilled margins less than 1m in width.

Where the Tumut-Wee Jasper Road crosses the Coolac Serpentinite Belt (G.R. 234 041, Tumorrama 1:25 000), a tectonic inclusion of granodiorite, that is enclosed within schistose serpentinite of the Coolac Serpentinite Belt, contains enclaves of metaserpentinite. Marshall & Franklin (1992) conversely indicated that, whereas the Young Granodiorite abuts the Coolac Serpentinite Belt for more than 50km, it transgresses the Coolac Serpentinite Belt and is shallowly discordant to the regional strike between the townships of Coolac and Young. They suggested that the relationships were consistent with the Young Granodiorite intruding the Coolac Serpentinite Belt subsequent to the latter being emplaced as a sub-vertical sheet-like mass along the eastern margin of the Tumut Synclinorial Zone. They found that, although generally steep, the contact is locally shallow and irregular and has a well-defined chilled and/or hydrothermally altered margin. The intrusive relationships locally give way to tracts of mylonitised granodiorite and S-C fabrics in the adjacent Coolac Serpentinite Belt, both commonly exhibiting an east-side up reverse component. In shear zones away from the faulted contact, and in places adjacent to the intrusive contact, S-C fabrics in the Coolac Serpentinite Belt record a sinistral movement-sense which predated the intrusion and upthrust of the Young Granodiorite (Marshall & Franklin 1992).

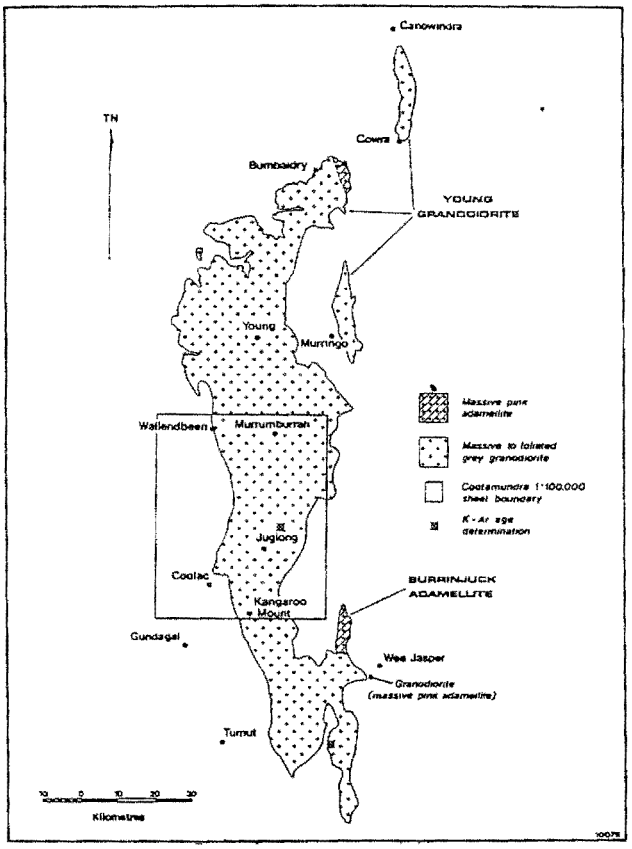

Figure 3.3 Location and extent of the Young Batholith (from Basden *et al.* 1974).

According to Marshall & Franklin (1992) the complex part-intrusive/part-faulted contact between the Coolac Serpentinite Belt and Young Granodiorite is consistent with emplacement of the Young Granodiorite at a high crustal level by surge tectonic processes (Hollister & Crawford 1986). They contended that any interpretation involving the Coolac Serpentinite Belt being thrust against the Young Granodiorite is inconsistent with the field relationships. Were a thrust tectonic model applicable to emplacement of the Coolac Serpentinite Belt, the imbricate architecture must have been established before the Silurian when, at least in the Tumut region, steeply-dipping portions of thrust faults were reactivated during emplacement of the Young Granodiorite. The generation, upward migration and intrusive/fault emplacement of the Young Granodiorite against the Coolac Serpentinite Belt, perhaps reflect components of east-west extension and shortening that accompanied the inferred (e.g. Basden 1990) opening and inversion of the Tumut Trough.

Warner *et al.* (1992) stated that mylonitic granodiorite extends up to 2km east from the NNW trending contact with 10m of ultramylonite passing outward into 100m of orthomylonite followed by 1000m of protomylonite. They reported that the ultra- and orthomylonites are discontinuously developed, the most intense mylonitisation is not always at the contact, and portions of the granodiorite in the mylonitic tract can be unmylonitised. It would seem that some parts of the tract have Type I S-C mylonite (Lister & Snoke 1984) with a well-defined extension lineation, whereas in other parts, the lineation is weak to absent. S-C relationships, the extension lineation and microscopic kinematic indicators suggest that the eastern boundary of the ENE dipping Mooney Mooney Fault System is a high angle (60 to 90°), reverse fault structure; where the extension lineation plunges north it has a dextral component, and a sinistral component where it plunges southeast. The change from dominantly sinistral to dextral coincides where the Mooney Mooney Fault System converges with the Jugiong Shear Zone.

Dupen (1986) and Harris (1987) reported the same movement senses from the Young Granodiorite and Coolac Serpentinite Belt across the Mooney Mooney Fault System, whereas Stuart-Smith (1988) expressed a contrary view. It is reasonable to suggest that the event reflecting the emplacement of granodiorite could overprint the older Coolac Serpentinite Belt emplacement signature. However, serpentinite readily forms S-C fabrics, and, in the absence of proof of overprinting, the significance and interpretation of local S-C fabrics is contentious.

During the present study, many dyke-like bodies of fine-grained aplitic granodiorite/diorite were found enclosed within either relatively unfoliated harzburgite or schistose serpentinite of the Coolac Serpentinite Belt; some are over 100m east of the Young Granodiorite/Coolac Serpentinite Belt boundary. The aplitic bodies are generally fine-grained, felsic, quartz-rich and biotite-free, and contain discrete zones (of weak to moderate intensity) of foliation. Fibrous tremolite commonly overprints the other minerals.

The dyke-like bodies found during the present study could not be traced into the main mass of the Young Granodiorite, but Harris (1987) and Stuart-Smith (1990a) record comparable bodies, some of which were connected to the main granodiorite mass.

(a) Along the Hume Highway road-cutting at the contact between the Coolac Serpentinite Belt and Young Granodiorite, now unfortunately covered over, Harris (1987) found blocks of massive gabbro (1-2m across) completely enclosed within unfoliated granodiorite. Observation confirmed by B.J. Franklin (*pers. comm.*).

(b) Stuart-Smith (1990a) found the following:

  (i) 5km SE of Mungi homestead (in the north of the belt) dykes and an irregular-shaped body (100m across) of granodiorite intrude massive harzburgite and are separated from the main mass of the Young Granodiorite by a 5m wide mylonite zone.

  (ii) 2km N and S of Mungi homestead, small stocks of granodiorite intrude both the Coolac Serpentinite Belt and North Mooney Complex. The granodiorite has a fine-grained narrow (<1cm) chilled margin surrounding coarse-grained granodiorite. Observation confirmed by both B.J. Franklin and B. Marshall (*pers. comm.*).

  (iii) Where the Tumut-Wee Jasper Road crosses the serpentinite belt, a tectonic inclusion of Young Granodiorite contains xenoliths of serpentinite. Observation confirmed personally and by B. Marshall (*pers. comm.*).

The petrographic similarity of these bodies to the Young Granodiorite has also been observed by others (e.g. Harris 1987; Stuart-Smith 1990a). Also, Ashley (1973: p.106) stated that rocks from two granodiorite tectonic inclusions within the Coolac Serpentinite Belt were chemically similar to rocks from the main mass of the Young Granodiorite.

Petrology

(For detailed petrographic descriptions, see Appendix 3PD)

The granodiorite has a uniform composition throughout the region (Basden 1990), despite porphyritic phases occurring near the eastern and southern contacts with the Goobarragandra Volcanics and, rarely, within the main mass. Nearly every thin-section exhibits some sign of deformation (Basden 1990); quartz variously displays undulose extinction, sutured grain boundaries and recrystallisation, while plagioclase and biotite are commonly bent and/or kinked. In the vicinity of the western contact- the principal foliation, a mylonitic foliation, varies from weak to moderately intense, is defined by the preferred orientation of biotite and lenticular aggregates of quartz (Franklin 1975), and becomes increasingly intense within discrete internal and marginal shear zones.

Enclaves composed of fine-grained biotite, feldspar and minor quartz occur in most outcrops (Basden 1990) and possess sharp to gradational contacts. In thin-section, they are hypidiomorphic granular and consist of plagioclase (65%), biotite (25%) and quartz (10%) along with minor epidote, chlorite and sericitic alteration (Basden 1990). These "microgranitoid-xenoliths" (Vernon & Flood 1982) are restricted to high-level plutons and perhaps formed by the quenching of more mafic "globules" in the host granitoid magma (Vernon 1983).

Basden (1990) stated that the Young Granodiorite is typically S-type according to the classification of De La Roche *et al.* (1980) and White & Chappell (1983). Areas of porphyritic granodiorite, with volcanic inclusions and aplitic dykes, occur in the central parts of the main mass and are consistent with exposure close to the roof.

3.4 GENERAL FEATURES OF THE COOLAC SERPENTINITE BELT

The Coolac Serpentinite Belt was named the "Coolac-Goobarragandra Serpentine Belt" (Golding 1962) and subsequently the "Coolac Serpentine Belt" (Golding 1966, 1967). The Coolac Serpentinite Belt, Honeysuckle Beds and North Mooney Complex were collectively interpreted as the Coolac Ophiolite Suite (Ashley *et al.* 1979), but the contentious nature of this (Stuart-Smith 1990) has resulted in the present author adopting Golding's (1966, 1967) definition of the "Coolac Serpentinite Belt". The type section is along the valley of Brungle Creek from G.R 235 044 to G.R 229 029 (Basden 1990)."

The Coolac Serpentinite Belt extends as a continuous body from the Hume Highway in the north to 1 km south of "Federal Park" (G.R 265 865) in the south (Figure 3.4), after which it continues southward as small isolated pods to G.R. 305 783. The overall strike length is 63km (Basden 1990). The width is 3.5km at Red Hill, but only 10m where it crosses the Goobarragandra river (Ray 1977). It extends at least 5km below the surface (Leven *et al.* 1991) and its contacts dip steeply (70° to vertical) to the west. It therefore comprises a near-vertical, sheet-like body of variably serpentinised peridotite.

3.4.1 Surface outcrop of rock types

Outcrop of the Coolac Serpentinite Belt, is good on the steep slopes of the Honeysuckle Range, but less well exposed on the top of the range, particularly in pine plantations (e.g. at Red Hill). It forms variably serpentinised harzburgite block-like masses that are generally 1-3m across and which show no preferred orientation. Schistose serpentinite crops out well within the creek drainage on the sides of the hills and, where better exposed, forms discontinuous vertical, sheet-like masses up to 1.5m high. Plagiogranites and albitites occur as white dyke-like masses readily observable within the much darker harzburgite and serpentinite, whereas wehrlites, lherzolites and hornblendites are hard to distinguish. Gabbros, and all but the large masses of rodingites, crop out poorly. The chromitites are marked by mine workings and/or prospect pits. Serpentinised dunites can be distinguished by their bleached-yellow colour, but fresh dunites are hard to distinguish from other ultramafic rocks.

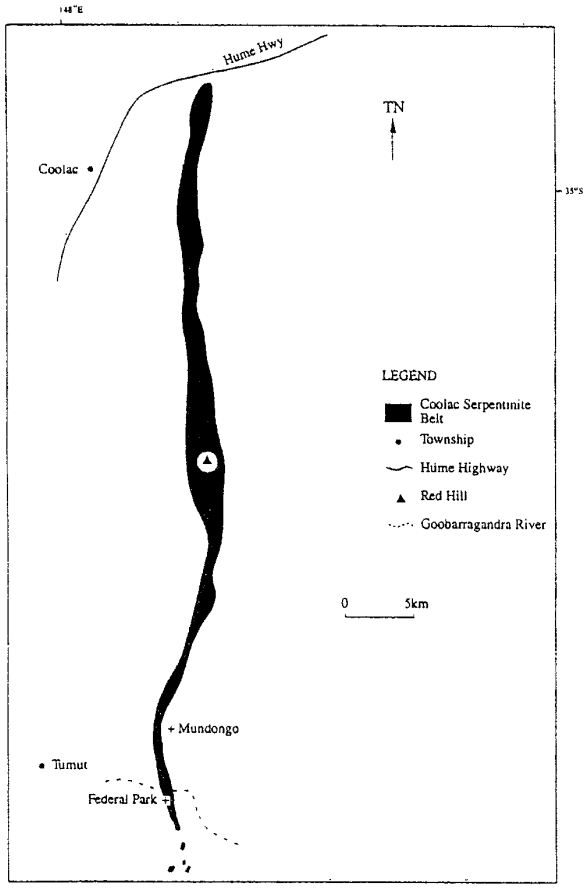

Figure 3.4 Location and extent of the Coolac Serpentinite Belt (adapted from Basden 1990).

3.4.2 Internal Features

The Coolac Serpentinite Belt contains a range of internal features and structures, these including: tectonic inclusions, intrusive rock bodies, the western schistose margin, primary layering, internal shear zones, and podiform chromitite bodies (Chapter 9).

(a) Tectonic inclusions

Tectonic inclusions are bodies of rock that have become detached or isolated from their source by tectonic disruption, and are enclosed or included in the surrounding rock" (Bates & Jackson 1980). Such tectonic inclusions abound in the western schistose margin but are less common within the southernmost part of the Coolac Serpentinite Belt. They range from <1m to 1400m long and up to 170m wide, and are either equidimensional or have their longer plan dimension parallel to the trend of the belt (Ashley 1973a). The bodies commonly consist of gabbro and plagiogranite, but chromitite, wehrlite, diorite, amphibolite, albitite, granodiorite, metabasalt, metadolerite, rhyodacite and rare metasedimentary bodies exist (Ashley 1973a).

Metasedimentary bodies are restricted to within 250m of the western boundary of the belt (i.e. the faulted contact with the Honeysuckle Beds), along with metabasaltic, metadoleritic and rhyodacitic bodies, and comprise a tectonically incorporated association. Features which are evidence of a tectonic emplacement include:

(i) the bodies have sheared margins;

(ii) the long axis of the bodies trend parallel to the trend of the serpentinite belt;

(iii) the metamorphic grade (and history) of the bodies is clearly different to that of the surrounding ultramafic rocks (e.g. the amphibolites); and

(iv) tectonic emplacement is the only mechanism that can explain their present position within the surrounding ultramafic rocks (e.g. the metasedimentary rocks).

(b) Intrusive rock bodies

It seems more likely that many of the gabbro and plagiogranite bodies represent late-stage intrusions of fractionated melts rather than being tectonic emplacements. Similarly, the chromitite bodies and associated dunites appear to have crystallised at their present location and even the highly brecciated chromitites appear to have moved little from their sites of crystallisation (Graham *et al.* 1993a).

Rodingite "dykes' abound, particularly near the podiform chromitite deposits in the north of the belt. They appear to be "rootless" and have been interpreted as pockets of residual gabbroic magma that subsequently underwent calcium metasomatism (Golding 1970; Ashley *et al.* 1972), or as metasomatised basic dykes and/or tectonic inclusions. Other rock types occurring as dyke-like masses are chlorite rock, pyroxene gabbro, plagiogranite and albitite. Features which are evidence of intrusive emplacement include:

(i) they do not have sheared margins;

(ii) most are unfoliated and massive;

(iii) they occur within massive, as well as schistose harzburgite and serpentinite; and

(iv) many contain inclusions of adjacent wallrock.

Also, it is hard to envisage a process whereby relatively small bodies are thrust into massive harzburgite.

(c) The Western Schistose Margin

The western margin of the Coolac Serpentinite Belt from the northernmost extremity to 4km south of Brungle Creek east of Brungle (see Figure 1.4), consists of a tract (100-800m wide) of schistose serpentinite with "tectonic inclusions" and blocks of massive serpentinite and partially serpentinised and variably foliated harzburgite; it has been termed "the western schistose margin" (Ashley 1973a, 1975). From 4km south of Brungle Creek, the tract occupies the entire width of the Coolac Serpentinite Belt and its southern satellite bodies (Basden 1990). According to Stuart-Smith (1990b), widespread S-C fabrics developed during sinistral strike slip movement in the mid-Devonian. In the vicinity of Mount Lightning, zones of schistose (S-C fabric) serpentinite alternate with relatively massive (unfoliated) porphyroclastic harzburgite across the full width of the belt, but their intensity increases from east to west.

The western schistose tract has the characterisitics of a melange and from here onward will be termed the "Western Tectonic Melange Zone" (WTMZ).

(d) Primary Layering

Mineralogical layering (of a primary magmatic origin) occurs within the massive porphyroclastic harzburgite and is defined by orthopyroxene-rich and orthopyroxene-poor layers (Jeffreson 1982; Basden 1990), which vary from 2 to 15cm in thickness (Lohan 1982). In-situ layering is rare, but it is present in many disoriented blocks.

(e) Internal Shear Zones

Discrete zones of moderately to highly schistose (S-C fabric) serpentinite are widespread throughout the Coolac Serpentinite Belt. They range from a few centimetres wide and a few metres long, through to continuous zones over 25m wide and more than 500m long. Some of the larger zones contain trains of small, ovoid "residuals" of massive serpentinite which help to define S within the S-C fabric. Prominent zones are well-exposed on the north-western slope of Mount Lightning (Gundagai 1: 25 000 sheet G.R. 138 253), where they form well-defined lineaments when viewed on air photos and from the ridge north of the Murrumbidgee River.

3.5 PETROGRAPHY AND TEXTURAL/STRUCTURAL EVOLUTION

(For detailed petrographic descriptions, see Appendix 3PD)

3.5.1 Harzburgites

Harzburgites of the Coolac Serpentinite Belt are ultramafic rocks with a porphyroclastic texture and at least 10% visible orthopyroxene (as fresh, or partially to completely serpentinised shape-preserved orthopyroxene grains) along with minor clinopyroxene and hornblende. Fresh, moderately serpentinised, and completely serpentinised relatively massive harzburgites are all common. The harzburgites collectively comprise 80-85 volume per cent of the entire belt, this rising to 95% if only the eastern half is considered. Foliated varieties characterise internal shear zones and the Western Tectonic Melange Zone (Figure 3.5).

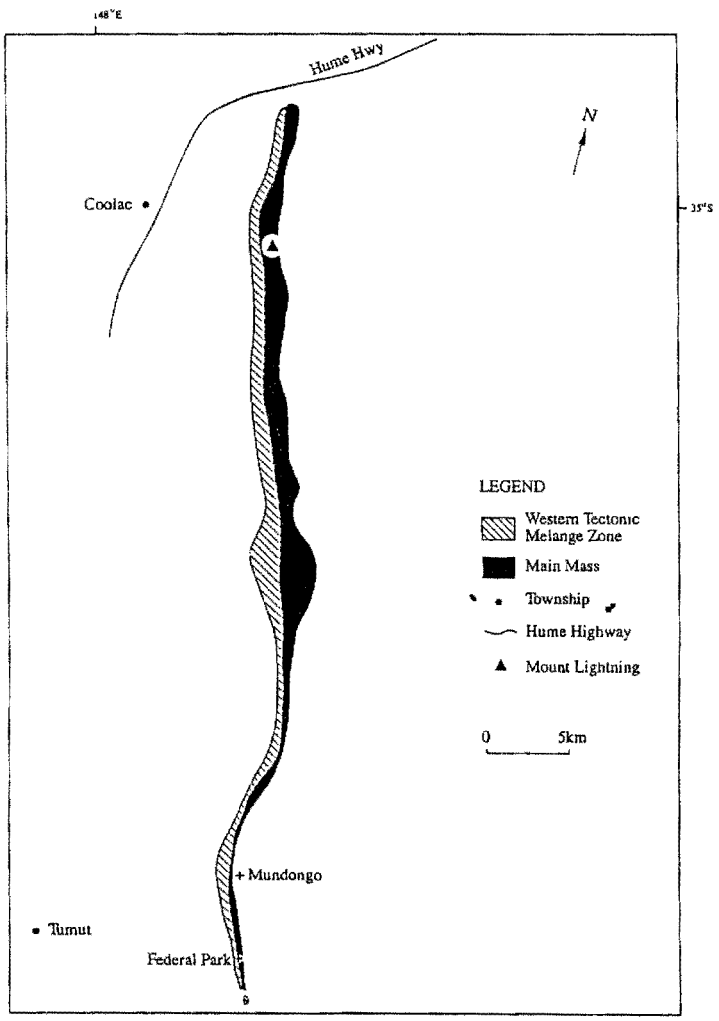

Figure 3.5 Location and extent of the Western Tectonic Melange Zone of the Coolac Serpentinite Belt.

Fresh harzburgite exhibits a porphyroclastic texture (Plate 3.2) and consists of more than 30% statically recrystallised olivine (with subgrain development) along with porphyroclasts of orthopyroxene, rare porphyroclasts of clinopyroxene, and accessory chrome spinel. Moderately serpentinised harzburgite also exhibits a pseudoporphyritic porphyroclastic texture and has less than 30% fresh olivine (Plate 3.3). Completely serpentinised harzburgite lacks relict olivine, always contains porphyroclastic orthopyroxene (or its pseudomorphs) and has mesh (Plate 3.4), sub-mesh, or feathery decussate texture.

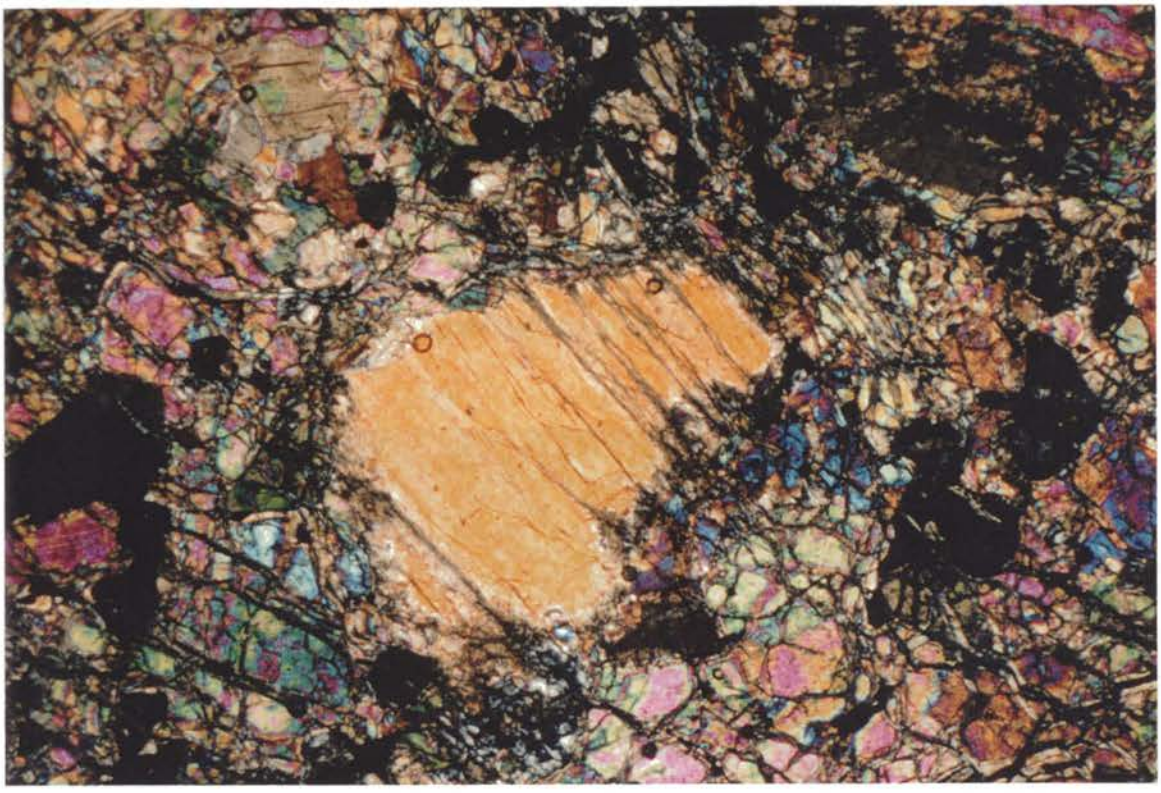

Plate 3.2 Fresh harzburgite with recrystallised olivine, exhibiting a pseudoporphyritic porphyroclastic texture.
Sample No ML032 UXP F.O.V 3.5mm

Plate 3.3 Moderately serpentinised harzburgite exhibiting a pseudoporphyritic porphyroclastic texture.
Sample No ML027 UXP F.O.V 3.5mm

Plate 3.4 Completely serpentinised harzburgite exhibiting a mesh texture.
Sample No ML028 UXP F.O.V 3.5mm

The porphyroclastic texture of mantle harzburgites results from recrystallisation during high temperature solid-state flow, and primarily accommodates ductile simple shear in the asthenosphere during sea-floor spreading (Bartholomew 1993; Boudier & Nicolas 1995). Based on experimental work and the type of olivine slip system involved (Carter & Ave Lallement 1970; Nicolas *et al.* 1980; Nicolas & Christiansen 1987), such flow requires temperatures of 1000-1100°C and pressures of 20MPa (Suhr 1993), this being significantly below the experimentally determined melting temperature of peridotite (Takahashi & Kushiro 1983; Nicolas 1989). If harzburgite crystallised from a melt at 1300-1350°C in an anhydrous environment, or even just below 1200°C in a hydrous environment (Nicolas 1989), recrystallisation at 1000-1100°C involves mineralogical and/or textural metamorphic retrogression.

Thus, as also concluded by Ray (1977), porphyroclastic texture in the Coolac Serpentinite Belt is interpreted as the textural product of deformation and metamorphism within the aesthenosphere. Suhr (1993) classified such texture as a 'type 3 microstructure', implying low strain at high temperature, followed by a weak low temperature overprint.

The development of elongate, aligned olivine grains (with intergranular space-fill serpentine) within some of the partially serpentinised harzburgites of the Coolac Serpentinite Belt (Plate 3.5) is controversial. The grains could have stretched during a localised pre-serpentinisation high strain event and then become affected by lower temperature serpentinisation processes. If so, they equate with the mylonitic 'type 6 microstructure' (Suhr 1993), supposedly developed under moderate strain conditions at 900 - 1000°C (Suhr 1993) and classified as lithospheric (e.g. Nicolas 1986; Ceuleneer *et al.* 1988). Alternatively, the grains could be part of a lower temperature syn-serpentinisation texture that formed by :

(a) grain-boundary related fracturing of the olivine grains, due to the reduction of lithostatic pressure that accompanied uplift from lower mantle to crustal levels;
(b) fluids migrating through the intergranular porosity and reacting with the olivine to form intergranular chrysotile;

(c) development of localised high strain zones, leading to the progressive stretching of the olivine grains within these zones and coalescence of the intergranular chrysotile (possibly accompanied by new chrysotile fibre growth).

The probable solution is ductile elongation (pre-fracturing) at high temperature with the active olivine slip system being (101) [100], then fracturing during low temperature extension concurrent with serpentinisation.

Plate 3.5 Elongate aligned olivine grains within partially serpentinised harzburgite.
Sample No ML037 UXP F.O.V 3.5mm

Mesh-texture mimics the high temperature porphyroclastic texture and involves pseudomorphous replacement of fractured olivine grains by lizardite cores and chrysotile rims (Wicks 1984). X-ray diffraction analyses of moderately and completely serpentinised harzburgites confirm that the Coolac Serpentinite Belt serpentine-group minerals are lizardite 6T and chrysotile 2M, consistent with a temperature range of 100 - 300°C (e.g. Coleman 1971; also see Ray 1977). More recently, O'Hanley and Wicks (1995) ascribed retrograde serpentinisation to temperatures below 250°C at $P_{(H2O)}$ of less than 1kb. Uncommon veinlets of prehnite cross-cut completely serpentinised

harzburgite at Mount Lightning (Graham 1990) and suggest limited amounts of either post-serpentinisation hydrothermal alteration or ongoing decay of the temperature regime.

Wicks (1984) contended that, before serpentinisation, harzburgites must undergo fracturing to allow ingress of serpentinising fluids, although concurrent and interdependent fracturing and fluid infiltration (e.g. Sibson 1996) could be a more realistic model, so it follows that the fresh harzburgite "blocks" have resisted fracturing and serpentinisation-related fluid infiltration. Laurent and Hebert (1979) ascribed retrograde serpentinisation to downward infiltration of sea-water through deep fractures in the oceanic lithosphere, thereby resulting in the replacement of olivine and orthopyroxene by lizardite+chrysotile+magnetite (Evans 1977). However, such grain-scale replacement also requires pervasive ingress of sea-water, as would be facilitated by grain-scale hydraulic fracturing, so it would seem that deep-reaching master fractures, coupled to pervasive grain-scale fracturing, are necessary for wide-ranging serpentinisation. With further evolution, some shear zones develop within serpentinised harzburgite and contain well-developed S-C fabrics with chrysotile-fibre development. Subsequently, chrysotile/magnetite veinlets cross-cut the post-serpentinisation shear zones, and are, in turn, cut by prehnite veinlets (above) and even the latter are locally displaced by small shear planes (Graham 1990). Thus, in summary, the harzburgites of the Coolac Serpentinite Belt have undergone textural and fabric changes over temperatures ranging from around 1100°C to approximately 100°C and also record several deformational events.

3.5.2 Dunites

Dunites are ultramafic rocks with a granular to porphyroclastic texture, containing greater than 90% olivine (or olivine/serpentine combinations) and 2-10% chromite. They comprise <0.5% by volume, of the Coolac Serpentinite Belt and are more common in the eastern half, and are extensively serpentinised. They occur as irregular bodies (approx. 5m across) or small dyke-like masses (a few metres in length), are relatively unfoliated, and lack sheared margins. Dunites hosting podiform chromitite deposits are described in Chapter 9.

The Coolac Serpentinite Belt dunites can be subdivided into relatively fresh and completely serpentinised groups but, unlike the harzburgites, transitional types seem not to exist. Fresh dunites

have more than 85% unaltered olivine and granular textures (Plate 3.6), whereas completely serpentinised dunites lack fresh olivine grains and have a well-developed mesh texture (Plate 3.7).

Like fresh harzburgites, the granoblastic to porphyroclastic texture of fresh dunites can be equated with the 'type 3 microstructure' (low strain high temperature, with a weak low temperature overprint) of Suhr (1993). This suggests recrystallisation temperatures of 1000-1100^{o}C under a deviatoric stress of some 20MPa. Serpentinisation varies from weak to intense. XRD studies reveal that the serpentine-group minerals comprise Al-rich lizardite and chrysotile 2M. The onset of serpentinisation resulted in the intergranular replacement of olivine by chrysotile 2M.

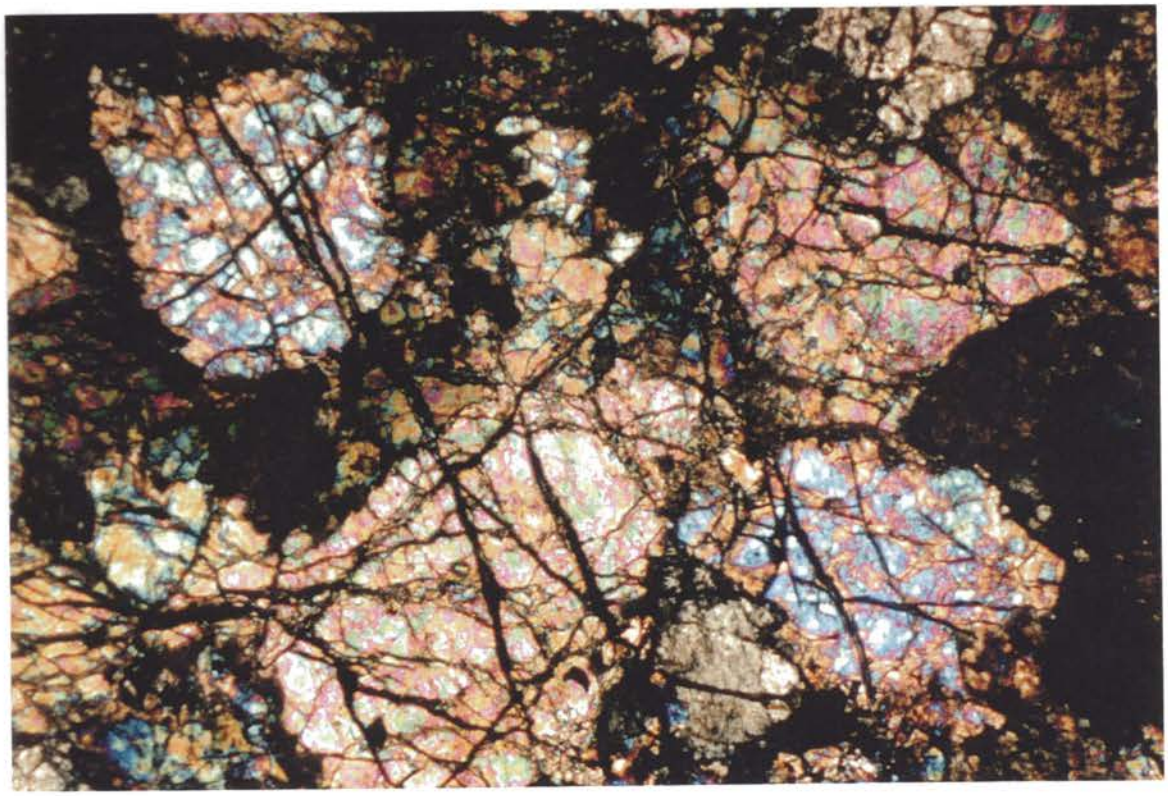

Plate 3.6 Fresh dunite exhibiting a granoblastic texture and extremely fractured grains with magnetite fracture-fill.
Sample No 123 UXP F.O.V 3.5mm

Plate 3.7 Serpentinised dunite exhibiting a well-developed mesh texture.
Sample No 85 UXP F.O.V 3.5mm

Continuation of this process led to replacement of the remaining olivine cores by Al-rich lizardite (e.g. O'Hanley & Wicks 1995), orthopyroxene was replaced by fibrous chrysotile around the rims, and within fractures and cleavage. Ongoing serpentinisation is evidenced by mesh texture and cross-cutting chrysotile veinlets. Talc/magnesite replacements of lizardite/chrysotile may also have formed during serpentinisation (Coleman 1977) or by later hydrothermal alteration (Ashley 1997). The assemblage lizardite+chrysotile+magnetite is ascribed to early stage low temperature serpentinisation ($<250 \pm 25^{\circ}C$ at a $P_{(H2O)}$ of < 1kb - O'Hanley & Wicks 1995) from sea-water infiltration (e.g. Laurent & Hebert 1979), prior to emplacement in continental crust (e.g. Moody 1979).

In summary, dunites, like the harzburgites, experienced a complex history which began in the upper mantle with high temperature ductile deformation, and was followed by continuing lower temperature brittle deformation within the lithosphere during serpentinisation.

3.5.3 Pyroxenites/Wehrlites/Hornblendites

Pyroxenites, wehrlites and hornblendites are rare within the belt and are generally restricted to its western margin (Ashley *et al.* 1971). They occur as lenticular bodies, up to several hundred metres long and 30m wide, within schistose serpentinite (Basden 1990). They also form rare dyke-like bodies (up to 10m x 3m), cross-cutting massive serpentinite (Basden 1990), with their long axes approximately paralleling the trend of the belt (i.e. approx. 335°). Elongate dyke-like bodies also occur within a tectonic melange block at Mundongo (G.R. 229 931).

The pyroxenites have >70% clinopyroxene, while the wehrlites have up to 80% olivine; both contain up to 15% amphibole (Basden 1990). Only meta-pyroxenites were found within the Coolac Serpentinite Belt during the present study. Hornblendites display a porphyroclastic, pseudoporphyritic texture.

The secondary mineral assemblage noted in the metapyroxenites consisted of dark brown hornblende rims with pale green amphibole cores (species not determined), actinolite, chlorite, epidote and minor chrysotile. The co-existence of actinolite and hornblende in these rocks is indicative of the transition from the upper greenschist to lower amphibolite facies of regional metamorphism (Miyashiro 1994). Hornblendes have pale green amphibole cores and dark brown rims (Plate 3.8), consistent with an amphibolite facies overprint. However, the "reverse" zonation could alternatively reflect:

(a) brown hornblende being due to lower granulite to amphibolite facies metamorphism and then experiencing selective core replacement during subsequent lower greenschist facies metamorphism; or
(b) lower greenschist facies metamorphism being followed by moderate grade thermal overprint; or
(c) the pale green cores being magmatic hornblende.

Alternative (b) is rejected because thermal overprints elsewhere in the Coolac Serpentinite Belt are confined to the western margin, close to I-type granite plutons (Basden 1990). No such pluton is observed in the mapped area. Alternative (c) is rejected because magmatic hornblende in hornblendites is typically brown (B. Franklin, pers. comm. 1998). Alternative (a), is therefore the most plausible explanation for the observed zonation.

Plate 3.8 Amphibole grains within metapyroxenite with pale green cores and dark brown rims.
Sample No BF92/51 PPL F.O.V 3.5mm

Although there is need for microprobe data to substantiate the amphibole species present, the author did not have necessary funding for such quantitative electron microprobe analysis. The amphiboles consist of dark brown hornblende rims which, if replacing magmatic clinopyroxene, could be consistent with amphibolite to lower granulite facies metamorphism within the upper mantle, and pale green amphibole cores (Plate 3.8). The dark brown hornblende could alternatively be late magmatic (e.g. Ashley 1973a).

Allowing that the pale green amphibole cores reflect greenschist facies metamorphism, it follows that actinolite fringes on clinopyroxene and hornblende grains could represent a second period of greenschist facies metamorphism (Miyashiro 1994) (Plate 3.9) or ongoing re-equilibration during metamorphic decay.

Actinolite fringes on clinopyroxene and hornblende grains could represent a second period of greenschist facies metamorphism (e.g. Miyashiro 1994) (Plate 3.10). However, it might alternatively reflect ongoing re-equilibration under protracted greenschist facies conditions.

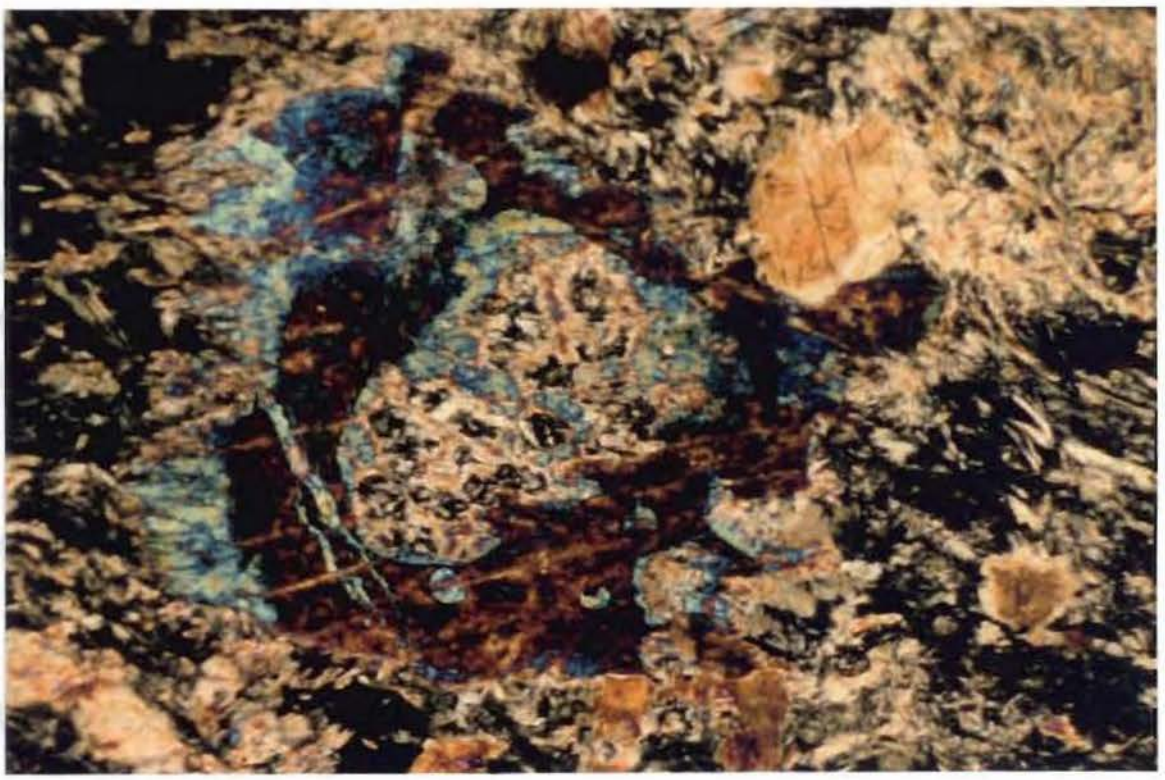

Plate 3.9 Serpentine cores in hornblende within metapyroxenite.
Sample No BF92/51 UXP F.O.V 3.5mm

Plate 3.10 Actinolite fringes around hornblende within metapyroxenite.
Sample No BF92/51 UXP F.O.V 3.5mm

Serpentine within the groundmass probably replaced olivine and seemingly obliterated the magmatic olivine texture. Late-stage low temperature (lower greenschist facies) alteration is indicated by epidote within the groundmass and platy colourless chlorite replacing and overprinting the ragged and corroded actinolite fringes (e.g. Miyashiro 1994). In summary, the magmatic and metamorphic history consists of:

(a) crystallisation of magmatic clinopyroxenite (clinopyroxene+olivine+chrome spinel);
(b) amphibolite to lower granulite facies metamorphism within the upper mantle environment (replacement of clinopyroxene by brown hornblende), or late magmatic crystallisation of brown hornblende.
(c) greenschist facies metamorphism and serpentinisation within the oceanic environment (replacement of the cores of brown hornblende by pale green hornblende, fringes of tremolite/actinolite, replacement of olivine by serpentine);
(d) low temperature alteration (development of chlorite and epidote).

Greenschist facies metamorphism overprinted any evidence of prior deformation. There is no evidence of deformation accompanying metamorphism (b), the high grade event, although undulose brown hornblende is consistent with deviatoric stress at relatively high temperature. With regards to deformation accompanying the greenschist facies metamorphism, none of the mineral grains (even fibrous amphibole) display preferred orientation or other evidence of strain.

3.5.4 Serpentinites

Serpentinites are the second most common rock type in the Coolac Serpentinite Belt. They are ultramafic rocks that lack fresh olivine and other magmatic minerals (with the exception of minor chrome spinel), exhibit a secondary serpentinisation texture, and contain less than 20 modal % talc and/or magnesite. Schistose and massive varieties occur throughout the belt, and are particularly common in the Western Tectonic Melange Zone. The massive variety occupies equidimensional blocks (up to a few metres in diameter) and lenses (up to 10m in maximum dimension) embedded in schistose serpentinite (see section 3.4.2), an indication of the distribution being conveyed by a strip-map along the crest of Mount Lightning (Figure 3.6).

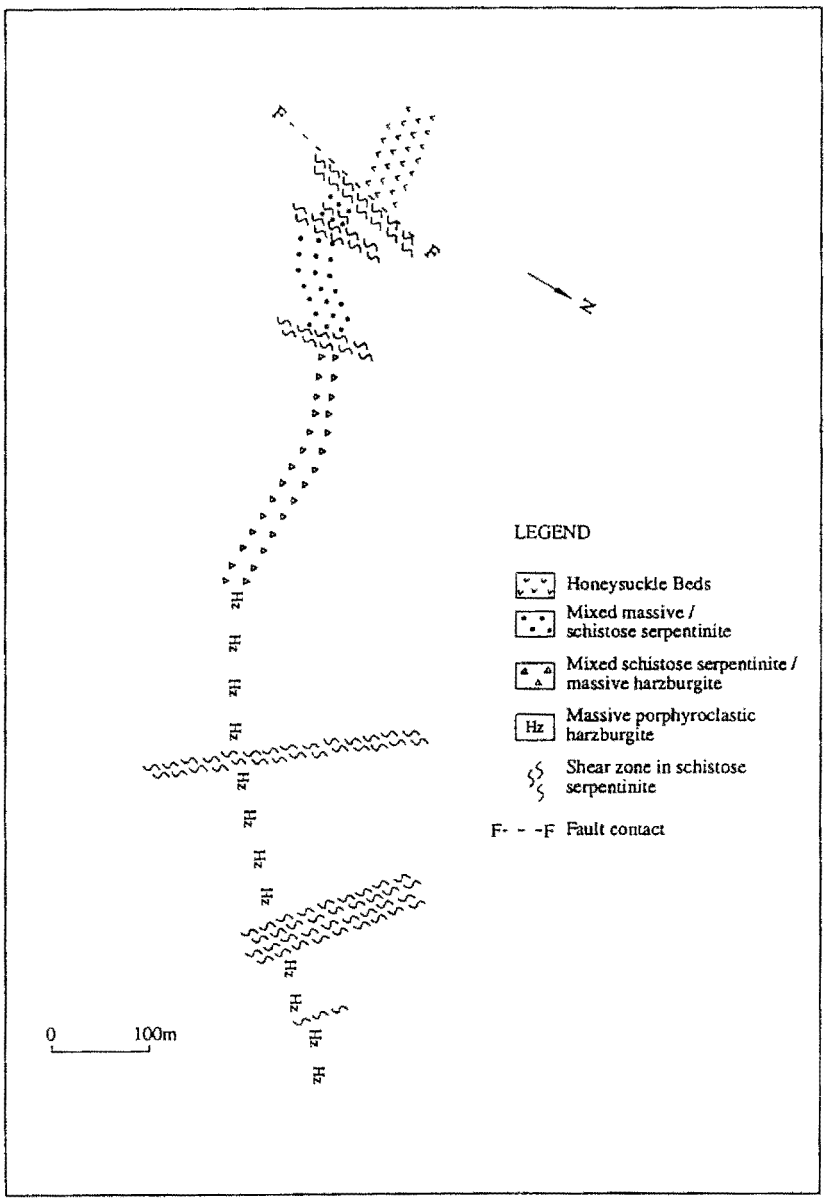

Figure 3.6 Strip-map showing the distribution of massive and schistose serpentinite along the crest of Mount Lightning.

According to Ashley (1973a), the massive serpentinites exhibit a well-developed "mesh texture". This is preserved in schistose serpentinites as lenticular relicts but it is destroyed in highly schistose rock, where the foliation is defined by the preferred crystallographic orientation of sub-fibrous chrysotile serpentine and linear aggregates of magnetite. Massive varieties in fact, have Serpentine pseudoporphyroclastic, sub mesh, or mesh textures. Both serpentinite varieties have cross-cutting veinlets of chrysotile/magnetite and decussate and feathery non-oriented serpentine grains.

X-ray diffraction analysis confirms that the most common serpentine-group mineral in massive serpentinite is lizardite (Al-rich lizardite 1T, lizardite 1T and lizardite 6T). Chrysotile 2M and chromite also occur, but chrysotile 2M is more common in schistose serpentinite (simply due to the greater volume of chrysotile veinlets) along with lizardite 1T, lizardite 6T and minor talc. Antigorite was identified in intensely sheared schistose serpentinites at the contact between the Coolac Serpentinite Belt and the Honeysuckle Beds at G.R. 223 030 and is common in the contact aureole of the Bogong Granite (Ashley 1973a; Irving & Ashley 1976).

The presence of lizardite and chrysotile suggests that the serpentinites formed at temperatures of less than 250°C and at a $P_{(H2O)}$ of less than 1kb (O'Hanley & Wicks 1995), while antigorite on the western boundary of the Coolac Serpentinite Belt indicates higher temperatures (>260°C - O'Hanley & Wicks 1995). An extended period of serpentinisation is indicated by the many differing generations of chrysotile/magnetite veinlets. The presence of tremolite indicates that low greenschist facies regional metamorphism has also occurred (e.g. Miyashiro 1978). The tremolite grains are cross-cut by a later generation of magnetite veinlets, and so must have formed during ongoing serpentinisation. The presence of relict orthopyroxene porphyroclasts indicate that the precursor rock type for virtually all of the Coolac Serpentinite Belt serpentinites was porphyroclastic harzburgite. Later-stage alteration is evidenced by cross-cutting talc grains.

Ashley (1973a) stated that "the transformation of peridotite to massive serpentinite in the Coolac ultramafic belt appears to have occurred with little small-scale deformation". However, serpentinisation requires fracturing and infiltration of sea-water (e.g. Laurent & Hebert 1979), thereby resulting in development of the greenschist or lower grade facies assemblage chrysotile+lizardite+magnetite (e.g. Wicks 1984). Subsequently, the massive serpentinites underwent more fracturing and developed a fibrous chrysotile fracture-fill.

S-C fabrics developed in localised zones of high shear strain and displacements on shear planes are minimal (<5mm) as evidenced by fractured chrome spinel grains. Although movement senses obtained from S-C fabric relationships can be used to determine the overall emplacement history within serpentinites (e.g. Offler & Williams 1987), during the present study, conflicting movement senses were found over a few metres in a number of areas within the Coolac Serpentinite Belt. This

is borne out by previously obtained results. In a more detailed study of the S-C relationships within the Coolac Serpentinite Belt and adjoining rock units, Stuart-Smith (1990) recognised a major Early Silurian sinistral strike-slip movement followed by a Mid-Devonian sinistral strike-slip movement and finally, a mid-Devonian dextral strike-slip movement. Conflicting results were obtained by Warner *et al.* (1992) who reported a Late Silurian sinistral strike-slip movement followed by an Early Devonian sinistral strike-slip movement.

3.5.5 Talc-carbonate rocks

Schistose and massive talc-carbonate rocks are minor components of the Coolac Serpentinite Belt. They are serpentinised ultramafic rocks that lack olivine and other primary minerals (except minor chrome spinel), have low temperature metamorphic textures, and contain more than 20% talc and/or magnesite. Ashley (1969) recognised talc-antigorite-chromite schists, talc-bearing metaserpentinites, magnesite-bearing metaserpentinites and talc-tremolite-magnetite-chromite schists, but a two-fold division into talc-rich (>75% talc) and rare magnesite-rich (>40% magnesite) metaserpentinites is used in the present study.

Talc-rich rocks occur in zones of highly schistose serpentinite within the Coolac Serpentinite Belt (Ashley 1969) and talc-rich metaserpentinites are the result of thermal metamorphism of the Coolac Serpentinite Belt adjacent to the Bogong granite (Ashley *et al.* 1971). For example, on the Bombowlee Creek road (G.R. 234 965), talc and magnesite-rich metaserpentinites occupy highly schistose narrow (<lm) zones, and highly schistose, talcosic metaserpentinite abuts the Bogong Granite at the Goobarragandra Copper Mine (G.R. 267 864).

The talc-carbonate rocks result from post-serpentinisation hydrothermal alteration and shearing along contacts. Both talc and magnesite replace and crosscut the serpentine-group minerals within highly schistose zones and reaction zones developed at contacts with the felsic intrusions. The original magmatic texture was destroyed by serpentinisation and associated development of S-C fabrics. The contacts were the locus for periodic reactivation and hydrothermal fluid channeling, which, according to Ashley (1997) resulted in magnesite deposition at minimum temperatures of 165-285°C. However, more generally, Laurent & Hebert (1979) indicated that talc and magnesite could reflect groundwater infiltration at temperatures below 100°C, so this possibility for the

Coolac Serpentinite Belt occurrences should be borne in mind. In the magnesite-deficient rocks, the CO_2 fugacity was too low for the development of magnesite (Deer *et al.* 1985).

3.5.6 Gabbros

Although Ashley *et al.* (1971) stated that small tectonic inclusions of gabbro occur within all parts of the Coolac Serpentinite Belt except the southern portion, many are igneous intrusions with intrusive boundaries rather than tectonic inclusions with tectonic boundaries(see section 3.4.2). The intrusions/inclusions, which are particularly common in the Western Tectonic Melange Zone, have the following outcrop patterns:

(a) discontinuous, boulder-like outcrop which just penetrates the surface (e.g. G.R. 145 255);

(b) relatively large masses (5-10m in diameter) of leucogabbro/gabbro containing dyke-like bodies of metabasalt, pegmatitic veins and patches of hornblende gabbro (e.g. G.R. 234 965);

(c) dyke-like bodies (up to 10m in length and 4m in width) within schistose serpentinite (e.g. G.R. 138 253; 234 965);

(d) dyke-like bodies within a block of tectonic melange at Mundongo - the block also contains dyke-like bodies of pyroxenite and metabasalt, and blocky massive serpentinite, all within a matrix of schistose serpentinite (e.g. G.R. 229 931).

The gabbros are of two main types, those with cumulus textures and those with granular textures, but both can occur in the same outcrop (e.g. G.R. 234 965). Cumulus gabbros have a post-cumulus space-fill texture (Plate 3.11) and range in composition from rare leucogabbro (with >85 modal% plagioclase - e.g. Bombowlee Creek, G.R. 234 965) to equally rare clinopyroxene (with Cpx>Hbl - e.g. Bombowlee Creek, G.R. 234 965) and common hornblende gabbros (with Hbl>Cpx - e.g. G.R. 234 917, where a hornblende gabbro has been intruded by an aplitic granite dyke of Young Granodiorite). Granular gabbros have allotriomorphic (Plate 3.12) or hypidiomorphic granular textures and comprise leucogabbro, and hornblende, clinopyroxene and completely altered gabbros. Leucogabbro is common in the central part of the Coolac Serpentinite Belt but rare elsewhere; hornblende gabbro is widespread and the most common type within the belt; only one occurrence (G.R. 234 965) of clinopyroxene gabbro was found during the present study. The completely altered gabbros, which are rare and tend to be confined to the central part of the belt, resemble hornblende gabbro in hand specimen, but are strongly altered and veined in thin-section.

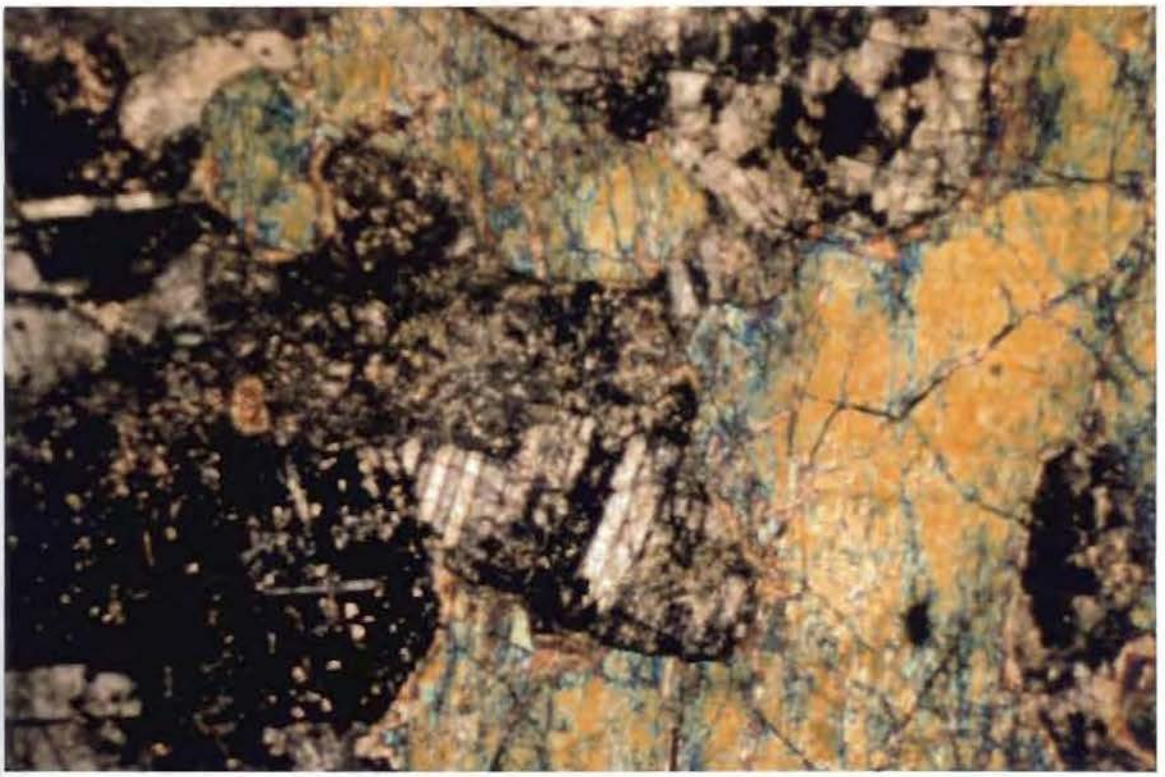

Plate 3.11 Cumulus gabbro exhibiting a post-cumulus space-fill texture.
Sample No 238b UXP F.O.V 3.5mm

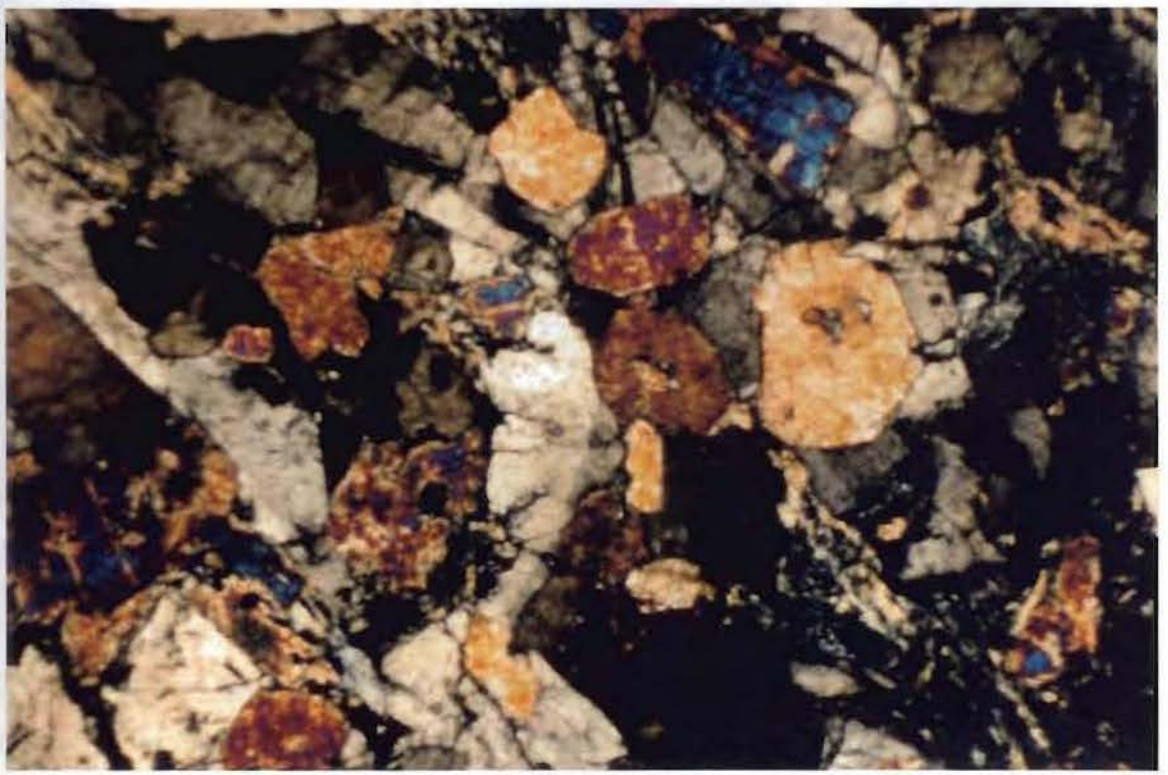

Plate 3.12 Granular gabbro exhibiting an allotriomorphic granular texture.
Sample No 156c UXP F.O.V 3.5mm

Electron microprobe funding was not available for the analysis of the amphibole grains within these rocks. The occurrence of brown hornblende grains around cores of colourless clinopyroxene (Plate 3.13) could be due to either late-stage magmatic crystallisation or upper amphibolite to lower granulite facies metamorphism (the preferred explanation). Green hornblende fringes on the brown hornblende formed under middle amphibolite facies conditions, while rare fringes of blue-green amphibole on the green hornblende probably indicate lower amphibolite facies conditions (e.g. Miyashiro 1994). Franklin (1975) ascribed similar fringes in the North Mooney Complex gabbros to sodic metasomatism, because the blue-green amphibole is Na-enriched, particularly compared to the brown-green hornblendes. Finally, tremolite/actinolite and rare chlorite replacements of all hornblende types are consistent with partial re-equilibration under greenschist facies regional metamorphic conditions (e.g. Miyashiro 1994)."

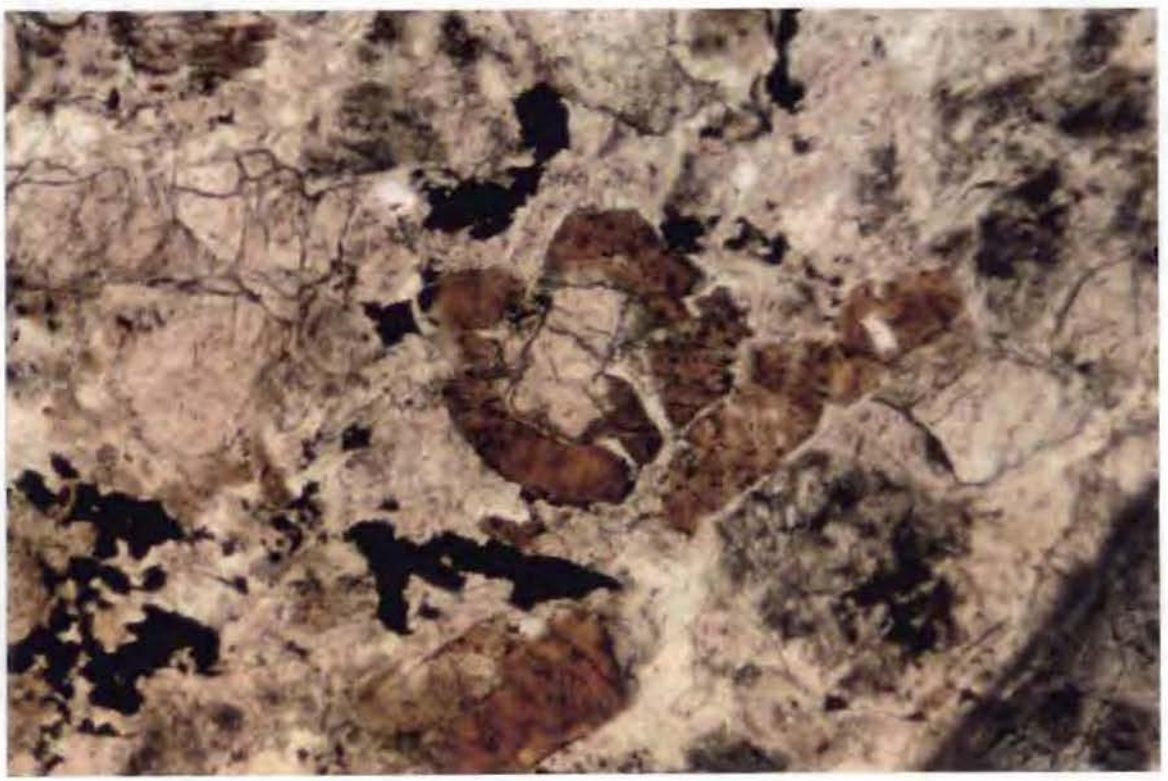

Plate 3.13 Brown hornblende surrounding cores of colourless diopside within gabbro.
Sample No BF92/53 PPL F.O.V 1.5mm

XRD studies of all types of gabbro show that the plagioclase is principally albite. During metamorphism, the original calcic plagioclase released its calcium, the latter then contributing to the low temperature (e.g. <300°C) development of the assemblage of epidote, grossular,

clinozoisite, prehnite, carbonate and quartz under low greenschist down to subgreenschist (prehnite-pumpelleyite facies) conditions (e.g. Miyashiro 1994).

Most gabbros are massive and unfoliated in hand specimen, but there is evidence of ductile and brittle deformation in thin-section. The ductile event occurred pre-alteration in that primary plagioclase and hornblende exhibit bending (Plate 3.14) and undulose extinction; the brittle event is evidenced by abundant veinlets with fracture-fill assemblages comprising prehnite, grossular, epidote, clinozoisite, albite/epidote/quartz and chlorite. Thus, following the ductile deformational event, brittle deformation preceded or was concurrent with inflow of fluids, which locally remobilised Mg, Na, Ca and Si.

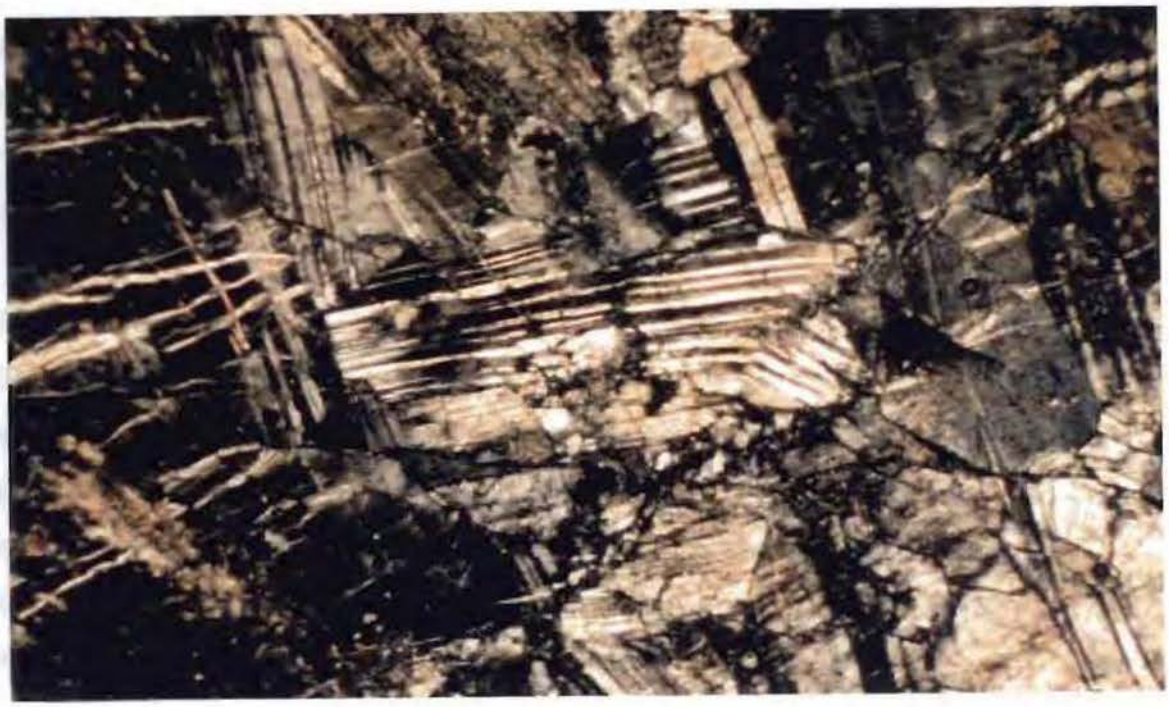

Plate 3.14 Bent and micro-faulted plagioclase twin lamellae within gabbro.
Sample No 238c UXP F.O.V 3.5mm

In summary, the gabbros show the effects of protracted metamorphism under conditions ranging from upper amphibolite/lower granulite facies, down to greenschist and subgreenschist (prehnite-pumpelleyite facies). The lower temperature metamorphism resulted in the release of magnesium and calcium leading to the related development of alteration assemblages variously comprising: tremolite/actinolite, Mg-chlorite, albite, epidote, grossular, clinozoisite, prehnite, quartz and carbonate.

3.5.7 Plagiogranites and albitites

Plagiogranites and albitites are minor components of the Coolac Serpentinite Belt. The plagiogranites are felsic intrusive rocks that contain >20% quartz, <10% mafic minerals and <10% alkali feldspar; the albitites contain <20% quartz, <10% mafic minerals and <10% alkali feldspar.

Ashley *et al.* (1983) recognised autochthonous (or intrusive) and allochthonous (or tectonic) plagiogranites. Intrusive plagiogranites crop out poorly and field relations are unclear (Ashley *et al.* 1983) though they appear to occur as small irregularly-shaped apophyses, plug-like masses and dykes. Tectonic plagiogranites form boldly outcropping elongate lensoidal bodies (up to 1.4km long) with sharp tectonic contacts against the enclosing serpentinite (Ashley *et al.* 1983). In the present study, plagiogranites were mainly encountered in the central and western parts of the Coolac Serpentinite Belt, where they occur as dyke-like bodies (up to 100m long and 5-10m wide) within schistose serpentinite. In some cases, the bodies consist of complex basalt/diorite and plagiogranite/leucogabbro/hornblende gabbro/basalt lithologies.

High to moderate temperature (750-400°C) metamorphic events were not recognised, but there is limited mineralogical and textural evidence (below) for lower temperature (~ 300°C) metamorphism. The metamorphism developed well-formed muscovite and albite after calcic plagioclase, while ongoing metamorphism resulted in tremolite/actinolite and chlorite replacements of primary hornblende, and overprinting grains and veinlets of tremolite/actinolite, chlorite, clinozoisite and epidote. Such an assemblage is consistent with greenschist facies regional metamorphism (e.g. Miyashiro 1994)."

Widespread sutured grain boundaries (Plate 3.15), subgrain development, and undulose extinction in quartz, and sutured boundaries and bent and kinked twin lamellae in plagioclase is evidence of widespread ductile deformation, while intense fracturing is evidence of brittle deformation. It would seem that the plagiogranites and albitites of the Coolac Serpentinite Belt underwent ductile-brittle deformation. The latter allowed fluid infiltration and the development of cross-cutting chlorite and tremolite, and veinlets of clinozoisite."

Plate 3.15 Strongly sutured grain boundaries in quartz and albite within plagiogranite.
Sample No BF91/20 UXP F.O.V 3.5mm

3.5.8 Rodingites

Rodingites from the Coolac Serpentinite Belt were previously described by Golding (1962, 1966, 1969), Ashley *et al.* (1971), Ashley (1973), Golding & Ray (1975a and b) and Ray (1977). "Rodingite" was first used by Bell *et al.* (1911) to describe coarse-grained gabbroic-looking rocks that were hosted by serpentinite, at the Roding River, New Zealand, and contained diopside (diallage), grossular and prehnite. However, following Ray (1977), this term is here used for all calc-silicate rocks occurring within the ultramafic rocks of the Coolac Serpentinite Belt.

Ray (1977) classified the rodingites of Mount Lightning into two groups: group one is predominantly composed of garnet and/or vesuvianite and chlorite and hosted by serpentinite or serpentinised ultramafic rock; group two is composed of zoisite, prehnite, garnet and chlorite and occurs at the contacts between variolitic spilite and serpentinite. Group one comprises variably striking dyke-like bodies, (up to 15m long and 2m wide) that have intrusive relationships with their host rocks, whereas group two includes dyke-like bodies and subrounded pods (0.5 to 3m in

maximum dimension) that trend parallel to the general strike of the Coolac Serpentinite Belt and although sharply abutting the serpentinite, have a 0.1m wide marginal zone of tremolite-actinolite rock; the contact with the variolitic spilites is obscure (Ray 1977). According to Ray (1977), group one dyke-like rodingites have relict textures consistent with gabbroic, doleritic and basaltic parents, and show variably distributed proportions of minerals from their contacts to their centres. They become mineralogically simple, or even monominerallic, have increasingly abundant vesuvianite relative to garnet, and show decreasing abundant relict clinopyroxene towards the centre.

In the present study, rodingites were found throughout the Coolac Serpentinite Belt but are particularly common in the northern half. The bodies have the following forms:

(a) dyke-like bodies (up to 10m long, 4m wide, and striking about 300°) within schistose serpentinite and porphyroclastic harzburgite;
(b) small veinlets (up to 30mm in width) within highly schistose serpentinite and porphyroclastic harzburgite;
(c) small rounded bodies (<0.3m across) of massive rodingite within schistose serpentinite;
(d) small (<2m in diameter) to relatively large (at least 15x10m) plug-like bodies within schistose serpentinite and porphyroclastic harzburgite;
(e) irregularly-shaped pod-like masses (up to 20m long and containing inclusions of serpentinite) within schistose serpentinite;
(f) dyke-like bodies (up to 4m across and containing inclusions of chromitite) within chromitite.

Irrespective of group (one and two of Ray 1977), they are granoblastic (defined by interlocking grains of the constituent phases), decussate (defined by interlocking elongate grains of zoisite and/or talc and chlorite), domainal (defined by interlocking grains of chlorite-zoisite-grossular in discrete bands between bands dominated by clinopyroxene), and banded (defined by variation in grain-size within discrete bands).

Thin-sections reveal little about the mineralogy of many rodingites found during the present study, so XRD methods were also used. Phases identified by XRD (Table 3.1) are vesuvianite, hydrogrossular, relict augite, magnesite, goethite, prehnite, serpentine group minerals (antigorite, lizardite, Al-rich lizardite) and chlorite group minerals (clinochlore IIb, chamosite, nimite IIB, Fe

clinochlore, ferroan clinochlore IIb). Based on XRD and thin-section work, the following mineralogical subdivision of rodingites from the Coolac Serpentinite Belt is presented:

(a) diopside-grossular dominant,

(b) clinozoisite dominant (clinozoisite+garnet assemblages),

(c) chlorite-rich (chlorite+garnet±diopside, chlorite+diopside assemblages),

(d) vesuvianite dominant,

(e) grossular dominant (garnet+serpentine, garnet+clinozoisite assemblages),

(f) clinopyroxene (diopside) dominant.

No.	Main assemblage	Minor phases
MLA	Grossular+Goethite	
ML033	Diopside+Augite	Fe-Clinochlore
ML042	Grossular+Clinochlore IIb+Diopside	
70	Nimite IIb+Grossular+Diopside	
76	Clinochlore IIb+Diopside	Vesuvianite
77	Diopside+Ferroan Clinochlore IIb	
84	Grossular+Clinochlore IIb+Diopside+Vesuvianite	
91	Grossular+Clinochlore IIb	
92	Clinochlore IIb+Prehnite+Diopside	
93	Grossular+Chamosite	
94a	Vesuvianite+Magnesite	Grossular
94b	Vesuvianite+Clinochlore IIb	Diopside
94xls	Chamosite	
95	Clinochlore IIb+Diopside	Vesuvianite
104d	Vesuvianite+Diopside	
104d	Vesuvianite	
104d	Vesuvianite+Al-Lizardite	Grossular+Diopside
174	Hydrogrossular+Calcite	
228a	Clinochlore IIb+Grossular	
228b	Clinochlore IIb	
228c	Clinochlore IIb+Grossular	
229	Vesuvianite+Hydrogrossular+Grossular	Zoisite+Clinozoisite
230	Hydrogrossular+Antigorite	
230	Grossular+Lizardite	
231	Clinozoisite+Hydrogrossular	Antigorite
231	Grossular+Clinochlore IIb	

Table 3.1 XRD-determined rodingite assemblages of the Coolac Serpentinite Belt.

The diopside-grossular and zoisite dominant rodingites are common throughout the Coolac Serpentinite Belt and exhibit decussate (zoisite dominant), granoblastic (Plate 3.16) and rare banded textures.

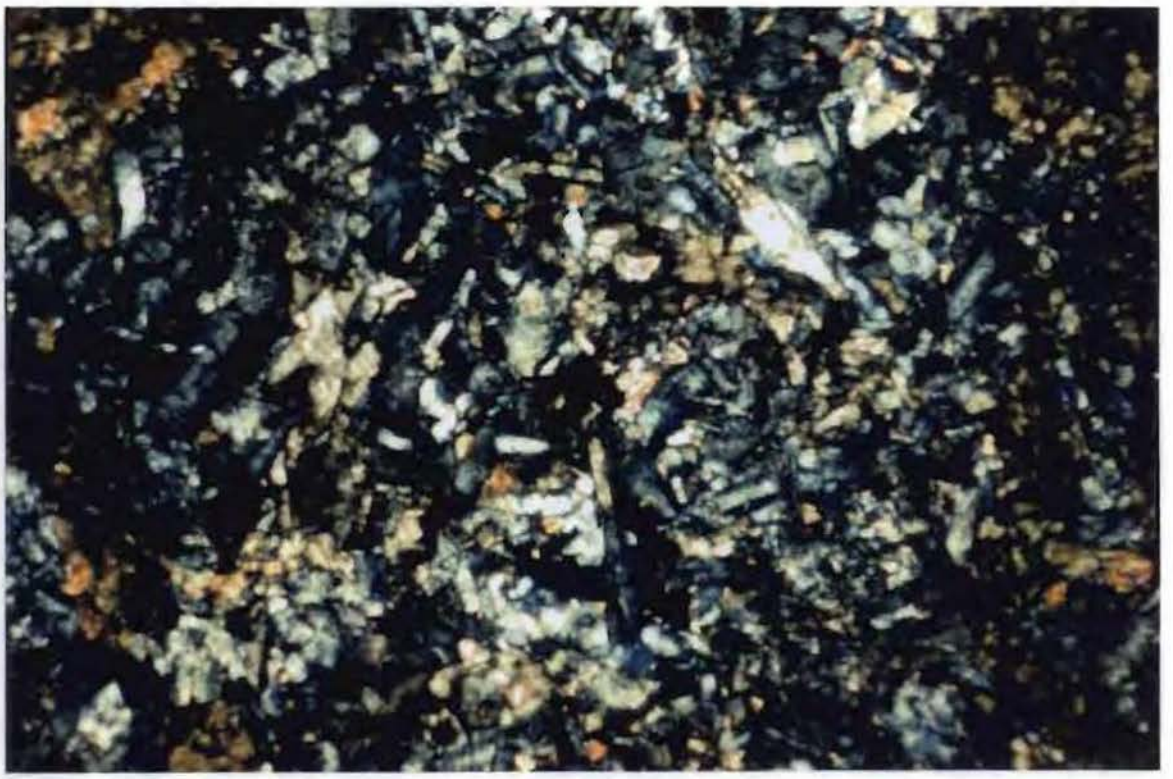

Plate 3.16 Zoisite-dominant rodingite exhibiting a granoblastic texture.
Sample No 73 UXP F.O.V 3.5mm

Chlorite-rich rodingites are uncommon and exhibit granoblastic domainal or decussate textures while rare grossular-zoisite rodingites consist of interlocking elongate zoisite and aggregates of grossular.

Grossular dominant rodingite has only been found at Mount Lightning (G.R. 138 253). It is entirely composed of grossular and forms schistosity-parallel vein-fillings in schistose serpentinite (Plate 3.17). The contact between the grossular veinlets and serpentinite is sharp and the rodingite is massive and unfoliated.

Other than "primary" diopside, rare augite and plagioclase, all the phases result from "rodingitisation" which, based on the mineralogy (above), occurred under conditions of the lower greenschist facies (e.g. Miyashiro 1978; O'Hanley *et al.* 1992). Many of the diopside grains exhibit

moderate to strong undulose extinction, have common triple junction grain boundaries, and/or are fractured and locally disaggregated. Rare opaque grains are also fractured and cross-cut by veinlets of chlorite and grossular. Such chlorite-dominated veinlets are common throughout some of the rodingite bodies (e.g. those at G.R. 154 255) and define a weakly developed planar fabric which parallels the NNW trend of the Coolac Serpentinite Belt.

Plate 3.17 Grossular rodingite veinlets within schistose serpentinite.
Sample No 98 UXP F.O.V 3.5mm

The parental rocks firstly underwent progressive ductile-brittle deformation (based on undulose, bent and fractured diopside and diallage development in relict diopside) and then experienced fluid infiltration and related rodingitisation. Ongoing or later fracturing accompanied rodingitisation as the rodingites are cross-cut by veinlets of chlorite and grossular.

3.5.9 Other rock types

Other rock types of the Coolac Serpentinite Belt whose relationship to the groups described above are uncertain include amphibolite, olivine hornfels, metabasalt, chlorite-rich rock and granitoid. Diorite, metadolerite and various metasedimentary rocks have also been recorded (Ashley 1973).

(a) Amphibolite

Amphibolites within the Coolac Serpentinite Belt were ascribed to the tectonic incorporation of moderate to high grade metamorphosed basalts and gabbros (Ashley 1973a). During the present study, a foliated amphibolite with a well-developed N-S trending mineral lineation was found as small (1 x 0.5m in diameter) outcrops adjacent to leucogranite in the vicinity of the Goobarragandra Copper mine. The mineral assemblage (brown/green hornblende, diopside, plagioclase, quartz, epidote and tremolite) (Plate 3.18) is indicative of the amphibolite facies (e.g. Miyashiro 1994). The rocks have partially retrogressed to the greenschist facies (as evidenced by tremolite fringes on hornblende and epidote alteration of plagioclase – e.g. Miyashiro 1994). Ductile deformation is evidenced by hornblende-defined planar and linear fabric elements, highly strained (with extreme undulose extinction) plagioclase, and recrystallised quartz grains with well-developed triple-junction grain boundaries.

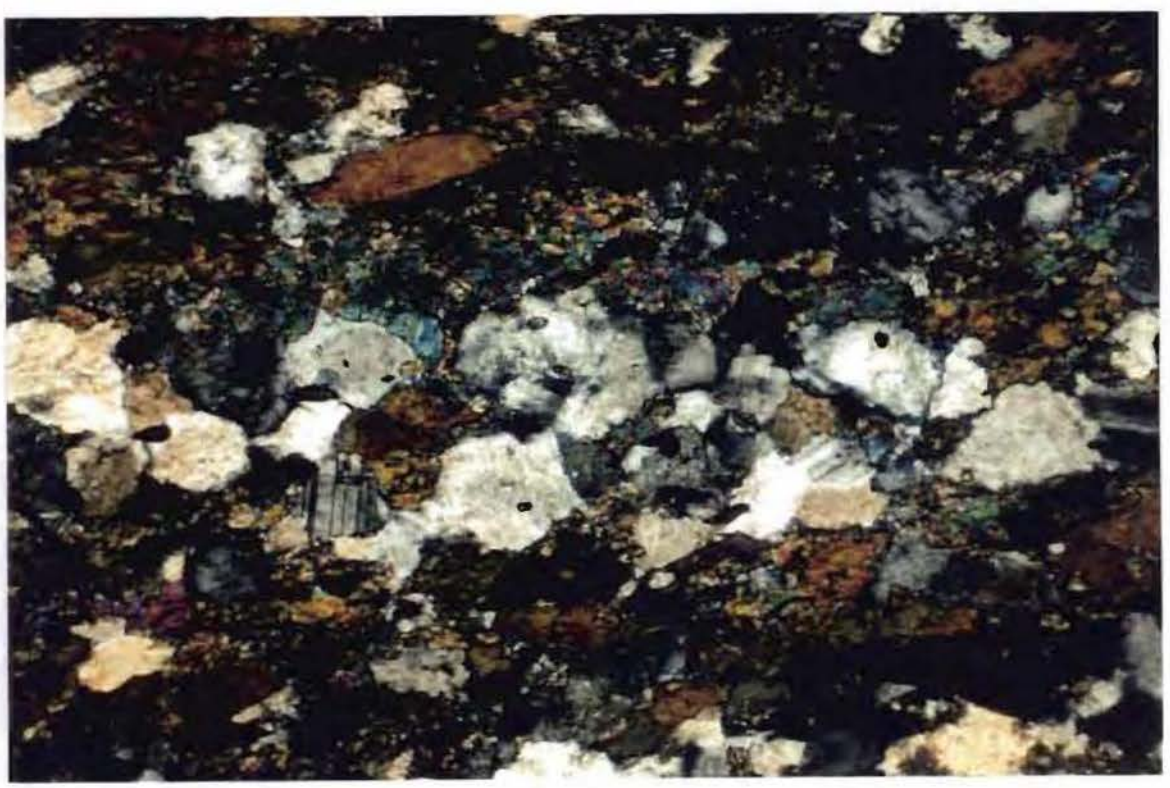

Plate 3.18 Hornblende-diopside-plagioclase-quartz-epidote amphibolite exhibiting a banded texture.
Sample No BF92/43 UXP F.O.V. 3.5mm

(b) Olivine hornfelses

Olivine hornfels is confined to three main areas (Ashley 1973a):

(a) along the Goobarragandra road, near the homesteads "Lameroo" and "Beaverbrook";

(b) along Pattens Ridge, southwards from the Goobarragandra Copper Mine for some 2km; and

(c) the vicinity of the Bogong Copper Mine and extending some 1-1.5km west and northwest.

Olivine hornfels occurs adjacent to the Bogong Granite and is interpreted as the product of contact metamorphism. Ashley (1973a) and Irving & Ashley (1976) suggested that the patches of hornfels reflect contact metamorphism of the Coolac Serpentinite Belt by the Bogong Granite to the hornblende hornfels facies (e.g. 550-700°C). Partial retrogression to greenschist facies is shown by talc rims on some of the olivine. There is no evidence for the presence of a metamorphic fabric before hornfelsing, but fractured olivine and green spinel grains are consistent with late brittle deformation.

(c) Metabasalts

Metabasalt occurs as numerous small (<0.5m across) blocks within schistose serpentinite near the Coolac Serpentinite Belt/Honeysuckle Beds contact on Mount Lightning and as small (<5m long and 0.5m wide) dyke-like bodies within a tectonic mélange block in a quarry near Mundongo Peak (G.R. 229 931). The only relict primary grains are plagioclase and clinopyroxene (most probably augite) , while metamorphic assemblages include the occurrence of cross-cutting veinlets of quartz-albite and chlorite replacements after actinolite (Plate 3.19), all indicative of the lower greenschist facies metamorphism of basaltic rocks (e.g. Miyashiro 1978). Ductile deformation is evidenced by the occurrence of bent plagioclase grains and stretched epidote-filled amygdules. Later brittle deformation is evidenced by abundant cross-cutting veinlets. Alteration associated with this deformation was pervasive as evidenced by the occurrence of epidosites.

(d) Chlorite-rich rocks

Chlorite-rich rocks from the Coolac Serpentinite Belt were ascribed to complete metasomatism of serpentinites during serpentinisation (Ashley 1973a). During the present study, such rocks occurred as dyke-like bodies (up to 11m long and 3m wide) that strike N-S within both massive and schistose serpentinite. They are composed of chlorite and minor clinozoisite (indicative of the lower

greenschist facies – e.g. Miyashiro 1994), and exhibit a decussate texture. Cross-cutting veinlets of Mg-chlorite and clinozoisite suggest that fracturing accompanied metasomatism."

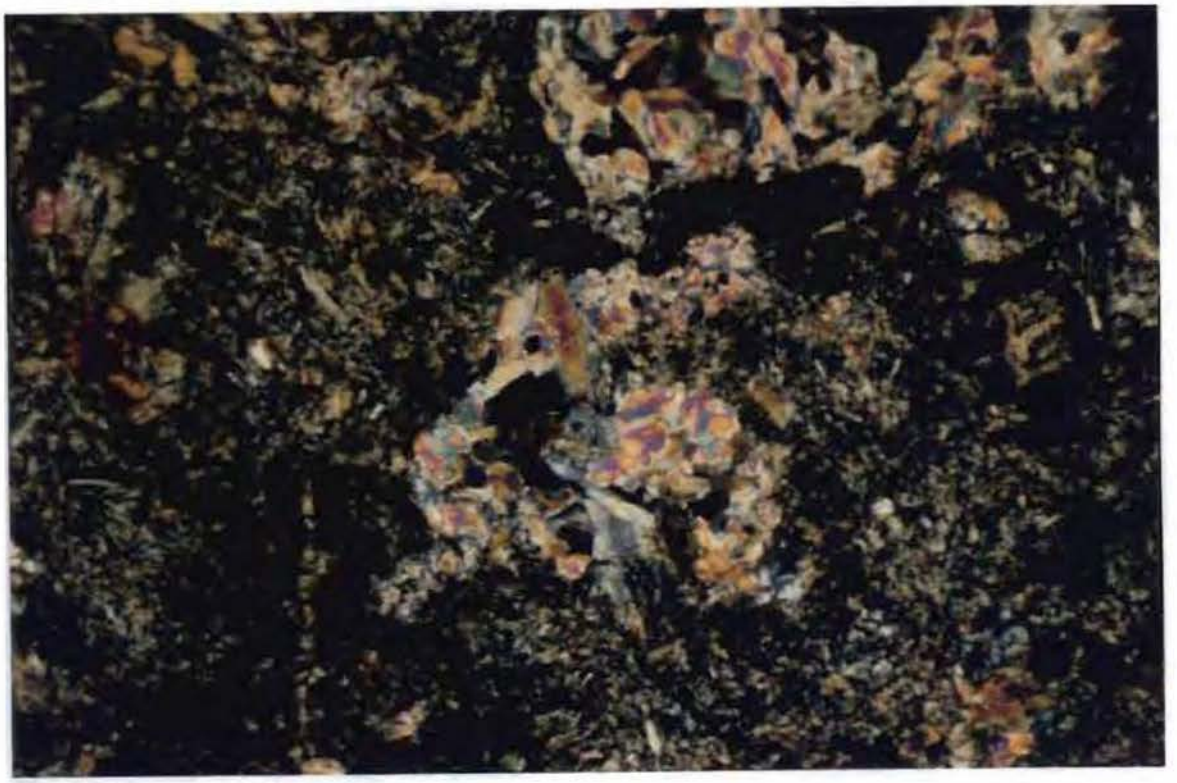

Plate 3.19 Amygdaloidal metabasalt.
Sample No BF92/49 UXP F.O.V 3.5mm

(e) Granitoids

N-S trending dyke-like masses of felsic leucogranite occurs in the vicinity of the Goobarragandra Copper Mine and a tectonic inclusion (Ashley 1973) of quartz-free diorite and granitic rocks occurs near McAlpines Copper Mine. The granitic intrusions have undergone low temperature regional metamorphism as evidenced by the occurrence of albite and thin veinlets and fracture-linings of chlorite. This metamorphism may have been of either prehnite-pumpelleyite or lower greenschist facies conditions. Minor deformation is inferred from moderate to strong undulose extinction in plagioclase and quartz and fracture-fill veinlets of chlorite (Plate 3.20)."

In the granitoid tectonic inclusions, replacement of biotite by chlorite and development of intergranular chlorite and cross-cutting fibrous tremolite (e.g. Miyashiro 1978) occurs. The mineral assemblage preserved in these rocks is indicative of lower greenschist facies metamorphism (e.g. Miyashiro 1978). Behaviour near the brittle-ductile transition of plagioclase is supported by

strongly bent multiple twin lamellae, moderate undulose extinction and ragged grain boundaries, and intense cataclasis of plagioclase and alkali feldspar. Fracturing concurrent with feldspar cataclasis is evidenced by chlorite in intragranular space-fillings and tremolite.

Plate 3.20 Bent plagioclase twin lamellae and fracture-fill chlorite veinlets within felsic granitoid.
Sample No BF92/44 UXP F.O.V 3.5mm

3.6 STRUCTURE OF THE COOLAC SERPENTINITE BELT

3.6.1 Primary layering in the main harzburgite mass

Primary layering within the Coolac Serpentinite Belt harzburgites (e.g. Jeffreson 1982; Lohan 1982; Graham *et al.* 1991, 1993) is defined by variation in the olivine to orthopyroxene ratio (resulting in olivine-rich and orthopyroxene-rich layers). This can be expressed by a variable response to weathering such that the orthopyroxene-rich layers form a prominent positive relief. Two different types of grading are present within the layers (Jeffreson 1982):

(a) a reduction in the percentage of the orthopyroxene grains in two directions away from a central core;

(b) simple grading composed of orthopyroxene-rich layers grading into orthopyroxene-poor layers.

The pyroxene-poor layers are dunitic in composition (<1% orthopyroxene) and vary in thickness from 2-5cm, whereas pyroxene-rich layers are peridotitic in composition (25-30% orthopyroxene) and vary in thickness from 5-15cm (Lohan 1982). Neither layer types shows preferred crystallographic orientation of orthopyroxene. Smaller scale layering, consisting of 1-3cm thick orthopyroxene-rich and olivine-rich bands, occurs within the main layering (Jeffreson 1982). Examples of this layering (Plate 3.21) occur in blocks throughout the belt, but in-situ examples are rare (Lohan 1982). Nevertheless, the layering is discontinuous (generally only a few metres), is more obvious in the massive porphyroclastic than in the intensely serpentinised harzburgites (Lohan 1982), and is far more common in the eastern half of the belt.

Plate 3.21 Outcrop of primary layering within harzburgite. Bold relief consists of orthopyroxene-rich layers while negative relief consists of olivine-rich layers.

The layering generally dips at 60° towards the ENE. An apparent in-situ block of porphyroclastic harzburgite displaying this layering occurs at G.R. 138 350. The layering strikes at 300° and dips at 69° towards 030°. Reported orientations of this layering are presented in Figure 3.7.

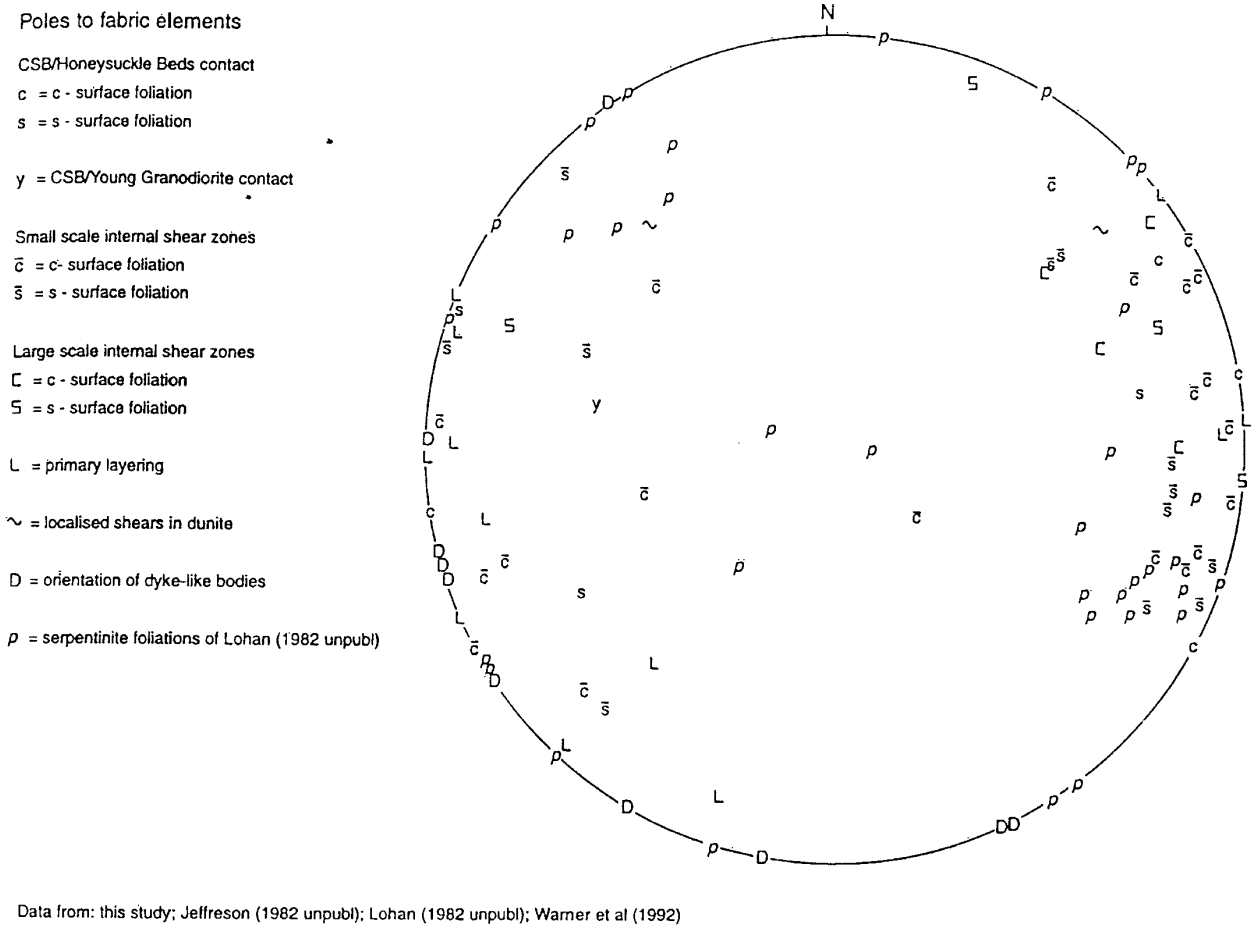

Figure 3.7 Poles to major structural elements of the Coolac Serpentinite Belt (equal area projection) (data from this study; Jeffreson 1982; Lohan 1982; Warner *et al.* 1992).

Microscale observations are derived from Lohan (1982). Layering is defined by varying amounts of orthopyroxene (<1 to 40%) and completely serpentinised olivine. A variably-developed, preferred orientation of the orthopyroxene grains exists in some samples and defines a "foliation" at moderate angles (<30°) to the strike of the primary layering.

Discontinuous primary compositional layering is a common feature of alpine-type peridotites and is similar to rhythmic cumulate layering within continental layered mafic-ultramafic complexes such as the Skaergaard intrusion of Greenland and the Bushveld Complex of South Africa (Dick & Sinton 1979). These authors described such layering from the Josephine peridotite of Oregon and the Red Mountain peridotite of New Zealand (pp. 404-405) as follows:

" It is difficult to trace the layering for great distances..... but it appears to disappear along strike, passing into large areas of massive unlayered harzburgite..... In outcrop, the layers typically consist of rhythmically alternating bands of pyroxene-poor and pyroxene-rich harzburgite a centimetre or more thick, primarily defined by variations in olivine to pyroxene ratios..... All gradations are found from alternating layers of pyroxene-rich and pyroxene-poor harzburgite to alternating layers of pyroxenite and dunite..... Typical layer boundaries are sharp. Gradations in grainsize or phase proportions between adjoining layers do occur, and these resemble, in some aspects, the graded bedding found in magmatic sediments.....In both peridotites, the predominant orientation of the layering is near vertical rather than horizontal.....the compositional layering appears to be the oldest feature preserved."

Nicolas (1989) pointed out that this type of layering is essentially parallel to the plane of mineral flattening except in areas of folding. He stated that possible causative mechanisms include:

(a) magmatic differentiation by gravitational settling;
(b) tectonically induced mechanical segregation;
(c) metamorphic differentiation;
(d) oscillatory processes of nucleation and in-situ crystallisation; and
(e) tectonic transposition of dykes and veins of dunite and orthopyroxenite within the main harzburgite mass.

Mechanism (a) seems unlikely because harzburgite is refractory mantle residue and lacks cumulate textures (e.g. Nicolas 1989). Furthermore, the discontinuous nature of the layering within the Coolac Serpentinite Belt is inconsistent with this mechanism.

Mechanism (b) requires development of systematic high and low strain zones within the upper mantle harzburgite during a phase of tectonic activity; evidence of such a tectonic event is not preserved.

Mechanism (c) necessitates selective dissolution and reprecipitation of orthopyroxene during a penetrative deformation event that produced high and low strain zones. Dick & Sinton (1979) favoured such a mechanism, but there is no evidence in the Coolac Serpentinite Belt for such

foliation producing processes. Again, the discontinuous nature of the layering and its gradational relationship to massive harzburgite is inconsistent with such a mechanism.

Mechanism (d) was proposed for the development of the layering in the Coolac Serpentinite Belt (Jeffreson 1982; Lohan 1982). In such a process, the primary layering is produced by the advancing solidification front "trapping" the crystallising orthopyroxene-rich layers between the already crystallised olivine-rich layers. This process has been proposed (McBirney & Noyes 1979) for continuous rhythmic layering in the Skaergaard intrusion.

Mechanism (e) was advocated by Nicolas (1989). He contended that early-formed dunite and orthopyroxenite dykes would be disrupted and rotated towards parallelism with the foliation plane (a plane of mineral elongation) within the harzburgite. He ascribed this to high temperature plastic flow within the upper mantle as it migrated away from the mid-ocean ridge. Although a mineral elongation lineation is commonly associated with layering within the Coolac Serpentinite Belt (e.g. Jeffreson 1982), the geometry and scale of the layering, together with the gradation of layers into massive harzburgite make this mechanism unlikely.

Assuming that the harzburgite was variably molten, then (d) (oscillatory processes of nucleation and in-situ crystallisation) seems the most likely explanation for this type of layering within the Coolac Serpentinite Belt.

3.6.2 Serpentinite foliations

Serpentinite foliations are of a secondary nature and help to determine the emplacement history of the Coolac Serpentinite Belt. They define S-C relationships (e.g. Berthe *et al.* 1979; Lister & Snoke 1984) and, can be classified as Type I S-C mylonites. Lister and Snoke (1984) note that, in Type I S-C mylonites, S-surfaces are related to the accumulation of finite strain and are defined by an anastomising mylonitic foliation whereas C-surfaces are related to localised high shear strain and comprise cross-cutting shear bands and displacement discontinuities (Lister & Snoke 1984) (Figure 3.8).

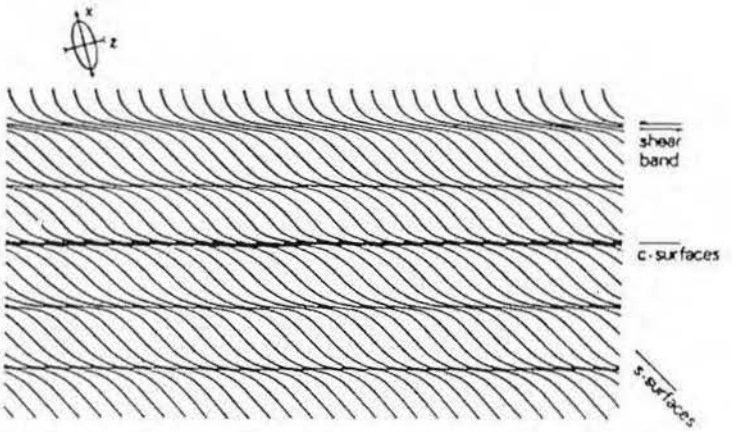

Figure 3.8 Type I S-C mylonites (from Lister & Snoke 1984).

In thin-section, the Type I S-C fabrics developed in variably serpentinised harzburgite and schistose serpentinite, have S defined by interlocking sigmoidal-shaped anastomising fibrous serpentine while C consists of more widely-spaced (generally in the range of 1-5cm) sub-parallel bands of fibrous serpentine (Plate 3.22). S becomes shallowly oblique to C before terminating abruptly against it. Mesoscopic linear elements observed include slickenfibres on both S and C and slickenlines.

Plate 3.22 S-C fabric within serpentinite defined by subparallel bands of fibrous chrysotile and magnetite veinlets.
Sample No ML036 UXP F.O.V 3.5mm

The Type I S-C fabrics of the Coolac Serpentinite Belt are mainly distributed:

(a) along the Coolac Serpentinite Belt/Young Granodiorite contact;

(b) along the Coolac Serpentinite Belt/Honeysuckle Beds contact;

(c) in large-scale internal shear zones;

(d) in small-scale internal shear zones; and

(e) in localised shear zones in serpentinised dunite.

Orientation data for these and other structures were shown in Figure 3.7. It would seem that:

(a) most data groups plot into broad regions rather than discrete confined areas;

(b) the majority of S-C fabric orientations in small-scale internal shear zones are steeply to vertically dipping, trending NNW-NNE;

(c) the large-scale internal shear zones have a more discrete distribution (though this could reflect the limited data), are steeply to vertically dipping, and trend NNW;

(d) the limited data shows that the Young Granodiorite/Coolac Serpentinite Belt contact is steeply dipping and trends NNE, while S-C data from the Honeysuckle Beds/Coolac Serpentinite Belt contact plot in the same regions as the small-scale internal shear zones;

(e) the dyke-like bodies, although usually trending subparallel to the main S-C fabric orientation within the ultramafic rocks, are highly oblique in some cases, suggesting they are cross-cutting dykes rather than tectonic inclusions.

Stuart-Smith (1990) stated that, at micro-scale, the C-surfaces in the serpentinites have a fibrous character, whereas the S-surfaces are platy. He noted that serpentine fibres within the C-surfaces are aligned sub-perpendicular to the S-C intersection and that S and C developed synchronously. The present study suggests that the Type I S-C fabrics, vary with rock type and intensity of development.

Discussion

The serpentinite foliations are of secondary tectonic origin, most likely related to the emplacement of the Coolac Serpentinite Belt (Jeffreson 1982), and began to form during the onset of serpentinisation.

For serpentinisation to initiate, brittle fracturing and brecciation of the fresh harzburgite (possibly as a function of cooling) must create permeability pathways for the infiltration of low-temperature seawater (e.g. Laurent & Hebert 1979). Large volumes of largely H_2O-dominant fluids (e.g. O'Hanley & Wicks 1995) infiltrated these pathways and reacted with olivine and orthopyroxene (e.g. Wicks 1984), thereby inducing serpentinisation (see section 3.5.4). During the early stages of serpentinisation, localised high strain zones developed S-C fabrics. Continuing deformation with ongoing serpentinisation enhanced these fabrics. The formation of the Western Tectonic Melange Zone and the Young Granodiorite/Coolac Serpentinite Belt contact is ascribed to continuing deformation during the late stages of serpentinisation associated with emplacement of the Honeysuckle Beds and Young Granodiorite.

The S-C relationships developed within both the Coolac Serpentinite Belt and Young Granodiorite have been used to construct tectonic models for the progressive emplacement of the Coolac Serpentinite Belt and Young Granodiorite at their present sites (e.g. Stuart-Smith 1990; Warner *et al.* 1992). Serpentinite readily deforms even under low temperature and becomes schistose, whereas the only mineral in the granodiorite that can easily become oriented and define a foliation is the biotite. As deformation within the granodiorite evolved from ductile to brittle, strain partitioned from the granodiorite into the adjacent serpentinite. Also, relative movement directions indicated by the S-C fabric relationships within the ultramafic rocks of the Coolac Serpentinite Belt can be highly variable over only a few metres, signifying a localised movement direction. There is also little evidence for any substantial movement along internal shear zones within the serpentinite (in fact, all available evidence points to movements of only a few mm).

3.6.3 Summary of the main structural elements of the Coolac Serpentinite Belt

(a) On its eastern contact, the Coolac Serpentinite Belt is variously intruded by or faulted against the Young Granodiorite.

(b) On its western boundary, there is a complex faulted contact with the rocks of the Honeysuckle Beds.

(c) The harzburgite exhibits a compositional layering that is interpreted as magmatic and is therefore the earliest structure formed.

(d) The harzburgite has a foliation that is defined by flattened orthopyroxene and olivine and is ascribed to plastic flow - it is the earliest secondary tectonic foliation in these rocks.

(e) Serpentine foliations (S-C fabrics) are developed within internal shear zones and on both contacts of the belt. S and C have broadly similar orientations, consistent with them forming within the same ductile-brittle environment during protracted serpentinisation.

(f) The S-C fabrics within serpentinites in internal shear zones record both sinistral and dextral oblique slip movement. Both movement lines are consistent throughout the belt suggesting that there were either two events that formed S-C fabrics or that they are coeval and represent opposing movements on the east and west faces of more resistant blocks. S-C fabrics within serpentinite on the western contact with the Honeysuckle Beds consistently recorded sinistral oblique slip movement.

CHAPTER 4: THE WAMBIDGEE SERPENTINITE BELT

4.1 INTRODUCTION

The Wambidgee Serpentinite Belt, like the Coolac Serpentinite Belt, is steeply-dipping and of alpine-type. It is topographically subdued (Plate 4.1) and clearing for agricultural purposes has disturbed most exposure. It consists of schistose and massive metaserpentinite and encloses other bodies of variably altered ultramafic, mafic and felsic rock. The belt, contains previously mined deposits of talc, and the only operating magnesite mine in this region of Australia (Figure 4.1). Podiform chromitites are uncommon and sporadically distributed.

Plate 4.1 Typical low-lying topography of the Wambidgee Serpentinite Belt. Fontenoy chromite mine, west of Wombat. Viewed from the south.

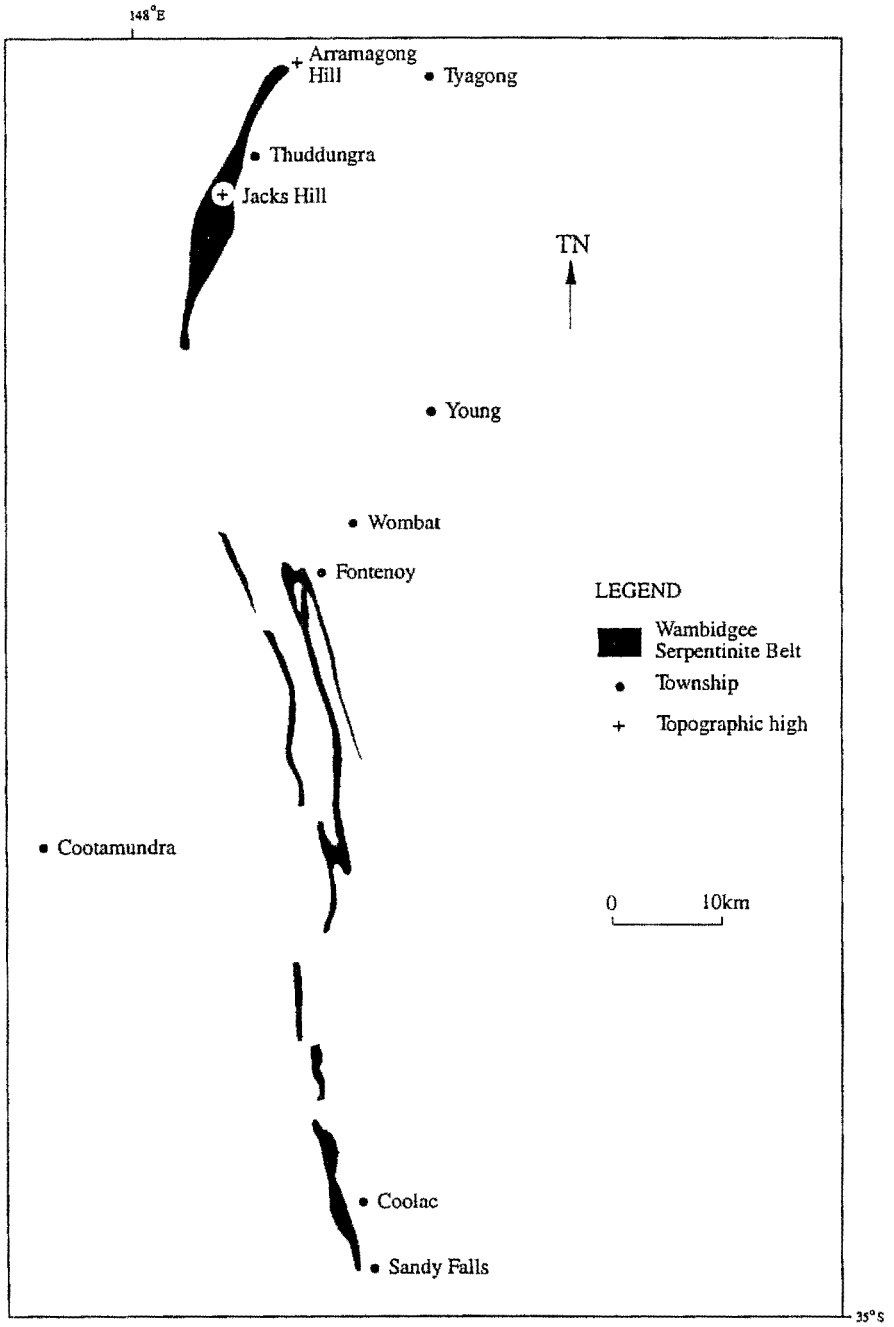

Figure 4.1 Location of the Wambidgee Serpentinite Belt (adapted from Fitzpatrick 1976).

4.2 THE WESTERN CONTACT AND ABUTTING ROCKS

The southern portion of Wambidgee Serpentinite Belt has faulted contacts with the Jindalee Beds (Figure 4.2). The northern portion, which crops out poorly other than near Fontenoy and the Thuddungra mine (Figure 4.3), has more complex relationships. In the Fontenoy area, the belt, which has been termed the "Fontenoy Serpentinite" (Cooper 1985), is faulted against mylonitic

Young Granodiorite. In the Thuddungra area, it is faulted to the west against metasedimentary rocks of the Jindalee Beds, and these in turn are faulted against metasedimentary and metavolcanic rocks of the Blowering Formation some 1.6 to 2.5km further west (Reynolds 1993). To the east, the Wambidgee Serpentinite Belt in this area is faulted against mylonitic Young Granodiorite.

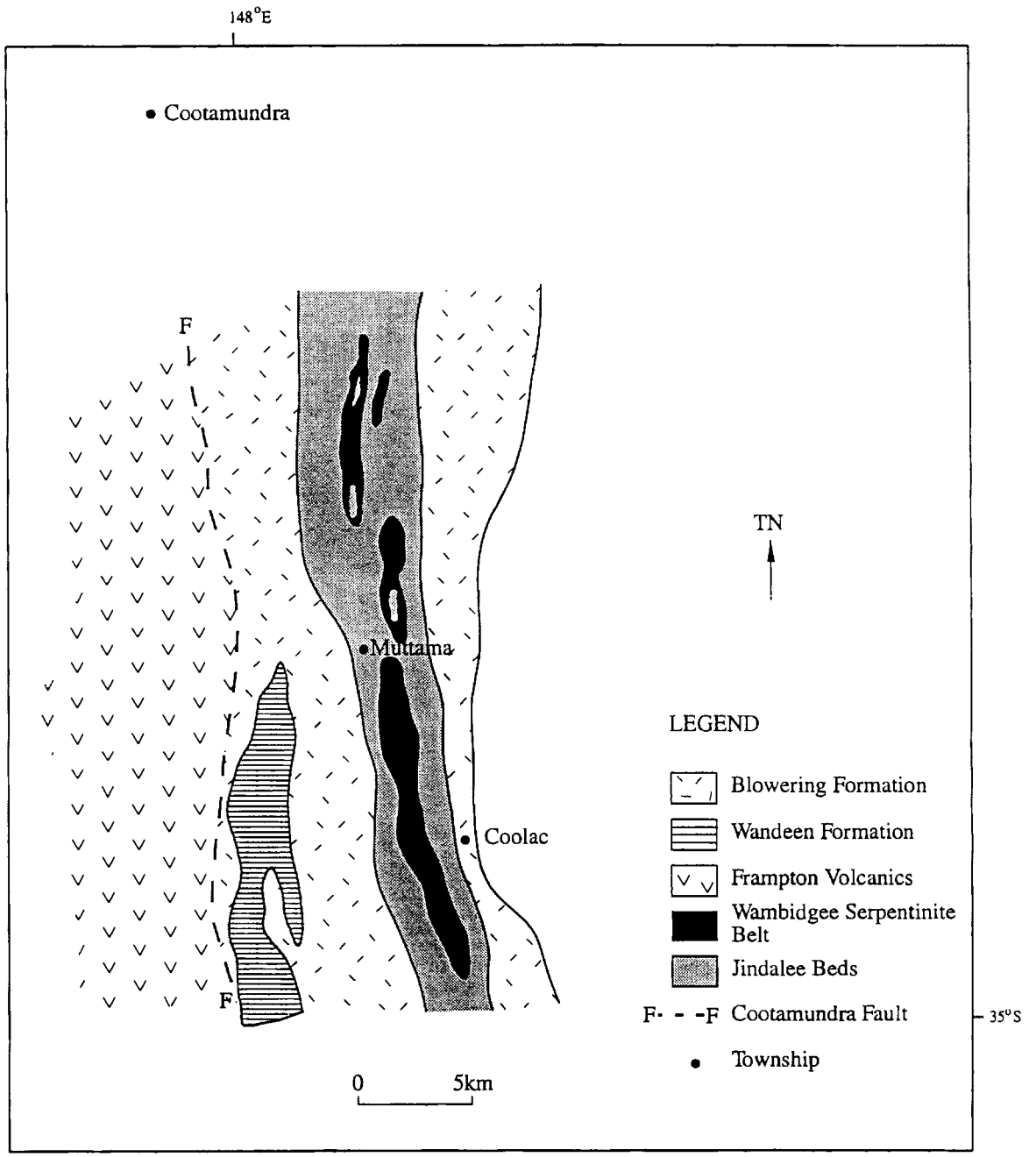

Figure 4.2 Geology of the southern portion of the Wambidgee Serpentinite Belt (adapted from Fitzpatrick 1976).

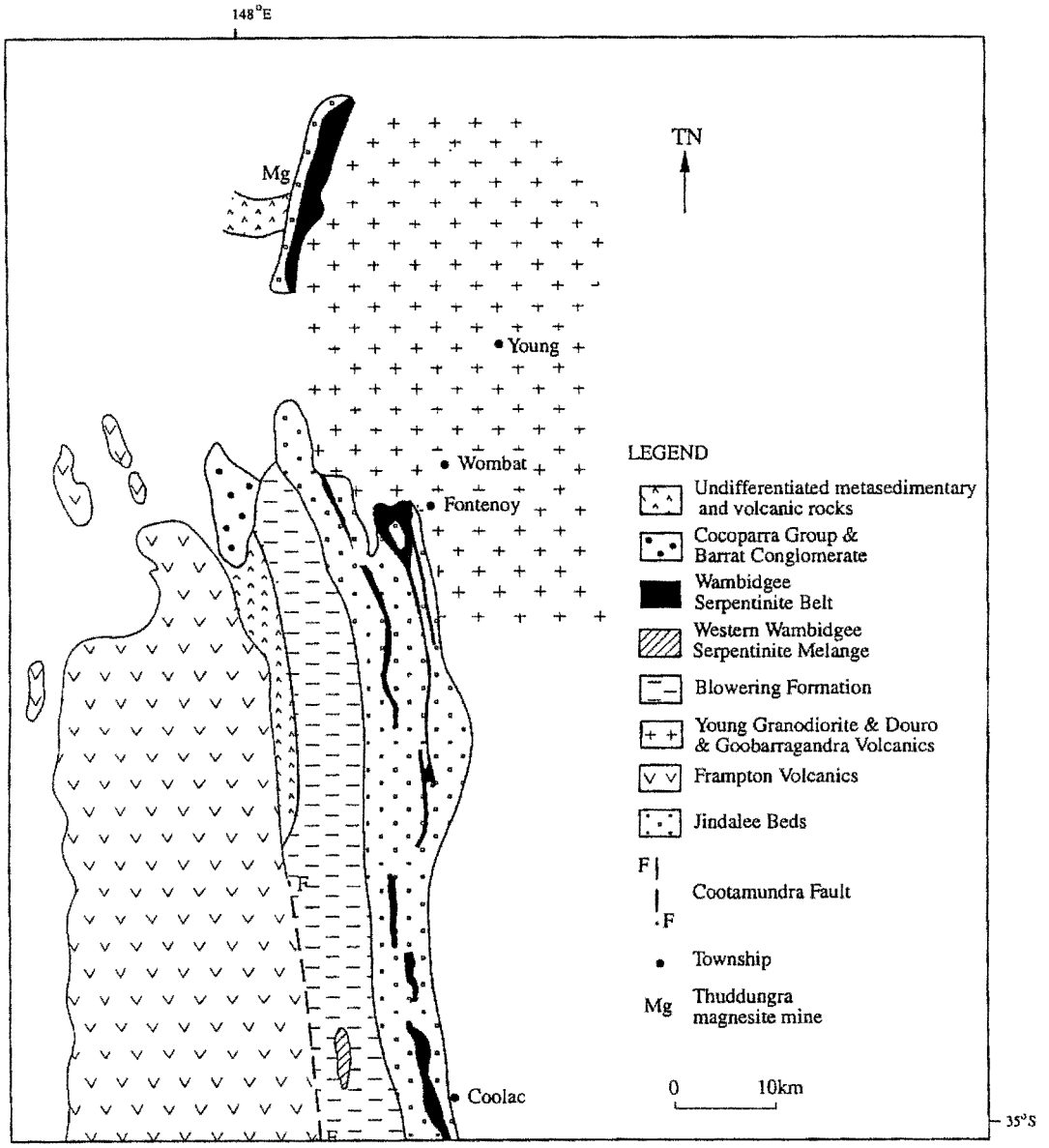

Figure 4.3 The northern portion of the Wambidgee Serpentinite Belt (adapted from Fitzpatrick 1976).

4.2.1 The Jindalee Beds

The Jindalee Beds are thought to represent the basement and be of Cambro-Ordovician age (e.g. Basden *et al.* 1974; Scheibner 1985). They form a linear north-south trending belt (Figure 4.4) and extend as far north as the Grenfell region (Basden *et al.* 1974). In general, the Jindalee Beds exhibit faulted contacts, although in the south of the belt, they are intruded by aplitic and lamprophyric dykes of the Young Granodiorite. There is a strong spatial association between the Jindalee Beds and Wambidgee Serpentinite Belt (Figure 4.4).

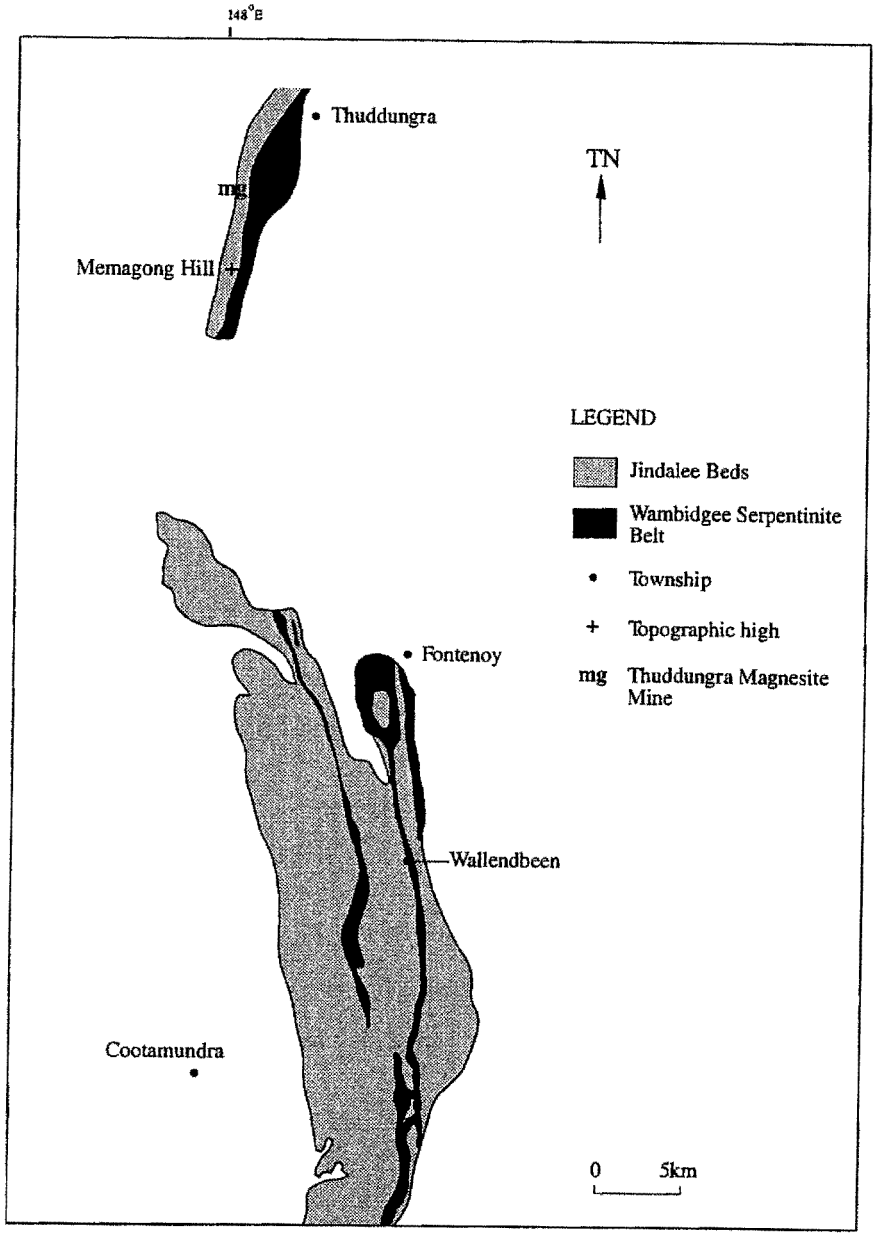

Figure 4.4 Distribution of the Jindalee Beds (adapted from Fitzpatrick 1976).

The Jindalee Beds can be divided into sub-units of quartzite, quartz-magnetite rock, chert, limestone, metapelite and metabasite. Petrographic data are presented in Appendix 4PD.

Quartzite is widespread and consists dominantly of recrystallised quartz with minor graphite and magnetite and/or hematite (Plate 4.2).

Plate 4.2 Folded micaceous quartzite from the Jindalee Beds.
Sample No 58 UXP F.O.V 3.5mm

Quartz-magnetite rock (>10% magnetite) contains fine-grained granoblastic quartz and magnetite and/or hematite, together with minor biotite, stilpnomelane and fibrous amphibole (Basden *et al.* 1974). In outcrop and hand-specimen, it has a similar appearance to the banded iron formations of the Broken Hill region (e.g. Stevens & Stroud 1983). Although the quartz-magnetite rock generally occurs as thin layers and pods within the Jindalee quartzite, Reynolds (1993) described a quartz-magnetite sequence in the Thuddungra area as 3.5km in extent along strike and up to 0.4km thick.

Chert (metachert) is relatively uncommon, but has been recorded by Macklin (1985) and Jones (1991). Although most of the metachert is intercalated with the Jindalee quartzite, Jones (1991) noted that it forms tectonic blocks within the Wambidgee Serpentinite Belt.

Basden *et al.* (1974) reported a lenticular limestone body within metabasite near Coolac. The body is better termed a dolomitic marble, and consists of recrystallised calcite/dolomite showing a granoblastic fabric with intergranular diopside, quartz, tremolite, and minor talc. The present study

has revealed that the marble body is a tectonic block, with intensely slickensided boundaries against the enclosing metabasites.

Metapelite and metapsammite are almost as common as quartzite to the north and west of Coolac, and most probably throughout the region. They crop out poorly and are generally interbedded with quartzite. Wilson (1993) observed phyllite along the contact with the Wambidgee Serpentinite Belt. Cooper (1985) found quartz-muscovite schists (up to 40% muscovite) in the Fontenoy area, where the present author found knotted quartz-muscovite-chlorite schist.

Both intrusive and extrusive metabasite is intercalated with other lithologies of the Jindalee Beds. Intrusives consist of pyroxene metagabbro and metadolerite while extrusives are metabasalt and rare meta-andesite. The metabasalt can be sub-divided into actinolite-albite-epidote schists, actinolite schists, amphibole-albite rocks, chlorite-epidote-albite schists and chlorite-epidote-zoisite rocks. In some areas, the metabasalt forms units over a kilometre in length and up to 200m in width. Amphibolite is rare in the southern portion of the Jindalee beds but common in the far north near the Thuddungra mine (Figure 4.3). It is diverse in nature, varying from fine to coarse-grained, massive to foliated, and commonly banded. At Memagong Hill (south of Thuddungra), an amphibolite layer (within quartzite) is 3.5km long and 30m wide. Metagabbro is relatively uncommon. The bodies are foliated at contacts but are otherwise massive.

Basden *et al.* (1974) stated that the metabasites of the Jindalee Beds underwent greenschist facies metamorphism, but this is an oversimplification. South of Coolac, Parker (1993) recorded mid-upper greenschist facies as indicated by sodic plagioclase+epidote in metabasalt (without chlorite), whereas saussuritised plagioclase+chlorite+epidote+actinolite in metagabbro indicated lower greenschist facies conditions. To the north and west of Coolac, Jones (1991) and Wilson (1993) reported that the metabasites had undergone mid-greenschist to lower amphibolite facies (staurolite zone) metamorphism based on the presence of metamorphic hornblende and diopside. The metamorphic peak was at least 500°C - the transition temperature of actinolite to hornblende, regardless of pressure (e.g. Jones 1991). Further north, around Cootamundra, Cooper (1985) stated that the amphibolites had undergone upper greenschist to lower amphibolite facies metamorphism, while around Thuddungra, assemblages in metabasites indicated upper greenschist facies, but

ranged to upper amphibolite on the basis of amphibole occurrences (Reynolds 1993). Overall, the common occurrence of actinolite fringes on metamorphic hornblende is consistent with an interpretation in which the region attained upper amphibolite facies conditions and was then variably retrograded to greenschist facies. The occurrence of abundant fine-grained almandine within the metabasalts at Pettitts (G.R. 059 310) is indicative of the upper greenschist facies under medium pressure conditions (e.g. Miyashiro 1978).

The metapsammites and metapelites also record a variable metamorphic history. Basden *et al.* (1974) stated that the quartz-magnetite rocks reached amphibolite facies conditions. South of Coolac, abundant biotite in metapelite is consistent with greenschist facies (biotite zone) conditions (Parker 1993), whilst around Coolac, diopside+quartz+calcite+tremolite+talc in marble (Plate 4.3) requires amphibolite facies conditions. Near Cootamundra, Macklin (1985) stated that metapelites had attained greenschist facies (almandine zone) conditions, but he also recorded cordierite retrogressing to chlorite. As the occurrence of almandine is compositionally restricted in low pressure conditions, Macklin (1985) stated that these rocks were of a very limited composition, metamorphosed under low pressure, high geothermal gradient conditions.

Plate 4.3 Cross-cutting tremolite grains in marble from the Jindalee Beds
Sample No PJ2 UXP F.O.V 1.5mm

In summary, the Jindalee Beds experienced temperatures, which may have reached upper amphibolite facies and retrograded to the now widespread lower greenschist facies conditions.

Basden *et al.* (1974) stated:

"The rocks of the Jindalee Beds have been extensively affected by several episodes of deformation and metamorphism. Repeated or continuous deformation is indicated by refolded folds, strong crenulation of axial plane cleavage which originally developed during isoclinal folding, and transposition."

Although this statement is generally true, the intensity and nature of deformation vary as a function of rock type. Quartzites are intensely deformed, whereas the metabasites are mildly deformed. Macklin (1985) recorded three distinct periods of deformation:

D1 involved isoclinal folding and development of a layer-parallel hinge surface cleavage, a bedding/cleavage intersection lineation and a mineral elongation lineation;

D2 generated tight to open folding with a hinge surface crenulation cleavage (S2);

D3 produced regional-scale kink bands which re-oriented the earlier foliations.

South of Coolac, Parker (1993) recognised D1 and possibly D2. Dl is represented by a strong slaty cleavage in the metapelites and a distinct N-S trending foliation in the metabasites (e.g. Parker 1993). To the north and east of Coolac, Jones (1991) noted that Dl in metapelite produced a domainal cleavage defined by quartz-rich (Q) domains within a continuous mica-rich (M) domain, and D2 generated a preferred orientation and domainal distribution of biotite (Jones 1991). He mentioned that open to tight D2 folds are common. North of Cootamundra, Cooper (1985) found two distinct fold styles:

(a) large-scale (10's to 100's of metres across) tight to isoclinal folds with axial surfaces dipping 50-90° towards the W/SW and hingelines plunging at approximately 20° S/SE;

(b) superimposed on these large-scale folds are smaller wavelength (0.1 to 5m) isoclinal folds.

Around Thuddungra, the most prominent foliation trends N-NNE, is steeply dipping, and is most likely an S2 cleavage (Reynolds 1993).

Based on the above results, the Jindalee Beds have undergone two periods of intense, widespread deformation followed by a period of less intense, irregularly distributed, deformation.

4.2.2 The Frampton Volcanics

The main body of Frampton Volcanics occurs some 6km west of the main Wambidgee Serpentinite Belt. The rocks are separated from the Jindalee Beds by the Blowering Formation and the Cootamundra Fault. A small infaulted block of the Frampton Volcanics also occurs within the Western Wambidgee Serpentinite Melange (Figure 4.5). The contacts of the Frampton Volcanics are ambiguous and their stratigraphic position within the region is uncertain (Skilbeck *et al.* 1992), although a U-Pb zircon date of 428 ±6 Ma has been obtained (Stuart-Smith 1990).

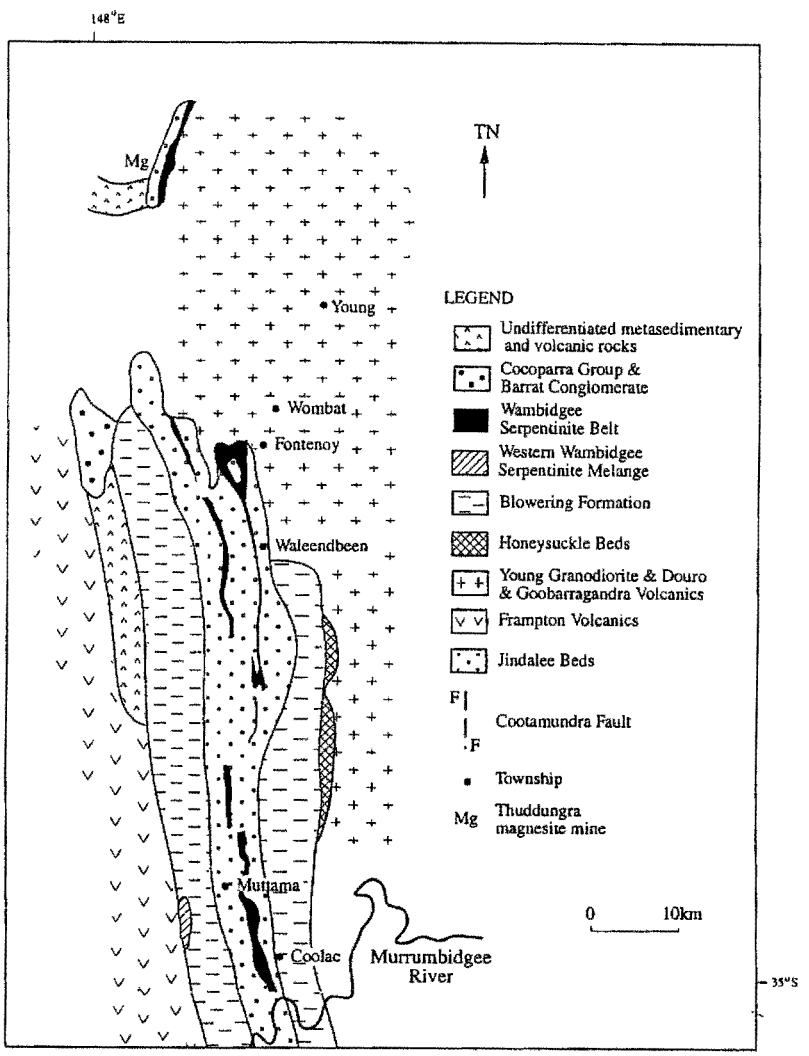

Figure 4.5 Distribution of the Frampton Volcanics (adapted from Fitzpatrick 1976).

The Frampton Volcanics are a silicic volcanic sequence with minor intercalations of conglomerate and rare fine-grained sedimentary rocks in the southern region (e.g. Stuart-Smith & Dadd 1993). These authors indicate that the volcanic rocks are rhyolitic to rhyodacitic crystal-rich vitric tuff with minor dacitic tuff and rare andesite and basalt. They stated that conglomerates range from oligomictic (with locally-derived volcanic clasts) to polymictic (with clasts of arenite, siltstone, volcanic rocks, limestone and rare granite). Metamorphic biotite and sericite in the volcanic rocks (Basden *et al.* 1974) are consistent with the biotite zone of greenschist facies regional metamorphism (e.g. Miyashiro 1978).

A common weak to strong foliation trends N-S, dips steeply west and in many cases is parallel to bedding. In the volcanic rocks, this spaced foliation is defined by the planar preferred orientation of micaceous minerals wrapping-around phenocrysts. In the sedimentary rocks it occurs as a continuous (in siltstones) to spaced (in conglomerates) cleavage. Ekers (1992) recognised an S2 foliation but this was not found to occur near the boundary with the Wambidgee Serpentinite Belt, Western Wambidgee Tectonic Melange and Gundagai Serpentinite Belt by either Parker (1993) or Wilson (1993).

4.3 THE EASTERN CONTACT - YOUNG GRANODIORITE

From Coolac to Cootamundra (Figure 4.6), the Young Granodiorite generally crops out 3-5km east of the Wambidgee Serpentinite Belt, intervening units are the Jindalee Beds and Blowering Formation. However, in the Fontenoy area, the Blowering Formation is not developed and the Wambidgee Serpentinite Belt and Jindalee Beds abut the Young Granodiorite. In the Thuddungra area, contacts between the Wambidgee Serpentinite Belt and Young Granodiorite are covered by alluvium although metabasic rocks of the Jindalee Beds generally occur between the Wambidgee Serpentinite Belt and Young Granodiorite in this area (Figure 4.6).

Dyke-like felsic bodies related to the Young Granodiorite and mafic dykes of unknown affinity have intruded the Wambidgee Serpentinite Belt, Blowering Formation and Jindalee Beds (Figure 4.6).

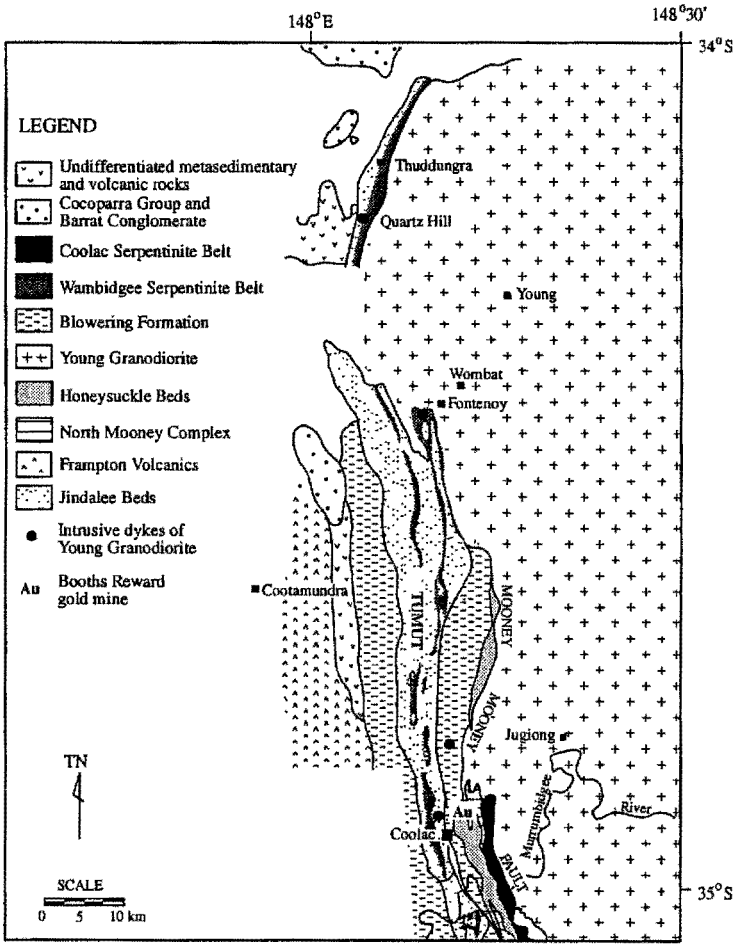

Figure 4.6 Distribution of the Young Granodiorite along the eastern contact of the Wambidgee Serpentinite Belt (adapted from Fitzpatrick 1976).

Contact relationships

From south to north, details of the dykes and Young Granodiorite (for petrographic descriptions, see Appendix 4PD) as pertaining to the contact, are:

(a) A small granodioritic body intrudes metapelite and metapsammite of the Jindalee Beds north of Coolac (Figure 4.6; G.R. 056 401). In the same vicinity, near the Booths Reward Gold Mine, the Jindalee Beds metasedimentary rocks are cut by aplitic and mafic (lamprophyric) dykes.

(b) Aplitic and mafic (lamprophyric) dykes intrude metasedimentary rocks of the Blowering Formation, 1km east of the Wambidgee Serpentinite Belt (Figure 4.6) about 10km north of Coolac. The aplitic dykes are massive and devoid of xenoliths, whereas the mafic dykes are coarse-grained and contain xenoliths of siltstone and quartzite whereas the aptitic dykes are massive and devoid of xenoliths. Other variants of the Young Granodiorite in this area are quartz monzodiorites.

(c) The Young Granodiorite in the Fontenoy area (Figure 4.6) varies from massive, through gneissic, to mylonitic, the latter forming 15-50m wide zones; all have the same mineralogy but progressively contain more abundant alteration phases (Cooper 1985). The gneissosity is defined by the preferred orientation and distribution of biotite wrapping around quartz and feldspar augen. Similarly, the mylonitic foliation is defined by the preferred rientation and distribution of biotite wrapping around cataclased quartz and feldspar. Regardless of deformation state, xenoliths abound and consist of biotite and biotite-quartz segregations, small vein quartz blebs, and ellipsoidal to spherical tonalitic bodies (Cooper 1985). "Rounded" elongate enclaves (up to 0.4m) of banded Jindalee quartzite also occur within protomylonite of this area (Plate 4.4).

(d) In the Quartz Hill area, south of Thuddungra (Figure 4.6), two varieties of the Young Granodiorite are found. Away from the main contact, the granodiorite is weakly foliated and even-grained. In a zone some 200-300m in width at its western margin, the granodiorite is porphyritic and strongly foliated. It has identical mineralogy to the more massive variety away from this margin, but has recrystallised quartz and strongly aligned grains of biotite defining a strong foliation. Also in this area, unfoliated mafic amphibolites become strongly schistose and exhibit a well-defined linear fabric at the contact.

Dykes in the Fontenoy area include metasomatised aplites in talcosic metaserpentinite; the dykes range in composition from unaltered aplite to quartz-oligoclase-actinolite rock (Cooper 1985).

Reynolds (1993) concluded that microgranites within the Wambidgee Serpentinite Belt (Figure 4.6) are an integral part of the belt, but their mineralogy and mode of occurrence are more consistent with dykes associated with the Young Granodiorite.

The chlorite, epidote, actinolite, zoisite, sericite and muscovite alteration assemblages suggest that the Young Granodiorite has undergone greenschist facies metamorphism (e.g. Miyashiro 1994). The greater intensity of alteration in the more foliated varieties suggests that the metamorphism was either synchronous with or subsequent to the deformation. There is no definitive evidence for either case as a number of the secondary metamorphic minerals do not show an overly strong preferred orientation and also, such a preferred orientation could be formed by mimetic alteration

Plate 4.4 Enclave of Jindalee Beds quartzite within foliated Young Granodiorite, Warrenoy, west of Fontenoy. Viewed from the south, looking north.

Most deformation within the Young Granodiorite is focused along its margins. In the Fontenoy area (Figure 4.6), the gneissosity has a mean strike of 330° and dips that vary some 20° either side of vertical (Cooper 1985). In the Cootamundra region (Figure 4.6), the foliation strikes 360° and dips subvertically (Macklin 1985). Thus, the gneissosity has approximately the same orientation as the dominant regional foliation for this part of NSW.

Microstructural evidence of deformation within the granodioritic and aplitic rocks includes:

(a) moderately bent and micro-faulted plagioclase twin lamellae (Plate 4.5),

(b) the relatively large quartz grains exhibit undulose extinction and subgrain development and have strongly sutured grain boundaries (Plate 4.6),

(c) the relatively small quartz grains are equant and polygonal in shape,

(d) aggregates of sub-parallel biotite grains wrap around both quartz and feldspar augen, and

(e) some muscovite grains are bent and exhibit moderate undulose extinction (Plate 4.7).

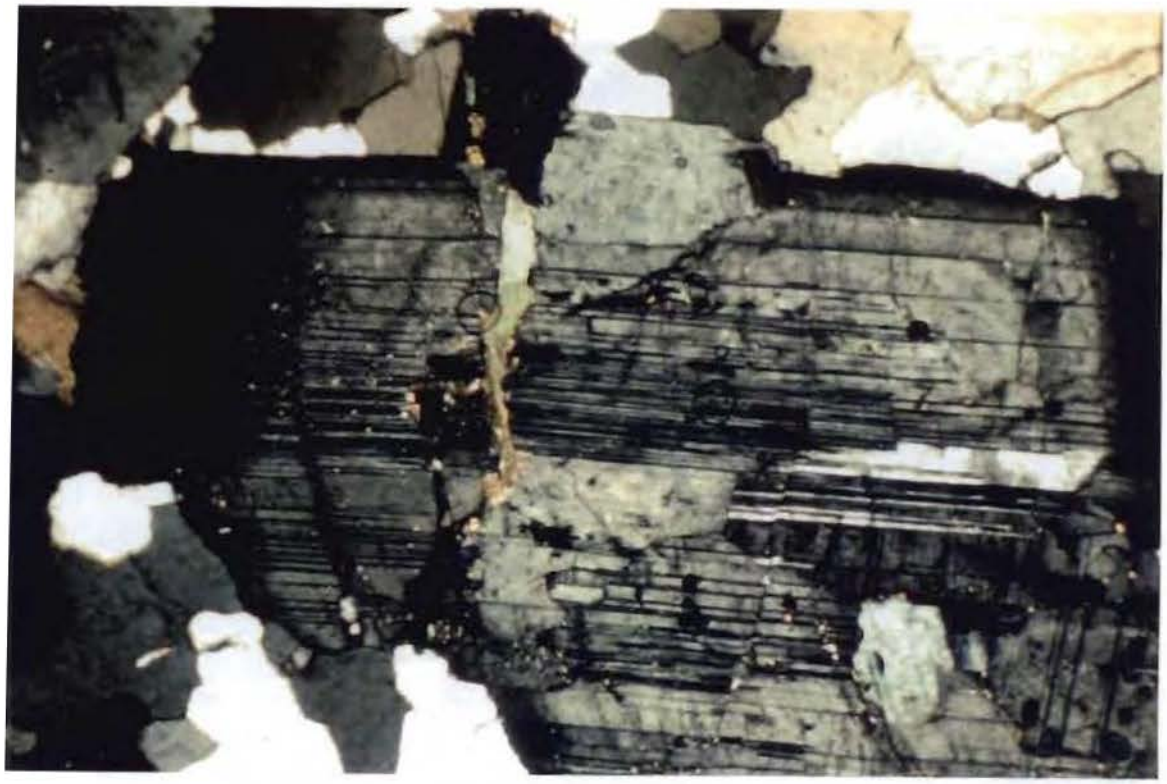

Plate 4.5 Bent and micro-faulted plagioclase twin lamellae within Young Granodiorite.
Sample No 223 UXP F.O.V 1.5mm

Plate 4.6 Strongly sutured grain boundaries of large quartz grains within mylonitised Young Granodiorite.
Sample No 200 UXP F.O.V 1.5mm

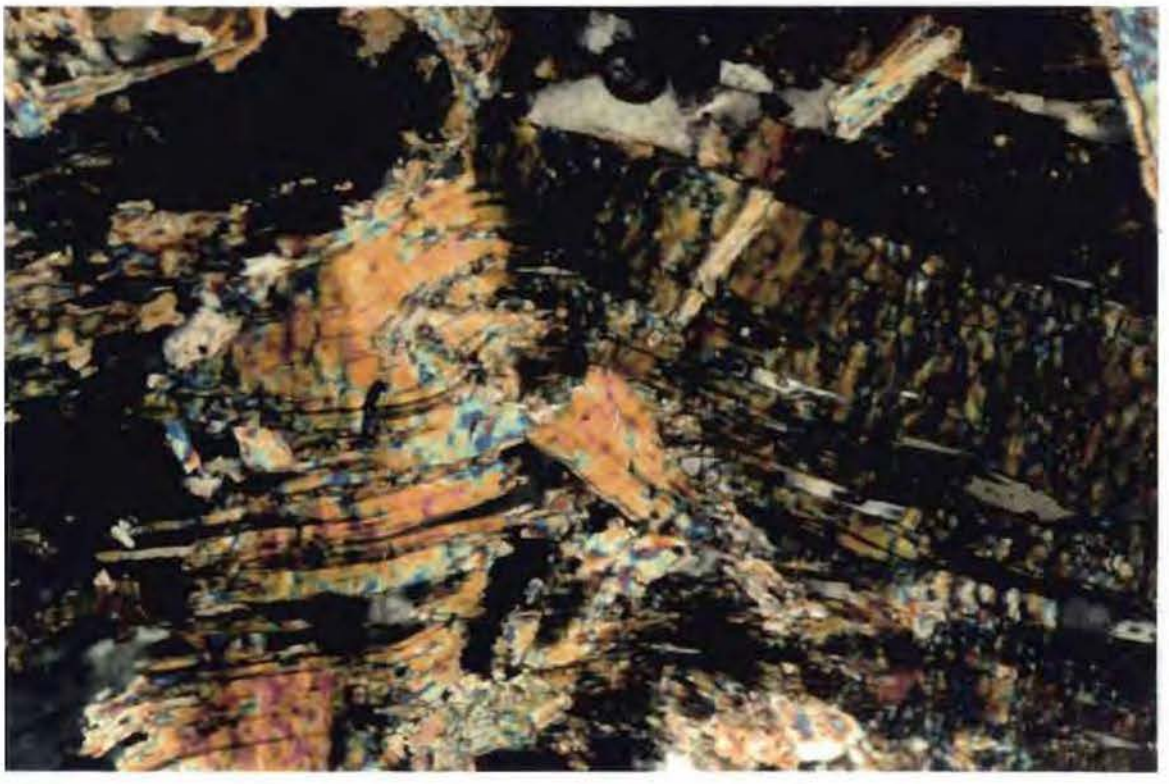

Plate 4.7 Bent muscovite grains within Young Granodiorite.
Sample No 223 UXP F.O.V 1.5mm

In summary, the Young Granodiorite contains evidence for one major deformation associated with intrusion and thrust emplacement against the Jindalee Beds and Wambidgee Serpentinite Belt. The deformation appears to have been part of a major regional event. Ductile deformation associated with silicic dyke rocks, west of the main contact, suggests that the dykes were still hot while being deformed.

The main contact between the Wambidgee Serpentinite Belt and the Young Granodiorite is faulted, based on the development of mylonite in the Young Granodiorite. However, dykes of Young Granodiorite within the Wambidgee Serpentinite Belt and Jindalee Beds to the west of this main contact, together with the irregular transgression of the contact by the Young Granodiorite north of Fontenoy, suggest a partially intrusive relationship. Thus, the Young Granodiorite has a faulted/intrusive contact with the Wambidgee Serpentinite Belt and Jindalee Beds, similar to that reported (e.g. Marshall & Franklin 1992; Warner *et al.* 1992) between the Young Granodiorite and Coolac Serpentinite Belt further south.

4.4 GENERAL FEATURES OF THE WAMBIDGEE SERPENTINITE BELT

The Wambidgee Serpentinite Belt is a linear belt of dominantly schistose and massive metaserpentinites which discontinuously outcrops for approximately 110km, from Sandy Falls in the south (Basden *et al.* 1974) to Jacks Hill (near Thuddungra) in the north (Figure 4.7 and see Figure 4.1).

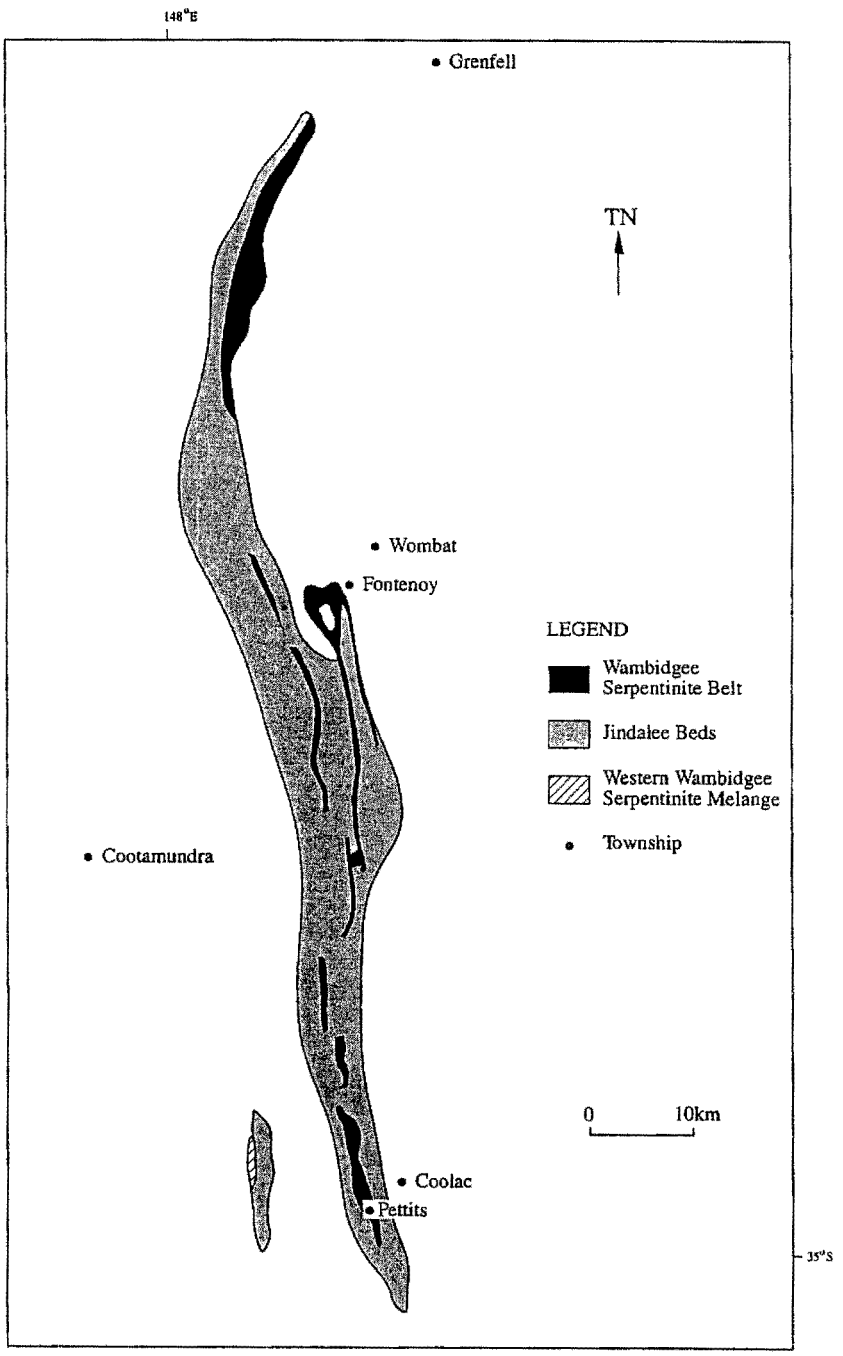

Figure 4.7 Extent and distribution of the Wambidgee Serpentinite Belt (from Fitzpatrick 1976).

All metabasic igneous rocks within this belt (regardless of their emplacement mechanisms) are an integral part of it; Young Granodiorite and Jindalee Beds within this belt are not part of it. Basden *et al.* (1974) give a type section for the Wambidgee Serpentinite Belt from G.R. 038 339 to G.R. 058 339, to the west of Coolac, where the belt attains a maximum width of 1.9km. More generally, it varies between 0.5 to 1km in width. A possible northward extension of the belt exists at Arramagong Hill (west of Tyagong), where serpentinised harzburgite has been recorded (Warren *et al.* 1995).

Although its contacts with other rocks are not exposed, the Wambidgee Serpentinite Belt appears to be steeply-east dipping (80° to vertical) and, like the Coolac Serpentinite Belt, is a dominantly ultramafic steeply-dipping, NNW-trending linear belt.

4.4.1 Surface outcrop of rock types

Outcrop is moderately good at the southern end of the Wambidgee Serpentinite Belt where the belt forms a prominent ridgeline, defined by a series of large hills. It is poor elsewhere, other than around Jacks Hill (Figure 4.6). At outcrop scale, the serpentinites form steep-dipping sheet-like masses, the plagiogranites and rodingites form small (<0.5m across) rounded masses just rising above the soil, and the metabasic rocks form positive relief as dyke-like bodies within the serpentinite. Chromitite locations are marked by old mine and prospect dumps.

4.4.2 Internal structure

As with the Coolac Serpentinite Belt, the Wambidgee Serpentinite Belt contains diverse lithologies and has a complex internal structure, including primary layering, massive and schistose serpentinites, and tectonic inclusions/intrusive masses.

(a) Primary layering (as detailed in section 4.6.1)

Primary layering has been found in the Fontenoy region (G.R. 058 896), where it can be traced for approximately 100m. The layering occurs within moderately massive unfoliated serpentinite and is defined by alternating Opx-rich and Opx-poor bands (Plate 4.8) that range in thickness from 4 to 40mm and, in some cases, are size-graded. In places, the layering is gently folded with interlimb angles of 150°. Dips range from 60/337° to 10/110°.

Plate 4.8 Layering within serpentinised peridotite defined by bastised orthopyroxene-rich layers (bold relief) and serpentine-rich layers (negative relief). Warrenoy, west of Wombat.

(b) Massive and schistose serpentinites

Serpentinites have no clear-cut geographic distribution within the Wambidgee Serpentinite Belt. Massive serpentinite is cut by discrete zones of schistose (S-C fabric) serpentinite that tend to be <1m thick. Such zones can be traced for over a kilometre (e.g. at Coolac Hill G.R. 045 337) and are spaced in the order of 2-10m. Schistose serpentinite contains discontinuous residuals (0.1-0.2m) of unfoliated serpentinite, and forms narrow (a few metres wide) continuous zones (e.g. G.R. 058 896) throughout the Wambidgee Serpentinite Belt. Within these zones, the C-surface is the dominant fabric element. These zones are commonly associated with cross-cutting chrysotile vein fibres, talc mineralisation and the development of cross-cutting tremolite.

(c) Tectonic inclusions?

As in the Coolac Serpentinite Belt, the Wambidgee Serpentinite Belt contains bodies of various lithologies within serpentinite. Such bodies include chromitite, dunite, gabbro, amphibolite, chlorite rock, plagiogranite and rodingite. Unfortunately, their contacts are usually obscure and make

discrimination between intrusion and tectonic emplacement extremely difficult. However, at G.R. 066 291, a chromitite body within massive serpentinite has its long axis at a high angle to the trend of the belt. Similarly, dyke-like bodies of chlorite rock occur at "Sunnybrae" (G.R. 042 410) and, at Jacks Hill (G.R. 972 194), a small (5m) mass of unfoliated plagiogranite occurs in serpentinite, which contains tremolite near and on the contact. These bodies may have been magmatically emplaced whereas others were tectonically emplaced.

4.5 PETROGRAPHY AND TEXTURAL/STRUCTURAL EVOLUTION

(For detailed petrographic descriptions, see Appendix 4PD)

4.5.1 Primary ultramafic rocks

The primary ultramafic rocks of the Wambidgee Serpentinite Belt are those which have either retained their primary igneous mineralogy, or lost their primary minerals but retained their igneous textures, allowing identification of the precursor rock types. On this basis, the Wambidgee Serpentinite Belt originally contained dunite, harzburgite, hornblende clinopyroxenite, hornblendite and layered peridotite. These rock types, with the exception of layered peridotite (found only in the central part) and dunite (usually associated with podiform chromitite), lack systematic distribution.

The preceding rock types occur as lenticular bodies (a few metres in maximum dimension) within massive or schistose metaserpentinite, their longest axis commonly parallel to the schistosity. This is particularly well illustrated by a long (nearly 100m) narrow (less than 4m) lens of layered hornblendite/peridotite located at G.R. 039 891. Conversely, the layered peridotite at Fontenoy (Figure 4.6; as mentioned above) forms a shallowly undulating body and is an exception to the lenticular geometry.

Microscopically, completely serpentinised dunite has a well-developed mesh texture and lacks pyroxene (Plate 4.9), whereas completely serpentinised harzburgite has >10% bastite pseudomorphs after orthopyroxene in a matrix of serpentine (Plate 4.10). Rare primary layering (above and section 4.6.1) occurs in the Fontenoy region. Hornblende metaclinopyroxenite is restricted to Jacks Hill, north of Thuddungra, while hornblendite occurs in the Fontenoy district, where it is coarse-grained (Plate 4.11) and also at Jacks Hill, where it is fine-grained.

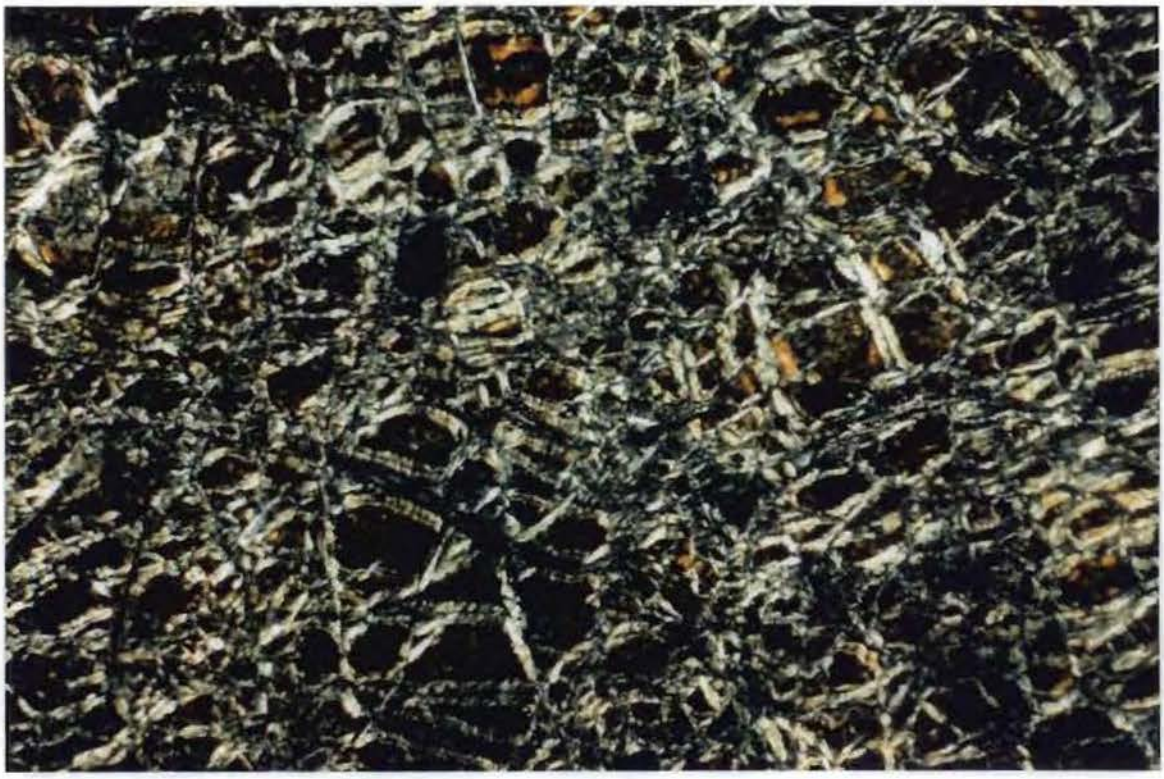

Plate 4.9 Serpentinised dunite exhibiting a mesh texture.
Sample No BF92/10b UXP F.O.V 3.5mm

Plate 4.10 Bastised orthopyroxene grains within serpentinised harzburgite. Lizardite and chrysotile are in the matrix.
Sample No BF91/27a UXP F.O.V 3.5mm

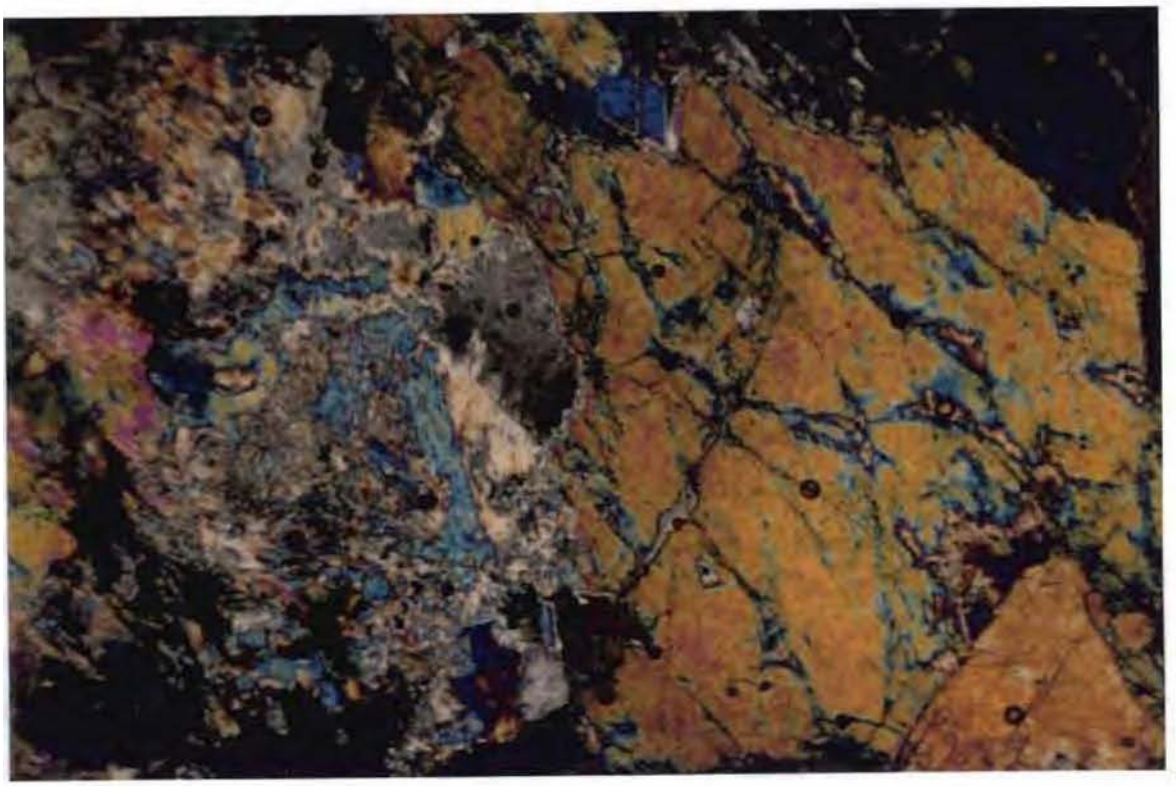

Plate 4.11 Coarse-grained hornblendite.
Sample No 65 UXP F.O.V 3.5mm

Layered peridotite (above and section 4.6.1) occurs in the Fontenoy region, where two variants exist. The most common consists of completely serpentinised rhythmically layered peridotite (alternating Opx-rich and Opx-poor layers) (section 4.6.1) within schistose and massive serpentinite. The less common comprises weakly serpentinised, simply layered peridotite (also Opx-rich and Opx-poor layers) and occurs as a layer within a hornblendite unit (section 4.6.1). The more common variant has a number of distinct types of layers (section 4.6.1).

The primary ultramafic rocks of the Wambidgee Serpentinite Belt have, in cases, been completely altered and, at best, only retain relict primary phases. The intensity of metamorphism varies along the belt with upper greenschist facies to lower amphibolite facies assemblages dominating the southern and central parts, and upper amphibolite facies with a lower amphibolite facies overprint dominating the northern part.

The dunites of the Wambidgee Serpentinite Belt have been completely serpentinised, so the pre-serpentinisation evolution is difficult to determine. The dominant assemblage of lizardite 6T+chrysotile+magnetite (Plate 4.9) is ascribed to an early stage of low temperature (less than 250 $^{\pm}$ 25°C at a $P_{(H_2O)}$ of less than 1kb - (O'Hanley & Wicks 1995) serpentinisation through the infiltration of sea-water in an oceanic environment (e.g. Laurent & Hebert 1979) before emplacement into continental crust (e.g. Moody 1979). However, Wicks (1984) stated that before sea-water infiltration could occur, there must have been brittle failure at least enhanced by hydraulic fracturing between and through grains to facilitate the intensity of serpentinisation. Thus, on this basis, the dunites of the Wambidgee Serpentinite Belt underwent brittle fracturing at a distance from where they formed and seawater infiltration and concurrent hydraulic fracturing resulted in their complete serpentinisation.

The serpentinised harzburgite contains relict orthopyroxene and chrome spinel grains (Plate 4.10) that enable reconstruction of the pre-serpentinisation history. The pseudo-porphyroclastic texture (Chapter 3, section 3.5.1) mimics the high temperature porphyroclastic texture that is ascribed to recrystallisation of original magmatic harzburgite (e.g. Bartholomew 1993; Chapter 3, section 3.5.1). This was followed by brittle failure and ongoing hydrofracturing under conditions above 250°C and $P_{(H_2O)}$ >1kb, and below 450°C (e.g. O'Hanley 1996) during which infiltrating sea-water resulted in the replacement of olivine and orthopyroxene by antigorite +magnetite (e.g. Evans 1977). Subsequent to antigorite formation, a period of brittle failure accompanied development of chrysotile and tremolite veinlets, a sequence of events which essentially parallels that found in harzburgite of the Coolac Serpentinite Belt (Chapter 3, section 3.5.1).

Hornblende metaclinopyroxenites have a granoblastic metamorphic texture and consist of a high-grade metamorphic assemblage partially overprinted by a low-grade assemblage. There is no clear evidence to suggest the nature of the pre-cursor assemblage except that clinopyroxene porphyroblasts may well be relict primary grains. The occurrence of fine-grained clinopyroxene and moderately pleochroic brown hornblende around the clinopyroxene porphyroblasts is ascribed to lower granulite facies metamorphism (e.g. Miyashiro 1994). Assuming an igneous parent, the metamorphism would have been retrogressive and could have been a function of the cooling history.

Tremolite overprinting hornblende is ascribed to upper greenschist to lower amphibolite facies metamorphism (e.g. Miyashiro 1994).

The hornblendites of the Wambidgee Serpentinite Belt have been variably altered. Those only weakly affected retain a cumulus texture and have a mineral assemblage of hornblende, diopside, actinolite, talc and chlorite (Plate 4.11), indicative of an original magmatic assemblage of hornblende and diopside, partially overprinted by greenschist facies metamorphism (i.e. actinolite, talc and chlorite) (e.g. Miyashiro 1994). In contrast, those more intensely affected exhibit a fine-grained metamorphic granular texture and a mineral assemblage of hornblende, diopside, orthopyroxene, actinolite and talc. Development of the granular texture is ascribed to recrystallisation of diopside, orthopyroxene and hornblende under upper amphibolite-lower granulite facies metamorphism (e.g. Miyashiro 1994). The occurrence of cross-cutting actinolite and talc is ascribed to upper greenschist facies retrograde metamorphism (e.g. Miyashiro 1994)."

The layered peridotites of the Wambidgee Serpentinite Belt have been variably serpentinised. The weakly serpentinised type, have a mineral assemblage of olivine, orthopyroxene, tremolite and chlorite and retain an igneous cumulus texture (Plate 4.12). The presence of cross-cutting tremolite and chlorite is ascribed to mid-greenschist facies metamorphism . In contrast, the strongly serpentinised layered peridotites consist of rare bastitised orthopyroxene, relict clinopyroxene, antigorite, talc, chlorite, tremolite and abundant secondary accessory magnetite (Plate 4.13). Although they retain primary layering, they exhibit a metamorphic decussate texture.

Orthopyroxene grains rimmed by hornblende are ascribed to upper amphibolite facies metamorphism (e.g. Miyashiro 1994). Antigorite formed at temperatures above 260°C, but below 450°C (e.g. O'Hanley 1996). The occurrence of cross-cutting tremolite+chlorite is ascribed to greenschist facies retrograde metamorphism (e.g. Miyashiro 1994).

Plate 4.12 Cumulus texture of weakly serpentinised layered peridotite.
Sample No 65 (L) UXP F.O.V 3.5mm

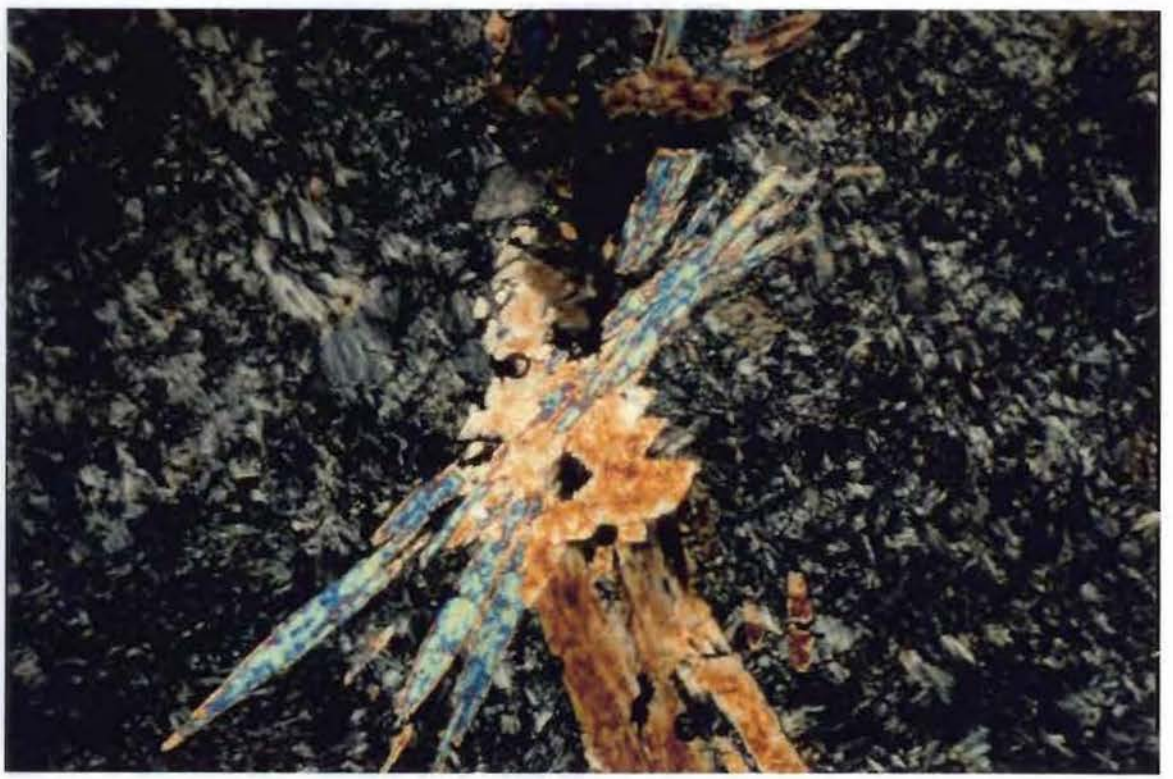

Plate 4.13 Cross-cutting tremolite within serpentinised layered peridotite.
Sample No 225B UXP F.O.V 3.5mm

4.5.2 Serpentinites

Massive and schistose serpentinites dominate the Wambidgee Serpentinite Belt. Massive varieties generally occur as "blocks" and lenses surrounded by the schistose variety. However, in certain places (e.g. at G.R. 043 460) schistose serpentinite is completely lacking. In such cases, narrow S-C fabric zones (<0.2m across), mostly composed of talc, occur within the massive serpentinite.

Primary phases are rare within the serpentinites, but where present, include olivine, chrome spinel and completely bastitised orthopyroxene grains. Secondary metamorphic phases are common (almost ubiquitous in every outcrop) and comprise tremolite, talc, Mg-chlorite and rare magnesite. On textural grounds, the serpentinites may be subdivided into massive and schistose types.

XRD studies on both massive and schistose serpentinites from the Wambidgee Serpentinite Belt confirm that a number of serpentine polymorphs exist, dominated by antigorite and chrysotile. The non-oriented serpentine matrix within the serpentinites, has been identified as antigorite using this method. Chrysotile 2M and chrysotile 20 occur within the chrysotile veinlets and Al-rich lizardite 1T is common within the Jacks Hill area in the north of the belt.

The serpentinites of the Wambidgee Serpentinite Belt are more correctly termed "metaserpentinites", as they are dominantly composed of antigorite with cross-cutting patches and veinlets of tremolite. The latter are indicative of medium pressure upper greenschist-lower amphibolite facies metamorphism (e.g. Miyashiro 1994; O'Hanley & Wicks 1995). The presence of chrysotile veinlets of a number of generations indicates that serpentinisation was an ongoing process (e.g. Wicks & Plant 1979). The rocks are now dominantly composed of antigorite which is ascribed to serpentinisation above 250°C and a $P_{(H_2O)}$ of less than 1kb (e.g. O'Hanley & Wicks 1995). Secondary cross-cutting talc and magnesite developed at temperatures below 100°C by the percolation of CO_2-enriched groundwaters through the rocks (e.g. Laurent & Hebert 1979).

The serpentinites of the Wambidgee Serpentinite Belt have been variably deformed. In the more massive varieties, deformation is defined by the occurrence of veinlets of tremolite, cross-cut by veinlets of chrysotile and magnetite, all of which developed synchronous to serpentinisation by brittle fracturing. In the schistose varieties, deformation is largely defined by the nature of the S-C

fabric present and the occurrence of veinlets. This deformational history is somewhat different. Brittle/ductile deformation either pre- or synchronous to serpentinisation led to the initiation of an S-C fabric. Following the formation of matrix antigorite, further brittle/ductile deformation led to the development of veinlets of a number of different generations and the enhancement of the S-C fabric.

4.5.3 Talc-carbonate rocks

Talc-carbonate rocks are common throughout the Wambidgee Serpentinite Belt. In the past, talc has been commercially mined from such rocks at Muttama and Wallendbeen. A large magnesite deposit, unrelated to these rocks and of recent sedimentary origin (e.g. Diemar 1998), is exploited at the Thuddungra Magnesite Mine (Plate 4.14)."

Plate 4.14 View of the West Main Pit, Thuddungra Magnesite Mine looking south.

Although talc-carbonate rocks occur throughout the belt, they are restricted to either discrete small-scale (0.1-0.2m in width and a few metres in length) cross-cutting shear zones within serpentinite, or to contacts between the Wambidgee Serpentinite Belt and either quartzites of the Jindalee Beds (Muttama talc mine), or intrusive felsic igneous rocks (Quartz Hill) (Figure 4.8). In the contact-related occurrences, the talc-carbonate rocks occur as discrete lenses and may be up to 50m in length and 5m in width.

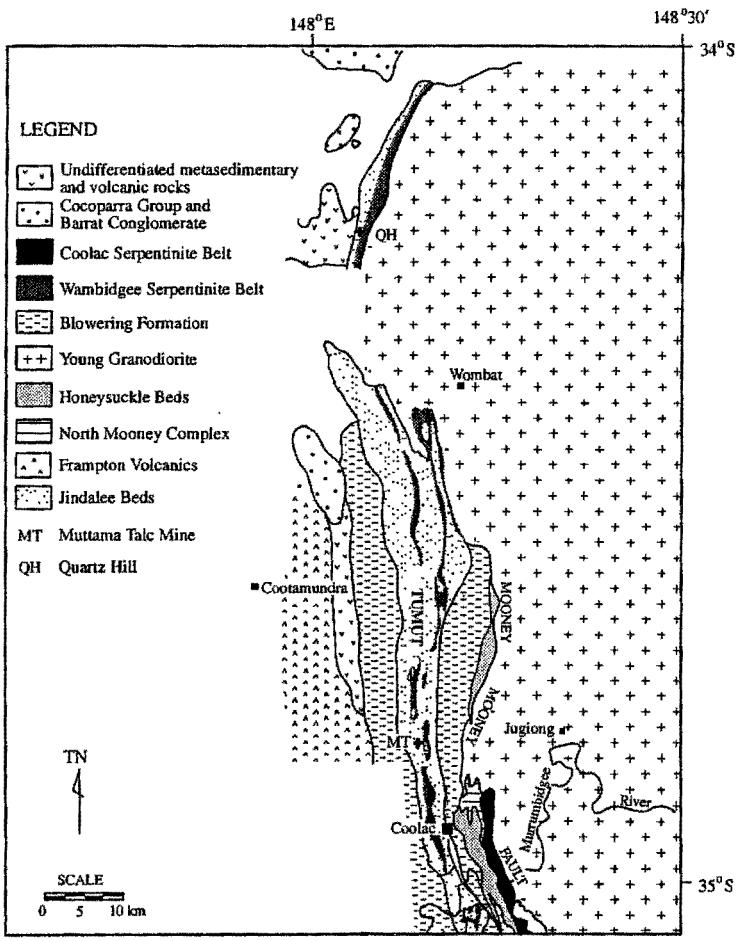

Figure 4.8 Location of main outcrops of talc-magnesite rocks within the Wambidgee Serpentinite Belt (adapted from Fitzpatrick 1976).

The talc-carbonate rocks of the Wambidgee Serpentinite Belt are divided into three groups based on dominant mineral assemblage:

(a) talc+magnesite rich metaserpentinites

(b) talc-rich metaserpentinites

(c) magnesite-rich metaserpentinites

In the talc+magnesite-rich metaserpentinite (Plate 4.15), initial brittle fracturing concurrent with serpentinisation of the primary ultramafic rocks led to the development of antigorite above 250°C and a $P_{(H_2O)}$ of less than 1kb (e.g. O'Hanley & Wicks 1995). Brittle fracturing after serpentinisation produced channelways for the passage of hydrothermal fluids which resulted in the development of talc and magnesite over a minimum temperature range of 165-225°C (e.g. Ashley 1997).

Plate 4.15 Talc+magnesite rich metaserpentinite exhibiting a granoblastic decussate texture.
Sample BF92/73 UXP F.O.V 3.5mm

The talc-rich metaserpentinites have undergone a similar metamorphic/structural history to the talc+magnesite-rich metaserpentinites.Magnesite is lacking, most likely because the fugacity of CO_2 was too low (e.g. Deer *et al.* 1985). Their schistosity is ascribed to brittle-ductile deformation pre- and/or syn-serpentinisation.

The magnesite-rich metaserpentinites (Plate 4.16) have undergone a similar metamorphic/structural history to the above rocks except that the fugacity of CO_2 was high enough to allow development of magnesite (e.g. Deer *et al.* 1985).

Plate 4.16 Magnesite porphyroblast within magnesite-rich metaserpentinite.
Sample No BF92/69 UXP F.O.V 3.5mm

4.5.4 Tremolite-rich metaserpentinites

These are metaserpentinites of the Wambidgee Serpentinite Belt which contain greater than 30% tremolite. The tremolite is of metamorphic origin and cross-cuts the matrix serpentine. These rocks have been found in the far north of the belt (i.e. in the vicinity of the Thuddungra magnesite mine and Jacks Hill) where they are common. In all occurrences, the tremolite-rich metaserpentinite occurs as narrow lenses within metaserpentinite or amphibolite.

The tremolite-rich metaserpentinites have a simple mineralogy and the dominance of tremolite and antigorite (Plate 4.17) is indicative of upper greenschist facies metamorphism (e.g. Miyashiro 1978). However, the rocks were initially composed of primary phases, which retrogressed during greenschist facies metamorphism, with the development of antigorite above 250°C (e.g. O'Hanley & Wicks 1995). Later brittle fracturing resulted in the development of veinlets of fibrous tremolite. Low temperature alteration is evidenced by talc cross-cutting all other phases and is ascribed to the passage of post-serpentinisation hydrothermal fluids through these rocks at minimum temperatures of 165-225°C (e.g. Ashley 1997).

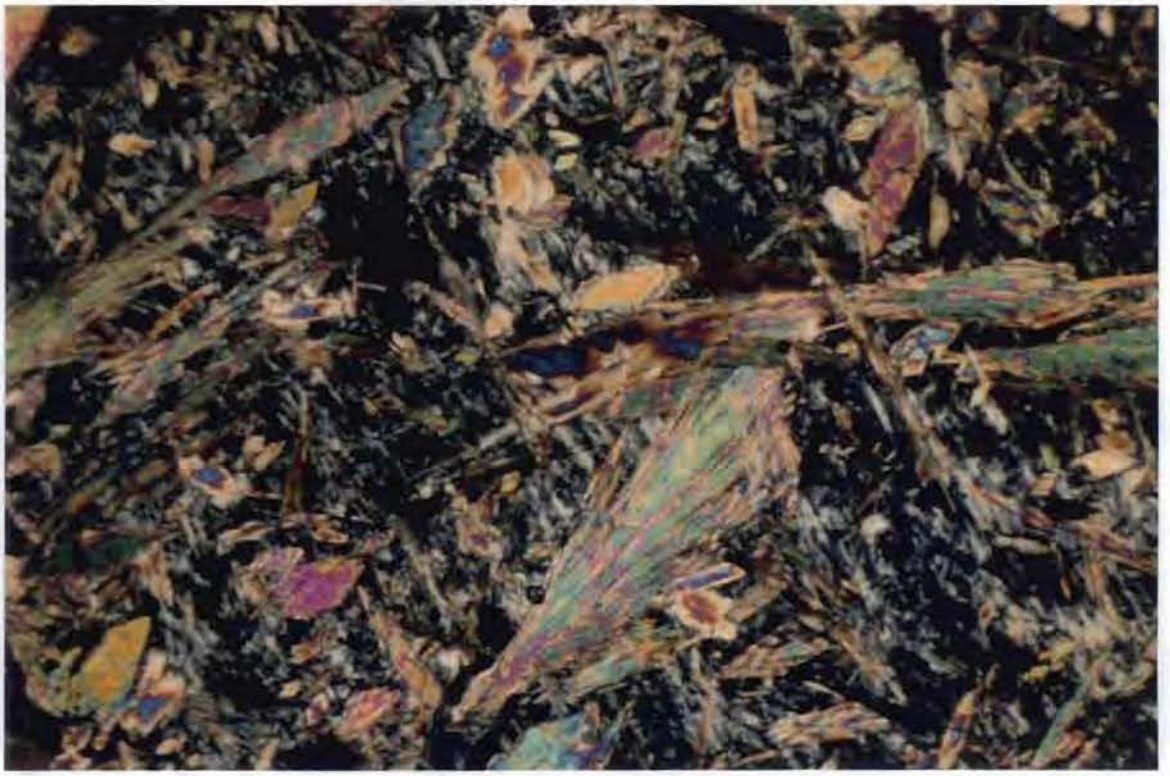

Plate 4.17 Cross-cutting tremolite within tremolite-rich metaserpentinite.
Sample No BF91/32d UXP F.O.V 3.5mm

4.5.5 Gabbros

Gabbros are essentially composed of mixtures of plagioclase, clinopyroxene, and hornblende and have an igneous texture. They may be divided into clinopyroxene-rich and hornblende-rich types. Gabbros of both types occur within the same outcrop and lack systematic distribution. They are common in both the central and northern parts of the belt but have not been found in the south. The gabbro bodies occur as small (<0.5m) to large (50m) generally dyke-like (i.e. with moderate length to width ratios) bodies within either schistose or massive serpentinite, though contact relationships are not clear. Many of the gabbros are unfoliated at meso-scale, but where they occur close to faulted contacts with the Young Granodiorite, they become schistose and finer-grained.

The initial metamorphism/deformation of the clinopyroxene-rich gabbros produced partial recrystallisation of plagioclase and quartz and bent clinopyroxene and plagioclase grains. Ongoing metamorphism resulted in the partial cleavage-related replacement of diopside by tremolite/actinolite, the saussuritisation of calcic plagioclase, and the development of zoisite and epidote, indicative of greenschist facies metamorphism (e.g. Miyashiro 1978). This was followed by the development of cross-cutting tremolite/actinolite (Plate 4.18).

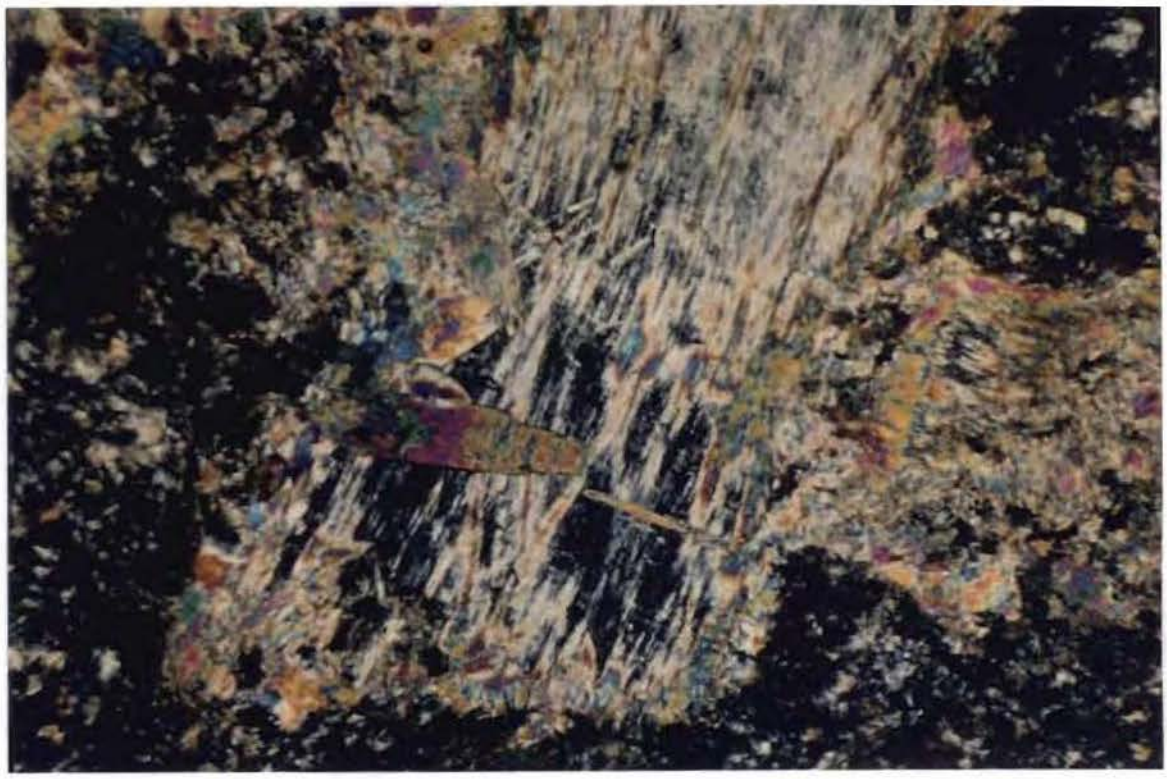

Plate 4.18 Cross-cutting tremolite/actinolite within clinopyroxene gabbro.
Sample No BF92/3 UXP F.O.V 3.5mm

Hornblende-rich gabbros have undergone the same metamorphic/deformation history as the clinopyroxene-rich gabbros. However, from textural evidence (Plate 4.19), phlogopite formed before the development of the tremolite/actinolite, epidote and zoisite.

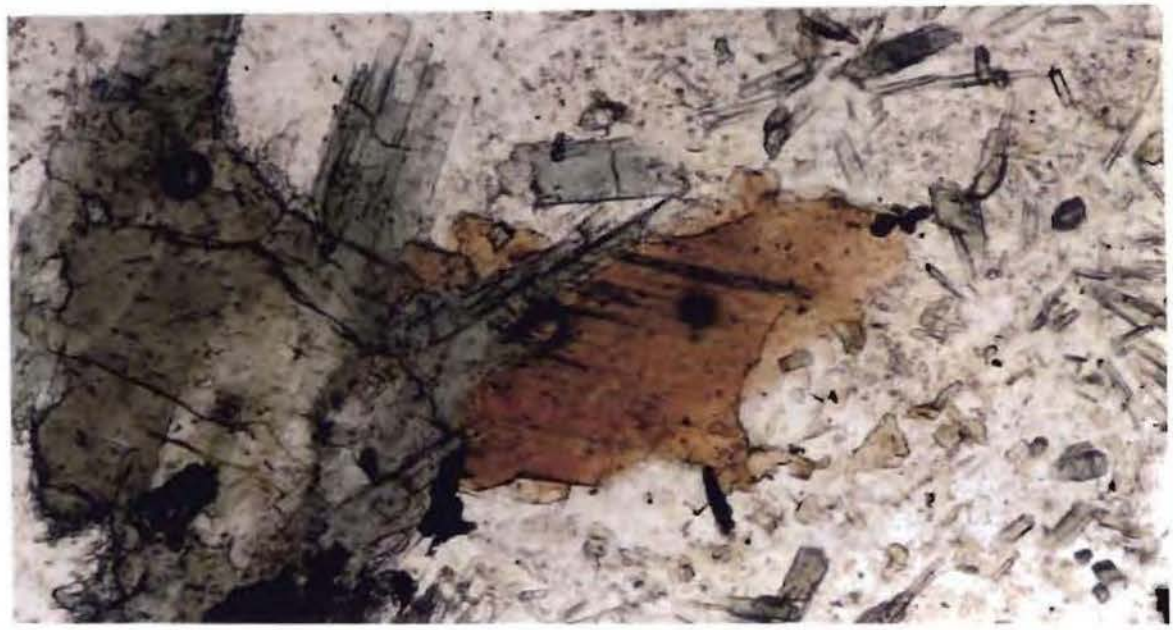

Plate 4.19 Phlogopite grains within hornblende gabbro.
Sample No 182b UXP F.O.V 1.5mm

Due to the intensity of alteration, the early metamorphic/deformational history of the completely altered gabbros cannot be determined. All that can be said is that they experienced a period of intense greenschist facies metamorphism (e.g. Miyashiro 1978) as indicated by the assemblage albite+epidote+zoisite+chlorite+quartz, followed by the development of cross-cutting tremolite.

4.5.6 Plagiogranites

Plagiogranites are composed of quartz and albitised plagioclase (determined by XRD methods) with minor tremolite-actinolite and chlorite and have a granular texture. They commonly contain angular enclaves of amphibolite (Plate 4.20) and form small (a few metres in maximum dimension), plug-like masses in the central and northern parts of the belt with unclear contact relationships against massive or schistose serpentinite. Plagiogranites are massive and unfoliated at meso-scale.

Contacts between the plagiogranites and amphibolite enclaves are generally sharp and planar (Plate 4.21). Isolated aggregates of hornblende (from the enclaves), occur within the plagiogranites.

Plate 4.20 Enclaves of amphibolite within plagiogranite.
Sample No BF91/33f

Plate 4.21 Contact between plagiogranite (left) and amphibolite enclave (right).
Sample No 33Fa UXP F.O.V 3.5mm

XRD studies confirm that the plagiogranites are composed of mixtures of quartz, albite, tremolite/actinolite and epidote, this assemblage being indicative of greenschist facies metamorphism (e.g. Miyashiro 1978). Initial deformation associated with the metamorphism led to the development of subgrains in the plagioclase and quartz, bent plagioclase twin lamellae. The development of cross-cutting cataclasite may have been synchronous or later (Plate 4.22). Cross-cutting aggregates of tremolite/actinolite and chlorite reflect metasomatic reactions between the plagiogranite and surrounding ultramafic wall rocks (e.g. Linder *et al.* 1992).

Because the amphibolite enclaves contain assemblages (see section 4.5.7) indicative of amphibolite facies partly retrograded to greenschist facies metamorphism, they must have reached their peak metamorphic grade before intrusion and incorporation into the plagiogranites.

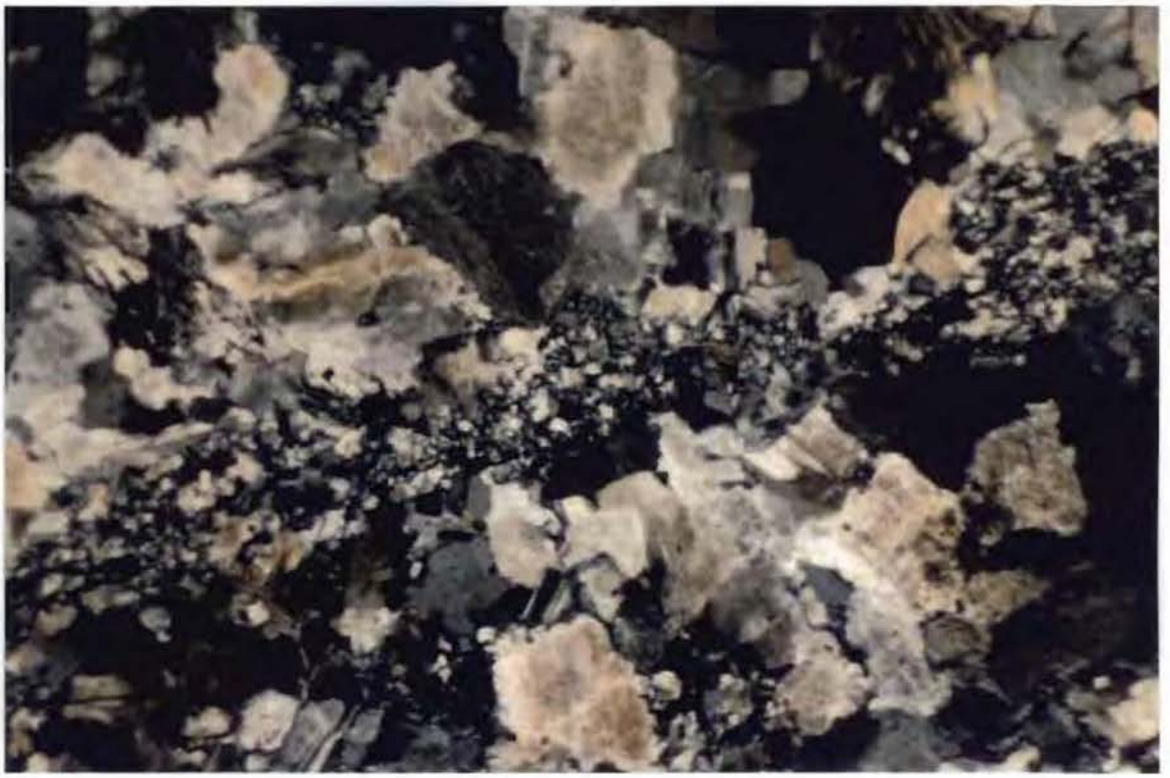

Plate 4.22 Cross-cutting narrow cataclasite zones within plagiogranite.
Sample No BF91/33f UXP F.O.V 3.5mm

4.5.7 Amphibolites

The amphibolites of the Wambidgee Serpentinite Belt are principally composed of amphibole and plagioclase and have a metamorphic texture. They can be divided into:

(a) types with relatively non-oriented grains,

(b) types with relatively oriented grains, and

(c) layered amphibolites

Amphibolites are common in the northern part of the belt and rare elsewhere. They occur as small (<0.5m maximum dimension) to relatively large (up to 30m in length and 15m in width) dyke-like bodies (i.e. with a large length to width ratio) within massive and schistose serpentinite. Although relatively massive at meso-scale and lacking sheared boundaries, they become progressively more schistose close to the faulted contact with the Young Granodiorite.

The amphibolites have been metamorphosed such that their igneous precursors cannot be accurately determined. The non-oriented amphibolites reached middle amphibolite facies conditions (e.g. Miyashiro 1978), as evidenced by green-brown hornblende around cores of colourless clinopyroxene. They then underwent greenschist facies retrogression, based on alteration of plagioclase to mixtures of epidote+albite+quartz and the occurrence of cross-cutting actinolite and chlorite. The oriented and layered amphibolites have undergone a similar metamorphic history but retrograde coarser-grained actinolite crystals are cross-cut and overprinted by finer-grained actinolite.

The more intensely deformed amphibolites contain bent and fractured hornblende, and have a polygonal texture with well-developed triple-junction grain boundaries shown by plagioclase and quartz. The oriented amphibolites exhibit a schistose texture defined by aligned hornblende and secondary actinolite grains which wrap-around the plagioclase and quartz. The layered amphibolites exhibit a gneissic texture defined by hornblende-rich and hornblende-poor zones (Plate 4.23).

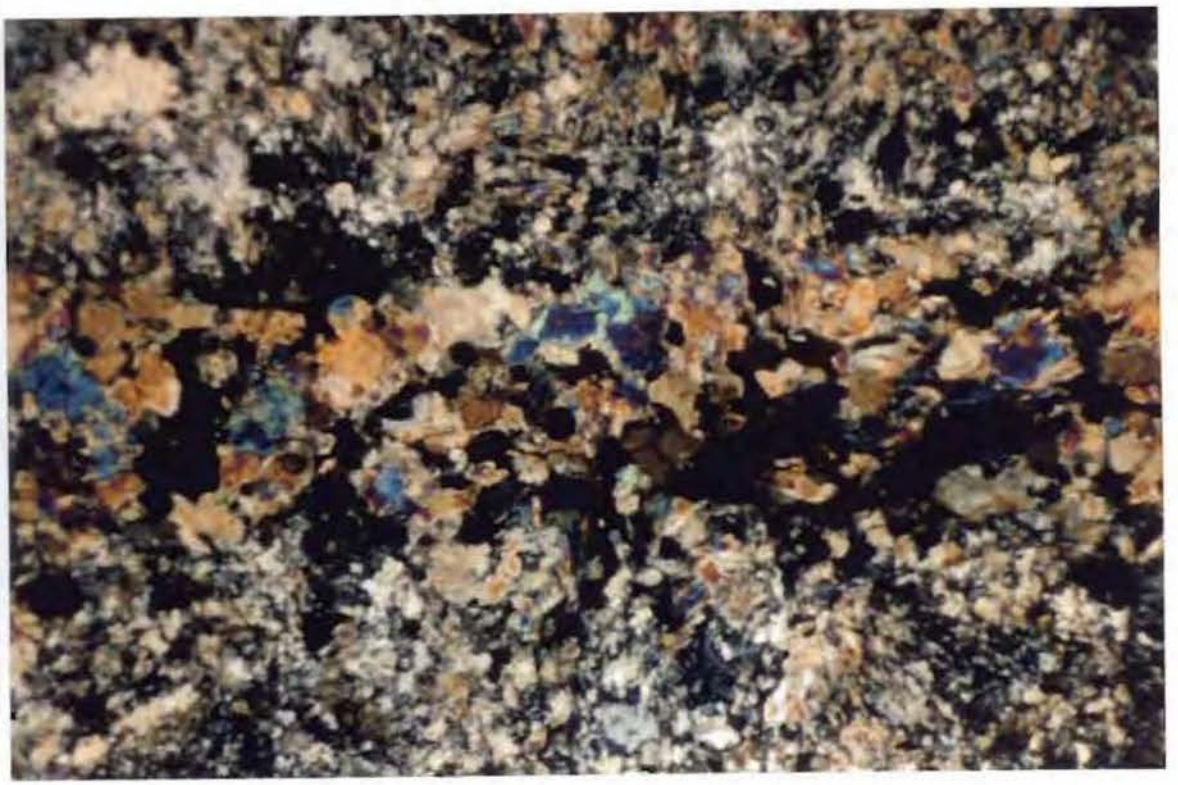

Plate 4.23 Fine-scale layering within layered amphibolite.
Sample No 190b UXP F.O.V 3.5mm

4.5.8 Tremolite/Actinolite rocks

Tremolite/actinolite rocks consist of more than 80% tremolite and/or actinolite and have a decussate non-oriented texture. They can be divided into tremolite-rich and actinolite-rich types.

Although very restricted in their distribution, they are prominent at the Muttama talc mine (G.R. 025 508) and the Borrow Pit of the Thuddungra magnesite mine (G.R. 970 186). They occur as relatively undeformed, discrete, narrow (<0.2m in width) zones at contacts between plagiogranite, metagabbro and quartzite, with enclosing serpentinite. It is therefore likely that they formed metasomatically (e.g. Curtis & Brown 1969; Linder *et al.* 1992). Their near monominerallic nature precludes accurate determination of the metamorphic grade, beyond saying that they have reached the lower to middle greenschist facies (e.g. Miyashiro 1978).

4.5.9 Chlorite rocks

Chlorite rocks contain more than 80% chlorite and have a decussate texture. They are of minor occurrence, but are widely distributed as lens-shaped (up to 5m in length and 2m in width) bodies within schistose serpentinite. Contacts between the chlorite rocks and the schistose serpentinites are sheared.

As the chlorite rocks are almost monominerallic, it is difficult to constrain their metamorphic grade and history, beyond stating that they have at least undergone low grade metamorphism.

Although most of the chlorite rocks are relatively massive and undeformed at meso-scale, some contain narrow and discrete cross-cutting shear zones at micro-scale, defined by chlorite grains with their long axis at 60° to the shear zone walls within a matrix of dominantly non-aligned chlorite (Plate 4.24). Some of the rocks are cut by veinlets of Mg chlorite+calcite suggesting that Mg-metasomatism resulted when Mg was released from the surrounding ultramafic rocks.

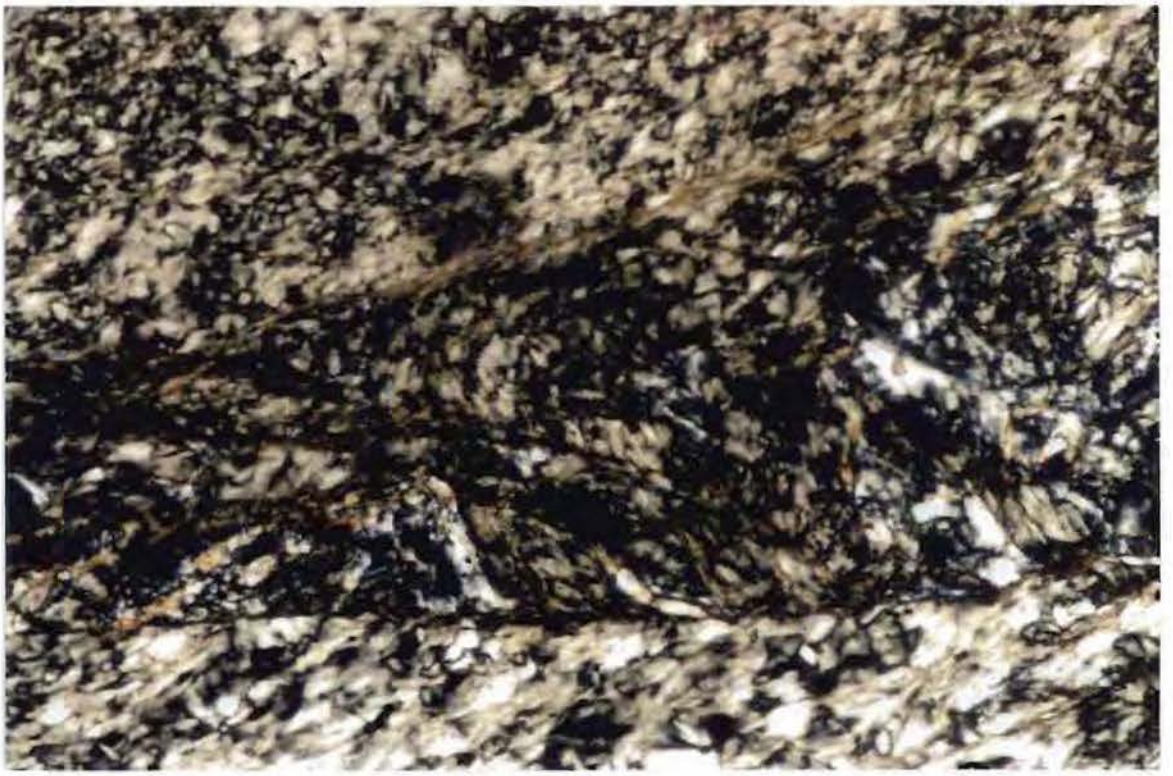

Plate 4.24 Micro shear zone defined by aligned chlorite grains within chlorite rock.
Sample No BF91/28c UXP F.O.V 1.5mm

4.5.10 Other rock types

This group includes those rock types that occur within the Wambidgee Serpentinite Belt (generally within serpentinite) but do not belong in any of the preceding groups. The group is diverse and comprises felsic volcanic tuffs, metabasalts, actinolite hornfelses, actinolite-chlorite rocks, chlorite-zoisite-talc rocks, rodingites and olivine-amphibole-chlorite hornfelses. Some of these are likely to be tectonically incorporated inclusions whereas others may be reaction zone products or possible intrusives, etc.

Felsic volcanic tuffs

Felsic volcanic tuffs have been found at one locality (G.R. 058 896) in the central part of the belt where they occur as strongly lineated rocks (up to 10m x 4m) within layered serpentinised peridotite. They have reached lower to middle greenschist facies as evidenced by the assemblage albite+quartz+actinolite+zoisite (e.g. Miyashiro 1978). Deformation accompanied the metamorphism and resulted in the partial recrystallisation and alignment of the plagioclase and quartz phenocrysts and the development of a fine-grained quartzofeldspathic matrix and synkinematic actinolite. Ongoing greenschist facies metamorphism partially altered some of the plagioclase to zoisite and developed relatively fine-grained actinolite.

Metabasalt

Rare metabasalts occur in the southern and northern extremities of the belt where they form small (max. 0.5 to 5m) dyke-like bodies within massive or schistose serpentinite. The presence of relatively abundant fine-grained almandine and hornblende (Plate 4.25) indicates upper greenschist to lower amphibolite facies metamorphism (e.g. Miyashiro 1978). Retrogression to lower greenschist facies is evidenced by abundant cross-cutting actinolite. Deformation late in the first metamorphic event resulted in the bending of hornblende grains. During retrogressive metamorphism, veinlets and grains of zoisite and epidote developed, and hornblende was largely replaced by actinolite.

Plate 4.25 Fine-grained almandine and cross-cutting actinolite within metabasalt.
Sample No BF92/16b PPL F.O.V 1.5mm

Actinolite hornfels

Actinolite hornfels has been found in the central part of the belt (G.R. 039 891) where it forms small (<0.5m) lensoid bodies. Contact relationships with the surrounding rock types are unclear. The near-monominerallic nature precludes determination of the precursor igneous rock type. Abundant actinolite and minor chlorite are consistent with lower to middle greenschist facies metamorphism (e.g. Miyashiro 1978).

Actinolite-chlorite rocks

Actinolite-chlorite rocks occur in the northern part of the belt (G.R. 970 186) at the contact between mafic amphibolite and serpentinite. They have a lepidoblastic, decussate texture (Plate 4.26) and have undergone low to middle greenschist facies metamorphism (e.g. Miyashiro 1978). They may be metasomatic reaction zone rocks. however, field evidence is inconclusive.

Plate 4.26 Lepidoblastic, decussate texture within actinolite-chlorite rock.
Sample No BF91/32c UXP F.O.V 3.5mm

Chlorite-zoisite-talc rocks

Chlorite-zoisite-talc rocks are moderately common in the southern part of the belt but have not been found elsewhere. They occur as small lens-shaped (a few metres in maximum dimension) bodies near the contacts of Jindalee Beds quartzite and serpentinite. They are strongly layered (Plate 4.27) and the original igneous texture has been obliterated by metamorphic recrystallisation. The mineral assemblage suggests that the rocks reached the lower greenschist facies of metamorphism (e.g. Miyashiro 1978). They are interpreted by the author as having formed by metasomatism between ultramafic rocks and adjacent quartzites (e.g. see also Linder *et al.* 1992). Minor deformation led to the development of veinlets of tremolite+muscovite+chlorite+zoisite+vesuvianite.

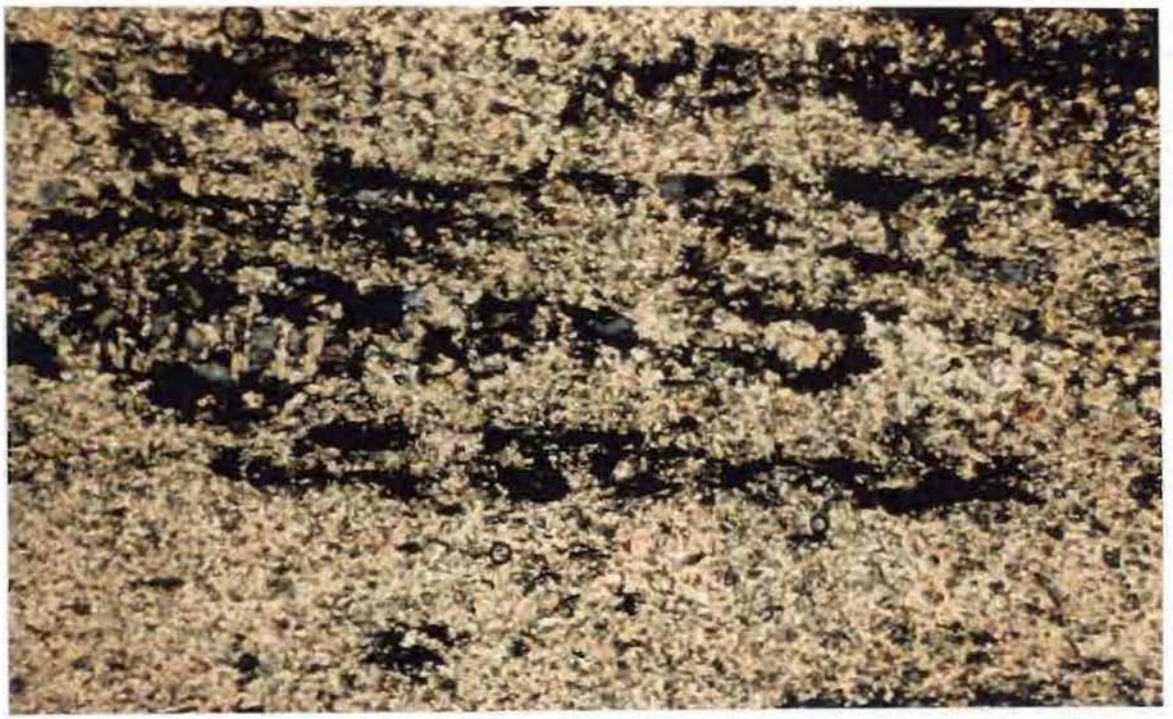

Plate 4.27 Fine-scale layering within chlorite-zoisite-talc rock.
Sample No BF92/72 UXP F.O.V 3.5mm

Rodingites

Rodingite occurs as a small lens (<0.5m) within serpentinite in the southern part of the belt (G.R. 037 398). It contains diopside, which is probably a relict primary phase from a pre-cursor clinopyroxene gabbro (e.g. Dubinska 1995) rather than an early metamorphic phase (e.g. Schandl *et al.* 1990; O'Hanley *et al.* 1992). This is supported by clinopyroxene gabbros elsewhere in the belt lacking evidence of metamorphic diopside. Plagioclase has altered to zoisite, Mg-chlorite and talc, indicative of lower greenschist facies metamorphism (e.g. O'Hanley *et al.* 1992). Deformation is recorded by bent exsolution lamellae and brecciated diopside grains (Plate 4.28).

Olivine-amphibole-chlorite hornfels

Olivine-amphibole-chlorite hornfels occurs as isolated lenses (a few metres in maximum dimension) within chlorite rock at only one locality (G.R. 050 880). It has formed from peridotite and originally consisted of olivine and clinopyroxene. High temperature hydrous metamorphism resulted in the replacement of clinopyroxene by pink (?manganiferous) hornblende (Plate 4.29) under hornblende hornfels or amphibolite facies conditions (e.g. Miyashiro 1978). Deformation accompanied retrogressive greenschist facies metamorphism and developed micro shear zones, and induced rim and fracture replacement of olivine and some hornblende by Mg-chlorite

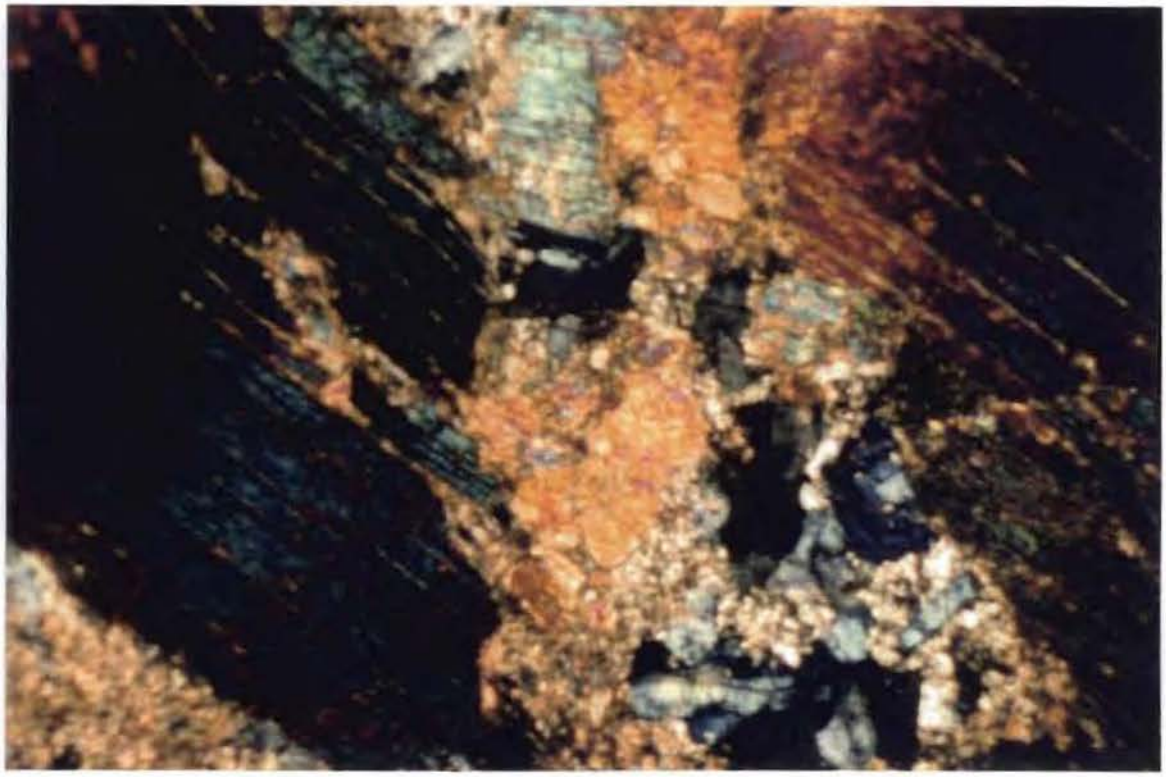

Plate 4.28 Brecciated diopside grains within rodingite.
Sample No BF92/26c UXP F.O.V 3.5mm

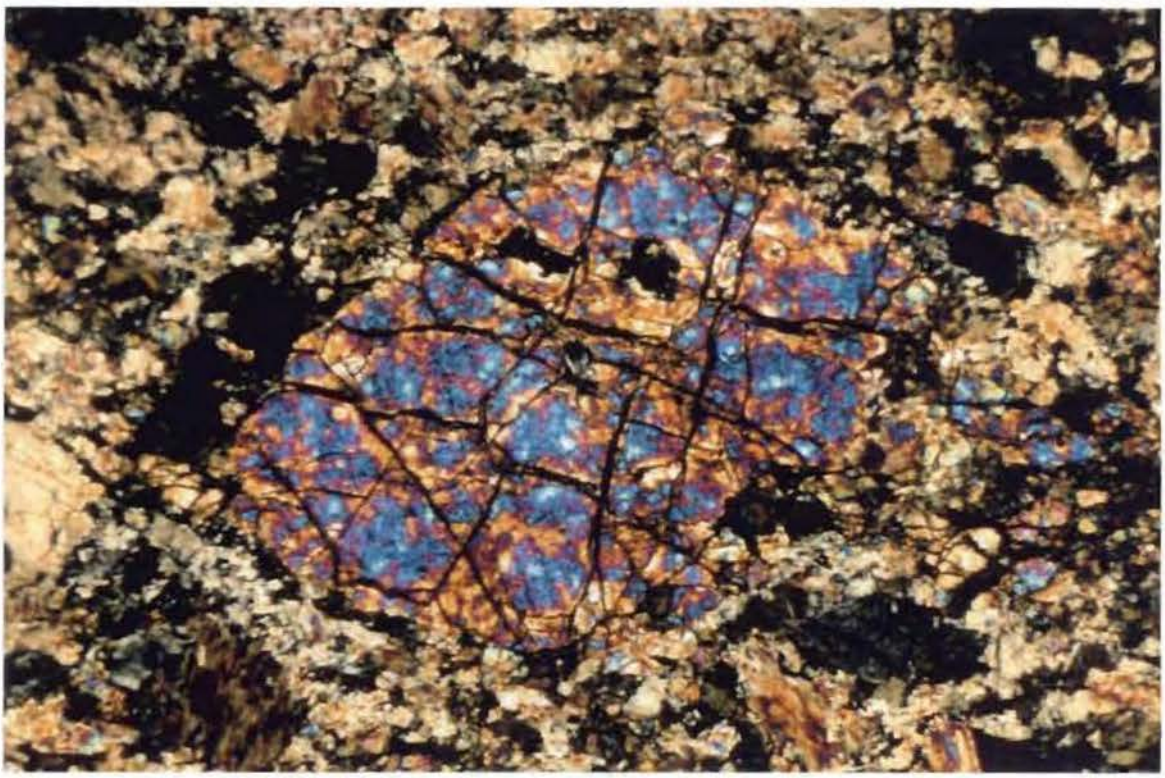

Plate 4.29 Porphyroblastic olivine within olivine-amphibole-chlorite hornfels.
Sample No BF92/8 UXP F.O.V 3.5mm

4.6 STRUCTURE OF THE WAMBIDGEE SERPENTINITE BELT

4.6.1 Primary layering

Primary layering is restricted (see section 4.5.1) and is defined by variation in:

(a) the olivine to orthopyroxene ratio (defining both olivine-rich and orthopyroxene-rich layers);

(b) the hornblende to olivine+orthopyroxene+clinopyroxene ratio (defining both hornblendite and peridotite layers);

(c) the serpentine to secondary amphibole ratio (defining both serpentine-rich and amphibole-rich layers);

(d) grain-size (defining fine-grained and coarse-grained layers, similar to sedimentary graded layering);

(e) the secondary mineralogy (a reflection of the vertical variation in the primary mineralogy);

Layered ultramafic rocks have been found only in the central portion of the belt in the Fontenoy region (Figure 4.9) (G.R. 039 891 and G.R. 058 896) where they are common.

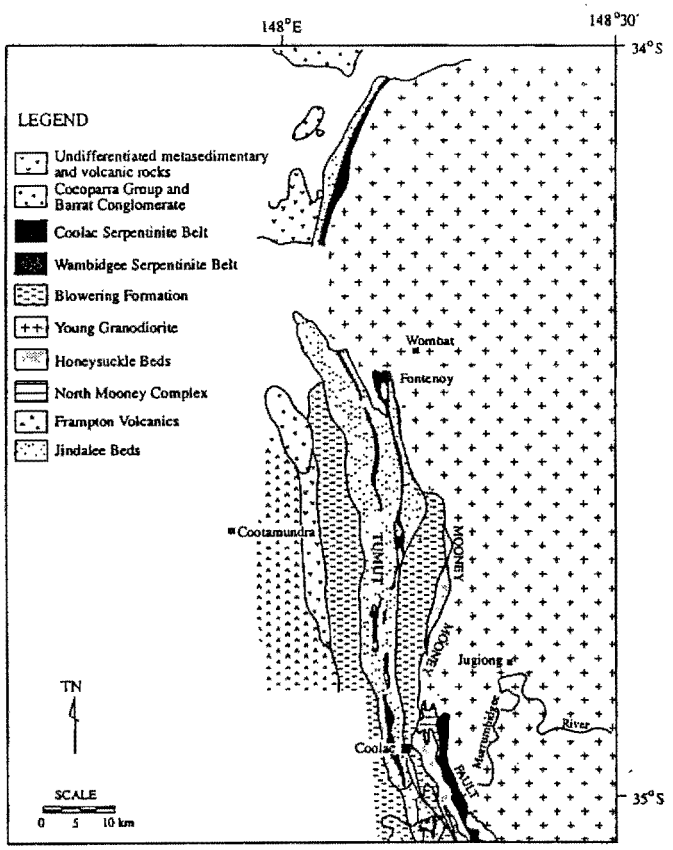

Figure 4.9 Location of the Fontenoy region of the Wambidgee Serpentinite Belt (adapted from Fitzpatrick 1976).

Two main types occur:

(a) Folded hornblendite/peridotite

This consists of folded hornblendite layers within partially serpentinised peridotite. The layering, which is defined by different hornblende/olivine+orthopyroxene+clinopyroxene ratios involves rhythmic (e.g. Park 1989) repetition of two layer types. Type 1 is composed of partially serpentinised olivine, orthopyroxene, clinopyroxene and minor amphibole; type 2 comprises amphibole with minor partially serpentinised olivine. The layers vary in thickness from 4 to 35mm. Layer contacts are generally sharp. Minor, late-stage serpentine-filled shear fractures occur. The folds are asymmetric, range from tight to isoclinal, exhibit intense limb attenuation and are ascribed to magmatic slumping. In thin section, types 1 and 2 exhibit postcumulus overgrowth texture, while secondary tremolite has variably replaced orthopyroxene and clinopyroxene. Layer interfaces are sharp, but there is no evidence that they are microshears. This layering is akin to magmatic cumulate layering within layered mafic-ultramafic complexes (e.g. Jackson 1967; McBirney & Noyes 1979). Despite much debate, there is strong support for such layering being produced by the processes of fractional crystallisation and magmatic differentiation (e.g. Irvine 1982).

(b) Layered serpentinised peridotites

These rocks exhibit primary layering defined by both serpentine/secondary amphibole ratios and grainsize variations (Plate 4.30). The layering is planar to gently curviplanar, varies from 5 to 40mm in thickness, and the layers maintain a fairly constant thickness along strike. The layers vary in colour from yellow-green and emerald-green for the serpentine-dominated layers to brown-black for the amphibole-dominated layers.

Finely layered serpentinised peridotite is a variant comprising distinct layers (Figure 4.10) that are based on variation in:

(a) grain-size;

(b) the colours of the serpentine and amphibole minerals present; or,

(c) the serpentine/amphibole ratio.

The layering varies in thickness from 1 to 10mm, is planar and maintains constant orientation; the grainsize of the serpentine minerals varies from aphanitic to 0.25mm.

Plate 4.30 Layering defined by bastised orthopyroxene-rich layers and serpentine-rich layers within serpentinised layered peridotite. Locality 224, Warrenoy.

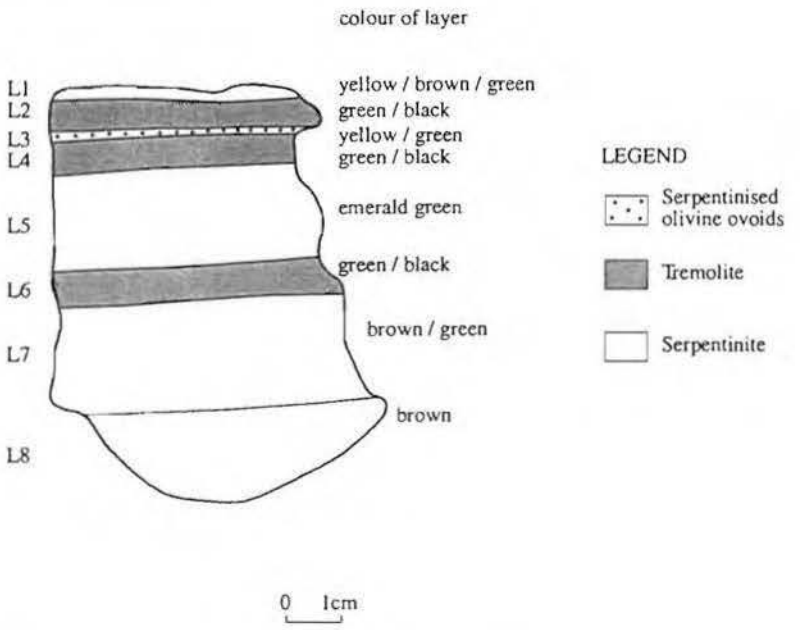

Figure 4.10 Sketch of finely-layered serpentinised peridotite from the Fontenoy region of the Wambidgee Serpentinite Belt (locality 224).

In thin section, rock of this type consist of feathery antigorite (up to 99%), relict and bastitised orthopyroxene grains (up to 15%) and rare, relict clinopyroxene, talc and ferroan chlorite, together with common secondary tremolite. The following types of microscale layering are distinguishable:
(i) bastised orthopyroxene-rich layers;
(ii) antigorite-rich layers;
(iii) amphibole-rich layers; and,
(iv) tremolite+Mg-chlorite layers.
Contacts between the orthopyroxene-rich and orthopyroxene-poor layers vary from sharp to diffuse in that isolated bastitised orthopyroxene grains occur within antigorite. Contacts between amphibole-rich and antigorite-rich layers are diffuse in that aggregates of amphibole grains occur within the antigorite-rich layers. The tremolite+Mg-chlorite layers have diffuse contacts against amphibole-rich layers.

XRD studies of completely serpentinised layered peridotites of the Fontenoy region confirmed the microscale observations by showing that the primary mineralogy of layers is reflected in the serpentinised products. Thus:

Layer 1: antigorite
Layer 2: antigorite+chrysotile
Layer 3: lizardite 6T
Layer 4: chrysotile 20
Layer 5: antigorite+tremolite
Layer 6: tremolite+chrysotile

This layering, although far more closely-spaced, is akin to primary layering within the Coolac Serpentinite Belt (section 3.6.1). Despite doubt regarding the genesis of the layering within the Coolac Serpentinite Belt and other upper mantle peridotites, the circumstantial evidence suggests that it was produced by primary magmatic processes.

4.6.2 Serpentinite foliations

Type I S-C fabrics are found within the serpentinised ultramafic rocks, schistose serpentinites, discrete zones within the massive serpentinites and in talcosic metaserpentinites. The S-surfaces are usually defined by interlocking sigmoidal-shaped anastomising fibrous serpentine and the C-surfaces by more widely-spaced (generally in the range of 10 to 30mm) sub-parallel bands of fibrous serpentine. The S-surfaces merge into or are terminated abruptly by the C-surfaces. The foliations have not been investigated in any detail during the course of this study, but where found, the C-surface is the dominant mesoscale structure. The foliations trend 350-050° and are steeply dipping (70° W).

The foliations, which are believed to be related to the emplacement of the belt, began forming during the onset of serpentinisation. Initially, brittle fracturing and brecciation of the original primary ultramafic rocks occurred, creating permeability pathways for the infiltration of low temperature sea-water (e.g. Laurent & Hebert 1979). Large volumes of H_2O-dominant fluids (e.g. O'Hanley & Wicks 1995) infiltrated these pathways and, by reacting with olivine and pyroxene (e.g. Wicks 1984) resulted in serpentinisation. During the early stages, localised high strain zones developed S-C fabrics (e.g. Lister & Snoke 1984), which were enhanced by continuing deformation along with ongoing serpentinisation. The nature of the Young Granodiorite/Wambidgee Serpentinite Belt contact is ascribed to strain partitioning from the granodiorite into the adjacent serpentinite as deformation within the granodiorite evolved from ductile to brittle.

CHAPTER 5: THE GUNDAGAI SERPENTINITE BELT

5.1 INTRODUCTION

The Gundagai Serpentinite Belt is a discontinuously outcropping alpine-type serpentinite belt extending as a ridge both north and south of Gundagai (Figure 5.1). It consists of massive and schistose metaserpentinite and contains variably altered minor lithologies such as clinopyroxenite, gabbro and chlorite rock. The Gundagai Serpentinite Belt has been mined for tremolite-asbestos and gold.

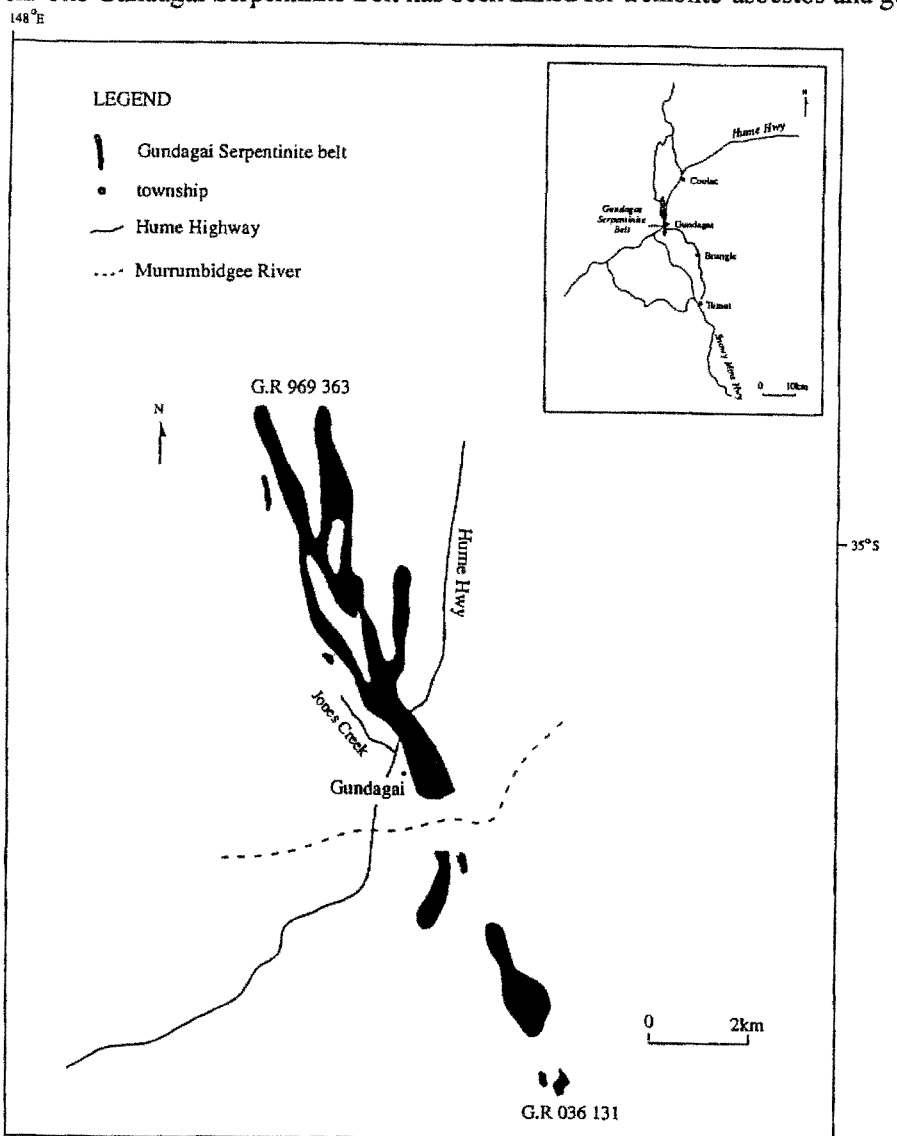

Figure 5.1 Location and extent of the Gundagai Serpentinite Belt (adapted from Basden 1990).

5.2 THE WESTERN CONTACT AND ABUTTING ROCKS

The Gundagai Serpentinite Belt abuts or closely approximates the following units along its western contact. The units from east to west (Figure 5.2) are: the Jindalee Beds; Jones Creek Diorite and breccia; and the Wandeen Formation and Frampton Volcanics. The Jindalee Beds and Frampton Volcanics were described in Chapter 4 and will receive no further comment. The Jones Creek Diorite has been included with the Jindalee Beds by Basden *et al.* (1974) and Basden (1990). However, it actually post-dates them and should therefore be treated separately.

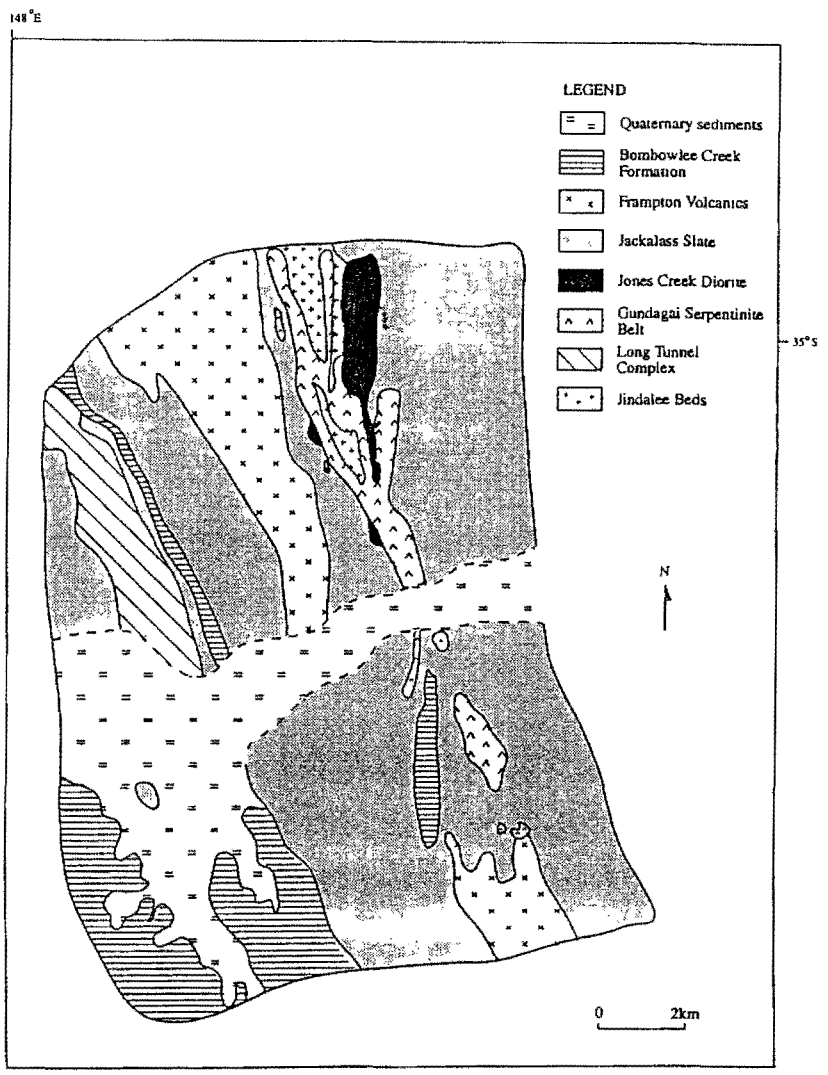

Figure 5.2 Geology of the Gundagai Serpentinite Belt and adjoining units (adapted from Basden 1990).

5.2.1 The Jones Creek Diorite and breccia

(Detailed petrographic descriptions are in Appendix 5PD)

The Jones Creek Diorite is composed of massive and nodular hornblende diorite, with the nodules comprising cognate inclusions which are thought to have formed by disruption of subsolidus material under ongoing magmatic flow (Winward 1972). However, Giddey (1995), showed that two subparallel NNW trending belts of massive diorite are separated by the Gundagai Serpentinite Belt and quartzites of the Jindalee Beds, and that the nodular variety is a volcanic breccia. The breccia occurs as two small and one large body within the Gundagai Serpentinite Belt (Figure 5.3), near contacts with metapelitic rocks of the Jindalee Beds.

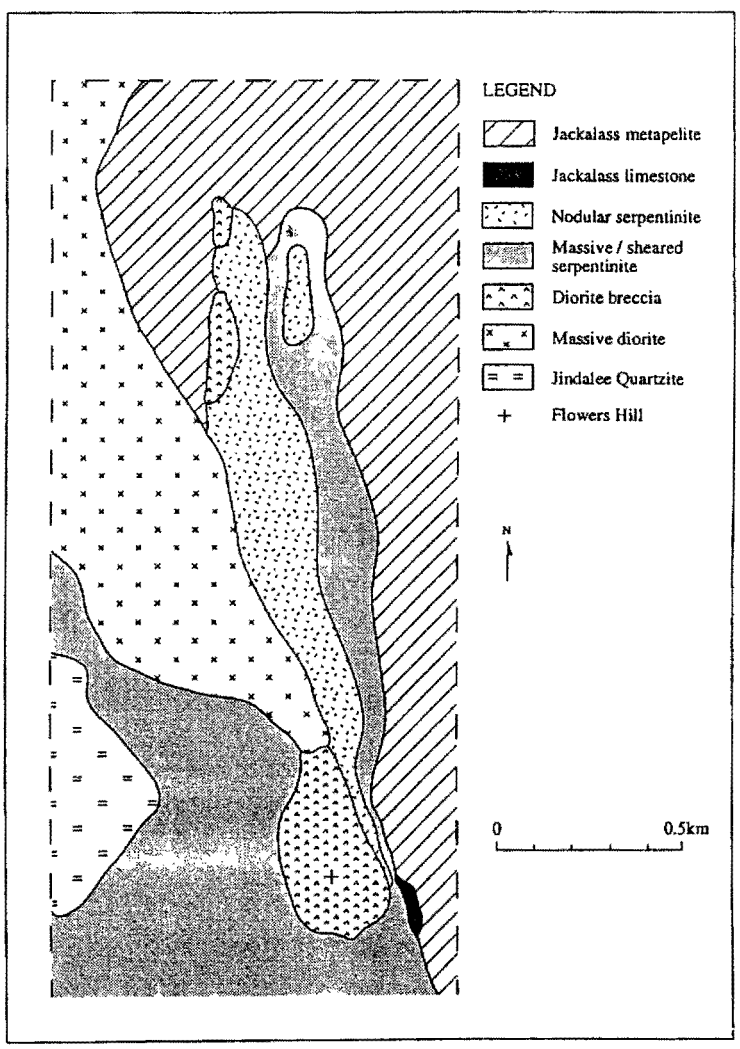

Figure 5.3 Distribution of the Jones Creek Diorite breccia and nodular serpentinite (Giddey 1995).

Both authors agree that all contacts of the Jones Creek Diorite are faulted. However, as most of the Jones Creek Diorite is massive and unfoliated, it is likely to be an allochthonous fault-bound block. There is no evidence to suggest that it is an integral part of the Jindalee Beds.

The massive section of the Jones Creek Diorite consists of hornblende diorite and metahornblendite (G.R. 999 245); the latter occurring as segregations within the hornblende diorite mass. The best exposure of the nodular section or "Jones Creek breccia" is on Flowers Hill at G.R. 002 218 (Plate 5.1). It consists of angular to subrounded, relatively large (150mm maximum) moderately rounded fragments of hornblende andesite, microgabbro, quartzite and metapelite, in a chlorite+epidote+actinolite+quartz matrix (Plate 5.2). The matrix appears to be volcanic in nature as it consists of phenocrysts of partially resorbed plagioclase and ragged hornblende in a finer-grained groundmass. Because the "Jones Creek breccia" contains clasts of metasedimentary Jindalee Beds and Jones Creek hornblende diorite, it is considered to be a subvolcanic plug formed after the Jindalee Beds. An alternative explanation, though one not favoured by this author, involves it being a proximal polymictic breccia of sedimentary rather than volcanic origin (Ashley, pers. comm. 1998).

Plate 5.1 Outcrop of the Jones Creek Diorite breccia on Flowers Hill, north of Gundagai. Viewed from the north-west, looking south-east.

Plate 5.2 Rounded fragments of hornblende andesite within Jones Creek Diorite breccia on Flowers Hill, north of Gundagai.

5.2.2 The Wandeen Formation

The ensuing description is based on Warren *et al.* (1995).

The unit is a northerly-trending imbricate package of mafic volcanic and mafic-sourced volcanogenic epiclastic sedimentary rocks, Jindalee Beds and Gundagai Serpentinite Belt. The Cootamundra Fault separates it from the Frampton Volcanics to the west and to the east it is faulted against well-cleaved siltstone of the Blowering Formation. The unit has previously been grouped with the Jindalee Beds by Basden *et al.* (1974). The mafic volcanic rocks are dominantly porphyritic, vesicular, microlitic, pyroxene basaltic andesite. Polymictic conglomerates in the volcanogenic epiclastic sequence include abundant basaltic and basaltic-andesite fragments, crenulated schist, metaquartzite, chert, porphyritic rhyolite, porphyritic pyroxene-plagioclase dacite, and siltstone. The sandstones include quartz, mafic rock fragments, chert/metaquartzite and detrital carbonate, and the siltstones comprise poorly-sorted quartz, plagioclase, epidote, carbonate and chert/metaquartzite clasts.

The siltstones and conglomerate matrix have a well-developed slaty cleavage that dips to the west. Bedding is only poorly developed and, where found, dips steeply westward. The mineralogy is indicative of at least the prehnite-pumpellyite facies metamorphism e.g. Miyashiro, 1994). Warren *et al.* (1995) believe that these rocks are Early Silurian in age and equate them with either the conglomerates of the Frampton Volcanics (e.g. Skilbeck *et al.* 1992) or the Brungle Creek and/or Wermatong metabasalts which are found much further to the south. The clastic rocks are locally derived from basaltic rocks within the unit and/or the nearby Jindalee Beds, and the polymictic conglomerates most likely represent near-source mass flow deposits.

The Wandeen Formation was investigated by the present author at G.R. 969 363. Talcosic metaserpentinite of the Gundagai Serpentinite Belt is faulted against volcaniclastic sandstone to the east, and basaltic meta-andesite to the west. The mineral assemblage of albite+actinolite+chlorite+epidote+zoisite within the basaltic meta-andesite is indicative of greenschist facies metamorphism (e.g. Miyashiro 1978).

5.3 THE EASTERN CONTACT AND ABUTTING ROCKS

The Gundagai Serpentinite Belt is faulted on its eastern contact against a 2.5-3km wide tract of dominantly metapelitic rocks, within which are small pods of quartzite, metabasalt/meta-andesite, limestone, and Jones Creek breccia (Figure 5.2). Giddey (1995) assigned the tract to the Jindalee Beds, whereas Basden (1990) termed it the Jackalass Slate. The contentious nature of the tract is further demonstrated by parts of it being assigned to the Bumbolee Creek Formation (Lightner 1977), the Frampton Volcanics (Fortowski 1981), the Blowering Formation (Nethery 1975) and the Jindalee Beds (Stevens 1975). The present author has opted for the Jackalass Slate, as the metasedimentary rocks are less deformed and metamorphosed than the Jindalee Beds.

5.3.1 The Jackalass Slate

The unit was named after the type section at Jackalass Slate Quarry (G.R. 043 141; Basden 1990). Structural complexity has prohibited determination of a stratigraphic succession within the unit (Basden

1990). Contacts with the Jindalee Beds and Gundagai Serpentinite Belt are faulted, those with the Frampton Volcanics are disconformable or unconformable, and those with the overlying Bumbolee Creek Formation are conformable (Basden 1990). The pods of quartzite, metabasalt/meta-andesite and limestone may well be infaulted.

The Jackalass Slate is dominated by slate and siltstone, which have a well-developed sub-vertical cleavage and elongation lineation, and form prominent upright tombstone-like outcrops. They range from unbedded to thinly bedded (<10mm), and have poorly developed sedimentary structures at mesoscale, such that younging is hard to determine (Basden 1990). The rocks consist of recrystallised quartz, plagioclase, amphibole, magnetite, chlorite, biotite and sericite (Basden 1990; Giddey 1995) and are tuffaceous (Nguyen 1977). Volcaniclastic rocks occur interbedded with these metapelites in the northern part of the eastern Jackalass Slate Belt (Giddey 1995), and euhedral plagioclase grains within these rocks indicate a proximal source (Giddey 1995). Sandstones are of minor occurrence within the Jackalass Slate, occur as interbeds in the slates and siltstones, are tuffaceous in character (Nguyen 1977) and range in composition from andesitic to rhyodacitic. Phenocrysts of angular quartz and plagioclase, opaques, biotite and pyroxene? are set in a fine-grained foliated matrix of recrystallised quartz, sericite, biotite, and epidote (Basden 1990).

The conglomerates are up to 300m in thickness, and are polymictic conglomerates with clasts of quartzite, quartzose sandstone, jasper, acid volcanics, limestone, quartz and granitic rocks. The clasts are almost always flattened and elongate parallel to the dominant foliation and lineation (Basden 1990). Dolomitic marble occurs at several localities within the Jackalass Slate, with the two largest bodies occurring at the Tumut Marble Quarry (G.R. 076 730) and Gilmore Marble Quarry (G.R. 092 739)(Basden 1990). In general, the marbles are strongly foliated (with the foliation defined by chlorite-rich layers) and are composed of strongly recrystallised calcite/dolomite. A small pod of dolomitised marble was investigated in the course of the present study (G.R. 004 215). This body crops out between serpentinite of the Gundagai Serpentinite Belt and the metapelitic rocks described above.

The volcanic rocks of the Jackalass Slate include meta-andesite, quartz-feldspar porphyries and feldspar porphyries (Basden 1990). The andesitic rocks are porphyritic and contain phenocrysts of plagioclase and amphibole in a groundmass of plagioclase, hornblende, recrystallised quartz, epidote, opaques, chlorite and biotite (Basden 1990). A small "pod-like" body of dacitic tuff within the metasedimentary sequence occurs at G.R. 015 175.

As rocks in the unit commonly contain chlorite, biotite, phengitic muscovite and epidote, they have probably undergone metamorphism to the middle greenschist facies (e.g. Miyashiro 1994).

5.4 GENERAL FEATURES OF THE GUNDAGAI SERPENTINITE BELT

The Gundagai Serpentinite Belt extends some 23km from G.R. 036 131 in the south to G.R. 969 363 in the north (Figure 5.1). Any rock body (regardless of composition, origin or mode of emplacement) within the belt is deemed an integral part of it. The type section is 5km north of Gundagai, between G.R. 074 740 and G.R. 083 740 (Basden *et al.* 1974). The Gundagai Serpentinite Belt has a maximum width of 1.8km and comprises a relatively continuous northern belt (10km in length) and a discontinuous southern belt. The former is associated with large slices (maximum dimensions of 3.5 x 1km) of metasedimentary Jindalee Beds and Jones Creek Diorite. The latter (southern) belt consists of 5 separate bodies (the largest is 2.5km x 1km), enclosed within Jackalass Slate metasediments. Overall, the Gundagai Serpentinite Belt is a steeply-W dipping, NNW-trending, sheet-like alpine-type serpentinite belt, similar to the Wambidgee Serpentinite Belt and Coolac Serpentinite Belt.

5.4.1 Surface outcrop

Outcrop is good in the northern part of the belt between Flowers Hill (G.R. 001 218) and G.R. 994 238 to the north. In the southern half of the belt, outcrop is poor, particularly between Flowers Hill and the southern bank of the Murrumbidgee River, where much of the land is occupied by the township of Gundagai.

The schistose serpentinites form near vertical, sheet-like outcrops up to 2m in height. Primary ultramafic and talc-carbonate rocks occur as lenses within schistose serpentinite. Metagabbro, metabasalt, plagiogranite and chlorite rock generally crop out poorly, as dyke-like masses within schistose serpentinite.

5.4.2 Internal Structure

The Gundagai Serpentinite Belt consists of massive serpentinite "kernels" in a schistose serpentinite matrix (e.g. Hume Highway at G.R. 004 207). The internal structure comprises:

(a) thin zones (<100mm wide and <200mm long) of schistose NNW-trending serpentinite dominated by an S-C fabric cutting massive serpentinite,

(b) blocks of massive serpentinite (up to 0.5m in maximum dimension) within schistose serpentinite,

(c) bodies (up to 15 x 10m and with the long axis parallel to the trend of the belt) of metagabbro, metabasalt, chlorite rock, clinopyroxenite, harzburgite, tremolite rock and plagiogranite within schistose S-C fabric serpentinite. Some are schistose and contain an S-C fabric similar to that in the enclosing serpentinite. Although the emplacement mechanism is unclear (due to lack of non-tectonised contacts), they were in-place before the development of the common S-C fabric.

(d) a tract (1.63 x 0.25km) of nodular serpentinite (described below) restricted to the western boundary of the northern half of the belt (G.R. 000 240, G.R. 000 210) (Figure 5.3).

5.5 PETROGRAPHY AND TEXTURAL/STRUCTURAL EVOLUTION

5.5.1 Primary ultramafic rocks

The primary ultramafic rocks of the Gundagai Serpentinite Belt are identified by their primary textures and/or minerals. They can be subdivided into metaharzburgites, metapyroxenites and metaperidotites and occur as remnant "cores" in massive or schistose serpentinite within the southern part of the belt. Possible primary layering (defined by differential olivine/orthopyroxene ratios) in metaharzburgite was found at one locality (G.R. 015 175) in the southern part of the belt. The layering strikes at 285° and dips very shallowly (10°) to the west.

The metaharzburgites have a relict porphyroclastic texture, contain >5% bastitised orthopyroxene and are predominantly massive. The metapyroxenites contain >80% clinopyroxene and <15% olivine and have a granoblastic to porphyroclastic texture. Metapyroxenite has been found at G.R. 992 218 in the northern part and at G.R. 016 174 in the southern part of the belt. The metaperidotite is composed of serpentine and talc and has only been found in the southern part of the belt (G.R. 001 205).

The primary ultramafic rocks of the Gundagai Serpentinite Belt have experienced different degrees of serpentinisation and alteration. Metaperidotite and metaharzburgite has been almost completely serpentinised (with relict chromian spinel the only remaining primary phase) whereas metapyroxenite contains unaltered diopside that is bent and microfractured within an unstrained anigorite-talc matrix (Plates 5.3, 5.4). It would seem that serpentinisation requires fracture-induced inter- and intra-granular permeability (e.g. Wicks 1984).

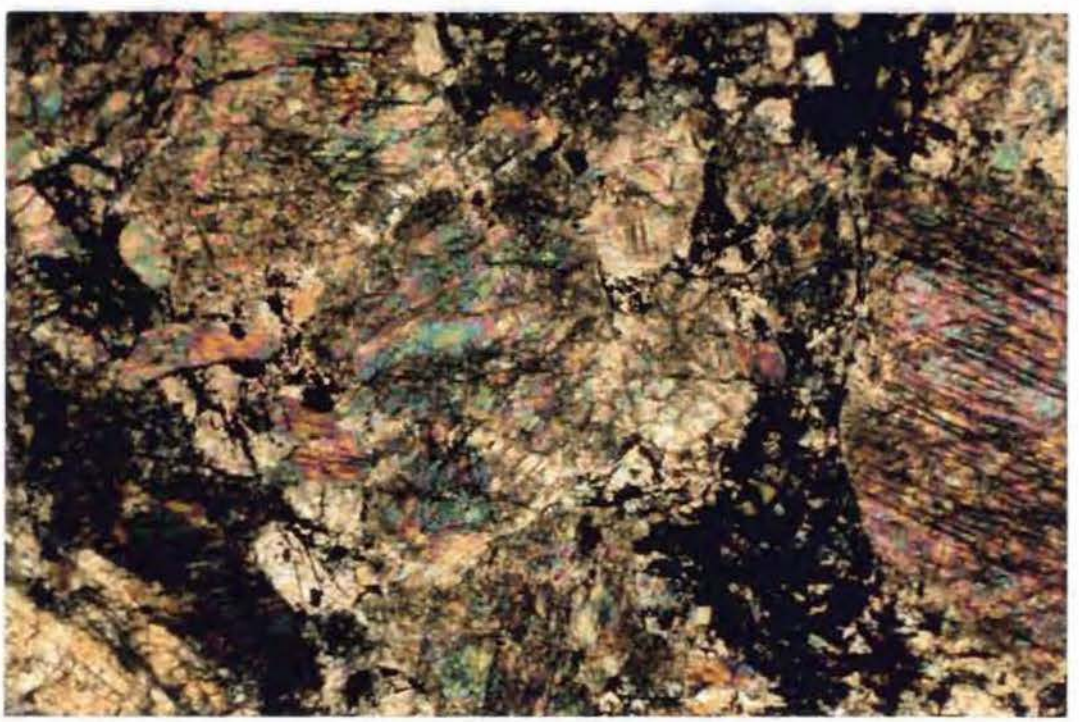

Plate 5.3 Bent and micro-faulted diopside grains with fracture-fill of antigorite+talc within meta-clinopyroxenite.
Sample No 203 UXP F.O.V 3.5mm

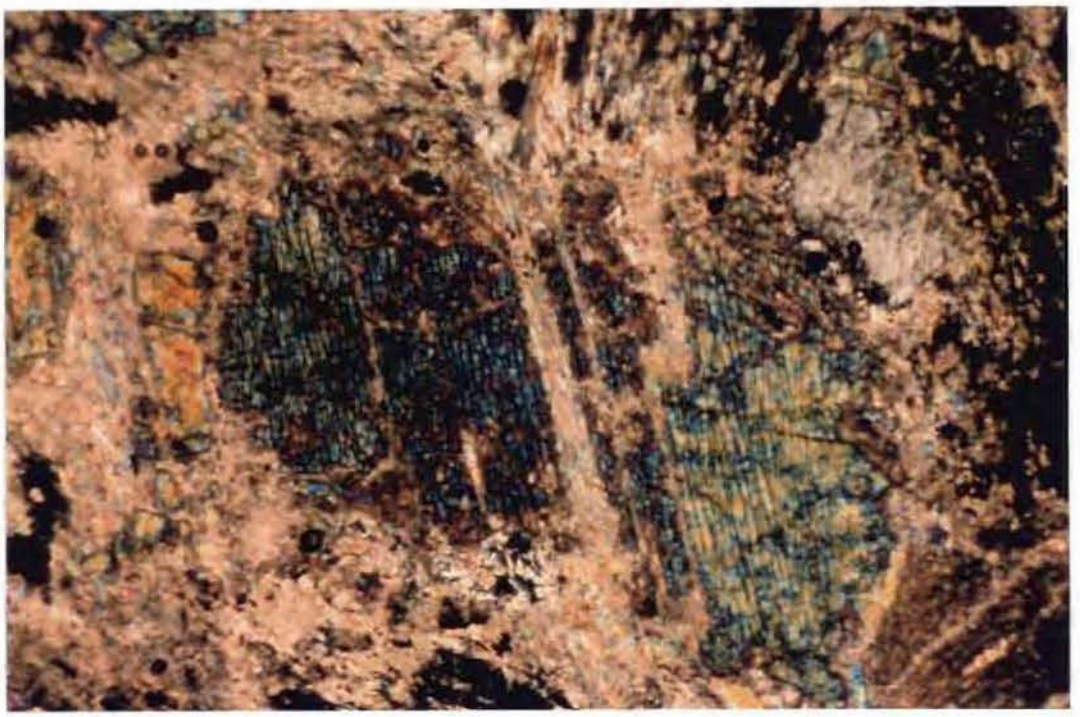

Plate 5.4 Bent and micro-fractured diopside grains within metapyroxenite.
Sample No 216 (b) UXP F.O.V 3.5mm

Thus, as the rocks cooled below 450°C (e.g. O'Hanley 1996), downward infiltration of sea-water (e.g. Laurent & Hebert 1979) led to the replacement of olivine and orthopyroxene by antigorite and further enhanced permeability through the hydraulic fracturing process. The occurrence of cross-cutting talc and/or magnesite is ascribed to hydrothermal fluid channeling at minimum temperatures of 165-285°C (Ashley 1997).

Intergranular chlorite, which probably grew concurrent with the initial fracturing and antigorite formation, is overprinted by cross-cutting tremolite. However, the latter is incompatible with retrogression during ongoing temperature decay, and is ascribed to a prograde event that induced metasomatic exchange between metapyroxenites and enclosing felsic country rocks (e.g. Linder *et al.* 1992) at temperatures of 580 to 650° C (e.g. Pfeifer 1987).

5.5.2 Serpentinites

Massive and schistose serpentinites are the most common rock types within the Gundagai Serpentinite Belt and occur in intimate association, generally as lenses of massive serpentinite in a matrix of schistose serpentinite. Nodular serpentinite, another variant, is highly restricted in occurrence. Whereas the massive and schistose serpentinites lack systematic spatial distribution, the nodular variety is restricted to two lenses in the northern part of the belt (Figure 5.3). The larger lens (1.9 x 0.25km) is fault-bound to the west against breccia and hornblende diorite of the Jones Creek Diorite, while to the east it has a sheared contact with massive/sheared serpentinite (Giddey 1995). The small lens (3 x 0.05km) is enclosed within massive/sheared serpentinite. The intensity of serpentinisation precludes petrographic determination of the parent ultramafic rocks.

XRD studies confirm that the non-oriented fine-grained "matrix serpentine mineral" in the massive and schistose varieties is antigorite, that the cross-cutting veinlets are chrysotile and that talc is a common minor phase. XRD analysis of the nodular serpentinite confirms that the nodules comprise antigorite+tremolite+chrysotile+magnetite, whereas the matrix consists of tremolite+antigorite+lizardite+magnetite.

As with the Wambidgee Serpentinite Belt (Chapter 4, section 4.5.2), the Gundagai Serpentinite Belt is dominated by antigorite (Plate 5.5). The original olivine, orthopyroxene and chrome spinel assemblages have retrogressed under greenschist facies conditions, to antigorite, but several generations of chrysotile veinlets demonstrate that serpentinisation was an on-going process (e.g. Wicks & Plant 1979) facilitated by hydraulic fracturing. Based on textural relationships, tremolite in the nodular serpentinites formed after magnesite. However, there is no clear evidence to suggest whether it formed before or after the chrysotile veinlets. Linder *et al.* (1992) ascribed tremolite formation to metasomatic reactions between the ultramafic rocks and enclosing felsic country rocks and Pfeifer (1987) estimated its temperature of formation to be 580-650°C. Cross-cutting talc and/or magnesite probably occurred due to hydrothermal fluid channeling at minimum temperatures of 165-285°C (Ashley 1997).

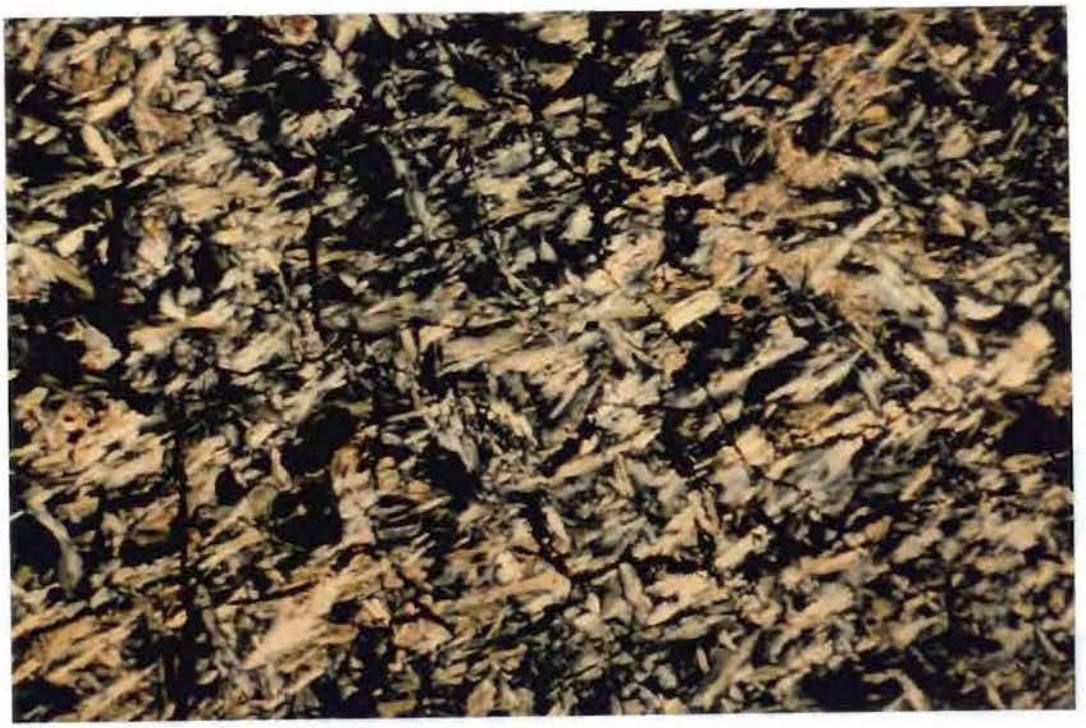

Plate 5.5 Feathery decussate texture of antigorite within massive serpentinite.
Sample No BF92/63 UXP F.O.V 3.5mm

Late-stage fracturing of massive serpentinite is evidenced by veinlets of magnesite and talc. Schistose serpentinites exhibit an S-C fabric defined by the preferred orientation and distribution of chrysotile veinlets (Plate 5.6)

Plate 5.6 S-C fabric within serpentinite defined by discontinuous fibrous chrysotile veinlets.
Sample No 215 (b) UXP F.O.V 3.5mm

Giddey (1995) described the nodular serpentinites as breccias but the preservation of a coherent "mesh-texture" within the matrix (Plate 5.7) does not support this interpretation. The subsequent history involved fracturing and the formation of tremolite and chrysotile veinlets that cross-cut nodules and matrix (Plate 5.8).

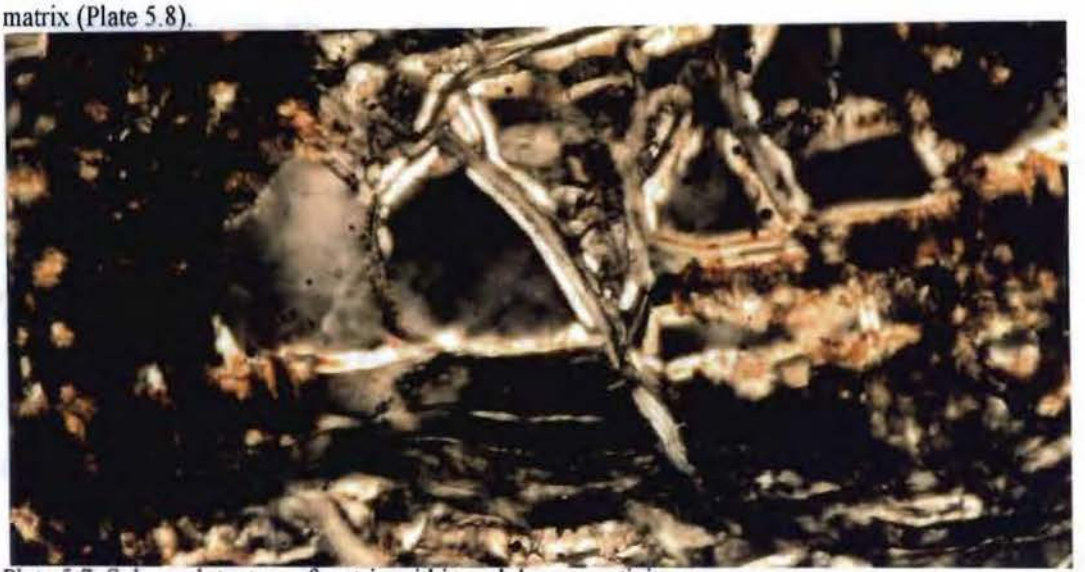

Plate 5.7 Sub-mesh texture of matrix within nodular serpentinite.
Sample No 273a UXP F.O.V 1.5mm

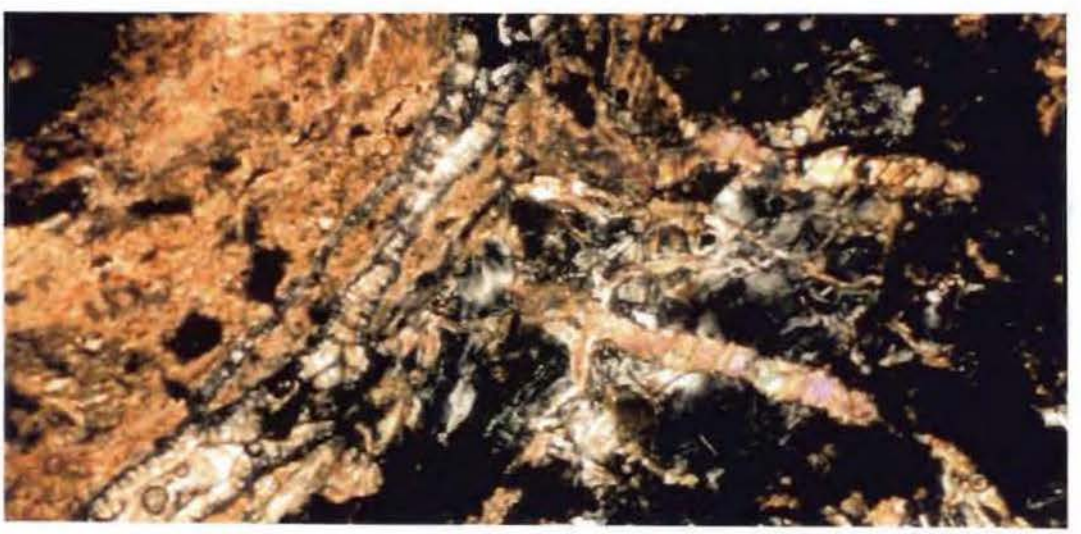

Plate 5.8 Cross-cutting tremolite veinlets within nodular serpentinite.
Sample No 273b UXP F.O.V 3.5mm

5.5.3 Talc-carbonate rocks

The talc-carbonate rocks contain >20% talc+carbonate and are derived from an ultramafic protolith. Three types are recognised:

(a) talc and/or magnesite rich meta-ultramafic rocks,

(b) talc-carbonate rocks, and

(c) talc schists.

The talc and/or magnesite rich meta-ultramafic rocks are of minor, but widespread occurrence as narrow zones, lenses, or "blocks" within schistose serpentinite. The talc-carbonate rocks are also of minor occurrence in the southern part of the belt where they form lenses (maximum dimensions 50 x 10m) within schistose serpentinite. Talc schists are rare, have been found at only three localities, and occur as small (maximum dimensions 5 x 2m) lenses within schistose serpentinite. The talc and/or magnesite-rich meta-ultramafic rocks can be subdivided into metapyroxenites and metaserpentinites while the talc-carbonate rocks can be subdivided into massive and foliated varieties.

Serpentinisation of the metapyroxenites precludes determination of the early deformational history. Textural evidence suggests talc formed first and was then overprinted by fibrous actinolite-tremolite. This suggests that talc was formed by fracture-related percolation of CO_2-rich hydrothermal fluids at the final stages of serpentinisation (e.g. Wicks and Whittaker 1977; Ashley 1994), whilst the cross-cutting fibrous actinolite/tremolite formed during prograde metamorphism by the metasomatic reaction between ultramafic rocks and enclosing felsic country rocks (e.g. Linder *et al.* 1992) at temperatures of 580-650°C (e.g. Pfeifer 1987). Unlike talc, the formation of magnesite is ascribed to the percolation of CO_2-rich groundwater at temperatures below 100°C (e.g. Laurent & Hebert 1979).

In metaserpentinites, which were originally composed of olivine, orthopyroxene, clinopyroxene and chrome spinel, antigorite formed between 450°C and 250°C (e.g. O'Hanley & Wicks 1995; O'Hanley 1996). Magnesite, talc and chlorite (Plate 5.9) then formed during retrogressive lower greenschist facies metamorphism (e.g. Miyashiro 1978).

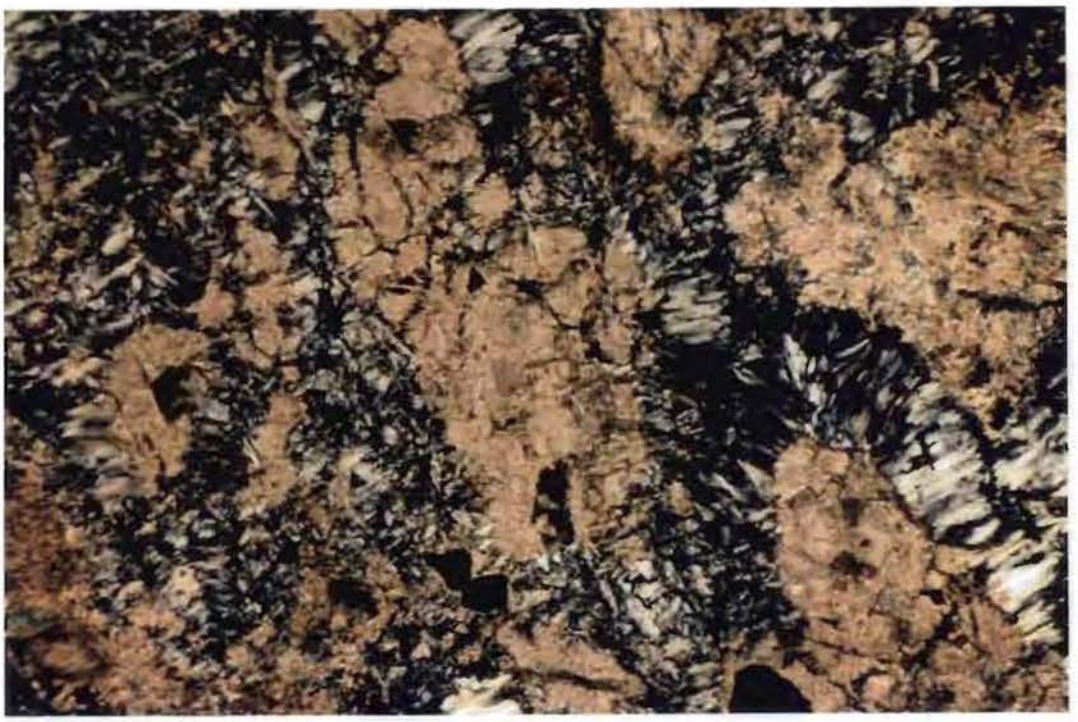

Plate 5.9 Overprinting magnesite and talc within metaserpentinite.
Sample No BF92/57 UXP F.O.V 3.5mm

In the massive talc-carbonate rocks, the early history is obscured. Relict chrome spinel grains provide some indication of the early deformation. It would seem that pre-serpentinisation fracturing was followed by weak post-serpentinisation brittle-ductile deformation.

In the foliated talc-carbonate rocks, antigorite formed at 450-250°C (e.g. O'Hanley & Wicks 1995; O'Hanley 1996). The antigorite-tremolite assemblage is cross-cut by talc and magnesite, which define S-C fabrics and are ascribed to the infiltration of CO_2-enriched fluids either during lower greenschist facies metamorphism (e.g. Miyashiro 1978) or groundwater flow at temperatures below 100°C (e.g. Laurent & Hebert1979).

The talc schists underwent much the same history as the foliated talc-carbonate rocks and then experienced a kink band-forming ductile event (Plate 5.10).

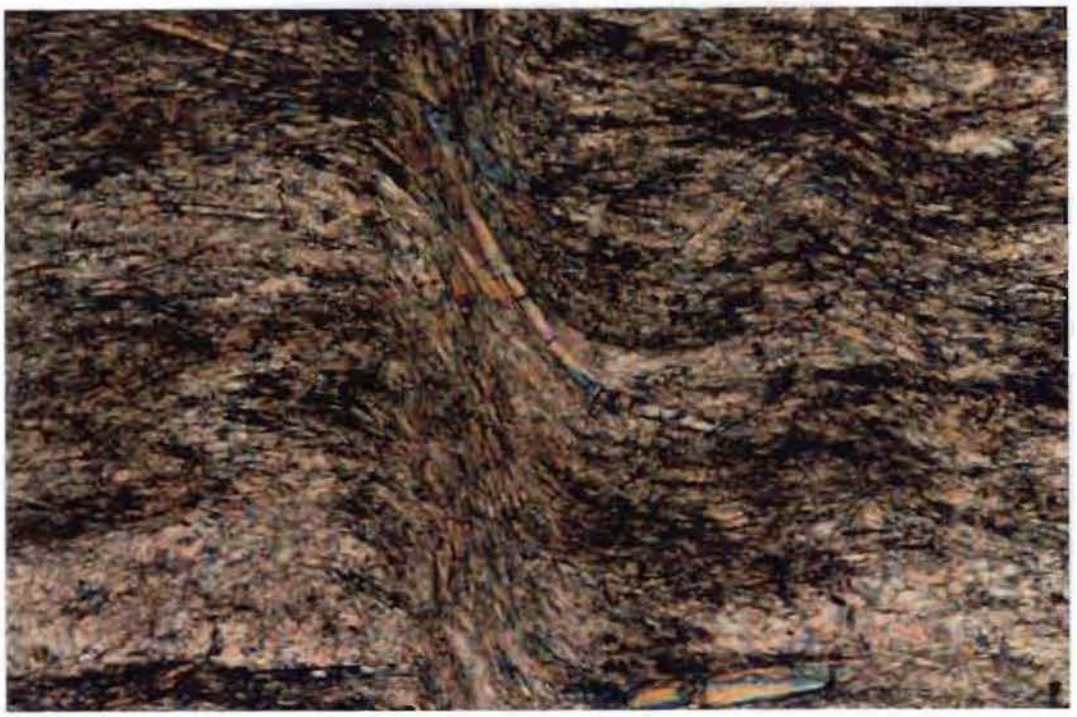

Plate 5.10 Micro kink bands or crenulations within talc-tremolite schist.
Sample No BF91/38c UXP F.O.V 1.5mm

5.5.4 Chlorite rocks

Because the chlorite rocks tend to have >90% chlorite, their protoliths tend to be petrographically indeterminable. The chlorite rocks occur in the southern part of the belt where they are widely distributed as dyke-like lens-shaped bodies (maximum dimensions 15 x 10m) within schistose serpentinite. Based on XRD analysis, they are dominantly composed of clinochlore IIb. Massive and schistose varieties of chlorite rock have been recognised.

The metamorphic/deformational history prior to chloritisation, cannot be determined. Textural evidence indicates that fine-grained chlorite is overprinted by coarse-grained chlorite which was itself overprinted by zoisite in massive varieties (Plate 5.11) and talc in schistose varieties. Evidence of deformation in massive varieties is limited to the parallel alignment of some of the chlorite grains, whereas in schistose varieties it has formed the main foliation.

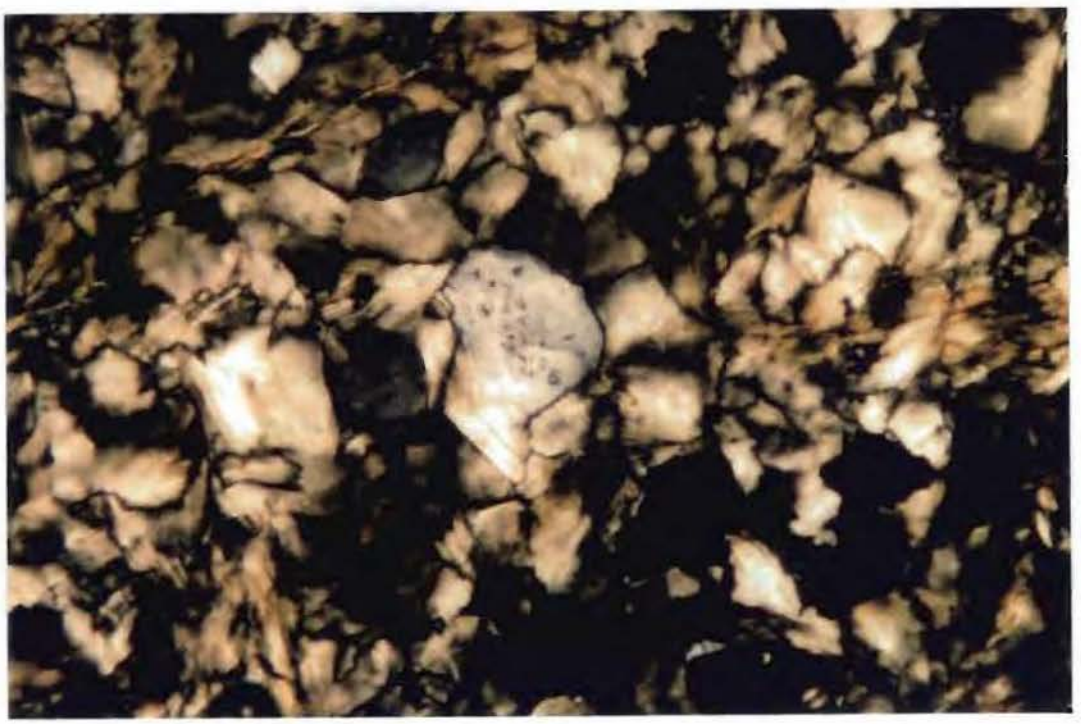

Plate 5.11 Zoisite overprinting chlorite within massive chlorite rock.
Sample No BF91/38d UXP F.O.V 1.5mm

5.5.5 Felsic plutonic rocks

Felsic plutonic rocks range from quartz-poor tonalites to quartz-rich granitoids on the IUGS classification scheme (e.g. Le Maitre 1989) and may also include plagiogranites. They occur as rare elliptical bodies (maximum diameter 5m) within schistose serpentinite in the southern part of the belt, contain mafic enclaves and tend to be foliated in places.

They all have the same mineral assemblage and textures but in varying proportions. Two groups are recognised:

(a) *tonalites* with <50% quartz and >10% amphibole,

(b) *quartz-rich granitoids* with >50% quartz and <5% amphibole.

(a) Tonalites

These rocks were originally composed of plagioclase+quartz+hornblende. Initial metamorphism resulted in the development of blue-green amphibole (Plate 5.12) overprinting brown-green hornblende, and a fine-grained plagioclase+quartz matrix. Accompanying deformation took place under decaying P/T conditions such that ductile behaviour (as evidenced by aligned and bent brown-green hornblende grains) gave way to a brittle overprint (as evidenced by micro-faulting in plagioclase (Plate 5.13) and development of the granular quartz+plagioclase matrix). Later and/or ongoing deformation produced chlorite pressure fringes on amphibole and sulfides, and chlorite veinlets.

(b) Quartz-rich granitoids

These were originally composed of quartz+plagioclase+minor hornblende and like the tonalites (above), have experienced greenschist facies metamorphism and deformation. This is expressed by an alignment of the Na-amphibole grains, bending fracturing and subgrain development in plagioclase, development of the granular plagioclase+quartz matrix, formation of cataclasite seams, and development of quartzofeldspathic veinlets.

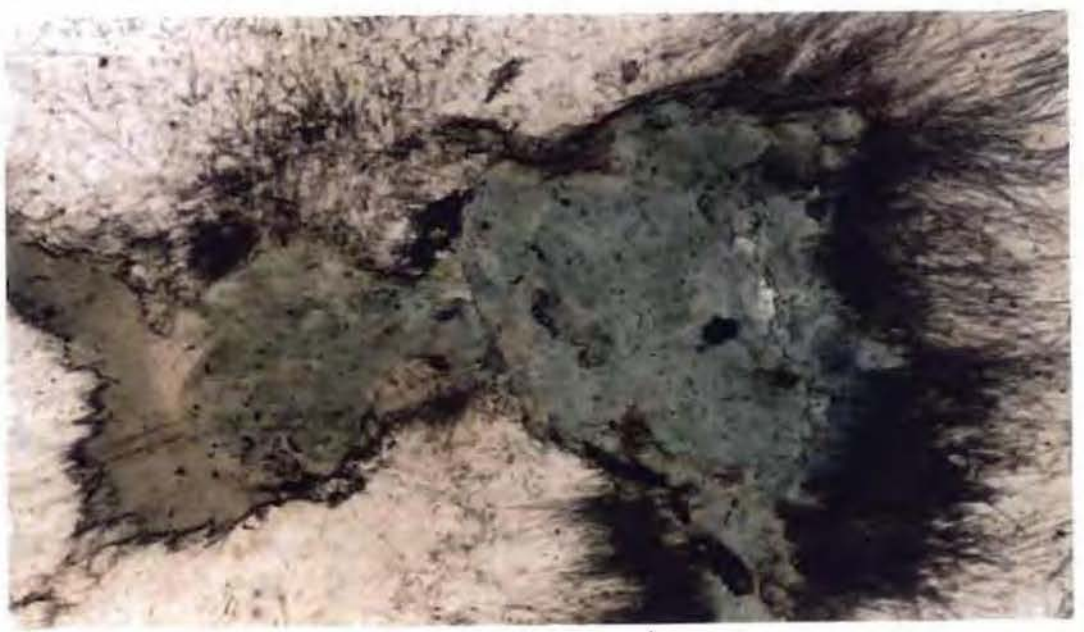

Plate 5.12 Blue-green hornblende overprinting brown-green hornblende in tonalite.
Sample No BF92/65 PPL F.O.V 1.5mm

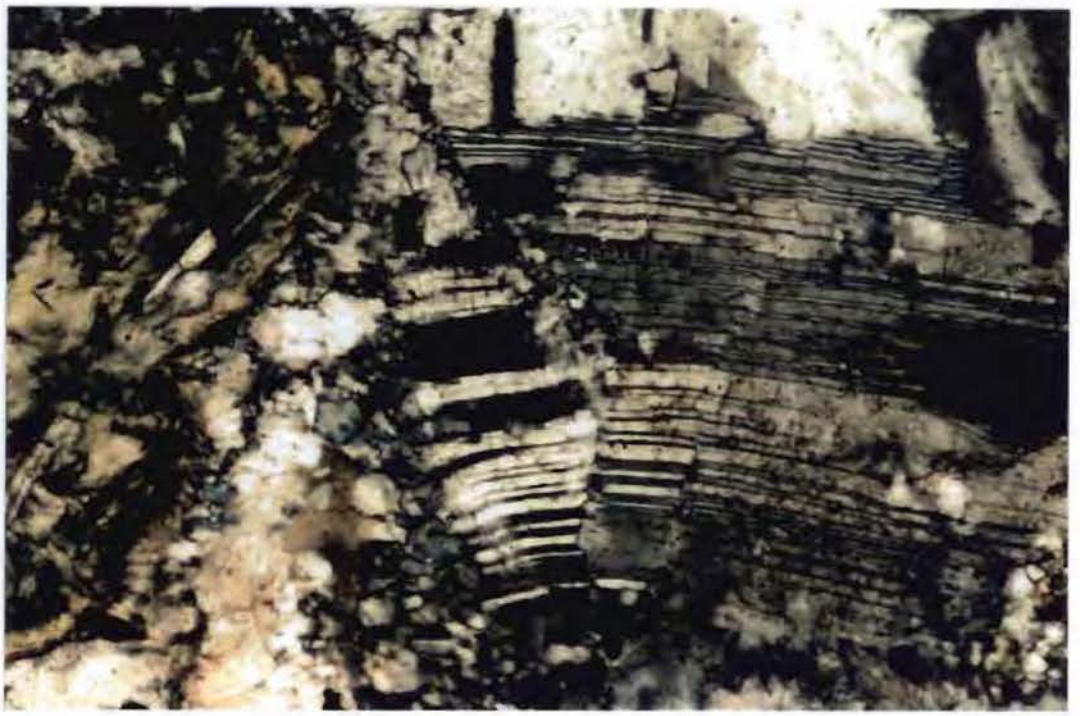

Plate 5.13 Bent and micro-faulted plagioclase twin lamellae in tonalite.
Sample No BF92/65 UXP F.O.V 1.5mm

5.5.6 Other rock types

This group includes all other rock types that could not be placed in the above groups. They comprise rare, small isolated bodies of metabasalt, metagabbro, amphibole rock, vitric lithic ash fall tuff and hybrid felsic/mafic rock, within schistose serpentinite.

Metabasalt

There are two occurrences of metabasalt in the northern part of the belt. The mineral assemblages (Plate 5.14) are indicative of greenschist facies metamorphism (e.g. Miyashiro 1994). Initial deformation was of a ductile-brittle character, which resulted in bending and cracking of the plagioclase phenocrysts and bent tremolite/actinolite grains.

Plate 5.14 Albite+zoisite+chlorite+epidote metamorphic assemblage in metabasalt.
Sample No 179 UXP F.O.V 3.5mm

Metagabbro

Two occurrences of metagabbro have been found. The one in the northern part of the belt is a small lens (maximum dimensions 5 x 1m) of indeterminate contact relationship with the nearby massive serpentinite; the one in the southern part of the belt is poorly exposed and of unknown geometry. Both have undergone greenschist facies metamorphism and accompanying ductile-brittle deformation that developed subgrains in plagioclase, bent and microfaulted hornblende (Plate 5.15) and plagioclase twin lamellae, strained and recrystallised intergranular quartz and developed cross-cutting epidote/zoisite.

Amphibole rock

Amphibole rock at G.R. 974 270 within the northern part of the belt has undergone low grade metamorphism as indicated by the presence of tremolite/actinolite (e.g. Miyashiro 1978). Textural relationships indicate that primary (?) amphibole was overprinted by metamorphic epidote and then the pervasive tremolite/actinolite. Accompanying ductile-brittle deformation resulted in bent, microfaulted and fractured hornblende (Plate 5.16), bent tremolite/actinolite grains, and quartzofeldspathic veinlets.

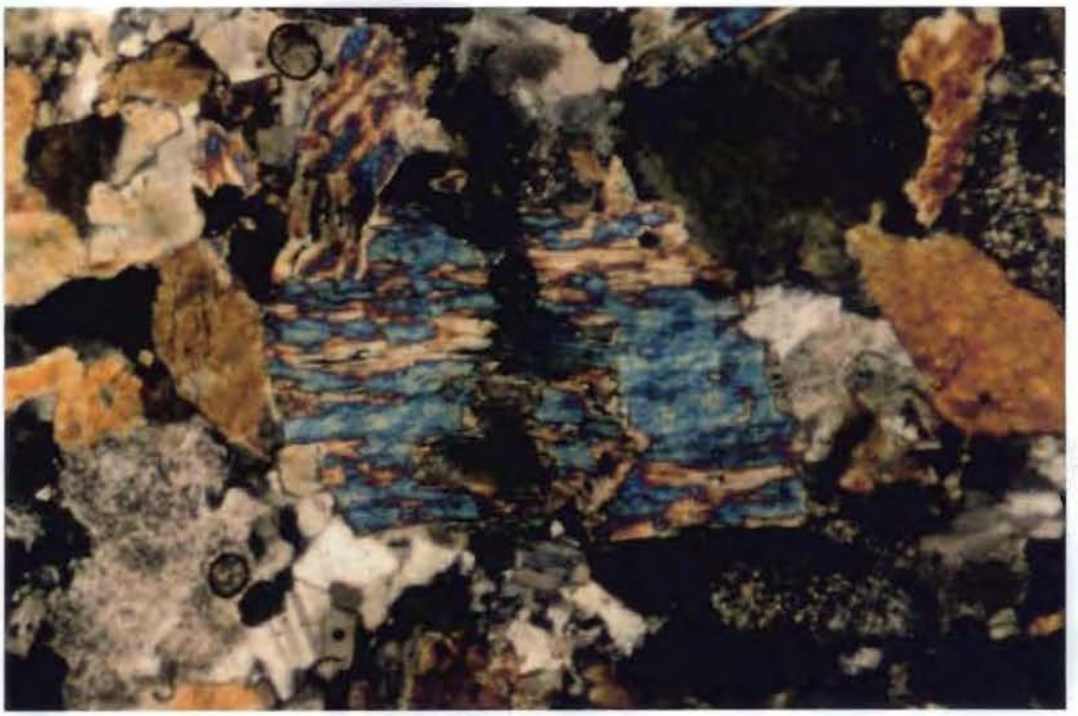

Plate 5.15 Bent and micro-faulted hornblende in gabbro.
Sample No 283 UXP F.O.V 1.5mm

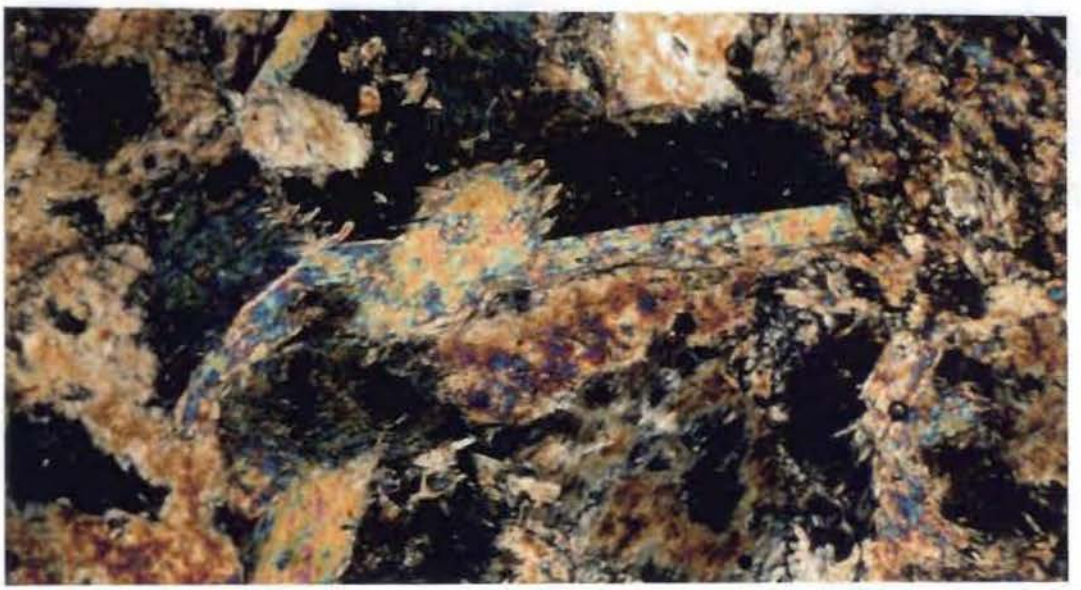

Plate 5.16 Bent hornblende within amphibole rock.
Sample No 202 (a) UXP F.O.V 3.5mm

Vitric lithic ash fall tuff

A well-cleaved, poorly exposed lens of vitric lithic ash fall tuff (Plate 5.17), occurs within schistose serpentinite at G.R. 014 167 in the southern part of the belt, associated with intense quartz veining. The presence of phengitic mica indicates lower greenschist facies metamorphism(e.g. Miyashiro 1994).

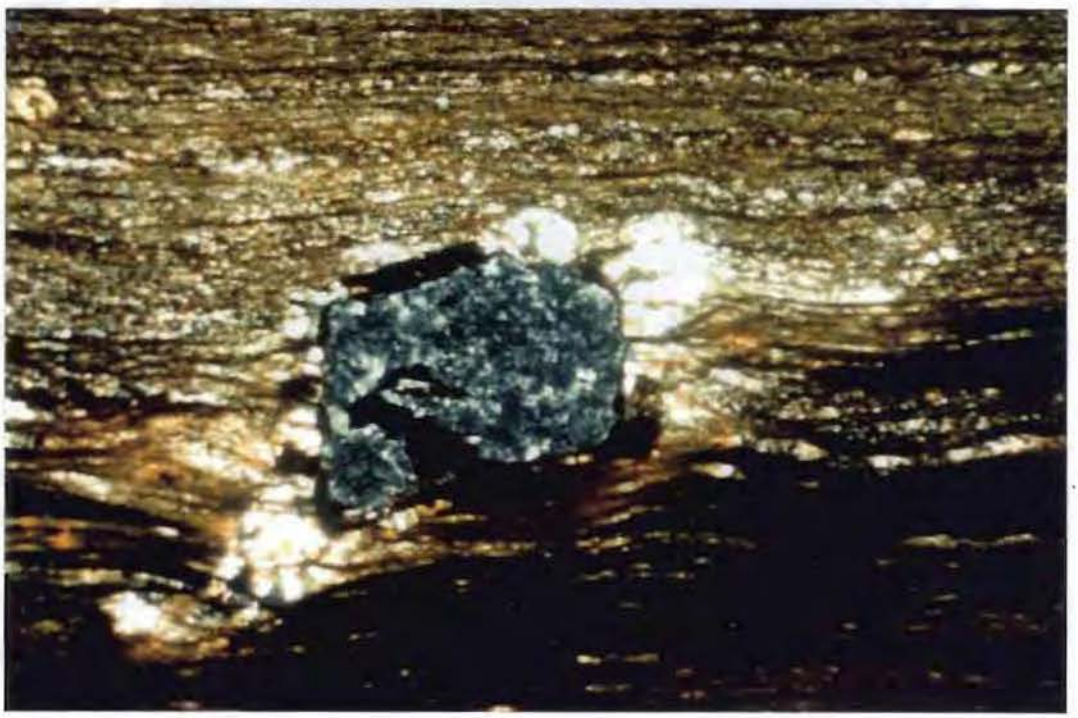

Plate 5.17 Laminar banded texture in meta ash fall tuff.
Sample No 221 UXP F.O.V 3.5mm

Hybrid felsic/mafic rock

A hybrid felsic/mafic rock occurs in a road-cutting on the Hume Highway (G.R. 001 205) where it forms an isolated narrow lens-shaped body (maximum dimensions 4 x 2m) within schistose serpentinite. This rock could derive from a plagiogranite body with a high proportion of metabasaltic enclaves. Low grade metamorphism and deformation have developed a foliation consisting of quartz-plagioclase domains (i.e. original plagiogranite component) separated by chlorite-sulfide domains (i.e. original metabasaltic component). Subsequent to or concurrent with plagiogranite disruption, syntectonic

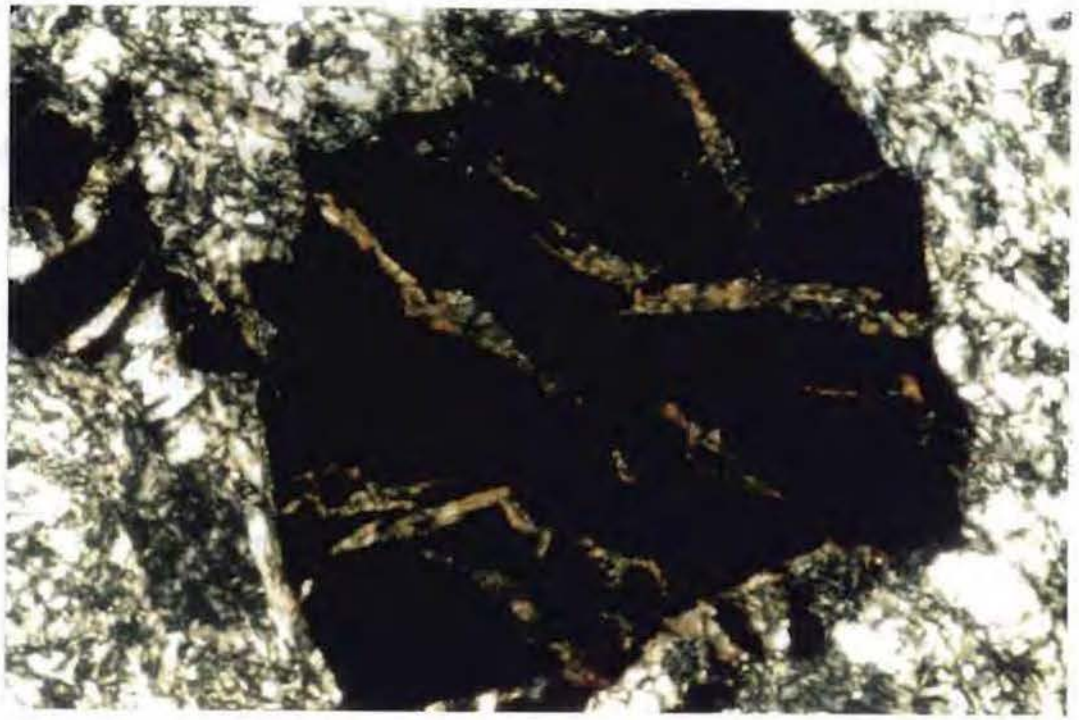

Plate 5.18 Fractured sulfide grain in chlorite matrix within hybrid felsic/mafic rock.
Sample No BF92/60 UXP F.O.V 1.5mm

recrystallisation/ crystallisation (ductile) and fracturing (brittle) of quartz, plagioclase, chlorite and sulfides took place (Plate 5.18).

5.6 STRUCTURE OF THE GUNDAGAI SERPENTINITE BELT

5.6.1 Serpentinite foliations

During the course of this study, the orientations of serpentinite foliations (Figure 5.4) were measured throughout the belt. The foliations comprise C-surfaces defined by regularly-spaced, consistently oriented shear planes, and S-surfaces, the sinuous foliation which merges into the C-surfaces. The data show:

(a) the distribution is similar to that obtained from the Coolac Serpentinite Belt (Figure 3.7);

(b) S and C are similarly oriented; and

(c) the main orientation trends NNW-NNE and dips steeply, similar to the other serpentinite belts.

(d) Although the orientation data recorded by the serpentinites of the Gundagai Serpentinite Belt are highly variable, the dominant movement sense is dextral (with equal proportions of oblique and strike slip movement)."

The above suggests that the foliations were formed by the same tectonic event as that which formed the S-C fabric foliations in the other serpentinite belts. The general orientation is also akin to the Siluro-Devonian regional foliation (see Basden 1990). It is concluded that the major deformation accompanied progressive serpentinisation (particularly the last stage of serpentinisation) and can probably be correlated with emplacement of the belts in their current continental position.

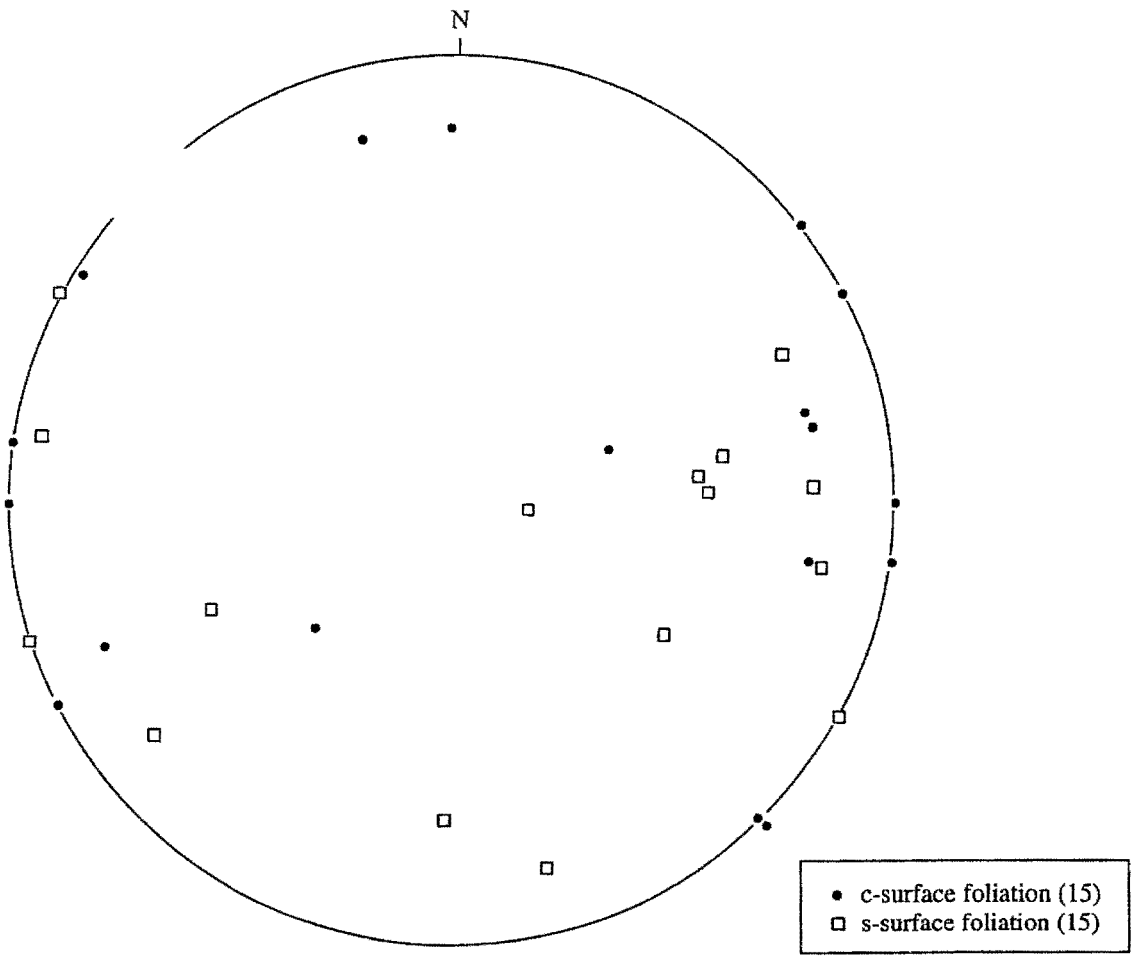

Figure 5.4 Poles to small-scale internal shear zones within serpentinite of the Gundagai Serpentinite Belt (equal area projection).

CHAPTER 6: THE TUMUT PONDS SERPENTINITE BELT

6.1 INTRODUCTION

The Tumut Ponds Serpentinite Belt occupies rugged, highly vegetated terrain (Plate 6.1) and has been little studied. A number of widely-spaced outcrops were mapped during the present study. Like the Coolac and Wambidgee serpentinite belts, it is steeply-dipping and of alpine-type, comprises schistose and massive serpentinite, and a diverse assemblage of minor rock types. It is defined as that NNW-trending belt of dominantly ultramafic rocks extending from east of Batlow south to Cabramurra (Figure 6.1). The proposed type section follows the Link Road from G.R. 273 265 to G.R. 264 273 (Cabramurra 1:25 000 sheet). The known length is approximately 24km (up to 43km is possible), while a maximum width ranges from 10m near the Brandy Mary Spur (Ravine 1:25 000 sheet), to 1.25km at G.R. 264 273 (Cabramurra 1:25 000 sheet) (Figure 6.1).

Plate 6.1 Typical rugged terrain occupied by the Tumut Ponds Serpentinite Belt. Locality 157, looking north.

In the Yarrangobilly 1:25 000 sheet, the main western belt extends from G.R. 580 135-580 140 to G.R. 430 193-430 195, and a small eastern belt occurs around G.R. 559 149. In the Ravine 1:25 000 sheet, it also splits to form a western belt from G.R. 430 193 to G.R. 398 202, and a larger eastern belt from G.R. 420 209 to G.R. 342 240. Overall, the belt consists of narrow (2m to 10m in width) zones of S-C fabric schistose serpentinite, relatively massive serpentinite, and small (maximum dimensions of 26x1.5m) bodies of chlorite rock, rodingite and gabbro, within schistose serpentinite.

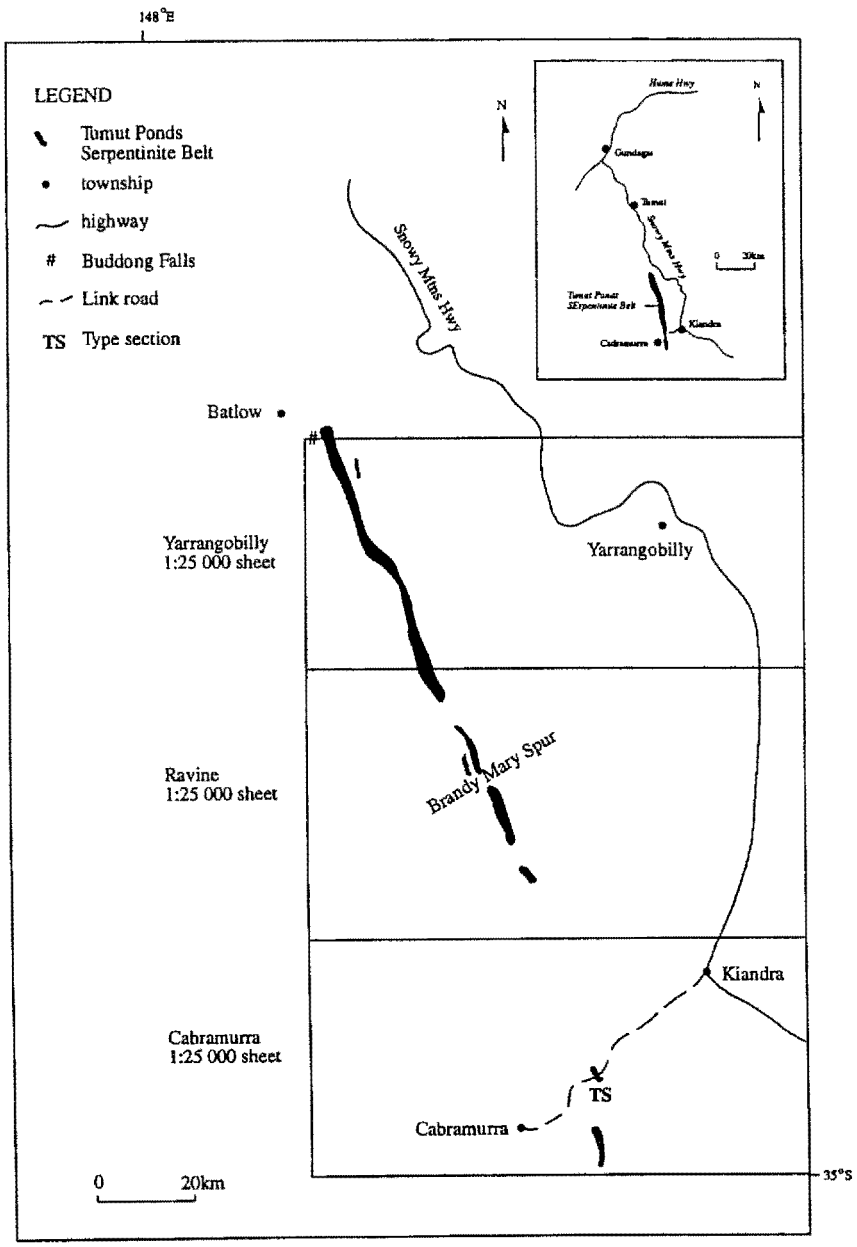

Figure 6.1 Location and extent of the Tumut Ponds Serpentinite Belt (from Degeling 1977).

6.2 NATURE OF CONTACTS

The Tumut Ponds Serpentinite Belt lies within and is bounded to the east and west by components of the Gilmore Fault Zone. In the Link Road area (G.R. 274 264, Cabramurra 1:25 000 sheet), the eastern boundary consists of a relatively large body of foliated coarse-grained hornblende clinopyroxenite in fault contact against cleaved quartz-veined fine-grained laminar metasiltstones of the Tumut Pond Group and O'Hares Beds; cleavage subparallels bedding and becomes more intense towards the contact. The western boundary consists of S-C fabric schistose serpentinite, also faulted against weakly cleaved, fine-grained, laminar metasiltstones of the Tumut Pond Group and O'Hares Beds. Orientation data for structural elements throughout the belt are in Table 6.1.

In the Buddong Falls area (around G.R. 147 545, Yarrangobilly 1:25 000 sheet), both the eastern and western boundaries consist of S-C fabric schistose serpentinite faulted against interbedded metabasalt/chert/metasiltstone. On the eastern boundary, the moderately foliated metabasalts and metasiltstones run sub-parallel to the trend of the belt and become more intensely foliated at the faulted contact (Table 6.1.) The metabasaltic rocks comprise two distinct types:

(a) fine-grained massive granular-textured metabasalts, and

(b) quench-textured metabasalts

A small body of serpentinite occurs at G.R. 148 559 on the Yarrangobilly 1:25 000 sheet. Its eastern boundary consists of S-C fabric schistose serpentinite abutting relatively unfoliated metabasalts and fine-grained metasedimentary rocks. The contact has a strike of 185° and dips at 70° towards 095°. S-C fabric schistose serpentinite on the western boundary is faulted against strongly cleaved, fine-grained metasiltstones. At the contact, cleavage is relatively shallow-dipping (some 40°), but becomes vertical some 5 to 10m away from the contact.

Although the Tumut Ponds Serpentinite Belt occupies heavily vegetated terrain, outcrop is good. Schistose serpentinite forms prominent sheet-like lenses or narrow zones within massive serpentinite. Massive serpentinite outcrops as either small blocks within a matrix of schistose serpentinite or large continuous bodies. Primary ultramafic rocks are rare, outcrop poorly, and occur as small lenses. Other rock types exist as discrete lenses (commonly boudinaged) within schistose serpentinite, or as lenses and small masses within massive serpentinite.

Rock Type	Grid Reference	Foliation	Strike	Dip
siltstone	291 254	S1	011	78 towards 281
hingeline		F2 folds		Plunge 78 towards 180
siltstone	287 233	S2		80 towards 292
hingeline		F2 folds		Plunge 80 towards 122
siltstone	290 227	S1	014	86 towards 104
		S2	094	80 towards 183
hingeline		F2 folds		Plunge 80 towards 110
serpentinite	264 273	slickenlines		Plunge 30 towards 070
serpentinite	266 274	s-surface	356	60 towards 266
		c-surface	324	72 towards 235
serpentinite	265 270	c-surface	330	42 towards 240
		s-surface	301	30 towards 211
siltstone	274 264	S1	329	86 towards 245
clinopyroxenite		c-surface	355	80 towards 085
		s-surface	129	80 towards 215
serpentinite	269 267	s-surface	334	60 towards 290
		c-surface	000	vertical
serpentinite	148 546	c-surface	006	60 towards 290
		s-surface	100	24 towards 190
serpentinite	150 548	c-surface	024	40 towards 294
		s-surface	024	75 towards 294
		slickenlines		Plunge 20 towards 320
serpentinite	142 545	c-surface	000	80 towards 090
		s-surface	010	vertical
serpentinite	148 559	c-surface	010	58 towards 290
		s-surface	358	vertical
		c-surface	144	vertical
		s-surface	163	vertical
		c-surface	352	80 towards 080
		s-surface	334	vertical
siltstone		S1	333	40 towards 245
fault contact		fault	185	70 towards 085

Table 6.1 Orientation data for structural elements within the Tumut Ponds Serpentinite Belt and adjoining rock units.

6.3 PETROGRAPHY AND TEXTURAL/STRUCTURAL EVOLUTION

(For detailed petrographic descriptions, see Appendix 6PD)

6.3.1 Primary ultramafic rocks

The primary ultramafic rocks exhibit a primary magmatic texture and are extremely rare, with only one outcrop, a highly sheared body of hornblende clinopyroxenite, occurring in the southern part of the belt (G.R. 274 264 Yarrangobilly 1:25 000 sheet). It consists of coarse-grained (10-20mm) interlocking diopside and intergranular brown/green hornblende (5-10%), and is ascribed to high temperature upper amphibolite facies metamorphism (e.g. Miyashiro 1994). It consists of coarse-grained (10-20mm) interlocking diopside and intergranular brown/green hornblende (5-10%). Blue-green amphibole/actinolite fringes and replacement grains are indicative of retrogressive lower amphibolite facies metamorphism (e.g. Miyashiro 1994), during which brittle-ductile deformation gave rise to fractured, microfaulted and bent hornblende and amphibole/actinolite grains, and replacement (Plate 6.2) and fracture-fill of tremolite/actinolite (Plate 6.3).

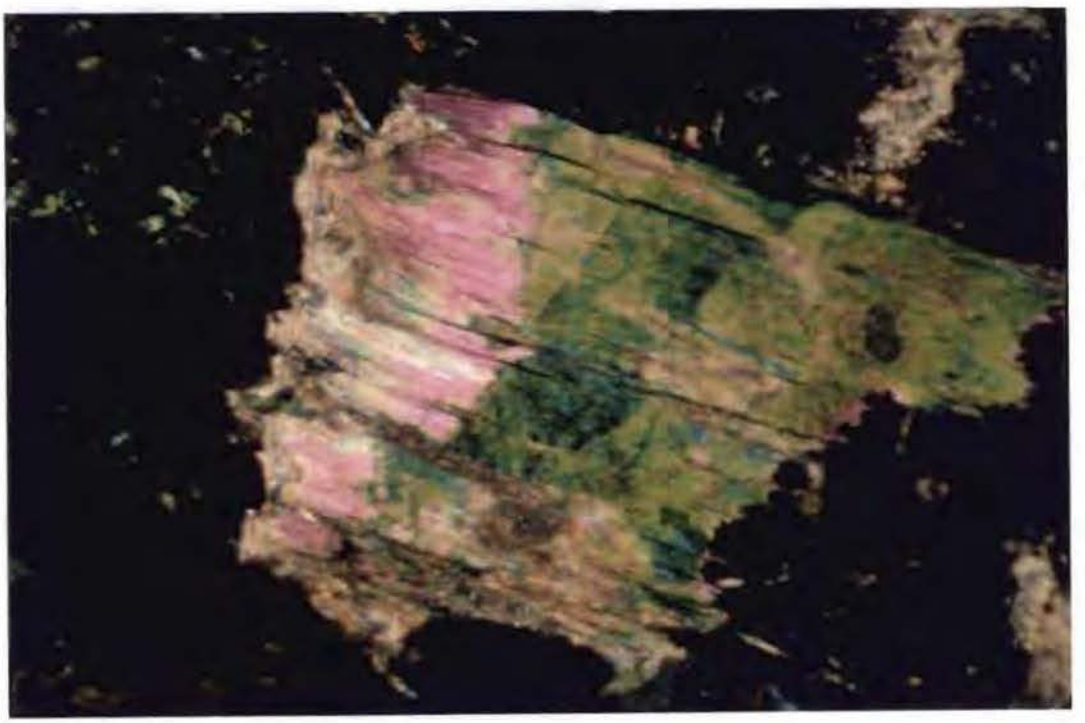

Plate 6.2 Tremolite fringes around blue-green actinolite within meta-clinopyroxenite.
Sample No 249 UXP F.O.V 3.5mm

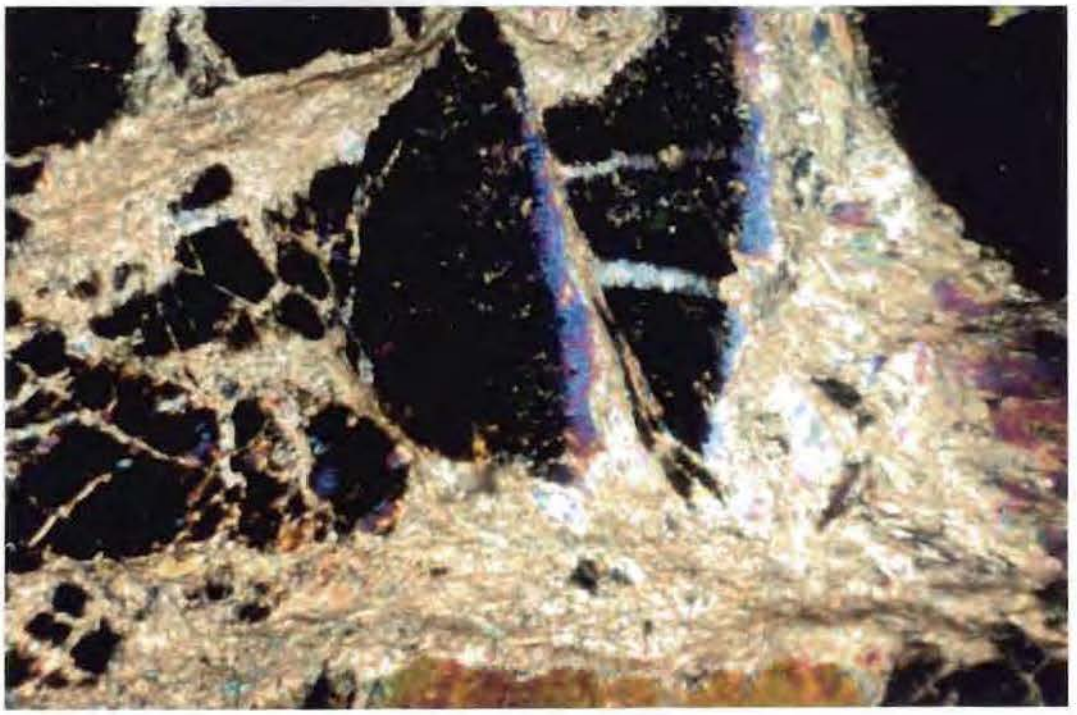

Plate 6.3 Fracture-fill actinolite within diopside in meta-clinopyroxenite.
Sample No 249 UXP F.O.V 3.5mm

6.3.2 Serpentinites

Massive and schistose serpentinites comprise at least 98% of the belt, and are the "matrix" to all other rock types. The schistose serpentinites occur as:

(a) elongate (hundreds of metres in length) narrow (maximum widths of 2 to 10m) "sheet-like" bodies; and,

(b) narrow (20 to 100mm in width) discrete zones in massive serpentinite.

The massive serpentinites exist as:

(a) boulder and block-like, relatively small (maximum dimensions of 10 x 5m) masses embedded in a matrix of schistose serpentinite; and,

(b) relatively large (hundreds of metres in length and tens of metres in width) generally elongate bodies within schistose serpentinite.

All serpentinite bodies are oriented sub-parallel to the trend of the belt and appear to have no set systematic areal distribution.

XRD studies of samples confirm that all three serpentine polymorphs exist. However, the schistose serpentinites are dominated by chrysotile 2M and chrysotile 2O, whereas the massive serpentinites generally consist of chrysotile 2M and lizardite 1T. Antigorite is a minor constituent, restricted to the southern half of the belt and commonly associated with talc and magnesite.

The occurrence of relict chromian spinel (Plate 6.4) and serpentine pseudomorphs after orthopyroxene (Plate 6.5) is consistent with a serpentinite origin as upper mantle harzburgites. Serpentinisation caused replacement of olivine and orthopyroxene by lizardite+chrysotile+magnetite at 250 $\pm$ 25°C at a $P_{(H_2O)}$ of less than 1kb (e.g. O'Hanley & Wicks 1995). The occurrence of antigorite, talc and magnesite in the southern half of the belt is attributed to prograde (higher temperature) serpentinisation of the lizardite+chrysotile+magnetite assemblage (e.g. Wicks 1984). Chrysotile and chlorite veinlets (Plate 6.6) and the main S-C fabric developed in the schistose serpentinites are ascribed to brittle deformation during retrogressive greenschist facies metamorphism (e.g. Miyashiro 1994), whilst cross-cutting tremolite grains reflect ongoing mid-greenschist facies metamorphism.

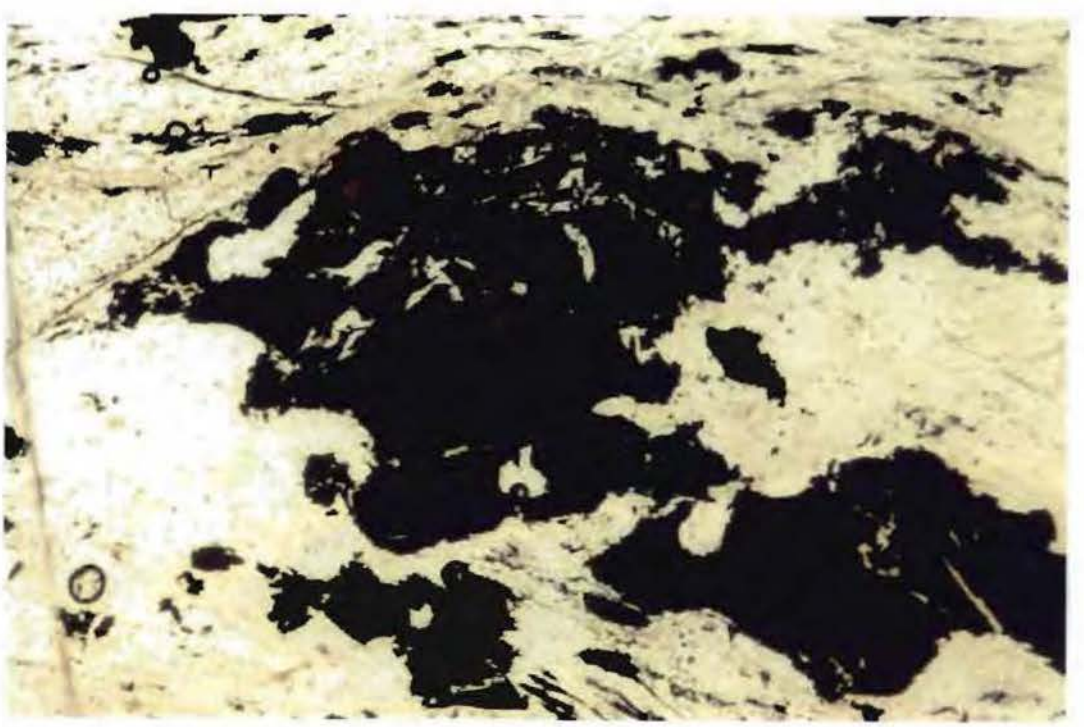

Plate 6.4 Relict chrome spinel within schistose serpentinite.
Sample No BF92/22 PPL F.O.V 1.5mm

Plate 6.5 Bastised orthopyroxene grains within massive serpentinite.
Sample No 258 UXP F.O.V 3.5mm

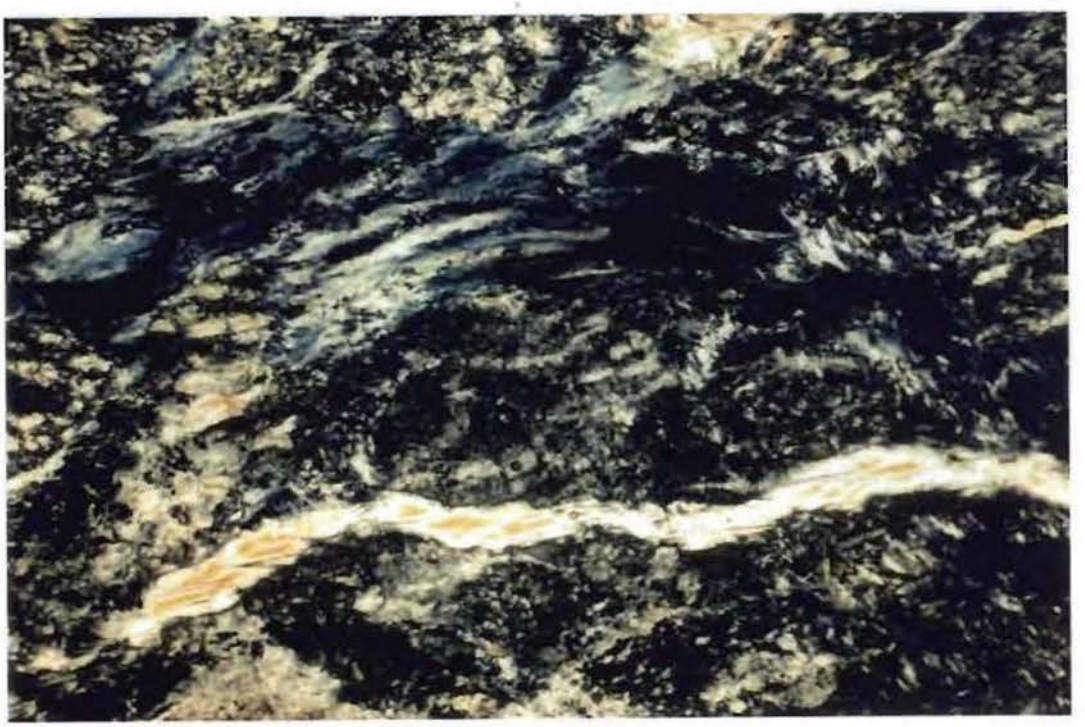

Plate 6.6 Cross-cutting chrysotile/chlorite veinlets within massive serpentinite.
Sample No 258 UXP F.O.V 3.5mm

6.3.3 Talc-carbonate rock

The talc-carbonate rock contains >50% talc and/or magnesite and is only found at one locality (G.R. 264 273; Cabramurra 1:25 000 sheet) in the southern half of the belt. It constitutes narrow (<0.3m) vein-like bodies and patches within massive and schistose serpentinites and consists of talc+magnesite+chrysotile 2M (XRD determination).

Talc and magnesite, which replace and cut across the serpentine group minerals (Plate 6.7) reflect hydrothermal fluid channeling and alteration at minimum temperatures of 165-285°C (Ashley 1997).

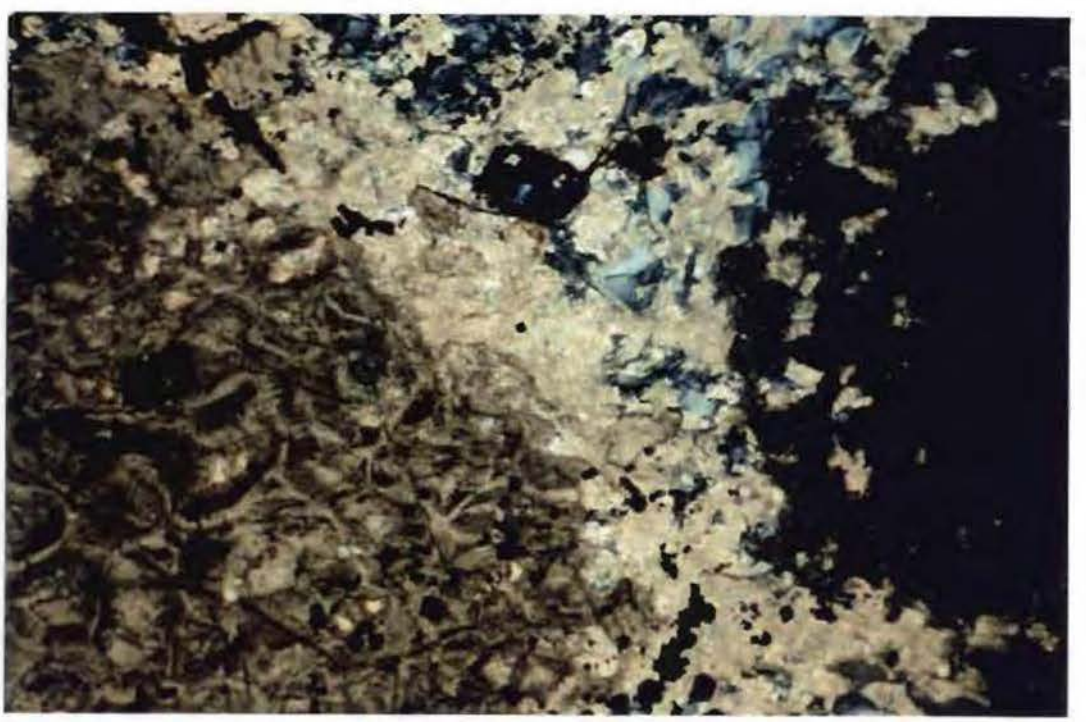

Plate 6.7 Magnesite and talc overprinting serpentine within talc-magnesite rock.
Sample No 245 UXP F.O.V 3.5mm

6.3.4 Gabbro

Gabbro is only found at one locality (G.R. 143 545; Yarrangobilly 1:25 000 sheet) within the northern half of the belt, where it is moderately foliated and occurs as small (maximum dimensions 1 to 3m) lens-shaped bodies within schistose serpentinite.

The gabbro was originally composed of diopside and plagioclase with minor orthopyroxene. Saussuritisation of the original calcic plagioclase resulted from "ocean-floor metamorphism" (e.g. Miyashiro 1978), but this was followed by lower greenschist facies regional metamorphism during which diopside was bent and fractured and cross-cutting veinlets of chlorite, epidote, zoisite and quartz developed (Plate 6.8).

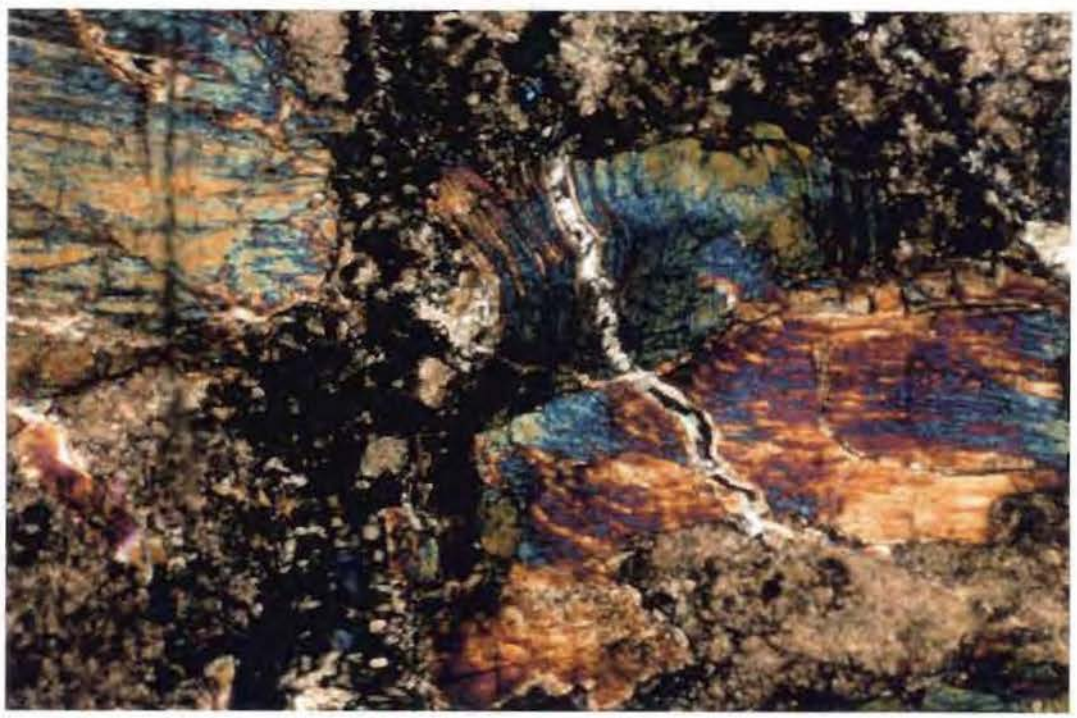

Plate 6.8 Bent and micro-faulted diopside grains with fracture-fill chlorite and zoisite within gabbro.
Sample No BF92/24 UXP F.O.V 1.5mm

6.3.5 Rodingites

Rodingites seem to be restricted to the northern half of the belt, where they occur as lens-shaped bodies (maximum plan dimensions 1 x 0.5m) or boudinaged dyke-like bodies (maximum dimensions of 26 x 1.5m) within schistose serpentinite. They are typically fine-grained and resemble fine-grained metabasalts in hand-specimen.

XRD studies enable subdivision of the rodingites into those containing:

(a) grossular, and

(b) diopside-grossular rodingites.

The former are composed entirely of grossular, whereas the latter, although dominantly diopside and grossular, also contain prehnite, hornblende and serpentine.

The rodingites are interpreted as metasomatically altered pyroxene gabbros. They contain relict primary diopside, but the calcic plagioclase has been altered and replaced. Fracturing was necessary to allow fluid infiltration and related rodingitisation; ongoing deformation resulted in veinlets of epidote/zoisite. Rodingitisation is equated with the initial stages of serpentinisation (e.g. Schandl *et al.* 1990; Dubinska 1995) at temperatures below 300 $\pm$ 36°C and $P_{(H_2O)}$ of 0.8kb (e.g. O'Hanley *et al.* 1992).

6.3.6 Metabasalts

Metabasalts are those basaltic rocks occurring within the boundaries of the belt, regardless of either their emplacement mechanism or origin. They have been found at only two localities in the northern half of the belt around G.R. 143 545 (Yarrangobilly 1:25 000 sheet), where they occur as small (maximum dimensions of only a few metres) lens-shaped masses within schistose serpentinite. The metabasaltic rocks include:

(a) quench-textured metabasalts, and

(b) meta-basaltic/andesitic tuffs.

The quench-textured metabasalts were originally assemblages of calcic plagioclase, clinopyroxene and olivine. Albitisation of the calcic plagioclase and replacement of original ferromagnesi

minerals by actinolite, took place under conditions that, on mineralogical grounds, indicate low grade greenschist facies metamorphism (e.g. Menzies *et al.* 1977; Miyashiro 1978). Cross-cutting epidote and chlorite (Plate 6.9) and localised brittle fracturing in actinolite-dominant veinlets are consistent with ongoing greenschist facies metamorphism and deformation.

The meta-basaltic/andesitic tuffs were originally composed of mafic lithic fragments up to 10mm in diameter) and broken crystal fragments of calcic plagioclase and hornblende set in a glassy(?) groundmass. The replacement of hornblende by actinolite, saussuritisation of calcic plagioclase and occurrence of veinlets of actinolite, quartz and epidote/zoisite (Plate 6.10) are all consistent with "ocean-floor metamorphism" (e.g. Miyashiro 1994). However, the cross-cutting veinlets may also have been produced during the same deformational event which developed cleavage in the less competent adjacent metasiltstones."

6.3.7 Chlorite rocks

Chlorite rocks (i.e. rocks with >90% chlorite) have been found in both the northern (at G.R. 143 545; Yarrangobilly 1:25 000 sheet) and southern (at G.R. 264 273; Cabramurra 1:25 000 sheet) parts of the belt. In the southern occurrence, the chlorite occurs as apparently randomly distributed patches (20 – 50mm in maximum dimension) within massive and schistose serpentinites, whereas in the northern locality, it forms discrete lenses (5m maximum dimension) within schistose serpentinite.

XRD studies show that the chlorite-dominant patches are composed of clinochlore IIb, whereas the chlorite lenses comprise ferroan clinochlore Ia.

Plate 6.9 Albite-epidote-chlorite-zoisite metamorphic assemblage in metabasalt.
Sample No BF92/26 UXP F.O.V 3.5mm

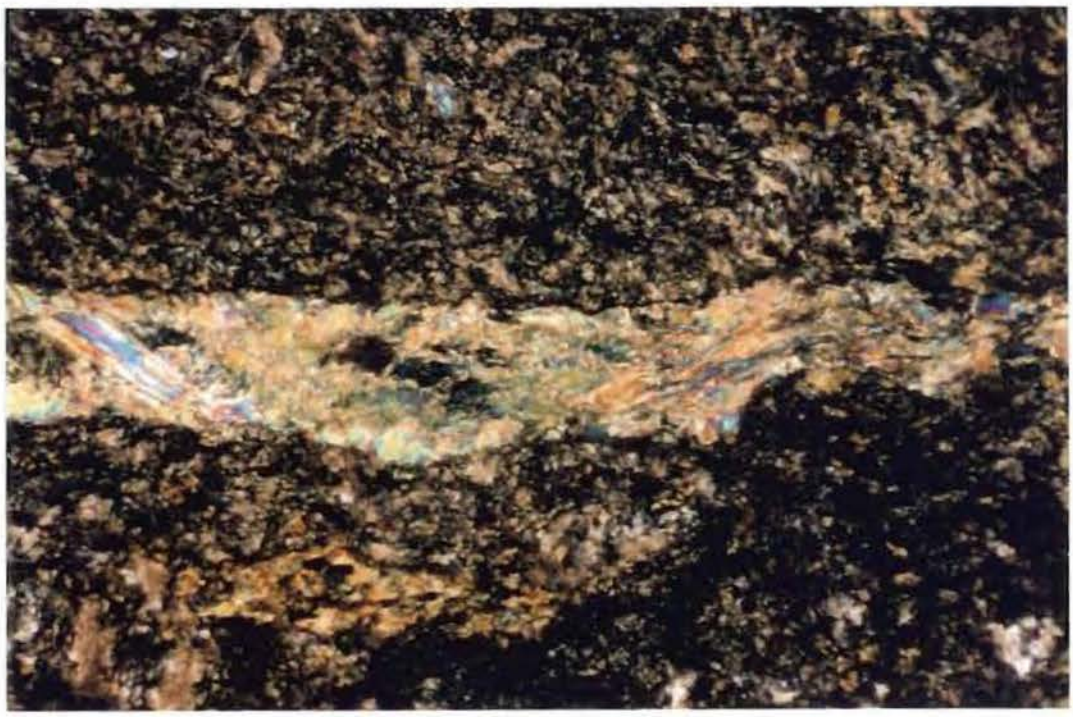

Plate 6.10 Actinolite-chlorite veinlets in meta-andesitic tuffs.
Sample No BF92/21 UXP F.O.V 3.5mm

6.4 STRUCTURE OF THE TUMUT PONDS SERPENTINITE BELT

6.4.1 Serpentinite foliations

The serpentinite S-C fabrics occur throughout the belt. Orientation data (Figure 6.2) show that:

(a) the majority of the S-C fabric orientations are steeply to vertically dipping and trend NNW-SSE;

(b) S and C are similarly oriented;

(c) the S-C fabric orientations are similar to those from the other serpentinite belts of the region (see Figures 3.7 and 5.4).

(d) internal shear zones within serpentinite of the Tumut Ponds Serpentinite Belt dominantly record dextral oblique slip movement. Minor dextral strike slip and sinistral oblique slip movements have also been recorded. S-C fabrics on the eastern contact of the belt dominantly record dextral oblique slip movement.

Micro-scale observations show that the foliations developed late in the serpentinisation process and, as the cleavage in the surrounding metasedimentary rocks approximates the trend of the belt, this probably accompanied emplacement of the belt into continental crust near to its present position.

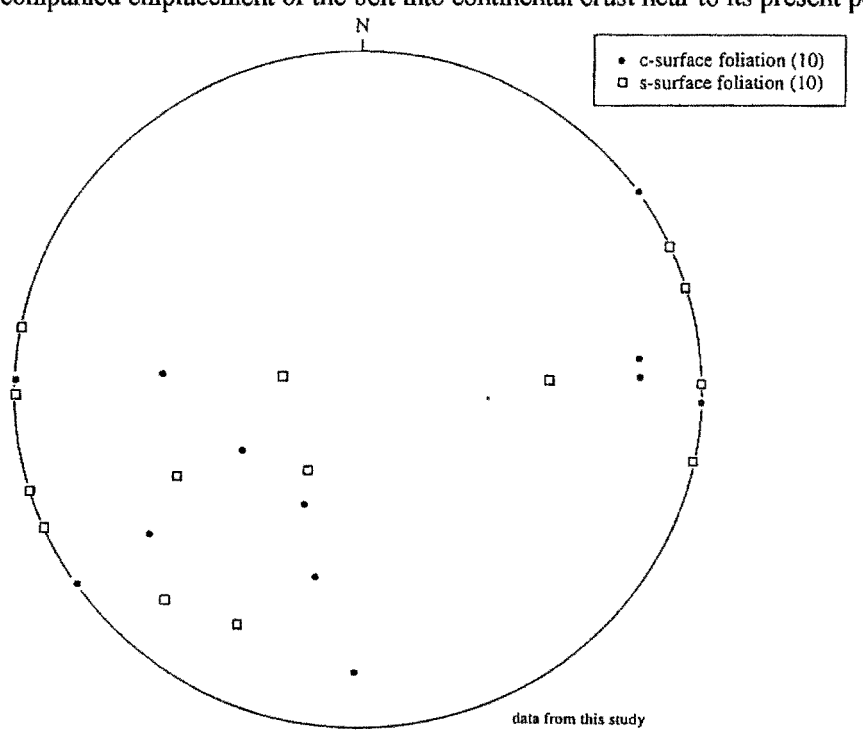

Figure 6.2 Poles to small-scale internal shear zones within serpentinite of the Tumut Ponds Serpentinite Belt (equal area projection).

CHAPTER 7: OTHER SERPENTINITE BELTS OF THE REGION

7.1 THE EURONGILLY SERPENTINITE BELT

The Eurongilly Serpentinite Belt crops out discontinuously near Sheridan's Corner and Eurongilly, approximately 20km south-east of the township of Junee (Figure 7.1). The type section (Warren *et al.* 1995) is at G.R. 568 613. The same authors suggested that the discontinuous outcrops are parts of a continuous body which extends for at least 6km and is up to 0.5km wide. The Eurongilly Serpentinite Belt trends approximately NNW-SSE, is relatively elongate and appears to be steeply-dipping.

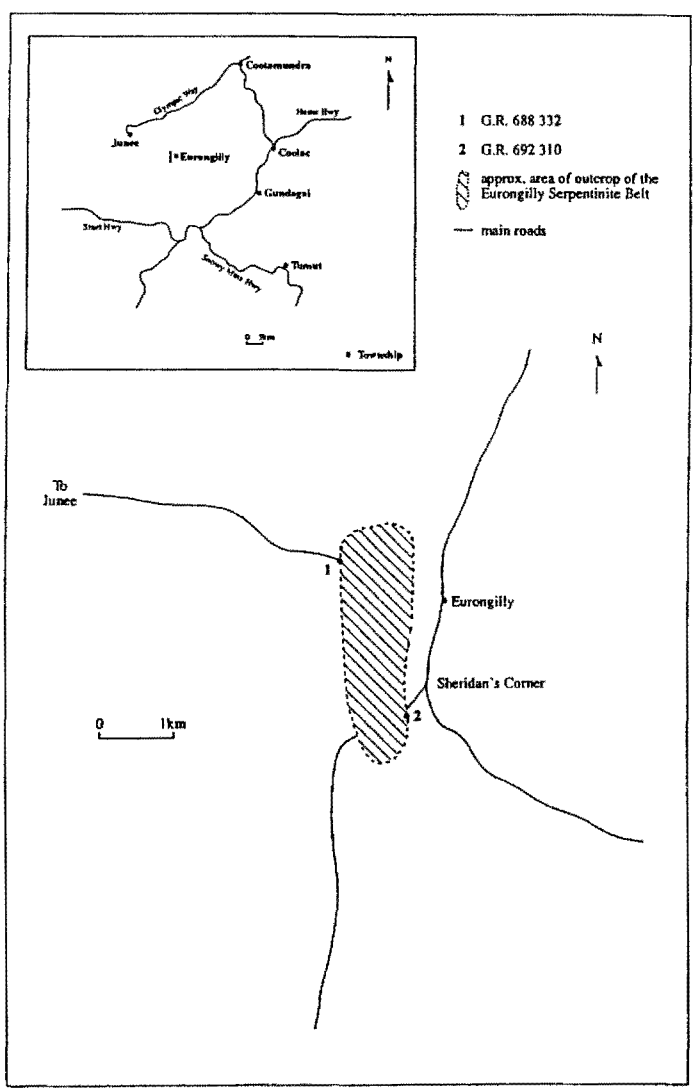

Figure 7.1 Location and extent of the Eurongilly Serpentinite Belt.

7.1.1 Nature of contacts

To the west, the belt is faulted against the Wagga Group, which comprises foliated, recrystallised micaceous quartzites with a strong domainal texture defined by mica-rich (M-domains) and quartz-rich (Q-domains) zones (e.g. G.R. 692 310; Junee 1:25 000 sheet). The rocks are similar in appearance to micaceous quartzites of the Jindalee Beds.

7.1.2 Petrography and textural/structural evolution

(Detailed petrographic descriptions are in Appendix 7PD)

The two areas examined during the present study contain distinctly different lithologies.

G.R 692 310 (Junee 1:25 000 sheet)

Outcrop (Figure 7.1) consists largely of olivine pyroxene meta-hornblendite, hornblende meta-lherzolite, and their alteration/ weathering derivatives which are carbonate-rich metaserpentinite.

G.R. 688 332 (Junee 1:25 000 sheet)

Outcrop (Figure 7.1) consists of massive and moderately foliated (S-C fabric) serpentinite.

The primary ultramafic rocks at G.R. 692 310 were lherzolites, with minor hornblendites. Initial serpentinisation resulted in the replacement of olivine by antigorite at temperatures above 250 ± 25°C and a $P_{(H2O)}$ of less than 1kb (e.g. O'Hanley & Wicks 1995), but below 450°C (e.g. O'Hanley 1996). Later, chlorite and actinolite developed (Plate 7.1) and was followed by crosscutting talc and magnesite. Finally, brittle fracturing was accompanied by the formation of veinlets of carbonate, quartz and goethite by groundwater movement."

At G.R.688 332, intense fracturing and serpentinisation was marked by replacement of the primary minerals by antigorite at temperatures >250°C ± 25°C and <450°C and P_{H2O} <1kb (e.g. O'Hanley & Wicks 1995; O'Hanley 1996) (Plate 7.2). In places localised high strain zones lead to the formation of an S-C fabric foliation.

Plate 7.1 Actinolite-chlorite veinlet within lherzolite.
Sample No. BF91/41g UXP F.O.V 3.5mm

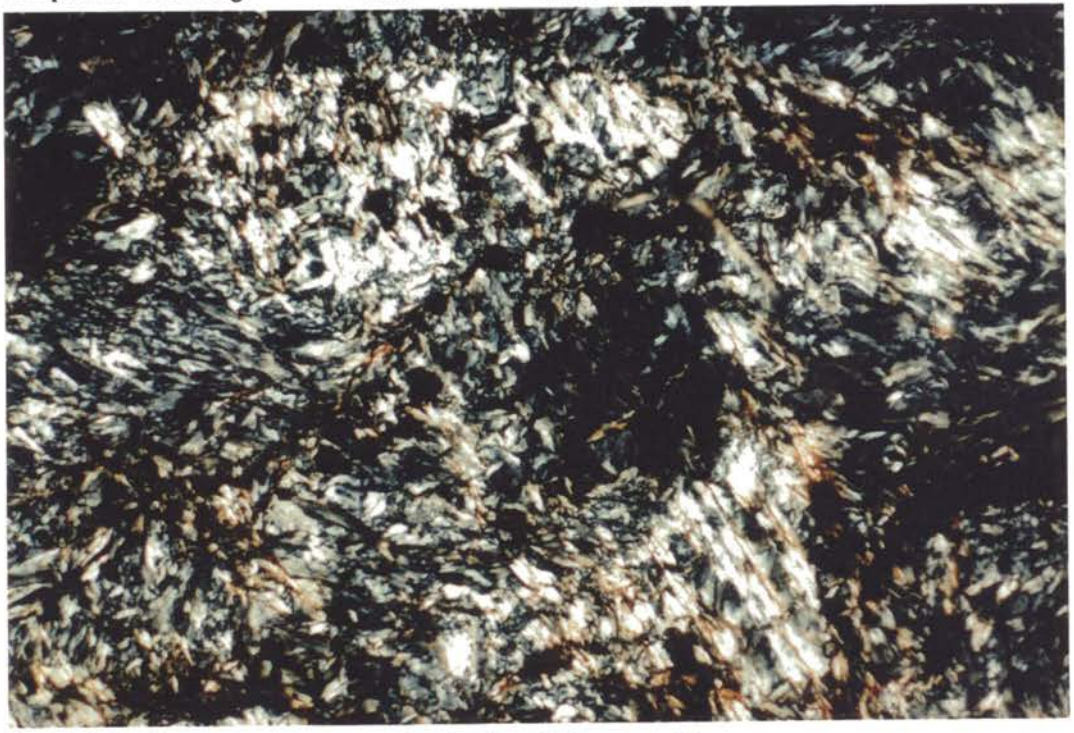

Plate 7.2 Feathery decussate texture of antigorite within serpentinite.
Sample No. BF91/44b UXP F.O.V 3.5mm

7.2 THE DARBALARA SERPENTINITE BELT

The Darbalara Serpentinite Belt is a small and highly discontinuous serpentinite belt which occurs near Darbalara (G.R. 108 231; Gundagai 1:25 000 sheet), approximately 10km north-east of the township of Gundagai (Figure 7.2). Warren *et al.* (1995) included this body within the Wambidgee Serpentinite Belt (some 4km to the north-west), but the author prefers to treat it separately. The belt crops out from at least G.R. 098 240 in the north to G.R. 108 231 in the south with a maximum length of 1.5km and a width of at least 100m (Figure 7.2). It is a steeply-dipping alpine-type serpentinite belt and has a type section at G.R. 108 231 (Gundagai 1:25 000 sheet).

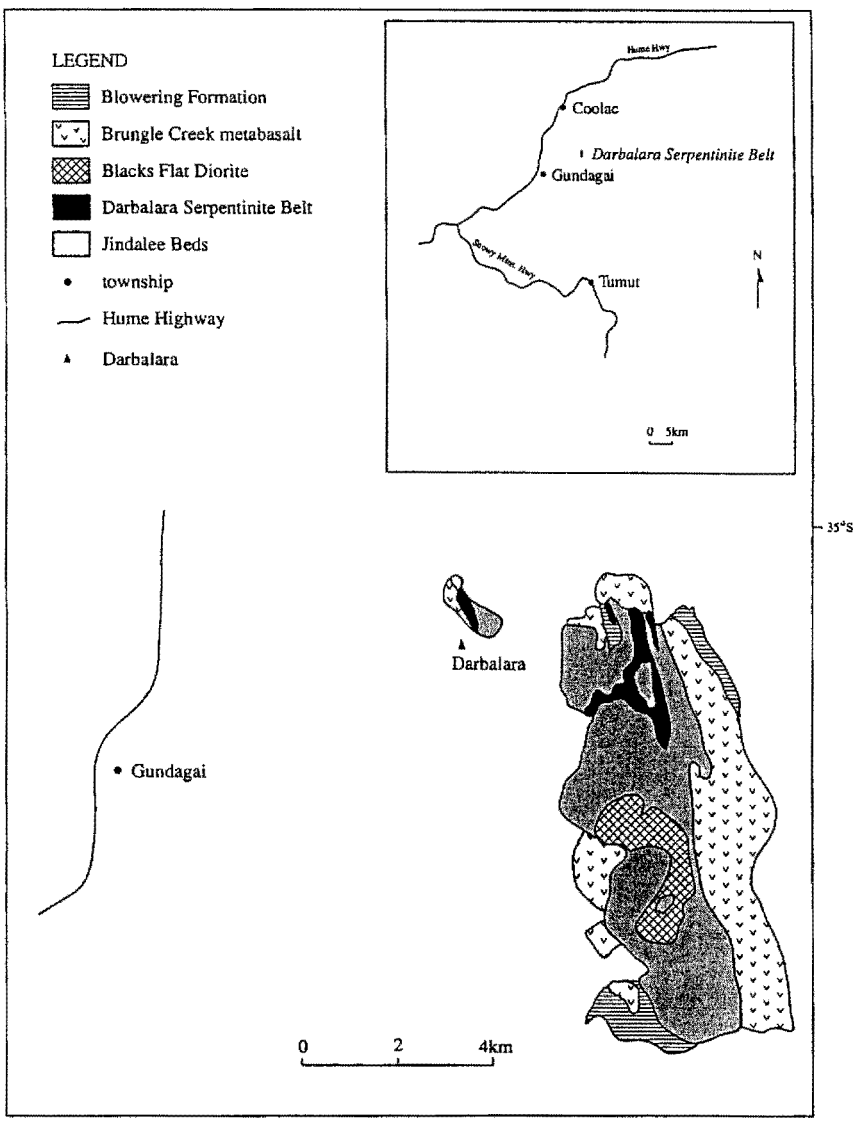

Figure 7.2 Location and geology of the Darbalara Serpentinite Belt (adapted from Basden 1990).

7.2.1 Nature of contacts

The Darbalara Serpentinite Belt is enclosed within metasedimentary and metavolcanic rocks of the Jindalee Beds. At G.R. 098 240, relatively massive serpentinite is faulted against foliated and lineated quartzites and has an S-C fabric that parallels foliation in the quartzites. At G.R. 108 231, a lens (<5m in width) of massive serpentinite is fault bound between a sequence of metabasalt, quartzite and metasiltstone in the east and well-cleaved metasiltstone in the west (Figure 7.3).

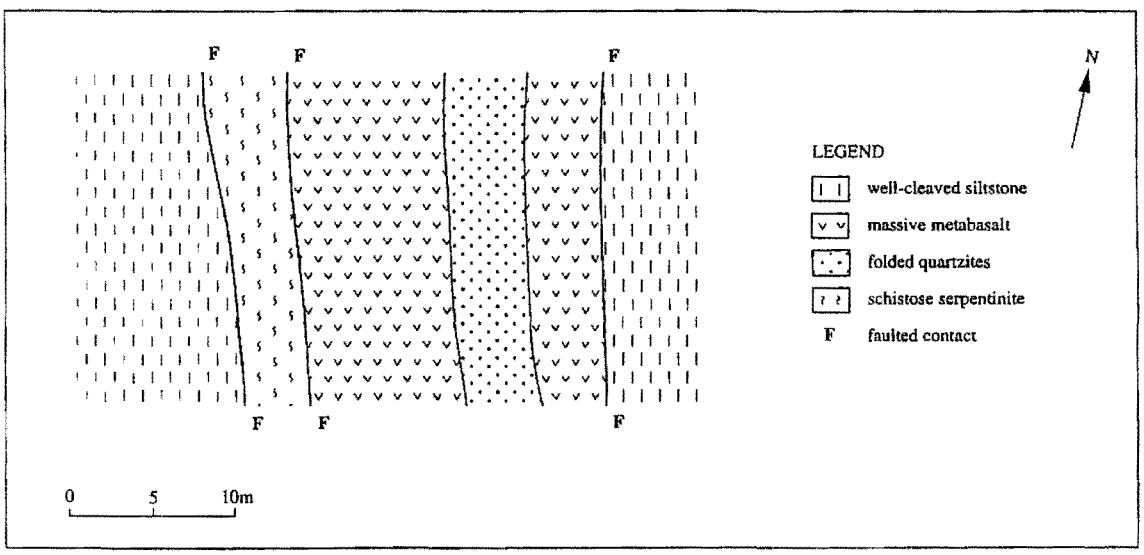

Figure 7.3 Simplified geology at G.R. 108 231: Darbalara Serpentinite Belt.

7.2.2 Petrography and textural/structural evolution

XRD studies on serpentinite samples from G.R. 098 240 show that the serpentinite is largely composed of antigorite and chrysotile, along with possible minor lizardite. A body of meta-hornblendite, associated with similar massive serpentinite, occurs at G.R. 108 231.

The initial period of serpentinisation of the primary ultramafic rocks was retrogressive and resulted in the development of antigorite at temperatures above 250°C ± 25°C and <450°C and P_{H_2O} <1kb (e.g. O'Hanley & Wicks 1995; O'Hanley 1996). However, the hornblendite provides evidence of an early upper greenschist to lower amphibolite facies metamorphism, as igneous brown hornblende has been replaced by fibrous brown-green metamorphic hornblende (e.g. Miyashiro 1994). Later, perhaps after the antigoritic serpentinisation event, retrogressive greenschist facies metamorphism resulted in fracture-related replacement of hornblende by zoisite.

7.3 THE WESTERN WAMBIDGEE SERPENTINITE MÉLANGE

The Western Wambidgee Serpentinite Mélange is an imbricate thrust package that contains a large ultramafic component. It is located 7.2km to the west of Coolac around G.R. 350 993 (Coolac 1:50 000 sheet) (Figure 7.4) and, according to Wilson (1993) it has a mappable length of 3.8km and a width of 1.1km. Within the unit (Figure 7.5), the main serpentinite body within the mélange has a maximum length of 1200m and a maximum width of 60m.

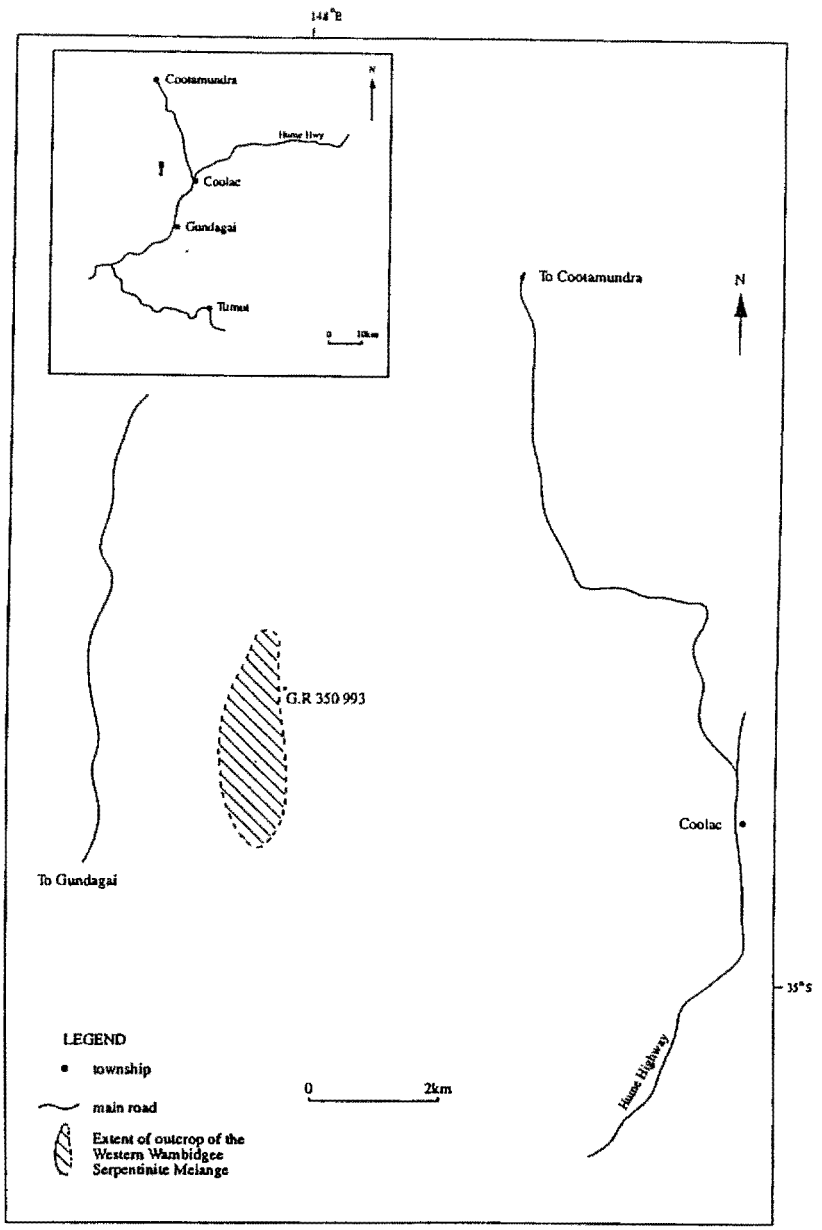

Figure 7.4 Location and extent of the Western Wambidgee Serpentinite Mélange.

7.3.1 Nature of contacts

The mélange includes slices from the Wambidgee Serpentinite Belt, Jindalee Beds, Frampton Volcanics and Blowering Formation, all of which have indeterminate contacts due to poor exposure (Figure 7.6). In the simplified interpretative map (Figure 7.5), massive serpentinite is shown faulted against the Blowering Formation (Fences Creek Conglomerate) on the east, while the western boundary is marked by unfoliated rhyolite of the Frampton Volcanics abutting metasiltstones of the Jindalee Beds.

7.3.2 Surface outcrop

Although contacts are poorly to not exposed, outcrop is quite good other than in the central part of the unit. Ultramafic rocks and metagabbros form prominent elongate lens-shaped bodies near the eastern boundary. A small (<10m) body of plagiogranite is associated with these rocks and forms "boulder-like" masses within serpentinite. The Jindalee Beds outcrop quite prominently along the western boundary of the unit.

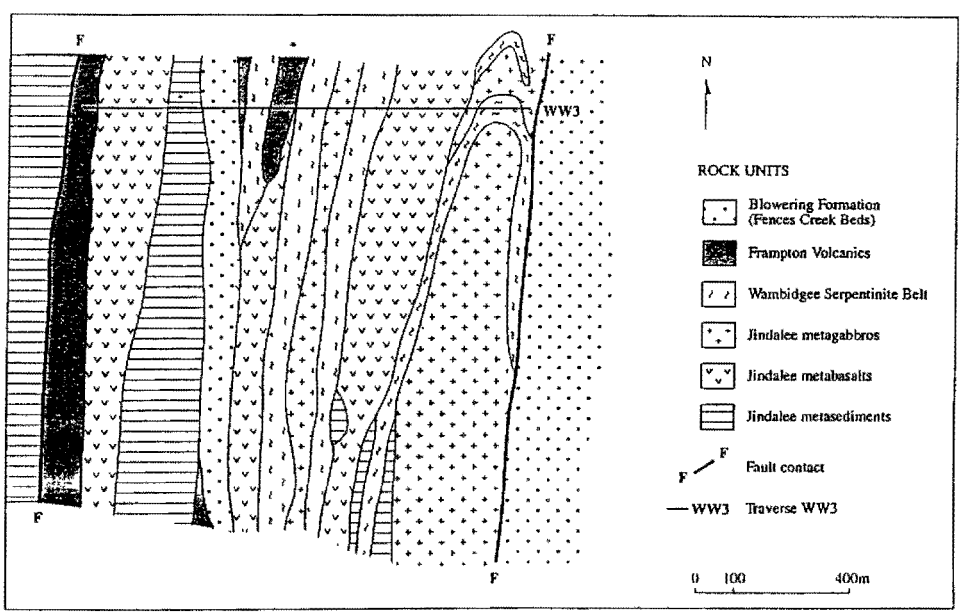

Figure 7.5 Simplified geology of the Western Wambidgee Serpentinite Melange (adapted from Wilson 1993).

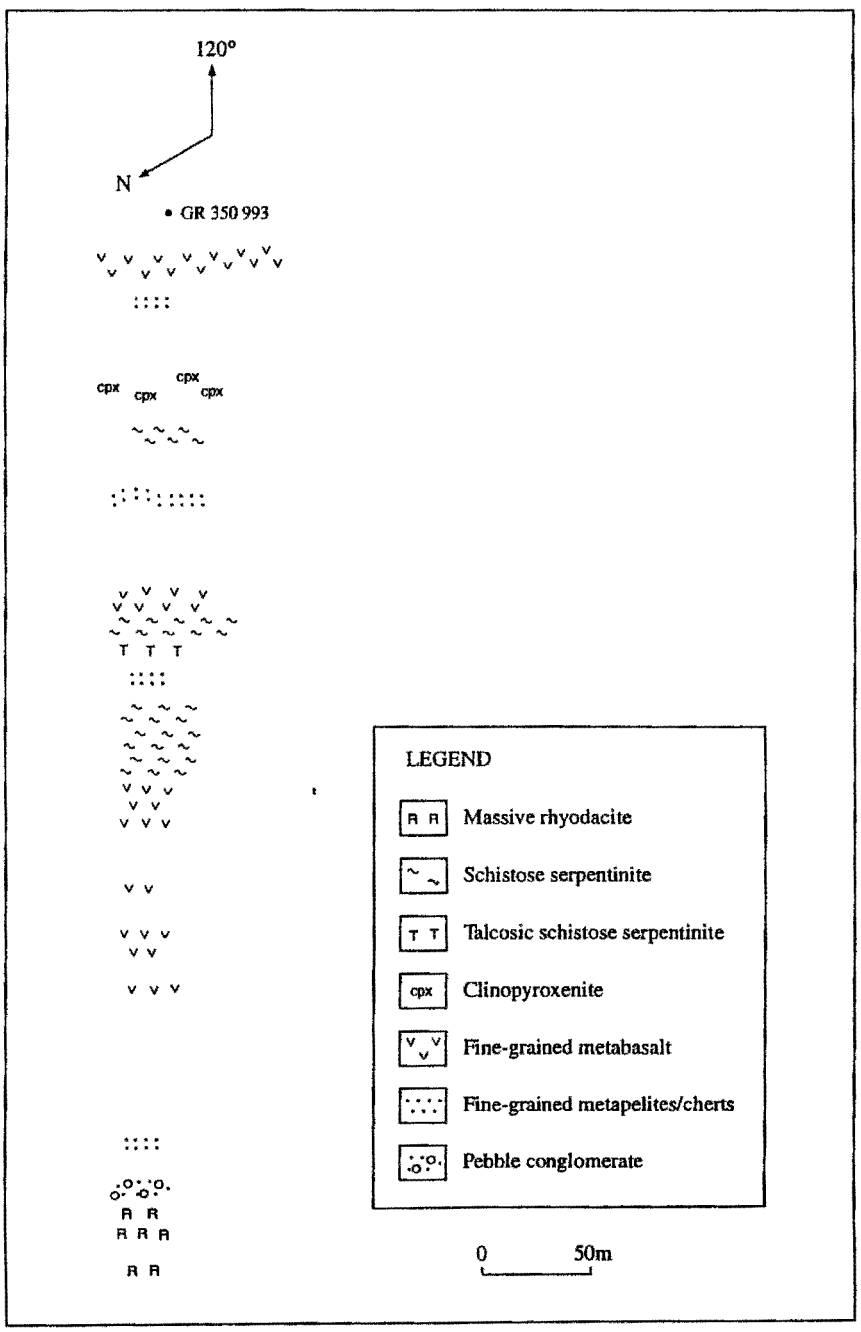

Figure 7.6 Outcrop geology of traverse WW3: Western Wambidgee Serpentinite Mélange.

7.3.3 Petrography and textural/structural evolution

(For detailed petrographic descriptions, see Appendix 7PD)

The primary ultramafic rocks of the Western Wambidgee Serpentinite Mélange are dominated by clinopyroxene and vary in composition from clinopyroxenite to lherzolite using the IUGS classification scheme (e.g. Le Maitre 1994). The pyroxene is relatively fresh, whereas olivine has been completely serpentinised and/or altered to talc. Fractured, micro-faulted and bent diopside grains, and the development of cataclasite zones result from deformation preceding and/or accompanying the upper greenschist facies metamorphism that is indicated by the assemblage serpentine+talc+chlorite+tremolite within these rocks (e.g. Miyashiro 1994). However, pyroxenite near the western margin of the unit exhibits an even-grained granoblastic texture (Plate 7.3) that is attributed to high temperature metamorphism, of at least upper amphibolite facies. Subsequent to this, fracturing under lower greenschist facies conditions is indicated by fracture-fill chlorite (e.g. Miyashiro 1994).

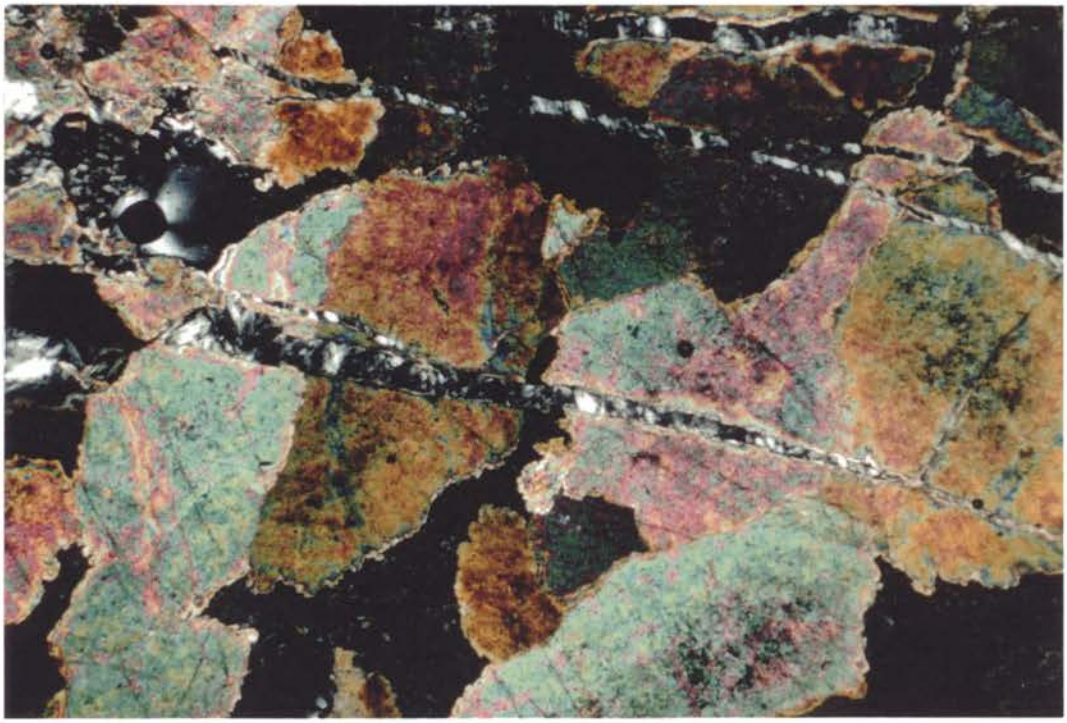

Plate 7.3 Metapyroxenite exhibiting a granoblastic texture along with fracture-fill Mg-chlorite.
Sample No 171 UXP F.O.V 3.5mm

Foliated and massive serpentinites (Figure 7.5) form discrete lenses in which the dominant serpentine group minerals (based on XRD) are Al-rich lizardite 1T and chrysotile. Massive pseudoharzburgitic serpentinites have a pseudoporphyritic decussate mesh texture (Plate 7.4), while schistose serpentinites are characterised by S-C fabrics that are considered to mark high strain zones coeval with serpentinisation. The assemblage lizardite 1T+chrysotile is indicative of retrogressive serpentinisation (e.g. Wicks 1984) at temperatures below 250 ± 25°C and $P_{(H_2O)}$ of 1kb (e.g. O'Hanley & Wicks 1995). Magnesite is ascribed to infiltration of low temperature CO_2-enriched groundwaters (e.g. Laurent & Hebert 1979).

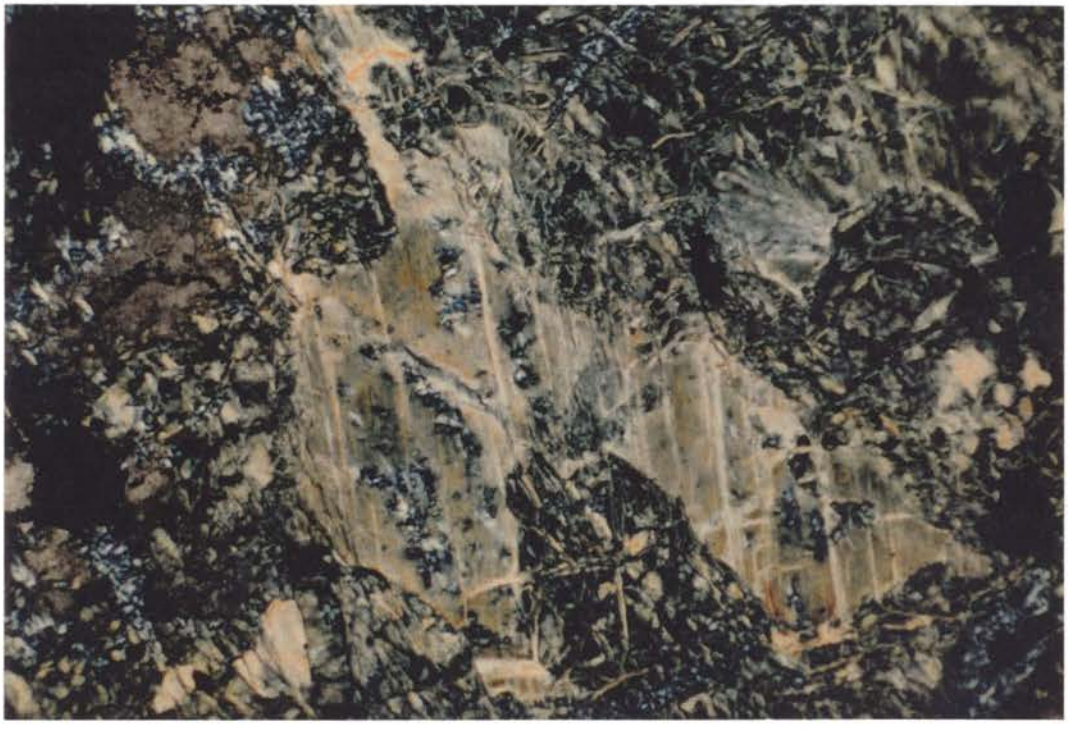

Plate 7.4 Pseudoporphyritic decussate sub-mesh texture of massive serpentinite.
Sample No BF92/17c UXP F.O.V 3.5mm

Talc schists occur in discrete zones on the western boundary of the unit (Figure 7.5). They contain relict chromian spinel (Plate 7.5) which supports derivation from an ultramafic parent and are fractured, providing possible evidence for an early deformational event. Talc could have formed either by hydrothermal fluid channeling (Ashley 1997) or from CO_2-enriched serpentinising fluids which reacted with the primary ultramafic rocks (e.g. Wicks & Whittaker 1977). Regardless of the process, the schistose texture reflects the one-time existence of high strain zones.

Gabbros occur near the eastern contact and central part of the unit. Most are strongly sheared, metamorphosed and altered. The gabbros can be subdivided into hornblende-clinopyroxene gabbros and completely altered gabbros. All gabbro bodies are intimately associated with ultramafic rocks (Figure 7.5). The partial to complete replacement of calcic plagioclase, hornblende and diopside by the assemblage albite+epidote+chlorite+actinolite (Plate 7.6) is indicative of greenschist facies metamorphism (e.g. Miyashiro 1978). Ductile-brittle deformation within the gabbros was localised in nature and textural evidence (Plate 7.6) indicates that it was synchronous with the greenschist facies metamorphism.

A plagiogranite body was found within schistose serpentinite at G.R. 990 337. It contains mafic enclaves with sharp contacts against the plagiogranite (Plate 7.7) and is undeformed apart from minor cataclasite zones (Plate 7.8). The latter developed prior to alteration, as the greenschist facies alteration assemblage of chlorite+zoisite+tremolite/actinolite cross-cuts the cataclasite zones (Plate 7.8). The development of tremolite/actinolite may be due to Mg-metasomatism during serpentinisation of the enclosing ultramafic rocks (e.g. Linder *et al.* 1992). Thus, if this interpretation is correct, it follows that the plagiogranites were emplaced in the ultramafic rocks prior to serpentinisation.

Plate 7.5 Fractured relict chrome spinel within talc schist.
Sample No BF92/17a PPL F.O.V 1.5mm

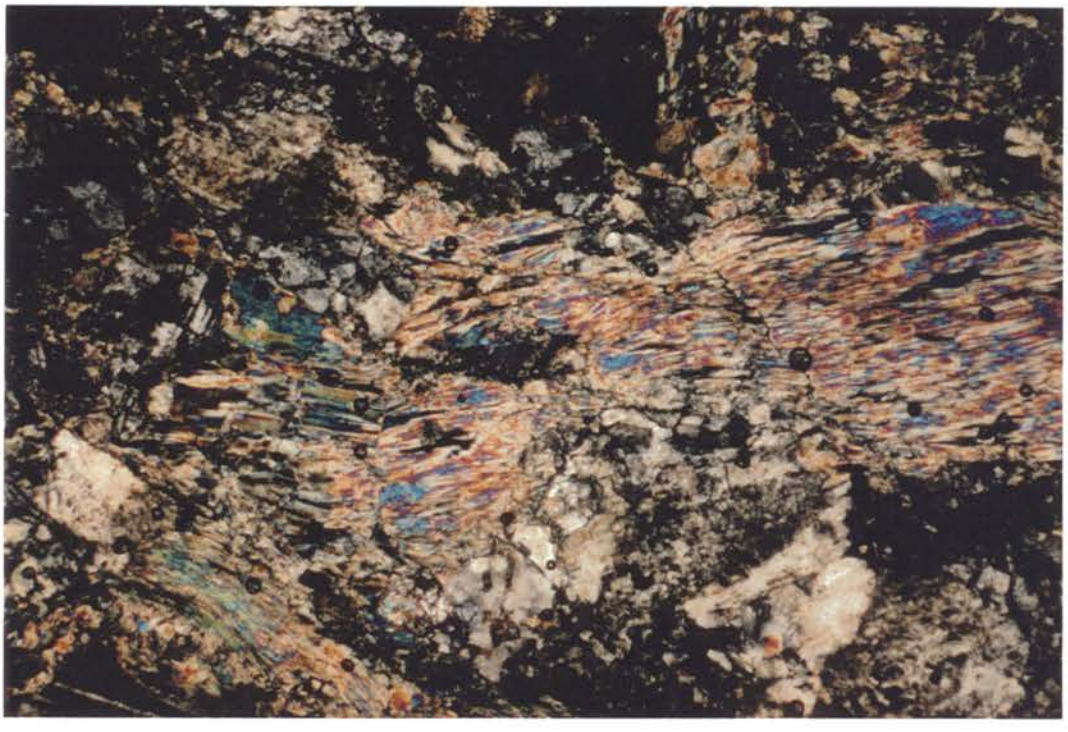

Plate 7.6 Kink bands in tremolite/actinolite pseudomorph after hornblende within gabbro.
Sample No 170a UXP F.O.V 3.5mm

Plate 7.7 Contact between plagiogranite (left) and metabasalt enclave (right).
Sample No 169a UXP F.O.V 3.5mm

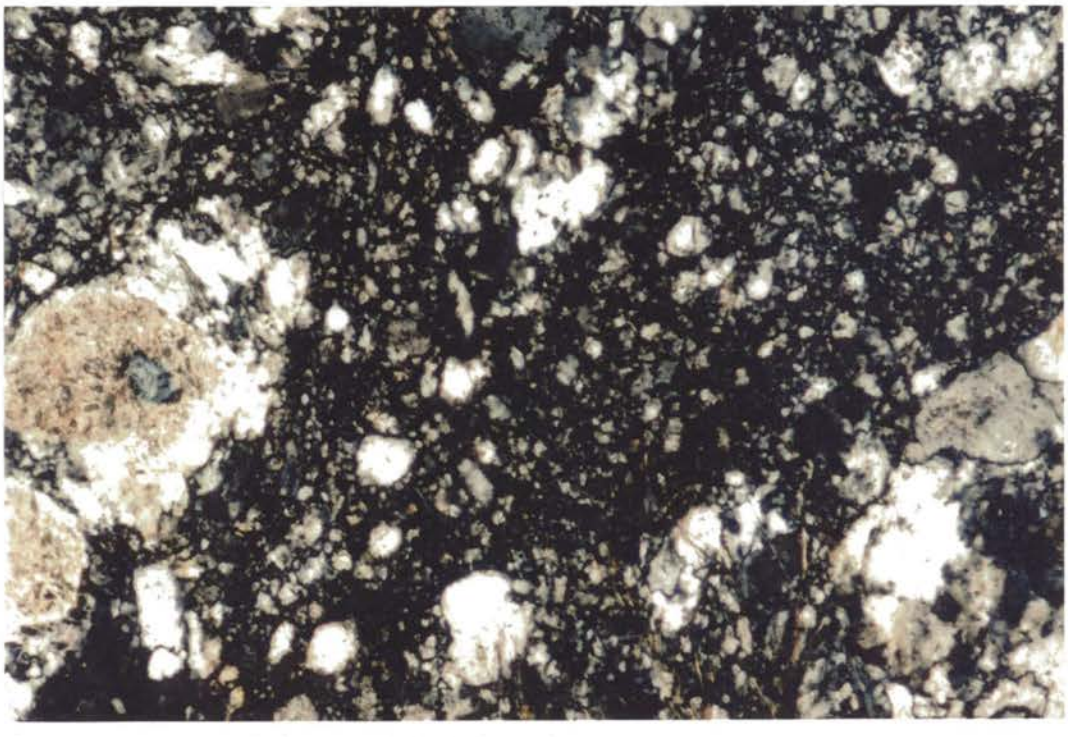

Plate 7.8 Narrow cataclasite zone within plagiogranite.
Sample No 169b UXP F.O.V 1.5mm

The metabasalts of the mélange can be genetically subdivided into those occurring as discrete lenses and those constituting enclaves within plagiogranite. Those occurring as discrete lenses are widespread and are believed to have been derived from the Jindalee Beds. They are dominantly amygdaloidal, although minor amounts of pillow basalt were observed, and have undergone lower greenschist facies metamorphism based on the assemblage albite+chlorite+quartz (Plate 7.9) (e.g. Menzies *et al.* 1977; Miyashiro 1994).

The metabasalts forming enclaves within the plagiogranite consist of actinolite and albite, indicative of greenschist facies metamorphism (e.g. Miyashiro 1994), and must have undergone fracturing and disruption prior to being incorporated by the plagiogranite.

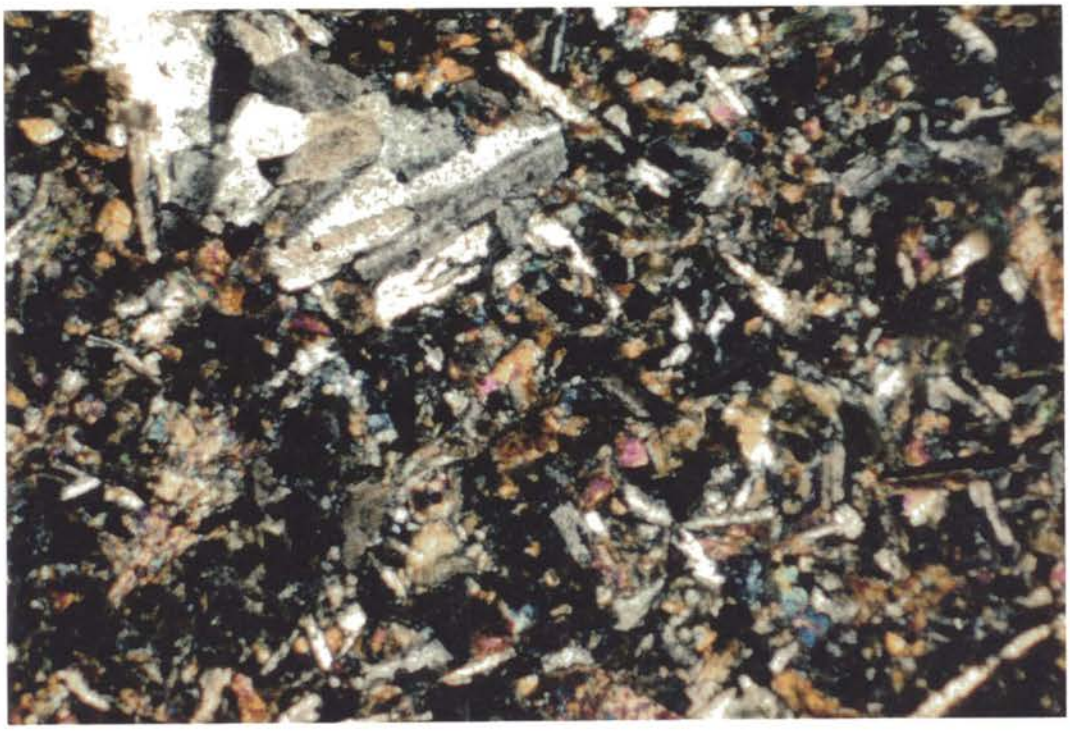

Plate 7.9 Albite-epidote-zoisite-chlorite metamorphic assemblage in metabasalt.
Sample No BF92/15b UXP F.O.V 3.5mm

Dacitic tuffs occur close to the western margin and near the centre of the unit (Figure 7.5). They are generally fine-grained and, in places, may be flow-banded and well-laminated. They are believed to have been derived from the Frampton Volcanics and now consist of the assemblage albite+quartz+zoisite+chlorite (Plate 7.10), indicative of greenschist facies metamorphism (e.g. Miyashiro 1994).

Rare quartzites are restricted to the eastern margin of the unit. They are highly recrystallised, strongly foliated, and are almost certainly derived from the Jindalee Beds. Other strongly foliated metasedimentary rocks within the western half of the unit and have been assigned to the Jindalee Beds by Wilson (1993).

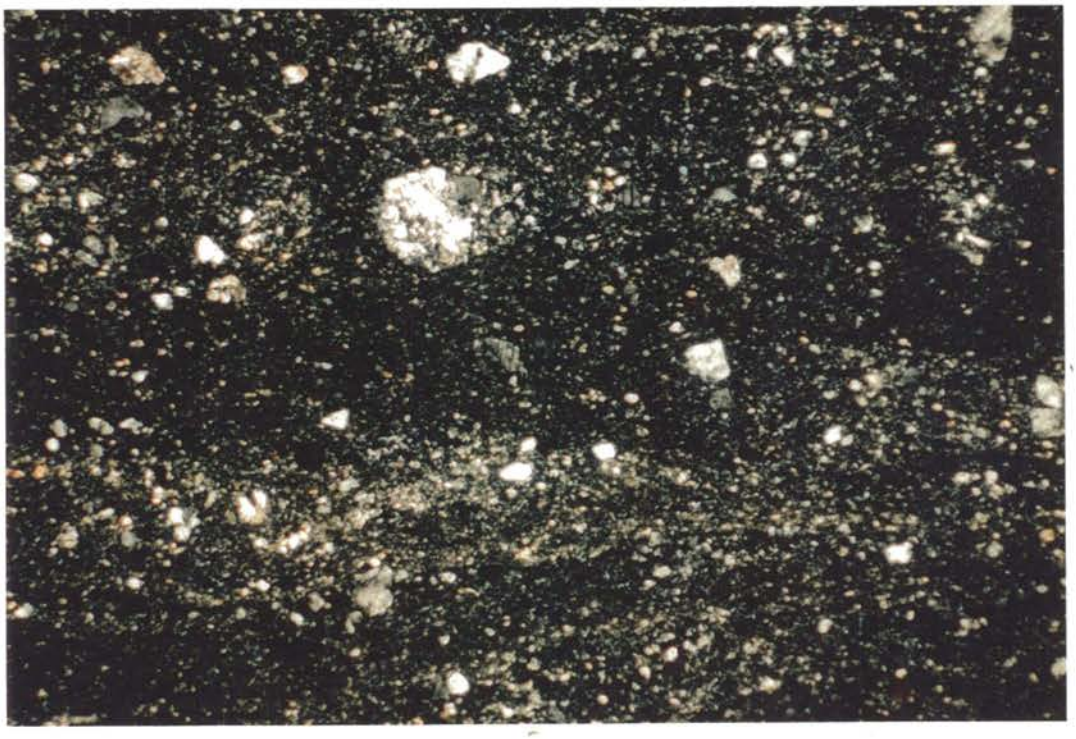

Plate 7.10 Laminar banded texture of meta-dacitic tuff.
Sample No WW4 (b) UXP F.O.V 3.5mm

7.3.4 Classification as a tectonic mélange unit

Greenly (1919) used "mélange" for a group of mixed rock types, now termed the Gwna mélanges (Wood 1974). They are believed to have formed by fragmentation of rock units followed by mixing with other units (e.g. Cloos 1984; Vollmer & Bosworth 1984; Raymond 1984). Raymond (1975, 1984) defined 'mélange' as:

'*a body of rock mappable at a scale of 1:24 000 or smaller and characterised both by the lack of internal continuity of contacts or strata and by the inclusion of fragments and blocks of all sizes, both exotic and native, embedded in a fragmented matrix of finer-grained material*'.

The Western Wambidgee Serpentinite Mélange satisfies most of the criteria in this definition with the exception that the differing rock types occur as discrete lenses, rather than blocks embedded within a finer-grained matrix. They constitute a discrete mappable unit and there is a lack of internal continuity. Based on Raymond (1984), the Western Wambidgee Serpentinite Mélange best classifies as a tectonic mélange.

CHAPTER 8: GEOCHEMICAL CHARACTER OF THE SERPENTINITE BELTS AND ASSOCIATED UNITS

8.1 PRIMARY ULTRAMAFIC ROCKS

The ultramafic rocks of the various serpentinite belts were analysed for their major, minor, trace and rare earth element geochemistries in order to identify any significant variation both within and between the various serpentinite belts, and to make comparison with similar rocktypes from other well-studied ophiolite occurrences.

8.1.1 Major and minor element geochemistry

Geochemical data for dunites and serpentinised dunites from the Coolac and Wambidgee serpentinite belts are shown in Table 8.1. Serpentinised dunite has a broader range in SiO_2, Fe_2O_3, FeO, MgO, CaO, H_2O, CO_2, Cr and Ni than weakly serpentinised dunite, and the latter is more enriched in TiO_2, Al_2O_3 and V. Serpentinised dunite from the Coolac and Wambidgee serpentinite belts has no significant compositional differences.

The compositions of harzburgite from the Coolac Serpentinite Belt are shown in Table 8.2. The data show that harzburgite is depleted in TiO_2, CaO, Cr, V, and the REE compared with dunite, and is similar in composition to serpentinised harzburgite.

Peridotite from the Tumut Serpentinite Province varies widely in composition (Table 8.3), particularly with respect to Fe_2O_3, MgO, CaO, CO_2, Cr and Ni. The compositional spread spans the range from harzburgite to pyroxenite.

lherzolite has been mapped in the Coolac, Wambidgee and Eurongilly serpentinite belts. Compared to harzburgite, dunite and peridotite, lherzolite is enriched in SiO_2, TiO_2, Al_2O_3, CaO, Na_2O, Ba, Sr, Ga and Zr, and depleted in MgO, Cr and Ni (Table 8.3). Compositional variation in lherzolite from the different belts is shown by SiO_2, Fe_2O_3, MgO, CO_2, Cr, Ni, V, Ba and Sr; lherzolite from the Eurongilly Serpentinite Belt is depleted in Cr and Ni compared to that from the Coolac and Wambidgee serpentinite belts.

Sample N	123	141	122	133b	135b	156b	ARC12	MU3899*	MU3864*	ARC15
Belt	CSB	CSB	CSB	CSB	CSB	CSB	CSB	CSB	CSB	WSB
Rocktype	WS Dun	WS Dun	Serp Dun	Serp Dun	Serp Dun	Serp Dun	Serp Dun	Serp Dun	Serp Dun	Serp Dun
SiO2	41.85	40.18	38.01	40.34	39.35	40.8	46.17	37.39	41.22	40.43
TiO2	0.3	0.09	0.02	0.01	b.d	0.01	0.11	0.01	0.03	0.02
Al2O3	1.59	5.76	1.13	0.23	0.17	0.37	2.03	0.78	0.98	1.52
Fe2O3	6.33	3.81	10.04	5.47	7.34	8.75	2.44	3.28	2.21	6.07
FeO	6.09	5.17	0.61	0.65	0.15	0.82	2.68	4.26	5.56	1.41
MnO	0.17	0.13	0.08	0.1	0.09	0.06	0.14	0.2	0.14	0.07
MgO	31.35	32.46	34.3	40.48	38.34	35.62	29.68	41.62	43.31	37.9
CaO	8.01	6.2	0.03	0.03	0.02	0.26	8.01	0.34	1.53	0.02
Na2O	b.d	0.03	b.d	b.d	b.d	b.d	0.04	b.d	0.04	b.d
K2O	b.d	0.01	b.d	0.01	b.d	b.d	0.01	b.d	b.d	b.d
P2O5	0.01	b.d	b.d	b.d	b.d	b.d	b.d	0.01	0.01	b.d
H2O+	4.58	6.62	12.8	11.99	14.29	12.17	8.2	11.19	5.43	12.23
CO2	0.12	0.08	0.05	0.23	0.2	0.44	0.13	0.11	0.05	0.08
H2O-	0.29	0.19	3.01	1.78	1.49	1.6	0.61	0.53	0.11	0.72
Cr	3276	2038	6876	1651	1866	1618	4955	2581	2868	3233
Ni	1101	1217	3339	2814	2651	3030	1585	2170	2234	3138
V	159	77	44	5	7	13	43	18	31	78
Cu	9	49	14	1	2	b.d	3	6	20	b.d
Pb	8	5	25	4	5	7	20			5
Zn	63	41	65	7	12	14	28	49	52	14
Rb	1	3	b.d	b.d	b.d	b.d	b.d			b.d
Ba	b.d	b.d	b.d	b.d	b.d	b.d	20			9
Sr	6	37	1	2	2	1	8			1
Ga	4	4	1	b.d	b.d	1	4			3
Nb	b.d	b.d	1	b.d	b.d	b.d	2			b.d
Zr	9	3	2	1	1	23	14			1
Y	10	4	1	b.d	1	2	2			b.d
Th	2	b.d	9	b.d	2	1	8			1

* data from Ashley 1973a
b.d = below detection limit
WS = weakly serpentinised

Table 8.1 Major and minor element analyses of dunites.

Table 8.2 Major and minor element analyses of harzburgites.

Sample No	74	139	ARC5	MLH01	G449-A*	MU3826*	MU3891*	MU3833*	MU2898*	MU3841*	MU3952*	MU3901*	MU3875*
Belt	CSB	CSB	CSB	CSB	CSB	CSB	CSB	CSB	CSB	CSB	CSB	CSB	CSB
Rocktype	Serp Harz	Wserp Harz	Serp Harz	Wserp Harz	Serp Harz	Serp Harz	Serp Harz	Serp Harz	Serp Harz	Serp Harz	Serp Harz	Serp Harz	Serp Harz
SiO2	40.57	40 08	43.84	41.57	41.79	42.47	39 47	43.51	40 13	42.42	42.56	41.97	42.29
TiO2	0.03	0	0 02	0.04	0 05	0 02	0 01	0 01	0.01	0.02	0.01	0 01	0.02
Al2O3	1.66	0.71	1.14	1.54	2.28	1 22	1 5	1 64	1 39	0.54	1 67	1.48	1.65
Fe2O3	5.31	4.97	7.46	2.91	1.4	1.83	4 52	1 57	2 41	5.74	1 35	2 79	2.44
FeO	2.06	2.04	0 49	5.01	6.25	5.22	3 11	6.34	5.21	3.61	6.32	4.76	5.24
MnO	0.12	0.11	0 13	0.13	0.11	0.15	0 1	0.14	0 13	0.22	0.15	0.14	0.14
MgO	38.5	39.16	29.78	41.85	39.52	37.2	39 17	41.28	41.23	37.54	40.91	40.27	40 4
CaO	0.01	0.02	1 09	1 85	2.35	1 6	0 49	1 52	0.37	1.05	1.56	1.42	1.73
Na2O	b.d	b.d	b.d	b.d	0.05	0 02	b d	0 01	b d	b.d	0 03	0 01	0.01
K2O	0.01	b.d	0.01	b.d	0.04	b.d	b d	0 02	0.01	0 01	0 04	0.04	0 02
P2O5	b.d	b.d	b d	b.d	b.d	0.01	b.d	0.01	0 01	0.01	0 01	0.01	0 01
H2O+	12.21	13.12	13.12	5.58	5.45	9.6	10 89	3.79	8.9	8.61	5.92	7.25	5.66
CO2	0.05	0.14	0.09	0 69	0 09	0.07	0.05	0 02	0.13	0.34	0.09	0.03	b.d
H2O-	0.56	0.63	3.97	0.25	0.03	0.09	0.24	0.09	0.27	0.1	0.16	0.17	0 34
Cr	2883	2436	2943	2881	2600	2672	2848	3013	2806	2951	2887	2899	2987
Ni	2426	2066	2520	2220	1340	1853	1995	2169	2113	2409	1996	2123	2079
V	53	26	42	47		30	54	41	45	4	46	34	42
Cu	2	4	2	5		82	5	21	14	11	16	16	24
Pb	5	3	5	4									
Zn	57	38	33	38		64	38	17	54	53	56	47	50
Rb	4	b d	1	b.d									
Ba	10	b.d	10	10									
Sr	1	2	3	4									
Ga	1	b d	3	3									
Nb	1	b.d	b.d	b.d									
Zr	b d	b d	b d	b.d									
Y	2	b d	1	1									
Th	1	1	b d	b d									

(Data source this thesis , Ashley 1973a, Basden 1990)

b d = below detection limit, wser = weakly serpentinised

Table 8.3 Major and minor element analyses of other primary ultramafic rocks.

Sample No	155c	155f	BF92/15a	61b	BF92/17b	BF91/33e	164	65	161b	161d	41e	41g	41d
Belt	CSB	CSB	WSB	WSB	WSB	WSB	WSB	WSB	GSB	GSB	ESB	ESB	ESB
Rocktype	Pyrox	Pyrox	Wehr	Wehr	Pyrox	Lherz	Perid	Hornbl	Perid	Perid	Lherz	Lherz	Lherz
SiO2	45.48	43.78	52.8	50.68	53.2	51.06	40.03	47.92	43.36	38.83	29.93	39.16	45.91
TiO2	0.62	0.43	0.05	0.07	0.08	0.75	0.01	1.02	0.1	0.04	0.47	0.86	0.29
Al2O3	16.46	9.77	1.03	1.48	1.85	4.65	0.51	8.38	1.65	0.87	4.47	4.91	6.84
Fe2O3	5.65	2.26	1.83	3.33	2.5	1.72	2.17	2	4.36	8.81	2.17	11.01	3.25
FeO	2.99	7.75	2.77	3.28	3.04	6.04	3.57	4.79	2.04	3.24	8.64	7.86	5.42
MnO	0.12	0.18	0.12	0.14	0.16	0.15	0.12	0.11	0.1	0.1	0.29	0.15	0.12
MgO	7.96	21.41	19.67	20.22	18.67	16.83	38.32	19.18	26.24	31.41	11.74	12.11	14.31
CaO	18.66	7.5	18.97	17.8	17.91	15.81	0.13	11.14	10.29	4.21	15.82	13.82	12.8
Na2O	0.45	0.43	0.04	0.06	0.19	0.72	b.d	1.94	b.d	b.d	0.02	0.34	0.47
K2O	0.03	0.04	b.d	b.d	0.01	0.05	b.d	0.14	b.d	b.d	0.01	0.07	0.16
P2O5	0.09	0.07	0.02	0.01	0.02	0.02	b.d	0.04	0.01	b.d	0.03	0.01	0.02
H2O+	2.32	6.42	2.58	3.19	2.4	2.21	9.85	3.12	6.66	10.04	2.68	2.55	3.98
CO2	0.04	0.02	0.13	0.08	0.26	0.14	5.02	0.18	4.32	2.24	23.24	6.25	6.64
H2O-	0.12	0.32	0.31	0.58	0.63	0.31	0.24	0.28	0.84	0.9	0.19	0.25	0.52
Cr	1060	1719	3197	2467	2290	3177	2538	960	3334	1663	910	165	596
Ni	138	1258	233	233	174	486	2027	956	925	1299	135	94	116
V	202	127	73	104	119	236	21	206	79	62	281	743	169
Cu	10	12	9	10	7	166	5	7	14	30	9	40	16
Pb	7	4	6	5	10	7	2	6	4	9	44	13	9
Zn	41	85	20	27	33	40	30	46	34	36	233	65	50
Rb	1	1	b.d	b.d	1	1	b.d	1	b.d	1	b.d	3	3
Ba	b.d	b.d	9	17	32	14	6	86	4	b.d	26	31	66
Sr	742	8	23	21	19	36	4	240	47	18	197	182	273
Ga	15	10	b.d	3	2	6	b.d	10	2	b.d	8	16	6
Nb	2	3	b.d	b.d	b.d	b.d	b.d	5	b.d	b.d	b.d	b.d	b.d
Zr	66	51	2	1	2	23	1	22	3	2	17	13	14
Y	18	15	2	2	3	14	b.d	9	2	1	8	6	6
Th	2	2	1	1	3	2	b.d	1	1	1	b.d	b.d	b.d

(Data source: this thesis; Ashley 1973a*; Basden 1990*)

b.d = below detection limit

Table 8.3 (continued) Major and minor element analyses of other primary ultramafic rocks.

Sample No	39	ARC14	MU3828*	M680/852*	MU3953*	MU3940*	MU3942*	MU3863*	MU3829*	MU3928*	MU3862*	MU3896*
Belt	MMSB	WSB	CSB	GSB	CSB	CSB	CSB	CSB	CSB	CSB	CSB	CSB
Rocktype	Wehr	Perid	Lherz	Pyrox	Wehr	Wehr	Wehr	Wehr	Wehr	Wehr	Wehr	Wehr
SiO2	43.58	41.68	44.71	49.3	47.59	44 17	46.11	37.01	46.97	46.25	50.52	39.84
TiO2	0.1	b.d	0 39	0.1	0.21	0.31	0.07	0.15	0 31	0.16	0 32	0 16
Al2O3	1.2	0.5	2 66	1.76	2.05	2.45	0.98	3.79	2 41	1.7	3.14	4 44
Fe2O3	5.68	7.33	3.67	4.11	2.8	4.89	3.91	8 66	4 35	5.22	2.01	4 91
FeO	3.07	1.3	5.42	3 08	2.5	2 79	3 39	7.11	3.72	4 02	3.55	3.96
MnO	0.12	0.11	0.2	0.15	0.15	0.13	0.16	0.23	0.15	0.16	0.14	0 16
MgO	32.84	35.95	26.25	17.3	24.38	27.04	24.67	29.97	21 99	24 48	21 39	33 82
CaO	2.36	0.27	12.44	18.5	14.72	10.92	14.99	4.99	15.78	13.58	17.66	3.41
Na2O	b.d	b.d	0.31	0.14	0.26	0.18	0.18	0 06	0.27	0.21	0.51	0.19
K2O	0.01	b.d	0.03	0.08	0.03	b.d	b d	0.01	0.02	b.d	0 04	0 04
P2O5	b.d	b.d	0.03	0.01	0.02	0.01	0 02	0.01	0.03	0.03	0.04	0 03
H2O+	10.47	12.24	4.26	1.4	4.12	6.27	3.88	7.39	3 83	4 43	1.75	9 64
CO2	0.38	0.11	0.06	1.92	0.1	0.14	b.d	0 08	0.13	0.05	0.1	0.05
H2O-	0.76	1.58	0.26	1.55	0.27	0.65	0.34	0 65	0 4	0 08	0.22	0 29
Cr	3012	2570	2055	1600	1986	2118	1797	2890	1758	1816	2699	2519
Ni	1355	2370	824	289	637	993	319	1217	583	408	739	1606
V	65	27	140	90	117	163	73	68	179	96	190	46
Cu	129	13	65	9	33	106	26	544	31	37	65	16
Pb	6	4	3	2	6	6	11	10	8	3	5	4
Zn	81	28	61	30	35	32	34	139	42	43	32	58
Rb	b.d	b.d	b.d	b d	b.d	b d	b.d	2	b d	b d	b.d	b d
Ba	17	16		50								
Sr	2	2	13	76	15	9	14	12	14	14	23	16
Ga	4	3	5	6	b.d	2	b d	2	b d	4	5	3
Nb	b.d	b.d		1								
Zr	2	b.d	11	10	5	8	2	4	9	b d	15	15
Y	3	b.d	9	7	5	6	3	2	8	4	10	5
Th	b.d	b d	b d	4	b d	b d	b d	b d	3	b d	b.d	b d

(Data source: this thesis; Ashley 1973a*, Basden 1990*)

b d = below detection limit

Compared with dunite, harzburgite and peridotite, pyroxenite is enriched in SiO_2, TiO_2, Al_2O_3, CaO, Na_2O, V, Ba, Sr, Zr and Y, and depleted in Fe_2O_3, FeO, MgO, Cr and Ni (Table 8.3). Pyroxenites from the Wambidgee and Gundagai serpentinite belts have similar compositions but differ from that of the Coolac Serpentinite Belt, which is enriched in TiO_2, Al_2O_3, FeO, Na_2O, V, Ni, Ga, Zr and Y, and depleted in SiO_2 and Ba.

Wehrlite occurs in all serpentinite belts and is similar to the lherzolite and pyroxenite (Table 8.3). Wehrlites from different belts are chemically similar with only minor variation in SiO_2, Fe_2O_3, FeO, MgO, CaO, Na_2O, H_2O, Cr, Ni and Cu.

Only one true hornblendite has been found within the Tumut Serpentinite Province. Compared to other primary ultramafic rocks, it is enriched in TiO_2, Al_2O_3, Na_2O, V, Ba, Sr, Zr and Y, and depleted in Fe_2O_3, MgO, Cr and Ni (Table 8.3).

8.1.2 Variation diagrams

Variation diagrams were constructed to investigate the relationships between the various ultramafic rocks of the Tumut Serpentinite Province. On all diagrams, the harzburgite data plot in restricted fields.

Mg# vs SiO_2 (Figure 8.1)

Weakly serpentinised harzburgite and serpentinised harzburgite of the Coolac Serpentinite Belt and the serpentinised dunites and peridotites from all the serpentinite belts plot in the same area. However, the weakly serpentinised dunites of the Coolac Serpentinite Belt can be differentiated, because of their distinctly lower Mg#. Lherzolite, pyroxenite, wehrlite and hornblendite, which are enriched in SiO_2, and have low and variable Mg#, cover a broad region, distinct from that of the dunites, harzburgites and peridotites.

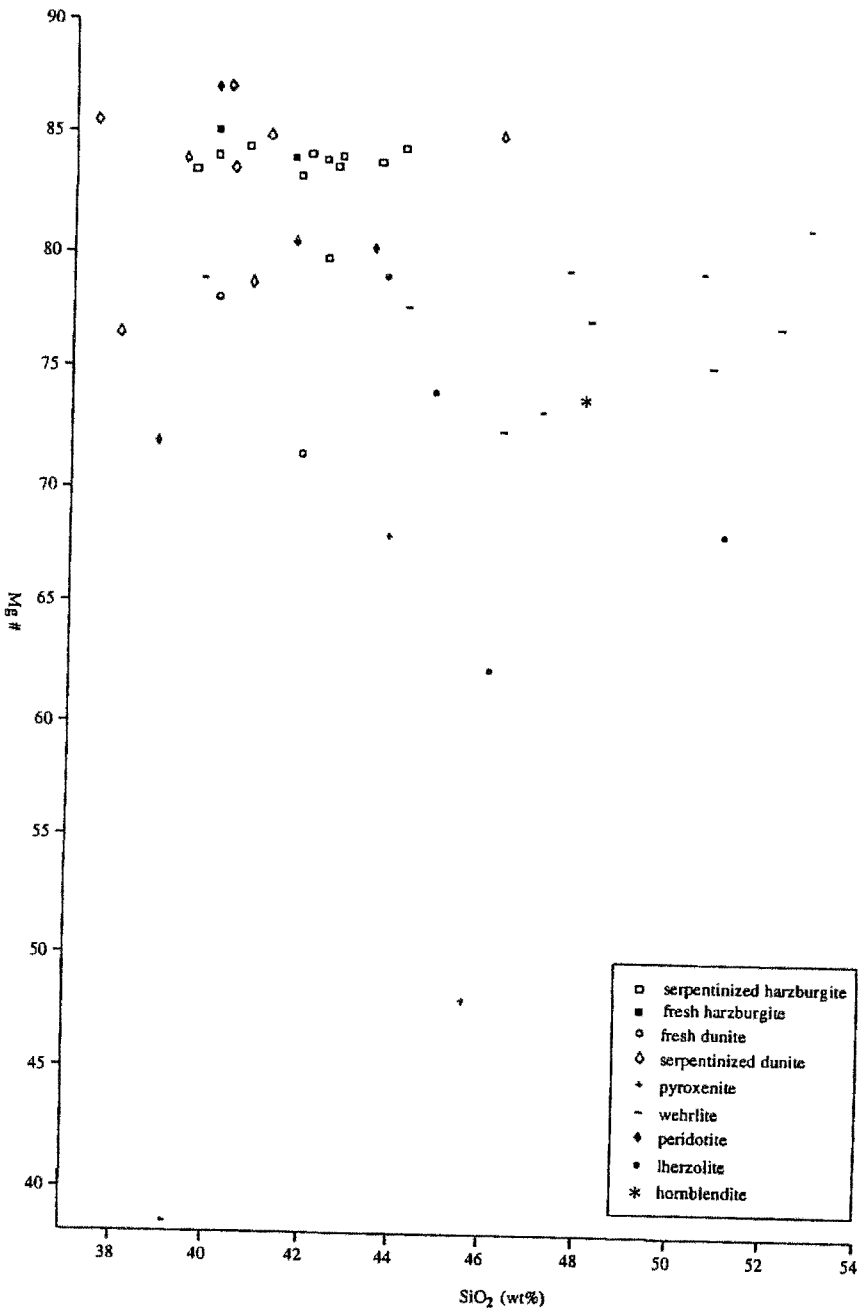

Figure 8.1 Mg# vs SiO_2 diagram for the primary ultramafic rocks of the Tumut Serpentinite Province (data from Tables 8.1, 8.2 and 8.3).

Mg# vs CaO (Figure 8.2)

Serpentinised dunites plot in the same area as the weakly serpentinised and serpentinised harzburgites of the Coolac Serpentinite Belt. However, as weakly serpentinised dunites are enriched in CaO compared to their serpentinised equivalents, they plot in a different area. Peridotites plot either with the harzburgites and serpentinised dunites, or, close to the weakly serpentinised dunites. Lherzolites, wehrlites and pyroxenites, which are enriched in CaO, plot in the same general area but distinct from the dunites, harzburgites and peridotites. Hornblendite plots in an intermediate position between weakly serpentinised dunite and serpentinised peridotite, and pyroxenite, wehrlite and lherzolite.

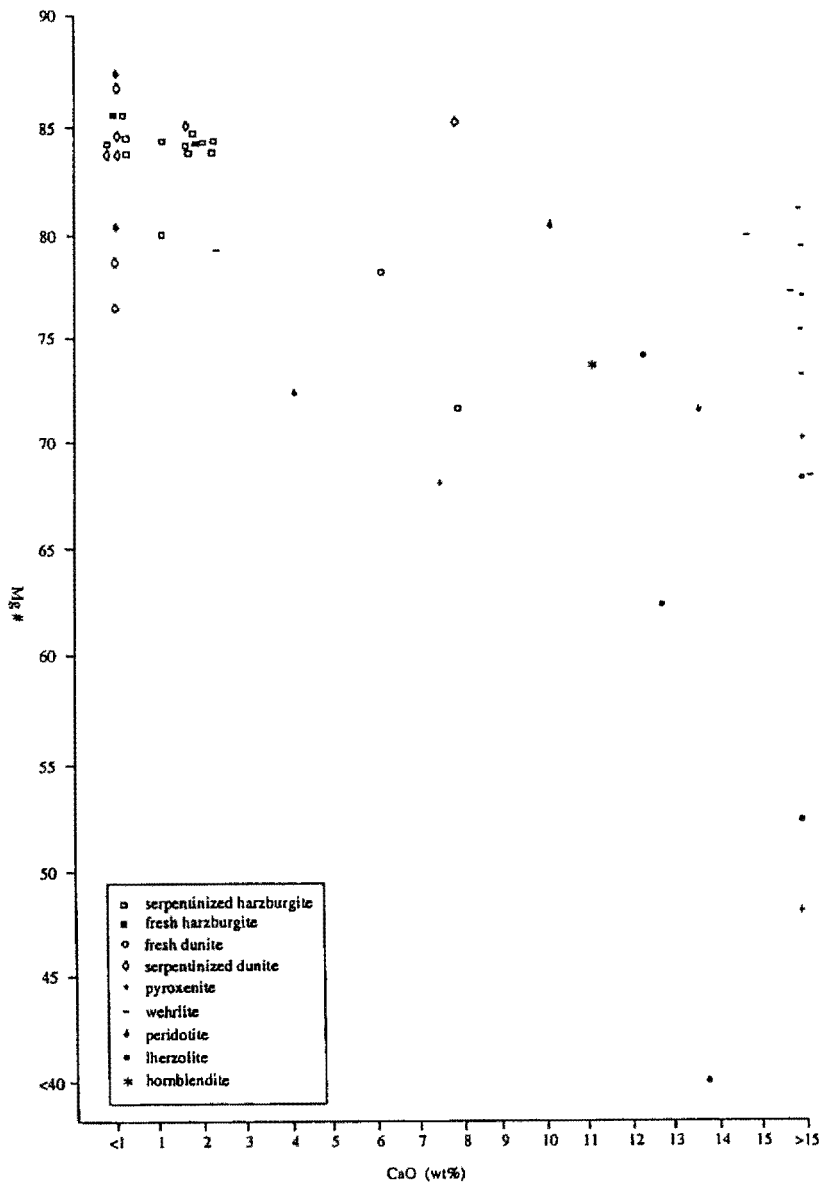

Figure 8.2 Mg# vs CaO diagram for the primary ultramafic rocks of the Tumut Serpentinite Province (data from Tables 8.1, 8.2 and 8.3).

Cr vs SiO_2 (Figure 8.3)

Weakly serpentinised and serpentinised dunites of the Tumut Serpentinite Province plot in different areas from the weakly serpentinised and serpentinised harzburgites of the Coolac Serpentinite Belt and the peridotites. Serpentinised dunites have more highly variable concentrations of Cr than the weakly serpentinised dunites and plot over a wide area. Because they contain more SiO_2, lherzolites of the Coolac and Wambidgee serpentinite belts plot together with the pyroxenites, wehrlites and hornblendite, and are separate from the dunites, harzburgites and peridotites. Because of their very low concentration of Cr, lherzolites from the Eurongilly Serpentinite Belt plot well away from all other analyses.

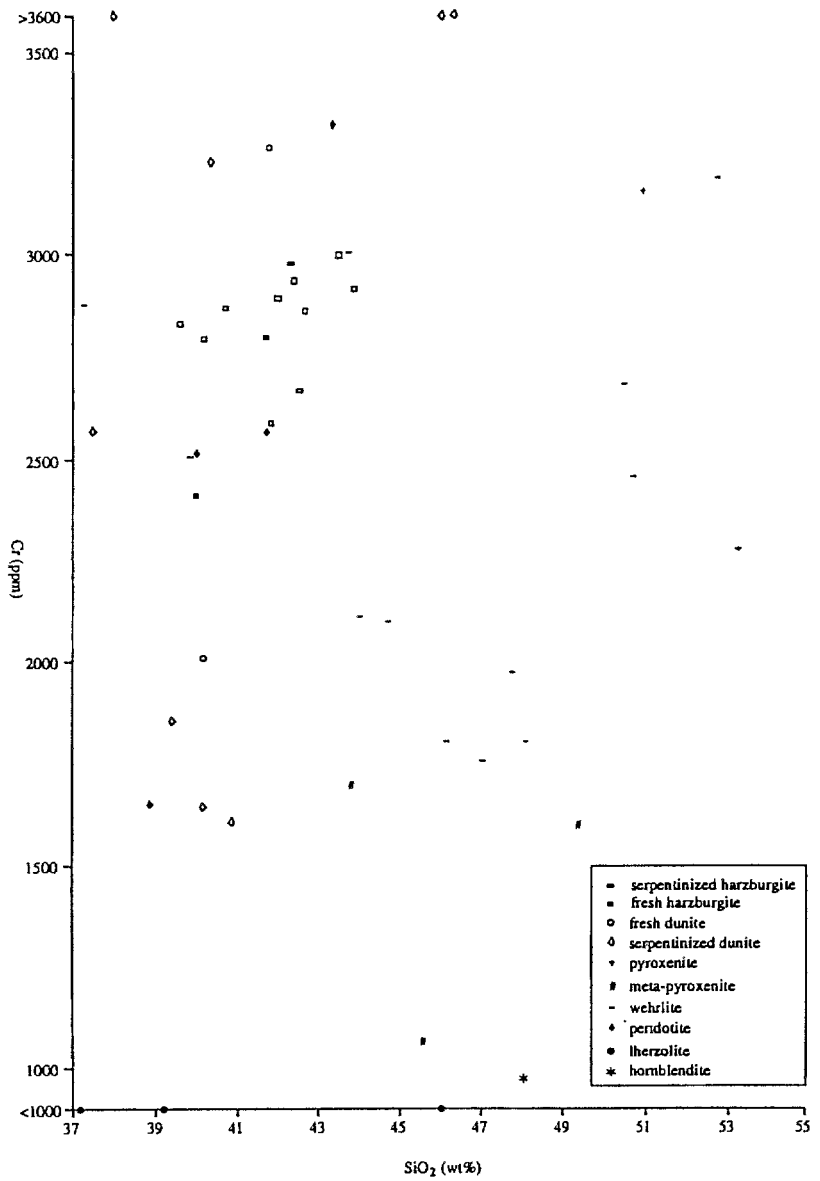

Figure 8.3 Cr vs SiO_2 diagram for the primary ultramafic rocks of the Tumut Serpentinite Province (data from Tables 8.1, 8.2 and 8.3).

Ni vs SiO_2 (Figure 8.4)

Weakly serpentinised dunites plot in a confined area while serpentinised dunites cover a wider area because of their highly variable and higher concentrations of Ni. Both the weakly serpentinised and serpentinised harzburgites of the Coolac Serpentinite Belt again plot in the same discrete field. Some peridotites plot in the same area as the harzburgites, whereas others plot in the same general area as the wehrlites, pyroxenites, lherzolites and hornblendite.

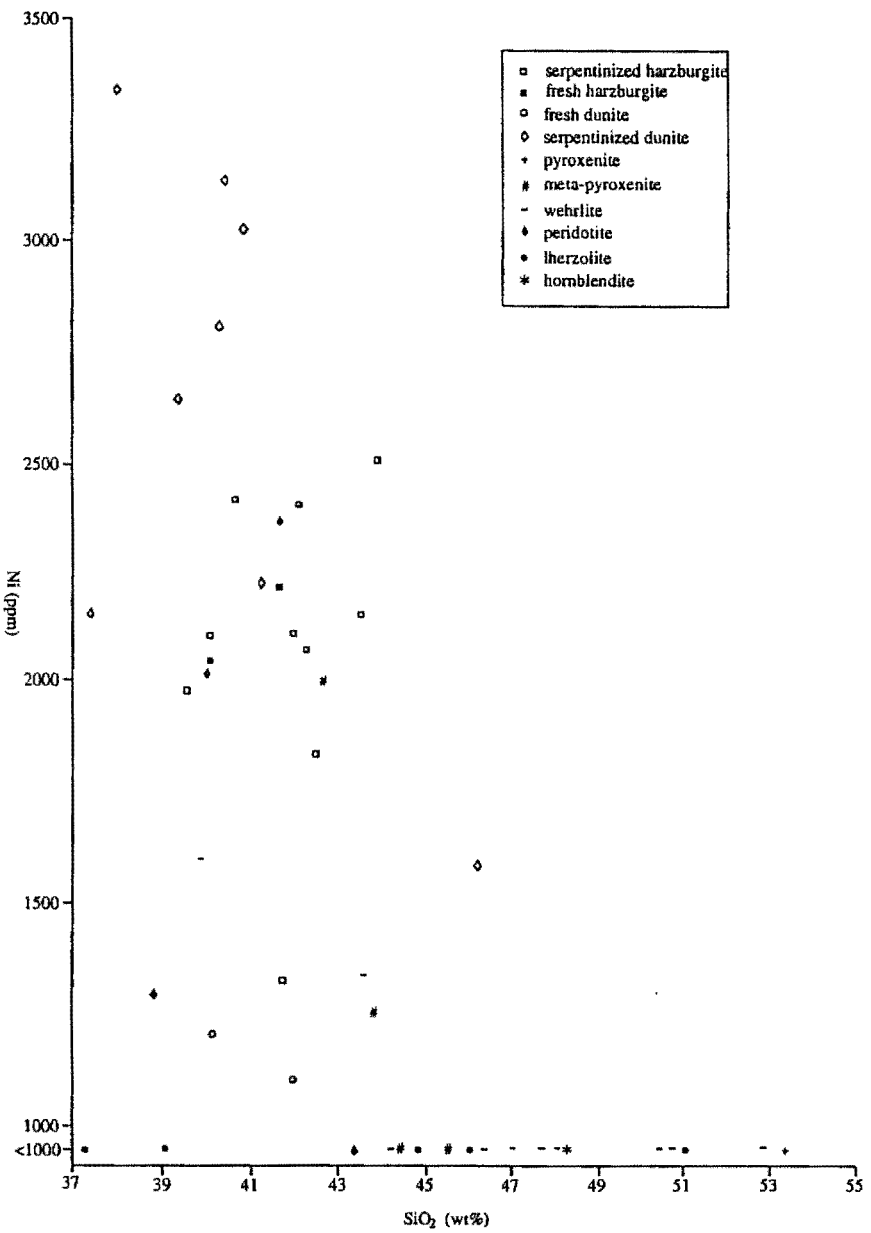

Figure 8.4 Ni vs SiO_2 diagram for the primary ultramafic rocks of the Tumut Serpentinite Province (data from Tables 8.1, 8.2 and 8.3).

8.1.3 REE and trace element geochemistry (Table 8.4)

Weakly serpentinised dunites of the Coolac Serpentinite Belt have low total REE concentrations and are slightly LREE-enriched. Serpentinised dunites from all belts also have low total REE concentrations, are enriched in La, Ce, Sb and As and depleted in Nd, Sm, Eu, Tb, Ho, Yb, Lu, Hf and Sc relative to weakly serpentinised dunites.

Harzburgites have very low total REE concentrations (on the detection limit). Compared to the dunites, they are REE-depleted. Serpentinised harzburgite is enriched in Sb and As, and depleted in Sc relative to weakly serpentinised harzburgite. The low Sc concentration in the completely serpentinised harzburgites compared to the weakly serpentinised harzburgites was also found within the Coolac Serpentinite Belt harzburgites by Ashley (1973a).

Two peridotites and a pyroxenite vein within the serpentinised layered peridotite, from the Fontenoy area of the Wambidgee Serpentinite Belt, were analysed for REE and trace elements. All are more enriched in total REE than the dunites and harzburgites. The serpentinised layered peridotite is similar to the weakly serpentinised peridotite, but the pyroxenite vein contains more REE. Both the pyroxenite vein and its serpentinised layered peridotite host are enriched in Sb and As compared to weakly serpentinised peridotite.

The low concentrations of incompatible elements and the rare earth elements within these rocks are similar to those found within tectonised peridotite of many ophiolite complexes (e.g. Coleman 1977). Nickel is hosted by olivine and pyroxene (e.g. Coleman 1977), nickel alloys (e.g. awaruite) and sulfides (e.g. heazlewoodite), the latter probably hosting the Co concentrations. The low concentrations of REE are due to the small modal proportions of clinopyroxene and plagioclase, the most likely REE-host minerals within ultramafic rocks (e.g. Menzies 1976). The low concentrations of Sc, Ti and V also reflect the low clinopyroxene content; this being the main host of Sc in such rocks (e.g. Ashley 1973a). The concentrations of As and Sb is ascribed to the disseminated arsenides and antimonides within fracture-fill assemblages.

Table 8.4 Rare earth and trace element analyses of primary ultramafic rocks.

Sample No	MLA01	123	135b	139	155c	155f	211	BF91/33e	34	36	65	65	225avein
Belt	CSB	CSB	CSB	CSB	CSB	CSB	CSB	WSB	WSB	WSB	WSB	WSB	WSB
Rocktype	WS Hz	WS Dun	S Dun	WS Hz	F Pyrox	A Pyrox	S Dun	Lherz	S Dun	S Dun	Hornbl	Perid	Pyx vein
La	0.09	1.01	0.05	0.1	6.06	4.86	0.51	2.3	1.54	0.49	9.2	0.53	4 18
Ce	0.28	0.82	b.d	0.3	12.91	9.01	1.73	7.21	3.39	1 04	18.63	1.86	13.06
Nd	b.d	3.22	b.d	b.d	8 81	6.93	1.49	6.28	2.19	b d	9.14	1.96	11.37
Sm	0.08	1.19	0 04	0.06	2.42	1.77	0.51	1.98	0.55	0 16	1.79	0.69	3.68
Eu	0 05	0.25	b.d	0.06	0.87	0 54	0.14	0.54	0 1	0.05	0 53	0.24	0.5
Tb	b.d	0.23	b.d	b.d	0 51	0 45	0 11	0 31	0 1	b d	0.23	b.d	0.61
Ho	b.d	0.28	b.d	b.d	0.7	0.61	0.16	0 42	0 11	b.d	0.25	b.d	0 42
Yb	0.16	0.73	0.04	0.07	1.63	1.17	0.41	0.85	0.19	0.06	0.6	0.36	0.61
Lu	0.03	0.11	b.d	0.01	0.22	0.14	0 06	0.1	0.02	0.01	0.09	0.043	0.08
Sb	b.d	b.d	b.d	b.d	0.52	b.d	b.d	0.21	b.d	0.65	b.d	b d	0.7
As	b.d	b.d	b.d	b.d	b d	0.86	0.92	b.d	3 63	5.35	b.d	b.d	3.18
Cr	2650	2660	2170	2428	876	1440	3800	2660	46900	3259	814	885	3210
Co	113	158	117	100	67.3	86.6	108	75.6	118	85.5	91.1	71.2	120
Au	b.d	b.d	b.d	b.d	b.d	b.d	b.d	12	b d	b.d	b.d	b.d	19.5
Hf	0.19	0.31	b.d	b.d	1.95	1.26	b.d	1.94	b.d	b d	0.84	0.59	2.26
Ir	b.d	b.d	b.d	b.d	b.d	b d	b d	b d	15 8	b.d	b.d	b d	b.d
Sc	10.2	37.6	3.65	5 76	32.3	22.5	4 58	51.1	5.2	8.34	28 1	24.3	18 4
Ta	0 37	0.28	b.d	b.d	0.58	b.d	b d	b d	b.d	0.21	0.28	b.d	1.64
Th	b.d	b.d	b d	b.d	1.66	1 19	b.d	0.38	b d	b d	0.48	b.d	b d

(Data source: this thesis)

b.d = below detection limit

Table 8.4 (continued) Rare earth and trace element analyses of primary ultramafic rocks.

Sample No	225aPerid	WW2	WW3	BF92/15a	BF92/17b	203	215	216	41d	41g	39	141	234	249
Belt	WSB	WWSM	WWSM	WWSM	WWSM	GSB	GSB	GSB	ESB	ESB	MMSB	NMC	NMC	TPSB
Rocktype	S Perid	Ol Webs	Pyrox	Pyrox	Pyrox	Pyrox	S Harz	Pyrox	Lherz	Lherz	Wehrl	WS Dun	Peg Pyx	A Pyrox
La	1.72	0.39	1.1	0.39	0 44	0.39	0 18	1.06	2.27	1.87	0.65	0 37	0.55	3.9
Ce	3.73	1.07	2.67	1.35	0.99	1.32	0 61	1.41	6 92	6.03	0 82	1.05	1 8	10.8
Nd	2.3	1.02	1.75	1.29	1.23	1.42	b.d	1 9	6.29	6.2	1.12	1 02	1.72	8.53
Sm	0.7	0.41	0.55	0.41	0 48	0 63	0.17	0.58	1.94	2.38	0.3	0.35	0.58	2.61
Eu	0.19	0.15	0.15	0.11	0.12	0.26	0.06	0.17	0.63	0.64	0 17	0 14	0.2	0.83
Tb	0.14	0.1	0.11	b.d	0 11	0.14	b.d	0.1	0.28	0.43	b.d	b.d	b.d	0 42
Ho	0.16	0.13	0.15	0.11	0.13	0.15	b.d	0 12	0.32	0.36	0.11	0.13	b d	0.4
Yb	0.15	0.19	0.31	0.15	0.32	0.16	0 14	0.21	0 39	0.47	0.27	0.35	0.372	0 64
Lu	0 02	0.02	0 04	0.02	0.04	0.02	0.02	0.02	0.03	0.06	0.03	0.05	0.052	0.08
Sb	0.31	0.17	0.41	0.7	0.32	b.d	3.62	0.63	1.94	1.63	0.78	b.d	b.d	b.d
As	1.63	b.d	b.d	b.d	b.d	2.18	54.2	5.31	5 46	6.99	7.62	b.d	b.d	b.d
Cr	1690	1190	1800	2790	1880	2280	1460	1580	475	138	2600	1910	2990	1500
Co	88	49.7	62.9	58.7	53.4	82 4	109	73.1	65 8	75.2	78.3	111	57 4	60 9
Au	b d	b.d	b.d	b.d	b d	b.d	b.d	b d	b.d	b.d	b d	b.d	b d	b.d
Hf	b.d	b.d	b d	b.d	b.d	b.d	b.d	b.d	0 46	0.63	b d	b d	b d	0 49
Ir	b.d	b.d	b.d	b.d	b d	b d	b.d	b d	b.d	b.d	b d	b.d	b d	b.d
Sc	7.08	57.6	75.8	39 5	58.9	42	4.47	38.2	68 3	73 9	42	21 9	58	64
Ta	b.d	b.d	b.d	b.d	0 35	0 44	b.d	b d	0.32	0.6	0.32	b d	0 82	b.d
Th	b d	b.d	b.d	b.d	b d	b d	b d	b d	b d	0 35	b d	b.d	b d	b.d

(Data source: this thesis)
b.d = below detection limit

Chondrite-normalised REE data for dunite, harzburgite and peridotite, and their serpentinised equivalents, are presented in Figure 8.5. Salient points include:

(a) Most patterns are flat to slightly concave downward, the principal exception being a serpentinised dunite;

(b) Weakly serpentinised and serpentinised harzburgites are depleted, whereas two out of three weakly serpentinised and serpentinised dunites and peridotites are enriched;

(c) A Ce trough is exhibited by one of the weakly serpentinised dunite samples;

(d) Minor Eu troughs characterise one of the peridotites and several of the serpentinised dunites;

(e) An Eu peak is shown by one of the weakly serpentinised harzburgites.

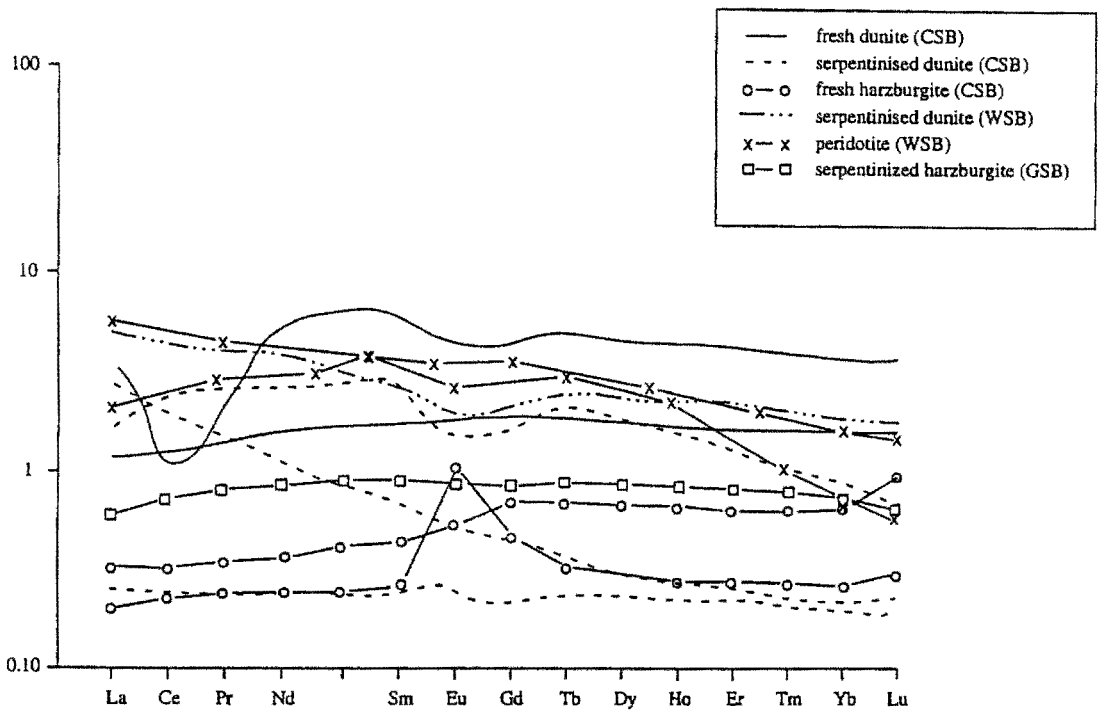

Figure 8.5 CN-REE diagram for the dunites, harzburgites and peridotites (data from Table 8.4)

Lherzolites are enriched in total REE compared to the harzburgites and dunites (Table 8.4). Lherzolites from the Wambidgee and Eurongilly serpentinite belts have similar REE and trace element geochemistry, whereas lherzolite from the Western Wambidgee Serpentinite Melange is significantly depleted. All are LREE-enriched with significant concentrations of Sb, Hf and Sc.

Pyroxenites are enriched in total REE concentrations compared to most of the other primary ultramafic rocks (Table 8.4). Pyroxenites from the Coolac Serpentinite Belt are more enriched in total REE compared to those from the other belts. All pyroxenites are also LREE-enriched and contain significant Sb, As, Sc and Ta.

Wehrlites are enriched in total REE compared to the dunites and harzburgites but depleted compared to the lherzolites and pyroxenites. They are moderately enriched in total REE and, like all of the other primary ultramafic rocks from the Tumut Serpentinite Province, are LREE-enriched (Table 8.4). The wehrlites also contain significant concentrations of Sb, As and Sc.

The single hornblendite analysis is highly enriched in total REE compared to all of the other primary ultramafic rocks (Table 8.4). It most resembles the REE geochemistry of the pyroxenites from the Coolac Serpentinite Belt and also contains significant concentrations of Hf, Sc and Ta.

Chondrite-normalised REE data for lherzolite, pyroxenite, wehrlite and hornblendite, and their serpentinised equivalents, are presented in Figures 8.6 and 8.7. Salient points include:

(a) Nearly all patterns are flat to moderately convex upward, but hornblendite is moderately concave upward;
(b) All are enriched;
(c) Ce troughs are exhibited by a pyroxenite and a wehrlite;
(d) Eu troughs are exhibited by a lherzolite, tthree clinopyroxenites and a wehrlite;
(e) A minor Eu peak is shown by a wehrlite.

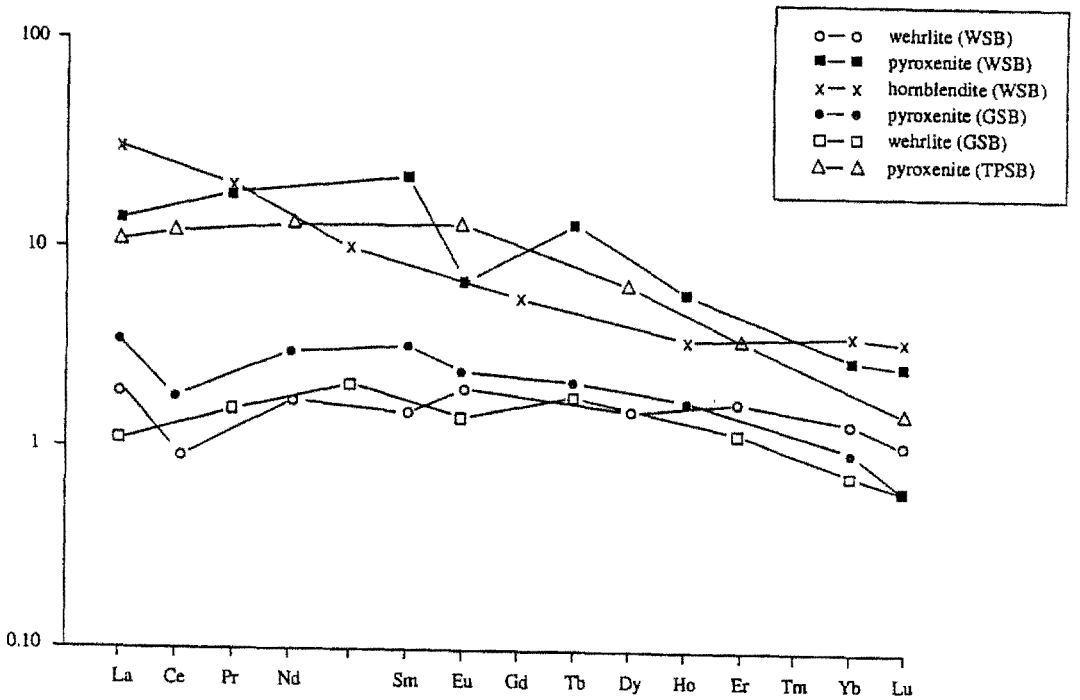

Figure 8.6 CN-REE diagram for the pyroxenites, wehrlites and hornblendite (data from Table 8.4).

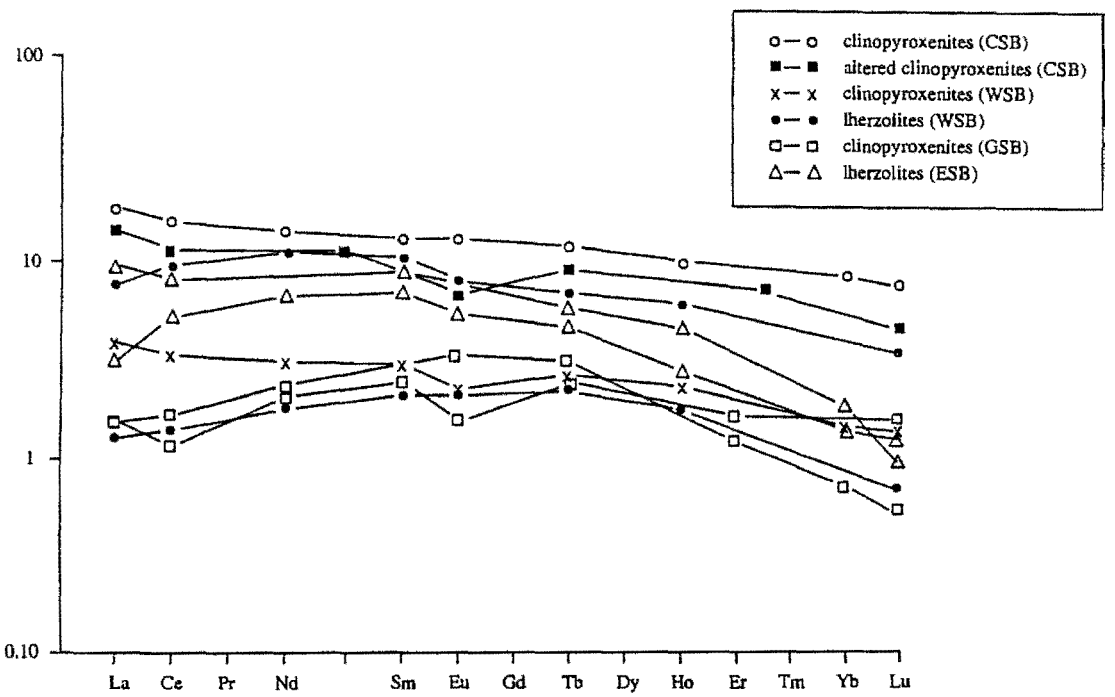

Figure 8.7 CN-REE diagram for the lherzolites and clinopyroxenites (data from Table 8.4).

8.1.4 Discussion

Dunites

Major element geochemistry shows that serpentinisation induced localised remobilisation of SiO_2, Fe_2O_3, FeO, MgO, CaO, Cr and Ni, gains in H_2O and CO_2, and losses in TiO_2, Al_2O_3 and V. This partly confirms the study of Graham *et al.* (1994), who reported that progressive serpentinisation of the primary ultramafic rocks of the Coolac Serpentinite Belt caused substantial decreases in Al_2O_3, FeO and CaO, and small increases in Ni and V. Localised remobilisation of Cr and Ni is further supported by the distribution of dunite and serpentinised dunite on the Cr vs SiO_2 and Ni vs SiO_2 diagrams (Figures 8.3, 8.4 respectively).

The results are in general accordance with those of Ashley (1973a) and Ashley *et al.* (1979) who found that serpentinisation of the Coolac Serpentinite Belt resulted in relatively constant total Fe, MgO, SiO_2, Cr and Ni, a decrease in Al_2O_3 and CaO, and gradual decreases in Mn, Ti, Sc, Cu and Zn. Ashley (1973a) also found that S and H_2O^+ increased significantly during serpentinisation. This in accords with Coleman (1977) who reported that serpentinisation is generally isochemical and that the only introduced component is H_2O.

Because weakly serpentinised dunite from the Coolac Serpentinite Belt has a distinctly lower Mg# than the weakly serpentinised harzburgite that hosts it, they are precluded from having the same parental magma. This is further confirmed on the Cr vs SiO_2 and Ni vs SiO_2 diagrams (Figures 8.3, 8.4) where the weakly serpentinised dunite and harzburgite of the Coolac Serpentinite Belt have separate distributions.

REE and trace element data suggest that serpentinisation of dunite was accompanied by La, Ce, Sb and As gains and, just possibly, Sm, Eu, Hf and Sc losses. Overall, weakly serpentinised and serpentinised dunites have low total REE abundances, in keeping with dunites of the Semail Ophiolite (Pallister & Knight 1981), Troodos Ophiolite (Kay & Senechal 1976) and alpine peridotites in general (Loubet *et al.* 1975). The flat CN REE patterns for dunites from the Tumut Serpentinite Province are similar to those from the Troodos Ophiolite (Kay & Senechal 1976), the Point Sal Ophiolite (Menzies *et al.* 1977), serpentinised dunites from Western Norway (Garmann *et al.* 1975) and alpine peridotites in general (Loubet *et al.* 1975).

Serpentinised dunites and a weakly serpentinised dunite from the Tumut Serpentinite Province have Eu troughs. Most dunites from the Semail Ophiolite exhibit –ve Eu anomalies, although there are a few +ve exceptions (Pallister & Knight 1981), whereas most peridotites from the Troodos Ophiolite have +ve Eu anomalies (Kay & Senechal 1976). Alpine type peridotites generally lack anomalies, but a –ve Eu anomaly in the Lizard Complex of Cornwall is an exception (Loubet *et al.* 1975). Menzies *et al.* (1977) found that dunites from the Point Sal Ophiolite lack anomalies, yet serpentinised dunites from west Norway have weak –ve Eu anomalies (Garmann *et al.* 1975). The -ve Eu anomalies of dunites from the Coolac Serpentinite Belt are ascribed to crystallisation from a MORB-type melt within small dyke-like conduits, such that Eu was lost to the harzburgite host.

Negative Ce anomalies have been ascribed (Menzies *et al.* 1977) to interaction with sea-water, but this cannot apply to weakly serpentinised dunite, which has experienced negligible serpentinisation. Neal & Taylor (1989) attributed a -ve Ce anomaly within a weakly serpentinised peridotite xenolith from a lamprophyre, to the input from pelagic sediment subducted into the mantle. However, more data are needed before any particular model can be seriously considered.

Harzburgites

Fresh harzburgite is a highly depleted rock (Nicolas 1989) and, because of this, has only a small concentration of mobile elements. Serpentinised harzburgite, therefore, differs little in composition from the fresh parent. The low concentration of alkalies within the harzburgites of the Coolac Serpentinite Belt was also found by Ashley (1973a), Franklin (1975) and Ray (1977). Ashley (1973a) stated that serpentinisation of the harzburgites resulted in decreases of Al_2O_3 and CaO and gradual decreases in Mn, Ti, V, Sc, Cu and Zn, as also substantiated by the present study. Both Ashley (1973a) and Coleman (1977) found that ultramafic rocks maintain a relatively constant composition during serpentinisation, with the only added components being H_2O and possibly S. The overall composition of the Coolac Serpentinite Belt harzburgites (Table 8.2) is akin to that of harzburgites from other well-studied ophiolites (e.g. Coleman 1977)."

The depleted harzburgites (both weakly serpentinised and serpentinised) plot in a discrete field on the variation diagrams, well away from other primary ultramafic rocks. Their low total REE concentration is similar to those for harzburgites from the Semail Ophiolite (Pallister & Knight

1981), Troodos Ophiolite (Kay & Senechal 1976), Othris Ophiolite (Menzies 1976), Point Sal Ophiolite (Menzies *et al.* 1977) and alpine peridotites in general (Loubet *et al.* 1975). Likewise, their flat CN REE patterns, and +ve Eu anomalies (weakly serpentinised harzburgite only), are similar to those reported from the Troodos Ophiolite (Kay & Senechal 1976; Menzies 1976) and alpine peridotites in general (Loubet *et al.* 1975). The REE depletion is consistent with the lack of significant concentrations of clinopyroxene and plagioclase (the two main REE "collectors" in ultramafic rocks - Menzies 1976).

Because the harzburgites of the Tumut Serpentinite Province are highly depleted, partial melting would be incapable of creating a substantially more "enriched" magma, even if a large portion of the harzburgite was involved.

Peridotites

The composition of the weakly serpentinised peridotites largely reflects the Cpx to Ol ratio and therefore spans the range from harzburgite (depleted in Cpx) to pyroxenite (enriched in Cpx). Conversely, the Fe_2O_3 and CO_2 contents reflect the degree of serpentinisation. These factors are embodied in the variation diagrams (Figure 8.1 and 8.2).

The relative enrichment in REE of peridotite compared with harzburgite and dunite reflects the higher concentration of Cpx, as is to be expected (e.g. Garmann *et al.* 1975; Menzies 1976). Because the serpentinised peridotite has a similar REE chemistry to weakly serpentinised peridotite it would seem that the REE have been generally immobile during serpentinisation. The enrichment of the serpentinised layered peridotite in Sb and As strongly suggests that the two elements were concentrated (and hence, mobile) during serpentinisation.

The flat CN REE pattern for weakly serpentinised peridotite (Figure 8.5) is similar to the weakly serpentinised harzburgite and dunite, and also to peridotites from the Troodos Ophiolite (Kay & Senechal 1976) and alpine-type peridotites in general (Loubet *et al.* 1975). The downward CN REE curve for the serpentinised layered peridotite is similar to serpentinised dunites from West Norway (Garmann *et al.* 1975) and lherzolites from the Massif Central (Menzies 1976).

Lherzolites

The overall major element chemistry of the Tumut Serpentinite Province lherzolites shows that they are far less depleted than harzburgites, dunites and peridotites, and formed from a more evolved melt (Figure 8.2). The high concentrations of Cr and Ni in lherzolites from the Coolac and Wambidgee serpentinite belts is consistent with derivation from the same magma as the dunites and peridotites. However, lherzolite from the Eurongilly Serpentinite Belt has distinctly lower Cr and Ni concentrations than ultramafic rocks in general (Wyllie 1967) and mantle sequence lherzolites from the Halmahera Ophiolite (Ballantyne 1992), in particular. This requires that the Eurongilly lherzolite formed from a Cr and Ni-depleted source and suggests a different geotectonic environment from that of the lherzolites from the other belts. Significantly, the Eurongilly Serpentinite Belt is the westernmost belt and lies 50km west of the Wambidgee Serpentinite Belt.

The high concentration of REE within lherzolite reflects the abundance of clinopyroxene, this mineral being the "sink" for REE and Sc within ultramafic rocks (Neal & Taylor 1989; Menzies *et al.* 1977). Despite the low Cr and Ni contents, of the Eurongilly Serpentinite Belt lherzolite, the trace element geochemistry is indistinguishable from lherzolites in the other serpentinite belts (Figure 8.7).

The concave upward CN-REE patterns of most of the lherzolites, are similar to those from the Troodos and Othris ophiolites (Menzies 1976), whereas the Eurongilly Serpentinite Belt lherzolite has some similarity to those of the Massif Central (Menzies 1976). The -ve Eu anomaly of one lherzolite sample from the Eurongilly Serpentinite Belt is ascribed to removal of plagioclase from the lherzolite-forming magma (e.g. Pallister & Knight 1981 - for the Semail Ophiolite).

Pyroxenites/Wehrlites

The overall difference in major element chemistry between the pyroxenites/wehrlites of the Tumut Serpentinite Province and the harzburgites, dunites and peridotites is simply a reflection in the differing modal proportion of Cpx (Figure 8.2). Compared to pyroxenites from the other belts, those from the Coolac Serpentinite Belt are enriched in a number of elements, some mobile (e.g. Na_2O) and some immobile (e.g. Zr). The enrichment and depletion in the mobile elements such as Na_2O and CaO can be attributed to serpentinisation of the pyroxenites within the Coolac Serpentinite

Belt, which are significantly more serpentinised/altered than those from the other belts. However, the enrichment in immobile elements such as Ti and Zr, within the pyroxenites of the Coolac Serpentinite Belt compared to those of the other belts cannot be due to serpentinisation/alteration, but must instead be due to a difference in the source magma from which these pyroxenites were derived.

Wehrlites from all the different serpentinite belts are similar and this is ascribed to their formation under similar geotectonic conditions from similar source magmas. Differences are attributed to differing degrees of alteration. The difference in composition of the pyroxenite/wehrlite in Cr compared to the other ultramafic rocks, is attributed to the modal amount of Cr-spinel. The highly variable concentrations of Ni within the pyroxenites reflects differing modal proportions of olivine (i.e. the Ni "sink" within ultramafic rocks) (Figures 8.3 and 8.4).

Differences in REE concentration between pyroxenite, wehrlite, and lherzolite is mainly due to differing concentrations of Cpx which is the main "sink" for the REE within ultramafic plagioclase-deficient rocks (Neal & Taylor 1989) (Figures 8.6 and 8.7). This is also reflected in the concentration of Sc within these rocks, which increases in concentration with increasing modal proportion of clinopyroxene (Menzies *et al.* 1977). Pyroxenite from the Coolac Serpentinite Belt is more enriched in REE.

Pyroxenites of the Point Sal Ophiolite exhibit weak upward CN REE patterns (Menzies *et al.* 1977) with moderate +ve Eu anomalies. However, those from the Tumut Serpentinite Province differ from this in having flat curves with no anomalies or strongly concave upward curves. Some of these pyroxenites also exhibit weak -ve Eu anomalies, and a pyroxenite sample from the Gundagai Serpentinite Belt exhibits a moderate -ve Ce anomaly.

Wehrlites from the Tumut Serpentinite Province exhibit similar patterns (much like the pyroxenites from the Gundagai Serpentinite Belt and Tumut Ponds Serpentinite Belt) though have weak +ve and -ve Eu anomalies, and one sample also exhibits a weak -ve Sm anomaly and a moderate -ve Ce anomaly (Figure 8.6).

Hornblendite

Hornblendite differs in major element composition from other primary ultramafic rocks of the Tumut Serpentinite Province. This is ascribed to the formation of the hornblendite in a hydrous environment from a more evolved (e.g. enriched in Ti, Al, Na, Zr and Y; depleted in Mg, Fe, Cr and Ni) magma.

The high relative enrichment in REE of this hornblendite compared to the other primary ultramafic rocks of the Coolac Serpentinite Belt is ascribed to differing mineralogy (i.e. hornblende-rich) and from it having crystallised with a higher proportion of trapped interstitial liquid (Kay & Senechal 1976) (Figure 8.6).

Lack of an Eu anomaly within the CN REE pattern for the hornblendite suggests that both plagioclase accumulation and plagioclase removal were not operating during its crystallisation from the source magma.

8.2 SERPENTINITES

8.2.1 Major and minor element geochemistry

Analytical data for massive and schistose serpentinite from the various belts of the Tumut Serpentinite Province are presented in Table 8.5. The majority of the serpentinites are compositionally similar, regardless of host belt and whether they are massive or schistose.

Despite the overall compositional similarity, there are minor variations. Schistose serpentinites of the Coolac Serpentinite Belt are depleted in Al_2O_3, FeO, MnO, CaO, Cr, Ni, V, Cu and Zn compared to the massive serpentinites. Conversely, schistose serpentinites of the Wambidgee and Tumut Ponds serpentinite belts contain more FeO and Ni than the massive varieties. Most of the serpentinites contain minor amounts (generally, <3 modal%) of other secondary phases such as tremolite, talc and magnesite, which may account for some of the compositional variation in these rocks.

8.2.2 Variation diagrams

On the Mg# vs SiO_2 diagram (Figure 8.8), serpentinites overprint the field of weakly serpentinised harzburgites and peridotites. This is consistent with principally harzburgite and to a lesser extent peridotite, being the precursor primary ultramafic rocks for the serpentinites from the Tumut Serpentinite Province. The dispersion due to serpentinisation is consistent with the accompanying enrichment in SiO_2 and, to a lesser extent, MgO.

Table 8.5 Major and minor element analyses of serpentinites.

Sample No	BF91/33a	BF91/27a	30	MU3878*	MU3827*	MU3888*	MU3929*	MU3890*	MU3961*	MU3905*	MU3909*	MU3856*	MU3949*
Belt	WSB	WSB	WSB	CSB	CSB	CSB	CSB	CSB	CSB	CSB	CSB	CSB	CSB
Type	Mass	Mass	Schist	Mass	Mass	Mass	Mass	Mass	Mass	Mass	Mass	Mass	Mass
SiO2	40.26	41 61	28 53	40 39	41.64	43 03	41.87	39 39	38 77	40 27	40 69	39.96	40 04
TiO2	0.07	0.04	0 02	b d	b.d	0.01	b d	0.01	0.02	b d	0 09	0.02	0 01
Al2O3	4.12	1.47	0.8	0.46	0.15	1 07	0.92	1.38	1.07	0.52	2.06	0.86	1.06
Fe2O3	5.21	3.73	4	4.84	4.04	2 84	3 08	5.38	7.53	7.15	4.15	4.95	5.31
FeO	1.63	2 7	3.87	2.31	3.52	3 39	3.19	2.38	3	0.62	3.24	2.47	2.39
MnO	0.04	0.06	0.07	0.07	0.14	0.08	0.07	0.15	0.07	0 07	0 11	0.11	0 13
MgO	35.96	37.99	36 77	39 38	37.43	36.3	39 42	39.09	38.24	37.41	38.32	38.48	38.58
CaO	0.06	0.03	0.07	0 03	0.04	0.71	0.01	0.02	0 01	0 01	0 03	0.06	0.01
Na2O	b.d	b.d	b.d	b.d	b.d	0.03	b d	b.d	b.d	b.d	b.d	b.d	b.d
K2O	0.01	b.d	b.d	b.d	0.04	b.d	b.d	b.d	b.d	b d	b.d	b.d	0 02
P2O5	b.d	b.d	b.d	b.d	0.01	0.01	b.d	0.01	0.01	0.01	0.04	0.01	b.d
H2O+	12.74	12.44	5.07	12.05	11.87	11 67	11.24	12.4	11.2	13.12	11.66	12.2	12.16
CO2	0.24	0 07	19.75	0.12	0.05	0.16	0.2	0.04	0.11	0.17	0.18	0.05	0.05
H2O-	0.87	0.71	0.38	0 46	0.24	0.22	0.2	0.26	0 36	0.8	0.05	0.25	0.54
Cr	3054	2517	7361	2319	2575	2772	2443	2872	2403	2333	2618	2454	2701
Ni	3192	2263	2114	1949	2728	2151	1893	2154	1613	2161	1920	2110	2198
V	65	27	28	9	5	23	13	33	11	5	24	27	4
Cu	b.d	2	4	6	5	5	17	3	1	9	1	2	35
Pb	5	3	3										
Zn	42	29	30	39	60	44	47	57	39	29	47	43	85
Rb	b.d	b.d	b.d										
Ba	11	14	6										
Sr	2	b.d	1										
Ga	4	3	4										
Nb	1	b.d	b d										
Zr	6	7	1										
Y	7	4	b d										
Th	b d	2	b d										
U	2	1	1										

(Data source: this thesis ; Ashley 1973a; Basden 1990)

b.d = below detection limit

Table 8.5 (continued). Major and minor element analyses of serpentinites.

Sample No	TPA-4	157a	162a	46d	GUN001	46c	38i	60	BF91/38a	M680/845*	46b	63	55
Belt	TPSB	TPSB	GSB	GSB	GSB	GSB	GSB	GSB	GSB	GSB	GSB	WSB	WSB
Type	Schist	Mass	Mass	Mass	Mass	Mass	Mass	Mass	Mass	Mass	Mass	Mass	Mass
SiO2	39.86	39 81	42.37	32.65	43 72	41 42	39 99	31.86	43 38	36.2	53.54	42.53	35.69
TiO2	0.02	b.d	0.02	0.01	0.02	0.01	0.03	b d	0.04	0 02	0.02	b.d	0.02
Al2O3	0.84	0.75	0.61	0.18	1.48	0 44	0 57	0.2	0 72	0.32	0.99	0 4	0.52
Fe2O3	6.54	5.34	4.57	6 3	6.32	4.36	5.84	7.79	5 02	4.35	5.27	7.94	5 43
FeO	1.25	1.04	1	1.83	1.83	2.05	2.06	1.14	2.03	1.67	1.18	1.02	2.16
MnO	0.09	0.02	0.04	0.21	0.08	0.06	0 08	0.15	0 04	0.1	0.07	0 11	0.09
MgO	38.57	39.61	39.28	39 86	31 62	38.49	35.58	36 09	36.4	39 5	31.27	36.18	39 43
CaO	0.01	0 01	b.d	0.17	0.09	0.81	1.51	3.06	0 06	0.07	0.04	0.95	0.08
Na2O	b.d	b.d	b.d	b.d	b.d	b.d	b.d	b.d	b.d	b.d	b.d	b.d	b d
K2O	b.d	b.d	b.d	b.d	b.d	b.d	b.d	b.d	b.d	0.02	b.d	b.d	b.d
P2O5	b.d	b.d	b.d	b.d	b.d	b.d	b.d	b.d	b.d	b.d	b.d	b.d	b.d
H2O+	12.69	12.9	12.14	8.99	12.99	11.39	11.69	9.83	12.23	9.96	7 48	10 64	9.86
CO2	0.05	0 1	0.05	9.56	0 1	1.47	2.68	9 73	0.27	6.7	0.17	0.09	6.55
H2O-	0.91	0.7	0 32	0.38	3.57	0.38	1.12	0.53	0.97	0.25	0 71	0.33	0.2
Cr	2434	3400	1734	2054	1967	1962	1616	2627	1451	1600	2453	2905	2192
Ni	2625	2489	3168	1933	2667	2221	2418	2711	2216	2120	2267	1280	2153
V	25	25	24	14	31	10	30	13	30	5	18	22	24
Cu	b.d	b d	14	8	32	8	73	2	95	b d	22	2	17
Pb	3	9	3	2	5	2	5	3	4	b.d	b.d	8	1
Zn	53	30	16	21	48	21	40	17	18	16	30	41	25
Rb	b.d	b.d	b.d	b d	b.d	b.d	b.d	b.d	b d	1	b.d	b.d	b.d
Ba	b.d	b.d	b.d	9	27	6	13	103	15	b d	35	34	10
Sr	1	b d	1	1	6	10	51	169	2	2	2	3	2
Ga	1	1	b.d	b.d	1	2	3	b d	3	0	5	2	2
Nb	b d	b.d	b.d	b d	1	b d	b.d	b d	b.d	b d	b.d	b.d	b d
Zr	2	1	1	b d	6	b d	b.d	b d	2	b d	1	2	b d
Y	1	b d	1	b d	8	b.d	1	b d	1	b d	b d	3	b d
Th	b.d	b d	1	1	1	b d	b d	1	b d	b.d	b d	b.d	b d
U	b d	b d	b d	b d	b d	b.d	b d	b d	b d	b d	b d	b d	2

(Data source: this thesis ; Ashley 1973a; Basden 1990)

b.d = below detection limit

Table 8.5 (continued) Major and minor element analyses of serpentinites

Sample No	V60*	G1765*	V811*	V1037*	149a	MU3893*	MU3908*	MU3871*	V1011*	44b	BF92/17c	BF91/32g
Belt	CSB	CSB	CSB	CSB	CSB	CSB	CSB	CSB	CSB	ESB	WWSM	WSB
Type	Mass	Mass	Mass	Mass	Schist	Schist	Schist	Schist	Schist	Mass	Mass	Trem
SiO2	40.24	39.71	39.07	39.82	39.25	40 95	43.42	42 19	39 92	42 74	36.31	48.42
TiO2	b.d	0.02	b.d	0.03	0 01	b d	b.d	0 01	0 03	0.02	0.01	0.02
Al2O3	1.96	0.34	1.31	1.12	0 86	0.17	0.34	0.44	0.04	0 75	0.4	2.45
Fe2O3	4.8	8.51	4 98	5.27	8.23	5.54	0.84	4.37	7.53	4.72	4.14	2.77
FeO	3.35	0.84	3.15	2.8	0 97	1.76	1.49	1.23	2 15	1.67	3.6	3.47
MnO	0.92	0.06	1.01	0.11	0.07	0.08	0 05	0.06	0 06	0.08	0 07	0.06
MgO	36.88	36.67	37.76	38.78	37.91	38 67	41.12	38.26	38.52	38.08	37.26	29.23
CaO	2.29	b.d	0.81	0.54	0.12	b.d	b.d	0.01	0.18	0 06	0.03	5.66
Na2O	b.d	0.01	b.d	0.04	b.d	b d	b.d	b d	0.03	b d	b.d	b.d
K2O	b.d	b.d	b.d	0.02	b.d	b.d	b.d	b.d	0 02	b.d	b.d	b.d
P2O5	0.02	b.d	0.02	0.03	b.d	b.d	0.01	0.01	0 02	b.d	b.d	b d
H2O+	8.75	11.15	10.26	10.72	12.28	12.34	12 16	12.92	10 84	11.52	10.87	8.04
CO2	0.11	b.d	0.21	0.22	0.1	0.05	0.37	0 03	0.32	0.51	6.87	0.04
H2O-	0.23	1.9	0.25	0.08	0.71	0 57	0.36	0.64	0.04	0.32	0.53	0.48
Cr	3080	3760	3220		2634	1923	1975	2921		1396	2402	806
Ni	1730	3620			2625	2400	1783	2717		2177	2324	878
V					25	b d	b.d	3		89	22	23
Cu					b.d	3	2	11		11	2	89
Pb					5					2	3	4
Zn					26	53	31	46		34	29	17
Rb					b.d					1	1	b.d
Ba					b.d					22	43	16
Sr					2					3	3	16
Ga					1					4	b d	3
Nb					b d					b.d	b d	1
Zr					2					b d	1	1
Y					2					1	1	1
Th					1					b d	1	b d
U					b d					b d	b d	1

(Data source: this thesis ; Ashley 1973a*; Basden 1990*)

b.d = below detection limit

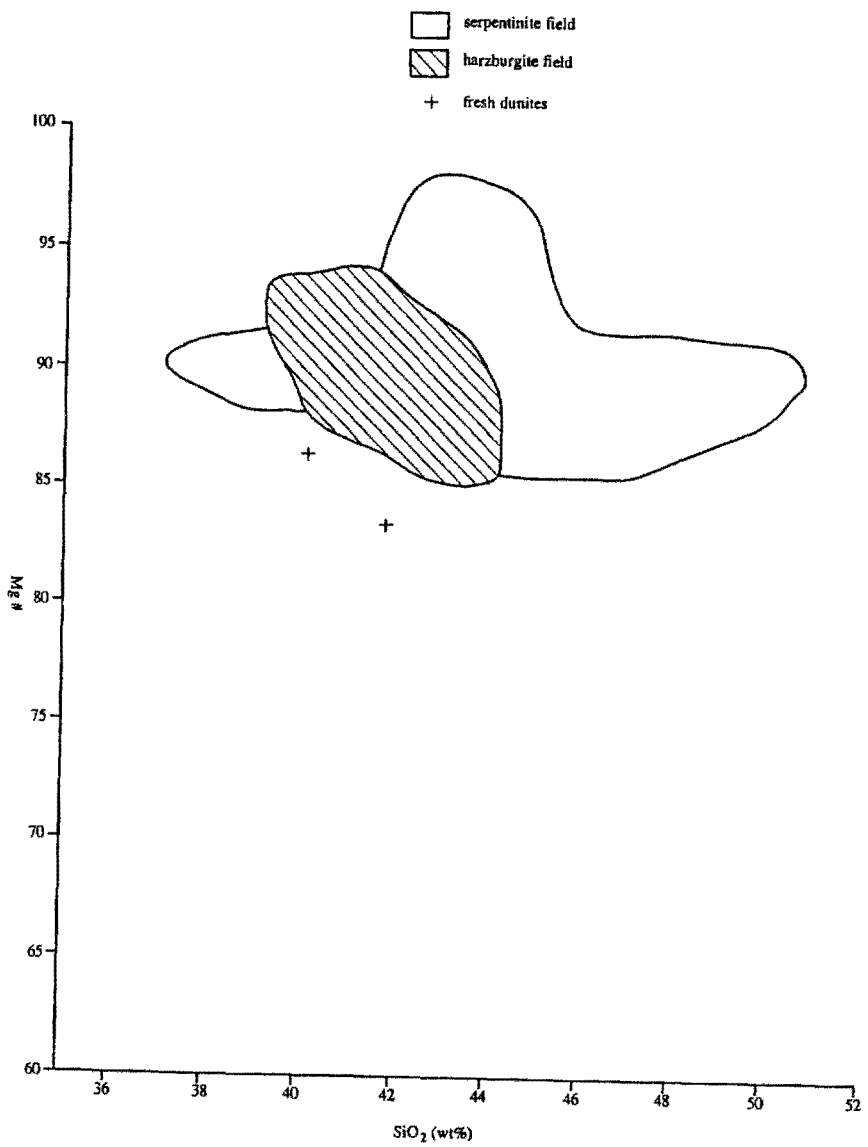

Figure 8.8 Mg# vs SiO2 diagram showing the fields for harzburgite, weakly serpentinised dunite and serpentinite (data from Tables 8.1, 8.2 and 8.5).

8.2.3 REE and trace element geochemistry

The massive and schistose serpentinites of the Tumut Serpentinite Province, like their parental harzburgites and peridotites, are highly depleted in the REE (Table 8.6). Compared to their parental ultramafic precursors, both varieties are relatively enriched in Sb, As, Co and Sc, while the schistose varieties are particularly enriched in Sb, As, Co, Sc and the LREE. Both Sb and As are most likely derived from a hydrothermal source as their concentrations are virtually negligible in the primary ultramafic rocks, whereas Sc was most likely derived from the breakdown of clinopyroxene in the primary ultramafic rocks (e.g. Ashley 1973a). Analysis 157a, a massive serpentinite from the Tumut Ponds Serpentinite belt is extraordinarily enriched in Au (6.1ppm). The gold most likely occurs as the metallic native metal and as a secondary phase in fracture-fill, as found within fracture-fill of the podiform chromitites of the serpentinite belts (see Chapter 9)."

The CN-REE patterns for the massive and schistose serpentinites are generally flat and lack anomalies (Figure 8.9). However:

(a) two massive serpentinites (one from each of the Wambidgee and Tumut Ponds serpentinite belts) and two schistose serpentinites (one from each of the Coolac and Tumut Ponds serpentinite belts) exhibit convex downward curves;
(b) a massive serpentinite from the Gundagai Serpentinite Belt and a schistose serpentinite from the Tumut Ponds Serpentinite Belt have strong Eu peaks;
(c) a massive serpentinite from the Wambidgee Serpentinite Belt and a schistose serpentinite from the Coolac Serpentinite Belt, have moderate Eu troughs.

8.2.4 Discussion

(a) Compositional similarity of harzburgite, serpentinised harzburgite, and massive and schistose serpentinite in terms of major elements, REE data and CN-REE patterns, convincingly demonstrate that the serpentinites have derived from parental harzburgite (and minor peridotite);
(b) The progression from harzburgite to serpentinised harzburgite to massive and schistose serpentinite, was accompanied by enrichments/depletions;
(c) Deformation accompanying development of schistose serpentinite seems to have resulted in additional La and Ce enrichment;

ıle 8.6 Rare earth and trace element analyses of serpentinites.

Sample No	149a	101a	BF91/30	173	177	BF91/33a	S1	BF91/38a	TPA-4	157a	245ms	252msus	258ms	252ss	258ss
Belt	CSB	CSB	WSB	WSB	WSB	WSB	WSB	GSB	TPSB	TPSB	TPSB	TPSB	TPSB	TPSB	TPSB
Type	schist	Mass	Schist	Schist	Mass	Mass	Trem	Mass	Schist	Mass	Mass	Mass	Mass	Schist	Schist
La	0.7	0.13	0.12	0.11	0.09	2.81	0.36	0 34	0.2	0.1	0.2	0.22	0.09	0.13	0.14
Ce	1.43	b.d	b.d	b.d	b.d	5.79	0.92	0.77	b.d	b.d	b d	0.55	b.d	b.d	b.d
Nd	b.d	b.d	b.d	b.d	b.d	3.54	b.d	b.d	b.d	b.d	b.d	b.d	b.d	b.d	b.d
Sm	0.17	0.09	0.09	0.09	0 08	0.81	0.15	0.18	0.05	0 08	0.04	0.13	0.05	0.04	0 05
Eu	0.04	b.d	0.04	b.d	b.d	0.18	0.1	0.28	0.09	b.d	b.d	0.05	b d	b.d	b.d
Tb	b.d	b.d	b.d	b.d	b.d	0.18	b.d	0.05	b.d	b.d	b d	b.d	b.d	b d	b.d
Ho	b.d	b.d	b.d	b.d	b.d	0.26	b.d	0.06	b.d	b.d	b.d	b.d	b.d	b.d	b.d
Yb	0.14	0.08	0.07	0.07	0.07	0.44	0.08	0.16	0.06	0.07	0.05	0.21	0.04	0.05	0 04
Lu	0.02	0.01	0.01	0.01	0.01	0.06	0.01	0 02	0.01	0.01	b d	0.03	b.d	b.d	b.d
Sb	b.d	0.1	0.74	3.29	1.37	0.58	0.42	1	0.54	0.15	5.82	2.01	2.62	1.25	2.62
As	2.4	0.5	18.7	5.39	7.17	3.88	1.18	13.5	1.23	0.58	37 7	2.24	2.1	2.15	3.25
Cr	2720	2830	6580	2330	2450	3160	6960	1900	2550	3210	2490	2050	2560	2340	2250
Co	169	93.9	113	100	93.4	90.8	91.9	91.6	94.2	88 4	135	128	77.2	106	86.2
Au	b.d	b.d	b.d	b.d	b.d	b.d	b.d	b.d	b.d	6.1	b.d	b.d	b d	b.d	b.d
Hf	b.d	b.d	b.d	b.d	b.d	0 2	b.d	b.d	b.d	b.d	b d	b.d	b.d	b d	b.d
Ir	b.d	b.d	b.d	b.d	b.d	b.d	b.d	b.d	b.d	b d	b.d	b.d	b d	b d	b.d
Sc	8.4	7.19	4.71	8.65	7.94	8 61	5 48	6.11	7.74	10 1	5 4	15.5	10	7.71	8.44
Ta	0.26	0.25	0.24	0.23	b.d	0.26	b.d	b d	b.d	b.d	b d	b d	b d	b d	b d
Th	0.35	b.d	b d	b.d	b d	0.48	b.d	b d	b d	b d	b d	b d	b d	b.d	b d

(Data source: this thesis)
b.d = below detection limit

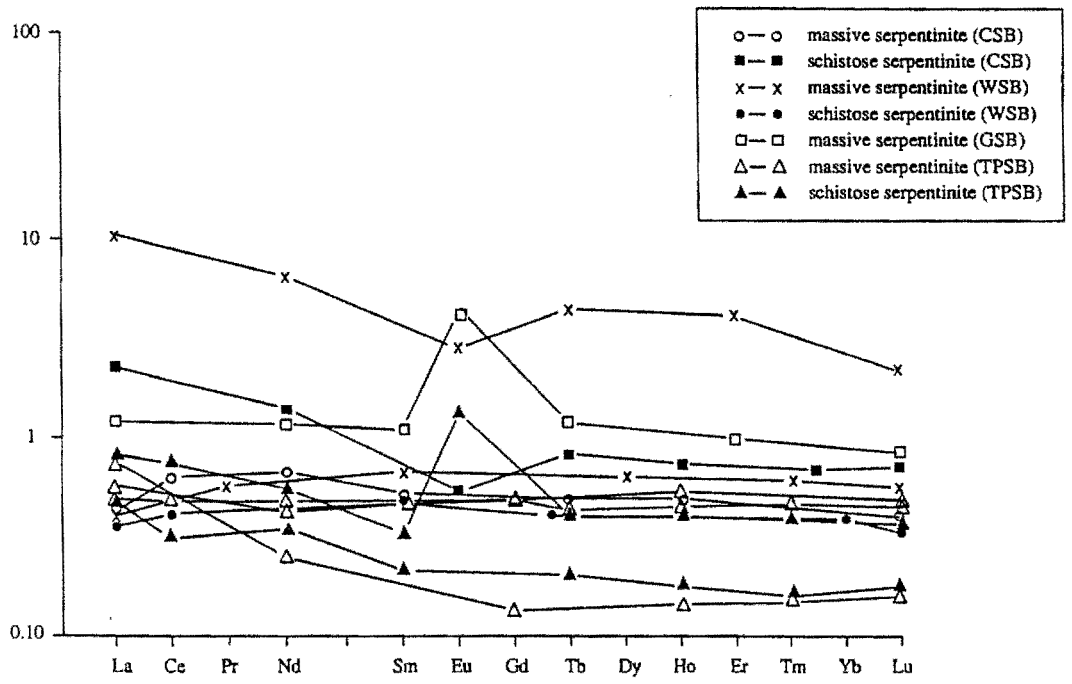

Figure 8.9 CN-REE diagram for serpentinites (data from Table 8.6).

(d) CN-REE patterns and Eu anomalies in a few harzburgite and serpentinised harzburgite samples have apparently carried over into massive and schistose serpentinite.

The occurrence of both enriched and depleted levels of SiO_2 and MgO in serpentinites compared to the host harzburgites and peridotites suggests that these elements were at least locally remobilised during the serpentinisation process. Enrichment of SiO_2 may be due to the formation of tremolite and talc within the serpentinites (e.g. Ashley 1973a). Ashley (1973a) found that total Fe, MgO, SiO_2, Cr and Ni generally remained constant during serpentinisation while Al_2O_3, CaO, Mn, Ti, V, Sc, Cu and Zn decreased. Perhaps the only components introduced during serpentinisation were H_2O^+ and S. Thus, Ashley (1973a) and, in a study of world-wide ophiolite occurrences, Coleman (1977), concluded that during serpentinisation, ultramafic rocks essentially retain their original composition. The present study reinforces this conclusion and shows that the concentrations of most trace and rare earth elements are similarly retained.

Massive serpentinite, like serpentinised harzburgite, exhibits flat CN REE patterns and lacks any significant anomalies. One massive serpentinite exhibits a strong +ve Eu anomaly, much like that for weakly serpentinised harzburgites from the Tumut Serpentinite Province and harzburgite from other ophiolites (Kay & Senechal 1976; Pallister & Knight 1981). However, others have a moderate downward CN REE pattern and one has a moderate -ve Eu anomaly.

The schistose serpentinites have similar CN REE patterns to the massive serpentinites. Again, this suggests that both types were derived from the same residual harzburgite parent. Like the massive serpentinites, some of the schistose serpentinites exhibit moderate downward CN REE patterns and weak -ve Eu anomalies.

8.3 TALC-CARBONATE ROCKS

8.3.1 Major and minor element geochemistry

Analytical data for talc-carbonate rocks of the Tumut Serpentinite Province are presented in Table 8.7. All belts show the same compositional range, other than in CO_2, which is depleted in the Coolac Serpentinite Belt and Western Wambidgee Serpentinite Melange and depleted to highly enriched in the Wambidgee and Gundagai serpentinite belts. In effect, talc-carbonate rocks of the Coolac Serpentinite Belt and Western Wambidgee Serpentinite Melange are dominated by talc, whereas those from the Wambidgee and Gundagai serpentinite belts contain varying amounts of both talc and carbonate.

With the exception of analysis 138g, the talc-carbonate rocks of the Tumut Serpentinite Province were derived from an ultramafic parent. The relatively high concentrations of Al_2O_3, Fe_2O_3, FeO and V, and low concentrations of Cr and Ni in analysis 138g suggests derivation from a mafic parent.

Table 8.7 Major and minor element analyses of talc-carbonate rocks.

Sample No	138g	150a	156g	BF92/17a	GUN002	160b	162b	162d	BF91/38c	BF91/29a	56	167a	167b	165b	BF91/28g	BF91/28e
Belt	CSB	CSB	CSB	WWSM	GSB	GSB	GSB	GSB	GSB	WSB	WSB	WSB	WSB	WSB	WSB	WSB
Rocktype	Carb rock	Ta Serp	Ta Serp	Ta Serp	Ta Carb	Ta Serp	Ta Serp	Ta Schist	Ta Schist	Ta Carb	Ta Serp	Ta Serp	Ta Serp	Ta Serp	Ta Carb	Ta Schist
SiO2	45.14	55.21	51.53	59 4	59.23	57 01	29 1	31 54	59.59	61 27	48 55	36.31	36.22	60.13	36.1	50.66
TiO2	0.42	0.01	0 02	b.d	b.d	0.01	0.01	0.02	0 01	0.01	b d	b.d	0.01	0.01	0 01	0.04
Al2O3	11.85	1.03	3.79	0.42	0.75	0.24	0.29	17.49	0 52	0.36	1.51	0.64	0 59	0.88	0 42	4.58
Fe2O3	1.34	5.94	1.42	0.95	3.59	9.46	6 43	1.45	0.97	8 02	3 46	2.34	5.01	1.9	1.7	2.66
FeO	3.62	2.3	3.27	3.37	1.01	1	1.71	6 15	3 52	1.12	4 45	4.44	2.02	3.11	4.46	4.79
MnO	0.37	0.1	0.07	0.05	0.03	0.02	0.1	0.1	0.07	0.03	0.08	0.06	0.09	0.04	0.07	0.26
MgO	9.11	28.25	24.86	25.87	29.35	27.98	36 21	31.1	26.26	22.5	30 41	37.25	38.75	28.93	34.37	22.35
CaO	26.21	0 65	9.23	5.58	0.02	0.01	0.23	0 01	4 85	0.07	1.23	0 13	0 47	0.02	0.11	8 83
Na2O	0.05	b.d	b.d	b d	0.09	0 1	0.09	0.32	b d	0 22	0 04	0.12	0.24	0.24	b.d	b.d
K2O	0.01	b.d	0.02	0 01	0 03	0.02	0.02	0.05	0 01	0.06	0 01	0.02	0.05	0.05	b.d	0.01
P2O5	0.09	b.d	b.d	b d	b.d	b.d	b d	b d	b.d	0.05	b.d	b.d	b.d	b.d	b.d	b.d
H2O+	2.39	5.09	5.49	4.02	5.37	4.5	2.61	12 44	4.02	5.48	7.96	8.6	9.32	5.26	3 45	5.73
CO2	0.05	0.97	0.05	0.05	0.1	0.01	24.04	0.03	0.04	0.33	1.98	9.8	8.21	0.05	19.38	0.16
H2O-	0.77	0 3	0.38	0.29	0.27	0.11	0.11	0.26	0.26	0.83	0.25	0.19	0.23	0.16	0.24	0.77
Cr	420	2878	2011	1882	2733	771	1679	1709	1022	3796	3684	2651	2081	1593	3257	277
Ni	494	1300	1997	1797	1432	1735	1545	1695	1861	1544	2081	2440	2167	951	1622	971
V	103	22	22	10	20	75	13	40	16	331	74	27	24	34	23	55
Cu	9	1857	4	13	25	12	1	19	16	13	25	8	2	32	5	9
Pb	7	3	3	4	3	5	2	5	3	5	5	5	3	4	1	6
Zn	32	826	31	34	49	56	14	51	46	33	50	25	28	28	34	69
Rb	1	b.d	1	1	b.d	b.d	b.d	b.d	b.d	b.d	b d	b.d	b d	b d	b.d	b d
Ba	9	b.d	b d	b d	1	b.d	b d	b d	5	7	65	b.d	3	1	8	23
Sr	6	1	3	3	1	1	3	b.d	9	3	56	3	10	1	1	21
Ga	9	1	6	b.d	b d	1	b.d	2	3	b.d	4	3	1	2	2	7
Nb	2	b.d	b d	b d	b.d	b.d	b d	b d	b d	b d	b d	b d	b.d	b d	b d	b d
Zr	51	1	3	1	2	3	1	3	2	1	b d	1	1	3	b d	6
Y	23	1	3	1	b d	2	b d	1	b d	3	2	b d	1	1	b d	6
Th	3	2	b d	b.d	1	2	1	1	b d	2	1	1	b d	b d	b d	1
U	b d	b.d	1	b d	b d	b d	b d	b d	1	b d	b d	b d	b d	b.d	b d	b d

(Data source this thesis)

b d = below detection limit

8.3.2 Variation diagrams

On the Mg# vs SiO_2 diagram (Figure 8.10), most samples fall within the field of serpentinites from the Tumut Serpentinite Province, but a few fall outside the serpentinite field due to higher SiO_2 contents at the same Mg#.

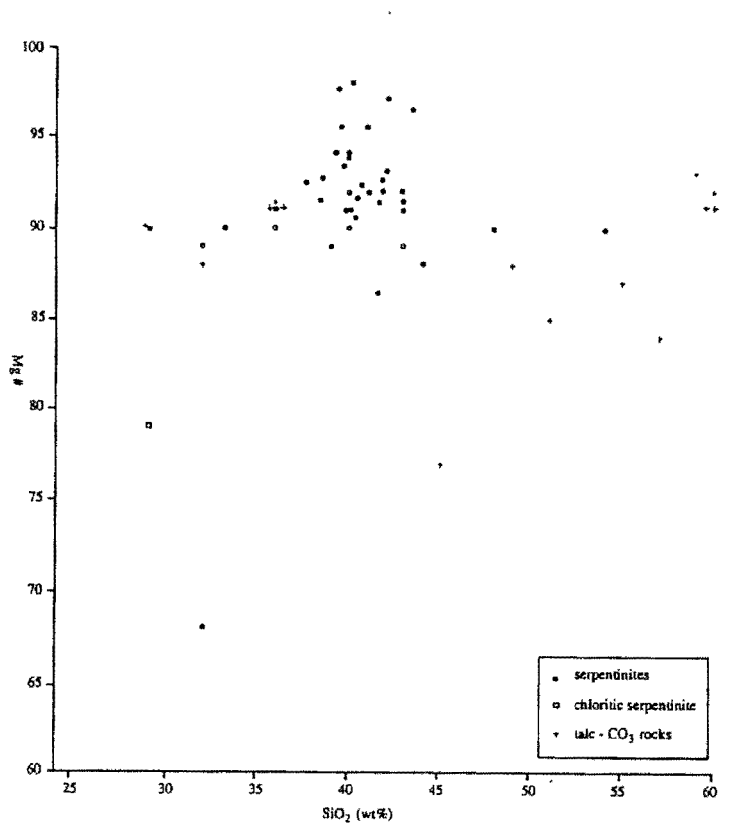

Figure 8.10 Mg# vs SiO_2 diagram for the serpentinites and talc-carbonate rocks (data from Tables 8.5 and 8.7).

8.3.3 REE and trace element geochemistry

The talc-carbonate rocks vary widely in REE and trace element concentrations (Table 8.8). As only a few samples have been analysed, great care must be taken when comparing results from the different belts. However, they appear to be either depleted in the REE (much like the serpentinites, harzburgites and peridotites of the Tumut Serpentinite Province) or enriched in them. Compared to the primary ultramafic rocks, they have anomalous concentrations of Sb and As, and one analysis

(BF91/28a) from the Wambidgee Serpentinite Belt is anomalously enriched in Au (9.8ppm). Anomalous concentrations of As, Sb and Au within serpentinites have been recorded from the Eastern Metals serpentinite-associated Ni-Cu-Zn deposit of Quebec, Canada (Auclair *et al.* 1993) and from alpine-type peridotites world-wide (e.g. Ashley 1997).

Sample No	150a	195	BF91/28a	162b	245tms
Belt	CSB	WSB	WSB	GSB	TPSB
La	0.42	1.01	1.94	0.08	2.39
Ce	0.65	0.83	3.22	b.d	6.06
Nd	b.d	2.05	3.89	b.d	3.54
Sm	0.1	0.67	1.15	0.07	0.89
Eu	0.05	0.2	0.26	0.03	0.1
Tb	b.d	0.14	0.18	b.d	b.d
Ho	b.d	0.15	0.23	b.d	0.24
Yb	0.08	0.23	0.53	0.05	0.54
Lu	0.01	0.03	0.07	b.d	0.07
Sb	0.19	0.11	0.45	0.85	1.42
As	2.28	1.43	74.4	2.7	4.92
Cr	3020	2490	212	2030	2770
Co	60.6	73.3	52.4	102	93.3
Au	b.d	b.d	9.8	b.d	b.d
Hf	b.d	b.d	b.d	b.d	b.d
Ir	b.d	b.d	b.d	b.d	b.d
Sc	4.53	3.28	10.3	4.02	9.76
Ta	0.31	b.d	b.d	0.28	b.d
Th	b.d	b.d	0.37	b.d	b.d

(Data source: this thesis)
b.d = below detection limit

Table 8.8 Rare earth and trace element analyses of talc-carbonate rocks.

CN REE patterns are either flat or weak downward curves (Figure 8.11). The sample from the Coolac Serpentinite Belt has weak Ce and Sm troughs. The two samples from the Wambidgee Serpentinite Belt have moderate to strong -ve Ce troughs and weak -ve Eu troughs. The sample from the Gundagai Serpentinite Belt lacks any anomalies while the sample from the Tumut Ponds Serpentinite Belt exhibits a striking –ve Eu trough.

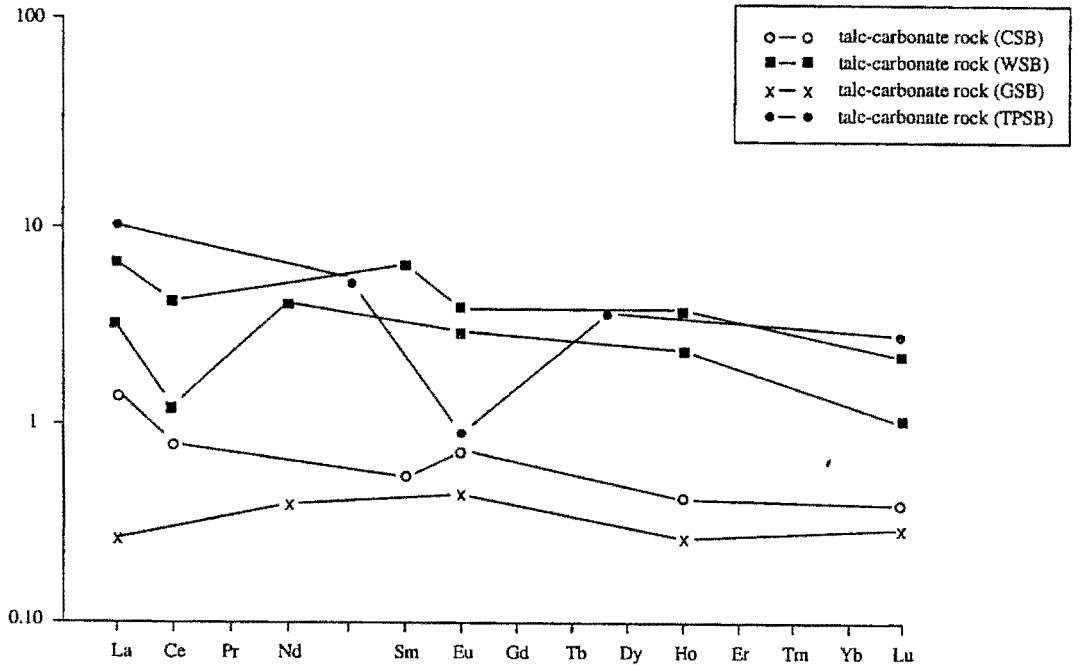

Figure 8.11 CN-REE diagram for the talc-carbonate rocks (data from Table 8.8).

8.3.4 Discussion

The range in major element composition of the talc-carbonate rocks is ascribed to differing modal proportions of the constituent phases. However, most have similar concentrations of the immobile elements Ti, Cr, Ni, Zr and Y, which suggests that they were derived from similar parental serpentinites and/or residual harzburgites/peridotites. Although the carbonate species were not identified, sample 138g from the Coolac Serpentinite Belt has high CaO concentration (26.21 Wt%) and relatively low MgO (9.11 Wt%) and FeO (3.62 Wt%) consistent with the carbonate being dolomite rather than magnesite. In contrast, the relative enrichment in CaO (4.85-9.23 Wt%) of some talcosic serpentinites and talc schists is probably due to relatively high proportions of tremolite.

The high concentration of CO_2 in talc-carbonate rocks within the Wambidgee and Gundagai serpentinite belts and its low concentration in the same rocks in the Coolac Serpentinite Belt and Western Wambidgee Serpentinite Melange suggests that CO_2 alteration of the serpentinites occurred in discrete zones, mostly along shear planes and contact zones between the belts and

enclosing quartz-rich country rocks (sections 3.5.5, 4.5.3, 5.5.3, 7.3). It is apparent that the parental rocktype for sample 138g from the Coolac Serpentinite Belt was either a mafic dyke rock or tectonic inclusion (section 3.5.5).

In a study of the Eastern Metals serpentinite-associated Ni-Cu-Zn deposit of Quebec, Canada, Auclair *et al.* (1993) reported that talc-carbonate rocks occurred at the contact between the serpentinites and country rocks and were associated with enrichment of Au, As and Sb. They ascribed the formation of these talc-carbonate rocks to the channeling of post-serpentinisation hydrothermal fluids along the fault contact between the serpentinites and Si-rich county rocks leading to intense metasomatic alteration of the serpentinites with enrichment in Au, Sb, As, La, Ce and Nd.

Likewise, Ashley (1997) reported that silica-carbonate alteration zones within serpentinites of the Great Serpentinite Belt, NSW, were associated with significant hydrothermal Au mineralisation and that this mineralisation was post-serpentinisation and formed by the periodic reactivation of faults (i.e. contacts with the surrounding country rocks) and channeling of hydrothermal fluids along these zones. Ashley (1997) suggested that the CO_2-bearing fluids were from a deep-seated source, introduced S, As, Sb, Hg and Au into the system, and had minimum temperatures of 165-225°C. As the talc-carbonate rocks of the Tumut Serpentinite Province are similar to those described by Ashley (1997) they are here ascribed to a similar genesis, thereby resulting in metasomatism of the serpentinites and relative enrichment in Au, Sb and As.

The talc-carbonate rocks vary in their concentration of the REE ranging from highly REE-depleted rocks (much like the harzburgites and serpentinites) to REE-enriched rocks (with higher REE concentrations than the pyroxenites, wehrlites, lherzolites and hornblendites). Although the database is small, it suggests that during the formation of these rocks by infiltration of CO_2-rich fluids through their protoliths, at least La, Ce, Nd, Sm and Eu were significantly mobilised, resulting in either the enrichment or depletion in these elements within the newly-formed talc-carbonate rocks.

The sample from the Gundagai Serpentinite Belt (162b) is almost identical to that from the Tumut Ponds Serpentinite Belt (245tms) but they have different La/Ce concentrations. As they both appear to have been originally derived from similar ultramafic rocks, all that can be said is that the enrichment or depletion in La and Ce must be due to either localised enrichment from a hydrothermal source, fluid flow variations within the serpentinite belt, or variations in the deformation rate along the flow paths.

CN REE patterns for talc-carbonate rocks are flat to weak downward curves, much like those for the harzburgites and serpentinites. However, the talc-carbonate rocks exhibit many varied anomalies ranging from weak to strong -ve Ce anomalies, weak to strong -ve Eu anomalies and non-existent to weak -ve Sm anomalies. This range in anomalies again attests to the possibility that the REE have been significantly mobilised during the percolation of CO_2-rich fluids through the precursor rock types.

8.4 GABBROS

8.4.1 Major and minor element geochemistry

Analytical data for the gabbros of the serpentinite belts is shown in Table 8.9. Gabbros from all belts are chemically similar. They vary widely in composition, due to differing plagioclase to diopside/hornblende ratios. The gabbros are also strongly enriched in Na_2O compared with K_2O.

8.4.2 Variation diagrams

Gabbros can be subdivided into:

(a) leucogabbros (rich in CaO and depleted in $MgO+FeO+Fe_2O_3$),

(b) gabbros (with near equal amounts of CaO and $MgO+FeO+Fe_2O_3$), and

(c) melanogabbros (depleted in CaO and enriched in $MgO+FeO+Fe_2O_3$).

This subdivision is graphically shown in Figure 8.12 by the circled areas.

Gabbros from the Micalong Swamp Complex are also shown on Figure 8.12 for comparison. Although they plot in the same area as those of the Tumut Serpentinite Province gabbros on this diagram, they are enriched in TiO_2 and depleted in both Cr and Ni as shown on the TiO_2 vs SiO_2 diagram (Figure 8.13). Differences between the two groups are also clearly shown on the Cr vs Ni diagram (Figure 8.14) where Micalong Swamp Complex gabbros plot in one small area on the bottom left corner of the diagram, whereas those from the Tumut Serpentinite Province cover almost the whole field and can be subdivided into Cr/Ni-rich gabbros, moderate Cr/Ni gabbros and Cr/Ni-depleted gabbros.

Gabbros from the Honeysuckle Beds, also shown on this last diagram (Figure 8.14) correspond closely with those of the Tumut Serpentinite Province.

A linear relationship between the various rock types of the Honeysuckle Beds (section 3.2.1) is shown on the Cr vs Ni diagram (Figure 8.15). This suggests that they are genetically related and have the same parental magma. Mafic dyke rocks of the North Mooney Complex are also shown, and seem to lie on the same trend, thereby suggesting that they relate to the Honeysuckle Beds and have intruded the North Mooney Complex.

Table 8.9 Major and minor element analyses of gabbros.

Sample No	156c	156d	97	146	155a	145	140b	118	116	BF92/3	BF92/9a	BF92/15b	157b
Belt	CSB	CSB	CSB	CSB	CSB	CSB	CSB	CSB	CSB	WSB	WSB	WWSM	TBSB
SiO2	49.68	47.29	43.14	47.98	50	44 85	55.65	48 89	54.32	61 87	46 41	48 08	46 95
TiO2	0.79	0.24	0.32	0.46	0 59	0.15	0 63	0 43	0.5	0 67	0 05	0 51	0 4
Al2O3	14.53	17.61	10.68	16.13	16.9	17.67	16.76	13.35	11 65	17.15	18.33	17.23	14.59
Fe2O3	1.52	0.85	1.23	2.26	2.13	1.45	2.34	0.67	0 64	1.45	0.79	2 04	1 52
FeO	5.83	3 42	6.95	5 8	4.59	2 1	4.28	4 07	5.27	1 16	2 02	3.44	4.04
MnO	0.14	0 11	0.17	0.14	0 15	0.07	0.15	0 09	0.11	0 14	0 06	0.18	0.17
MgO	10.15	9.95	20.5	10.52	9.91	10 45	5 57	9.05	10 85	2.66	13.04	8 7	9 49
CaO	9.18	14.7	10.5	12.23	6.85	21.31	5.79	20.38	10.01	7.31	15 88	9 18	18.46
Na2O	3.76	1.61	0.34	1.7	3.25	0.1	5.81	0.16	2.54	5.67	0.7	2.85	0.69
K2O	0.2	0.28	0.03	0.06	1 07	b.d	0.28	0 09	1.3	0.06	0.11	1.15	0.81
P2O5	0.13	0.01	0.08	0.06	0.08	0.02	0.11	0.03	0.07	0.32	0.01	0.19	0.01
H2O+	3.42	4	6.05	2.84	3.95	2.5	2.61	3.41	2.6	1.01	2.6	4.11	2.89
CO2	0.01	0.01	0.05	0.25	b.d	0.11	0 09	0.09	0 07	0.11	0 11	0.3	0 05
H2O-	0.24	0.23	0.37	0.23	0 48	0 2	0.4	0 03	0.25	0.21	0.2	0.26	0.16
Cr	648	933	1583	409	900	1972	137	651	1791	8	2934	100	848
Ni	251	275	881	114	210	296	91	169	238	4	491	44	156
V	224	118	152	221	154	111	207	167	200	93	92	285	210
Cu	15	19	7	35	27	36	5	12	16	9	65	55	43
Pb	2	5	4	6	21	4	4	6	5	10	10	1	6
Zn	45	34	56	40	76	18	42	31	37	69	18	62	42
Rb	9	12	1	2	70	1	10	1	32	2	2	16	17
Ba	296	108	7	25	160	11	138	12	355	154	72	183	549
Sr	587	221	72	190	180	480	118	15	314	772	89	1358	301
Ga	9	9	9	9	11	6	12	12	6	17	6	14	6
Nb	3	1	3	1	2	b d	3	2	3	14	b.d	b d	b d
Zr	52	6	53	19	69	b d	51	55	34	125	b.d	b d	7
Y	25	8	11	14	19	4	20	16	16	21	4	7	12
Th	3	2	1	2	2	1	2	3	2	12	1	1	2
U	b.d	b.d	b.d	b d	b.d	b.d	b d	1	b d	2	b d	b d	b d

(Data source: this thesis)

b d = below detection limit

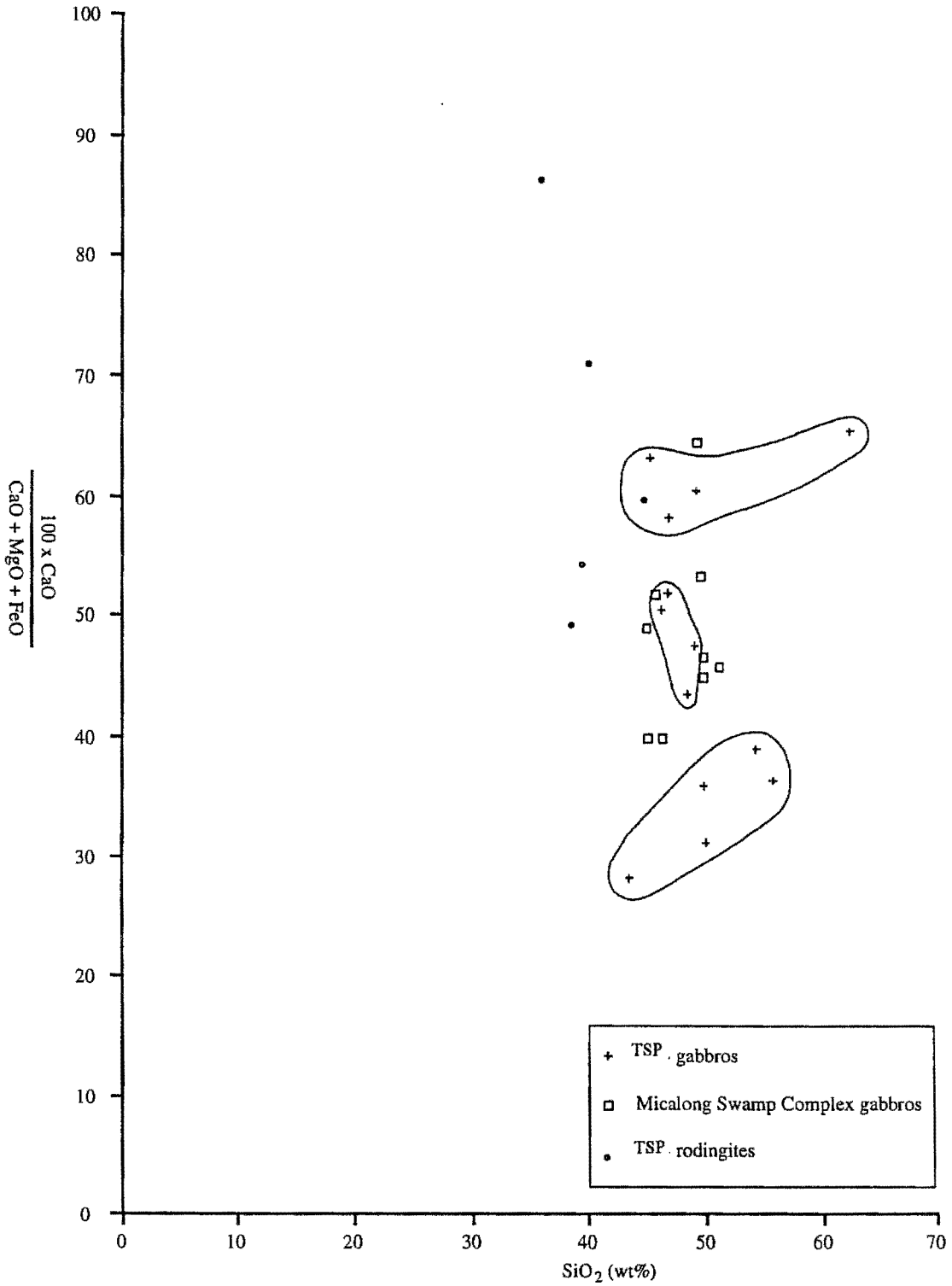

Figure 8.12 100xCaO/CaO+MgO+FeO vs SiO_2 diagram for the gabbros and rodingites of the Tumut Serpentinite Province and gabbros from the Micalong Swamp Complex (data from Tables 8.9 and 8.21; Callan 1984).

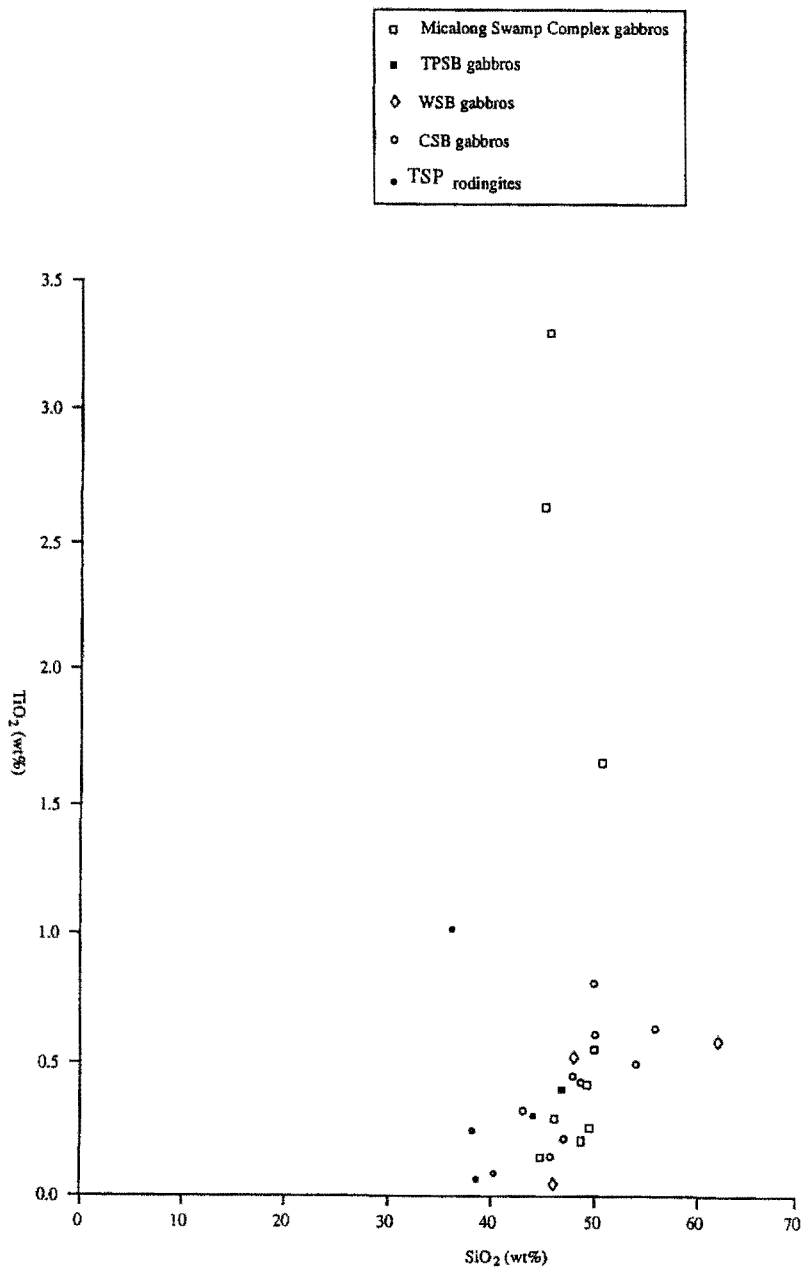

Figure 8.13 TiO_2 vs SiO_2 diagram for the gabbros and rodingites of the Tumut Serpentinite Province and gabbros from the Micalong Swamp Complex (data from Tables 8.9 and 8.21; Callan 1984).

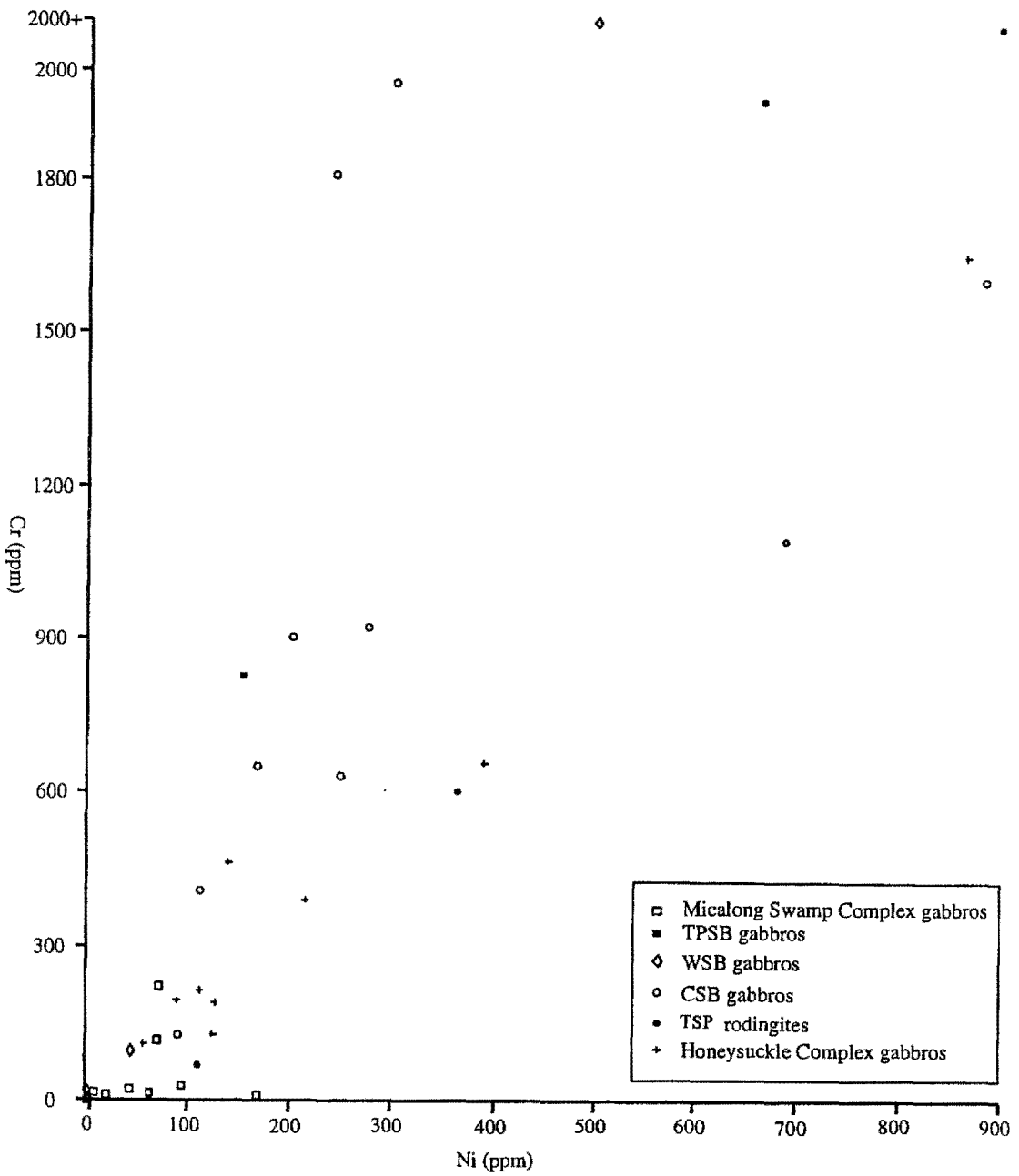

Figure 8.14 Cr vs Ni diagram for the gabbros and rodingites of the Tumut Serpentinite Province and gabbros from the Micalong Swamp Complex and Honeysuckle Beds (data from Tables 8.9 and 8.21; Callan 1984; Basden 1990).

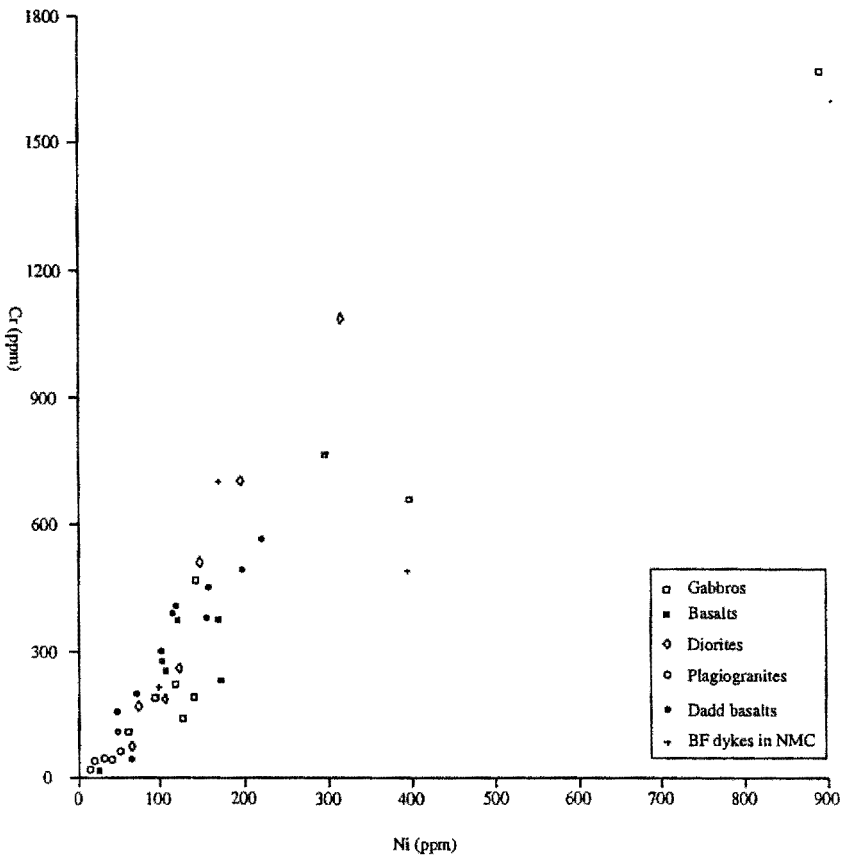

Figure 8.15 Cr vs Ni diagram for the various rock types of the Honeysuckle Beds and mafic dyke rocks of the North Mooney Complex (data from Table 8.13; Ashley 1973a; Franklin 1975; Dadd 1998).

8.4.3 REE and trace element geochemistry

Most gabbros from the Tumut Serpentinite Province are enriched in the LREE, La, Ce, Nd, Sm, Eu and Yb compared with the HREE (Table 8.10). Sc concentration is high. There is a wide range in the concentration of Cr, Ni, Ba, Sr and Zr.

Chondrite normalised REE data for the gabbros are presented in Figure 8.16. The salient points are:

(a) Most of the gabbros are REE enriched. They are moderately convex downward. One has a weak –ve Eu trough, one a strong –ve Eu trough, and one a weak +ve Eu peak;

Table 8.10 Rare earth and trace element analyses of gabbros.

Sample No	156d	116	238a	BF92/3	196Gab	BF92/15b	170	170b	157b	145	233	238peg/gab
Belt	CSB	CSB	CSB	WSB	WSB	WWSM	WWSM	WWSM	TPSB	NMC	NMC	CSB
La	1.13	5.35	0.79	26.42	0.28	3.7	9.21	9.31	0.54	0 44	0.81	6.31
Ce	3.2	11.01	1.69	56.93	0.92	10.9	17.97	18.59	1.61	1.39	1.83	16.3
Nd	2.6	6.82	1.14	33.01	b.d	8.56	10	11	1.99	1.25	1.57	12.2
Sm	0.92	2.01	0.31	6.46	0.28	2 16	2.23	2.21	0.97	0 45	0.55	4.03
Eu	0.36	0.75	0.23	1.52	0.15	0.9	0.71	0.5	0 48	0.14	0.26	1.2
Tb	0.2	0.46	b.d	0.74	b.d	0.4	0 4	0.39	0.3	b.d	b.d	0.93
Ho	0.27	0.63	b.d	0.82	b.d	0.47	0.45	0 47	0.44	b.d	0.21	1.23
Yb	0.65	1.5	0.167	1.84	0.14	0.85	0.97	0.93	1.15	0.27	0.5	2.75
Lu	0.09	0 19	0.024	0.25	0.02	0 09	0 14	0.12	0 18	0 035	0.074	0.4
Sb	b.d	b.d	b.d	b.d	b.d	b.d	0.27	0.53	0.38	b.d	b.d	b.d
As	b.d	b.d	b.d	2.49	b.d	b.d	b.d	0.98	b.d	b d	11.6	b.d
Cr	832	1594	126	6	1190	87.2	472	431	723	1160	1200	250
Co	39.3	49	38.9	63.8	67.6	47.9	63.8	62.3	61.5	66 1	50.1	54.8
Au	b.d	b.d	b.d	b.d	b.d	b.d	b.d	6.4	b.d	b.d	b.d	b.d
Hf	0.26	1.04	0.28	3.38	0.21	0.24	0.65	0 88	0 42	0.37	b d	3 19
Ir	b.d	b.d	b.d	b d	b.d	b.d	b.d	b.d	b d	b d	b.d	b.d
Sc	32.3	47.1	11.6	13.9	38.7	36	44.4	41 3	47 9	38 1	20 4	37.8
Ta	b.d	0.5	b d	0.96	0.21	b d	0 44	0.23	b.d	b d	b d	0 52
Th	b.d	1.59	0.28	12.3	b d	b d	1.05	1.25	b d	b d	b d	1 45

(Data source: this thesis)

b d = below detection limit

(b) One gabbro from each of the Coolac and Tumut Ponds serpentinite belt has moderate REE, Cr and Sc concentrations, and low Fe and Hf concentration. The curves are moderately convex upward and lack anomalies;

(c) One gabbro from the northern half of the Wambidgee Serpentinite Belt is depleted in REE and has a high concentration of Cr. It has a weak convex upward curve with a weak +ve Eu peak.

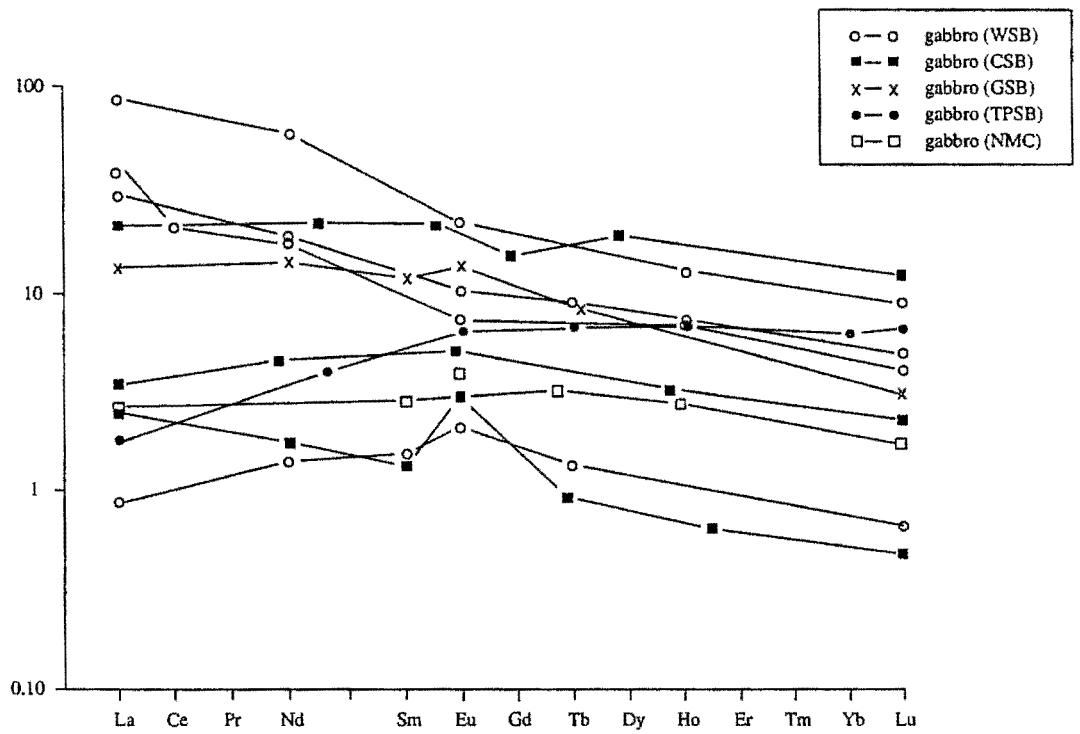

Figure 8.16 CN-REE diagram for the gabbros (data from Table 8.10).

8.4.4 Discussion

The range in composition of the Tumut Serpentinite Province gabbros (comprising a continuous series from leuco- to melano-gabbro) is ascribed to their differing clinopyroxene+hornblende/plagioclase ratios. It is not belt dependent as the range exists in all of the belts.

Although similar-looking gabbros occur within the Micalong Swamp Complex (Callan 1984), they are distinctly different from those of the Tumut Serpentinite Province in that they are more enriched in TiO_2 and more depleted in Cr and Ni (all three considered as immobile elements). Gabbros of the Honeysuckle Beds (Basden 1990) are similar to those of the Tumut Serpentinite Province and significantly different from those of the Micalong Swamp Complex. This suggests that the gabbros of the Honeysuckle Beds are geochemically akin and possibly genetically related to those of the Tumut Serpentinite Province.

The various rocktypes of the Honeysuckle Beds (Basden 1990) form linear trends on the Cr vs Ni variation diagram, thereby suggesting that they are genetically related and have the same source magma. Conversely, Dadd (1998) suggested (unsupported by evidence) that the intrusive rocks of this unit were unrelated to the Honeysuckle Beds and perhaps part of a younger sequence. Intrusive mafic dykes from the North Mooney Complex are also shown on this diagram, and as they coincide with the mafic volcanic rocks of the Honeysuckle Beds, this suggests that they are in fact mafic volcanic rocks of the Honeysuckle Beds which have intruded into hornblende gabbros of the North Mooney Complex.

Gabbros of the Tumut Serpentinite Province range from REE-depleted to REE-enriched, but this is not belt dependent (see above). High concentration of Sc within some of the gabbros is attributed to scavenging by clinopyroxene (Menzies *et al.* 1977).

CN REE patterns for many gabbros exhibit convex upward curves. Anomalies range from weak -ve to strong +ve Eu anomalies. These patterns differ from those of both cumulus and high-level gabbros from the Semail (Pallister & Knight 1981), Troodos (Kay & Senechal 1976), and Point Sal ophiolites (Menzies *et al.* 1977), all of which generally exhibit moderate concave-upward curves. CN REE patterns for the Tumut Province gabbros exhibit moderate +ve Eu anomalies indicative of plagioclase accumulation (Pallister & Knight 1981) and more rarely, weak -ve Eu anomalies indicative of plagioclase removal (Pallister & Knight 1981). The gabbros which exhibit moderate concave-upward curves with no significant anomalies and weak concave upward curves with a weak +ve Eu anomaly, are similar to those from the various ophiolites described above.

8.5 METABASALTIC ROCKS

8.5.1 Major and minor element geochemistry

The metabasaltic rocks of the Tumut Serpentinite Province vary widely in composition (Table 8.11), and the compositional range is present in all belts, generally characterised by enrichment in Al_2O_3, FeO, CaO, Na_2O, V, Cu, Zn, Ba, Sr, Nb, Zr and Y, and depletion in K_2O, Ga, Th and U.

For comparison, metabasalts from the Jindalee Beds and the Honeysuckle Beds were also analysed (Tables 8.12 and 8.13) and both groups are similar. Ashley (1973a) interpreted the basaltic rocks of the Honeysuckle Beds as representing low grade metamorphosed abyssal tholeiites whose chemistry suggested little fractionation following migration from the source region. Franklin (1975) noted that they were tholeiitic (rather than alkalic) and of ocean-floor origin, and suggested that metamorphism led to an increase in Fe^{3+}/Fe^{2+}, a decrease in Ca and Mg, and a possible increase in K. She also reported rare high-Mg basalts that were enriched in MgO, had lower Al_2O_3, and higher CaO/Al_2O_3 ratios than other basaltic rocks of the Honeysuckle Beds. Ray (1977) indicated that the spilitic basalts of Mount Lightning had a wide range in both major and trace element geochemistry but that they were consistently low in K_2O, TiO_2 and P_2O_5, and had high Na_2O/K_2O ratios. He suggested that they represented abyssal tholeiites.

Based on new trace element and REE analyses, Hellman & Henderson (1977) argued that the basaltic rocks of the Honeysuckle Beds could have formed in any of several tectonic settings including island-arc, continental margin or within-continent. To counter-act this, Ashley *et al.* (1979) provided substantial geochemical and field evidence to show that the basalts were tholeiitic and formed within a marginal basin environment, possibly a back-arc basin.

Dadd (1998) showed that the basaltic rocks of the Honeysuckle Beds range from little fractionated to highly evolved and that their geochemical affinity is to modern back-arc basin basalts formed within a subduction-related environment. She showed that, on various trace element discrimination diagrams, they plotted as island-arc and mid-ocean ridge basalts and that their REE geochemistry is most similar to back-arc basin basalts and enriched MORB. With regards to the effects of

metamorphism, Dadd (1998) showed that the scatter of Na, K and Ca on variation diagrams was due to redistribution during alteration.

With regards to basaltic rocks in world-wide ophiolite complexes, Coleman (1977) showed that they have a restricted geochemical composition being distinctly low in TiO_2 (0.5-2 Wt%), are mainly tholeiitic, and that any calc-alkaline tendencies are due to hydrothermal metamorphism."

8.5.2 Variation diagrams

On the compositional diagram of Winchester and Floyd (1977) (Figure 8.17), metabasaltic rocks of the Tumut Serpentinite Province plot as follows:

(a) Coolac Serpentinite Belt - close to the border between the andesite/basalt and subalkaline basalt field,

(b) Wambidgee Serpentinite Belt - predominantly in the andesite/basalt and subalkaline basalt fields,

(c) Tumut Ponds Serpentinite Belt - andesite/basalt and subalkaline and alkaline basalt fields,

(d) Jindalee Beds – close to the border between the subalkaline basalt and alkaline basalt field,

(e) Honeysuckle Beds - predominantly in the andesite/basalt field.

Using the Zr/Y vs Zr discrimination diagram of Pearce and Norry (1979), (Figure 8.18) metabasaltic rocks of the Tumut Serpentinite Province plot as follows:

(a) Coolac Serpentinite Belt - dominantly mid-ocean ridge and island arc basalts;

(b) Wambidgee Serpentinite Belt – dominantly mid-ocean ridge and within plate basalts;

(c) Tumut Ponds Serpentinite Belt – mid-ocean ridge basalts and within plate basalts;

(d) Jindalee Beds and Honeysuckle Beds – predominantly mid-ocean ridge/island arc basalt overlap, and within plate basalts.

Using the Ti vs Cr discrimination diagram of Pearce (1975) (Figure 8.19), most of the metabasaltic rocks of the Tumut Serpentinite Province, Jindalee Beds and Honeysuckle Beds plot as ocean floor basalts.

Using the $Nb^{x}2$-Zr/4-Y discrimination diagram of Meschede (1986) (Figure 8.20) metabasaltic rocks of the Tumut Serpentinite Province plot as follows:

(a) Coolac Serpentinite Belt - P-MORB and N-MORB basalts;

(b) Wambidgee Serpentinite Belt - predominantly VAB and N-MORB basalts;

(c) Tumut Ponds Serpentinite Belt - no clear distribution;

(d) Jindalee Beds - P-MORB basalts;

(e) Honeysuckle Beds - predominantly N-MORB and VAB basalts.

Using the Cr vs Ni diagram (Figure 8.21), metabasaltic rocks of the Tumut Serpentinite Province plot with the metabasaltic rocks of the Jindalee Beds, Honeysuckle Beds and mafic dyke rocks from within the North Mooney Complex, but although generally lying on the same trend as the metabasaltic rocks of the Micalong Swamp Complex, they are distinctly more enriched in Cr and Ni and are therefore more primitive.

On the Ti/Zr vs Zr discrimination diagram of Gamble *et al.* (1993), (Figure 8.22) the metabasalts of the Tumut Serpentinite province plot within the field of back-arc basin basalts from the Pacific rim region. This suggests that they originally formed within such a tectonic setting.

Sample No	140a	147	150b	BF92/14c	BF92/16	TPA2	TPA3	157c	159
Belt	CSB	CSB	CSB	WSB	WSB	TPSB	TPSB	TPSB	TPSB
SiO2	52.28	52.09	50.36	43.76	41.47	47.34	55.17	49.37	46.15
TiO2	0.65	0.58	1.01	2.15	1.61	1.97	0.7	1.9	1.77
Al2O3	17.68	14.14	15.04	12.26	13.75	11.03	15.16	13.5	14.96
Fe2O3	1.76	2.84	2.44	2.66	3.47	3.24	4.84	1.93	3.43
FeO	5.33	4.83	5.17	6.52	14	7.76	3.57	9.92	7.32
MnO	0.15	0.16	0.35	0.12	0.3	0.18	0.13	0.25	0.17
MgO	6.35	10.12	10.04	14.72	6.37	11.77	4.8	6.83	10.08
CaO	8.53	8.76	7.07	13.06	12.08	10.26	7.07	10.15	8.79
Na2O	3.76	4.37	3.83	1.96	3.73	1.68	4.03	3.57	2.85
K2O	0.68	0.15	1.27	0.21	0.47	0.24	2.13	0.35	0.69
P2O5	0.1	0.15	0.23	0.18	0.07	0.18	0.28	0.2	0.66
H2O+	2.25	1.71	2.62	2.77	2.17	4.01	1.9	1.78	2.23
CO2	0.06	0.05	0.42	0.07	0.03	0.03	0.05	0.07	0.05
H2O-	0.23	0.23	0.25	0.19	0.2	0.3	0.28	0.16	0.71
Cr	9	581	406	562	7	932	143	120	350
Ni	40	202	180	373	36	409	77	117	245
V	220	105	200	271	619	256	340	368	162
Cu	84	37	134	7	139	70	53	43	56
Pb	3	6	16	6	10	8	17	10	7
Zn	51	64	195	40	139	86	62	92	74
Rb	37	5	42	2	3	6	70	10	10
Ba	145	76	409	49	100	159	604	153	437
Sr	295	96	427	63	224	231	355	236	884
Ga	10	12	11	6	9	15	11	15	14
Nb	3	6	9	19	5	22	6	5	57
Zr	46	55	87	124	121	127	43	128	218
Y	19	19	27	30	39	24	12	45	24
Th	2	5	3	2	6	4	4	2	5
U	b.d	b.d	b.d	b.d	b.d	b.d	b.d	1	1

(Data source: this thesis)

b.d = below detection limit

Table 8.11 Major and minor element analyses of basalts.

Sample No	62b	BF92/12	163
SiO2	49.93	49.61	54.9
TiO2	0.61	2.35	2.76
Al2O3	15.58	13.71	12.02
Fe2O3	3.82	3.23	7.79
FeO	4.7	7.99	5.71
MnO	0.16	0.15	0.15
MgO	9.14	7.01	3.53
CaO	7.09	11.74	7.74
Na2O	3.84	2.09	0.92
K2O	1	0.12	0.03
P2O5	0.31	0.23	0.3
H2O+	3.93	1.53	3.36
CO2	0.03	0.15	0.41
H2O-	0.35	0.13	0.28
Cr	316	192	121
Ni	65	90	70
V	236	336	403
Cu	103	147	165
Pb	6	7	12
Zn	92	94	98
Rb	20	1	b.d
Ba	323	28	40
Sr	741	372	540
Ga	11	19	22
Nb	12	18	27
Zr	51	142	165
Y	17	29	46
Th	3	3	2

(Data source: this thesis)

b.d = below detection limit

Table 8.12 Major and minor element analyses of Jindalee Beds basalts.

Table 8.13 Major and minor element analyses of rock types from the Honeysuckle Beds

Sample No	BF92/18	81	108	109	107	BF29	MU3822*	MU3880*	MU3943*	MU3955*	MU3954*	MU3925*	MU3860*
Rocktype	Metabas	Metabas	Metabas	Metabas	Metagab	Metabas	Trondhj	Trondhj	Granodio	Trondhj	Trondhj	Trondhj	Albititite
SiO2	51.13	54.74	55.72	52.11	45.75	58.24	78 79	77.56	75 51	71.18	70 33	63.04	62.24
TiO2	0.76	0.84	0.88	1.07	0 36	0.94	0.04	0.05	0.27	0.29	0.34	0 76	0.65
Al2O3	17.31	15.62	14.76	15.05	13.34	17.16	12.95	13 42	11.58	15.64	16.75	18 53	18.54
Fe2O3	3.88	2.09	2.93	3.52	1.68	4.07	0.03	0.05	0.15	1.59	0.45	1.06	0.81
FeO	3.6	4.25	4.16	4.22	5.98	3.72	0.1	0 35	1.4	0 63	0.6	1.1	2.99
MnO	0.13	0.11	0 12	0.14	0.15	0.1	0.01	0 02	0.07	0.04	0.02	0.05	0.05
MgO	5.22	6.35	5.46	6.35	17.12	2.86	0.51	1.15	1.83	0.99	1.44	2.68	1.8
CaO	10.77	6.61	7.75	9.94	9 63	6.79	1.7	0.22	3 24	3.3	2.55	4 48	2.39
Na2O	1.95	6.28	5.69	4.36	0.81	4.53	5.6	6.36	3.87	6.33	6.93	8.06	9.34
K2O	0 68	0.06	0.07	0.33	0.2	0.11	0.37	0.31	2.62	0.03	0.34	0.32	0.09
P2O5	0.13	0.17	0.12	0.15	0.05	0.16	0.03	0.02	0.08	0.1	0.14	0 32	0.24
H2O+	3.4	2.72	2.38	2.71	5.01	1.77	0.16	0 38	0.45	0.32	0.68	0.64	0.74
CO2	1.14	0.16	0.01	0.01	b.d	0.04	b.d	0.13	0.15	b d	0.05	0.18	0.25
H2O-	0.21	0.27	0.39	0.23	0.34	0.22	0.04	0.07	0.25	0.1	0.15	0.16	0.06
Cr	69	811	375	317	1351	131	19	36	579	37	51	62	37
Ni	42	165	87	179	495	29	24	32	275	22	53	53	45
V	219	140	212	220	114	261	b.d	b.d	18	17	27	97	21
Cu	14	19	189	18	46	29	6	5	669	8	12	16	30
Pb	7	8	3	6	7	2	8	b.d	21	b.d	b d	b.d	2
Zn	59	57	50	63	78	19	3	15	1089	8	5	8	11
Rb	17	1	2	6	6	4	6	4	64	b.d	3	2	4
Ba	158	24	29	73	22	85							
Sr	221	115	116	81	74	276	249	305	161	358	383	326	207
Ga	14	14	13	15	11	18	12	9	11	12	12	14	11
Nb	7	7	2	4	1	4							
Zr	63	169	83	116	33	71	24	58	100	248	172	159	137
Y	21	31	28	31	10	29	11	2	28	22	10	23	29
Th	3	6	1	2	b.d	2	10	b d	10	7	7	3	4
U	b.d	b.d	1	1	1	1	4	b d	8	2	b d	b d	2

(Data source this thesis*, Ashley 1973a, Basden 1990)

[Ashley (1973a) included the intrusives as North Mooney Complex equivalents]

b d = below detection limit

Table 8.13 (continued) Major and minor element analyses of rock types from the Honeysuckle Beds

Sample No	MU3921*	MU3882*	MU3956*	MU3847*	MU3830*	MU3859*	MU3818*	MU3973*	MU3957*	MU3913*	MU3978*	MU3927*	MU3930*
Rocktype	Diorite	Diorite	Diorite	Diorite	Diorite	Diorite	Diorite	Meta-and	Dolerite	Metadol	Metabas	Metabas	Metabas
SiO2	60.8	58.63	56 03	54.71	54 4	53.04	52.67	60.02	49.27	48.97	50 62	53	54 87
TiO2	0.9	0.76	0.91	0.45	0 43	0.58	0.49	0.84	1.15	0.71	0 68	0 59	0.65
Al2O3	19.06	16.67	17.46	14.38	14.49	17 16	11.95	16.55	17.16	14.52	14 42	16.68	14 05
Fe2O3	0.81	1.07	1.22	0.79	1.03	1.01	1.77	2.28	1.38	1.73	5 15	1 21	3 43
FeO	1.75	3.94	3 99	4.31	4.33	5.51	4.76	5.05	6.19	5.57	3.28	4 78	3.3
MnO	0.05	0.1	0 1	0.13	0.13	0 15	0.14	0 14	0.16	0.24	0.21	0 15	0 2
MgO	3.56	6.12	6.23	8.66	10 42	7.12	13.7	3 46	9.05	12.73	7.81	7.17	8 65
CaO	6.5	5.78	5.56	11.38	9.34	10.04	9.72	5.32	10.89	9.8	14.36	12 41	11.65
Na2O	6.03	6.49	6.12	2.42	2.74	3.05	2.76	4.18	2.91	2.62	1.63	3.33	2.21
K2O	0.51	0.09	0.57	2	1 43	0.62	0.09	0 08	0.19	0.09	0.08	0.16	0.08
P2O5	0.4	0.15	0.32	0.1	0.08	0 1	0.1	0.26	0 14	0.13	0 38	0 17	0.19
H2O+	1	1.12	1.7	1.51	0.84	1.35	1.7	2.2	2.52	3 38	1.79	1.59	0.59
CO2	0.05	0.05	0.45	0.1	b.d	0.05	0.1	0 09	0.1	0.15	0 13	0.1	0.11
H2O-	0.07	0.06	0.22	0.19	0 03	0 08	0.14	0.14	0.13	0.1	0.14	0 11	0 04
Cr	78	247	173	514	706	191	1085	14	376	755		243	225
Ni	58	120	71	140	194	99	337	26	159	287		103	160
V	122	134	169	131	130	151	157	179	139	160		186	104
Cu	11	62	10	22	22	54	17	300	86	93		22	26
Pb	b.d	b.d	b.d	b.d	8	12	3	3	2	8	8	b d	7
Zn	12	28	18	35	50	59	45	40	66	86		51	64
Rb	5	2	7	78	59	20	b.d	b d	5	2	2	b.d	b.d
Ba													
Sr	610	388	404	230	206	172	270	482	267	269	192	555	205
Ga	14	12	16	10	12	15	10	20	15	8	12	13	14
Nb													
Zr	144	127	135	70	50	62	56	112	87	63	71	68	80
Y	27	24	23	17	13	16	14	22	27	19	41	18	20
Th	3	2	3	2	3	2	b d	3	2	2	3	2	5
U	2	b d	b d	b.d	b d	b d	b d	2	b d	b d	b d	2	2

(Data source this thesis*, Ashley 1973a Basden 1990)

[Ashley (1973a) included the intrusives as North Mooney Complex equivalents]

b d = below detection limit

Sample No	MU3934*	MU3885*	MU3895*	MU3972*	MU3885*	MU3920*	MU3861*	MU3842*	MU3834*	MU3922*
Rocktype	Metabas	Gabbro	Gabbro	Gab peg	Gabbro	Gabbro	Gabbro	Gabbro	Gabbro	Gabbro
SiO2	52.73	42.18	44.65	44.56	42.31	46.32	47.23	48.71	53.05	51.17
TiO2	1.02	1.41	0.23	3.33	2.97	0.83	0.47	0.49	0.45	0.52
Al2O3	16.61	15.28	9.49	16.11	13.28	17.73	19.84	20.16	13.84	16.04
Fe2O3	2.06	3.3	3.37	2.7	0.98	4.4	0.68	1.48	1.44	1.4
FeO	5.38	5.76	5.28	8.14	14.71	6.56	4.62	4.32	4.82	3.96
MnO	0.18	0.14	0.17	0.19	0.2	0.15	0.12	0.12	0.15	0.13
MgO	7.16	12.97	21.06	8.78	8.35	8.76	8.52	8.5	10.38	11.14
CaO	7.87	14.31	12.22	11.01	13.52	9.37	14.31	10.07	10.85	9.06
Na2O	5.03	0.93	0.33	2.93	1.48	2.09	1.59	3.1	2.15	3.44
K2O	0.21	0.18	0.11	0.15	0.08	1.57	0.87	0.9	1.8	0.74
P2O5	0.15	0.73	0.04	0.06	0.04	0.1	0.05	0.08	0.08	0.17
H2O+	2.15	2.49	2.01	1.97	1.97	1.81	1.41	1.87	1.35	1.6
CO2	0.08	0.18	0.31	0.29	0.06	0.25	0.1	0.15	0.05	0.17
H2O-	0.27	0.14	0.22	0.16	0.25	0.07	0.15	0.21	0.09	0.2
Cr	370	654	1660	218	192	104	132	195	468	392
Ni	131	393	879	113	126	62	125	86	134	209
V	169	413	131	629	1047	528	173	147	171	165
Cu	28	49	35	33	204	199	198	24	93	19
Pb	9	5	8	11	9	7	b.d	5	8	5
Zn	71	47	54	57	82	49	31	38	48	32
Rb	5	b.d	4	b.d	b.d	15	85	35	83	6
Ba										
Sr	131	172	192	284	141	696	436	561	172	681
Ga	12	13	4	14	15	14	13	12	11	12
Nb										
Zr	118	62	9	37	16	36	20	35	42	47
Y	27	34	8	40	15	9	12	10	15	13
Th	b.d	4	2	2	b.d	b.d	b d	2	b.d	2
U	2	b.d	b d	b.d	b.d	b.d	b.d	b.d	3	b.d

(Data source: this thesis*; Ashley 1973a; Basden 1990)
[Ashley (1973a) included the intrusives as North Mooney Complex equivalents]
b d = below detection limit

Table 8.13 (continued) Major and minor element analyses of rock types from the Honeysuckle Beds

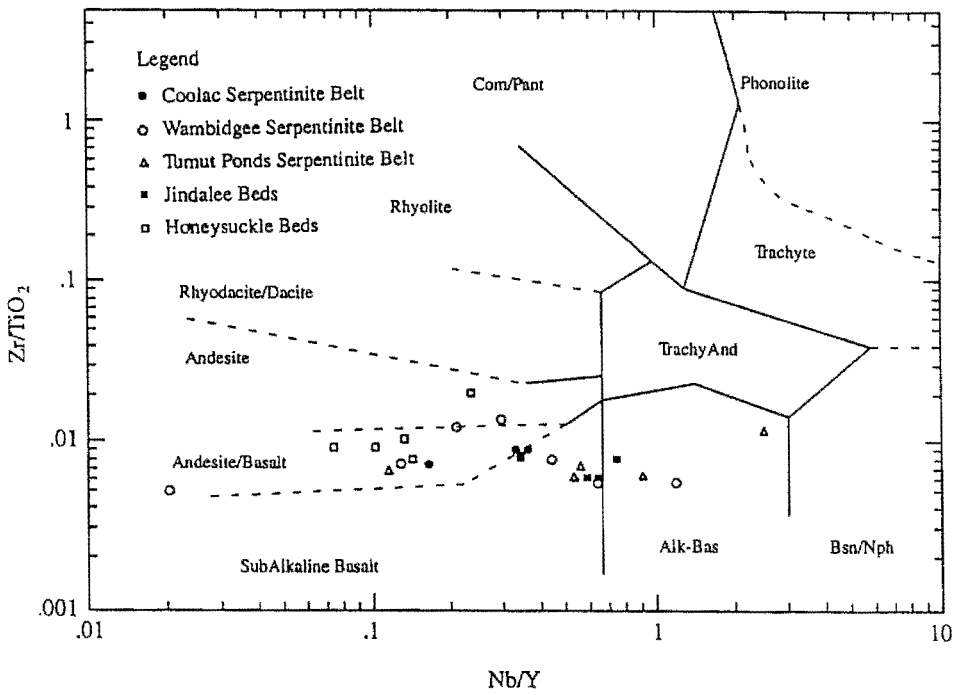

Figure 8.17 Zr/TiO_2 vs Nb/Y discrimination diagram of Winchester and Floyd (1977) for basalts from the Coolac, Wambidgee and Tumut Ponds serpentinite belts, Jindalee Beds and Honeysuckle Beds (data from Tables 8.11, 8.12 and 8.13).

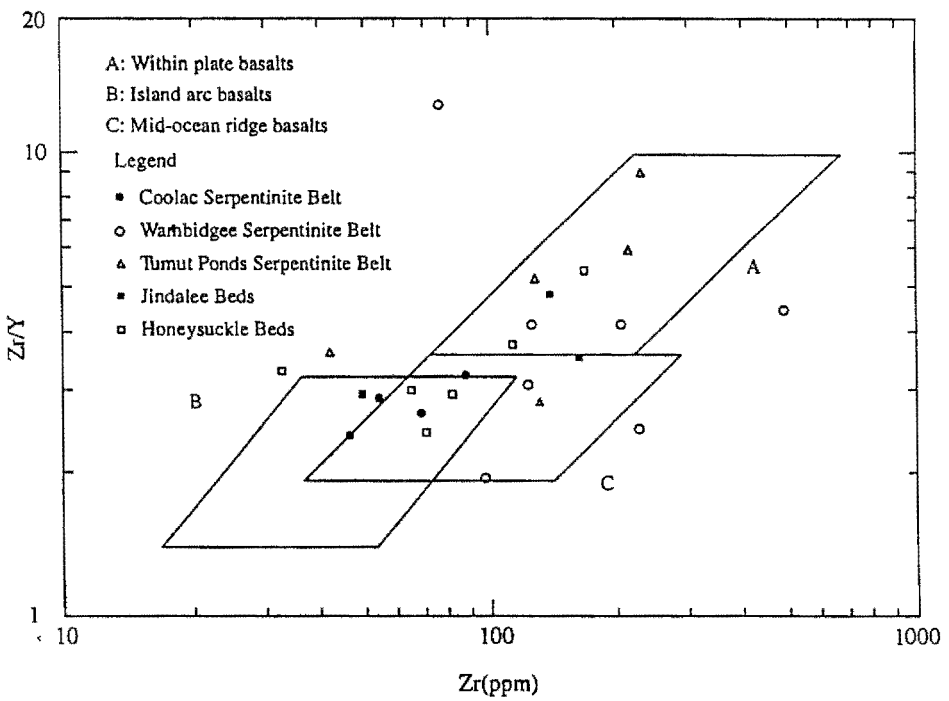

Figure 8.18 Zr/Y vs Zr discrimination diagram of Pearce and Norry (1979) for basalts from the Coolac, Wambidgee and Tumut Ponds serpentinite belts, Jindalee Beds and Honeysuckle Beds (data from Tables 8.11, 8.12 and 8.13).

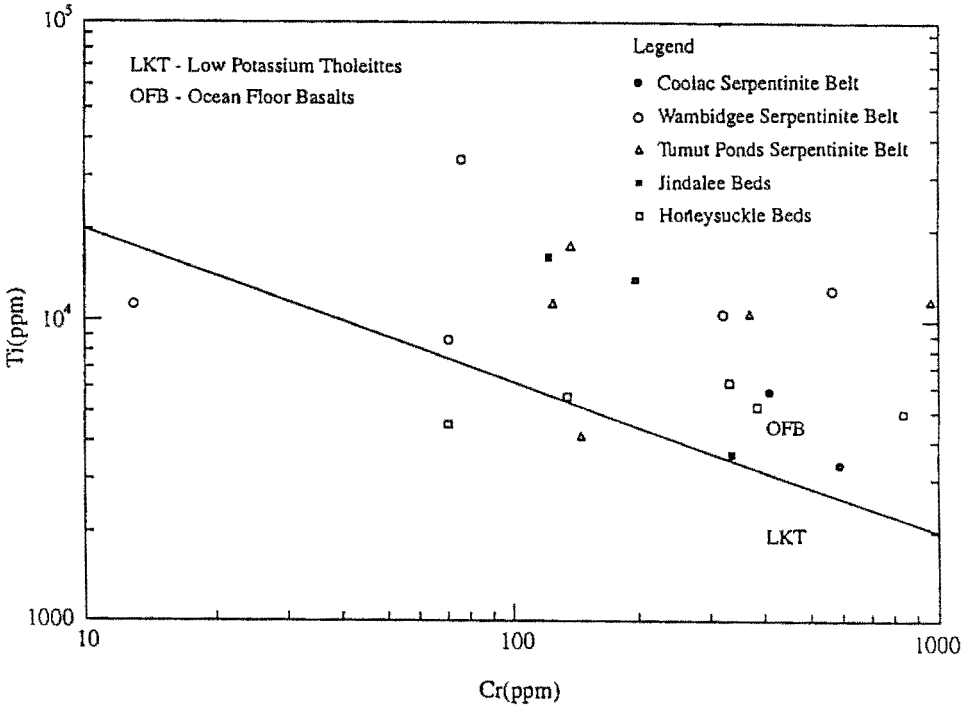

Figure 8.19 Ti vs Cr discrimination diagram of Pearce (1975) for basalts from the Coolac, Wambidgee, and Tumut Ponds serpentinite belts, Jindalee Beds and Honeysuckle Beds (data from Tables 8.11, 8.12 and 8.13).

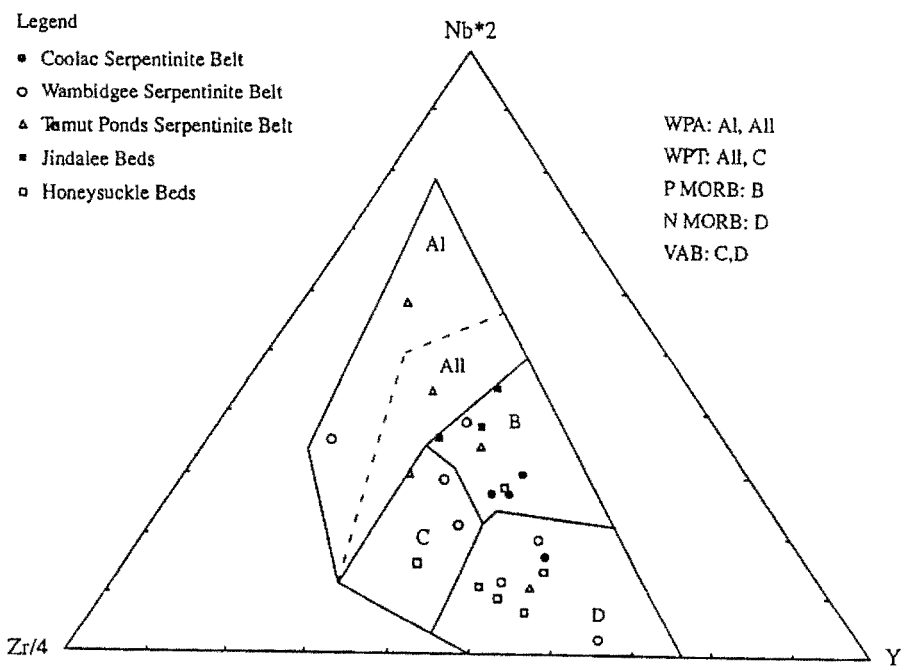

Figure 8.20 Nb*2-Y-Zr/4 discrimination diagram of Meschede (1986) for basalts from the Coolac, Wambidgee, and Tumut Ponds serpentinite belts, Jindalee Beds and Honeysuckle Beds (data from Tables 8.11, 8.12 and 8.13).

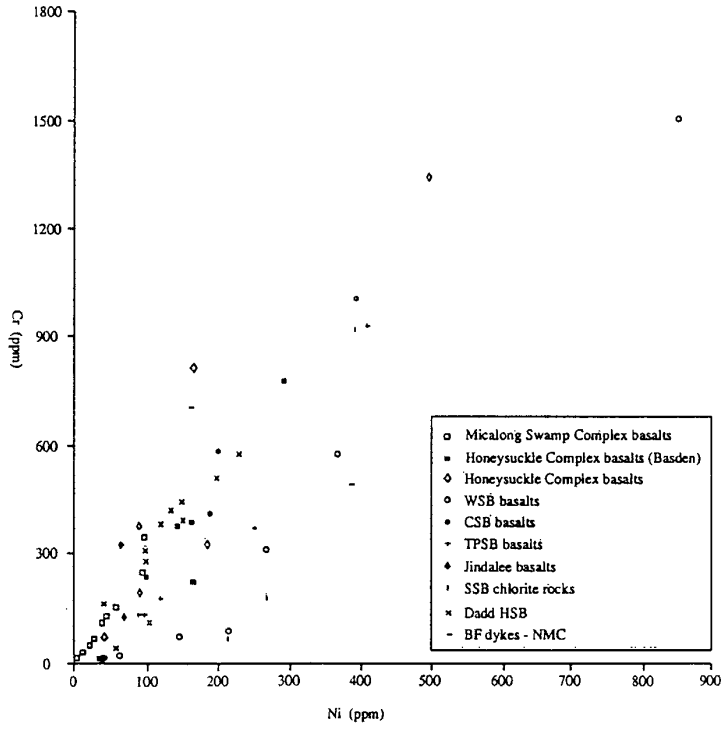

Figure 8.21 Cr vs Ni diagram for basalts and chlorite rocks from the serpentinite belts; basalts from the Honeysuckle Beds, Micalong Swamp Complex and Jindalee Beds; and mafic dyke rocks from the North Mooney Complex (data from Tables 8.11, 8.12, 8.13 and 8.19; Callan 1984; Basden 1990).

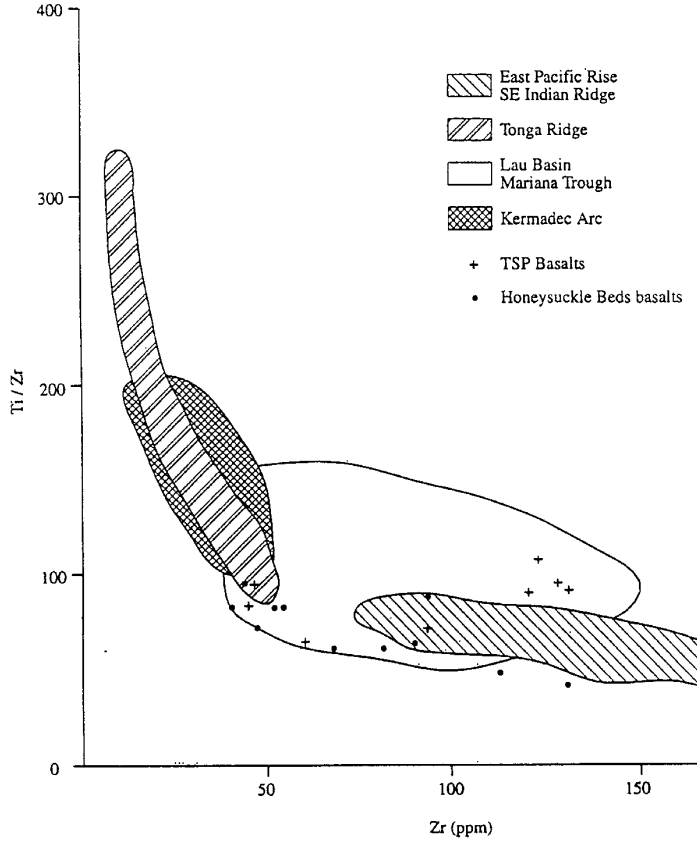

Figure 8.22 Ti/Zr vs Zr diagram of Gamble et al. (1993) for basalts from the Tumut Serpentinite Province and Honeysuckle Beds (data from Tables 8.11 and Dadd 1998).

8.5.3 REE and trace element geochemistry

Overall, metabasaltic rocks of the Tumut Serpentinite Province are moderately REE-enriched (Table 8.14) with respect to the ultramafics and the gabbros. Those from the Wambidgee Serpentinite Belt contain high REE concentrations, those from the Gundagai Serpentinite Belt contain moderate to high REE concentrations, and the single sample from the Western Wambidgee Serpentinite Mélange contains moderate REE concentrations. They also contain high contents of Co and Sc and variable concentrations of Hf and Ta.

REE and trace element geochemistry of metabasalts from the Jindalee Beds and Honeysuckle Beds (Table 8.14), in comparison with those from the Tumut Serpentinite Province, are more REE-enriched, but have similar trace element concentrations. However, it is emphasised that the number of analyses is small.

CN REE patterns (Figure 8.23) for metabasaltic rocks from most of the belts, and the Jindalee and Honeysuckle Beds vary from weakly convex downward curves to essentially planar; one metabasalt from the Wambidgee Serpentinite Belt has a small Eu trough.

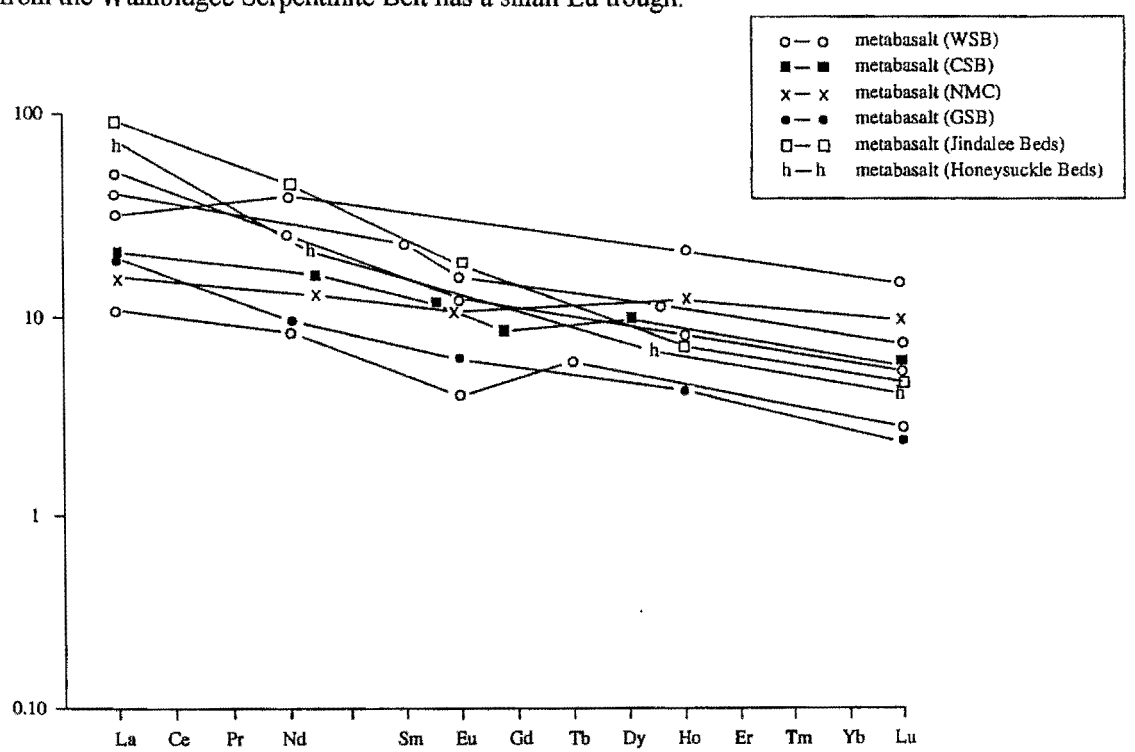

Figure 8.23 CN-REE diagram for metabasalts (data from Table 8.14).

Table 8.14 Rare earth and trace element analyses of basalts.

Sample No	BF92/16	182	169bas	201	179	235	62b	K92-679	235	238m/dyke
Belt	WSB	WSB	WWSM	GSB	GSB	NMC	Jindalee	Honeysu	TPSB	CSB
La	10.51	11.41	3.31	5.39	14.16	5.3	28.67	18.08	5.3	5.11
Ce	31.46	29.19	7.95	10.4	29.9	12.9	52.37	38.72	12.9	11.8
Nd	21	18.1	4.95	5.45	15.2	8.26	23.7	18.97	8.26	8.26
Sm	6.07	3.93	1.18	1.27	3.43	2.43	4.59	3.91	2.43	2.14
Eu	2.04	1.01	0.28	0.41	0.82	0.86	1.21	1.22	0.86	0.65
Tb	1.12	0.6	0.27	0.22	0.46	0.58	0.46	0.57	0.58	0.47
Ho	1.41	0.68	0.37	0.27	0.54	0.91	0.52	0.71	0.91	0.63
Yb	3.13	1.47	0.65	0.52	1.21	2.45	1.21	1.61	2.45	1.42
Lu	0.47	0.21	0.09	0.07	0.18	0.35	0.18	0.23	0.35	0.2
Sb	b.d	b.d	b.d	0.42	0.14	b.d	b.d	b.d	b.d	b.d
As	b.d	b.d	b.d	1.67	b.d	b.d	1.68	b.d	b.d	2.5
Cr	9.1	230	272	658	81.8	245	255	360	245	199
Co	66.6	60.6	85.3	66.9	50.6	48.4	58.3	38.6	48.4	52.3
Au	b.d	b.d	b.d	b.d	b.d	b.d	b.d	b.d	b.d	b.d
Hf	3.17	1.19	0.66	0.36	1.61	1.26	1.23	1.63	1.26	0.98
Ir	b.d	b.d	b.d	b.d	b.d	b.d	b.d	b.d	b.d	b.d
Sc	48.5	43.8	39	56.1	35.5	43.1	39.9	29.4	43.1	31.6
Ta	0.45	0.92	0.2	0.21	b.d	b.d	0.59	b.d	b.d	b.d
Th	2.13	0.64	0.9	0.65	1.92	b.d	3.09	4.95	b.d	0.96

(Data source: this thesis)

b.d = below detection limit

8.5.4 Discussion

Metabasaltic rocks of the Tumut Serpentinite Province vary widely in composition, but the variation is not belt dependent. The metabasaltic rocks are generally low in K_2O and enriched in Na_2O, as also found by Ray (1977) and Dadd (1998). This was ascribed to remobilisation during regional metamorphism by Ashley *et al.* (1979) and Dadd (1998), rather than representing a primary magmatic signature.

Metabasaltic rocks of both the Jindalee Beds and Honeysuckle Beds (Basden 1990) closely resemble those of the Tumut Serpentinite Province. With regards to the basaltic rocks of the Jindalee Beds, their geochemical similarity to the metabasaltic rocks of the Tumut Serpentinite Belt and Honeysuckle Beds does not in any way suggest a genetic relationship. The Jindalee Beds are an older basement terrane (e.g. Basden 1990). Using a range of variation diagrams, the metabasalts of the region fall into several different groups, but predominantly seem to be andesitic to subalkali and of mid-ocean ridge (MORB) affinity. This tends to be affirmed by the Ti vs Cr discrimination diagram in which most plot as ocean floor basalts. Zr and Y (on which many of the discrimination diagrams are based) are regarded as relatively immobile during metamorphism, but the scatter shown by some of the plots (e.g. Figure 8.18) suggests varying degrees of mobility. Dispersion arising from metamorphism and/or alteration has been noted by many workers in other regions (e.g. Hellman & Henderson 1977; Wang & Glover 1992), yet the diagrams continue to be employed because, if used cautiously and in conjunction with other geological data, they remain as in the case in the Tumut district, a useful basis for tectonic interpretation (e.g. Basden 1986, 1990). Having said this, the author emphasises that such diagrams do not work for continental flood basalts of eastern North America (Wang & Glover 1992), so should not be used alone in order to reconstruct the tectonic setting of basaltic rocks.

Relation to the Micalong Swamp Complex basalts

The Micalong Swamp Complex comprises bodies of gabbro, dolerite, diorite and metabasalt which generally occur to the east of the Tumut Serpentinite Province (Basden 1990). These bodies occur as dyke swarms within the Goobarragandra Volcanics but are themselves intruded by parts of the Young Granodiorite (e.g. Owen & Wyborn 1979). The rocks of the Micalong Swamp Complex have generally undergone lower greenschist facies metamorphism and are low-K tholeiites (Basden

1990). Owen & Wyborn (1979) reported a K-Ar hornblende age of 430 ± 9 Ma and Basden (1990) advocated formation from tholeiitic magmas rising-up peripheral rift zones associated with the early opening of the Tumut Trough to the west. The Micalong Swamp Complex is, in general, neither geographically nor tectonically related to the Tumut Serpentinite Province, and pre-dates its formation (see Chapter 11).

The Cr vs Ni variation diagram (Figure 8.21) shows that metabasaltic rocks of the Tumut Serpentinite Province, Jindalee Beds and Honeysuckle Beds, together with the mafic dyke rocks from the North Mooney Complex cover the same broad region. Those of the Micalong Swamp Complex plot in a more confined area of this diagram and as they are distinctly more depleted in Cr and Ni, are not likely to be genetically related to the others.

Metabasaltic rocks of the Tumut Serpentinite Province vary widely in REE abundances (Table 8.14), but the range is not belt controlled, even though the Wambidgee and Gundagai serpentinite belts, and the Western Wambidgee Serpentinite Melange have moderately REE-enriched metabasalts. Comparison with samples from the Jindalee Beds and Honeysuckle Beds shows that they are more REE-enriched, and that the Jindalee metabasalts are the most REE-enriched.

CN REE patterns (Figure 8.23) for the metabasaltic rocks of the Tumut Serpentinite Province vary from planar to moderate downward curves with non-existent to weak -ve Eu anomalies. The CN REE pattern for the metabasalts from the Jindalee Beds and Honeysuckle Beds are moderate downward curves (Figure 8.23) with no anomalies. However, all three groups of metabasalts are similar. CN REE patterns for the metabasaltic rocks of the Troodos Ophiolite (Smewing & Potts 1976) are generally flat to concave upward curves with no significant anomalies, so also are the patterns for MORB-type basalts (Pallister & Knight 1981).

However, CN REE patterns for tholeiitic basalts from Iceland, alkali olivine basalts from New Zealand, high alumina basalt and alkali olivine basalt from Japan, and spilitic metabasalts from India (Hellman & Henderson 1977), exhibit moderate to strong downward curves. Thus, despite exhibiting different CN REE patterns from those of other ophiolites, this does not preclude them from having formed in an ophiolitic environment. Indeed, REE patterns partly result from secondary

metamorphic or metasomatic activity (Hellman & Henderson 1977), so differences could reflect the metamorphism and alteration that have affected the Tumut Serpentinite Province metabasalts.

8.6 AMPHIBOLITES

8.6.1 Major and minor element geochemistry

The amphibolites of the Tumut Serpentinite Province are compositionally variable (Table 8.15), particularly with respect to SiO_2, Al_2O_3, Fe_2O_3, MgO, CaO, Na_2O, K_2O, H_2O and the minor elements Cr, Ni, V, Cu, Zn, Ba, Sr, Zr and Y.

8.6.2 Variation diagrams

Despite somewhat limited quantities of data, it would seem from the Cr vs TiO_2 diagram (Figure 8.24) that there are Cr-rich and Cr-poor groups of amphibolite. This is also shown on the Cr vs Ni diagram (Figure 8.25). On the Cr vs TiO_2 diagram (Figure 8.24), most of the amphibolites of Ashley (1973a) are far more enriched in TiO_2 than those analysed during the present study.and cannot be plotted on the diagram.

8.6.3 REE and trace element geochemistry

Only some of the amphibolites from the Wambidgee Serpentinite Belt have been analysed for REE and trace elements (Table 8.16). They vary widely from moderately to highly REE-enriched, are enriched in LREE relative to HREE (Table 8.16), and contain appreciable concentrations of Hf, Sc and Ta.

The CN REE patterns (Figure 8.26) show that there are enriched and highly enriched groups. The patterns range from convex upward curves in the enriched group, to flat or slightly convex downward curves in the highly enriched group.

Table 8.15 Major and minor element analyses of amphibolites.

Sample No	150c	151b	152b	152c	154a	BF92/14b	64	BF92/6b	BF92/8	*86	*527	*345	*304	*303
Belt	CSB	CSB	CSB	CSB	CSB	WSB	WSB	WSB	WSB	CSB	CSB	CSB	CSB	CSB
SiO2	31.12	58.65	39.77	50.2	41.8	43.6	56.17	48.18	41.78	50.46	47.74	49.12	48.59	48.54
TiO2	1.04	0.85	1.29	1.68	0.45	0.05	0.61	0.05	0.6	1.03	0.53	2.69	2.34	3.32
Al2O3	22.93	14.46	12.47	14.11	12.32	18.89	18.3	18.01	6.29	16.74	18.9	15.34	14.07	15.58
Fe2O3	8.53	1.73	4.7	1.99	3.97	0.99	1.25	0.73	4.76	2.26	0.89	2.55	2.31	1.36
FeO	6.65	6.97	8.82	6.92	6.94	2.26	3.62	1.76	5.97	5.64	5.65	7.99	9.23	10.79
MnO	0.31	0.16	0.18	0.21	0.33	0.05	0.1	0.04	0.16	0.16	0.14	0.2	0.23	0.25
MgO	24.12	4.25	22.26	5.32	24.59	13.77	4	11.18	27.27	8.56	9.54	7.03	7.94	5.26
CaO	0.67	6.61	4.94	14.29	6.06	13.73	6.43	17.58	5.57	9.09	12.4	9.11	10.19	9.7
Na2O	0.14	4.46	0.47	3.28	0.28	1.38	7.12	0.53	0.49	3.85	2.19	3.98	3.12	3.48
K2O	0.01	0.35	0.04	0.33	0.03	0.3	0.29	0.1	0.07	0.38	0.99	0.55	0.41	0.39
P2O5	0.33	0.26	0.17	0.24	0.15	b.d	0.28	0.01	0.07	0.16	0.08	0.37	0.32	0.49
H2O+	4.86	1.37	4.65	1.09	2.76	4.67	1.35	1.79	6.48	1.51	1.8	1.8	1.02	1.11
CO2	0.04	0.07	0.04	0.2	0.72	0.03	0.08	0.17	0.16	0.1	0.1	0.15	0.05	0.14
H2O-	0.23	0.21	0.3	0.19	0.15	1.01	0.29	0.15	0.32	0.11	0.05	0.16	0.15	0.24
Cr	617	71	1790	208	1686	3563	2	1669	2910	463	377	294	498	205
Ni	233	22	683	74	741	475	42	299	1554	302	131	249	145	56
V	323	305	193	259	175	81	217	98	139	178	173	280	281	302
Cu	35	66	4	1742	49	6	7	62	56	59	33	195	77	117
Pb	7	7	8	9	7	8	12	13	12					
Zn	109	98	158	139	104	38	27	16	72	62	49	102	223	242
Rb	2	9	b.d	7	1	5	5	4	2					
Ba	10	250	b.d	313	b.d	93	1199	85	161					
Sr	22	460	19	411	15	410	1969	99	92					
Ga	22	14	14	14	9	6	10	7	4					
Nb	13	4	9	13	6	b.d	13	b.d	11					
Zr	150	76	80	107	39	b.d	60	b.d	40					
Y	39	23	28	31	14	5	16	2	10					
Th	13	3	1	4	3	1	3	b.d	2					
U	1	b.d	1	2	1	b.d	1	b.d	1					

(Data source: this thesis; Ashley 1973a)

b.d = below detection limit

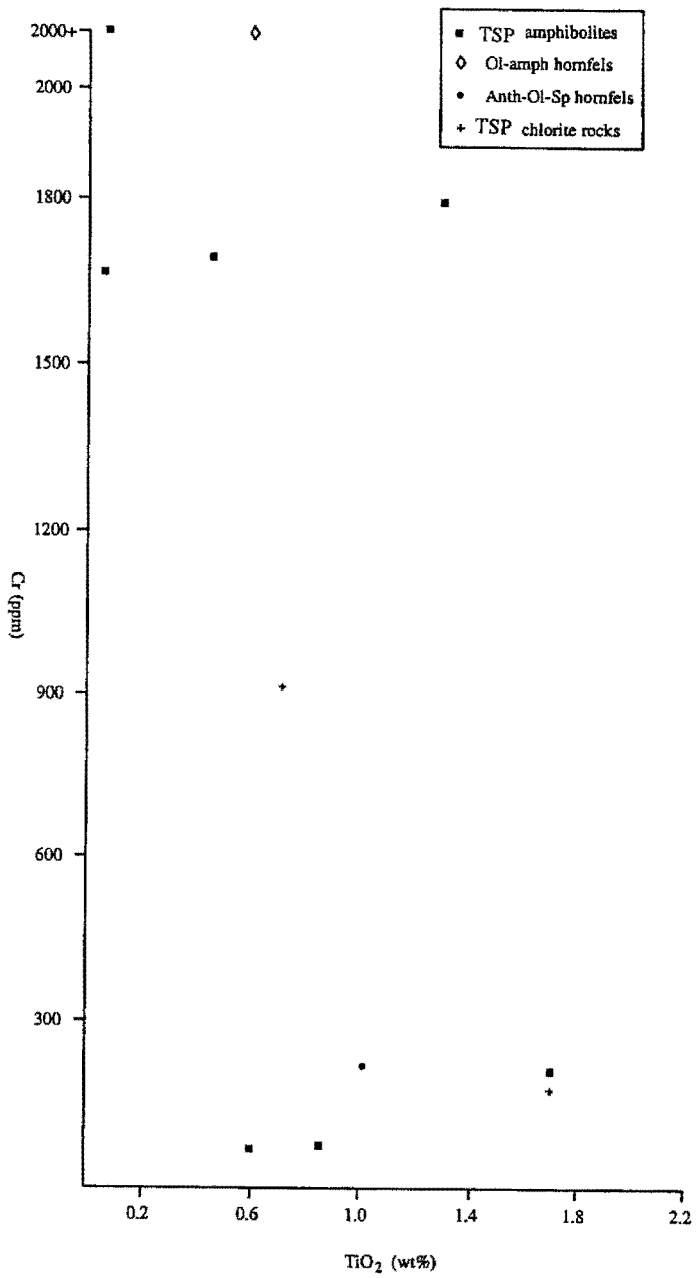

Figure 8.24 Cr vs TiO_2 diagram for amphibolites, chlorite rocks, olivine-amphibole hornfels and anthophyllite-olivine-spinel hornfels from the Tumut Serpentinite Province (data from Tables 8.15, 8.19 and 8.23).

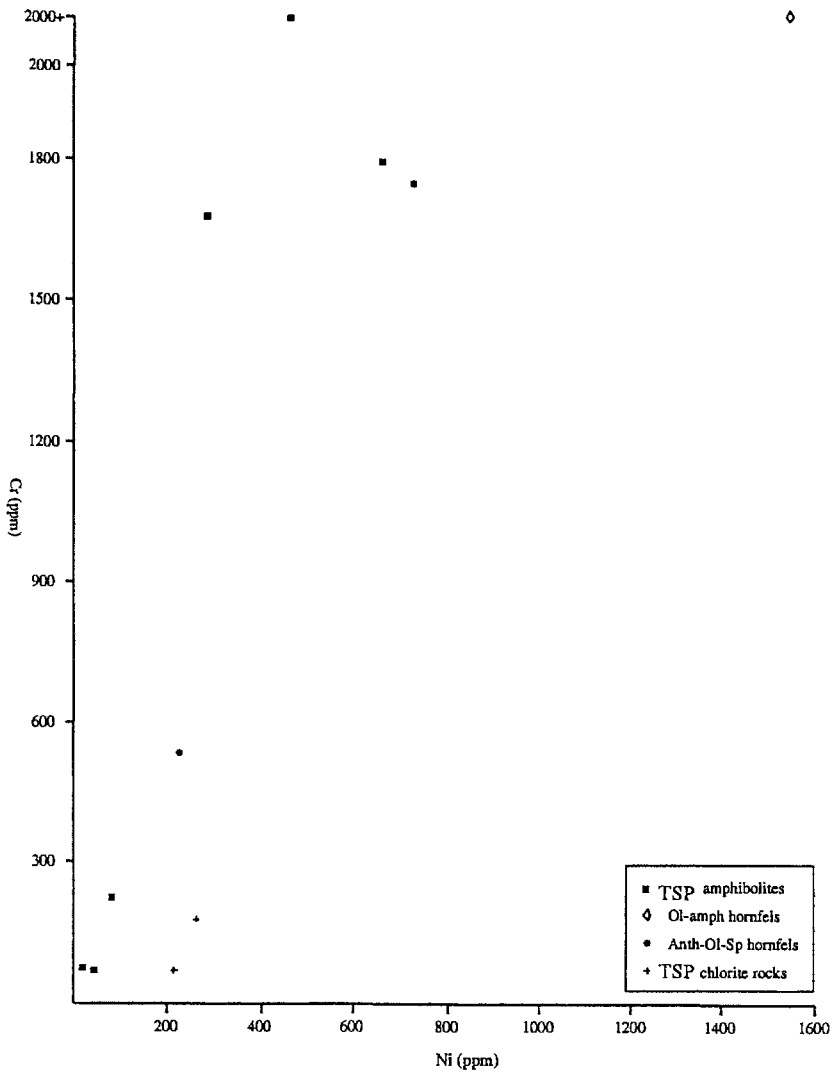

Figure 8.25 Cr vs Ni diagram for amphibolites, chlorite rocks, olivine-amphibole hornfels and anthophyllite-olivine-spinel hornfels from the Tumut Serpentinite Province (data from Tables 8.15, 8.19 and 8.23).

Sample No	193	187	188	196	190
Belt	WSB	WSB	WSB	WSB	WSB
La	12.2	57.71	22.79	0.43	0.97
Ce	29.58	91.54	42.43	1.49	2.99
Nd	20.05	39.14	19.28	1.59	2.45
Sm	5.67	7.56	3.54	0.73	0.8
Eu	1.74	2	0.9	0.35	0.31
Tb	1.09	0.84	0.64	0.24	b.d
Ho	1.27	0.87	0.8	0.36	0.242
Yb	2.81	2.23	1.81	0.9	0.57
Lu	0.38	0.32	0.28	0.11	0.079
Sb	0.2	b.d	b.d	b.d	b.d
As	b.d	b.d	b.d	b.d	b.d
Cr	174	3.1	2.8	643	246
Co	75.1	62.8	58.4	72.7	52.2
Au	b.d	b.d	b.d	b.d	b.d
Hf	3.84	2.16	2.11	0.32	b.d
Ir	b.d	b.d	b.d	b.d	b.d
Sc	36.9	31.8	13	48.3	33.3
Ta	1.23	0.4	0.59	b.d	b.d
Th	1.18	0.92	5.55	b.d	b.d

(Data source: this thesis)
b.d = below detection limit

Table 8.16 Rare earth and trace element analyses of amphibolites.

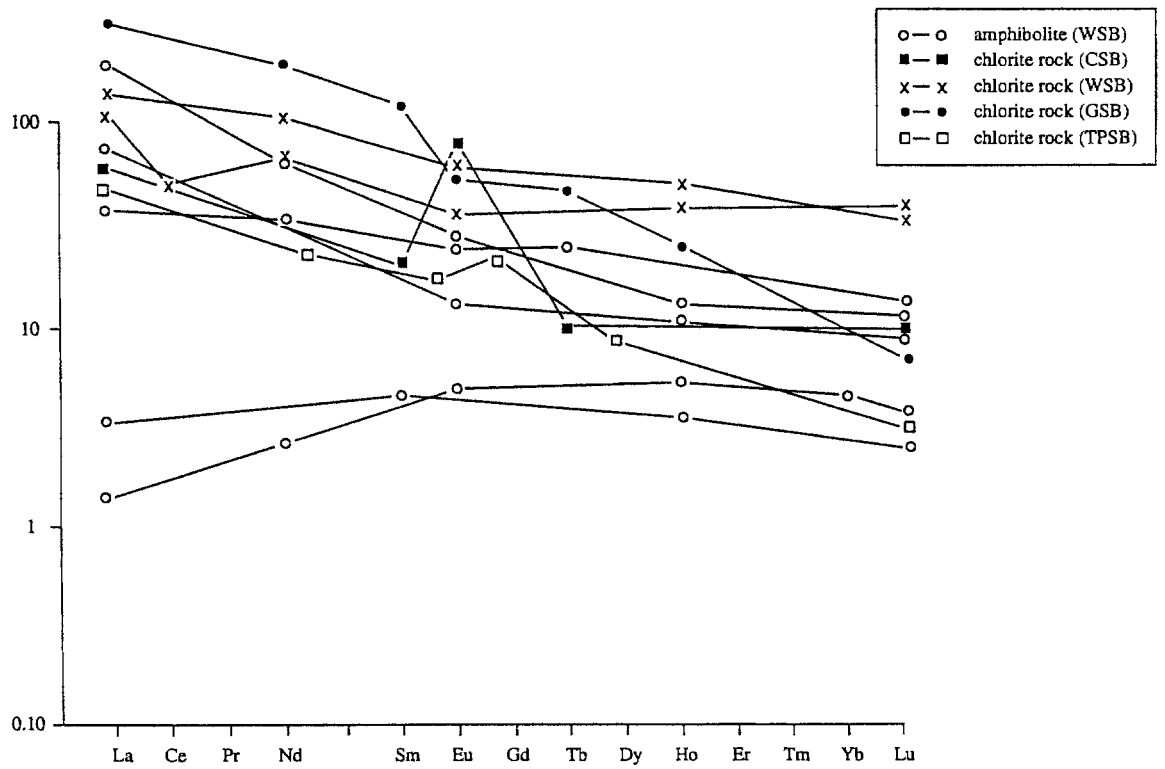

Figure 8.26 CN-REE diagram for amphibolites and chlorite rocks (data from Tables 8.16 and 8.20).

8.6.4 Discussion

The variation in major and minor element chemistry of amphibolites within the two belts from the Tumut Serpentinite Province is particularly expressed in the concentration of immobile elements such as Cr, Ni, and Zr. This is consistent with the variation reflecting magmatic rather than metamorphic/alteration causes; it requires that Cr-rich and Cr-poor types of magma characterise both belts.

The amphibolites of the Tumut Serpentinite Province vary widely in composition. Analyses BF92/14b and BF92/6b from the Wambidgee Serpentinite Belt have particularly low concentrations of TiO_2, P_2O_5, Ni and Zr compared to the other amphibolites while analysis 64, also from the Wambidgee Serpentinite Belt, has particularly high concentrations of SiO_2, Ba and Sr but is low in Cr and Ni. The wide range in chemical composition of amphibolites from the Tumut Serpentinite Province most likely reflects derivation from different protoliths, as proposed (Ashley 1973a) for amphibolites of the Coolac Serpentinite Belt. Ashley (1973a) ascribed these occurrences to the tectonic incorporation emplacement of metamorphosed and deformed oceanic crustal rocks (e.g.

basalts, gabbros, diorites, sediments) by rocks of the ophiolite suite. Samples BF92/14b and BF92/6b are chemically similar to some of the gabbros of the Tumut Serpentinite Province (Table 8.9) whereas sample 64 from the same serpentinite belt is chemically similar to diorites of the Coolac Serpentinite Belt (Table 8.17).

From the CN REE patterns of the amphibolites it would appear that either metamorphism has completely altered the original REE geochemistry of these rocks or, more likely, that these amphibolites were derived from different source rocks. Alternatively, REE concentrations may have increased as a result of loss of other elements through metamorphism.

8.7 PLAGIOGRANITES

8.7.1 Major and minor element geochemistry

Plagiogranites have only been found within the Coolac and Wambidgee serpentinite belts and the Western Wambidgee Serpentinite Melange. All are enriched in SiO_2, Al_2O_3 and Na_2O (Table 8.17).

They have Na_2O/K_2O ratios of 2.99 to 345, with the majority in the range of 100 to 250, and are typical oceanic plagiogranites, as defined by Coleman (1977). Their Zr contents reflect the presence of zircons from which meaningful magmatic crystallisation ages have been obtained (See Chapter 10).

8.7.2 Variation diagrams

Although these plagiogranites are confined to the serpentinite belts, other similar looking felsic granitic rocks occur widespread throughout this region. In order to differentiate the plagiogranites from other granitic rocks in the region, two main discrimination diagrams were constructed. On the $100xNa_2O/Na_2O+K_2O$ vs SiO_2 diagram (Figure 8.27), most of the plagiogranites occupy a different field from the Young Granodiorite. However, there is some overlap between the plagiogranites and the tonalites of the Micalong Swamp Complex. To further investigate this, a $100xMgO/MgO+FeO+Fe_2O_3$ vs SiO_2 diagram (Figure 8.28) was used; it shows that the plagiogranites are different from the tonalites of the Micalong Swamp Complex.

Table 8.17 Major and minor element analyses of plagiogranites and related rocks.

Sample No	79	BF91/20	153	BF91/33f	BF92/6a	161a	162c	1*	2*	4*	6*
Belt	CSB	CSB	CSB	WSB	WSB	GSB	GSB	CSB	CSB	CSB	CSB
Rocktype	Albitite	Plgran	Plgran	Plgran	Plgran	Alt Plgran	Plgran	Hr-Qt Dior	Hr-Qt Dior	Hr-Qt Dior	Trondhj
SiO2	70.47	74.4	79.69	64.93	60.76	46.15	64.81	58.63	60.1	60.85	66.36
TiO2	0.14	0.09	0.1	0.3	0.77	0.08	0.22	0.91	1.02	0.69	0.34
Al2O3	17.1	14.58	11.98	18.43	19.21	20.12	16.83	12.1	16.21	15.95	15.9
Fe2O3	0.13	0.3	0.06	0.43	1.69	0.87	1.7	1.82	0.66	0.91	0.76
FeO	0.27	0.48	0.13	1.17	0.37	3.98	1.58	3.97	4.12	3.01	2.4
MnO	b.d	0.03	0.01	0.02	0.16	0.1	0.06	0.05	0.1	0.19	0.02
MgO	0.47	0.4	0.08	1.16	1.7	15.89	1.33	5.34	3.52	3.63	2.33
CaO	0.71	0.51	0.27	2.59	8.2	0.34	2.38	8.02	7.03	6.58	2.51
Na2O	9.27	5.84	7.11	9.93	5.55	4.8	9.82	6.49	5.98	6.54	7.13
K2O	0.26	1.95	0.04	0.04	0.05	0.05	0.26	0.09	0.46	0.32	0.21
P2O5	0.04	0.01	0.01	0.16	0.3	b.d	0.06	0.19	0.1	0.01	0.08
H2O+	0.72	0.79	0.38	0.65	0.99	7.26	0.55	1.6	1.76	0.98	0.64
CO2	0.01	0.02	0.05	0.03	0.08	0.01	0.02	0.03	b.d	b.d	b.d
H2O-	0.25	0.19	0.19	0.22	0.21	0.27	0.18	0.19	0.01	0.17	0.18
Cr	7	2	1	1	10	2638	15	458	330	120	45
Ni	52	2	29	35	5	455	105	84	76	80	30
V	12	6	b.d	54	86	40	61	260	186	167	10
Cu	3	2	4	8	5	1	28	25	39	18	12
Pb	b.d	4	4	b.d	7	2	b.d				
Zn	3	16	2	12	55	39	25				
Rb	5	17	1	1	b.d	1	2	18	26	39	6
Ba	122	1663	23	67	113	26	326	176	192	176	385
Sr	303	576	49	575	1037	216	731	276	182	290	308
Ga	14	9	9	15	17	6	11				
Nb	9	4	8	10	15	b.d	4				
Zr	100	104	59	85	145	1	72	76	82	65	56
Y	7	2	11	16	22	1	11	19	27	29	18
Th	2	1	24	12	11	1	1				
U	b.d	b.d.	2	1	4	b.d	b.d				

(Data source: this thesis ;Ashley 1973a; Ashley et al. 1983)

b.d = below detection limit

Table 8.17 (continued) Major and minor element analyses of plagiogranites and related rocks

Sample No	7*	8*	9*	10*	13*	14*	15*	16*	17*	18*	19*	20*	21*
Belt	CSB	CSB	CSB	CSB	CSB	CSB	CSB	CSB	CSB	CSB	CSB	CSB	CSB
Rocktype	Trondhj	Qt Kerato	Trondhj	Trondhj	Trondhj	Trondhj	Trondhj	Trondhj	Trondhj	Trondhj	Trondhj	Trondhj	Trondhj
SiO2	67.24	68.17	68.85	69.62	71.32	72.02	72.41	73.14	73.82	75.11	75.31	77.06	77.54
TiO2	0.52	0.45	0.19	0.28	0.21	0.65	0.26	0.42	0.31	0.34	0.13	0 17	0 05
Al2O3	16.4	14.86	16.01	14.62	14.15	14.82	13.27	14.01	12.64	13.84	12.63	12 47	12 12
Fe2O3	1.82	2.06	1.01	1 94	0.86	1.62	1.68	0 82	1.75	0 48	0.31	1 47	0.2
FeO	0.91	2.44	2.53	1.24	1.29	1.21	0.74	0.62	0.82	1 04	1 62	1.2	0.76
MnO	0.1	0.56	0.04	0.1	0.01	0.14	0.18	0.04	0.09	0.16	0.08	0.01	0.01
MgO	1.82	1.04	1.31	1.96	1.3	1.06	0.92	0.66	0 68	0 48	1.13	0.73	0.51
CaO	1.64	3.85	3.2	1.92	1.56	1.89	2.33	1.81	2.42	1.07	1.92	0.99	2.03
Na2O	7.01	4.09	5.25	5 46	7.23	4.74	5.24	5.82	4.73	3.84	5.72	4.24	6 36
K2O	0.22	0.04	0.19	0.4	0.31	0.38	0.34	0.68	0.41	0.79	0.3	0.07	0.12
P2O5	0.07	0.07	0.3	0.03	0.1	0 12	0.12	0.04	0.09	0.11	0 19	0.41	0.14
H2O+	1.82	1.46	0.62	1.62	0 43	1.62	1.84	1.42	1.68	1.21	0.87	0.83	0 45
CO2	0.04	b.d	0.21	0.03	0.18	0.06	0.04	0.07	0.06	0 04	0.24	b.d	b.d
H2O-	1.04	b.d	0.05	0.4	0.16	0.63	0 68	0.74	0.74	0 69	0.2	b d	0.03
Cr	2	30	15	15	62	6	22	18	2	3	18	32	25
Ni	58	15	64	50	26	56	45	33	25	64	42	3	24
V	27	13	18	b.d	10	b.d	25	9	10	2	b d	5	b.d
Cu		b.d	25	b.d	40						b.d		3
Pb													
Zn													
Rb	6	8	5	6	b.d	b.d	4	2	b.d	b.d	b.d	9	b.d
Ba	205	68	324	150	450	122	108	160	180	79	290	33	265
Sr	475	225	196	300	154	372	728	536	225	290	200	133	350
Ga													
Nb													
Zr	105	85	28	75	170	86	49	145	51	180	200	114	137
Y	20	31	16	10	12	10	16	6	25	12	2	37	6
Th													
U													

(Data source: this thesis ;Ashley 1973a; Ashley et al. 1983)

b d = below detection limit

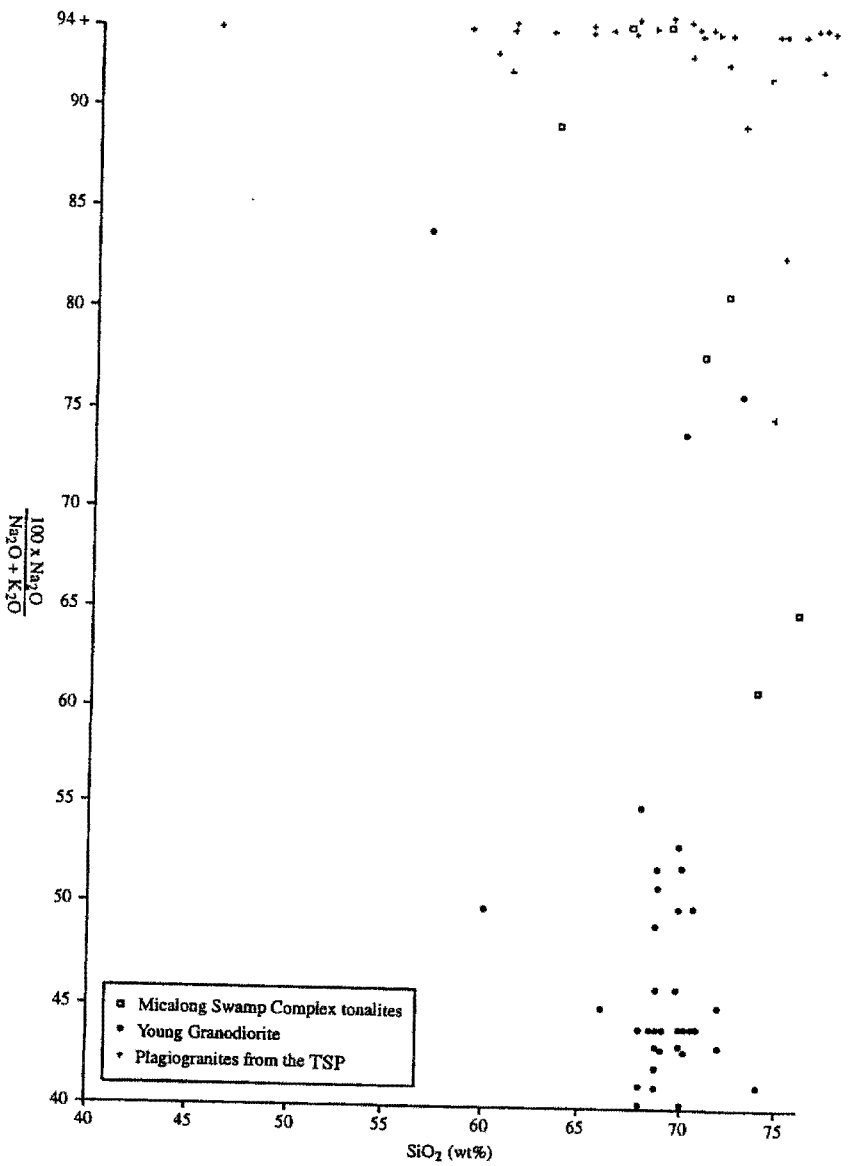

Figure 8.27 $100xNa_2O/Na_2O+K_2O$ vs SiO_2 diagram for plagiogranites and related rocks from the serpentinite belts; tonalites from the Micalong Swamp Complex; and granitic rocks from the Young Granodiorite (data from Table 8.17; Ashley *et al.* 1983; Callan 1984; Basden 1990).

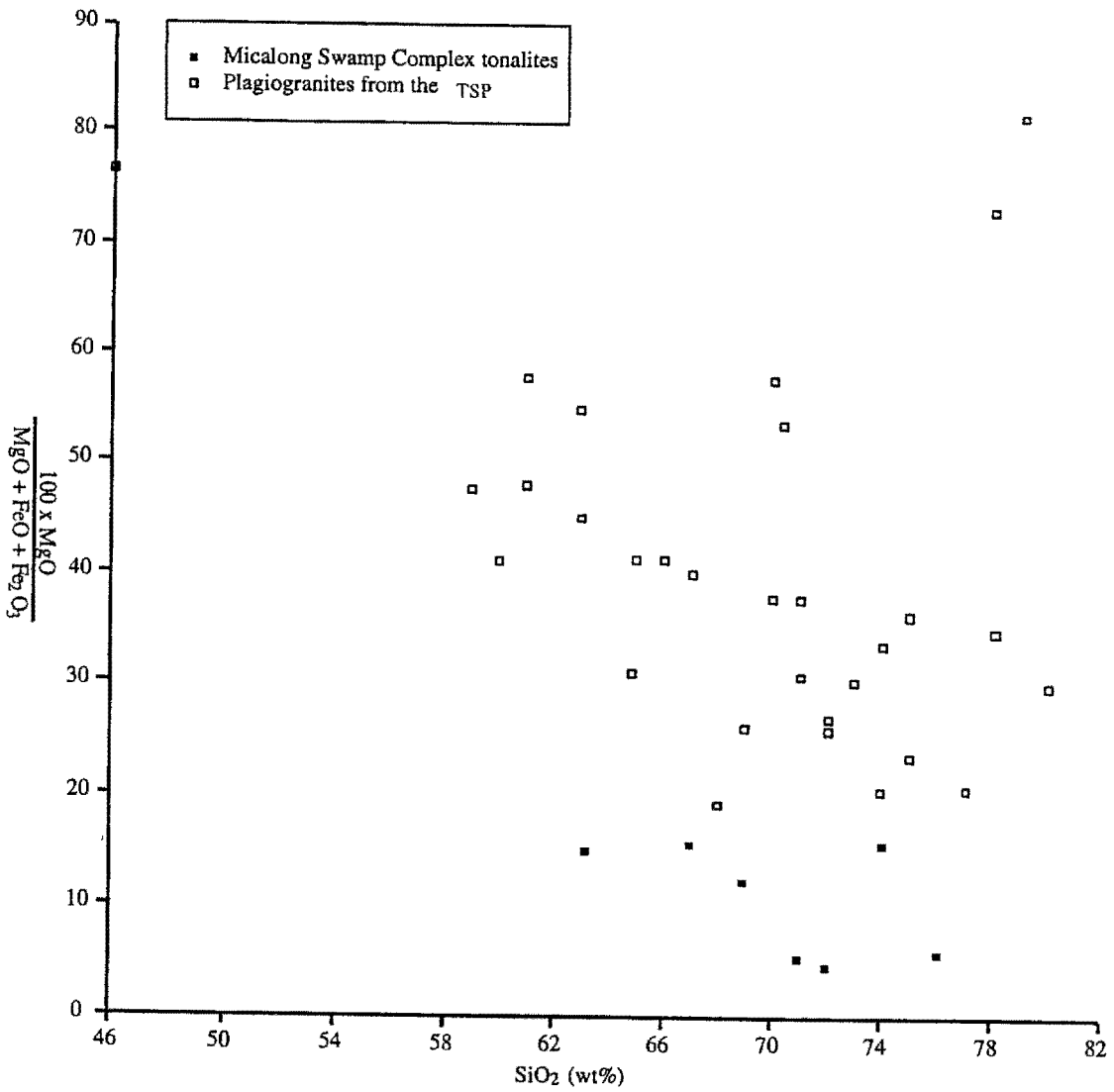

Figure 8.28 100xMgO/MgO+FeO+Fe_2O_3 diagram for plagiogranites and related rocks from the serpentinite belts; and tonalites from the Micalong Swamp Complex (data from Table 8.17; Callan 1984).

Sample No	BF91/20	BF92/6a	189	BF91/33f	169
Belt	CSB	WSB	WSB	WSB	WWSM
La	1.58	44.92	1.23	33.69	16.72
Ce	3.15	103.55	1.4	56.09	31.99
Nd	1.62	50.53	b.d	22.62	12.92
Sm	0.4	8.7	0.113	3.42	2.47
Eu	0.24	2.31	b.d	0.81	0.45
Tb	0.1	0.97	b.d	0.36	0.34
Ho	0.15	0.93	b.d	0.47	0.45
Yb	0.41	2.11	0.114	1.3	1.25
Lu	0.05	0.3	0.018	0.19	0.17
Sb	b.d	0.32	b.d	b.d	b.d
As	b.d	1.26	b.d	b.d	b.d
Cr	2	7.3	b.d	b.d	3
Co	94.1	64.5	46.3	70.4	87.7
Au	b.d	b.d	6.2	b.d	b.d
Hf	1.97	4.06	b.d	2.31	1.97
Ir	b.d	b.d	b.d	b.d	b.d
Sc	0.64	21.5	0.15	7.45	4.02
Ta	0.5	0.64	b.d	0.72	0.94
Th	b.d	12.1	b.d	5.72	5.8

(Data source: this thesis)
b.d = below detection limit

Table 8.18 Rare earth and trace element analyses of plagiogranites.

8.7.3 REE and trace element geochemistry

The plagiogranites from the Tumut Serpentinite Province are enriched in the LREE (Table 8.18), with the exception of the plagiogranite from the Coolac Serpentinite Belt which is 10X more depleted. They have variable Sc, and one sample from the Wambidgee Serpentinite Belt (BF 92/6a) contains anomalous Sb and As.

On the CN REE diagrams, the plagiogranites exhibit convex downward curves (Figure 8.29) with the exception of the sample from the Coolac Serpentinite Belt which is affected by a Eu peak. The only other anomalous sample is from the Wambidgee Serpentinite Belt and has an appreciable Eu trough.

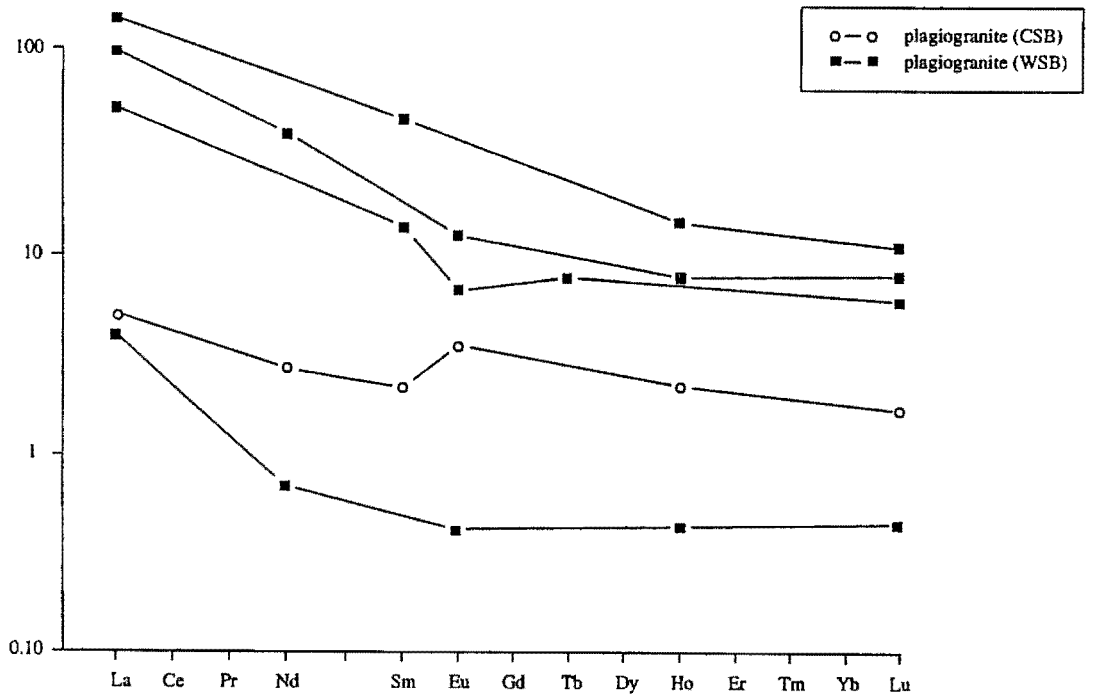

Figure 8.29 CN-REE diagram for plagiogranites (data from Table 8.18).

8.7.4 Discussion

The plagiogranites and related felsic rocks of the Tumut Serpentinite Province differ from the Young Granodiorite and felsic rocks of the Micalong Swamp Complex. They cannot therefore be tectonic inclusions of these bodies and are interpreted as integral parts of the serpentinite belts, as suggested by Ashley *et al.* (1983) and Graham *et al.* (1996). Sample 161a from the Gundagai Serpentinite Belt is unusually depleted in SiO_2, TiO_2, Nb and Zr, while enriched in Al_2O_3, FeO, MgO, Na_2O, H_2O, Cr and Ni. Petrographically, it is an albite-chlorite rock consisting of alternating chlorite- and albite-rich bands. It may well represent a reaction zone rock (e.g. Ashley 1973a) formed between serpentinite and plagiogranite/albitite.

The plagiogranites of the Tumut Serpentinite Province are similar in major element composition to those from the Volti Group of the Ligurian Alps (with 69-76Wt% SiO_2, high Na_2O and low K_2O, and low TiO_2) and the Sestri-Voltaggio Zone (with 60-75Wt% SiO_2, high Na_2O and low K_2O, and low TiO_2) (Borsi *et al.* 1996) even though the latter have been metamorphosed to the eclogite facies. They are also similar to those from the Canyon Mountain (with 69.7 to 76Wt% SiO_2, high

Na_2O and low K_2O, and low TiO_2) (Gerlach *et al.* 1981) and Josephine ophiolites (with 65 to 77% SiO_2, high Na_2O and low to moderate K_2O, and low TiO_2) (Barnes *et al.* 1996). The high K_2O concentration in sample BF91/20 from the Coolac Serpentinite Belt does not negate this rock from being a plagiogranite as those from the Josephine Ophiolite contain up to 1.85 Wt% K_2O (Barnes *et al.* 1996).

With regards to their REE composition, the plagiogranites of the Tumut Serpentinite Province (including the REE-depleted sample BF91/20 from the Coolac Serpentinite Belt; Table 8.18) encompass the range in REE concentrations of those from the Volti Group of the Ligurian Alps and the Sestri-Voltaggio Zone (both of which have high REE total concentrations) (Borsi *et al.* 1996), the North Apennines (with low to moderate REE total concentrations) (Borsi *et al.* 1996), Canyon Mountain (with moderate REE total concentrations) (Gerlach *et al.* 1981), and Josephine ophiolites (also with moderate total REE concentrations) (Barnes *et al.* 1996).

CN-REE profiles of plagiogranites from the various world localities described above cover a broad spectrum. Those from the Volti Group of the Ligurian Alps and the Sestri-Voltaggio Zone have flat profiles with significant Eu troughs (Borsi *et al.* 1996). Those from the North Apennines have flat profiles but with strong Eu peaks (Borsi *et al.* 1996). Those from the Canyon Mountain Ophiolite also have flat patterns (though some are weak concave upward curves) along with significant Eu troughs (Gerlach *et al.* 1981). Gerlach *et al.* (1981) also show CN-REE patterns for plagiogranites from various other ophiolites (e.g. the Tihama Asir, Coleman & Donato 1979; Smartville, Menzies *et al.* 1980; Troodos, Kay & Senechal 1976; Samail, Coleman & Donato 1979; Point Sal, Menzies *et al.* 1977; and Samail ophiolites, Pallister & Knight 1981) which exhibit flat to weak concave upward curves, all with Eu troughs. In contrast, plagiogranites from the Josephine Ophiolite are of three principal types, though most exhibit steep downward patterns with significant Eu troughs (Barnes *et al.* 1996). The curves for plagiogranites from the Tumut Serpentinite Province are mainly akin to those from the Josephine Ophiolite (Barnes *et al.* 1996), but the sample from the Coolac Serpentinite Belt with its weak downward pattern and significant Eu peak is more akin to ophiolites from the North Apennines.

Borsi *et al.* (1996) ascribe the Eu troughs to fractional crystallisation prior to emplacement of the plagiogranites as dykes; Pallister and Knight (1981) ascribed such troughs to the fractional crystallisation of clinopyroxene+hornblende and plagioclase and late stage liquid segregation and emplacement through filter pressing; and Menzies *et al.* (1977) suggested that only a small Eu trough anomaly will result from extensive plagioclase removal during early-stage magmatic fractionation. However, the fact that only one of the plagiogranites from the Wambidgee Serpentinite Belt exhibits a significant Eu trough, whereas other plagiogranites from the same belt lack such anomalies, suggests that primary magmatic processes (e.g. removal or accumulation of plagioclase within the melt) might not be the cause. Instead, the trough may be secondary and result from mobilisation of Eu during serpentinisation and related metasomatic alteration of the plagiogranites.

8.8 CHLORITE ROCKS

8.8.1 Major and minor element geochemistry

Only chlorite rocks from the Coolac and Wambidgee serpentinite belts have been analysed. They are characteristically low in SiO_2, Na_2O, K_2O and CO_2, have moderate concentrations of Fe_2O_3, MgO and Ni, and are rich in Al_2O_3, FeO, V, Zn, Nb, Zr, Y and Th (Table 8.19).

8.8.2 Variation diagrams

On the Cr vs Ni diagram (Figure 8.21), chlorite rocks plot alongside the metabasaltic rocks from the Coolac, Tumut Ponds, and Wambidgee serpentinite belts. Some of the chlorite rocks, particularly those from the Coolac Serpentinite Belt analysed by Ashley (1973a), are highly enriched in Cr and Ni, and differ from other chlorite rocks of the Tumut Serpentinite Province (Figure 8.21). It is most likely that they derived from altered ultramafic rocks rather than basalt (Ashley 1973a).

8.8.3 REE and trace element geochemistry

Compared with other rock types from the Tumut Serpentinite Province, the chlorite rocks are enriched in REE (Table 8.20). Those from the Coolac Serpentinite Belt have the lowest total REE concentrations, those from the Wambidgee Serpentinite Belt are intermediate, and those from the

Gundagai Serpentinite Belt have the highest concentrations. The chlorite rocks also have high concentrations of Hf, Sc and Ta.

The CN REE patterns of chlorite rocks (Figure 8.26) exhibit weak to moderate convex downward curves. That from the Coolac Serpentinite Belt has a strong Eu peak, the one from the Wambidgee Serpentinite Belt has a moderate Ce trough, and the one from the Gundagai Serpentinite Belt has a moderate Eu trough.

8.8.4 Discussion

Most of the chlorite rocks (with the exception of those from the Coolac Serpentinite Belt analysed by Ashley 1973a) are chemically similar to metabasaltic rocks of the Tumut Serpentinite province (Table 8.19; Figure 8.21). This suggests that most of these chlorite rocks were derived by metasomatism of basaltic rocks during intense lower greenschist facies metamorphism. The chlorite rocks of the Coolac Serpentinite Belt [as analysed by Ashley (1973a)] probably derived by metasomatism of ultramafic rocks (Ashley 1973a). The metasomatite was largely independent of the parental rocktype and commonly hosted epigenetic sulfides (Ashley 1973a).

The REE geochemistry of the chlorite rocks shows they are the most REE-enriched rocks of the Tumut Serpentinite Province. Hellman and Henderson (1977) show that chlorite is capable of increasing the La content of spilitic metabasalts by as much as four times through the process of adsorption. From the data above, this may also hold true for most of the REE, and particularly Ce, Nd and Sm.

The downward nature of the CN REE patterns (Figure 8.25) is similar to metabasalt from the Tumut Serpentinite Province (Figure 8.22); it is again consistent with metabasalts as the precursors to the chlorite rocks. The Eu troughs may be due to plagioclase removal from the melt (Pallister & Knight 1981), the Eu peaks to plagioclase accumulation within the melt (Pallister & Knight 1981) and the Ce trough to interaction of the metabasalts with sea-water (Menzies *et al.* 1977).

Sample No	BF91/28f	100	165a	BF91/32c	38b	134c*	*266	*643
Belt	WSB	CSB	WSB	WSB	GSB	CSB	CSB	CSB
SiO2	24.42	26.16	22.61	32	28.79	26.75	28.33	29.05
TiO2	1.74	0.71	5.9	2.85	1.84	0.92	0.13	0.42
Al2O3	21.46	20.25	17.47	15.99	15.54	19.56	21.8	17.57
Fe2O3	3.44	3.68	5.72	5.49	5.41	5.65	2.5	5.17
FeO	19.4	18.64	19.4	10.6	8.09	17.42	13.95	9.66
MnO	0.66	0.18	0.37	0.23	0.27	0.15	0.32	0.17
MgO	16.79	17.27	15.69	18.18	27.87	16.12	19.01	24.76
CaO	0.65	1.75	1.56	5.84	0.61	3.35	4.63	3.26
Na2O	b.d	b.d	b.d	1.12	b.d	0.02	b.d	0.08
K2O	0.01	b.d	0.01	0.11	b.d	b.d	0.03	b.d
P2O5	0.47	0.21	1.26	0.37	0.49	0.12	0.08	0.14
H2O+	11.29	11.01	10.06	7.49	11.83	10.14	10.05	10.56
CO2	0.04	0.03	0.04	0.02	0.06	0.1	0.19	0.05
H2O-	0.5	0.27	0.22	0.43	0.46	0.09	0.05	0.29
Cr	168	911	59	971	197		327	1427
Ni	257	388	215	806	291		586	920
V	540	292	674	328	420		3	224
Cu	2	b.d	15	b.d	16		11	26
Pb	11	9	10	8	5			
Zn	222	34	203	77	78		145	57
Rb	b.d	1	3	1	b.d			
Ba	27	b.d	30	30	b.d			
Sr	14	5	33	24	23			
Ga	16	12	8	16	19			
Nb	18	9	46	54	16			
Zr	226	67	479	145	144			
Y	91	25	107	40	35			
Th	6.32	2.93	4.98	2	7			
U	4	1	1	1	b.d			

(Data source: this thesis; Ashley 1973a)
b.d = below detection limit

Table 8.19 Major and minor element analyses of chlorite rocks.

Sample No	165a	BF91/28f	218	100	157ba
Belt	WSB	WSB	GSB	CSB	TPSB
La	43.97	32.05	104.73	20.39	19.1
Ce	100.74	40.36	218.05	40	41.3
Nd	64.28	40.36	115.54	18.93	25.6
Sm	17.62	9.75	23.71	3.7	6.7
Eu	4.46	2.54	4.11	5.57	3.13
Tb	2.76	1.99	2.2	0.46	1.05
Ho	3.69	2.65	1.79	0.72	1.1
Yb	7.82	6.55	1.99	1.99	2.5
Lu	1.07	1.01	0.22	0.3	0.37
Sb	b.d	b.d	b.d	b.d	b.d
As	1.89	10.1	1.7	b.d	b.d
Cr	58.5	168	302	911	4.9
Co	103	42.3	106	191	76.7
Au	b.d	b.d	b.d	b.d	13.4
Hf	11.5	5.88	5.6	1.32	2.15
Ir	b.d	b.d	b.d	b.d	b.d
Sc	47.6	50.8	44.5	42.8	40.1
Ta	3.23	1.21	1.23	0.43	b.d
Th	4.98	6.32	12.7	2.93	2.5

(Data source: this thesis)
b.d = below detection limit

Table 8.20 Rare earth and trace element analyses of chlorite rocks.

8.9 RODINGITES

8.9.1 Major and minor element geochemistry

Rodingites from the Coolac and Wambidgee serpentinite belts (Table 8.21) vary most widely in their concentrations of TiO_2, MgO, CaO, Cr, Ni, Cu, Sr, Zr Y and Th. Likewise, in a study of the rodingites on Mount Lightning within the Coolac Serpentinite Belt, Ray (1977) reported considerable chemical variation, being particularly low in SiO_2, total Fe, TiO_2, CO_2 and alkalies, but high in CaO. He divided the rodingites into two main groups based on their dominant mineralogy, which reflects their differing compositions. He termed these "Group 1" (those comparatively low in TiO_2, but high in Cr and Ni) and "Group 2" (those comparatively low in Cr and Ni but high in Al_2O_3, Sr, Y and Zr) rodingites. During the present study, most of the rodingites found conform to Ray's (1977) Group 1 rodingites.

8.9.2 Variation diagrams

On the 100xCaO/CaO+MgO+FeO vs SiO_2 diagram (Figure 8.12), the rodingites plot near the gabbros of the Tumut Serpentinite Province but are richer in CaO, but have less in SiO_2. On the Cr

vs Ni diagram (Figure 8.14), the rodingites plot similarly to gabbros from the various serpentinite belts and Honeysuckle Beds, but differ from those of the Micalong Swamp Complex.

8.9.3 REE and trace element geochemistry

The REE and trace element geochemistry (Table 8.22) indicate that the rodingites have moderate to high concentrations of REE. Some contain appreciable Co, Hf, Sc and Ta.

As with the REE concentrations, the REE CN patterns are of three main types (Figure 8.29). Relatively flat curves are exhibited by one rodingite from each of the Coolac and Tumut Ponds serpentinite belts. Convex upward curves are exhibited by three rodingites, one from each of the Wambidgee, Coolac and Tumut Ponds serpentinite belts, and a convex downward curve is shown by a rodingite from the Coolac Serpentinite Belt. Eu troughs are exhibited by two Coolac Serpentinite Belt rodingites, whereas the other sample from this belt has a Eu peak. Ce troughs are shown by one sample from each of the Coolac and Wambidgee serpentinite belts.

8.9.4 Discussion

The major element geochemistry (Table 8.21) shows that, although variable, rodingites from the Coolac Serpentinite Belt resemble those from the Wambidgee Serpentinite Belt. This variation occurs in both relatively mobile and immobile elements such as Ti, Cr, Ni, Zr and Y. Similar findings occurred in rodingites from the eastern part of the Jordanow-Gogolow serpentinite massif of Poland (Dubinska 1995).

The variation diagrams (Figures 8.12, 8.13 and 8.14) show that the rodingites are similar to the gabbros of the Tumut Serpentinite Province, but contain more Ca and less Si. This is similar to the findings of Honnorez and Kirst (1975) for rodingites from the Equatorial Mid-Atlantic Fracture Zones. These authors believe that the high H_2O content of rodingites (see Table 8.21), indicate that water pressure was almost equal to the total pressure at the time of their formation. Coleman (1967), Keusen (1972) and Leach and Rodgers (1978) also found that rodingitisation largely involved Ca-enrichment and near complete alkali depletion for rodingitised dykes enclosed within serpentinite. Schandl *et al.* (1989) similarly proposed that rodingitisation simply involves the addition of Ca and the removal of SiO_2 and alkalis from the protolith.

Sample No	94	ML042	144	121	BF91/26c
Belt	CSB	CSB	CSB	CSB	WSB
SiO2	35.61	38.14	38.75	40.38	44.27
TiO2	1.05	0.29	0.09	0.1	0.34
Al2O3	20.21	17.44	17.44	17.7	16
Fe2O3	1.17	0.61	1.34	0.79	2.46
FeO	1.27	2.03	2.61	1.69	3.25
MnO	0.08	0.03	0.09	0.14	0.11
MgO	3.86	17.11	14.7	8.79	10.39
CaO	33.29	18.13	19.97	26.9	20.64
Na2O	b.d	b.d	b.d	b.d	0.16
K2O	b.d	0.02	b.d	b.d	0.01
P2O5	0.23	0.01	0.01	0.02	0.02
H2O+	3.77	6.52	5.32	3.31	3.02
CO2	0.13	0.06	0.05	0.04	0.06
H2O-	0.24	0.53	0.32	0.6	0.23
Cr	65	2691	1091	1959	605
Ni	113	1286	677	667	357
V	159	105	94	67	162
Cu	10	6	8	54	44
Pb	30	4	4	6	8
Zn	24	4	44	21	30
Rb	1	3	1	1	1
Ba	b.d	5	10	b.d	37
Sr	43	4	53	4	84
Ga	5	2	6	5	12
Nb	16	b.d	b.d	b.d	b.d
Zr	384	27	2	4	7
Y	76	24	5	7	12
Th	39	2	1	2	1
U	5	b.d	b.d	b.d	b.d

(Data source: this thesis)
b.d = below detection limit

Table 8.21 Major and minor element analyses of rodingites.

Sample No	144	94	ML042	BF91/26c	157rod	256g/rod	257rod
Belt	CSB	CSB	CSB	WSB	TPSB	TPSB	TPSB
La	0.24	73.82	5.58	0.62	0.37	5.51	0.36
Ce	0.71	167.93	9.12	0.67	1.31	13.64	1.19
Nd	b.d	68.77	12.9	2.02	1.49	9.74	1.29
Sm	0.3	14.71	3.44	0.89	0.62	3.1	0.57
Eu	0.3	1.4	0.62	0.44	0.28	1.17	0.28
Tb	0.12	1.92	0.61	0.29	0.21	0.67	0.2
Ho	0.15	2.75	0.77	0.44	0.33	0.84	0.3
Yb	0.4	6.56	1.77	1.14	1.07	1.89	0.88
Lu	0.05	1.08	0.27	0.17	0.17	0.27	0.13
Sb	0.14	b.d	b.d	b.d	0.42	b.d	1.28
As	b.d	b.d	b.d	b.d	b.d	b.d	b.d
Cr	777	60.2	2440	509	732	22.2	995
Co	55.4	49	33.5	78.4	59.5	59.3	52.5
Au	b.d	b.d	b.d	b.d	5.6	b.d	34.4
Hf	0.2	12	0.64	0.29	0.9	1.97	b.d
Ir	b.d	b.d	b.d	b.d	b.d	b.d	b.d
Sc	26.9	29.9	38.4	39.2	39.6	22	46.6
Ta	b.d	1.63	0.35	0.36	b.d	b.d	b.d
Th	0.18	36.5	0.33	b.d	b.d	0.73	b.d

(Data source: this thesis)
b.d = below detection limit

Table 8.22 Rare earth and trace element analyses of rodingites.

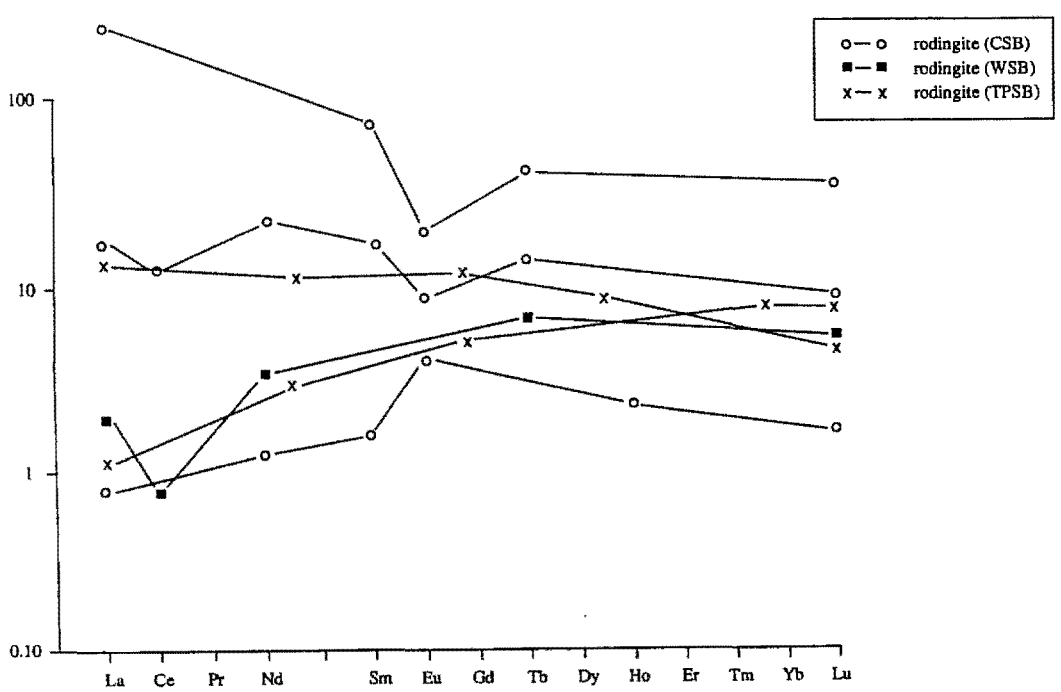

Figure 8.30 CN-REE diagram for rodingites (data from Table 8.22)

Both Ashley (1973a) and Ray (1977) found that the rodingites from the Coolac Serpentinite Belt were derived from a variety of protoliths and that the high concentration of CaO could have been inherited (Ray 1977). Ray (1977) stated that Group 1 rodingites were generally derived from gabbros but some may have come from dolerites and basalts, and that Group 2 rodingites were after spilitic basalts. This finding is supported by the present study. Most of the rodingites equate with Ray's (1977) Group 1 and are chemically similar to the gabbros of the Tumut Serpentinite Province. Ashley (1973a) concluded that rodingitisation was contemporaneous with serpentinisation and was due to metasomatic reaction between tectonic inclusions/dykes and the enclosing ultramafic host. He stated that such a process occurs at temperatures of 100-350°C at <6kb, and that the dominant fluid phase was H_2O, with low CO_2 activity.

The Cr vs Ni variation diagram (Figure 8.14) shows that the rodingites are akin to gabbros of the Tumut Serpentinite Province and Honeysuckle Beds, but plot away from the gabbros of the Micalong Swamp Complex. This suggests that the rodingites were derived from gabbros of the Tumut Serpentinite Province and/or Honeysuckle Beds.

The variability in the REE concentrations of the rodingites again reflects their derivation from gabbros of the Tumut Serpentinite Province. The REE data suggests that the variability is as much within as between belts.

The CN REE curves for the rodingites (Figure 9.29) exhibit greater variability and stronger anomalies than those from the Tumut Serpentinite Province gabbros (Figure 8.16). Thus, although they do not negate derivation from the gabbros, rodingitisation has profoundly affected the protolith and has led to significant remobilisation of at least some of the REE (e.g. Graham *et al.* 1994).

8.10 UNUSUAL ROCK TYPES

8.10.1 Major and minor element geochemistry

The anthophyllite-olivine-spinel hornfels from the Coolac Serpentinite Belt differs in overall chemistry from the olivine-amphibole hornfels from the Wambidgee Serpentinite Belt (Table 8.23),

in being enriched in Al_2O_3, Fe_2O_3, FeO, MgO, V, Zn, Ga, Nb, Zr, Y and Th, and depleted in SiO_2, CaO, Na_2O, K_2O and Rb. In contrast, the olivine-amphibole hornfels is enriched in FeO, MgO, CaO, Cr, Ni, Ba and Sr, and depleted in K_2O, Rb, Ga and Th. Ashley (1973a) and Irving & Ashley (1976) showed that the hornfels rocks from the Coolac Serpentinite Belt were characterised by low SiO_2 and relatively high Al_2O_3, total Fe, MgO, Cr, Mn, Ni, Sc, Ti, V and Zn. The anthophyllite-olivine-spinel hornfels from the Coolac Serpentinite Belt analysed in this present study conforms with this, whereas the olivine-amphibole hornfels from the Wambidgee Serpentinite Belt does not.

8.10.2 Variation diagrams

On the Cr vs TiO_2 diagram (Figure 8.23), the anthophyllite-olivine-spinel hornfels plots near the Cr-depleted amphibolites and chlorite rocks of the Tumut Serpentinite Province, whereas the olivine-amphibole hornfels plots near the Cr-enriched amphibolites.

On the Cr vs Ni diagram (Figure 8.24), the olivine-amphibole hornfels plots well to the right of the Cr-enriched amphibolites, whereas the anthophyllite-olivine-spinel hornfels plots close to the Cr-poor amphibolites and chlorite rocks.

8.10.3 REE and trace element geochemistry

The unusual rock types of the Tumut Serpentinite Province vary widely in their REE and trace element geochemistry (Table 8.24). The anthophyllite-olivine-spinel hornfels is REE-enriched and contains appreciable As, Co, Hf, Sc and Ta. The olivine-amphibole hornfels contains moderate REE concentrations along with appreciable Co. The amphibole-chlorite rock from the Wambidgee Serpentinite Belt is REE-enriched and has appreciable Co and Hf, while the zoisite rock from the Wambidgee Serpentinite Belt contains moderate REE concentrations along with significant Sb, Co, Hf and Ta.

The anthophyllite-olivine-spinel hornfels exhibits a convex downward CN REE pattern with a strong Eu trough, whereas the olivine-amphibole hornfels is convex downward but lacks any anomalies (Figure 8.31). The amphibole-chlorite rock is very similar to the anthophyllite-olivine-spinel hornfels, but the zoisite rock has an essentially flat CN REE pattern with no anomalies (Figure 8.31).

Sample No	BF92/8	150c
Belt	WSB	CSB
Rocktype	Ol-Am Hf	An-Ol-Sp
SiO2	41.78	31.12
TiO2	0.6	1.04
Al2O3	6.29	22.93
Fe2O3	4.76	8.53
FeO	5.97	6.65
MnO	0.16	0.31
MgO	27.27	24.12
CaO	5.57	0.67
Na2O	0.49	0.14
K2O	0.07	0.01
P2O5	0.07	0.33
H2O+	6.48	4.86
CO2	0.16	0.04
H2O-	0.32	0.23
Cr	2420	527
Ni	1554	233
V	139	323
Cu	56	35
Pb	12	7
Zn	72	109
Rb	2	2
Ba	161	10
Sr	92	22
Ga	4	22
Nb	11	13
Zr	40	150
Y	10	39
Th	0.51	12.2
U	1	1

(Data source: this thesis)

Table 8.23 Major and minor element analyses of unusual rock types.

Sample No	150c	174	171	BF92/8
Belt	CSB	WWSM	WWSM	WSB
Rocktype	ant-ol-sp	zois rock	Amph-Chl	Ol-Amph
La	32.7	9	23.35	8.29
Ce	72.84	23.05	53.42	17.13
Nd	28.28	15.66	33.17	8.59
Sm	5.8	4.7	8.26	1.76
Eu	0.61	1.49	1.03	0.53
Tb	0.97	0.88	1.09	0.25
Ho	1.16	1.16	1.48	0.33
Yb	2.99	2.3	3.9	0.79
Lu	0.42	0.32	0.56	0.12
Sb	b.d	1.44	b.d	b.d
As	1.94	b.d	b.d	b.d
Cr	527	101	75.6	2420
Co	88.2	47.2	32.6	121
Au	b.d	20.3	b.d	b.d
Hf	3.99	3.12	2.65	1.1
Ir	b.d	b.d	b.d	b.d
Sc	35.8	24.5	25.4	21.6
Ta	1.18	1.08	0.45	0.69
Th	12.2	1.04	2.73	0.51

(Data source: this thesis)

b.d = below detection limit

Table 8.24 Rare earth and trace element analyses of unusual rock types.

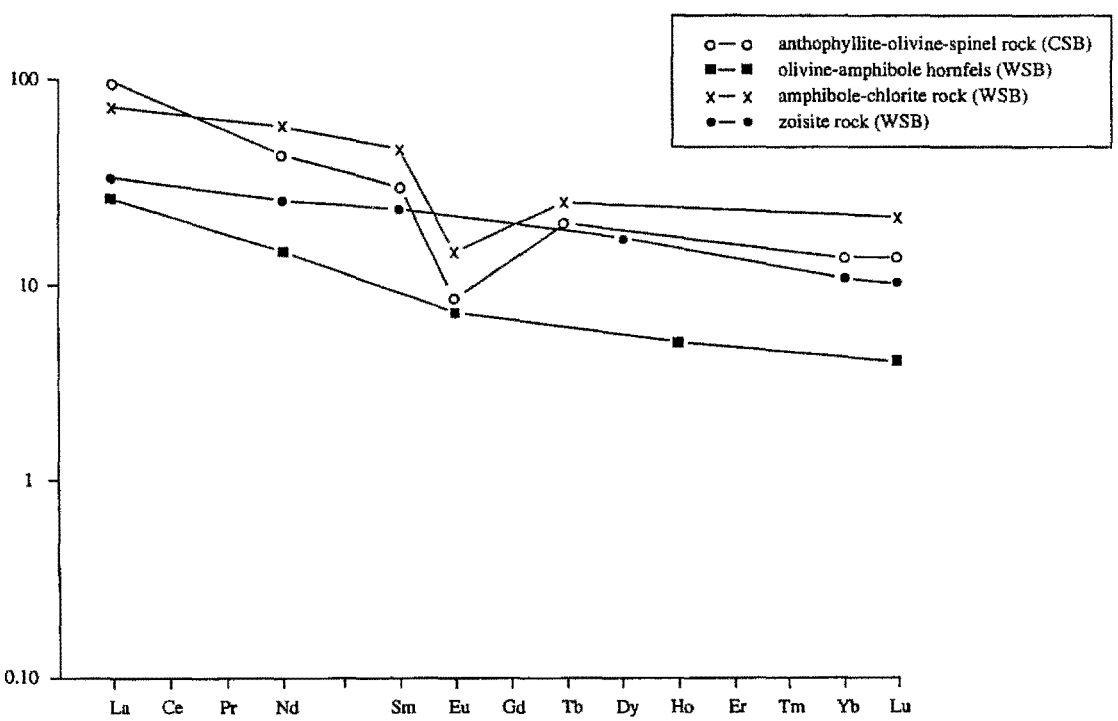

Figure 8.31 CN-REE diagram for unusual rock types (data from Table 8.24).

8.10.4 Discussion

The difference in composition of the anthophyllite-olivine-spinel hornfels and the olivine-amphibole hornfels reflects their differing mineralogy and protoliths. The chemistry of the olivine-amphibole hornfels is consistent with derivation from either a hornblende peridotite or hornblendite. In contrast, the anthophyllite-olivine-spinel hornfels contains pleonaste (Ashley 1973a; Irving & Ashley 1976) rather than chrome spinel and, in view of its chemical composition and ratios of the immobile elements such as Ti, Cr, Y, V and Zr, has probably derived from a mafic protolith. In that it plots with chlorite rocks and Cr-depleted amphibolites of the Tumut Serpentinite Province, and is spatially associated with metabasalts of the Honeysuckle Beds, it most likely formed by high temperature contact metamorphism of altered metabasaltic rocks (c.f. Irving & Ashley 1976).

Due to their differing mineralogies, the various unusual rock types vary widely in REE and trace element geochemistry. The anthophyllite-olivine-spinel hornfels has a similar REE concentration to metabasaltic rocks of the Tumut Serpentinite Province and Honeysuckle Beds (Tables 8.11 and 8.13). The olivine-amphibole hornfels has a similar REE composition to the hornblendite from the same belt, reflecting that most of the REE are contained within the amphibole minerals and that the olivine is highly REE-depleted. The amphibole-chlorite rock and zoisite rock have similar REE concentrations to the metabasaltic rocks from the Tumut Serpentinite Province, Jindalee Beds and Honeysuckle Beds, suggesting that they are derived from such metabasaltic rocks.

The strong downward CN REE pattern for the anthophyllite-olivine-spinel hornfels is similar to that for the metabasaltic rocks from the Tumut Serpentinite Province with the exception of the strong Eu trough (Figures 8.30 and 8.22). Dobbe (1994) ascribed the Eu trough, within similar cordierite-anthophyllite rocks from Tunabergs Sweden, to removal of Eu from the parental basaltic rocks during alteration. The CN REE pattern with no anomalies for the olivine-amphibole hornfels is akin to that for the hornblendite from the same belt (Figures 8.30 and 8.6) and suggests derivation from the same magma. The CN REE pattern and Eu trough for the amphibole-chlorite rock is similar to that for some of the metabasaltic rocks from the Wambidgee Serpentinite Belt (Figures 8.30 and 8.22), and suggests that it may be derived from them. The CN REE pattern for the zoisite rock is also akin to some of the metabasaltic rocks from the Wambidgee Serpentinite Belt (Figures 8.30 and 8.22), and also suggests derivation from this source.

8.11 CONCLUSIONS

Note: A detailed geochemical discussion has been made earlier in this Chapter, in the relevant section for each different rock grouping.

Primary ultramafic rocks of the Tumut Serpentinite Province have a very similar major, minor, trace and rare earth element geochemistry to similar rock types found within ophiolitic sequences throughout the world. They have formed in an oceanic environment floored by oceanic crust, and not in a continental environment. An exception to this is the lherzolite from the Eurongilly Serpentinite Belt which is more akin to lherzolite from mantle peridotites of southern Spain and northern Morocco which have been interpreted as forming in either transitional oceanic-continental crust (Bodinier *et al.* 1987) or purely continental crust (Platt & Vissers 1989).

Weakly serpentinised dunites, lherzolites, pyroxenites, wehrlites and hornblendites of the Tumut Serpentinite Province have a distinctly more evolved and enriched composition than their host harzburgite or peridotite (both of which are extremely depleted – Nicolas 1989). Although they cannot therefore have formed by partial melting of their hosts, they may reflect partial melting of the same source, with the residuum now comprising the extremely depleted harzburgite and peridotite. Fractional crystallisation of the partial melts would have progressively evolved more enriched compositions.

Serpentinisation of the primary ultramafic rocks of the Tumut Serpentinite Province has involved some mobilisation of elements, but the degree of mobilisation and the elements involved have largely been rock type dependant. In general, the ultramafic rocks have largely retained their original composition. The REE chemistry of Cpx-rich primary ultramafic rocks from the Tumut Serpentinite Province are largely unaffected by serpentinisation, despite the serpentinisation process introducing significant concentrations of H_2O, CO_2, Sb and As.

The overall similarity in composition of **massive and schistose serpentinites** with the weakly serpentinised and serpentinised harzburgites indicates that the serpentinites largely were derived from a harzburgitic parent and that serpentinisation was largely an isochemical process. In massive serpentinite, serpentinisation mobilised some SiO_2 and MgO, while in schistose serpentinites

development of the foliation induced a minor increase in the mobility of some elements. This led to the enrichment of schistose serpentinites in La, Ce, Sb and As relative to massive serpentinites.

Most of the **talc-carbonate rocks** of the Tumut Serpentinite Province have similar concentrations of immobile elements (Ti, Cr, Ni, Zr and Y) to the serpentinites and harzburgites. This suggests that, like the serpentinites, most of the talc-carbonate rocks have been derived from a harzburgitic parent. Nevertheless, some talc-carbonate rocks were probably derived from mafic rocks or tectonic inclusions. Based on the distribution of talc-carbonate rocks, CO_2 alteration primarily took place along shear planes and at the contact of the serpentinite belts with surrounding quartz-rich country rocks (particularly the Jindalee Beds quartzites). The CO_2 alteration would seem to have resulted in the significant mobilisation of La, Ce, Nd and Sm.

Gabbros of the Tumut Serpentinite Province can be divided into groups mainly on the basis of their Cpx-plagioclase ratios. It is not belt dependent as the range exists in all of the belts. Although similar-looking gabbros occur within the Micalong Swamp Complex (Callan 1984), they are distinctly different from those of the Tumut Serpentinite Province in that they are more enriched in TiO_2 and more depleted in Cr and Ni (all three considered as immobile elements). Gabbros of the Honeysuckle Beds (Basden 1990) are similar to those of the Tumut Serpentinite Province and significantly different from those of the Micalong Swamp Complex. This suggests that the gabbros of the Honeysuckle Beds are geochemically akin and possibly genetically related to those of the Tumut Serpentinite Province. Some of the gabbros have similar CN REE patterns to cumulus and high level gabbros (section 8.4.4) from other ophiolite complexes, thereby suggesting that they formed in an oceanic rather than a continental crustal environment.

Metabasaltic rocks of the Tumut Serpentinite Province vary widely in composition, but the variation is not belt dependent. The metabasaltic rocks are generally low in K_2O and high in Na_2O. This was ascribed to remobilisation during regional metamorphism by Ashley *et al.* (1979) and Dadd (1998), rather than representing a primary magmatic signature. Metabasaltic rocks of both the Jindalee Beds and Honeysuckle Beds (Basden 1990) closely resemble those of the Tumut Serpentinite Province. However, the Jindalee Beds are an older basement terrane and not genetically connected to the metabasaltic rocks of the Tumut Serpentinite Province. Also,

metabasaltic rocks of the Micalong Swamp Complex, which generally occur to the east of the Tumut Serpentinite Province as dyke swarms within the Goobarragandra Volcanics are low-K tholeiites (Basden 1990) of quite different chemical affinity, possibly formed from tholeiitic magmas rising-up peripheral rift zones associated with the early opening of the Tumut Trough to the west.

Using a range of variation diagrams, the metabasalts of the region fall into several different groups, but predominantly seem to be andesitic to subalkali and of mid-ocean ridge (MORB) affinity. This tends to be affirmed by the Ti vs Cr discrimination diagram in which most plot as ocean floor basalts. The interpretation is somewhat weakened by mobilisation probably induced by low greenschist to lower amphibolite facies metamorphism/metasomatism. This metamorphism/ metasomatism also appears to have led to significant REE mobilisation. However, using the Ti/Zr vs Zr discriminant diagram of Gamble *et al.* (1993), they clearly plot as back-arc basin basalts.

The large variation in overall geochemistry of the Tumut Serpentinite Province **amphibolites** (particularly in the immobile elements) and their subdivision into Cr-rich and Cr-poor groups cannot have been produced by metamorphism/alteration, but must have been inherited from their differing protoliths. The Cr-rich amphibolites may have been derived from gabbroic protoliths, whereas the Cr-poor amphibolites derived from basaltic protoliths, although some of the gabbros are Cr-poor. Amphibolite facies metamorphism of the protoliths led to significant mobilisation of the REE.

Plagiogranites of the Tumut Serpentinite Province are geochemically distinct from the granitic rocks of the Young Granodiorite and tonalites of the Micalong Swamp Complex. They are restricted to the serpentinite belts and are an integral part of them. Geochemically, the plagiogranites are similar in overall composition to plagiogranites from other ophiolite complexes. This similarity applies to the CN REE patterns and provides further support for origin in an oceanic rather than a continental geotectonic environment.

Most of the **chlorite rocks** (with the exception of those from the Coolac Serpentinite Belt analysed by Ashley 1973a) are chemically similar to metabasaltic rocks of the Tumut Serpentinite province.

This, along with their field occurrence as dyke-like bodies enclosed within serpentinites, suggests that they were initially basaltic/doleritic rocks, which have subsequently undergone intense low greenschist facies metamorphism/metasomatism. This chloritisation has led to enrichment in the REE, As and Hf, but, despite this, the CN REE profiles for the chlorite rocks are still similar to those of the metabasaltic rocks. The chlorite rocks of the Coolac Serpentinite Belt [as analysed by Ashley (1973a)] probably derived by metasomatism of ultramafic rocks.

The **rodingites** from the Coolac Serpentinite Belt were derived from a variety of protoliths and the high concentration of CaO may have been inherited (Ray 1977). Many of the rodingites found in the present study are also Si and alkali depleted and appear to have been generally derived from gabbros of the Tumut Serpentinite Province, but some may have come from dolerites and basalts Although the rodingites appear to have formed by rodingitisation of the gabbros, their CN REE patterns are more variable and have more intense anomalies. This is ascribed to the REE experiencing mobilisation during the rodingitisation process. Ashley (1973a) concluded that rodingitisation was contemporaneous with serpentinisation and was due to metasomatic reaction between the mafic rocks and an enclosing/adjacent ultramafic host. He stated that such a process occurs at temperatures of 100-350°C at <6kb, and that the dominant fluid phase was H_2O, with low CO_2 activity.

Although the **unusual rock types** of the Tumut Serpentinite Province largely consist of metamorphic/alteration mineral assemblages, their trace and REE geochemistry reflect their varying mineralogy and protoliths. The chemistry of the olivine-amphibole hornfels is consistent with its derivation from either a hornblende peridotite or hornblendite that underwent very high T contact? metamorphism such that a change in the major element chemistry resulted. In contrast, the anthophyllite-olivine-spinel hornfels contains pleonaste rather than chrome spinel and, in view of its chemical composition and ratios of the immobile elements such as Ti, Cr, Y, V and Zr, has probably derived from a mafic protolith that underwent high T metasomatism prior to contact metamorphism, resulting in major element changes and the removal of Eu. It plots with chlorite rocks and Cr-depleted amphibolites of the Tumut Serpentinite Province, and is spatially associated with metabasalts of the Honeysuckle Beds. Both the amphibole-chlorite and zoisite rocks were

initially metabasaltic rocks which were modified by upper greenschist to middle amphibolite facies metamorphism/metasomatism thereby modifying the major element chemistry.

Due to their differing mineralogies, the various unusual rock types vary widely in REE and trace element geochemistry. The anthophyllite-olivine-spinel hornfels has a similar REE concentration to metabasaltic rocks of the Tumut Serpentinite Province and Honeysuckle Beds (Tables 8.11 and 8.13). The olivine-amphibole hornfels has a similar REE composition to the hornblendite from the same belt, reflecting that most of the REE are contained within the amphibole minerals and that the olivine is highly REE-depleted. The amphibole-chlorite rock and zoisite rock have similar REE concentrations to the metabasaltic rocks from the Tumut Serpentinite Province, Jindalee Beds and Honeysuckle Beds, suggesting that they are derived from such metabasaltic rocks.

CHAPTER 9: GEOLOGY AND GENESIS OF THE PODIFORM CHROMITITE DEPOSITS

9.1 INTRODUCTION

Numerous small podiform chromitite deposits occur throughout the Tumut Serpentinite Province of NSW. They have produced more chromite ore than any other part of Australia, despite the overall production being negligible on a world-wide basis (Graham *et al.* 1996). By far the greatest contribution to date has been that of Golding (1966, 1975; Golding & Bayliss 1968; Golding & Johnson 1971) who worked on the overall chemistry and mineralogy of the podiform chromitite deposits of the Coolac Serpentinite Belt. Their main conclusions were that the chromitites are of podiform type, typical of alpine-type peridotites; they range widely in composition from Cr-rich to Al-rich, though generally exhibiting a bi-modal distribution; they sharply abut the surrounding harzburgite or are separated from it by a thin shell of dunite; they appear to be randomly distributed throughout the belt; disseminated chromitite may merge into the dunite; Al-rich chromitites are less deformed and younger than the Cr-rich chromitites; altered chromite is more enriched in Cr and total Fe, but less enriched in Al and Mg than the primary host; and the alteration of chromite resulted in the formation of Cr-chlorite, Cr-grossular and uvarovite.

Ashley (1973a) also worked on the chromitites and composition of Cr-spinel within their primary ultramafic rocks of the Coolac Serpentinite Belt. He found that the colour, texture and composition of the Cr-spinels depend on the hostrock, and that spinels in the harzburgite are compositionally distinct (poorer in Cr and Fe^{3+} and richer in Al) from those in the chromitites. Ray (1977) carried-out microprobe analyses of chromite grains and associated host silicates from the podiform chromitite deposits of Mount Lightning within the Coolac Serpentinite Belt. He concluded that they spanned the entire range of compositions found in the Coolac Serpentinite Belt; chemical variation is largely between rather than within chromitite pods; fluid interaction between the chromitites and mafic dyke rocks led to the formation of Cr-chlorite, Cr-grossular and rare Cr-vesuvianite during serpentinisation; and the microprobe analyses were in general accordance with the bulk rock chromitite analyses of Golding (1966).

Field and laboratory work on these deposits, together with the author's observations of the Shetland Island's podiform chromitite deposits (e.g. Prichard & Neary 1982; Prichard 1985) and evaluation of published genetic models, are used to evolve a genetic model pertinent to the Tumut Serpentinite Province and perhaps to podiform chromitite deposits in general. Much of the field and laboratory work has previously been published (Graham *et al.* 1996 - Appendix PUB).

Podiform chromitite bodies have been found within the Coolac and Wambidgee serpentinite belts (Figure 9.1). Most (over 60) are within the Coolac Serpentinite Belt and the remainder (6) within the Wambidgee Serpentinite Belt. They are widely distributed within the main harzburgite mass and the western schistose zone of the Coolac Serpentinite Belt (Figure 9.1). Most occur in the northern part of the Coolac Serpentinite Belt. The six deposits in the Wambidgee Serpentinite Belt are also irregularly distributed.

9.2 FIELD RELATIONSHIPS

Most of the chromite ore and, in some cases, the chromite-rich dunitic halo have been mined, or are covered by tailings (Plate 9.1), so only portions could be mapped and investigated in detail. The Coolac Serpentinite Belt chromite deposits range from approximately 1m to >30m in maximum plan dimension, are tabulate, and have a thin halo of relatively massive, serpentinised, chromite-rich dunite. This passes outward into a narrow zone of schistose serpentinite, and then into relatively unfoliated porphyroclastic harzburgite that dominates the belt. Uncommonly, the chromitite passes directly into altered, massive porphyroclastic harzburgite. Massive granoblastic rodingite dykes cut the chromitite deposits, and contain fragments of the other rock types (Plate 9.2).

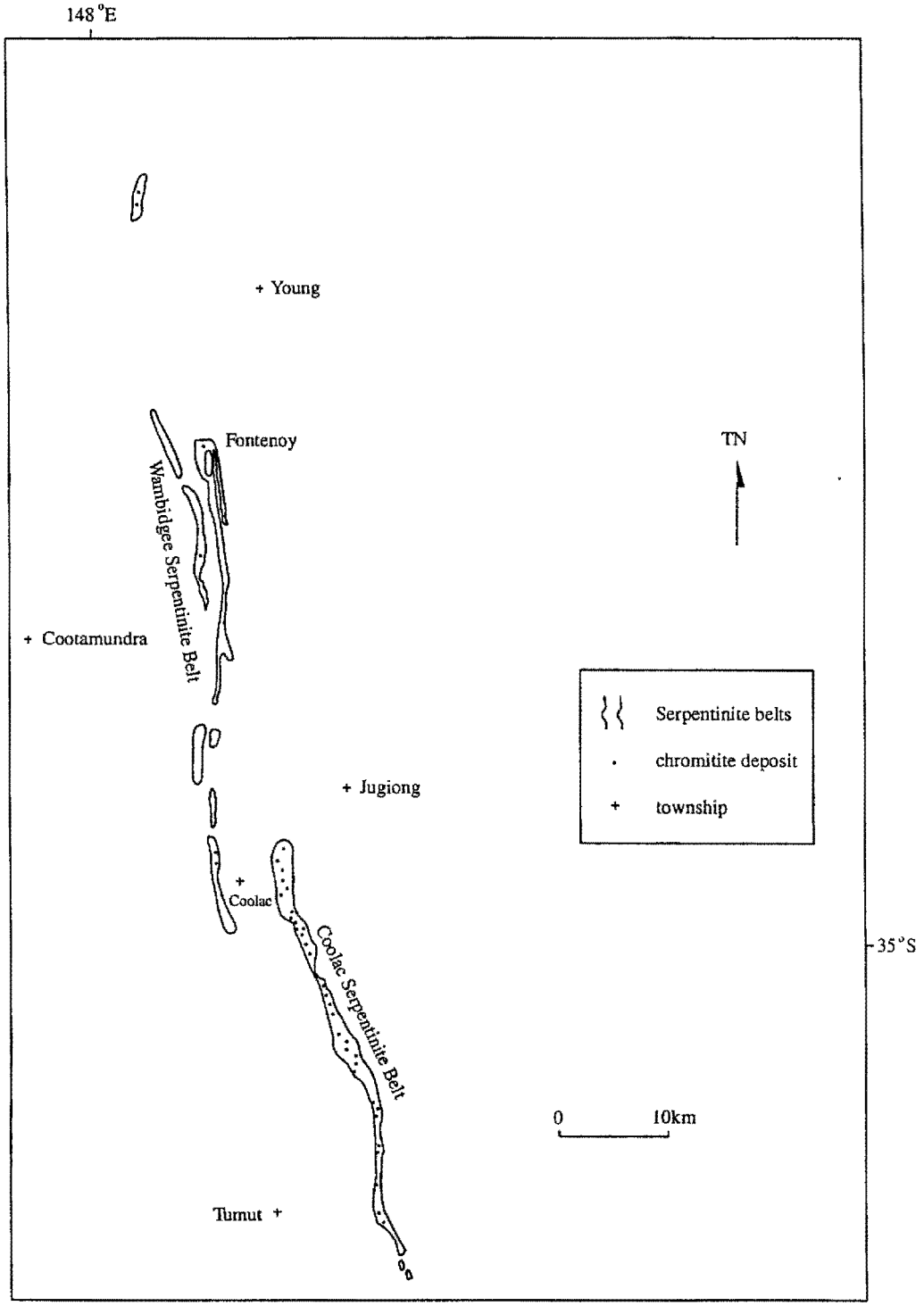

Figure 9.1 Distribution of podiform chromitite deposits within the Coolac and Wambidgee serpentinite belts (adapted from Golding & Johnson 1971).

Plate 9.1 Typical outcrop of the podiform chromitite deposits. Outcrops are serpentinised harzburgite. Locality 37, near Pettits. Viewed from the east.

Plate 9.2 Chromitite fragments within rodingite dyke of the MLA deposit. Viewed from the north-east. F.O.V 5m

Golding and Johnson (1971) indicated that the Coolac Serpentinite Belt chromitite bodies were ellipsoidal in shape with their short axes perpendicular to both the length of the belt and the secondary tectonic foliation. However, the three mappable bodies [the Mount Lightning Adit (MLA), Quilter's Open-Cut (QOC) (G.R. 146 261) and Mount Miller (MM) deposits (Figure 9.2) (G.R. 232 038)] are tabulate in shape and dip shallowly (20°NW), whereas the enclosing harzburgite mass is grossly vertical to steeply dipping (>60° WSW - Leven *et al.* 1991). Although not identified within the immediate vicinity of the deposits, primary layering, as defined by varying proportions of olivine and orthopyroxene, dips 60° ENE (see Chapter 3).

9.2.1 Mount Lightning Adit (MLA) deposit

The MLA deposit occurs on the northern slope of Mount Lightning in the northern part of the Coolac Serpentinite Belt (Figure 9.2). It consists of an adit driven into a relatively large pod of mainly massive polycrystalline chromitite. The chromitite has a thin (0.5 to 2m), essentially unfoliated, serpentinised dunitic halo, which is enclosed within a zone (approximately 5m thick) of schistose harzburgite (Figures 9.3 and 9.4). The transitional contact from dunite to chromitite comprises: chromite-bearing dunitic wallrock (<10% chromite), disseminated chromitite (10 to 20% chromite), nodular chromitite (20 to 60% chromite) and massive polycrystalline chromitite (>60% chromite). A small core of pegmatitic chromitite (subhedral to euhedral chromite, up to 20mm long, embedded in massive serpentine) occurs within the massive chromitite (Figure 9.3).

9.2.2 Quilter's Open-Cut (QOC) deposit

The QOC deposit occurs on the NNE slope of Mount Lightning, some 450m east of the MLA deposit (Figure 9.2). It consists of 3 main open-cuts (30m maximum dimension), only one of which is safely accessible (Plate 9.3). The mapped, accessible deposit has an encompassing zone of schistose dunitic serpentinite some 4m thick. Towards the southern end of the deposit the serpentinite contains diffuse-margined cores of massive, partially serpentinised, porphyroclastic harzburgite (Figure 9.5; Plate 9.4). Overall, the deposit comprises many small (<1m in length) tabulate vein-like bodies (Plates 9.5 and 9.6), that dip shallowly (20°NW) and have slickensided contacts with the dunitic serpentinite.

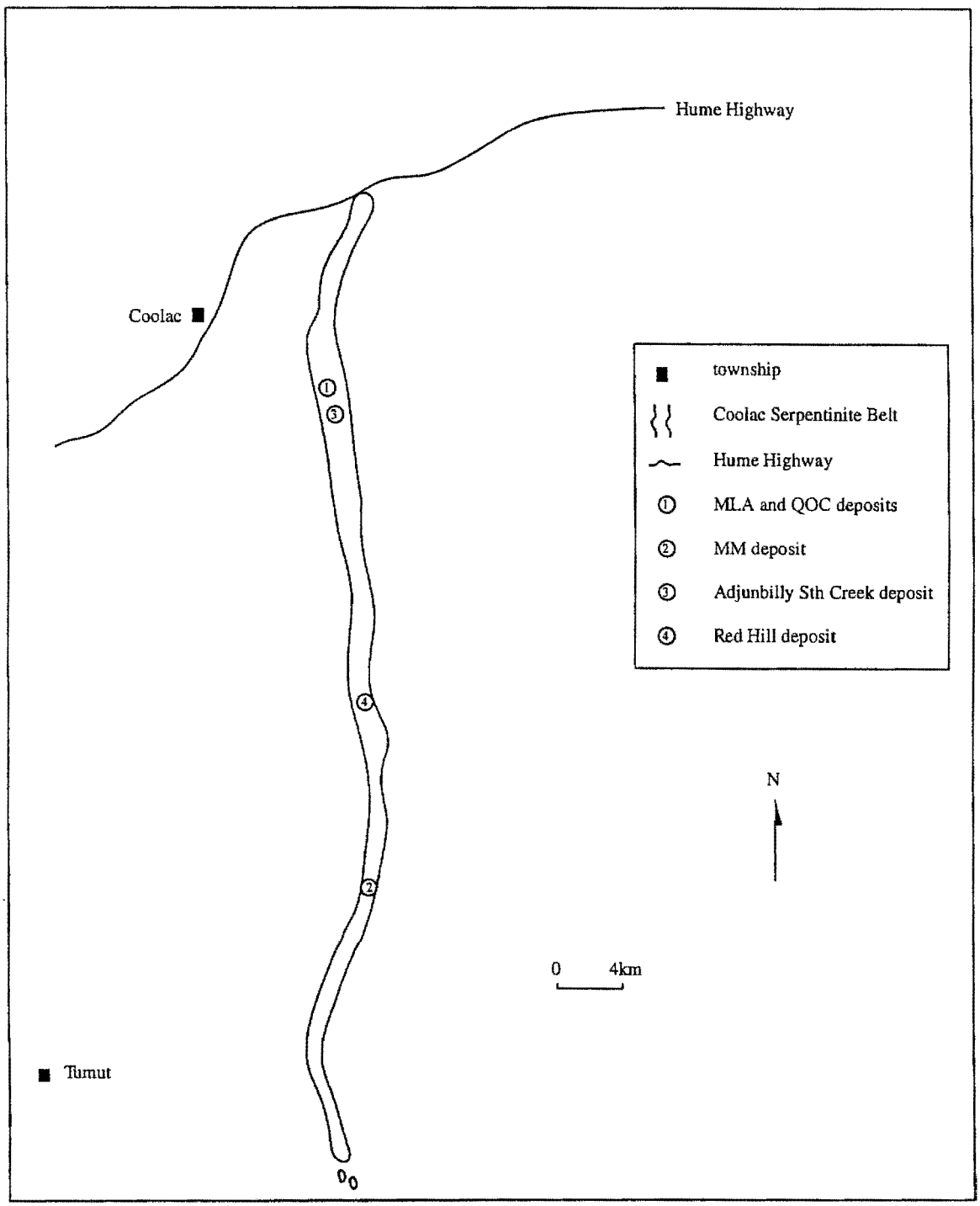

Figure 9.2 Location of the MLA, QOC, MM, Adjungbilly Sth Creek and Red Hill chromitite deposits.

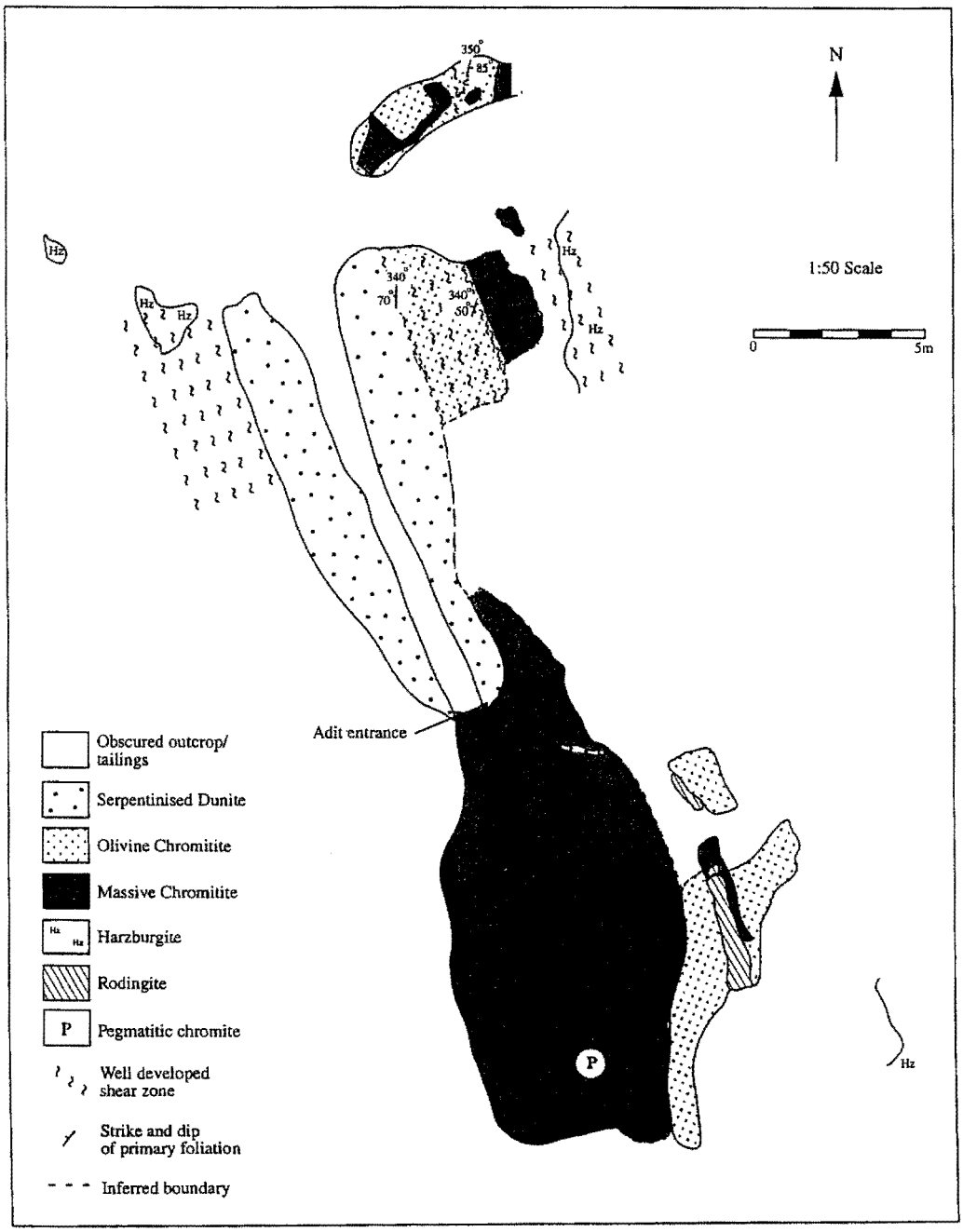

Figure 9.3 Plan view of the outcrop geology of the MLA chromitite deposit.

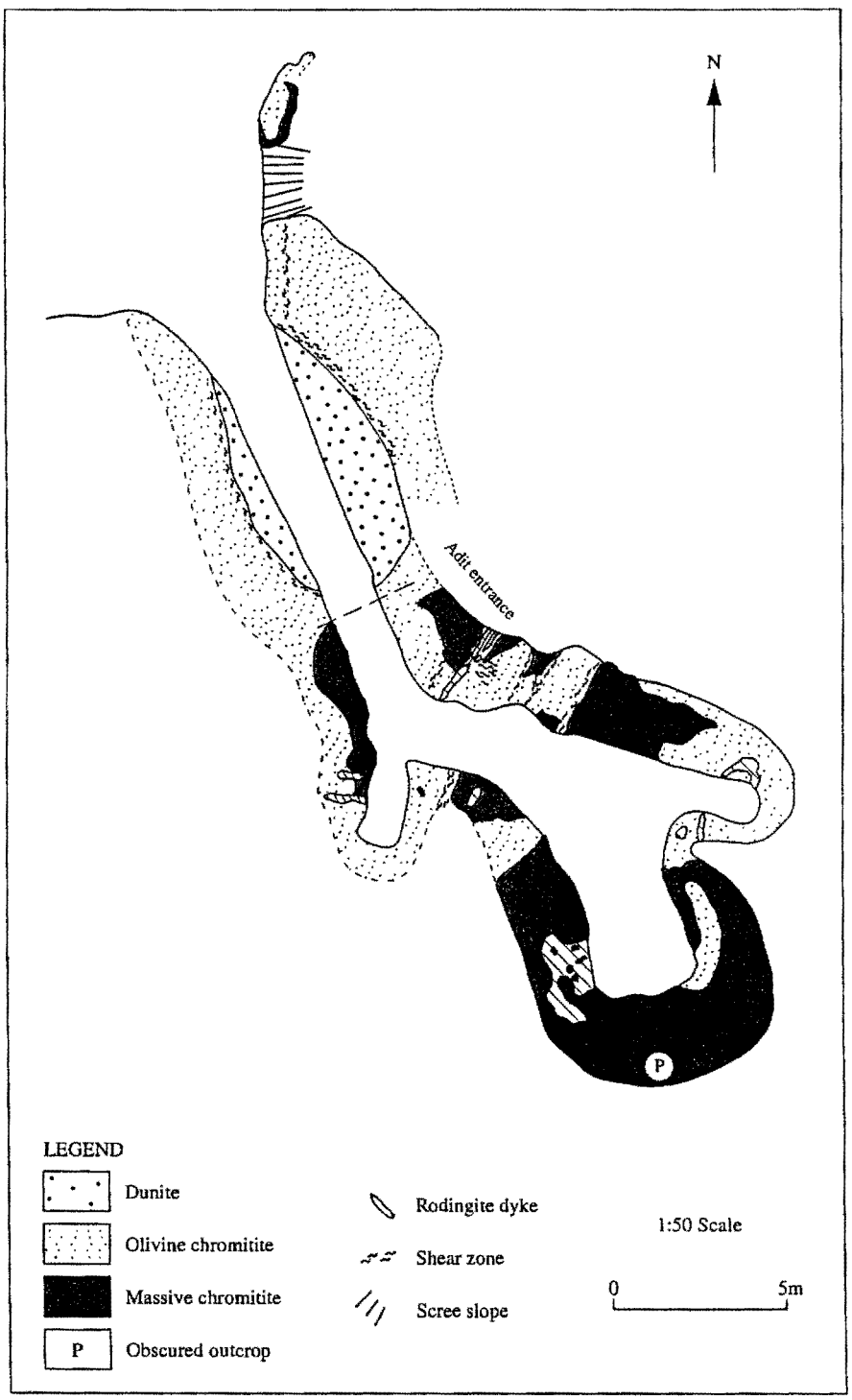

Figure 9.4 Plan of the walls of the MLA chromitite deposit.

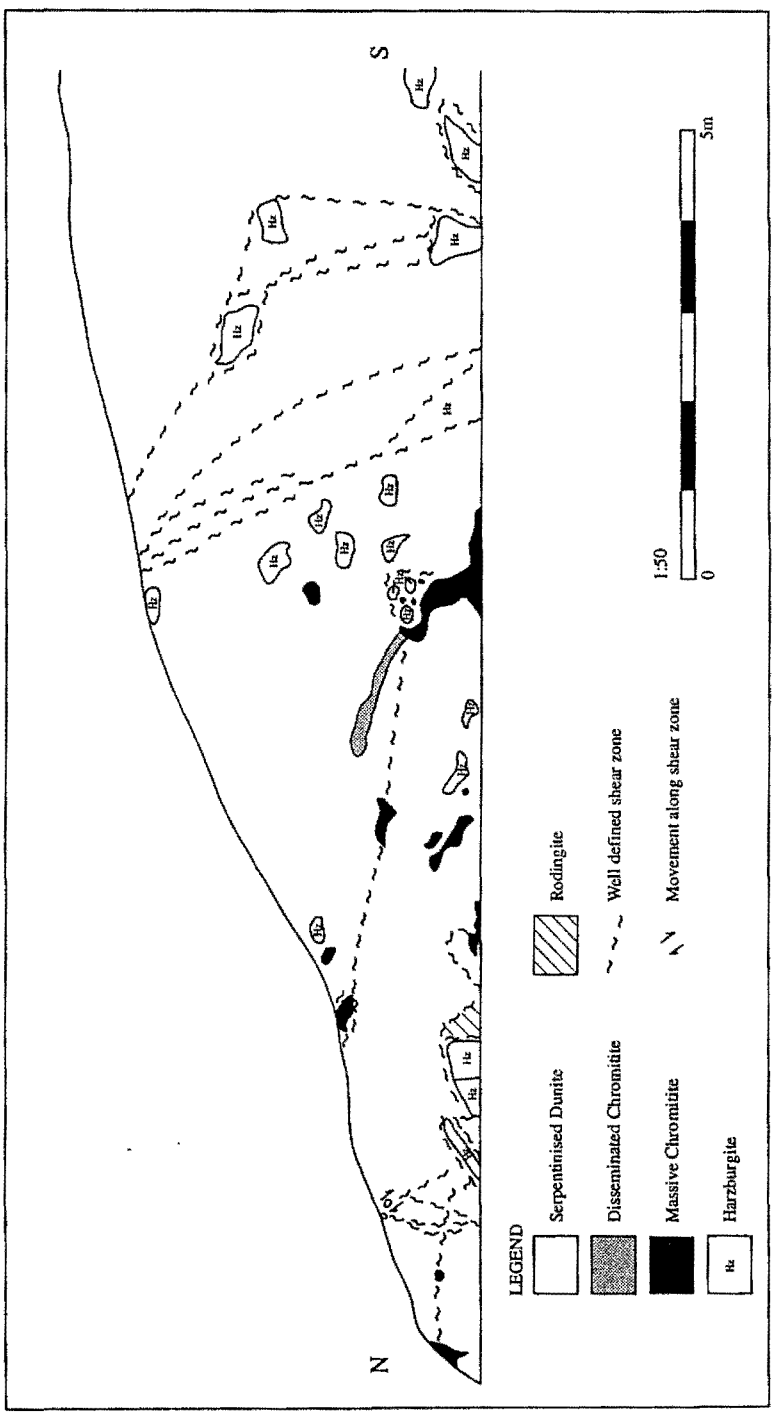

Figure 9.5 East wall geological section of the QOC chromitite deposit.

Plate 9.3 Quilter's Open-Cut, viewed from the north-east. Outcrop on the walls consists of blocks of unsheared harzburgite within serpentinised dunite.

Plate 9.4 Diffuse-margined core of unsheared harzburgite within serpentinised dunite. QOC deposit, viewed from the north-west.

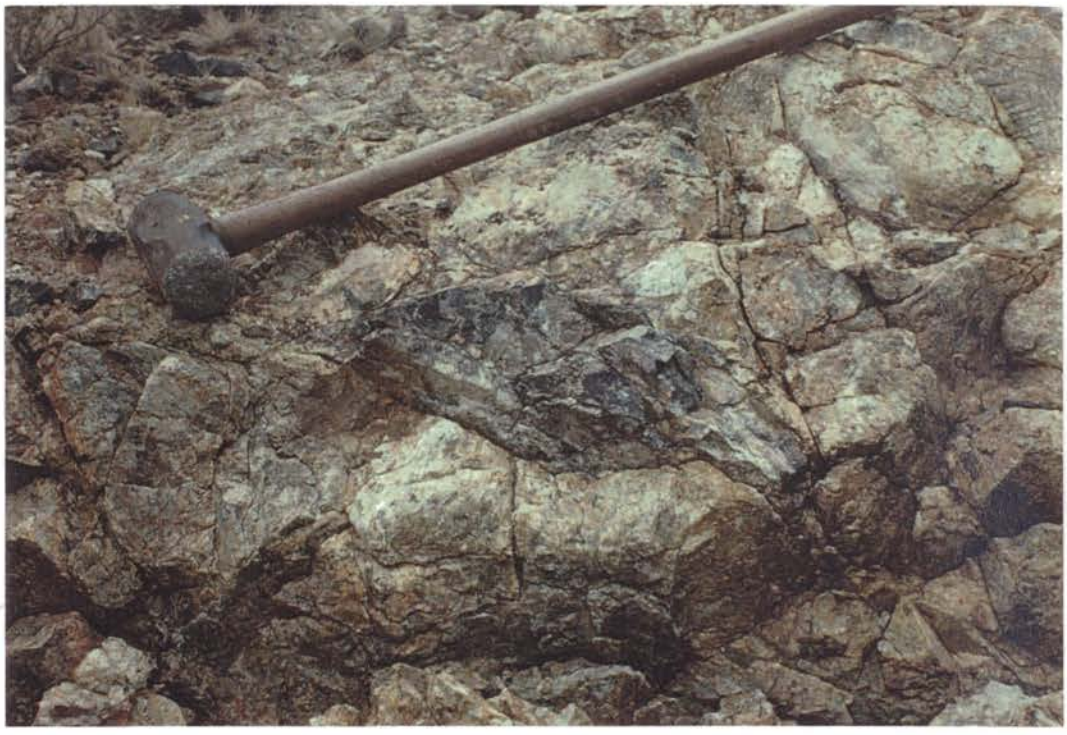

Plate 9.5 Small tabular chromitite body within serpentinised dunite. QOC deposit, viewed from the west.

Plate 9.6 Chromitite veins within serpentinised dunite. QOC deposit, viewed from the west.

9.2.3 Mount Miller (MM) deposit

The MM deposit occurs along a ridge, which is cut by Brungle Creek in the southern part of the Coolac Serpentinite Belt (Figure 9.2). The Emu Mine chromitite lies approximately 500m to the east and consists of a small but partially complete podiform chromitite body accessed by an adit. The MM chromitite has an unfoliated chromite-poor (<5% chromite) dunitic halo (0.2 to 2m thick), in turn enclosed by a zone (3m) of schistose harzburgite (Figure 9.6). The chromitite is mainly nodular and passes outward into disseminated chromitite and weakly chromitiferous dunite. The gradation, from nodular chromitite through to disseminated chromitite and weakly chromitiferous dunite, is graphically portrayed in Figure 9.6.

9.2.4 Observations from other deposits

At the Adjungbilly South Creek Deposit (Figure 9.2, deposit 211), the chromitite dips some 30° towards the SW and the strike of the body parallels the trend of the relatively unfoliated, serpentinised dunite wallrock. The dunite is 1-2m thick, passes outward into a few metres of schistose serpentinised harzburgite, and finally into massive porphyroclastic harzburgite. The chromitite body is 0.3-1m thick (other dimensions unknown) and mostly comprises coarse-grained orbicular chromitite.

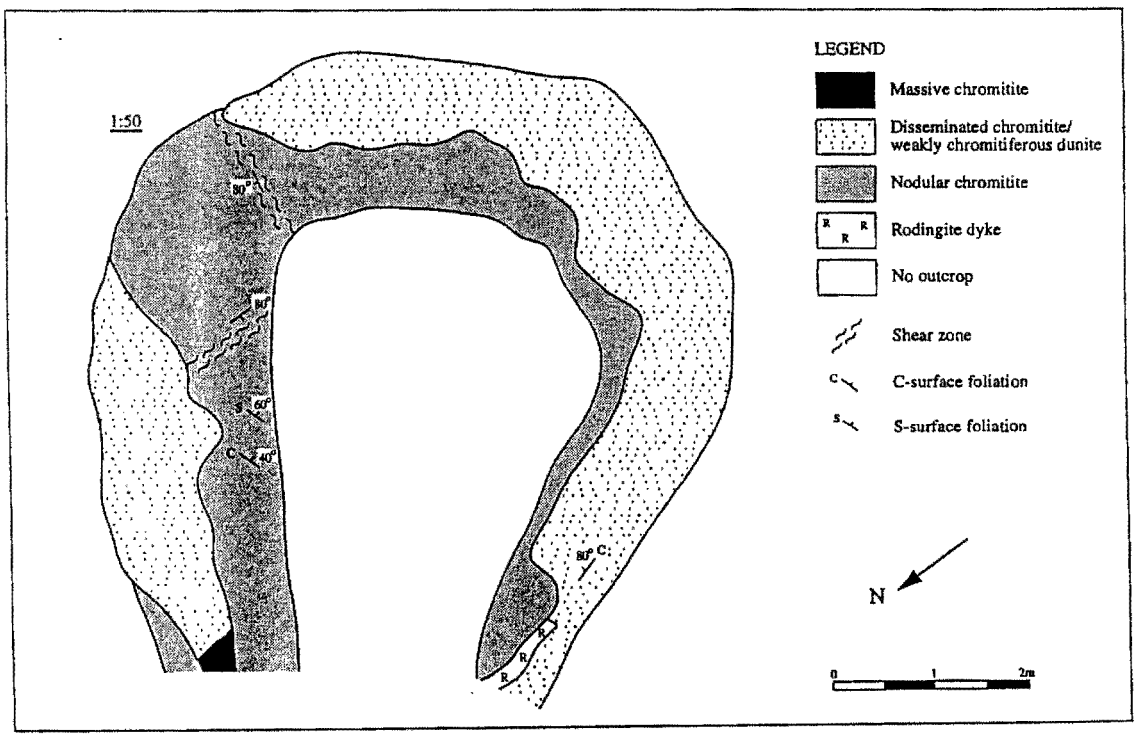

Figure 9.6 Plan of the walls of the MM chromitite deposit (see Figure 9.2 for location in belt)

At the Red Hill deposit (Figure 9.2, deposit 25), the chromitite body is hosted by highly veined, silicified dunite, within a tract of schistose serpentinite that varies from 1 to 5 m wide. Variably serpentinised massive porphyroclastic harzburgite occurs outside the shear zone. The only accessible chromitite dips 60° towards 270° within a 1.5m wide massive dunite envelope, in turn surrounded by similarly oriented schistose (S-C fabric) serpentinite. The contact between the dunite and schistose serpentinite is gradational, such that the foliation tails off from the serpentinite into the dunite. Small blocks of massive porphyroclastic harzburgite occur within the schistose serpentinite.

9.3 TEXTURAL STUDIES

Golding (1966, 1975) interpreted the podiform chromitites of the Coolac Serpentinite Belt in terms of cumulate ultramafic rocks and distinguished three distinct textural types: type 1 consisted of single crystal multifaceted chromite grains formed by sintering of chromite anhedra followed by overgrowths; type 2 consisted of polycrystalline ellipsoidal chromite nodules that developed from spherical precursors by plastic deformation and recrystallisation; type 3 comprised complex aggregates in which large aggregates of serpentine group minerals were surrounded by sub-aggregates of small chromite grains - this type of chromitite merges into the type 1 chromitite. Golding (1966, 1975) also reported that some of the grain boundary relationships between chromite and olivine (or its serpentinised equivalents) suggested penecontemporaneous crystallisation of both phases, that the chromitites had undergone metamorphism and deformation over a protracted period from just after initial crystallisation (with high T metamorphism and accompanying ductile deformation of chromite grains) to post-emplacement (with low T metamorphism and brittle deformation), and that the chromitites were of a polygenetic origin and more than one age. Ashley (1973a) ascribed the chromitite textures variously to primary (i.e. magmatic) and secondary (i.e. deformation/serpentinisation) processes. He noted that marginal slickensiding and internal cataclasis of chromitite pods were consistent with tectonic inclusion emplacement.

Textures of podiform chromitites are ambiguous, as many have been interpreted in terms of both primary magmatism (Leblanc 1980) and secondary tectonism (Gates 1991). Graham *et al.* (1993) subdivided the textural varieties of the Tumut Serpentinite Province chromitites into formational and post-formational textures. Formational textures comprise those largely developed during crystallisation of the chromitites, whereas post-formational textures are those imposed after crystallisation.

9.3.1 Mesoscale observations

(a) MLA deposit

Formational textures dominate this deposit. The disseminated chromitite (Plate 9.7) consists of cuspate or lobate anhedral chromite grains (<1mm to 10mm), and rare aggregates (up to 5mm) comprising smaller chromite grains in a matrix of alumian lizardite and chrysotile 2M (Plate 9.8); some of the chromite grains exhibit atoll texture. In places, trails of elongate chromite define planar and linear preferred orientations, and chromite-rich versus chromite-poor bands of different grain size define layering (Plate 9.9).

The nodules in nodular chromitite consist of atoll textured, angular to subrounded, equant ellipsoidal chromite grains within a matrix of serpentine (Plate 9.10). The nodules range from <1mm to 7mm in size, but are mainly 3-4mm across. They are evenly and closely spaced (<2mm) within the intervening serpentine.

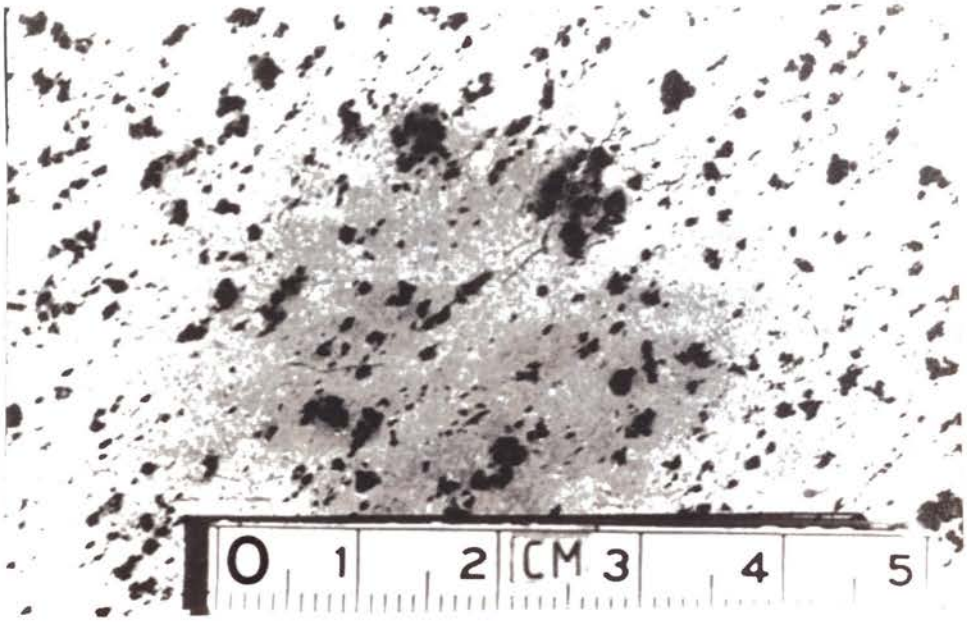

Plate 9.7 Disseminated chromitite from the MLA deposit.
Sample No MLA019

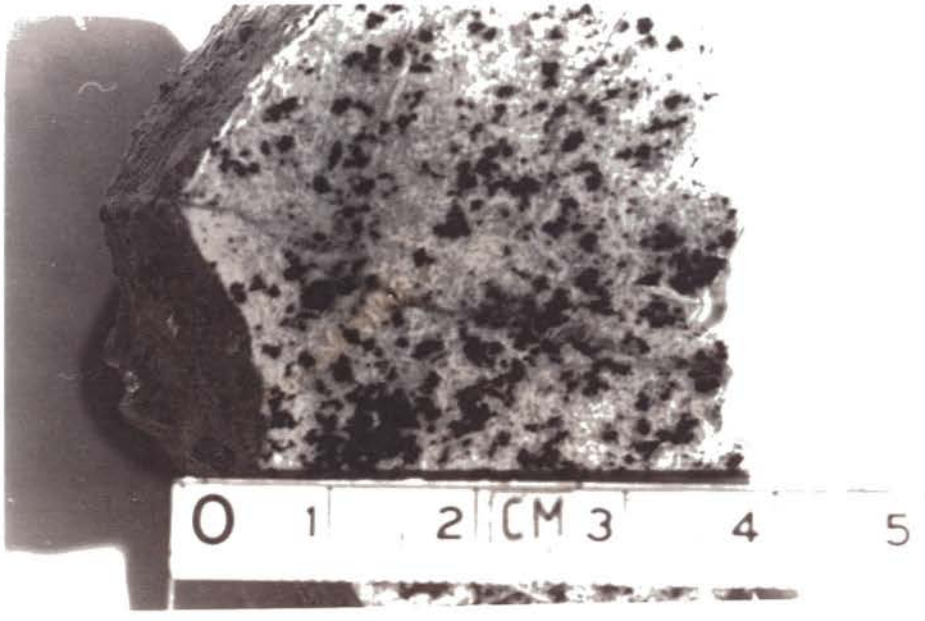

Plate 9.8 Aggregates of chromite within disseminated chromitite from the MLA deposit. Sample No MLA013

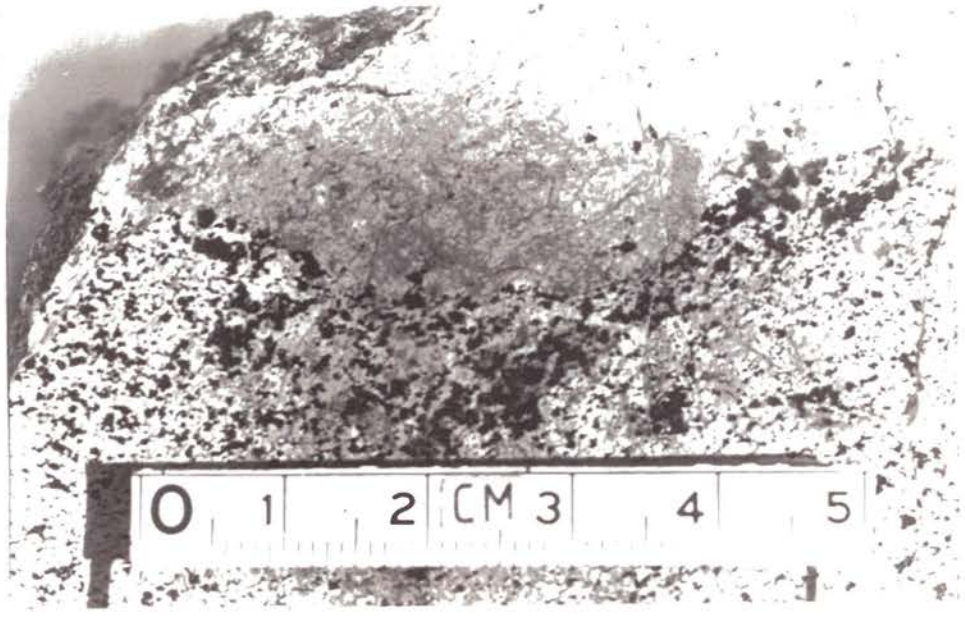

Plate 9.9 Banded disseminated chromitite from the MLA deposit. Consists of an upper dunite layer, and underlying chromite-rich band passing downward into disseminated chromitite. Sample No MLA017

Plate 9.10 Nodular chromitite from the MLA deposit.
Sample No MLA011

Massive polycrystalline chromitite consists of highly fractured, subrounded and closely packed chromite nodules, with less than 5% internodular space in-filled by serpentine (Plate 9.11).Post-formational textures are less prominent and range from discrete fractures to intense brecciation, in which the amount of dilation ranges from 0.5mm down to resolution limits. The fractures generally lack offsets and therefore have no significant shear component.

(b) QOC deposit

Whereas formational textures dominate and are well-preserved in the MLA deposit, the QOC deposit is dominated by post-formational deformational textures. This difference is primarily ascribed to the QOC chromitite comprising small, easily disrupted lenses within foliated (S-C fabric) serpentinised dunite.

Preserved formational textures include "vein-like" bodies composed of aggregates of highly fractured and brecciated angular chromite grains up to 2mm in diameter (Plate 9.6) (up to 0.4m wide, 0.1m thick, and of variable length in the range 0.3 to at least 2m). The dominant formational texture is massive polycrystalline chromitite and the dominant post-formational effect has been to change this into a compact micro-breccia (Sibson 1977) comprising highly angular, relatively equant, fractured chromite grains up to 1mm in diameter (Plate 9.12).

9.3.2 Micro-scale observations

(a) MLA deposit

The formational textures comprise poor- to well-developed chromite-olivine pseudo-net texture (Plate 9.13) progressing into polycrystalline chromitite (Plate 9.14), largely reflecting the increasing chromite/olivine ratio. Olivine grains range in size from 100um to 0.1mm, are well-rounded, ovoid, and commonly contain tiny (<2um) inclusions of nickel sulfides. Single and multiple ovoid-shaped serpentine pseudomorphs, after olivine, occur within the chromitite. Post-formational textures consist of fracturing and replacement relationships. Fracturing is systematic and includes a dominant orthogonal pair (Plate 9.15), striking parallel and normal to the long axis of the chromitite pod. The fractures have high aspect ratios (>1000) with lengths more than 10mm and widths less than 0.001mm. Cataclasis is marked at intersections, but there is no rotation of fragments and negligible offset (Plate 9.16).

Plate 9.11 Massive polycrystalline chromitite from the MLA deposit.
Sample No MLA018

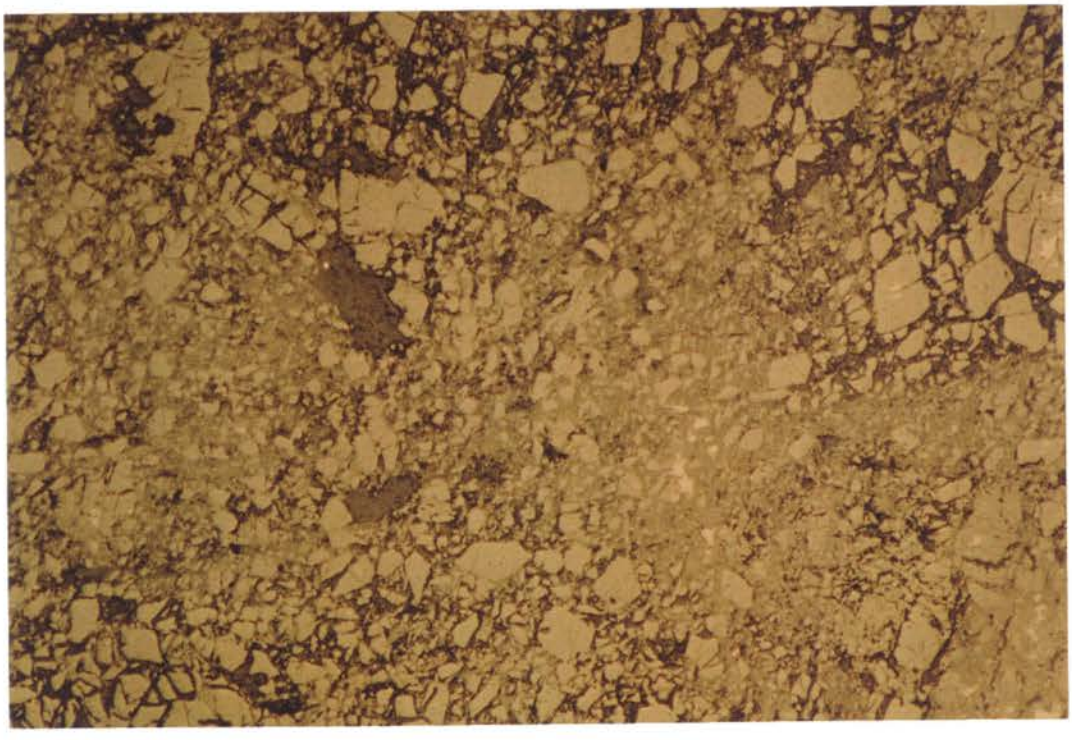

Plate 9.12 Compact microbreccia from the QOC deposit.
Sample No QOC003 PPL F.O.V 3.5mm

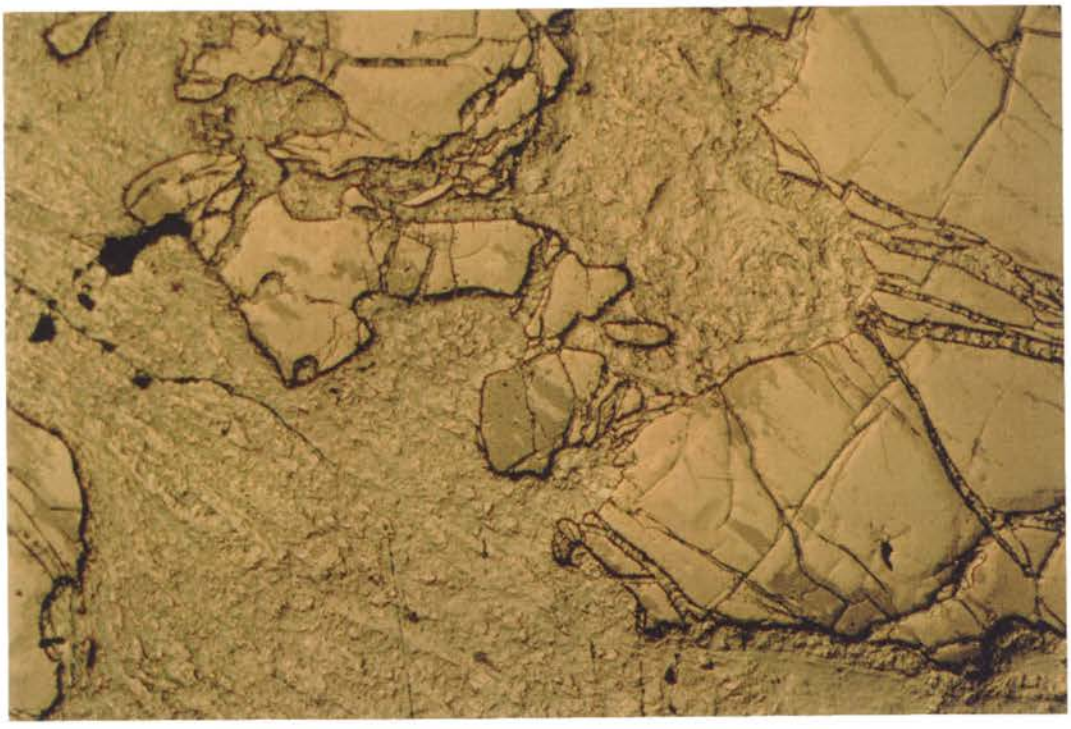

Plate 9.13 Chromite-olivine pseudo net texture from the MLA deposit.
Sample No MLA014 PPL F.O.V 3.5mm

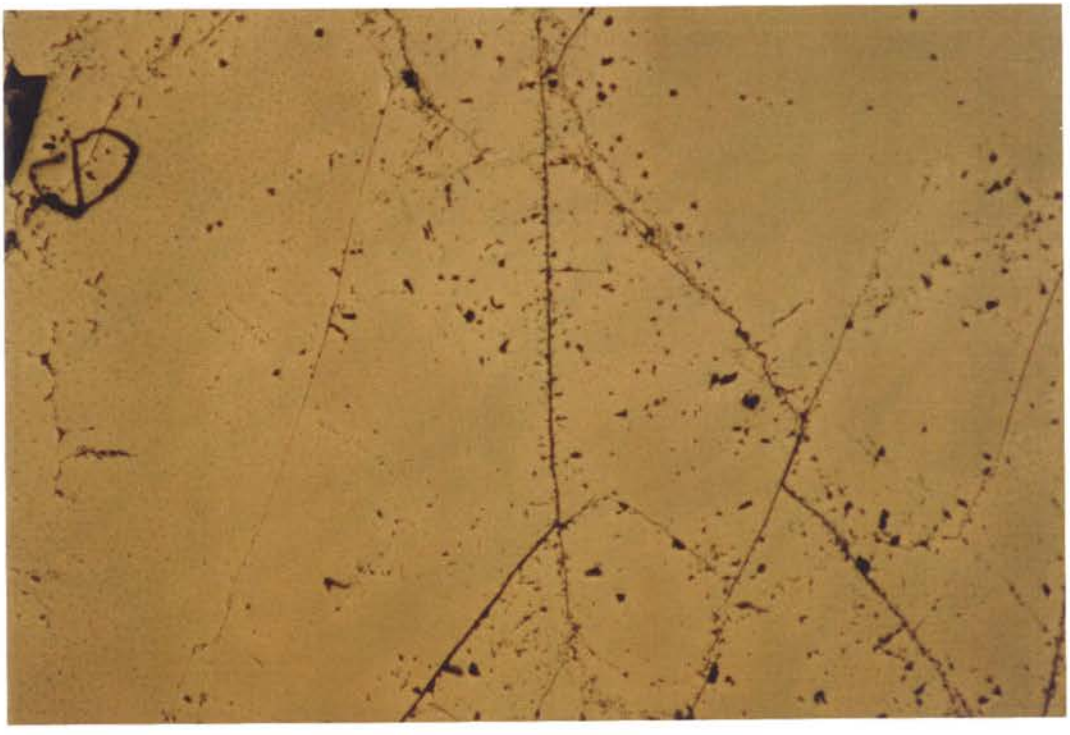

Plate 9.14 Well-developed massive polycrystalline chromitite from the MLA deposit.
Sample No MLA010 PPL F.O.V 3.5mm

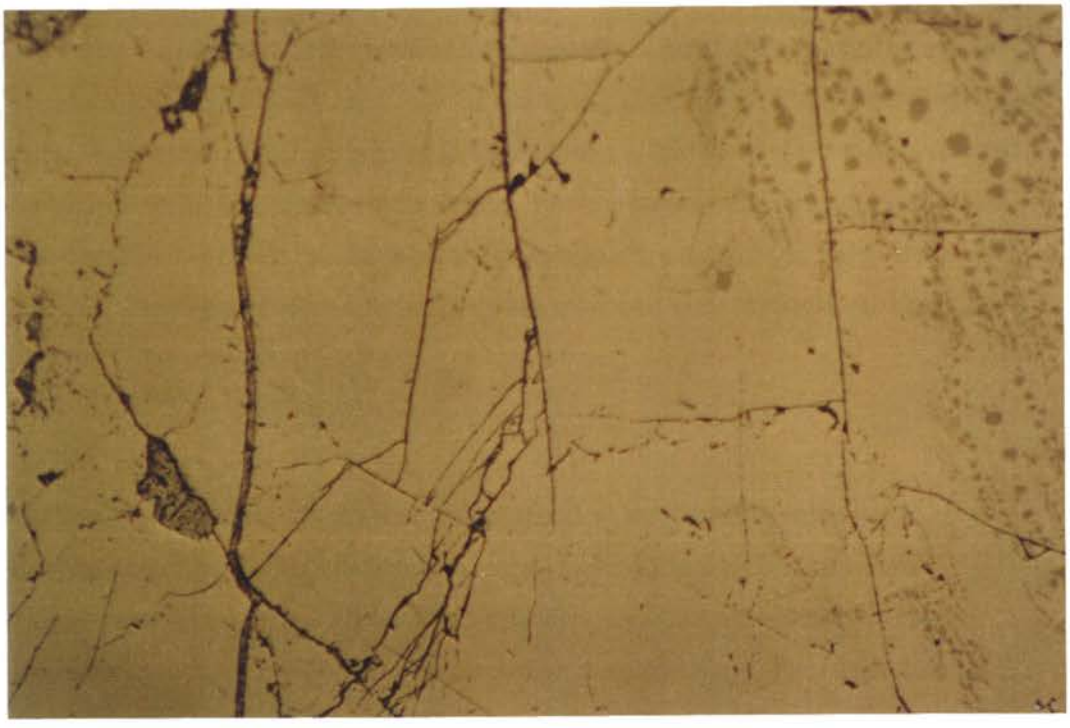

Plate 9.15 Orthogonal systematic fracturing within massive polycrystalline chromitite from the MLA deposit.
Sample No MLA018 PPL F.O.V 3.5mm

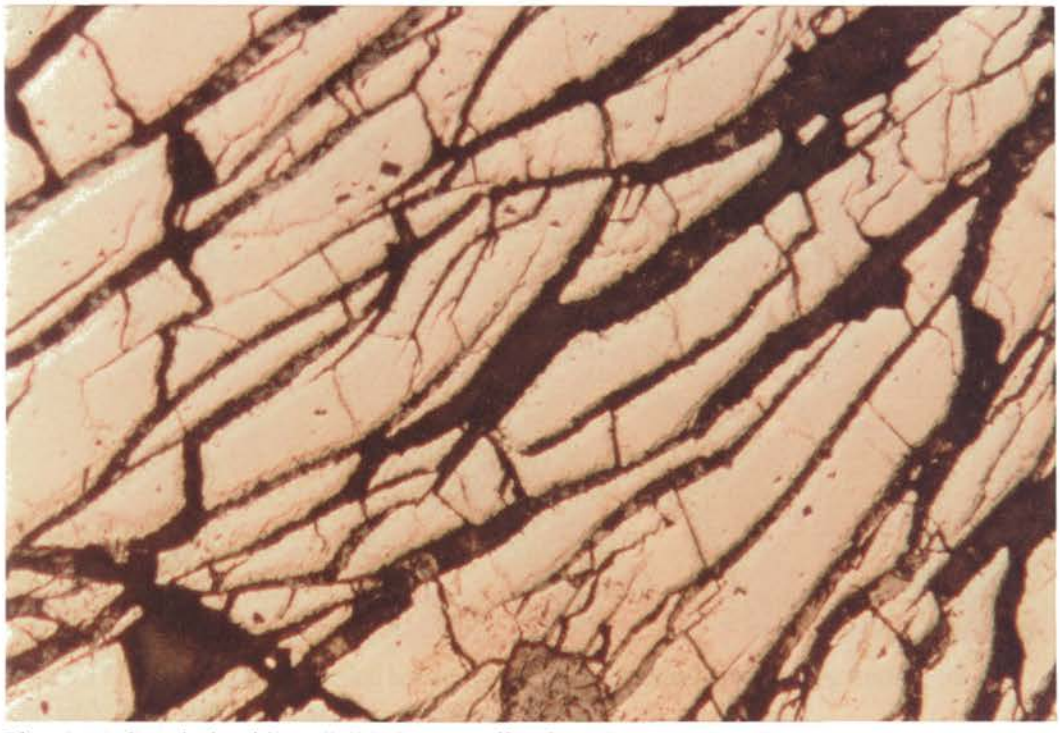

Plate 9.16 Cataclasis with negligible fracture offset from the MLA deposit.
Sample No MLA007 PPL F.O.V 3.5mm

In elongate chromite grains, one fracture of the orthogonal pair parallels the length. The chromite grains also have tails of fine-grained, euhedral magnetite grains trending parallel to the elongation direction. Ferritchromit replaces primary chromite adjacent to fracture-fill that comprises chrysotile, talc and magnesite, and secondary nickel sulfides. This is in keeping with Ashley (1973a, 1975) who concluded that the fracture-fill serpentine group minerals, nickel sulfides, and awaruite were co-genetic.The long axes of the nickel sulfide grains are normal to the chrysotile vein fibres, which are at 90° to the vein walls (Plate 9.17).

(b) QOC deposit

The dominant micro-scale textures are post-formational, as the chromitites are now crush microbreccias (Sibson 1977) with fragments ranging from 1mm to submicron size (Plate 9.18). The angular fragments have preserved their relative positions, consistent with dilation without significant rotation (Plate 9.19). Ferritchromit commonly replaces chromite along fractures and grain boundaries and the main fracture-fill comprises chrysotile, chromite fragments altered to ferritchromit, magnetite and awaruite.

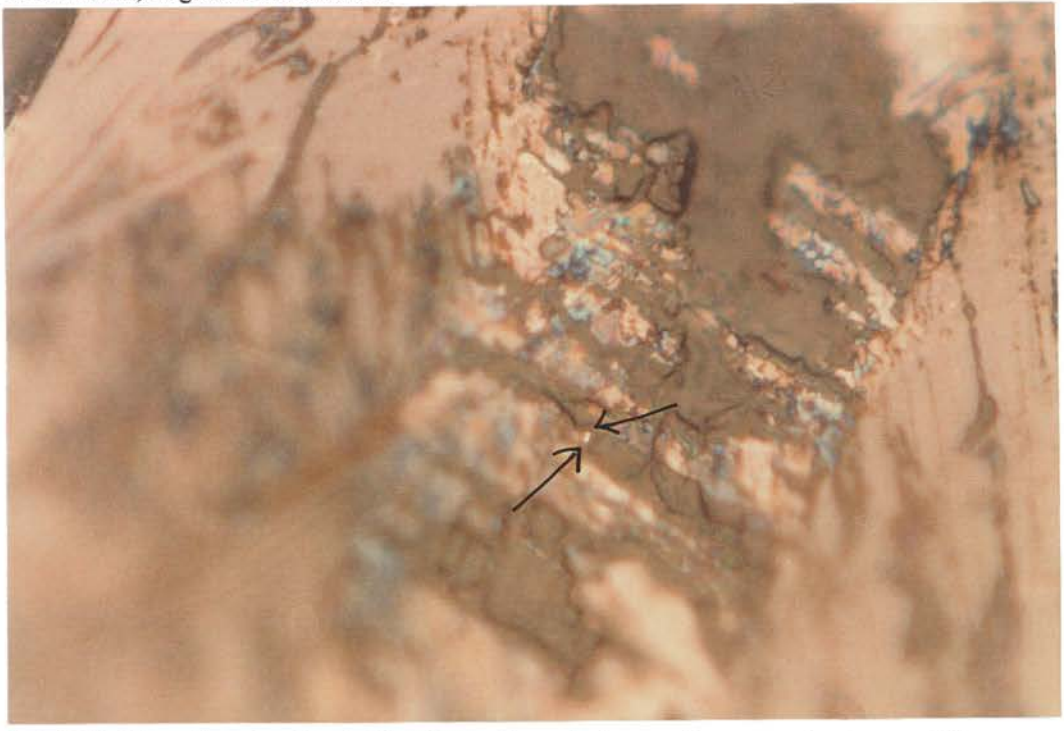

Plate 9.17 Tiny prismatic subhedral heazlewoodite grain (arrowed) cross-cutting fracture-fill chrysotile fibres within chromite. MLA deposit.
Sample No MLA006 PPL F.O.V 0.6mm

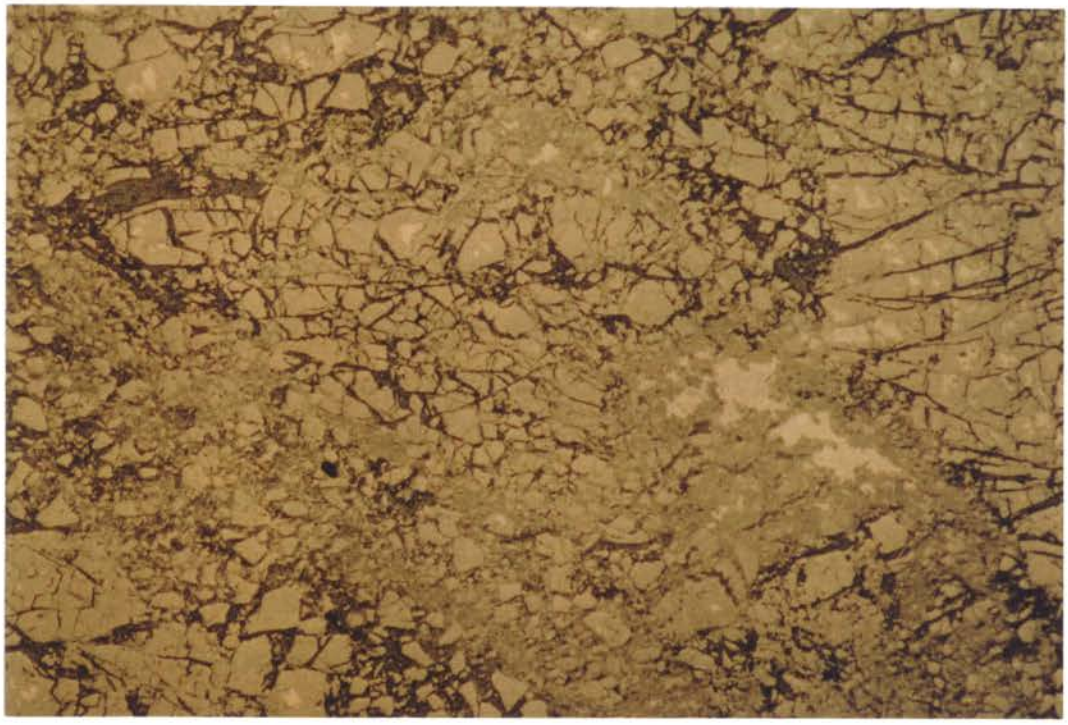

Plate 9.18 Crush microbreccia from the QOC deposit.
Sample No QOC003 PPL F.O.V 3.5mm

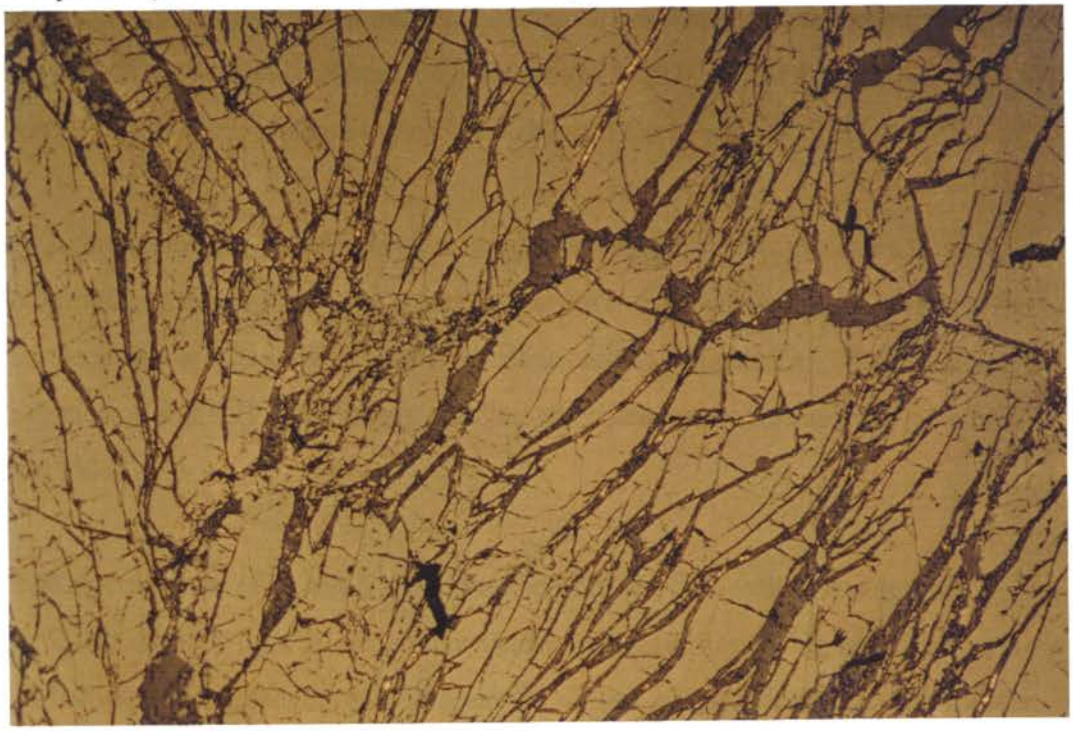

Plate 9.19 Dilation without significant fragment rotation within chromitite breccia from the QOC deposit.
Sample No QOC001 PPL F.O.V 0.6mm

9.4 BULK CHEMISTRY OF THE CHROMITITES AND ASSOCIATED DUNITIC WALLROCKS

Golding (1966) and Golding & Johnson (1971) conducted the first detailed whole-rock chemical analyses of chromitites from the Coolac Serpentinite Belt. Their findings are reported in section 9.1. The composition of the Coolac and Wambidgee serpentinite belt chromitites (Table 9.1; Figures 9.7 and 9.8), although almost a continuous spectrum from Cr-rich to Al-rich types, is divisible into:

1. Al-poor chromitites (7 to 13% Al_2O_3),
2. Al-rich chromitites (17 to 23% Al_2O_3), and
3. highly Al-rich chromitites (28 to 33% Al_2O_3).

Their distribution within the Coolac Serpentinite Belt (Figure 9.9) is such that: (i) highly Al-rich chromitites occupy the middle portion of the northern third of the belt; (ii) Al-poor chromitites occur along the western margin and throughout the southern third of the belt; and (iii) Al-rich chromitites occupy the remainder of the belt. All compositions (Figure 9.7) fall within or close to the ophiolitic chromitite field (Leblanc 1985) and are low in TiO_2 (0.13 to 0.28 wt%; Figure 9.8), as generally found within podiform chromitites (Leblanc & Ceuleneer 1992; Leblanc 1995).

Podiform chromitites within the Wambidgee Serpentinite Belt are too few to obtain a meaningful Cr/Al distribution. However, the central ones are classically ophiolitic (Figure 9.7), whereas the two southernmost deposits are less typically ophiolitic because of higher TiO_2, MnO and V_2O_3 concentrations (Table 9.1). Nevertheless, ophiolitic chromitites can contain up to 0.4 wt% TiO_2 (Ahmed 1984).

The high concentrations of Ti, Mn, V, Ni, Co and Sc within the bulk-rock chromitite analyses, compared with chromite from the electron microprobe analyses of Ray (1977), are not surprising as they partially reflect the chemistry of the fracture-fill silicates and rare secondary nickel sulfides and alloys.

The trace element analyses (Table 9.2) are reasonably constant within a deposit, but vary widely between deposits. Ga and Al_2O_3 are linked (Figure 9.10), consistent with Ga replacing Al in the chromite crystal lattice (Graham *et al.* 1996), and Zn and high Fe and/or Mg are linked, consistent with Zn replacing Fe^{2+} and/or Mg in the tetrahedral sites of the spinel structure.

Sample	[1]Type	Belt	[2]Locality A	[3]Locality B	Cr_2O_3	Al_2O_3	MgO	FeO	TiO_2	MnO	ZnO	V_2O_3
Detection limits (wt%)					0.01	0.01	0.01	0.01	0.01	0.01	0.01	0.01
35	M	CSB	C	W	53.1	7.68	16.4	20.83	0.13	0.26	0.10	0.10
25	M	CSB	C	W	51.1	9.57	16.6	15.82	0.26	0.27	0.05	0.10
24	M	CSB	C	M	49.4	12.60	16.5	14.27	0.19	0.22	0.04	0.16
137A	M	CSB	C	E	38.6	21.60	17.6	13.12	0.21	0.16	0.07	0.19
137B	D	CSB	C	E	28.7	16.20	18.5	10.07	0.20	0.12	0.05	0.12
133A	M	CSB	S	E	51.7	8.82	15.4	18.65	0.24	0.27	0.09	0.13
135A	M	CSB	C	M	48.9	9.9	17.7	14.40	0.14	0.16	0.05	0.16
39A	D	CSB	N	W	44.6	9.55	16.0	17.36	0.20	0.20	0.09	0.08
39C	M	CSB	N	W	48.8	10.0	12.7	16.08	0.28	0.24	0.08	0.09
69A	M	CSB	N	E	43.4	19.8	16.2	12.99	0.22	0.12	0.06	0.20
69B	D	CSB	N	E	29.0	20.9	21.5	10.71	0.21	0.12	0.02	0.15
104A	M	CSB	N	M	46.2	10.9	18.7	14.15	0.21	0.17	0.04	0.12
MLA007	M	CSB	N	M	27.8	23.5	22.6	11.87	0.16	0.11	0.04	0.18
MLA008	M	CSB	N	M	33.2	30.1	18.7	12.41	0.21	0.12	0.05	0.22
MLA010	M	CSB	N	M	31.9	28.8	19.6	12.08	0.21	0.12	0.05	0.21
MLA014	M	CSB	N	M	25.7	22.0	22.7	11.20	0.19	0.12	0.04	0.17
MLA018	M	CSB	N	M	34.6	32.2	17.8	12.49	0.25	0.12	0.06	0.21
QOC001	M	CSB	N	E	39.4	17.8	17.5	12.71	0.17	0.16	0.07	0.14
QOC003	M	CSB	N	E	38.6	12.9	15.9	12.99	0.17	0.18	0.05	0.12
35	H	CSB	C	W	31.0	5.37	22.1	14.27	0.10	0.18	0.07	0.08
MLA013	H	CSB	N	M	7.16	5.74	26.6	9.83	0.06	0.11	0.02	0.03
104B	H	CSB	N	M	0.48	0.17	37.0	7.66	0.02	0.13	0.02	0.01
QOC002	H	CSB	N	E	0.57	1.81	25.6	11.88	0.03	0.05	0.02	0.03
MLA017	H	CSB	N	M	3.09	4.00	15.2	11.10	0.05	0.05	0.02	0.03
24	H	CSB	C	W	2.27	3.34	31.1	5.18	0.14	0.15	0.04	0.01
25	H	CSB	C	M	2.58	0.65	31.4	6.44	0.02	0.10	0.03	0.02
138A	M	CSB	C	E	38.1	20.3	17.4	14.92	0.17	0.55	0.12	0.07
139A	M	CSB	C	E	54.3	7.88	15.3	13.57	0.13	0.17	0.04	0.04
139B	H	CSB	C	E	0.62	0.64	42.9	4.95	0.01	0.05	0.02	0.00
139V	V	CSB	C	E	38.9	7.88	23.5	13.22	0.08	0.14	0.06	0.06
ARC1	D	WSB	C	W	30.5	12.9	23.1	11.14	0.10	0.11	0.03	0.17
34A	M	WSB	C	W	41.4	21.1	19.8	12.86	0.14	0.12	0.04	0.23
ARC8	M	WSB	S	M	45.2	12.0	16.7	17.23	0.32	0.47	0.06	0.32
ARC9	M	WSB	S	M	41.2	12.8	16.1	18.78	0.34	0.40	0.07	0.32

[1] D = Disseminated chromitite M = Massive chromitite H = Hostrock dunite V = Vein chromitite

[2] Locality A: N = north C = central S = south

[3] Locality B: E = east M = middle W = west

Table 9.1 ICP-OES major and minor element analyses of the chromitites and associated dunitic host rocks from the Coolac and Wambidgee serpentinite belts (wt%).

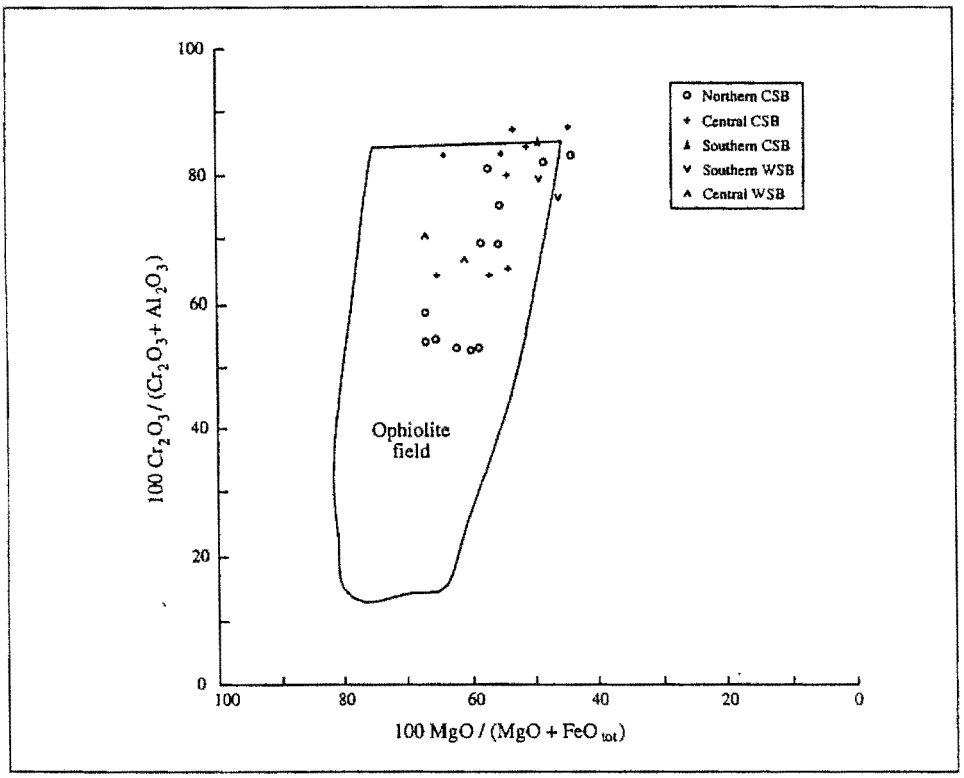

Figure 9.7 Compositional diagram for the Coolac and Wambidgee serpentinite belt chromitites with reference to the podiform chromitite field of Leblanc (1985) (data from Table 9.1).

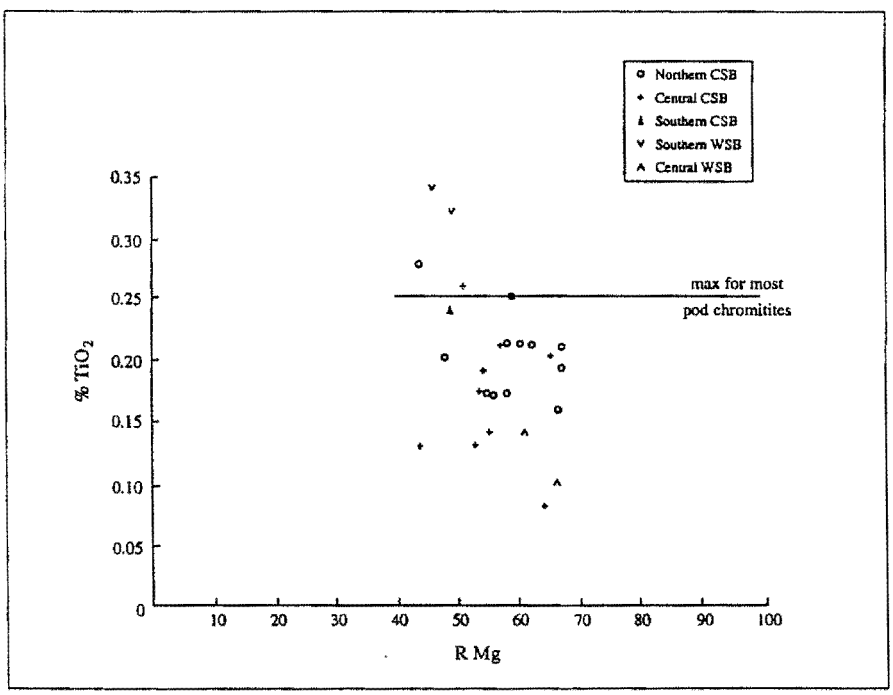

Figure 9.8 Wt% TiO_2 vs (100xMgO/MgO+FeO_{tot}) ratio for the Coolac and Wambidgee serpentinite belt chromitites (data from Table 9.1).

Table 9.2 XRF and neutron activation trace element analyses of the chromitites and associated dunitic hostrocks from the Coolac and Wambidgee serpentinite belts (results are in ppm).

Deposit	Type	Belt	Cu	Ga	Ni	Pb	Zn	Sb	As	Co	Sc
Detection limits (ppm)			1	4	2	3	2	0.2	1.0	1.0	0.05
34	D	WSB	17	25	2200	17	216	-	-	-	-
34a	M	WSB	16	36	2038	17	330	0.88	-1.0	215	4.88
35	M	CSB	12	18	1252	23	779	0.46	-1.0	272	5.40
37	M	WSB	27	15	1740	23	623	0.29	-1.0	221	5.59
25	M	CSB	15	21	1335	25	533	0.48	-1.0	229	4.60
24	M	CSB	16	18	1858	21	418	-	-	-	-
137a	M	CSB	19	34	1550	15	382	0.33	-1.0	195	6.32
137b	D	CSB	20	22	1191	16	201	-0.2	-1.0	171	16.10
133a	M	CSB	11	15	1342	22	731	0.22	-1.0	273	5.46
135a	M	CSB	16	12	1312	22	411	1.09	-1.0	228	5.94
39a	M	CSB	12	20	1934	21	729	-	-	-	-
39c	D	CSB	14	17	1142	24	699	0.62	1.91	223	4.90
69a	M	CSB	18	29	1415	17	291	0.38	-1.0	184	7.04
69b	D	CSB	19	24	1547	16	271	-	-	-	-
104a	M	CSB	17	23	1900	68	409	0.61	19.90	218	4.20
MLA	M	CSB	15 (1.87)	40.4 (7.30)	1827 (159)	14.4 (2.88)	354 (87)	-0.05 (0.31)	5.4 (2.39)	182 (13)	4.72 (0.76)
QOC	M	CSB	18 (1.4)	24 (5.66)	1245 (219)	15.5 (2.12)	494 (36)	0.51 (0)	6.12 (2.93)	193 (14)	5.13 (2.10)
138A	M	CSB	-	-	-	-	-	0.47	8.09	243	5.01
139A	M	CSB	-	-	-	-	-	0.41	-1.0	208	4.54
139V	V	CSB	-	-	-	-	-	0.22	-1.0	235	4.53
35	H	CSB	12	10	2511	17	336	-0.1	-0.5	205	4.41
MLA	H	CSB	21.5 (3.54)	10.5 (0.71)	4440 (619)	8 (1.4)	65 (13)	0.11 (0.30)	4.84 (0.13)	146 (6)	5.23 (0.48)
104B	H	CSB	5	-	3165	3	22	-	-	-	-
QOC	H	CSB	-	-	-	-	-	0.47	16.40	87.4	7.09
139B	H	CSB	-	-	-	-	-	-0.1	-0.5	96.30	4.79
36	H	WSB	-	-	-	-	-	0.65	5.35	85.50	8.34

Nb, Rb, Sr, Th, U, Y and Zr were analysed for but were essentially below the detection limit.

D = Disseminated chromitite M = Massive chromitite H = Hostrock dunite V = Vein chromitite

-ve sign indicates below detection limit.
Values are mean values with one standard deviation in brackets.

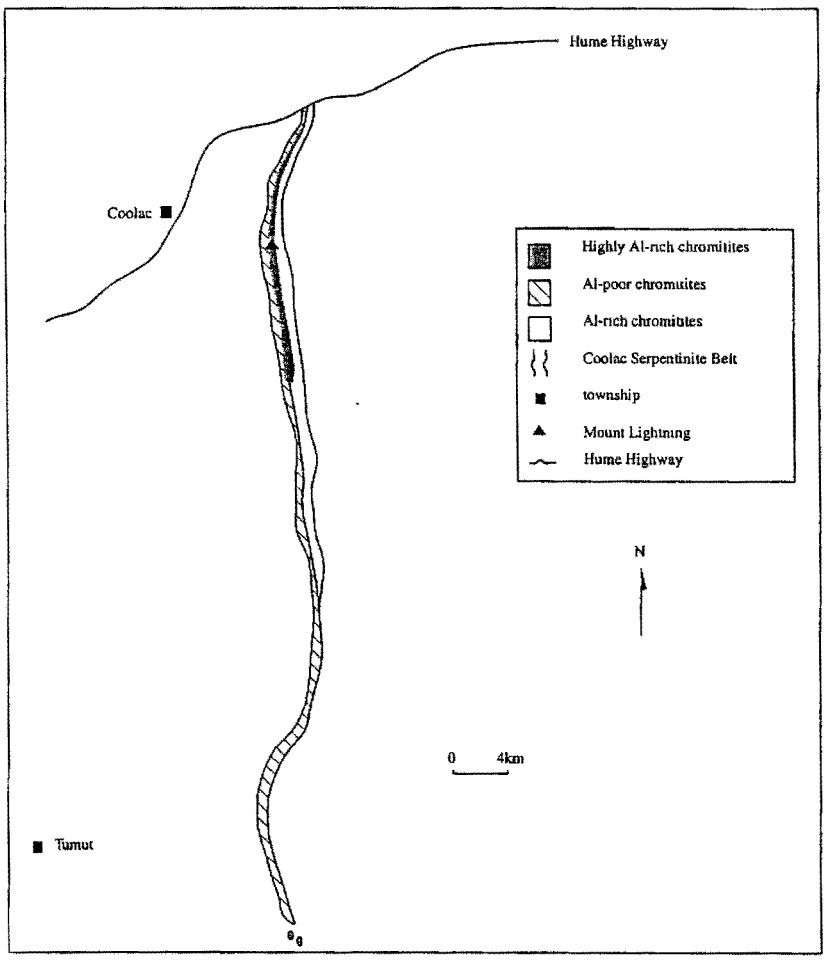

Figure 9.9 Distribution of chromitite types within the Coolac Serpentinite Belt (adapted from Golding & Johnson 1971) (data from table 9.1).

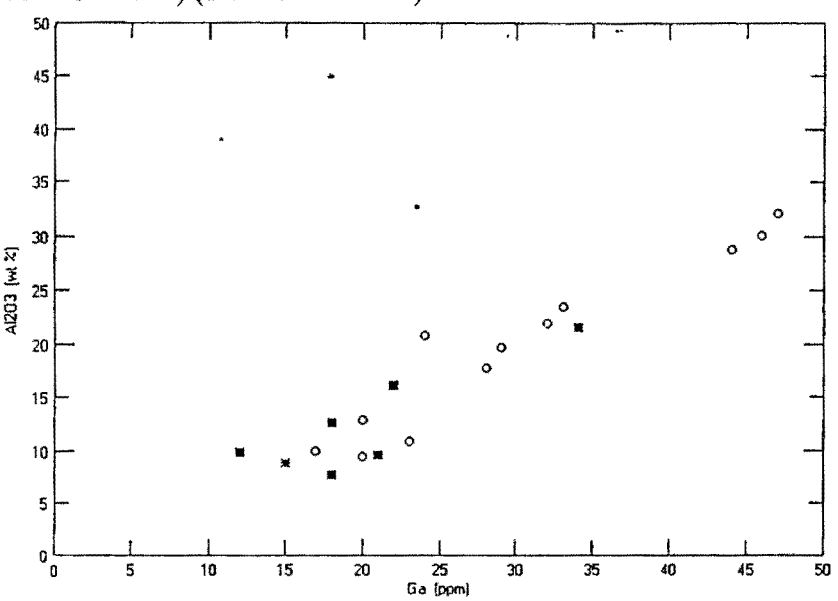

Figure 9.10 Al_2O_3 (Wt%) vs Ga (ppm) diagram for the Coolac and Wambidgee serpentinite belt chromitites (data from tables 9.1 and 9.2).

REE concentrations (Table 9.3) in all the chromitites are low (commonly below the detection limits). They appear to lack systematic geographic distribution and are of little use in understanding the geochemical evolution of the chromitites.

Most of the PGE analyses (Table 9.4) have low Os and Au values. The low Os is ascribed to errors resulting from rapid devolatilisation of Os during the fire assay procedure; whereas the low Au values are probably real. Ophiolitic chromitites are usually enriched in Os, Ir and Ru relative to Pt and Pd (Auge 1988; Leblanc 1995), and most of those from the Coolac Serpentinite Belt and Wambidgee Serpentinite Belts typically have this ophiolitic signature (Table 9.4). The MLA and QOC deposits (both within the Coolac Serpentinite Belt) are exceptions in that they are enriched in Pt and Au, such that the combined Au, Pt and Pd concentrations for the MLA deposit exceed the combined Ru, Ir and Os concentrations. The low Ir and Ru values (Table 9.4) in the alumina-rich MLA chromitites and the high values in the chromian-rich QOC, ARC7, ARC8 and ARC9 chromitites are consistent with Bacuta *et al.* (1990), who found similar results for podiform chromitites from the Acoje Block of the Phillipines. The results are also consistent with those of Yang & Seccombe (1993), who reported that Pt and Pd within fracture-fill hydrothermal assemblages reflected localised remobilisation from inclusions within chromite, whereas Ru, Os, Ir and Rh tended not to be remobilised. Localised remobilisation during serpentinisation would explain the concentration of Au, Pt and Pd within the podiform chromitites of the MLA and QOC deposits.

To further compare the chromitites, both within and between the serpentinite belts, and with ophiolitic podiform chromitites from elsewhere, chondrite-normalised (CN) spider diagrams (Figure 9.11) were constructed. The chondrite values are from Naldrett & Duke (1980), while the deposit data are from Crocket (1981), Page *et al.* (1982, 1986) and Prichard & Lord (1990). With the exception of the MLA chromitite, the CN PGE diagrams have positive slopes to Ru followed by negative slopes to Pt, in keeping with their ophiolitic signature (Barnes *et al.* 1985; Franklin *et al.* 1992). Less typical of ophiolitic occurrence is the relative Au enrichment in the MLA and QOC chromitites that Franklin *et al.* (1992) ascribed to remobilisation during serpentinisation.

Sample	Belt	Type	Locality A	Locality B	La	Ce	Sm	Yb
Detection limits (ppm)					0.1	1.0	0.05	0.1
35	CSB	M	C	W	0.05	-2	0.1	0.11
MLA	CSB	M	N	M	0.44 (0.14)	-2 (0)	0.07 (0.01)	-0.1 (0)
QOC	CSB	M	N	E	0.94 (0.39)	-2 (0)	0.22 (0.14)	0.23 (0.04)
69A	CSB	M	N	E	0.10	-2	0.10	0.11
137A	CSB	M	C	E	0.57	-2	0.08	0.11
137B	CSB	D	C	E	0.20	-2	0.10	0.12
135A	CSB	M	C	M	0.15	-2	0.09	0.12
104A	CSB	M	N	M	0.19	-2	0.09	0.13
133A	CSB	M	S	E	0.15	-2	0.10	0.14
25	CSB	M	C	W	0.28	-2	0.10	0.13
39C	CSB	M	N	W	0.32	-2	0.10	0.12
138A	CSB	M	C	E	0.23	-2	0.08	-0.1
139A	CSB	M	C	E	1.54	-2	0.12	0.16
139V	CSB	V	C	E	0.46	-2	0.09	0.10
37	WSB	M	S	M	0.38	-2	0.08	0.11
34A	WSB	M	C	W	0.18	-2	0.08	0.11
35	CSB	H	C	W	0.18	-2	0.09	-0.1
MLA	CSB	H	N	M	0.50 (0.21)	0.24 (1.75)	0.18 (0.02)	0.1 (0.007)
QOC	CSB	H	N	E	0.70	1.69	0.35	0.32
139B	CSB	H	C	E	0.33	0.74	0.11	0.08
36	WSB	H	S	E	0.49	1.04	0.16	0.06

Nd, Eu, Tb, Ho and Cu were also analysed but were found to be below the detection limits.

D = Disseminated chromitite M = Massive chromitite H = Hostrock dunite V = Vein chromitite

Locality A: N = north C = central S = south
Locality B: E = east M = middle W = west

-ve sign indicates below detection limits.
Values are mean values with one standard deviation in brackets.

Table 9.3 Neutron activation rare earth element analyses of the chromitites and associated dunitic hostrocks from the Coolac and Wambidgee serpentinite belts (results are in ppm).

Sample	Type	Belt	Au	Pt	Pd	Ru	Rh	Ir	Os
Detection limit (ppb)			2	0.5	0.5	0.5	0.5	0.5	2
MLA	M	CSB	9 (8.07)	17.92 (18.39)	4.25 (3.19)	10.83 (5.31)	2.67 (1.66)	16.42 (11.48)	0.33 (0.82)
QOC	M	CSB	2 (2.83)	5.25 (1.06)	3.25 (4.60)	86 (19.80)	6.25 (2.47)	34 (7.07)	1 (1.41)
MLSE 027	M	CSB	4	5	13	51	6	25	2
MLSE 027	D	CSB	4	3	1.5	27	5.5	16	-
QOC	H	CSB	4 (2.83)	8.5 (3.54)	5.5 (2.12)	8.5 (0.71)	1.75 (0.35)	5.5 (0.71)	1 (1.41)
MLA	H	CSB	3.5 (1.91)	5.38 (2.63)	3.13 (1.25)	7.75 (5.85)	1.5 (0.41)	7.25 (3.66)	-
2434	D	WSB	2	0.5	2	25	2.5	3.5	4
35	P	CSB	-	2.5	2.5	7	1	1	-
35	H	CSB	-	2	1	110	6.5	6.5	42
35	M	CSB	-	0.5	-	48	12	12	10
36	M	WSB	-	6.5	1.5	41	5	5	4
37	M	WSB	-	2.5	2	98	8.5	8.5	18
25	M	CSB	-	1	1	21	2	2	8
24	M	CSB	-	1	0.5	11	1.0	1.0	10
24	H	CSB	-	5	2	3.5	-	-	6
25	H	CSB	2	1.5	1.5	29	3.5	3.5	6
37	H	WSB	-	0.5	-	49	5.5	5.5	4
36	H	WSB	-	5.5	1	5	1	1	-
Detection limit			5	2	2	2	2	2	2
138a	M	CSB	<5	24	5	82	9	19	2
139a	M	CSB	10	16	6	140	14	24	4
139b	H	CSB	<5	4	<2	10	2	2	<2
139v	V	CSB	<5	26	8	86	10	20	2

D = Disseminated chromitite M = Massive chromitite H = Hostrock dunite V = Vein chromitite P = Enclosing harzburgite
Values are mean values with standard deviations in brackets.

Table 9.4 ICP-MS platinum-group element analyses of the chromitites and associated dunitic hostrocks from the Coolac and Wambidgee serpentinite belts (results are in ppb).

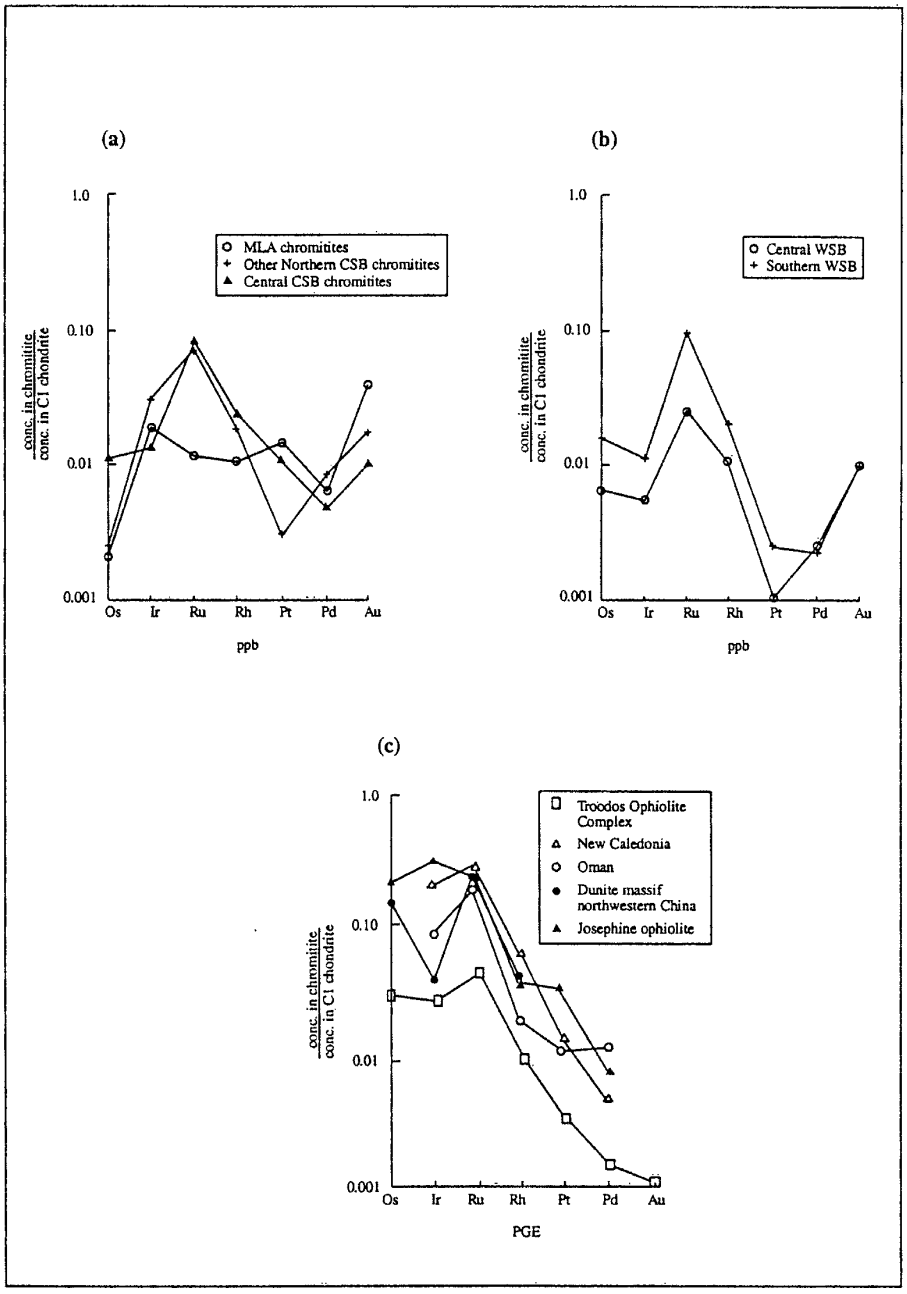

Figure 9.11 CN-PGE graph for the chromitites.

(a) CSB chromitites (data from table 9.4).
(b) WSB chromitites (data from table 9.4).
(c) Other ophiolite chromitites (data from Crocket 1981; Page *et al.* 1982, 1986; and Prichard & Lord 1990).
(chondrite values are those of Naldrett & Duke 1980).

9.5 PROBE CHEMISTRY OF THE CHROMITE GRAINS

Because the MLA and QOC deposits are respectively dominated by formational and post-formational textures, chromites from these end-member textural types were chosen for probe work. The electron microprobe analyses (Table 9.5) confirm that chromitite from the MLA deposit is Al-rich while that from the QOC deposit is Cr-rich. Fracture-related rims of secondary chromite (ferritchromit) contain far less Mg and Al and far more Fe than their parent grains (cf. Ashley 1975).

Sample	Part of Grain	Type	Mg	Al	Si	Ti	Cr	Fe	Ca	O	Total
QOC003	C	B	8.34 (0.04)	9.19 (0.04)	0.01 (0.008)	0.12 (0.01)	35.16 (0.13)	12.49 (0.21)	0.06 (0.05)	33.58 (0.07)	98.94 (0.31)
QOC003	R	B	8.35	9.12	0.02	0.13	35.21	12.57	0.13	33.62	99.14
QOC001	C	B	9.17 (0.10)	12.89 (0.64)	0.02 (0.008)	0.15 (0.017)	29.74 (1.10)	12.49 (0.41)	0.0025 (0.005)	34.93 (0.44)	99.38 (1.27)
MLA018	C	M	11.18 (0.02)	17.61 (0.16)	-	0.16 (0.01)	24.91 (0.06)	9.74 (0.06)	-	37.42 (0.16)	101.01 (0.30)
MLA007	R	M	10.21	16.53	0.02	0.15	25.71	11.22	0.01	36.63	100.47
MLA007	C	M	9.76 (1.31)	17.28 (0.30)	0.04 (0.04)	0.16 (0.007)	24.50 (0.25)	10.63 (0.12)	0.01	36.23 (1.10)	98.63 (2.62)
MLA007	Alt	M	4.76	3.12	3.12	6.20	23.65	21.37	0.12	29.45	91.79

B = Breccia Fragment M = Massive grain Alt = Ferritchromit C = Core R = Rim

Values are mean values with standard deviations in brackets.

Table 9.5 Electron microprobe analyses of selected chromite grains (Wt%).

Cr-rich chromitites are believed to represent more fractionated melts than Al-rich chromitites (e.g. Dick & Bullen 1984). This is clearly shown within these two above deposits, with the Cr-rich QOC chromitites being derived from a more fractionated melt than the Al-rich MLA chromitite. Also, the Cr# (Cr/Cr+Al ratio) is believed to be indicative of the tectonic setting of chromitite formation with Cr# <0.7 being indicative of a MOR setting and Cr# >0.7 being indicative of a subvolcanic arc setting (e.g. Dick & Bullen 1984; Arai 1994). The Cr-rich QOC chromitites have Cr# of 0.7-0.79, thus indicative of a subvolcanic arc setting, while the Al-rich MLA chromitites have a Cr# of 0.6, this indicative of a MOR setting. However, as these two deposits from the Coolac Serpentinite Belt are only a few hundred metres apart and are both enclosed within a thin dunitic shell in harzburgite, it is hard to envisage them as having formed within different tectonic settings. Obviously this ratio

may not be applicable here. In contrast, the chromian spinels within the harzburgites (Table 9.6) have Cr# of 0.38 to 0.40, much lower than that within both chromitite types.

Sample N	1	2	3
Belt	CSB	CSB	CSB
Cr2O3	25.5	26	26.5
Al2O3	40.6	42.3	39.3
Fe2O3	4.4	4.6	4.2
FeO	10.3	8.3	11.8
MnO	3.6	3.2	0.4
MgO	16.1	18.2	16.8
NiO		0.1	
TiO2			
Total	100.5	102.7	99

Table 9.6 Electron microprobe analyses of Cr-spinels within harzburgite (data from Ashley 1973a).

Semi-quantitative SEM analyses (Table 9.7) of discrete chromite grains from the Tumut Serpentinite Province show the chemistry variation both between and, to a lesser degree, within deposits. They confirm that discrete chromite grains and their chromitite hosts can be categorised as Cr-rich or Al-rich, and that ferritchromit reflects the composition of the parent chromite grain.

The PIXE proton probe results (Table 9.8) show that, relative to fracture-fill serpentine, the trace element geochemistry of selected chromites from the MLA and QOC deposits is enriched in Mn, Ni, Zn and Ga, and depleted in As and Cu. Although the QOC chromites contain more Zn and less Ga than MLA grains, their trace element geochemistry indicates little variation between and within deposits. This also applies to chromites from podiform chromitites of the Massif Du Sud, New Caledonia (McAndrew *et al.* 1987) which have a remarkably similar trace element composition to those from the MLA and QOC deposits (Graham 1990). Regardless of geographic location, it is thus conceivable that podiform chromitite deposits have similar trace element geochemistries. The relatively high concentrations of Au, Ru and Rh from the proton microprobe analyses may not represent "real values" and could be artifacts of data processing (Ashley pers. comm. 1998)."

Deposit	Belt	Type	Site	Mg	Al	Cr	Fe	Si
25A	CSB	B	C	9.17 (3)	7.10 (1.98)	62.93 (1.94)	221.56 (4.69)	-
25A	CSB	Alt	R	0.47 (0.20)	0.005 (0.007)	50.06 (42.67)	49.46 (42.86)	-
25A	CSB	Alt	C	0.29	0.02	25.22	74.48	-
25A	CSB	M	C	3.28 (0.33)	2.67 (0.07)	76.62 (15.13)	17.43 (15.09)	-
25A	CSB	Alt	f	0.18 (0.25)	-	43.02 (55.34)	56.81 (55.59)	-
24A	CSB	B	C	7.74 (4.71)	7.45 (4.04)	58.11 (1.79)	26.71 (8.05)	-
24A	CSB	M	C	10.17 (3.13)	9.46 (2.82)	58.79 (0.55)	21.58 (5.69)	-
24A	CSB	B	f	3.34	2.94	63.13	30.58	-
24A	CSB	B	S	4.13 (0.18)	3.69 (0.16)	63.64 (0.28)	28.55 (0.06)	-
35B	CSB	M	C	12.62 (0.59)	10.56 (3.50)	64.45 (1.02)	12.38 (1.88)	-
35B	CSB	M	S	3.45	2.23	54.26	40.06	-
137A	CSB	M	C	14.78 (1.07)	22.74 (1.06)	51.91 (2.21)	10.58 (0.08)	-
137A	CSB	B	C	13.50	29.35	47.14	10.01	-
137A	CSB	Alt	R	14.04	10.80	56.65	13.19	5.33
135A	CSB	B	C	10.66	7.59	59.93	21.82	-
36B	WSB	M	C	13.08	16.32	49.71	20.88	-
36B	WSB	Alt	C	14.71 (6.50)	15.17 (10.28)	42.57 (7.83)	23.08 (7.56)	4.47 (5.57)
36B	WSB	Alt	f	4.36	0.79	46.71	47.33	0.81
36B	WSB	B	C	15.65 (0.57)	21.30 (2.53)	48.66 (0.56)	14.39 (2.70)	-
36B	WSB	B	S	8.81	9.90	64.36	16.93	-
36B	WSB	B	f	22.28	20.46	34.20	9.83	13.23

B = Breccia Fragment M = Massive grain Alt = Alteration product S = Shear band
C = Centre of grain R = Rim of grain f = Along fractures

Values are mean values with standard deviations in brackets.

Table 9.7 Electron microprobe analyses of selected chromite grains from the Coolac and Wambidgee serpentinite belts (Wt%).

Sample	Type	Mn	Ni	Zn	Ga	Ge	As	Au	Ru	Cu	Rh
QOC003	B	>1000	690	675	32.6	3.5	3.7	7.6	-	-	-
QOC003	B	>1000	>1000	545	35.1	-	-	8.7	-	-	-
MLA018	M	>1000	>1000	513	65	-	-	6.4	3.4	-	-
MLA018	M	>1000	>1000	481	59.9	-	-	6.5	-	-	-
MLA018	M	>1000	>1000	409	57.6	-	-	5.0	-	5.8	-
QOC001	B	>1000	>1000	991	56.0	-	3.9	-	-	9.8	-
QOC001	B	>1000	>1000	628	41.4	-	-	12.7	-	-	-
MLA018	M	>1000	>1000	398	56.8	-	-	-	-	-	-
QOC001	B	>1000	>1000	874	55.0	-	-	11.4	-	-	-
QOC001	S	536	>1000	8.43	6.3	-	5.9	-	-	19.3	-
QOC003	M	>1000	980	581	30.7	-	4.9	-	4.2	-	6.8

B = Breccia fragment M = Massive grain S = Serpentine fracture-fill

Table 9.8 Proton microprobe analyses of selected chromite grains from the MLA and QOC deposits (results are in ppm).

9.6 PRIMARY INCLUSION MINERALOGY

Non-silicate inclusions in chromite grains range in diameter from 1 to 10um and consist of Al-rich chromite, PGE-bearing nickel sulfides (Plate 9.20) and palladian gold in decreasing abundance-order (Table 9.9). The Al-rich chromite occurs as trails of ovoid-shaped grains (1-2um across) along grain boundaries within Cr-rich chromite (Plate 9.21; Table 9.10).

Mineral	Fe	Ni	Cu	Os	Pt	Rh	S	As	Co	Ir	Total
Fe-Cu millerite	8.39 (1.72)	47.21 (8.12)	4.80 (0.70)	4.2 (2.01)	0.11 (0.04)	0.01 (0.13)	35.88 (6.06)	-	-	-	100.72 (15.37)
Millerite	3.90 (2.59)	46.6 (3.74)	-	0.08 (0.09)	-	-	27.11 (4.75)	-	0.04 (0.04)	0.04 (0.04)	77.82 (9.79)
Heazlewoodite	1.78 (0.76)	65.23 (6.95)	-	0.17 (0.16)	-	-	23.31 (3.56)	0.18 (0.13)	-	-	90.76 (9.83)

Table 9.9 Electron microprobe composition of primary sulfide and metallic inclusions in chromite (Wt%). Values in parentheses represent average standard deviation.

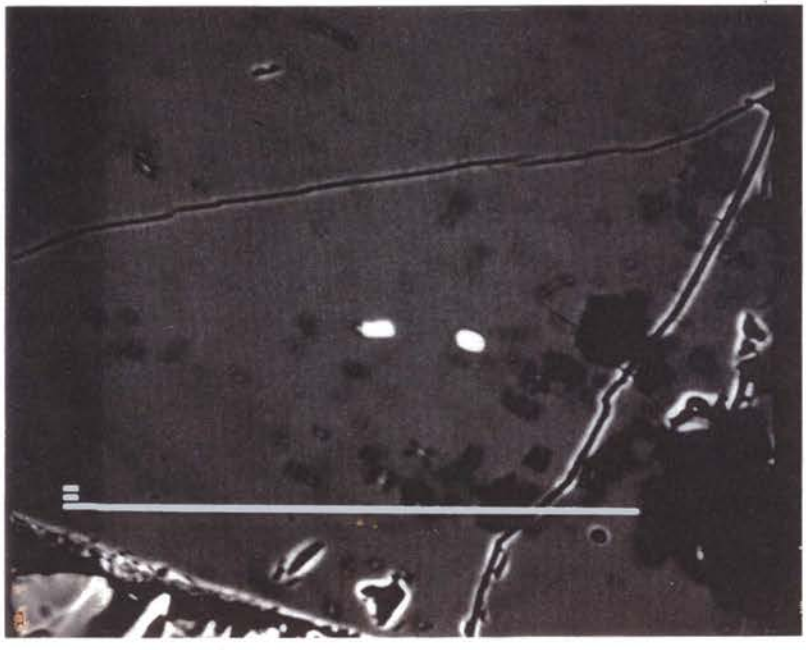

Plate 9.20 SEM image of PGE-bearing pentlandite inclusions within chromite from McAlpine's chromitite deposit.
Sample No DBchrom Scale bar 100um

Type	Mg	Al	Cr	Fe
I	6.62	38.66	46.95	7.78
H	14.02	21.99	53.47	10.52
I	5.42	34.15	40.41	14.24
H	10.66	7.59	59.93	21.82

Table 9.10 Electron microprobe analyses of Al-rich spinel primary inclusions (I) compared to that of the host chromite (H) (Wt%).

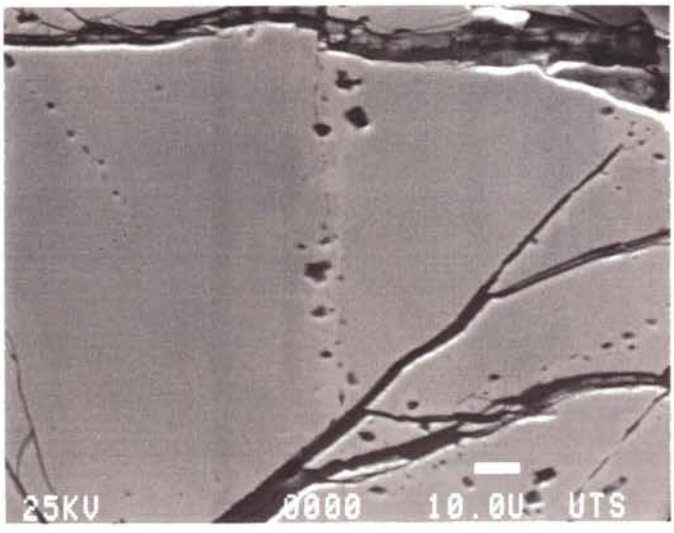

Plate 9.21 SEM image of Al-spinel inclusions within Cr-rich chromite.
Sample No 133 Scale bar 10um

Silicate inclusions consist of abundant olivine and two types of amphibole. Forsteritic olivine occurs as Ni-rich, Cr-bearing ovoid-shaped grains that typically contain more Ni than the chromite host; the Ni-enrichment is ascribed to subsolidus re-equilibration. Abundant pargasitic amphibole and rare inclusions of a member of the gedrite-anthophyllite group form prismatic euhedra (up to 20um in length) that lack compositional zoning (Plate 9.22) and are without reaction rims against the chromite host (Plate 9.23).

Rare composite inclusions, consisting of silicate/Ni-sulfide phases (Plate 9.24), consist of either Mg-Na amphiboles or diopside (the silicate phase) and millerite (the sulfide phase).

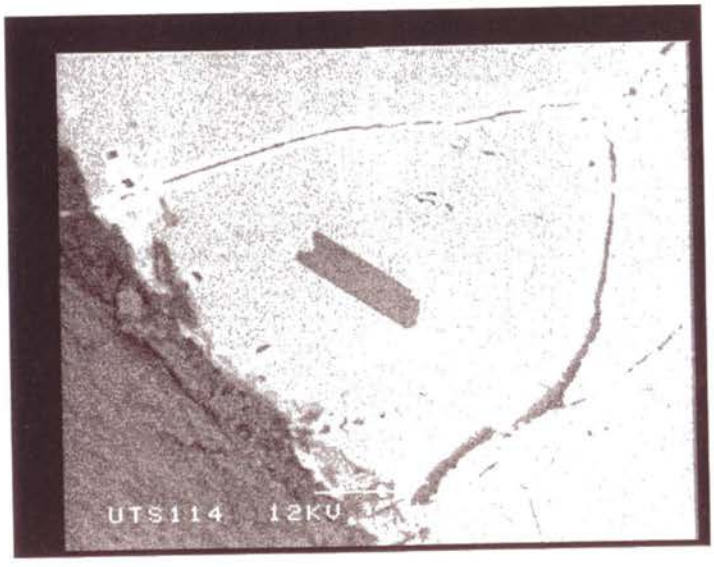

Plate 9.22 SEM im age of euhedral pargasitic amphibole inclusions within chromite.
Sample No 36 Scale bar 10um

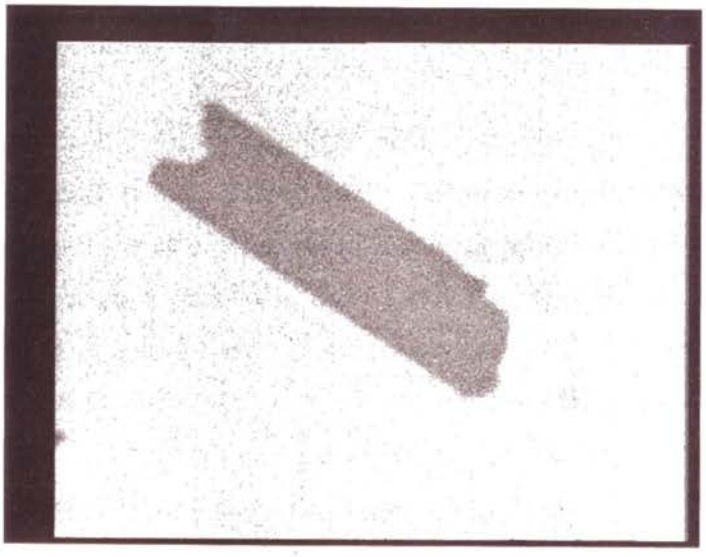

Plate 9.23 SEM image - enlargement of portion of Plate 9.22. Sharp contact between the pargasitic amphibole inclusion and host chromite.
Sample No 36 Scale bar 1um

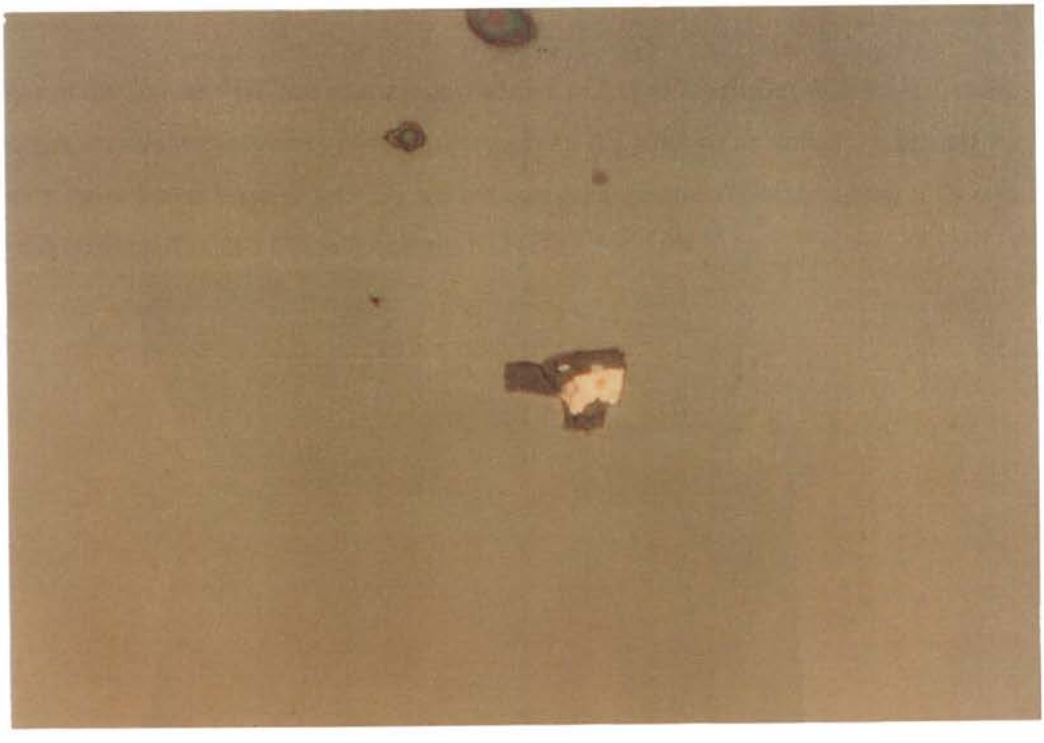

Plate 9.24 Composite silicate/Ni-sulfide inclusion within chromite.
Sample No 138d PPL F.O.V 0.6mm

9.7 FRACTURE-FILL MINERALOGY

9.7.1 Metallic phases

Many of the fracture-fill phases within the podiform chromitite deposits of the Coolac Serpentinite Belt were initially documented by Golding (1966) and are part of the minor opaque mineral assemblage from the ultramafic rocks of the Coolac Serpentinite Belt, as described by Ashley (1975). Nickel sulfide and Ni-Fe alloys are both common, but nickel sulfides dominate some deposits (e.g. the MLA deposit) whereas alloys dominate others (Table 9.11). Awaruite (Ni_2Fe to Ni_5Fe) is the most common alloy and occurs as discrete grains (typically 10-20um but up to 80um in diameter; Plate 9.25), grains rimmed by trevorite ($NiFe_2O_4$) and/or magnetite (Plate 9.26), and as rims on chromite grains. Millerite (NiS) is the most common nickel sulfide. It is PGE-rich, (Table 9.11), occurs as discrete subhedra and anhedra (up to 10um across; Plate 9.27), and forms atoll-shaped rim replacements of primary chromite. Heazlewoodite (Ni_3S_2) is the second most abundant nickel sulfide and, along with polydymite (Ni_3S_4), is PGE-bearing and occurs as euhedra (Plate 9.28) and atoll-shaped anhedra up to 15um in length. Pentlandite $(Fe,Ni)_9S_8$ is rare and lacks PGE, but one grain occurred within PGE-rich trevorite.

Other phases include: PGE-rich chalcopyrite ($CuFeS_2$), with up to 15wt% Os (Table 9.11), forming margins around chromite grains ; Pd-rich native gold (Au-Pd) which forms subhedral grains and "wires" up to 5um in length (Plate 9.29); and platinum group minerals (PGM) consisting of Os- and Ir-rich ruthenium (Table 9.10), palladium and Ni_3Pt (?).

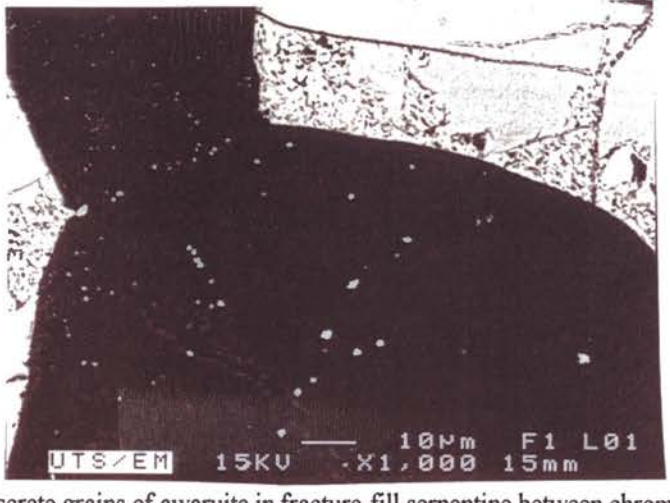

Plate 9.25 Discrete grains of awaruite in fracture-fill serpentine between chromite grains.
Sample No 69b Scale bar 10um

Table 9.11 Electron microprobe analyses of fracture-fill metallic phases in the chromitites (Wt%). (Poor totals due to either beam overlap or to small size of analysed grains).

Sample	Fe	Co	Ni	S	Os	Cu	Pt	Pd	Rh	Ir	As	Sb	Ru	Total
Ni_4S_3	0.71	-	67.20	27.61	-	-	-	-	-	-	-	-	-	95.52
$Ni_{13}S_{10}$	0.72	-	72.13	30.32	-	-	-	-	-	-	-	-	-	103.16
Millerite	0.91 (0.48)	0.007 (0.010)	47.31 (14.49)	23.70 (7.57)	0.07 (0.06)	-	0.01 (0.017)	0.017 (0.018)	0.013 (0.022)	0.034 (0.067)	0.072 (0.099)	-	-	72.73 (20.72)
Polydymite	0.7 (0.55)	0.005 (0.007)	43.84 (17.64)	33.82 (6.94)	0.07 (0.09)	-	-	-	-	0.06 (0.08)	-	-	-	78.48 (23.86)
Heazlewoodite	1.18 (0.98)	0.015 (0.013)	57.51 (11.42)	21.60 (3.97)	0.044 (0.055)	-	0.02 (0.04)	0.016 (0.024)	0.003 (0.007)	0.044 (0.08)	0.054 (0.099)	0.003 (0.007)	-	80.58 (14.97)
Ni_8S_5	0.44	-	54.40	17.72	0.06	-	0.04	-	-	0.06	-	-	-	72.76
Awaruite	21.73 (4.31)	0.83 (0.56)	64.90 (10.47)	0.16 (0.32)	-	-	-	-	-	-	-	-	-	87.65 (11.80)
Ruthenium	-	-	-	-	27.09 (0.18)	-	-	-	-	9.76 (0.19)	-	-	15.48 (2.62)	52.3 (2.99)
Chalcopyrite	28.64 (1.54)	0.0067 (0.011)	0.053 (0.023)	36.04 (1.59)	14.17 (1.25)	27.51 (2.08)	0.11 (0.11)	0.017 (0.029)	-	0.04 (0.07)	-	-	-	106.6 (5.65)

Values are mean values with standard deviations in brackets.

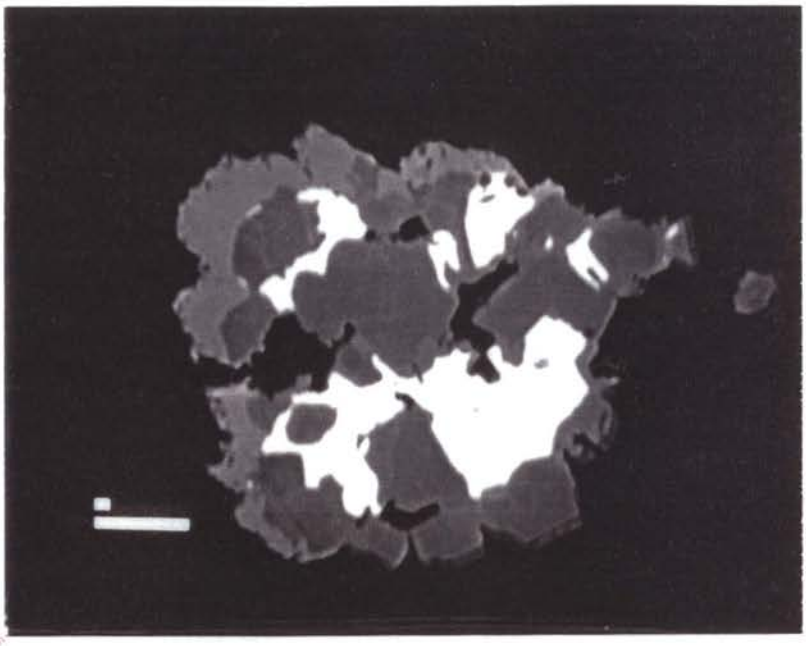

Plate 9.26 Sem image of composite awaruite (white)/trevorite (dark grey)/magnetite (light grey) grain within fracture-fill.
Sample No MC015 Scale bar 10um

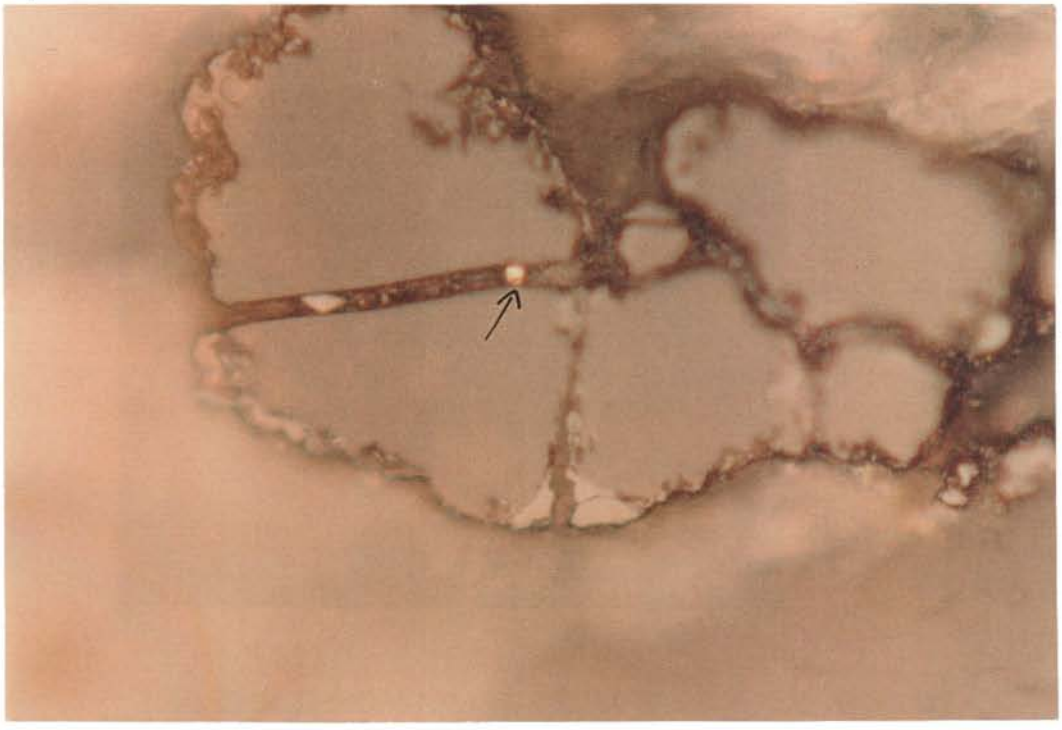

Plate 9.27 SEM image of discrete grain of subhedral equant millerite (arrowed) within fracture-fill.
Sample No MLA007 PPL F.O.V 0.6mm

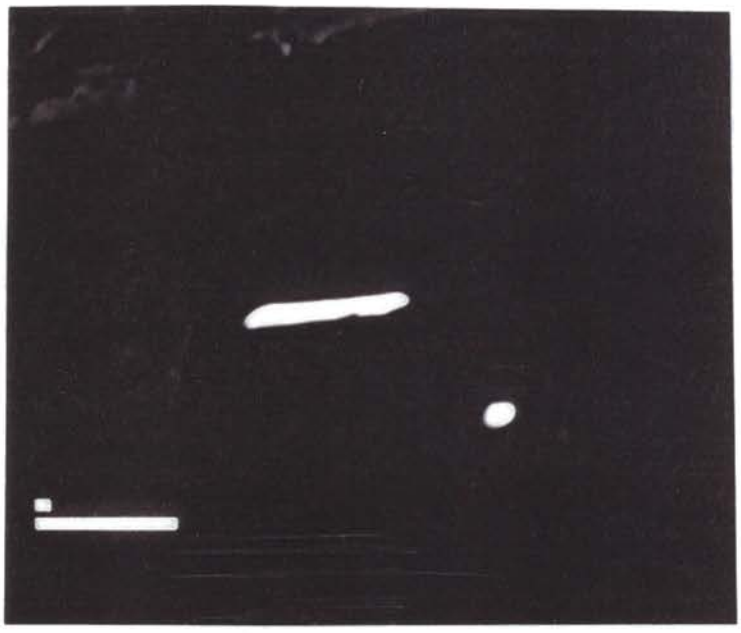

Plate 9.28 SEM image of euhedral prismatic heazlewoodite within fracture-fill.
Sample No MLA008 Scale bar 10um

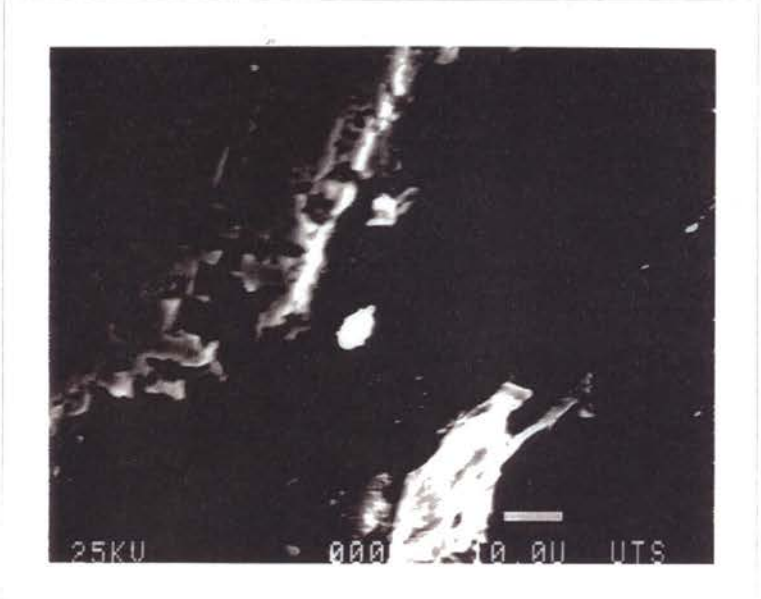

Plate 9.29 SEM image of palladian gold (bright white) within fracture-fill.
Sample No 69 Scale bar 10um

9.7.2 Oxide phases

The oxide phases in fractures between chromite grains are magnetite, trevorite and ferritchromit. Titaniferous and Ti-poor magnetite occur as equant-shaped subhedral grains and also as anhedral masses surrounding awaruite. Trevorite ($NiFe_2O_4$) commonly forms a rim between an awaruite core and outer rim of magnetite (Plate 9.26). Ferritchromit forms fracture-related replacement rims on primary chromite (Plates 9.30 to 9.32) and, in some of the disseminated chromitites of the Coolac Serpentinite Belt, almost completely replaces the primary chromite. The replacement developed during serpentinisation, as inferred from intergrowths between ferritchromit and serpentine (Plate 9.33). The reaction front is marked by the primary chromite being replaced by ferritchromit and then by mixtures of ferritchromit and Al-rich serpentine (Plate 9.34).

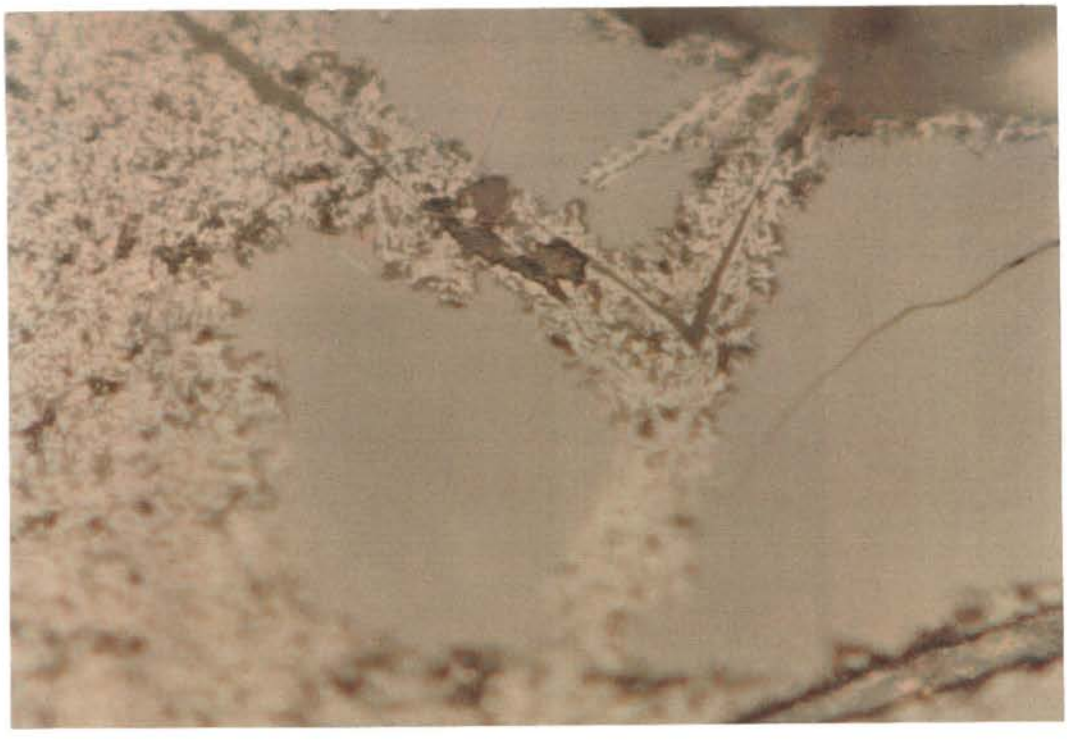

Plate 9.30 SEM image of fracture-related replacement of primary chromite (grey) by ferritchromit (pitted yellow-white).
Sample No MLA007 PPL F.O.V 0.6mm

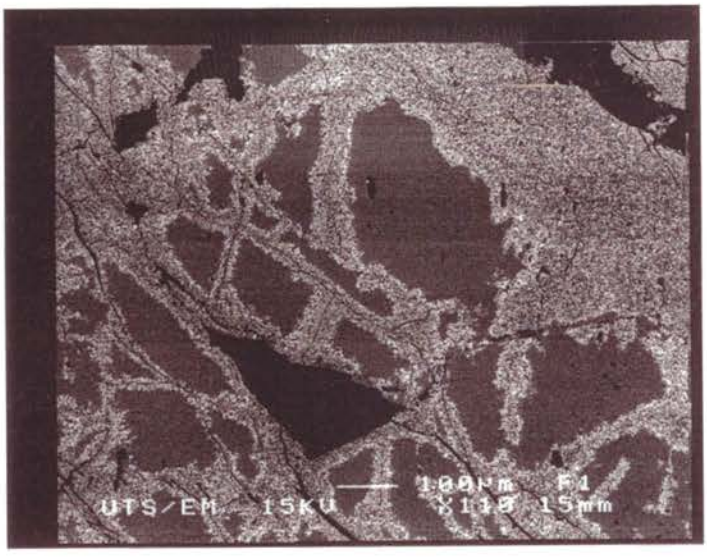

Plate 9.31 SEM image of fracture-related replacement of primary chromite (dark grey) by ferritchromit (pitted white).
Sample No 138b Scale bar 100um

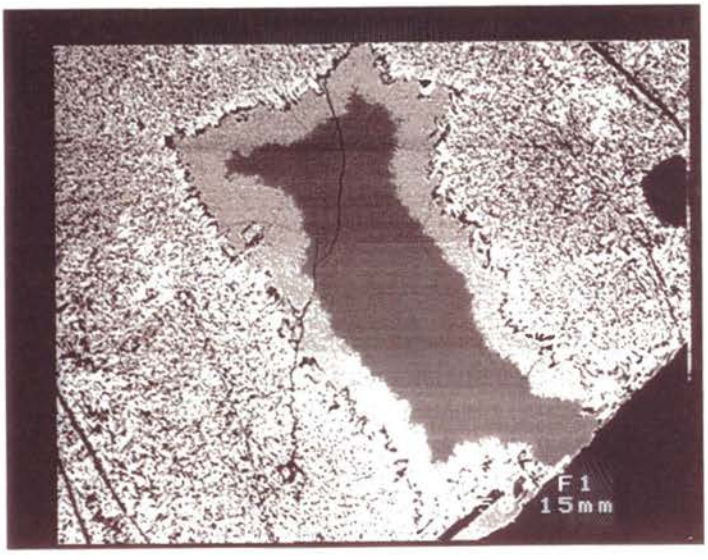

Plate 9.32 SEM image of fracture-related replacement of primary chromite (dark grey) by ferroan chromite (light grey) and ferritchromit (pitted white).
Sample No 138b Scale bar 10um

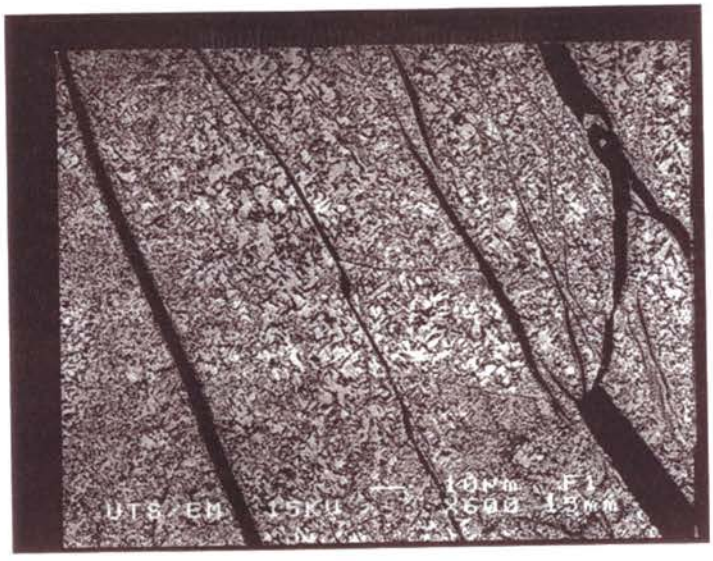

Plate 9.33 SEM image of intergrowth of ferritchromit (white) and serpentine (black).
Sample No 138b Scale bar 10um

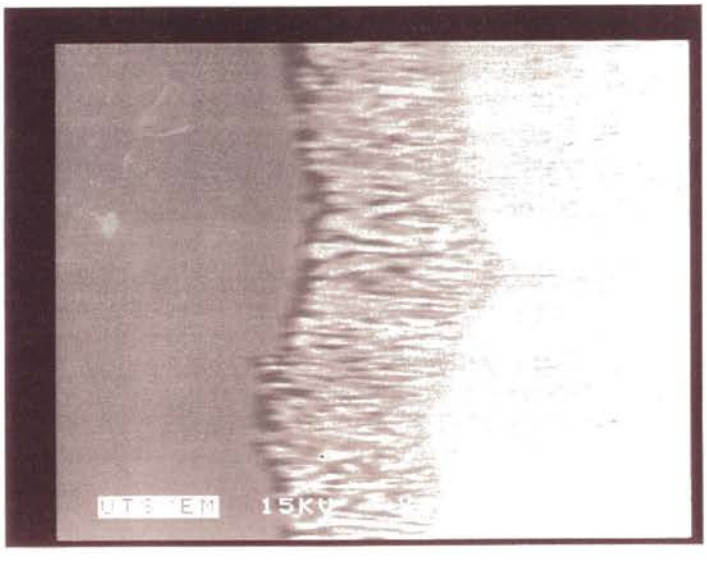

Plate 9.34 SEM image of reaction front of ferritchromit (white) replacement of primary chromite (grey).
Sample No 138b Scale bar 10um

9.7.3 Silicate phases

The fracture-fill serpentine minerals of the podiform chromitites vary between belts. Lizardite 6T and chrysotile 2M dominate the Coolac Serpentinite Belt, whereas antigorite dominates the Wambidgee Serpentinite Belt (Table 9.12).

Phases such as the various serpentine-group minerals, Cr-grossular, uvarovite, Cr-vesuvianite and Cr-chlorite were described from the Coolac Serpentinite Belt by Golding (1966), Golding & Bayliss (1968), Ashley (1973a) and Ray (1977). Clinochlore IIb commonly occurs as rims around the chromite grains (particularly in the more aluminous chromitites) and, in places, abundant talc pseudomorphs serpentine. Uvarovite garnet ($Ca_3Cr_2Si_3O_{13}$) defines slickenlines and also occurs as bright green rhombic dodecahedra, up to 5mm in diameter, within fractures in a few deposits (Graham & Colchester 1995). It is commonly associated with pink chromian clinochlore. Diopside in solid solution with diopsidic augite is a major fracture-fill phase within some of the deposits (Table 9.12; Plate 9.35). As serpentine group minerals overprint the diopside, the latter records an earlier alteration event (Plate 9.36).

Deposit	Serpentinite Belt	Wallrock	Serpentine mineralogy
MLA	CSB	dunite	Al-rich lizardite, chrysotile 2M
QOC	CSB	dunite	chrysotile 2M, Al-rich lizardite
24	CSB	serpentinite	antigorite, Al-diopside
25	CSB	dunite	lizardite 6T
34	WSB	dunite	lizardite 6T
35	CSB	dunite	lizardite 6T
36	WSB	serpentinite	antigorite
37	WSB	serpentinite	antigorite
39	CSB	dunite	chrysotile 2M, lizardite 6T
69	CSB	dunite	lizardite 6T
104	CSB	dunite	chrysotile 2M, lizardite 6T
133	CSB	dunite	lizardite 6T, chrysotile 2O
135	CSB	dunite	lizardite 6T, chrysotile 2O
137	CSB	serpentinite	lizardite 6T
138	CSB	dunite	lizardite 6T, chrysotile 2M
139	CSB	dunite	lizardite 6T
211	CSB	dunite	Al-rich lizardite, chrysotile 2M

Table 9.12 Summary of XRD-determined mineralogy of the hostrocks to the podiform chromitite deposits of the Coolac and Wambidgee serpentinite belts.

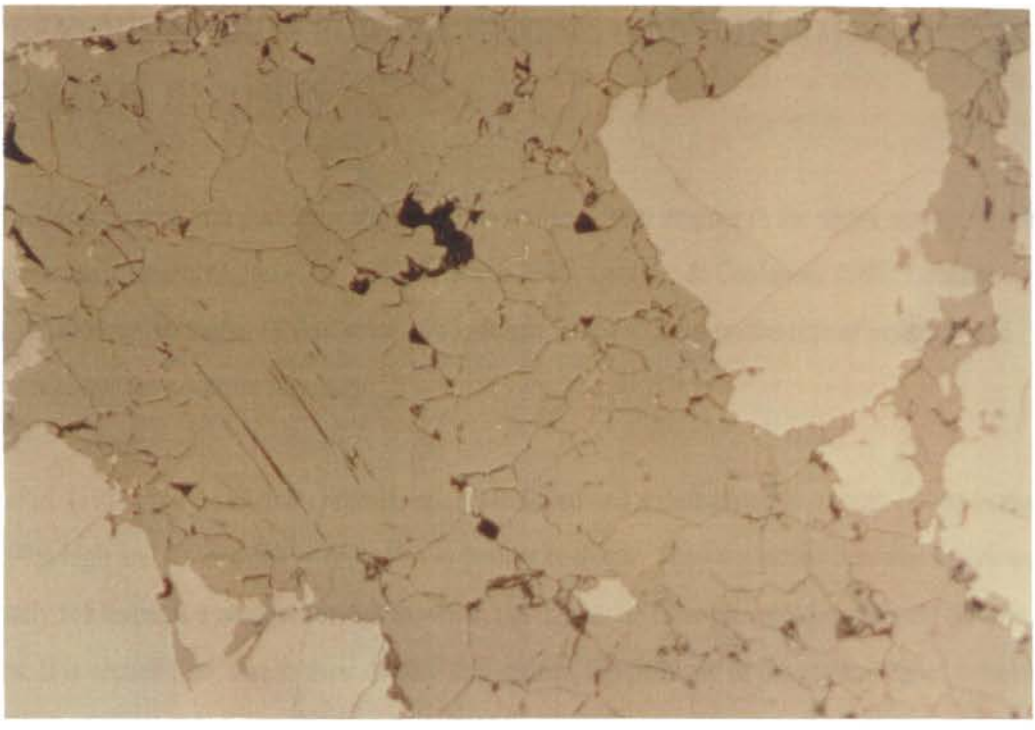

Plate 9.35 SEM image of fracture-fill diopside (dark grey) and serpentinised olivine (black) within chromite (light grey).
Sample No 137b PPL F.O.V 2mm

Plate 9.36 SEM image of replacement of fracture-fill diopside (light grey) by serpentine (black) within chromite (white).
Sample No 69b Scale bar 100um

9.8 PREVIOUS MODELS FOR THE GENESIS OF PODIFORM CHROMITITE DEPOSITS

Many authors believe that podiform chromitite crystallizes from magma in the upper mantle within an oceanic environment (Lago *et al.* 1982; Leblanc 1985; Leblanc & Ceuleneer 1992; Leblanc 1995). An alternative model (Johan *et al.* 1983; Johan 1986) focuses on the role of volatiles and advocates lower temperature formation.

Lago *et al.* (1982) proposed that chromite ore crystallised and accumulated in a large cavity (some 100-200m high and 2-5m thick) within a solid peridotite diapir. They suggested that this cavity was constantly fed through a narrow conduit in which the magmatic flow prevented settling of chromite nodules. It is argued that, due to their density differences, the pathway of the grains differs from the streamlines of the convective cell (caused by the thermal difference between the outflowing magma and the cold cavity wall), and this causes the chromite grains to collide with each other, leading to the formation of nodular chromitite by the coalescence of individual chromite grains.

Leblanc (1985) proposed that the upper mantle peridotites were solid when the chromitites crystallised in cross-cutting veins or sill-like conduits. He suggested that high temperature (1300°C) chromite-forming magma partially melted the surrounding peridotites, thereby generating the dunitic wallrocks. He also suggested that the chromite-forming magmas were generated at different times and from a range of parent magmas, this giving rise to compositional differences between pods in the same ultramafic belt.

Johan (1986) suggested that shear zones developed in the harzburgitic upper mantle and that, during an extensional event, magma invaded these zones of weakness and metasomatically transformed the harzburgitic wallrock to dunite. He argued that once the dunite had solidified, Cr-rich fluids penetrated along the centre of the dunite body and replaced the olivine from grain boundaries inward.

Roberts (1988) argued that podiform chromitite is restricted to suprasubduction zone (SSZ) ophiolites from marginal basins, rather than mid-oceanic ridge environments. He based this on the

reasonable belief that SSZ magmas are the more hydrated. Supposedly, the olivine phase volume would be greatly expanded, which, by allowing olivine and spinel to remain as liquidus phases for longer, would thereby increase the potential for chromitite development. He proposed that the Tethyan ophiolites are typical, in that the mantle sequences of the Semail, Troodos and Vourinos ophiolites contain large volumes of dunite cumulate, whereas gabbros are volumetrically more significant in mid-oceanic ridge mantle sequences. It would seem that magmas quickly pass-out of the olivine-spinel phase volume such that pyroxene-plagioclase assemblages crystallize.

Nicolas (1989) suggested that podiform chromitites and cumulate dunites within the layered cumulates of ophiolites are genetically linked, but that the podiform chromitites within the underlying mantle sequence formed in a very different environment. Nicolas (1989) supported Lago *et al.* (1982) by suggesting that podiform chromitites form in narrow dykes from basaltic magma rising through mantle diapirs below midocean ridges. In this model, magmatic flow prevents even the largest chromite nodule from crystal or gravity settling, whilst the reaction between the magma and peridotite wallrock produces the commonly observed dunitic shell. The chromite and olivine supposedly precipitated due to pressure release, an increase in the oxygen fugacity, or a temperature drop. Nicolas (1989) envisaged that the melt cooled to subsolidus temperatures at or just below the Moho, where most chromitite bodies are now located. He ascribed the formation of hydrous primary inclusions within chromite to downward permeation of water. This aided cooling, modified the local oxygen fugacity, and possibly increased chromite fractionation from the melt. Closure of the conduit induced plastic deformation of the chromitite and expelled most of the melt, but the remaining (trapped) melt crystallised as intercumulus diopside and amphibole or plagioclase between the chromite grains.

Paktunc (1990) argued that chromite within the upper mantle environment derives from incongruent melting of pyroxene and direct crystallisation from partial melts in small magma pockets. He suggested that podiform chromitites in ophiolites result from multistage melting of refractory peridotite, this producing boninitic melts. The latter then ascend through the upper mantle and interact with tholeiitic melts, such that chromite crystallizes and accumulates at the bottom of the small magma chambers. With ongoing expulsion of magma, chromite is left behind and incorporated in the refractory dunite. The chromitite and dunite will then move away from the ridge

axis and cool. Paktunc (1990) ascribed the nodular textures to plastic deformation of chromite-olivine mush, once most of the melt had been extracted.

Leblanc and Ceuleneer (1992) proposed that the chromitite dyke of Maqsad, Oman, crystallised in a sub-vertical magmatic conduit below an oceanic ridge. They contended that layering and compositional variations in the dyke reflect a multicellular convective system, which segregated various batches of chromite grains. They argued that the magma influx was of short duration (less than 2 months) and that the parental magma was an already fractionated (Ti-rich and PGE-poor) MORB-type. The hydrous fluids supposedly accompanied crystallisation of the chromite, this being consistent with the existence of fluid-rich, hydrous melts in the uppermost portions of the upper mantle.

Arai and Yurimoto (1994) concluded that podiform chromitites are most commonly formed in the shallow upper mantle beneath back-arc basins. They showed that the chromite chemistry of the chromitite and dunite are almost the same, whereas chrome spinels in the surrounding harzburgite are distinctly different. They considered that this was consistent with the chromitite and enveloping dunite being comagmatic and different from the surrounding harzburgite. They advocated melt infiltration to explain the chromitite and hostrock dunite. The first melt reacted with harzburgite to form the dunitic shell, and then interacted with an influx of more primitive MORB-type melt to form chromitite. Arai and Yurimoto (1995) showed that podiform chromitites have Cr/(Cr+Al) ratios >0.7, this being typical of chrome spinels from arc-related primitive magmas, but higher than those from oceanic peridotites and MORB-type magmas. The necessary conditions for formation of podiform chromitite within the upper mantle are listed as low pressure, high water vapor pressure, high temperature and compressional stresses, as found in island-arc settings. Supporting evidence is provided by the occurrence of chromitite xenoliths of podiform-type in the Takashima alkali basalt of the southwest Japan arc (Arai & Abe 1994).

Zhou *et al.* (1996) advocated chromitite formation from a boninitic magma produced by second-stage melting. They proposed that first-stage melting produced residual peridotite and a tholeiitic MORB-type melt at a mature spreading centre such as a mid-oceanic ridge. Second-stage melting deep within the residual peridotite mantle supposedly produced boninitic magma above a

subduction zone. This ascended through confined channels and interacted with the MORB-type, harzburgitic wallrock. Melt-dissolution of pyroxenes from the harzburgitic wallrock, led to the formation of the dunitic shell and incorporation of SiO_2 into the melt, and thereby resulted in precipitation of chromite and olivine as the melt moved into the chromite-olivine stability field.

For Coolac Serpentinite Belt chromitites, Golding and Johnson (1971) concluded:

(a) a poly-stage model was an attractive possibility;
(b) the features of the pods, the textures in the harzburgite and the contact between the chromitite and the harzburgite were in accordance with the pods being transported within tectonically mobile harzburgite;
(c) one type of chromite grain (i.e. either Cr- or Al-rich) formed in a different environment from the one in which the harzburgite crystallised whereas the other formed with the crystallising harzburgite;
(d) the Al-rich pods crystallised above the harzburgites and subsequently descended into them; and
(e) the Al-rich chromitites are younger than the Cr-rich ones.

Golding (1975) later concluded that the dunite cumulate was co-magmatic with the enclosed chromitite and that the textural variation between pods was consistent with discrete sites of chromite accumulation. He proposed that the chromitite and dunite formed in numerous small magma chambers that were developed sporadically and intermittently within and above pre-existing depleted mantle peridotite.

9.9 FEATURES OF THE TUMUT SERPENTINITE PROVINCE CHROMITITE DEPOSITS THAT MUST BE EXPLAINED BY ANY GENETIC MODEL

Any model for the formation and evolution of the Tumut Serpentinite Province podiform chromitite deposits must explain the following:

(a) chromitite bodies cross-cutting primary layering in the main harzburgite mass, consistent with them being near-vertical and dyke-like;

(b) a gradually increasing concentration of chromite from the margin to the core of the deposits;

(c) the tabular shape and generally small size;

(d) location within essentially unfoliated chromite-bearing dunitic envelopes, in turn within narrow zones of foliated harzburgite;

(e) diffuse-margined variably serpentinised harzburgite cores within some deposits;

(f) the occurrence and distribution of the three chromitite types within the Coolac Serpentinite Belt;

(g) the similar chemistry of the podiform chromitites and associated dunitic wallrocks;

(h) the occurrence and emplacement of vein-like chromitite bodies within some deposits;

(i) pegmatitic chromitite in the core of the MLA deposit;

(j) the presence, as primary inclusions within the chromite grains, of PGE-enriched nickel sulfide, forsteritic olivine, Al-rich spinel, complex nickel sulfide/silicate and hydrous pargasitic amphibole;

(k) localised slickensided faces and brecciation of the chromitite pods;

(l) cataclasis down to micron scale, together with negligible fragment rotation and substantial introduction of fracture-fill minerals;

(m) concentrations of Cr, Al, Mn, Ni, Co, Zn and Ga within the chromitites relative to the associated dunitic wallrocks and enclosing harzburgite;

(n) the variation in the distribution, shape and composition of the fracture-fill phases between the different deposits;

(o) the trends of the CN PGE curves for the podiform chromitites and associated dunitic envelopes; and

(p) the paucity of REE within the chromitites.

9.10 A GENETIC AND EVOLUTIONARY MODEL FOR THE TUMUT SERPENTINITE PROVINCE CHROMITITES

9.10.1 Discussion

Tectonic environment of formation: The high Cr and/or Al concentrations confirm that the Tumut Serpentinite Province chromitites are of podiform type (Dickey 1975), as do the reciprocal variations of Cr_2O_3 (25.7 to 54.1 wt%) and Al_2O_3 (7.68 to 32.2 wt%), and the small variation and low values of Fe^{+2}/Mg (Thayer 1964; Leblanc & Violette 1983). Further confirmation of an ophiolitic affinity is afforded by the chromitites plotting within the ophiolitic chromite field of Leblanc (1985), the large scatter of deposits on the plot of Cr/Cr+Al against Mg/Mg+Fe^{+2} (see Irvine 1967), and by the Coolac Serpentinite Belt chromitites having a low TiO_2 concentration (0.13 to 0.28 wt%) (e.g. Leblanc & Violette 1983; Leblanc & Ceuleneer 1992).

Geometric Aspects: the tabular shape of the Tumut Serpentinite Province chromitite bodies is typical of those in most ophiolites within the mantle sequence (e.g. Leblanc & Violette 1983; Auge 1987), whilst the small size is best explained by formation in dilatant cavities within the harzburgite and restriction of chromitite-forming conditions to these cavities (e.g. Lago *et al.* 1982).

The unfoliated chromite-bearing dunitic envelopes and outer zones of foliated harzburgite are consistent with the chromitite bodies and dunitic wallrocks developing subsequent to the main harzburgite mass (e.g. Leblanc 1985, 1995; Nicolas 1989; Leblanc & Ceuleneer 1992). A dunitic envelope is a common feature of ophiolitic podiform chromitites (e.g. Whittaker & Watkinson 1984; Ahmed 1984; Johan 1986) and, in some occurrences, interfingers with the enclosing harzburgitic peridotite (Leblanc 1986). Late emplacement of the chromitites is based on the dunitic wallrocks containing remnant cores of unfoliated harzburgite, that presumably reflect brecciation and partial assimilation/metasomatism of the harzburgite during migration of magma up the conduit (Boudier *et al.* 1988).

Wilshire and Kirby (1989), among many others, stated that brittle fracturing at high temperatures and pressures can only occur under high fluid pressures where $P_f - s_3 > T_o$ (where: P_f = fluid pressure, s_3 = local minimum principal stress and T_o = tensile strength of the harzburgite). They

proposed that volatile-rich fluids exsolved from mafic magma and promoted tensile fracture development thereby facilitating upward migration of these fluids and magma, and inducing metasomatic alteration of the wallrocks. For substantial brecciation of an otherwise ductile shear zone, local fluid pressure (P_f) would need to have been lithostatic or even supralithostatic. Brecciation could have resulted from implosion, at jogs or bends in the shear zone, accompanying a sudden drop in the fault P_f, relative to wallrock P_f, due to breaching of a less permeable cap (Sibson 1977, 1996; Hobbs & Ord 1987). **It is therefore proposed that the magmas were chromitiferous and that, during evolution from source, they metasomatically converted harzburgite to dunite and subsequently precipitated chromite due to a pressure drop.**

The hypothesis that the chromitites post-dated crystallisation of the hostrock peridotites is also supported by:

(a) the Tumut Serpentinite Province chromitites forming dyke-like bodies that cross-cut primary layering in the host peridotite (also see Grafenauer 1977; Leblanc & Ceuleneer 1992);

(b) the chemistry of the chromite in the chromitites and chromitiferous dunitic halo differs from that of chromite in the harzburgite host as reported by Ashley (1973a) and Ray (1977) for the Coolac Serpentinite Belt deposits;

(c) the occurrence of partially assimilated blocks of harzburgite within the dunitic wallrocks (e.g. Leblanc 1986; McAndrew 1989).

(d) the suggestion of Wilshire and Kirby (1989) that emplacement of a high-temperature magma would induce dyke-formation, permeate and react with the peridotitic wallrocks, and induce chemical changes in the peridotite by diffusion.

Johan (1986) suggested that the gradational contact between dunite and harzburgite for the Massif du Sud chromitites of New Caledonia was due to pervasive replacement of orthopyroxene by olivine. Lago *et al.* (1982) conversely suggested that the dunite resulted from localised melting of orthopyroxene. The diffuse-margined harzburgite cores within some of the Coolac Serpentinite Belt chromitite deposits are more consistent with unmelted residuals and thereby favour the interpretation of Lago *et al.* (1982).

The increasing chromite content from the margin to the core of podiform chromitites of the Massif du Sud, New Caledonia, was ascribed to chromite-forming fluids penetrating along olivine grain boundaries in the dunite and replacing the grains (Johan 1986). However, zonation could also result if chromite and olivine crystallised from the same magma, provided that chromite-bearing dunite formed at the margins of the magmatic conduit and gave way to increasing quantities of chromite towards the centre. Concurrent crystallisation of chromite and olivine is supported by the chemical similarity of chromite grains from the dunitic wallrocks and massive chromitites.

A progressively more reducing environment or increasing oxygen fugacity could influence chromite content, as with the formation of chromitite layers in mafic/ultramafic layered complexes (e.g. Hulbert & Von Gruenewaldt 1985; Campbell & Murck 1993). Thus, chromite within the massive chromitite cores (i.e. the last chromite to crystallise) could have formed under the least reduced conditions during periods of high oxygen fugacity. **It is therefore proposed that the increasing Cr content from margin to core reflects oxygen fugacity and Eh within the host cavity. Consequently, lack of, or weak zonation of the chromite content, suggest that a high oxygen fugacity and oxidised state existed throughout the period of crystallisation.**

The occurrence of vein-like chromitite masses and blocks of dunite within massive chromitite suggest that there were fluctuations in the environmental conditions (perhaps due to influxes of the same magma but with a higher volatile-rich hydrous fluid component - see below) during the formation of the deposits. The vein-like masses most likely formed by injection of semi-solid chromite-rich crystal 'mush', facilitated by volatiles exsolved from the magma. Dunitic blocks within massive chromitite are consistent with brecciation induced by the magmatic pulses, the latter perhaps also causing Eh fluctuation, and thereby enhancing precipitation of chromite.

Chemical Aspects: the developments of vein-like and pegmatoidal chromitite, and the presence of PGE-enriched nickel sulfides and primary inclusions of hydrous pargasitic amphibole collectively suggest that the chromitite-forming magma evolved a late-stage volatile-rich melt. Sintering (annealing recrystallisation - Hulbert & Von Gruenewaldt 1985) of chromite grains in the presence of the volatile-rich melt, cleared strain induced by stresses produced by the ongoing tendency of the conduit to close. The sintered chromite "trapped" droplets of the volatile-rich melt which

crystallised as pseudo-primary mineral inclusions, now observable as "primary inclusions" within the chromite. Lorand and Ceuleneer (1989) proposed that the volatile-rich melt represented exotic contamination, and was unrelated to the chromite-bearing magma. However, evidence of channel-ways for introduction of an unrelated fluid, metasomatic alteration products in the surrounding harzburgite mass, and a change in the chemistry or development of textural features within the Tumut Serpentinite Province chromitites (e.g. zonation of chromite and/or olivine grains) is lacking. Additionally, PGE-enriched nickel sulfide inclusions probably result from magmatic PGM (most likely, PGE alloys) reacting with sulfur in the volatile-rich melt. **It is therefore proposed that components of the poly-minerallic inclusions were derived from a volatile-rich differentiate of the chromite-forming magma.**

Fluid enhanced sintering led to postcumulus enlargement of chromite grains, thereby "trapping" the phases that are now seen as pseudo-primary mineral inclusions. Sintering can increase the chromite concentration by up to 20% (Hulbert & Von Gruenewaldt 1985) and, depending upon the amount of late volatile-rich melt present, will produce chromitites enriched or lacking in inclusions. Further evidence of a late-stage volatile-rich melt is provided by the upper stability limit (750 to 850°C) of the inclusions of gedrite-anthophyllite. The "liquid" inclusions must postdate the chromite-olivine crystallisation of 1200 to 1250°C (Lorand & Ceuleneer 1989), whilst the likelihood that they were present during sintering is supported by some of these inclusions defining linear trails that perhaps reflect former chromite grain boundaries.

The primary inclusion trails of Al-rich (high Al) chromite in Cr-rich (low Al) chromite seem to conform to the type II inclusions of Christiansen (1986). He suggested that their distribution is controlled by subgrain or grain boundaries. In turn, this seems to suggest that the trails result from diffusion of Al to subgrain boundaries during annealing. The concept is one of annealing exsolution of aluminous chromite.

Despite the chromitites having a parental magma rich in such elements as Cr, Al, Mg, Fe, Zn and Ni (Tables 9.1 and 9.2), the extreme concentration of chromite in chromitite deposits requires concentration processes beyond fractional crystallisation. The large concentration of chromite in a chromitite body requires that a very large volume of magma must have passed through the host-

cavity. Auge (1987) suggested that podiform chromitite bodies require a volume of magma at least 500 times greater than that of the chromitite. Similarly, Leblanc & Ceuleneer (1992) suggested that the volume of magma needed to produce the Maqsad chromitite dyke was at least 300 times the volume of the dyke. The precipitated chromite remains in the cavity due to the higher density of chromite compared to the magma (e.g. Lago *et al.* 1982). As the chromitite was emplaced subsequent to crystallisation of the peridotite hostrock (e.g. Brown 1982; Leblanc & Ceuleneer 1992), it follows that the chromitite derived from a different magma; most probably that which sourced the mafic units (layers 3a and 2) of the ophiolite.

Chromitites of the Coolac Serpentinite Belt may be subdivided into low-Al (i.e Cr-rich), intermediate-Al and high-Al groups that collectively form a continuous spectrum of Al concentrations (Section 9.4). Some authors (e.g. Leblanc & Violette 1983; Bacuta *et al.* 1990) suggested that many ophiolite belts have a bi-modal distribution of Cr-rich (low-Al) and Al-rich (intermediate and high-Al) chromitites. Leblanc & Violette (1983) also suggested that the bi-modal distribution of major elements is reflected in the trace elements, but in the Coolac Serpentinite Belt, the only obvious correlation is between increasing Zn and Ga, with increasing Al_2O_3. The previous suggestions seem to require different magmatic sources and times of formation, but the near-continuous spectrum of chromite compositions in the Coolac Serpentinite Belt chromitites seems to oppose this view and be more consistent with a progressively changing (time and space) source. **The present distribution of low-Al, intermediate-Al and high-Al chromitites within the Coolac Serpentinite Belt is considered to reflect the spatial distribution of a progressively fractionating MORB parental magma.**

The relative enrichment in REE in the dunitic wallrock over the chromitite is ascribed to small amounts of interstitial plagioclase (altered to clinochlore) in the dunite. The plagioclase crystallised from the melt along with the olivine and chromite, but seems to have been a minor early component, into which the LREE preferentially partitioned.

The trace element and REE compositions of the chromitites yield little insight into the genesis of the chromitite pods. The apparent variability of trace element concentrations throughout the belt is more consistent with localised redistribution during serpentinisation (Graham *et al.* 1995).

Although the REE have been traditionally regarded as being immobile during alteration, Pearce (1983) has shown that Sr, Rb, Th, Ce and Sm can be mobile during the dehydration of subducted oceanic crust. The REE can also be mobilised by carbonate-rich and/or halogen-rich hydrothermal fluids (Rollinson 1993). Evidence for such carbonate-rich hydrothermal fluids associated with alteration lies in the discrete zones of talc-carbonate rocks and patches of talc-carbonate alteration within some of the chromitites. Because Frey *et al.* (1985) and Bodinier *et al.* (1984) argued that serpentinisation does not overly affect the mobility of REE, some of the REE distribution in the chromitites could reflect remobilisation by carbonate-bearing fluids along discrete conduits during the late stages of serpentinisation (See Chapter 3). This could explain why the REE CN trends for the chromitites differ from those of the weakly serpentinised Maqsad chromitite deposit of Oman (Leblanc & Ceuleneer 1992), where well-defined Ce troughs and Eu peaks are ascribed to hydrothermal alteration.

Alternatively, the trace element distribution could reflect an inhomogenous distribution of these elements within the parent magma, while the REE depletion could result from partitioning of REE into the magma during crystallisation of olivine and chromite. However, the evidence opposes this. The chromitite types of the Coolac Serpentinite Belt are systematically distributed (section 9.4), so one would expect a similar distribution in their trace element concentrations, provided that these were controlled by processes such as trace element and REE partitioning, yet this parallelism is not found.

Turning to the PGE geochemistry, most of the Tumut Serpentinite Province chromitites (excluding the MLA deposit) have ophiolitic CN trends. Franklin *et al.* (1992) interpreted the substantial difference in CN curves between the MLA and QOC chromitites in terms of metahydrothermal remobilisation leading to Pt enrichment. This interpretation is supported by primary inclusions of PGE-bearing nickel sulfides in the chromitites versus discrete PGM phases in the secondary fracture-fill. Although circumstantial, the case for deriving the PGE in the PGM from the primary PGE-bearing sulfide phases is compelling. Similarly compelling is the circumstantial interpretation that primary inclusions of gold within the chromite grains are the source of more abundant Pd-rich secondary gold in the fracture-fill. Thus, the PGE and Au were released from the chromitites and dunitic and harzburgitic hostrocks during serpentinisation, and precipitated within the (Ramsay &

Huber 1983, 1987) breccia environment of the chromitite, supporting more extensive remobilisation and focusing. A similar model invoking hydrothermal remobilisation is invoked for the chromitites of the Great Serpentinite Belt, NSW, where Yang & Seccombe (1993) found that Pt and Pd phases occurred within the fracture-fill, whereas Ir-Ru phases only occurred as primary inclusions in chromite. Comparable processes have been described by Larocque & Hodgson (1995) for the release of 'invisible gold' in the Mobrun massive sulfide deposit, Canada."

The probe chemistry of the discrete chromite grains also supports chemical remobilisation during serpentinisation. The replacement of primary chromite by ferritchromit involves the loss of Al, Mg and Cr, and gain of Fe (Ashley 1975). This remobilisation is circumstantially expressed by the Cr-clinochlore rims on chromite, the existence of fracture-fill uvarovite garnet, and the development of Al-rich lizardite.

Post-crystallisation Aspects: the fracture-fill and fracture-related phases within the chromitites are diverse. Ferritchromit forms fracture-related rims on primary chromite grains but is postdated by nickel sulfides, magnetite and trevorite. An evolving fluid system was responsible for the formation and subsequent evolution of the chromitites and/or multiple injections of fluids of differing chemistry occurred during the serpentinisation process. Both olivine and chromite precipitated from the parental magma at an early stage (1200°C - Nicolas 1995). This magma was then progressively modified by incoming fluids as the magma conduit acted as a channelway by which fluids could escape deep crustal conditions by fracture flow in the direction of decreasing temperature (Ferry & Dipple 1991; Dipple & Ferry 1992). Thus, the initial magma of the conduit became progressively hydrothermal in nature with aqueous wave input. Hydrothermal fluids induced rodingitisation of gabbro and the localised remobilisation of Cr, leading to the formation of uvarovite and other secondary Cr-bearing phases (around 300 ± 36°C and below 0.8kb – O'Hanley *et al.* 1992), and localised remobilisation of metallic phases, PGE, REE and S occurred during late-stage serpentinisation (<250 ± 25°C and a $P_{(H2O)}$ of less than 1kb – O'Hanley & Wicks 1995), based on the mineralogy and textural relations of the fracture-fill phases. The formation of uvarovite at such relatively low temperatures is in conflict with earlier experimental work (e.g. Huckenholz 1975; Huckenholz & Knittel 1975; Clarke & Carswell 1977) which suggested temperatures of 855 ± 5°C. Textural and petrographic evidence within the chromitites of the Tumut Serpentinite Province

suggests uvarovite formation occurred during the early stages of serpentinisation/rodingitisation at temperatures of around 300 ± 36°C. As nearly all components involved in serpentinisation were locally derived from the chromitites and dunitic and harzburgitic wallrocks, it is likely that H_2O and CO_2 were the only introduced phases. Thus, to explain the present distribution of elements within the chromitites, it is necessary to invoke remobilisation of the trace elements, REE, Al, Cr, Mg, Fe and PGE, over distances in the order of mm to a few metres, based on the distribution of the fracture-fill phases.

The concept of an evolving fluid system within an oceanic environment is akin to that proposed by Kelley *et al.* (1993) for fluid evolution within submarine magmatic-hydrothermal systems at the MARK area of the Mid-Atlantic Ridge. In their model, Kelly *et al.* (1993) invoked initial fracturing of crustal gabbros at >700°C due to exsolution of volatile-rich phases from the magma, followed by the upward migration of these fluids along microfractures near the magma chamber margins. Further fracturing resulted during progressive cooling of the intrusion and allowed the downward passage of seawater-derived hydrothermal fluids at temperatures of >400°C. In fault-zone regions, multiple hydrothermal pulses involved compositionally and thermally (340-180°C) diverse hydrothermal fluids, which led to pervasive brecciation, alteration and remobilisation in the wallrock (Kelly *et al.* 1993).

Distributed fracturing and brecciation of oceanic crustal rocks could well be the upper crustal expression of deeper shear zones (Agar 1994). It is likely that fractures and their related fracture-fill phases developed rapidly, perhaps as high as 100m/s (Phillips 1972), under conditions of high strain rate (Agar 1994). Intense cataclasis in fault zones in quartzofeldspathic rocks occurs under conditions of P_L ~ 3-5kb and T~300°C (Sibson 1977), particularly where the fluid pressure approximates the lithostatic pressure. In a study of chromite grains from Oman, Christiansen (1985) showed that the chromite lacked preferred crystallographic orientation, consistent with the deformation involving brittle mechanisms. Similarly, in a later SEM study of chromite grains from the Oman, Vourinos (Greece) and Tiebaghi (New Caledonia) ophiolites, crystal plastic deformation of chromite grains was shown (Christiansen 1986) to be very localised (i.e. at the micron scale) and extremely uncommon, whereas cataclasis abounded. Christiansen (1986) ascribed the cataclasis variously to tectonic emplacement, serpentinisation, and later alteration, whereas Leblanc *et al.*

(1981) ascribed it to serpentinisation and, conversely, attributed pull-apart structures to plastic deformation at temperatures approximating 1000°C. For the chromitites of the Tumut Serpentinite Province, hydrothermal remobilisation began with early serpentinisation and rodingitisation (with localised remobilisation of Cr) at temperatures of around 300°C and continued down to <250°C.

Ductile deformation of chromite only occurs at high temperatures (e.g. 1000°C - Leblanc 1980) whereas quartz can be ductile down to ~300°C. Thus, from >850 - ~400°C, chromite and quartz have very different rheological behaviours, whereas from ~400°C downwards they both behave similarly. Deformation, involving localised brecciation and cataclasis of the pods, is confined to the smaller chromitite bodies (Graham *et al.* 1993) in the Tumut Serpentinite Province. The cataclasis is considered to express brittle deformation in the presence of the high fluid pressures that accompanied serpentinisation. The cataclasis facilitated localised remobilisation of metals, PGE, REE and S as a consequence of the increased surface area.

9.10.2 The proposed model

Based on the foregoing discussion, the following model is proposed for the evolution of chromitites of the Tumut Serpentinite Province. It has many similarities to those of Lago *et al.* (1982) and Leblanc and Ceuleneer (1992) because, of the many hypotheses proposed, theirs most closely fit the evidence from the Tumut Serpentinite Province.

(a) Production of a MORB magma by small amounts of partial melting (approx. 5-10%) of the rising aesthenosphere beneath a spreading centre.

(b) Upward percolation of the MORB, driven by magmatic pressure alone or by magmatic-pressure facilitated fracturing and dilation within jogs or bends in previously weakened zones of the upper mantle harzburgite. Initial reaction between the magma and wallrock harzburgite, particularly in dilatant bulges just below the Moho (i.e. the crust/mantle boundary) resulted in the metasomatic conversion of harzburgite to dunite.

(c) Concurrent and sequential to dunitic wallrock alteration, fluctuations in oxygen fugacity and/or magmatic pressure and/or temperature resulted in the periodic crystallisation of

chromite or olivine from the rising magma. Due to a relatively high thermal contrast between the rising magma and colder conduit walls, strong thermal convection was produced within the cavity, resulting in the mixing of the chromite and olivine and the retention of these phases within the confined cavity. Large volumes (~300-500 times the chromite volume as an order of magnitude) of magma must have passed through this cavity in order to produce the amount of chromite within the pods.

(d) Cessation of the relatively stable chromitite-forming system resulted from one or more of: changed environmental conditions (e.g. oxygen fugacity, magmatic pressure or ambient temperature); depletion/cessation of magma production; and accumulated chromite choking the pod and inhibiting thermal convection. Concurrent with, and sequential to breakdown in the stability of the system, late-stage hydrous melts exsolved from the chromite-forming magma (perhaps due to a pressure drop) and this, along with the confining pressure, induced sintering (annealing recrystallisation) of the chromite grains and development of various pseudo-primary inclusions.

(e) The chromitites were subsequently fractured and intruded by gabbroic magma (now rodingite dykes containing fragments of chromitites) that seemingly derived from a more fractionated MORB source than the chromitites.

(f) Soon after this, whilst all the rocks were still hot, tectonic emplacement of the harzburgite and contained chromitites was accompanied by progressive cataclasis, high-temperature alteration, and serpentinisation. With intensification of cataclasis by systematic hydraulic fracturing, more pervasive fluid invasion over a decreasing temperature range resulted in serpentinisation and the localised remobilisation of metals, PGE, REE and S. Under conditions of localised high sulfur fugacity and low oxygen fugacity, the fracture-fill comprised serpentine and sulfide species; when the reverse conditions applied, oxide species developed. The present distribution of fracture-fill minerals, major and minor elements, REE, PGE and trace elements is partly due to localised remobilisation during the serpentinisation process.

9.11 CONCLUSIONS

The podiform chromitites of the Tumut Serpentinite Province formed from an initial MORB-type magma. They crystallised within narrow cavities in ophiolitic upper mantle harzburgite under a stable dynamic system. The present distribution of the different chromitite types is due to the more aluminous chromitites forming from a more fractionated source. No evidence exists for the different chromitite types being derived from different source magmas.

Rodingitisation and serpentinisation of the Tumut Serpentinite Province occurred during progressive cooling of the chromitites and host rocks, and were accompanied by systematic brittle fracturing of the chromitites and the remobilisation of their chemical components.

CHAPTER 10: GEOCHRONOLOGICAL INVESTIGATIONS

10.1 INTRODUCTION

In order to constrain the age of the serpentinite belts, a range of igneous rocks were anlysed by to two different geochronological techniques, U/Pb zircon isotopics using the SHRIMP ion probe and whole-rock Nd/Sm isotopics. The rocks were investigated by petrographic and XRD techniques to select samples with minimum serpentinisation and alteration. Detailed field observations were made at each sample site to constrain the interpretation of geochronological data.

The first geochronological investigation on rocks of the Tumut Serpentinite Province was that of Webb (1980) who obtained a K-Ar hornblende age of 426 ± 6Ma on hornblende gabbro from the North Mooney Complex. Basden et al. (1987) and Basden (1990) interpreted this age as the age of crystallisation of the North Mooney Complex and, as a consequence, the age of the Coolac Serpentinite Belt. Initial results of U/Pb zircon data obtained during the present study were summarised and fully discussed in Graham *et al.* (1996a, 1996b – see Appendix PUB). The Nd/Sm data have not been published.

10.2 U/Pb ZIRCON ISOTOPE STUDIES

10.2.1 Introduction

In recent years, accurate U/Pb ages have been obtained from zircon grains derived from plagiogranite bodies within ophiolite sequences (e.g. Kimbrough *et al.* 1992; Encarnacion & Mukasa 1993; Aitchison & Ireland 1995; Borsi *et al.* 1996). This is usually supplemented by cathodoluminescence microscopy, which facilitates identification of zoning within the zircons and reveals the presence of inherited cores and/or young overgrowths. The combined techniques are extremely useful in determining the magmatic history of a wide range of igneous rocks.

The SHRIMP ion microprobe at the Research School of Earth Sciences (RSES) of the Australian National University (ANU) was used for these investigations. It was previously used successfully

by Aitchison *et al.* (1992, 1994) to determine U/Pb ages on plagiogranite bodies from the New England Fold Belt of NSW.

10.2.2 Sample Collection

Samples were collected from plagiogranite and related bodies identified during field mapping. Sites were selected on the basis of:

(a) presence of substantial 'in place' outcrop;

(b) comparative ease of sampling; and,

(c) ensuring an adequate geographic spread within individual serpentinite belts.

Samples were ultimately collected from three plagiogranite bodies within the Wambidgee Serpentinte Belt, and one plagiogranite body and one leucogabbro body from the Coolac Serpentinite Belt (Figure 10.1). Collection was made using a portable diamond saw and cold chisels. Each sample was labelled and separately bagged. Some 30-50kg was collected at each site to ensure adequate zircon recovery.

10.2.3 Geology of the Sample Sites

Sample BF91/20 (MAP: Tumorrama G.R. 225 032) - plagiogranite: : the sample site is located within the schistose western margin of the central part of the Coolac Serpentinite Belt, some 100m east of the faulted boundary between the Coolac Serpentinite Belt and the Honeysuckle Beds. The plagiogranite consists of an elongate (some 100m in length and 5m in width) body of weakly deformed plagiogranite with minor angular enclaves (<100mm) of metabasalt. Ashley (1973a) stated that the contacts show evidence of shearing and that a well-developed metasomatic reaction zone with development of talc- and chlorite-rich rocks is apparent on the eastern margin. These were not observed during the present investigation.

Sample BF91/33f (MAP: Bendick Murrell G.R. 972 186) - plagiogranite: the sample site is located within the centre of the northern part of the Wambidgee Serpentinite Belt. This plagiogranite consists of rounded masses (2m) of weakly foliated plagiogranite. The masses have slickensided outer surfaces and are interpreted as tectonic inclusions. Contacts between the plagiogranite masses and enclosing serpentinite are obscured.

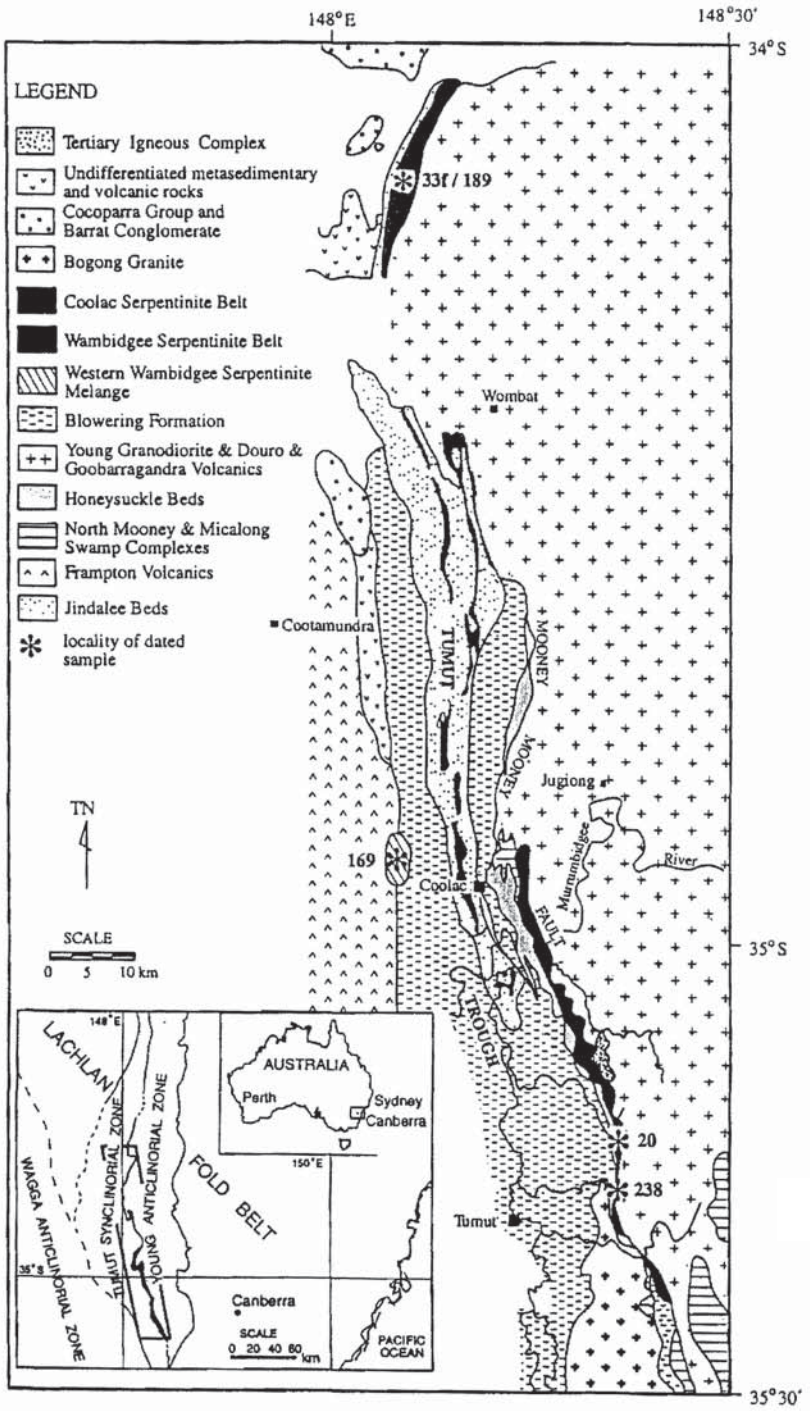

Figure 10.1 Location of the sample sites for U/Pb geochronology.

Sample 169 (MAP: Coolac G.R. 990 337) - plagiogranite: the sample site is located within the centre of the central part of the Western Wambidgee Serpentinite Melange. The plagiogranite consists of rounded masses (1m maximum dimension) of weakly foliated plagiogranite enclosed within highly schistose serpentinite. It contains minor angular enclaves of metabasalt and has slickensided contacts with the surrounding serpentinite.

Sample 189 (MAP: Bendick Murrell G.R. 972 194) - plagiogranite: the sample site is located within the eastern part of the northern section of the Wambidgee Serpentinite Belt. This plagiogranite occurs as an ellipsoidal fine-grained to pegmatitic segregation (of axial dimensions 5 x 2m) within schistose serpentinite. The body is rimmed by a zone of acicular tremolite, which may represent a metasomatic rim formed during serpentinisation. Further evidence of local metasomatism in the surrounding schistose serpentinite is indicated by the presence of margarite, a Ca-bearing mica.

Sample 238 (MAP: Lacmalac G.R. 234 965) - leucogabbro: the sample site is located within the western schistose margin of the central section of the Coolac Serpentinite Belt where leucogabbro occurs as a segregation within a complex leucogabbro/hornblende gabbro body which contains numerous elongate enclaves of metabasalt, and veins and patches of pegmatitic hornblende gabbro. The metabasaltic enclaves are both moderately fractured and brecciated with sharp contacts against the enclosing gabbro. The body has a faulted contact against schistose serpentinite on both sides; other lenticular bodies, variously consisting of metabasalt and hornblende gabbro and hosted by schistose serpentinite, are also present.

10.2.4 Petrography

The plagiogranites mostly exhibit an allotriomorphic granular texture, generally defined by interlocking grains of quartz and albitic plagioclase along with cross-cutting fibrous grains of tremolite and mica. The leucogabbro has an allotriomorphic granular texture defined by interlocking grains of diopside, hornblende and plagioclase, cut by fibrous tremolite. The mean modal composition of the plagiogranites is 60% quartz and 40% albite, with trace amounts of tremolite, Na-rich white mica, epidote and zircon. The plagiogranite from sample site BF91/20

differs from the others in that it contains 5% perthitic orthoclase. The leucogabbro consists of 85% albite, 5% diopside, 5% tremolite, 5% hornblende, and accessory zircon.

10.2.5 Sample preparation and analytical procedure

Samples were sliced on a diamond saw in order to remove any metabasaltic enclaves and crushed to a grainsize of less than 10mm at the University of Technology, Sydney (UTS). The grainsize was reduced to less than 200um and zircon concentrates obtained by heavy liquid separation techniques at the mineral preparation laboratories, CSIRO Division of Exploration and Mining, North Ryde.

The concentrates were sent to the Precise Radiogenic Isotope Services (PRISE) laboratories at the Research School of Earth Sciences, Australian National University. Zircons were hand-picked under a binocular microscope and mounted in epoxy along with a chip of the RSES standard zircon SL13. They were then sectioned and polished.

The zircons were analysed by Mark Fanning of PRISE using both SHRIMP I and SHRIMP II. Analyses consisted of 6 scans through the mass range. The SHRIMP data were reduced in a manner similar to that described by Williams & Claesson (1987) and Compston *et al.* (1992). Augmented uncertainties for the isotope ratios were calculated by Mark Fanning using software of T.R. Ireland (RSES)(pers. comm.) The observed coefficient of variation in the Pb/U ratio measured for the SL13 standard was 2.37% and 2.36%. Pb/U ratios were normalised to a value of 0.09279 for the $^{206}Pb/^{238}U$ ratio of this standard, equivalent to an age of 572 Ma for the standard. Uncertainties given for the individual analyses (both ratios and ages) are at the one sigma level, whereas uncertainties in the weighted mean ages are at 95% confidence limits.

10.2.6 Results

The results are presented in Tables 10.1 to 10.5 and in Figure 10.2, and the complete data are presented in Appendix 10UPBR. Figure 10.2 is a composite plot of all data. A weighted mean for these 48 analyses has excess scatter with a x^2 of 2.06. The weighted mean includes 10 analyses at around 430 Ma. If these 10 are excluded, a weighted mean of the $^{206}Pb/^{238}U$ ages for the remaining analyses has no excess scatter at 401.3 ± 3.4Ma. A weighted mean for the 10 analyses excluded in the mean above has no excess scatter at 431 ± 8 Ma.

The SHRIMP data reveal that, within error limits, all samples have a dominant age of zircon crystallisation of approximately 400 Ma. The second largest population of zircon ages is approximately 430 Ma. Cathodoluminescence studies revealed that the 430 Ma zircons form distinct cores within 400 Ma zircons (Plates 10.1 to 10.4) and are either inherited from the source of the plagiogranites or are a crustal contaminant.

Grain .spot	U (ppm)	Th (ppm)	Th/U	Pb* (ppm)	$^{204}Pb/^{206}Pb$	$^{206}Pb/^{238}U$	±	Age (Ma) $^{206}Pb/^{238}U$	±
1.1	490	79	0.16	28	0.002030	0.0612	0.0016	382.9	9.5
1.2	267	123	0.46	24	0.000186	0.0847	0.0023	524.2	13.4
2.1	198	177	0.89	15	-	0.0661	0.0017	412.4	10.6
2.2	133	135	1.02	9	0.000233	0.0607	0.0018	379.8	10.8
3.1	315	26	0.08	9	0.000447	0.0301	0.0008	191.3	5.2
4.1	447	142	0.32	28	0.000401	0.0649	0.0017	405.6	10.3
5.1	315	48	0.15	30	0.000010	0.1047	0.0027	641.8	15.5
6.1	407	88	0.22	26	0.000147	0.0667	0.0018	416.5	10.7
6.2	198	66	0.33	12	0.000859	0.0596	0.0023	372.9	13.7
7.1	459	230	0.50	31	0.000517	0.0694	0.0018	432.2	10.8
7.2	482	162	0.34	29	0.000915	0.0633	0.0017	395.3	10.2
8.1	320	118	0.37	20	0.000153	0.0642	0.0017	401.3	10.5
8.2	158	113	0.71	11	0.001148	0.0646	0.0019	403.5	11.7
9.1	633	180	0.28	38	0.004871	0.0672	0.0018	419.5	10.7
9.2	335	100	0.30	46	0.001117	0.1499	0.0043	900.2	23.9

Note : 1. - signifies no ^{204}Pb detected.
2. Uncertainties given at the one sigma level.
3. Correction for common Pb made on the basis of extrapolation to concordia along a mixing line with common Pb, following Tera & Wasserburg (1972), as outlined in Compston et al (1992).

Table 10.1 U-Pb isotope data for sample 238.

Grain .spot	U (ppm)	Th (ppm)	Th/U	Pb* (ppm)	$^{204}Pb/^{206}Pb$	$^{206}Pb/^{238}U$	±	Age (Ma) $^{206}Pb/^{238}U$	±
1.1	386	12	0.03	24	0.000456	0.0685	0.0032	427.2	19.6
2.1	428	10	0.02	25	0.000010	0.0638	0.0016	398.7	9.9
3.1	167	2	0.01	10	0.000334	0.0686	0.0023	427.4	13.8
4.1	259	6	0.02	15	0.001142	0.0635	0.0017	396.7	10.4
5.1	349	4	0.01	20	0.000444	0.0637	0.0017	397.8	10.2
6.1	1371	67	0.05	86	0.000682	0.0687	0.0017	428.3	10.3
7.1	1042	56	0.05	64	0.000464	0.0667	0.0017	416.1	10.1
8.1	5287	206	0.04	326	0.000100	0.0675	0.0020	421.1	11.9
9.1	1752	69	0.04	102	0.000494	0.0640	0.0030	399.9	18.5
10.1	1053	791	0.75	81	0.000350	0.0693	0.0024	431.9	14.6

Note : 1. Uncertainties given at the one sigma level.
2. Correction for common Pb made on the basis of extrapolation to concordia along a mixing line with common Pb, following Tera & Wasserburg (1972), as outlined in Compston et al (1992).

Table 10.2 U-Pb isotope data for sample 20.

Grain .spot	U (ppm)	Th (ppm)	Th/U	Pb* (ppm)	$^{204}Pb/^{206}Pb$	$^{206}Pb/^{238}U$	±	Age (Ma) $^{206}Pb/^{238}U$	±
1.1	455	185	0.41	30	0.000049	0.0653	0.0018	408.0	10.9
2.1	903	435	0.48	59	0.000025	0.0634	0.0016	396.4	9.6
3.1	2825	5061	1.79	315	0.000546	0.0805	0.0019	499.4	11.6
4.1	553	352	0.64	44	0.000079	0.0751	0.0019	467.1	11.5
5.1	575	143	0.25	168	0.000047	0.2874	0.0070	1629	35
6.1	353	34	0.09	21	0.000214	0.0627	0.0017	391.7	10.2
6.2	470	42	0.09	29	0.000818	0.0661	0.0019	412.5	11.4
7.1	3060	3906	1.28	276	0.000334	0.0721	0.0026	448.8	15.9
8.1	3809	4719	1.24	344	0.000055	0.0740	0.0035	460.4	21.2

Note : 1. Uncertainties given at the one sigma level.
2. Correction for common Pb made on the basis of extrapolation to concordia along a mixing line with common Pb, following Tera & Wasserburg (1972), as outlined in Compston et al (1992).

Table 10.3 U-Pb isotope data for sample 169.

Grain .spot	U (ppm)	Th (ppm)	Th/U	Pb* (ppm)	$^{204}Pb/^{206}Pb$	$^{206}Pb/^{238}U$	±	Age (Ma) $^{206}Pb/^{238}U$	±
1.1	310	27	0.09	18	0.000183	0.0632	0.0016	394.9	9.9
2.1	200	17	0.09	10	0.001266	0.0519	0.0014	326.4	8.8
3.1	453	55	0.12	27	0.000165	0.0631	0.0016	394.7	10.0
4.1	602	96	0.16	35	0.000066	0.0611	0.0016	382.1	9.4
5.1	778	120	0.15	51	0.000305	0.0693	0.0018	431.9	10.6
6.1	163	13	0.08	10	0.000287	0.0636	0.0017	397.5	10.6
7.1	2444	622	0.25	123	0.000576	0.0523	0.0013	328.5	7.9
8.1	435	34	0.08	28	0.000221	0.0701	0.0020	437.0	12.1
9.1	974	147	0.15	61	0.000157	0.0661	0.0017	412.6	10.3
10.1	969	111	0.11	59	0.000122	0.0654	0.0019	408.3	11.7
11.1	1004	155	0.15	62	0.000066	0.0656	0.0017	409.4	10.1
12.1	673	85	0.13	42	0.000627	0.0660	0.0017	411.8	10.2

Note : 1. Uncertainties given at the one sigma level.
2. Correction for common Pb made on the basis of extrapolation to concordia along a mixing line with common Pb, following Tera & Wasserburg (1972), as outlined in Compston et al (1992).

Table 10.4 U-Pb isotope data for sample 189.

Grain .spot	U (ppm)	Th (ppm)	Th/U	Pb* (ppm)	$^{204}Pb/^{206}Pb$	$^{206}Pb/^{238}U$	±	Age (Ma) $^{206}Pb/^{238}U$	±
1.1	710	162	0.23	42	0.000536	0.0622	0.0016	389.2	9.5
2.1	653	378	0.58	42	0.000010	0.0615	0.0016	384.5	9.8
3.1	411	230	0.56	29	0.000175	0.0661	0.0017	412.7	10.3
4.1	754	428	0.57	51	0.000118	0.0637	0.0016	397.8	9.9
5.1	545	288	0.53	38	0.000093	0.0661	0.0017	412.9	10.1
6.1	576	320	0.56	42	0.000097	0.0691	0.0017	430.7	10.5
7.1	471	233	0.50	34	0.000127	0.0689	0.0017	429.4	10.4
8.1	974	595	0.61	66	0.000007	0.0632	0.0016	395.1	9.4
9.1	772	554	0.72	52	0.000236	0.0628	0.0016	392.7	9.7
10.1	410	189	0.46	30	0.000024	0.0699	0.0019	435.3	11.5
11.1	499	259	0.52	34	0.000551	0.0653	0.0018	407.7	11.1
12.1	376	179	0.48	23	0.000382	0.0603	0.0024	377.5	14.6
13.1	832	547	0.66	59	0.000115	0.0655	0.0017	409.1	10.2
14.1	186	65	0.35	12	0.000941	0.0664	0.0021	414.5	12.6

Note : 1. Uncertainties given at the one sigma level.
2. Correction for common Pb made on the basis of extrapolation to concordia along a mixing line with common Pb, following Tera & Wasserburg (1972), as outlined in Compston et al (1992).

Table 10.5 U-Pb isotope data for sample BF91/33f.

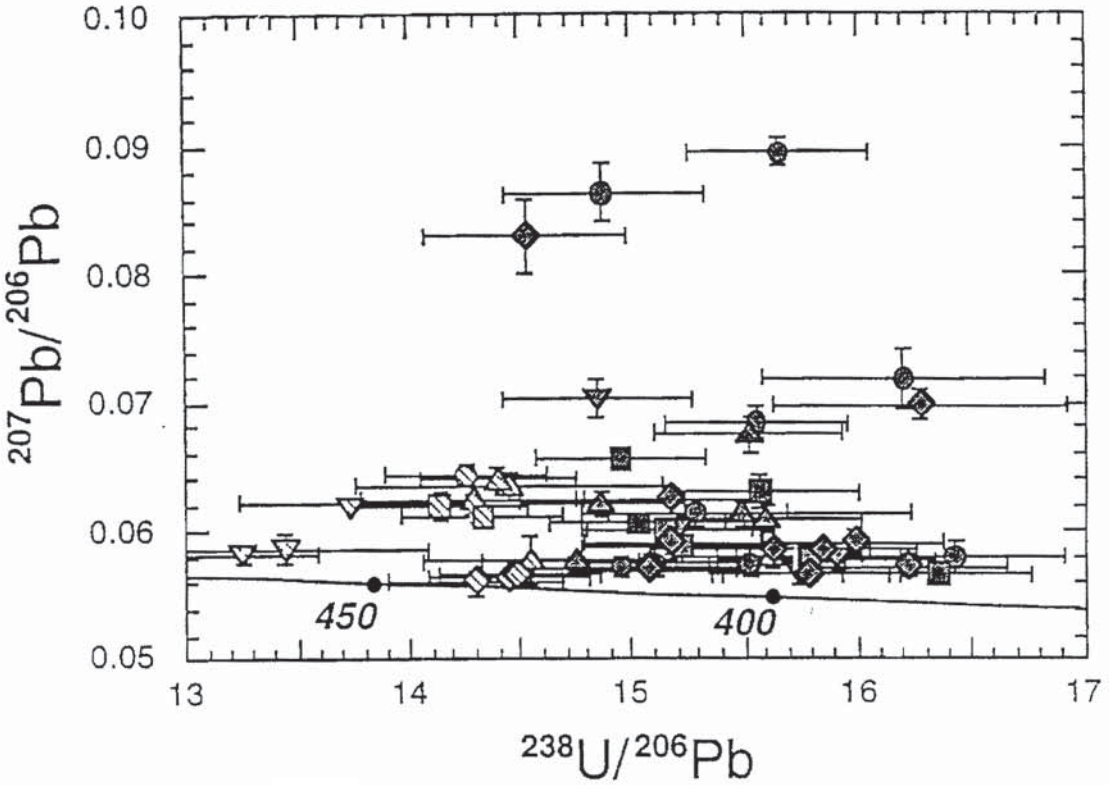

Figure 10.2 Composite Tera-Wasserburg concordia plot for the SHRIMP analyses of zircons from samples 238 (circles), 20 (triangles), 169 PLAG6 (inverted triangles), 189 (squares) and BF91/33f (diamonds). Analyses plotted, uncorrected for common Pb, with one sigma bar errors. A weighted mean of the ^{207}Pb corrected $^{206}Pb/^{238}U$ ages for 38 analyses gives a pooled age of 401.3 ± 3.4Ma (shaded symbols). Some 10 analyses are older at 431 ± 8Ma (striped symbols).

Plate 10.1 Cathodoluminescence image of zircon grains 1 and 2 from sample BF91/20. Scale bar is 100um

Plate 10.2 Cathodoluminescence image of zircon grains 4, 6 and 14 from sample BF91/33f. Scale bar is 100um

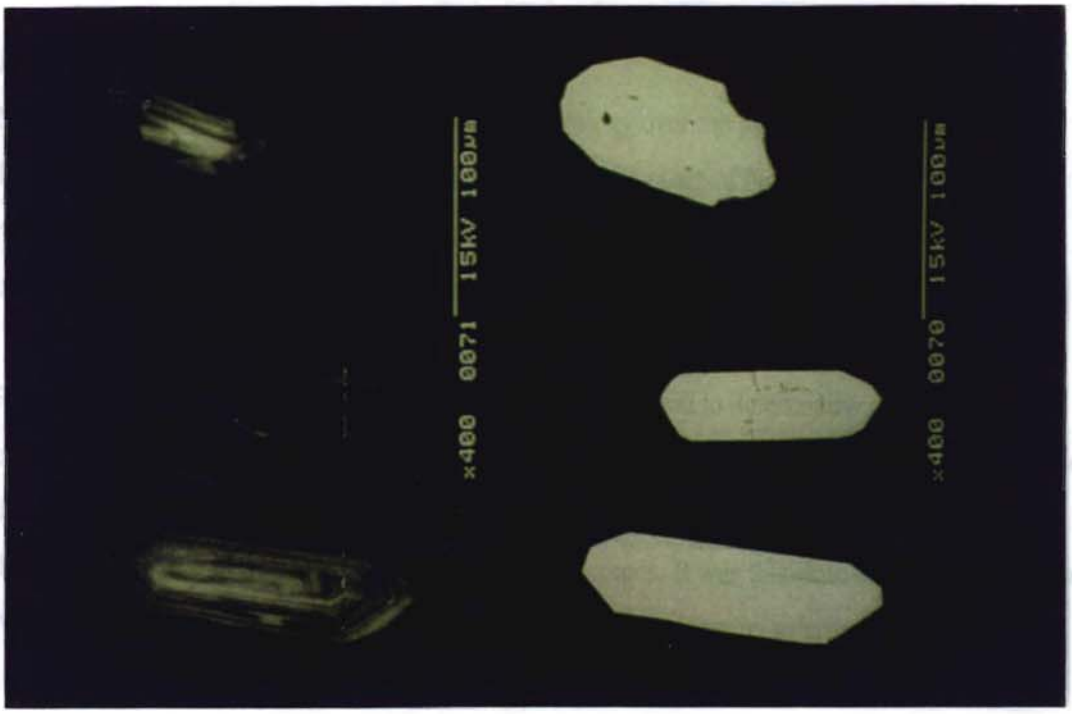

Plate 10.3 Cathodoluminesence image of zircon grains 6, 7 and 8 from sample 238. Scale bar is 100um

Plate 10.4 Cathodoluminesence image of zircon grain 9 from sample 238. Scale bar is 100um

10.3 Nd/Sm ISOTOPE INVESTIGATIONS

10.3.1 Introduction

Nd/Sm isotopes have only been used in igneous petrology over the past 20 years (e.g. Richard *et al.* 1976; De Paulo & Wasserburg 1976). This is because the range of Nd/Sm isotopes in igneous rocks and the natural variability of radiogenic ^{143}Nd is small, and requires the types of high-precision measurement (Cox *et al.* 1979) that were not possible prior to ca. 1975.

Rollinson (1993) stated that the Nd/Sm technique is best suited to determining the age of crystallisation of igneous rocks. The geochemistry of the Tumut Serpentinite Province rocks shows that the concentrations of Rb and Sr have been affected by alteration (See Chapters 3-8 of this thesis) and are unsuited to Rb/Sr age determination methods. It was therefore decided to investigate Nd/Sm isotope geochronology, particularly since this had the capacity to provide an independent check on the U/Pb zircon investigation, and yield important information on tectonic/petrogenetic evolution.

Nd/Sm geochronology is based on the construction of an isochron diagram, a bivariate plot of measured parent/daughter isotope ratios for a suite of cogenetic samples. Provided that the suite defines a linear array, its slope yields the age of crystallisation (Rollinson 1993).

10.3.2 Sample Selection

The samples were subdivided into four main groups (Table 10.6). Group 1 consisted of rocks from the North Mooney Complex. These were chosen as a "standard", because Franklin (1975) considered that the different rock types within the North Mooney Complex formed from a common parental magma. All selected North Mooney Complex rocks were fresh and had only undergone lower greenschist facies metamorphism. Group 2 consisted of samples from the Wambidgee Serpentinite Belt and the Western Wambidgee Serpentinite Melange. Group 3 consisted of samples from the Fontenoy area of the Wambidgee Serpentinite Belt and group 4 comprised samples from the Coolac Serpentinite Belt. Between 2 and 10kg of each rock type was collected for analysis.

GROUP ONE: THE NORTH MOONEY COMPLEX

141 Weakly serpentinised dunite (i.e. 90% fresh olivine)
145 Pyroxene gabbro - diopside, orthopyroxene, completely saussuritised plagioclase, clinozoisite, tremolite, chlorite)
233 Hornblende gabbro - Hornblende, diopside, plagioclase
234 Diopside xls
235 Basalt - calcic plagioclase, clinopyroxene, albite, actinolite, chlorite, epidote

GROUP TWO: THE WAMBIDGEE SERPENTINITE BELT

170 Pyroxene-hornblende gabbro - calcic plagioclase, hornblende, tremolite/actinolite, chlorite, epidote
188 Garnet-bearing amphibolite - hornblende, calcic plagioclase, actinolite, epidote, clinozoisite, almandine
BF91/33e Hornblende clinopyroxenite - diopside, hornblende, chlorite
BF91/33f Plagiogranite - albite, quartz, tremolite
BF92/16 Garnet-bearing metabasalt - actinolite, epidote, clinozoisite, almandine
WW2 Clinopyroxenite - diopside, orthopyroxene, tremolite

GROUP THREE: THE FONTENOY REGION OF THE WAMBIDGEE SERPENTINITE BELT

34 Completely serpentinised dunite
65Horn Hornblendite - hornblende, olivine, orthopyroxene
65Perid Peridotite - olivine, orthopyroxene, diopside, hornblende
225a Completely serpentinised layered peridotite
BF92/3 Gabbro - hornblende, albite, actinolite, epidote, clinozoisite, chlorite
BF92/6a Plagiogranite - albite, quartz, orthoclase, tremolite
BF92/8 Olivine-amphibole hornfels - olivine, manganoan amphibole

GROUP FOUR: THE COOLAC SERPENTINITE BELT

BF91/20 Plagiogranite - quartz, albite, orthoclase
123 Weakly serpentinised dunite (i.e. 90% olivine)
155c Altered clinopyroxenite - diopside, tremolite, epidote, chlorite
156 Metagabbro - albite, tremolite/actinolite. Epidote, clinozoisite, chlorite
238a Leucogabbro - albite, diopside, hornblende, tremolite/actinolite
238m/dyke Basalt - actinolite, epidote, saussuritised plagioclase
238peggab Pegmatitic gabbro - hornblende, completely saussuritised plagioclase

Table 10.6 List of samples used for Nd/Sm geochronology.

10.3.3 Geology of the sample sites

Group 1 samples: THE NORTH MOONEY COMPLEX (Figure 10.3)

Sample 141 - dunite *(MAP: Coolac G.R. 112 336):* the sample site is on the eastern boundary of the North Mooney Complex adjacent to the Coolac Serpentinite Belt. Dunite occurs as rare isolated patches within weakly schistose serpentinite.

Sample 145 - pyroxene gabbro *(MAP: Coolac G.R. 107 360):* the sample site is near the eastern boundary of the North Mooney Complex between it and the Coolac Serpentinite Belt. The pyroxene gabbro occurs as a lens-like mass with a faulted boundary to the east against partially serpentinised, weakly schistose harzburgite of the Coolac Serpentinite Belt, but the contact to the west is obscure.

Sample 233 - hornblende gabbro *(MAP: Coolac G.R. 099 368):* the sample site is near the western margin of the North Mooney Complex. The hornblende gabbro at this locality forms a fairly large (80 x 5m) and continuous outcrop. It contains angular metabasalt enclaves generally less than 0.1m in maximum dimension and is crossed by veins of pegmatitic hornblende gabbro.

Sample 234 - pegmatitic clinopyroxenite *(MAP: Coolac G.R. 105 365):* the sample site is located in the eastern half of the North Mooney Complex (Figure 10.3). It consists of a large mass of relatively fresh pegmatitic clinopyroxenite with the clinopyroxene grains as large as 150mm. The clinopyroxenite is crossed by veins and intrusive patches of pegmatitic hornblende gabbro.

Sample 235 - basalt *(MAP: Coolac G.R. 100 365):* the sample site occurs in the southern part of the North Mooney Complex (Figure 10.3). The basalt forms dyke-like bodies (2m x 25m+) which clearly cut massive hornblende gabbro.

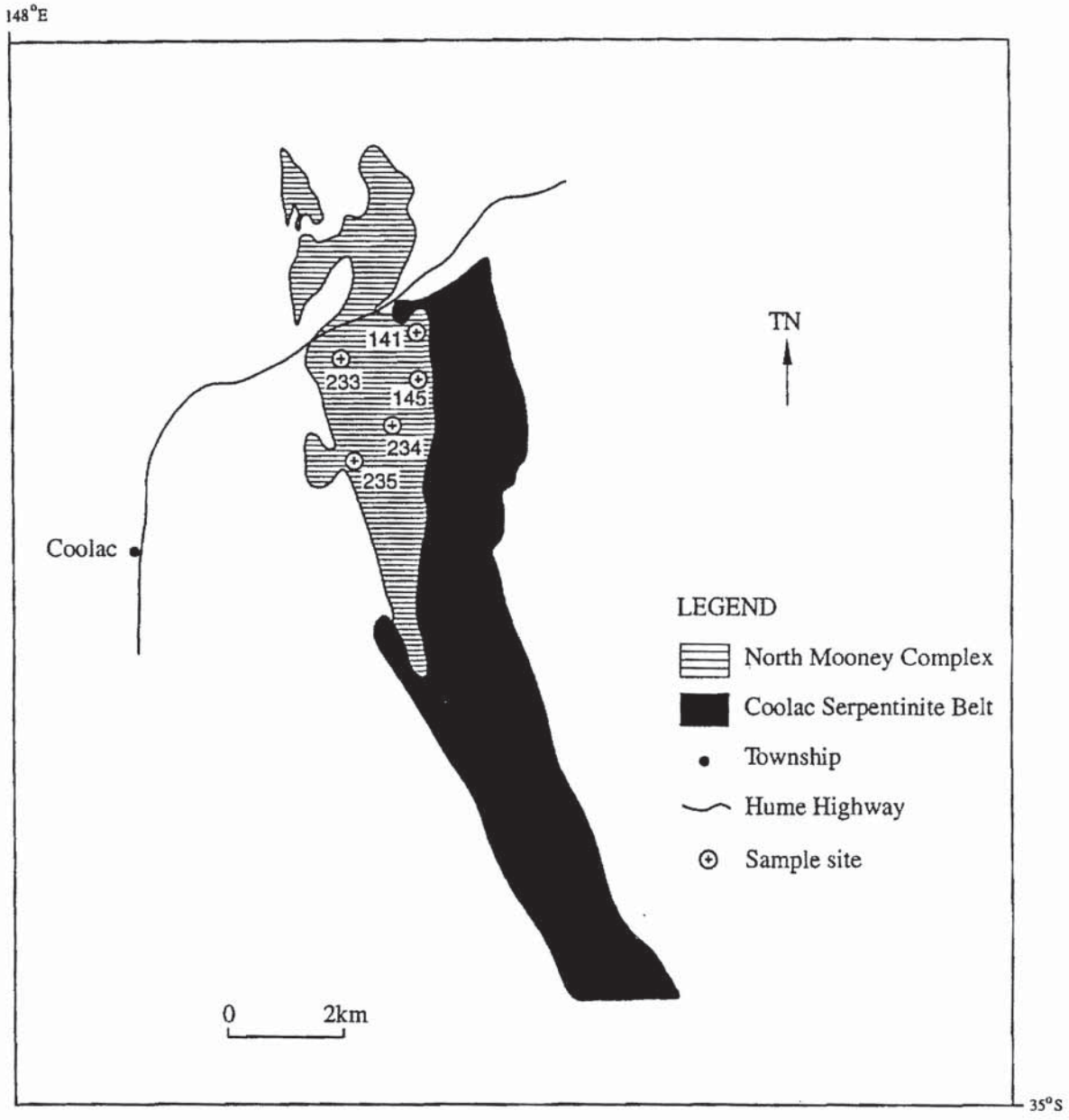

Figure 10.3 Nd/Sm sample locations within the North Mooney Complex.

Group 2 samples: THE WAMBIDGEE SERPENTINITE BELT (Figure 10.4).

Sample 170 - pyroxene-hornblende gabbro (MAP: Coolac G.R. 990 337): the site sampled lies within the eastern half of the northern section of the Western Wambidgee Serpentinite Melange. The gabbro forms an elongate (20-30m) and narrow (up to 4m) homogeneous body within highly schistose serpentinite.

Sample 188 - garnet-bearing meta-amphibolite (MAP: Bendick Murrell G.R. 972 198): the sample site is in the central part of the northern section of the Wambidgee Serpentinite Belt. The meta-amphibolite occurs as small, isolated blocks (maximum dimensions of some 1m) enclosed within highly schistose serpentinite.

Sample BF91/33e - hornblende clinopyroxenite (MAP: Bendick Murrell G.R. 972 186): the sample comes from the central part of the northern section of the Wambidgee Serpentinite Belt, where clinopyroxenite outcrops as small (maximum dimensions of some 1-2m) isolated patches enclosed within weakly foliated serpentinite.

Sample BF91/33f - plagiogranite (MAP: Bendick Murrell G.R. 972 186): this site was described in section 10.2.3.

Sample BF92/16 – garnet-bearing metabasalt (MAP: Coolac G.R. 059 310): the sample is from the eastern half of the southern section of the Wambidgee Serpentinite Belt. The metabasalt is a body some 5m wide and of indeterminate length within schistose serpentinite."

Sample WW2 - clinopyroxenite (MAP: Coolac G.R. 990 337): the sample site is located near the eastern boundary of the northern section of the Western Wambidgee Serpentinite Melange. The clinopyroxenite is at least 100m long but less than 2-3m thick. It is enclosed within highly schistose serpentinite.

Group 3 samples: FONTENOY REGION OF THE WAMBIDGEE SERPENTINITE BELT (Figure 10.4)

Sample 34 - serpentinised dunite (MAP: Young G.R. 035 883): the sample was collected in the central part of the Wambidgee Serpentinite Belt. It was associated with a small podiform chromitite deposit located within massive serpentinite; the contacts have been removed by mining.

Sample 65 - hornblendite and peridotite (MAP: Young G.R. 039 891): the sample site is in the western half of the central Wambidgee Serpentinite Belt). Hornblendite/peridotite forms a prominent dyke-like outcrop with a length of at least 100m and a width of 3-5m. The hornblendite occurs within this outcrop as rhythmic slump-folded layers (some 40mm in thickness) alternating, across sharp contacts, with layers of partially serpentinised peridotite. This layered body is enclosed within relatively massive serpentinite, though the contact between the two rock types is obscured.

Sample 225a - completely serpentinised layered peridotite (MAP: Young G.R. 058 896): this site is near the eastern margin of the central Wambidgee Serpentinite Belt. The peridotite outcrops as discontinuous, small (with maximum dimensions of some 1m) well-layered blocks. The layering is defined by differences in the proportions of serpentine pseudomorphs after enstatite and tremolite.

Sample BF92/3 - metagabbro (MAP: Young G.R. 058 896): the site is located near the eastern margin of the central part of the Wambidgee Serpentinite Belt. The metagabbro forms discontinuous, small (with maximum dimensions of some 1m) blocks and its contact with enclosing serpentinite is obscured.

Sample BF92/6a - plagiogranite (MAP: Young G.R. 058 896): this site occurs some 50m uphill from site BF92/3. The plagiogranite forms discontinuous, small (<0.5m) blocks, but contacts with the enclosing serpentinite and knotted quartz-mica knotted schists are obscured.

Sample BF92/8 - olivine-amphibole amphibolite (MAP: Young G.R. 050 880): the sample site is in the western section of the central part of the Wambidgee Serpentinite Belt. This unusual amphibolite appears to occur as a small tectonic block (approximate 20 x 20m) enclosed within massive serpentinite and associated with massive chlorite rock.

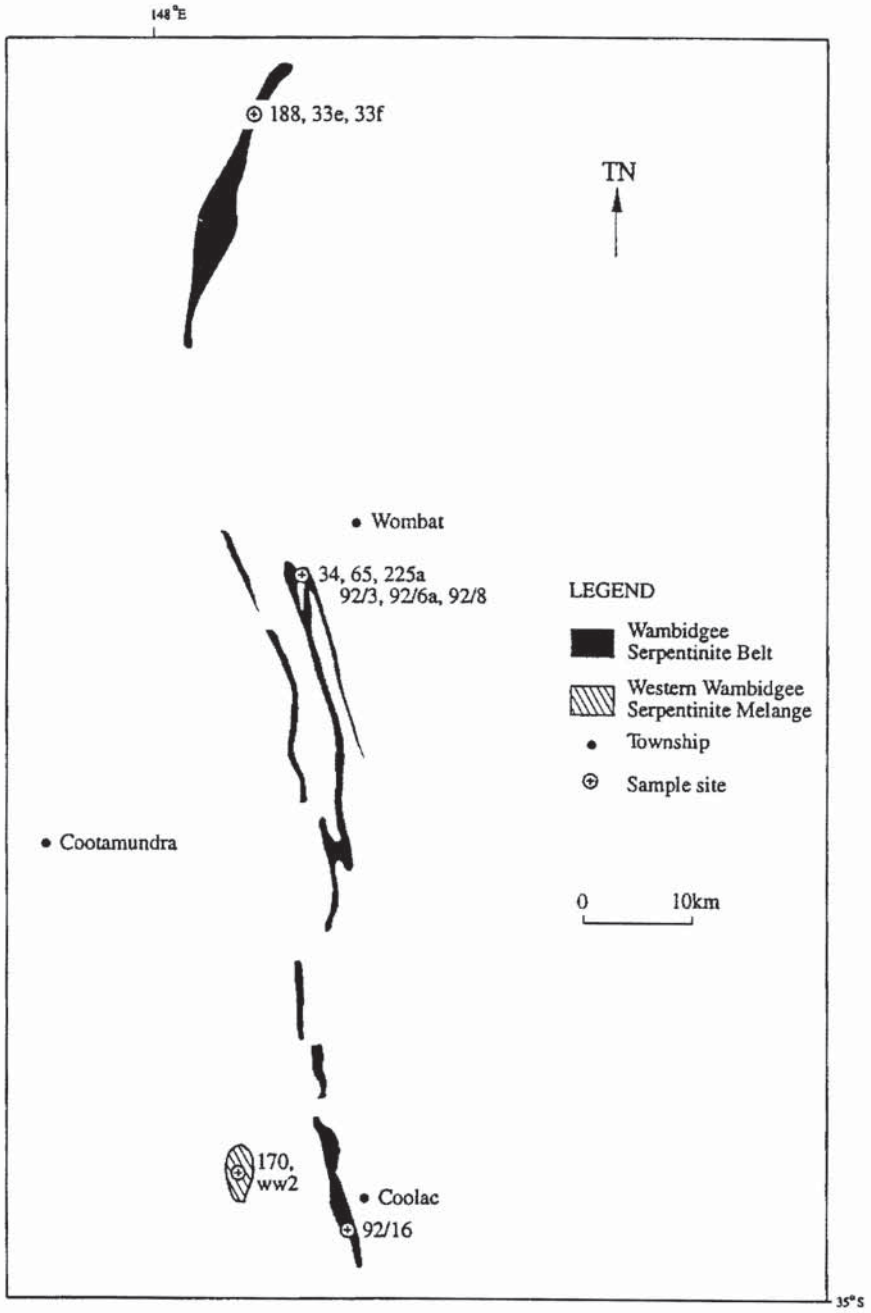

Figure 10.4 Nd/Sm sample locations within the Wambidgee Serpentinite Belt (including the Fontenoy region).

Group 4 samples: THE COOLAC SERPENTINITE BELT (Figure 10.5).

Sample BF91/20 - plagiogranite (MAP: Tumorrama G.R. 225 032): this site was described in section 10.2.3.

Sample 123 - dunite (MAP: Adjungbilly G.R. 141 255): the sample site comes from the western margin of the northern part of the Coolac Serpentinite Belt. The dunite forms small blocks (<0.5m)completely enclosed within schistose serpentinite. Contacts with the serpentinite are obscured.

Sample 155c - hornblendite (MAP: Lacmalac G.R. 229 931): hornblendite outcrops on the western margin of the central part of the Coolac Serpentinite Belt. It forms tectonic blocks (<2-3m) within schistose serpentinite.

Sample 156 - metagabbro (MAP: Lacmalac G.R. 234 965): the sample site is in the central section of the central part of the Coolac Serpentinite Belt. The metagabbro forms small tectonic blocks (<0.5-1m) in association with rodingite bodies within schistose serpentinite.

Sample 238a - leucogabbro (MAP: Lacmalac G.R. 234 965): the sample site was described in section 10.2.3.

Sample 238m/dyke - basalt (MAP: Lacmalac G.R. 234 965): the sample site was described in section 10.2.3.

Sample 238peggab - pegmatitic gabbro (MAP: Lacmalac G.R. 234 965): the sample site was described in section 10.2.3.

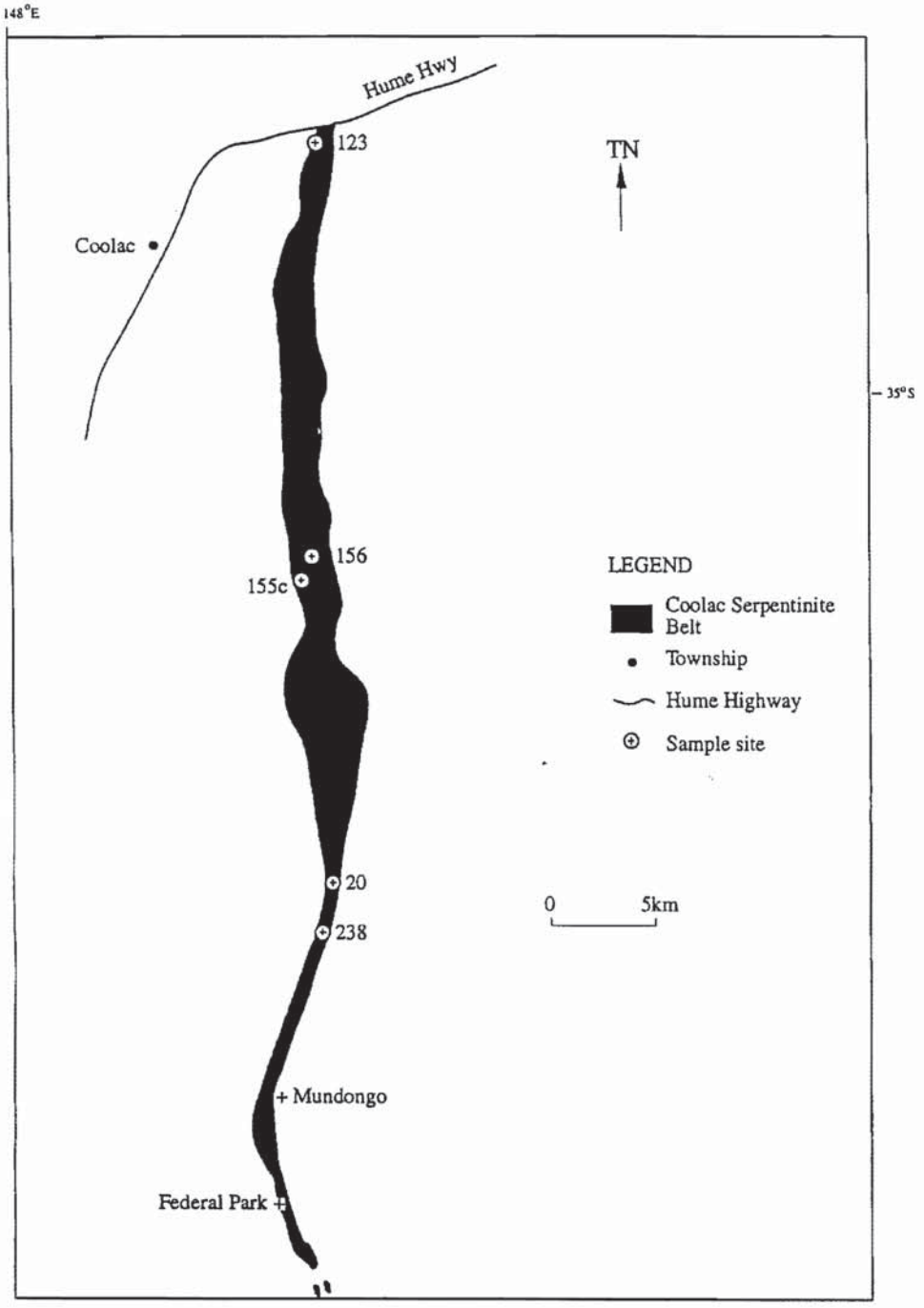

Figure 10.5 Nd/Sm sample locations within the Coolac Serpentinite Belt.

10.3.4 Petrography

Group 1: THE NORTH MOONEY COMPLEX

Sample 141 - dunite: this sample has a modal composition of olivine (85%), chrome spinel (2%), serpentine (13%), and accessory magnetite. A post-cumulus overgrowth texture is defined by interlocking embayed olivine grains. Chrome spinel forms inclusions within the olivine grains and serpentine occurs as fracture-fill.

Sample 145 - pyroxene gabbro: the modal composition is diopside (40%), orthopyroxene (2%), hornblende (3%), tremolite (5%), clinozoisite (10%), chlorite (10%), saussuritised plagioclase (30%) and rare magnetite. A pseudoporphyritic post-cumulus space-fill texture is defined by large grains of diopside and orthopyroxene in a finer-grained matrix of completely saussuritised plagioclase, clinozoisite, tremolite and chlorite. The tremolite also occurs as narrow fringes on the diopside and orthopyroxene grains.

Sample 233 - hornblende gabbro: this sample has a modal composition of plagioclase (55%), clinopyroxene (30%), hornblende (5%), clinozoisite (2%), tremolite/actinolite (5%), epidote (3%), accessory zircons, and rare sulphides. It has an allotriomorphic granular texture defined by large, interlocking, highly embayed grains of diopside, and post-cumulus space-filling plagioclase. The hornblende occurs as strongly zoned grains with brown cores and green rims. The tremolite/actinolite occurs as rim replacements on diopside and hornblende and as cross-cutting fibrous grains. Clinozoisite and epidote occur as partial replacements of the plagioclase.

Sample 234 - pegmatitic clinopyroxenite: this sample consists of large (up to 15cm in length), interlocking subhedral olive-green diopside grains.

Sample 235 - basalt: this sample has a porphyritic intersertal texture defined by randomly oriented phenocrysts of plagioclase and clinopyroxene in a fine-grained groundmass of albite, actinolite, chlorite and rare epidote. The clinopyroxene phenocrysts are surrounded by a narrow fringe of actinolite.

Group 2: THE WAMBIDGEE SERPENTINITE BELT

Sample 170 - pyroxene-hornblende gabbro: this sample has a modal composition of saussuritised plagioclase (50%), hornblende (20%), tremolite/actinolite (25%), chlorite (5%), epidote (<1%), dolomite (<1%), accessory magnetite and apatite. It has an allotriomorphic granular texture defined by interlocking plagioclase and hornblende, along with cross-cutting tremolite/actinolite, chlorite and epidote. The tremolite/actinolite also occurs as rim and partial to complete replacements of hornblende, while dolomite forms aggregates which partially replaces the plagioclase.

Sample 188 - garnet-bearing meta-amphibolite: this sample has a modal composition of plagioclase (65%), quartz (10%), almandine garnet (2%), hornblende (5%), actinolite (15%), epidote (3%), accessory clinozoisite and apatite. It has an allotriomorphic granular decussate texture defined by interlocking hornblende and plagioclase, along with cross-cutting actinolite, epidote and clinozoisite. Much of the original hornblende has been replaced by actinolite. The quartz is spatially associated with plagioclase which occurs as strongly sutured grains with well-developed triple-junction grain boundaries.

Sample BF91/33e - hornblende clinopyroxenite: this sample has a modal composition of diopside (40%), pink (possibly Mn-bearing) amphibole (45%), tremolite (10%), serpentine (5%), and accessory magnetite. It has a granoblastic texture defined by interlocking, moderately aligned grains of diopside and hornblende with cross-cutting fibrous tremolite and serpentine. In places, the hornblende is zoned, with brown/green cores and colourless rims. The tremolite also occurs as rim replacements on diopside and hornblende.

Sample BF91/33f - plagiogranite: this sample has a modal composition of albite (50%), quartz (40%), tremolite (8%), epidote (2%), accessory apatite and zircon. It has an allotriomorphic granular texture with interlocking plagioclase and quartz, and cross-cutting fine-grained fibrous tremolite. The epidote occurs as granular aggregates at the boundaries of plagioclase grains.

Sample BF92/16 - garnet-bearing amphibolite: this sample has a modal composition of actinolite (90%), clinozoisite (4%), almandine garnet (4%) and epidote (2%). It has a decussate granoblastic

texture defined by randomly oriented, plumose aggregates of actinolite, along with interstitial grains of epidote, clinozoisite and almandine garnet.

Sample WW2 - clinopyroxenite: this sample has a modal composition of diopside (80%), enstatite (10%), tremolite (5%), serpentine (5%), common accessory magnetite and rare apatite. It has a sheared granular domainal texture defined by interlocking and fractured, even-grained brecciated diopside and enstatite, with fracture and breccia fill by tremolite and serpentine. The magnetite occurs as narrow veinlets which cross-cut the other phases. The domainal texture is defined by narrow shear-bands throughout the rock which consist of fine-grained cataclastic fragments of diopside and enstatite in a matrix of tremolite and serpentine.

Group 3: FONTENOY REGION OF THE WAMBIDGEE SERPENTINITE BELT

Sample 34 - dunite serpentinite: this sample consists of completely serpentinised dunite. It is relatively chromite-rich (5-10%) and weakly sheared. No relict primary phases exist. XRD analysis shows that the serpentine consists of a mixture of lizardite and chrysotile.

Sample 65Horn - hornblendite: this sample has a modal composition of hornblende (70%), tremolite (30%) and accessory chlorite. It has a porphyroclastic poikiloblastic texture defined by large non-aligned interlocking hornblende with intergranular tremolite. The hornblende is heavily embayed, the embayments filled by fibrous tremolite, which also occurs as partial rim replacements on the hornblende.

Sample 65Perid - peridotite: this sample consists of two distinct layers, an olivine-orthopyroxene layer and an amphibole layer. The contact between the different layers is sharp and planar. The olivine-orthopyroxene layer has a modal composition of orthopyroxene (20%) and olivine (80%). The orthopyroxene occurs as large embayed grains within a matrix of smaller highly fractured olivine. The orthopyroxene has been partially replaced by fibrous tremolite and the olivine has been partially replaced by serpentine. The amphibole layer largely consists of tremolite pseudomorphs after orthopyroxene, along with minor interstitial small serpentinised olivine.

Sample 225a - serpentinised layered peridotite: this sample has a modal composition of bastitised orthopyroxene (15%), antigorite (85%), cross-cutting fibrous tremolite, and accessory magnetite. It has a layered decussate feathery texture defined by large, embayed grains of bastitised orthopyroxene in a matrix of non-aligned plumose aggregates of fine-grained antigorite and cross-cutting fibrous tremolite.

Sample BF92/3 - metagabbro: this sample has a modal composition of Ca-plagioclase (60%), hornblende (20%), quartz (5%), chlorite (5%), epidote (5%), actinolite (5%), and accessory clinozoisite, sphene and zircon. It has an allotriomorphic granular texture defined by moderately aligned, large grains of interlocking hornblende and plagioclase, along with cross-cutting grains and veinlets of actinolite, epidote, clinozoisite and chlorite. Many of the hornblende grains are replaced by fibrous actinolite and sphene occurs as inclusions within hornblende.

Sample BF92/6a - plagiogranite: this sample has a modal composition of albite (70%), quartz (15%), orthoclase (10%), tremolite (5%), accessory sphene, and cross-cutting veinlets of epidote/clinozoisite. It has an allotriomorphic granular texture defined by interlocking plagioclase, quartz and orthoclase, along with cross-cutting fibrous tremolite. The epidote/clinozoisite occurs as partial replacements of plagioclase and cross-cutting veinlets.

Sample BF92/8 - olivine-amphibole amphibolite: this sample has a modal composition of olivine (20%), pink (possibly Mn-bearing) amphibole (75%), chlorite (5%), and accessory chrome spinel. It has a porphyritic intersertal texture defined by large, highly fractured ovoid-shaped olivine in a fine-grained matrix of decussate pink amphibole and chlorite. The chlorite occurs as fibrous aggregates which cross-cuts the olivine and pink hornblende.

Group 4: THE COOLAC SERPENTINITE BELT

Sample BF91/20 - plagiogranite: this sample has a modal composition of quartz (50%), albite (38%), orthoclase (10%), white mica (1%), chlorite (1%), and accessory epidote, apatite and zircon. The overall texture is defined by interlocking quartz, albite and orthoclase, which are of highly variable grain-size. The chlorite and epidote occur as fracture-fill between the other phases and the Na-mica occurs completely enclosed within the feldspar.

Sample 123 - dunite: this sample has a modal composition of olivine (90%), clinopyroxene (2%), orthopyroxene (2%), chrysotile/lizardite (6%) and accessory magnetite. It has a granoblastic texture defined by interlocking, highly fractured olivine grains, which are separated from each other by magnetite and/or lizardite/chrysotile veinlets.

Sample 155c - hornblendite: this sample has a modal composition of hornblende (70%), serpentine (15%), chlorite (7%), actinolite (5%), epidote (3%), and accessory magnetite. It has a porphyritic granular texture defined by large grains of hornblende in a matrix of fine-grained serpentine and epidote. The actinolite occurs as rim-replacement on the hornblende whereas chlorite replaces hornblende and actinolite.

Sample 156 - metagabbro: this sample has a modal composition of Ca-plagioclase (45%), diopside (25%), hornblende (15%), tremolite (5%), clinozoisite (4%), Mg-chlorite (3%) and quartz (3%). It has an allotriomorphic granular texture defined by interlocking, non-aligned plagioclase, diopside, hornblende and quartz, along with cross-cutting fibrous tremolite and Mg-chlorite. Many of the plagioclase grains are moderately saussuritised..

Sample 238a - leucogabbro: this sample has a modal composition of albite (85%), diopside (5%), tremolite/actinolite (5%), hornblende (5%), and accessory zircon. It has a post-cumulus overgrowth texture defined by interlocking, moderately embayed grains of albite, diopside and hornblende, along with cross-cutting tremolite/actinolite. The tremolite/actinolite also occurs as partial to complete replacements of diopside and hornblende.

Sample 238m/dyke - basalt: this sample occurs as inclusions within the leucogabbro and is composed of a fine-grained mixture of actinolite, epidote and saussuritised plagioclase, exhibiting a granoblastic texture.

Sample 238peggab - pegmatititic hornblende gabbro: the pegmatitic hornblende gabbro consists of large (some 2cm across) euhedral equant-shaped hornblende in a fine-grained matrix of completely saussuritised plagioclase.

10.3.5 Sample Preparation and analytical procedure

Samples were selected following thin-section evaluation of the degree and intensity of alteration. They were crushed with a jaw crusher, washed thoroughly and cleaned in distilled water and acetone, and reduced to an average grain size of 150um with the aid of a ring grinder. These were initially sent to Becquerel Commercial Laboratories (Lucas Heights, Sydney), to obtain the concentrations of Nd and Sm (in each sample) by neutron activation techniques. They were subsequently forwarded for isotopic analysis to the Department of Earth Sciences at Carleton University, Ottawa, Canada, where determinations were made by Dr Brian Cousens using isotope dilution mass spectrometry. "Odd" or "unusual" isotopic data were checked by re-running the sample.

10.3.6 Results

The Nd-Sm isotopic concentrations are presented in Table 10.7. For low concentrations, the precision of the concentration data is approximately ±1%. However, because a mixed Sm-Nd spike was used, the precision of the $^{147}Sm/^{144}Nd$ ratio is approximately 0.5%.

The isochron plot for groups 2 and 3 has the best regression (Figure 10.6) and gives an apparent age of magmatic crystallisation of 341 Ma. This apparent young age is due to one sample with an anomalously high Sm/Nd ratio, which levers the line downwards. One outlier point detracts from this isochron. It corresponds to a serpentinised dunite from the Fontenoy area of the Wambidgee Serpentinite Belt (sample 34) which is strongly altered (See 10.3.5 above), which could explain its "anomalous" behaviour. However, an alternative possibility, and one favoured by Dr Brian Cousens (pers comm., November 1995), is that "old" Nd was added to sample 34 (subsequent to solidification), thereby lowering its initial $^{143}Nd/^{144}Nd$.

When groups 1-3 are plotted with the "outlier" points excluded, the array gives an age of 406 Ma (Figure 10.7). Adding group 4 samples has no effect on the line, initial $^{143}Nd/^{144}Nd$ or the calculated age. However, the low correlation coefficient involved suggests that this line could be an errochron (Rollinson 1993). The calculated initial eNd value of +5.3, falls below the depleted mantle evolution curve at 400 Ma (+7 to +8), this again suggesting that the rocks have a crustal component (Dr Brian Cousens, pers comm., November 1995).

Group 1 samples (i.e. the North Mooney Complex) with the outlier removed have a 400 Ma isochron but higher initial $^{143}Nd/^{144}Nd$ (0.51250) and eNd (+7.5) than the average of the 4 groups combined (0.51239 and +5.3). Groups 2-4 with the outliers omitted yields an age of 380 Ma with an initial $^{143}Nd/^{144}Nd$ of 0.51241 and eNd of +5.2.

When only the intrusive rocks (e.g. gabbro, plagiogranite, basalt) are examined, groups 2-4 yield an age of 392 Ma with a satisfactory fit. All intrusives (groups 1-4) yield an age of 399 Ma with a good fit (Figure 10.8).

Group	Sample	Nd	Sm	147Sm/144Nd	143Nd/144Nd meas	2-sigma
1	141	0.79	0.29	0.221	0.513042	37
	145	1.20	0.45	0.226	0.513003	19
	233	1.70	0.55	0.195	0.512921	22
	234	1.48	0.50	0.204	0.512765	25
	235	8.99	2.30	0.150	0.512878	22
2	170	10.29	2.10	0.123	0.512687	20
	188	16.98	3.30	0.118	0.512706	17
	BF91/33e	6.19	1.70	0.166	0.512752	19
	BF91/33f	22.51	3.45	0.093	0.512643	19
	BF92/16	21.08	5.73	0.164	0.512884	11
	WW2	1.50	0.47	0.189	0.512823	61
3	34	2.20	0.54	0.148	0.512371	22
	34 dup				0.512331	16
	65 horn	11.45	2.21	0.116	0.512639	12
	65 perid	2.22	0.88	0.240	0.512990	14
	225a	3.81	0.87	0.138	0.512724	27
	BF92/3	34.35	6.63	0.117	0.512729	10
	BF92/6a	50.34	8.69	0.104	0.512721	21
	BF92/8	6.33	1.38	0.132	0.512685	13
4	20	1.37	0.33	0.146	0.512785	34
	123	3.69	1.17	0.192	0.512611	50
	155c	7.69	2.06	0.162	0.512566	17
	156	10.62	2.90	0.165	0.512934	24
	238a	1.07	0.32	0.182	0.512793	50
	238 m/dyk	9.28	2.37	0.155	0.512891	18
	238 peggat	14.25	4.63	0.197	0.512976	14

Table 10.7 Nd/Sm isotopic concentrations.

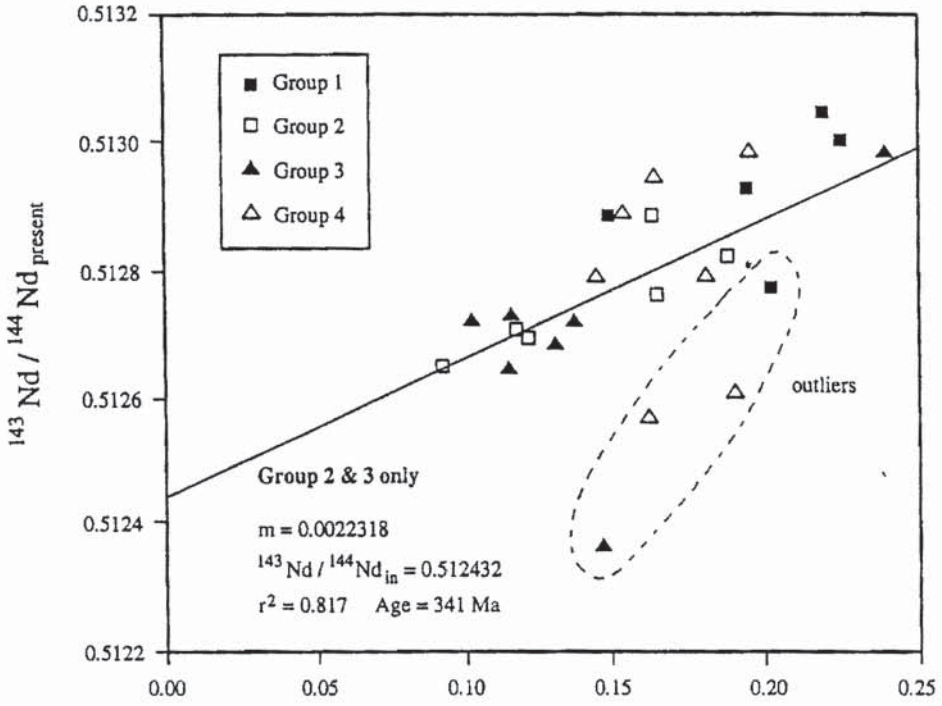

Figure 10.6 Nd/Sm isochron plot for groups 2 and 3.

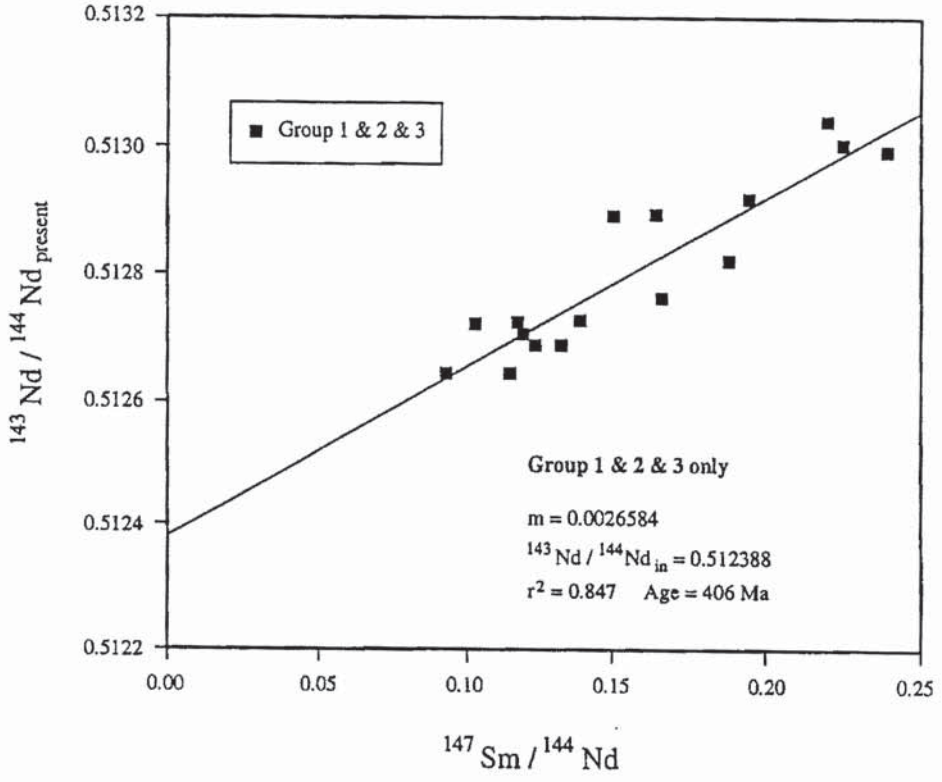

Figure 10.7 Nd/Sm isochron plot for groups 1-3 with outliers removed.

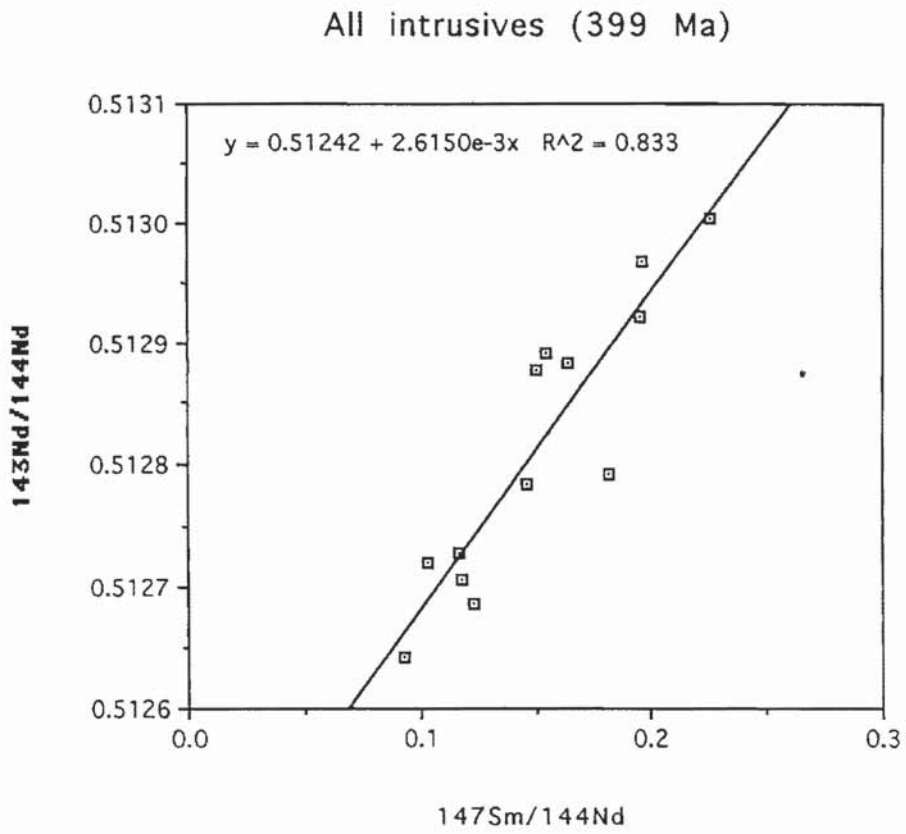

Figure 10.8 Nd/Sm isochron plot of intrusives (e.g. gabbro, plagiogranite, metabasalt) from all groups.

10.4 DISCUSSION

The SHRIMP data constrain the time of formation of ophiolitic rocks within the Tumut Trough region of the Lachlan Fold Belt. Within the error limits, the age data on all of the samples from the various named serpentinite belts overlap; and this, combined with the similar lithotectonic setting of the samples, suggests that the ophiolitic rocks from all of the named belts formed at about the same time. The age of approximately 400 Ma (early Devonian) is considerably younger than that previously proposed for crystallisation (426 ± 6Ma - Basden 1990) and emplacement (*ca.* 417 Ma - Basden 1990) of the Coolac Serpentinite Belt. The early Devonian zircon ages differ significantly from the Cambro-Ordovician (Stuart-Smith 1990) or Silurian (Scheibner 1985; Warner *et al.* 1992) ages proposed for the Coolac Serpentinite Belt, or the Cambro-Ordovician age proposed for the Wambidgee Serpentinite Belt (Stuart-Smith 1990; Basden 1990).

The North Mooney Complex, that supposedly intruded the Coolac Serpentinite Belt (Franklin 1975), has been interpreted as the youngest Silurian unit in the region (Warner *et al.* 1992). K-Ar

ages of 425 ± 6 Ma and 426 ± 6 Ma were obtained for hornblende from a gabbro in the complex (Basden *et al.* 1987). If these ages record magmatic crystallisation, or are in any way meaningful, the North Mooney Complex could not have intruded the Coolac Serpentinite Belt. This conclusion is contrary to the field relationships reported by Franklin (1975); it is also contrary to data presented in Chapter 8 where it was shown that the North Mooney Complex gabbros and metabasalts are geochemically the same as gabbros and metabasalts from the Honeysuckle Beds and the Coolac Serpentinite Belt, thereby suggesting formation from the one magma source.

Franklin (1975) suggested that the North Mooney Complex had intruded the Coolac Serpentinite Belt on the basis of a metasomatic zone between the two units. Similar metasomatic zones have been described from ultramafic bodies on the island of Unst, Shetland Islands, where they have been ascribed to diffusion caused by the passage of hydrothermal fluids between these bodies and the surrounding country rocks (Curtis & Brown 1969). Franklin (1975) also proposed an intrusive relationship on the basis of the occurrence of antigorite in the Coolac Serpentinite Belt at its contact with the North Mooney Complex, whereas lizardite and chrysotile predominate elsewhere in the belt. This was confirmed in the present study. Nevertheless, one would also expect to see gabbro and/or metabasalt dykes from the North Mooney Complex intruding the Coolac Serpentinite Belt. Although none were proven to transgress the interface, gabbroic and basaltic dykes are widely distributed within the Coolac Serpentinite Belt (see Chapter 3) and, as their geochemistry is almost identical to those from the North Mooney Complex and Honeysuckle Beds, there seems little doubt that magma representative of North Mooney Complex and Honeysuckle Beds has intruded the Coolac Serpentinite Belt. It follows that:

(a) parts of the complex must be substantially younger than the parts selected for dating - but this does not seem to be a serious possibility;

(b) the field relationships were inconclusive and/or misconstrued - not supported by the present work;

(c) the North Mooney Complex dates are incorrect – this seems to be the most likely explanation as both field and geochemical data suggest that the gabbros of the North Mooney Complex are genetically similar to those found within the Coolac Serpentinite Belt, one of which (sample 238) gave a U/Pb zircon age of approx. 400 Ma. Clearly, new age dates are required on the North Mooney Complex.

The Young Granodiorite has K-Ar ages of 417 ± 6Ma (Evernden & Richards 1962), 397 ± 16Ma (Thomson 1974) and 405 Ma (Pogson & Hillyard 1981). As the Young Granodiorite has been extensively affected by lower greenschist facies metamorphism (see Chapters 3 and 4), this event most likely re-set the K and Ar in these rocks such that the portions dated from the Young Granodiorite are in fact younger than their real age of crystallisation. However, on the basis of extensive field evidence, portions of the Young Granodiorite intrude the Coolac Serpentinite Belt (Harris 1987; Stuart-Smith 1990a; Marshall and Franklin 1992) and the Wambidgee Serpentinite Belt (this work), so it is possible that the Young Granodiorite is a composite intrusion with a range of ages of intrusion. A modern U/Pb zircon age determination for the intrusive portions of the Young Granodiorite would go toward resolving this matter, but did not form a core part of the present investigation.

The Bogong Granite, an I-type postkinematic granite intrudes and has contact metamorphosed serpentinite at the southern end of the Coolac Serpentinite Belt (Basden 1990). It has a K-Ar biotite age of 410 ± 16 Ma (Ashley *et al.* 1971), which overlaps that of most of the plagiogranites (Figure 10.9). Stuart-Smith *et al.* (1992) obtained a U-Pb zircon age of 411 ± 5 Ma on the chemically similar I-type Gocup Granite from which Richards *et al.* (1977) obtained a K-Ar muscovite age of 409 ± 2 Ma.

Compared to published age data from other rocks in the Tumut-Gundagai region (Figure 10.9), the zircon-crystallisation ages from plagiogranites of the Tumut Serpentinite Province are the youngest data from this part of the Lachlan Fold Belt. However, plagiogranite 20 from the Coolac Serpentinite Belt is older than the only published age for the Bogong Granite (Ashley *et al.* 1971). The inherited ages of all the plagiogranites overlap the ages published for the Goobarragandra Volcanics, Micalong Swamp Complex, North Mooney Complex, and the Frampton Volcanics. The evidence is thus conflicting and new age dates, particularly on the Bogong Granite, are required.

Conceivable explanations for the plagiogranite ages include:

(a) the zircons dated are metamorphic overgrowths of earlier-formed magmatic zircons. There is no evidence of a metamorphic event of sufficiently high temperature to form the postulated

overgrowths, and the zircons are of euhedral shape and have a magmatic morphology. The alternative is therefore rejected.

(b) the plagiogranites are younger than the serpentinite belts that host them. Because the plagiogranites occur as dyke-like bodies within the serpentinite belts, they must be at least marginally younger. The geochemistry of the plagiogranites (See Chapter 8) is clearly distinct from that of all other felsic intrusive rocks in the region, and so, if the plagiogranites are unrelated to the serpentinite belts, why are they exclusively hosted by them and why is the association generally recognised (e.g Menzies *et al.* 1977; Nicolas 1989)?

Inherited zircon cores within the magmatic zircons require that the magma from which the plagiogranite crystallised, must have had access to and incorporated "older" zircons. The fact that the age of these "inherited" zircons is the same as reported ages for the Goobarragandra Volcanics (Owen & Wyborn 1979), Micalong Swamp Complex (Owen & Wyborn 1979), North Mooney Complex (Webb 1980), and the Frampton Volcanics (Stuart-Smith *et al.* 1991), is consistent with these rocks (particularly the Frampton Volcanics, as their age is the only one based on U-Pb in zircon) being a source, or reflecting derivation from the source of the zircons. The problem of how these "older" zircons were incorporated by the plagiogranite-forming magma, bearing in mind that the magma formed within oceanic crust whereas the volcanic rocks clearly formed on a substrate of continental crust, will be addressed in Chapter 11.

If the "outlier" points are removed from the Nd/Sm data, it is difficult to distinguish between the suite from the North Mooney Complex, and that from the Tumut Serpentinite Province. The North Mooney Complex samples, minus the "outlier" point , would approximately yield a 400 Ma errochron; the initial $^{143}Nd/^{144}Nd$ would be 0.51250 and the eNd +7.5. The four groups combined (but without the "outliers") have an initial $^{143}Nd/^{144}Nd$ of 0.51239 and an eNd of +5.3. A line of best fit through the data for groups 2 to 4 (without the "outliers") yields a magmatic age of approximately 380 Ma, an initial $^{143}Nd/^{144}Nd$ of 0.512413 and an eNd of +5.2. However, it must be stressed that the results have much uncertainty and are only indicative of the formational age in the context of the highly reliable zircon data.

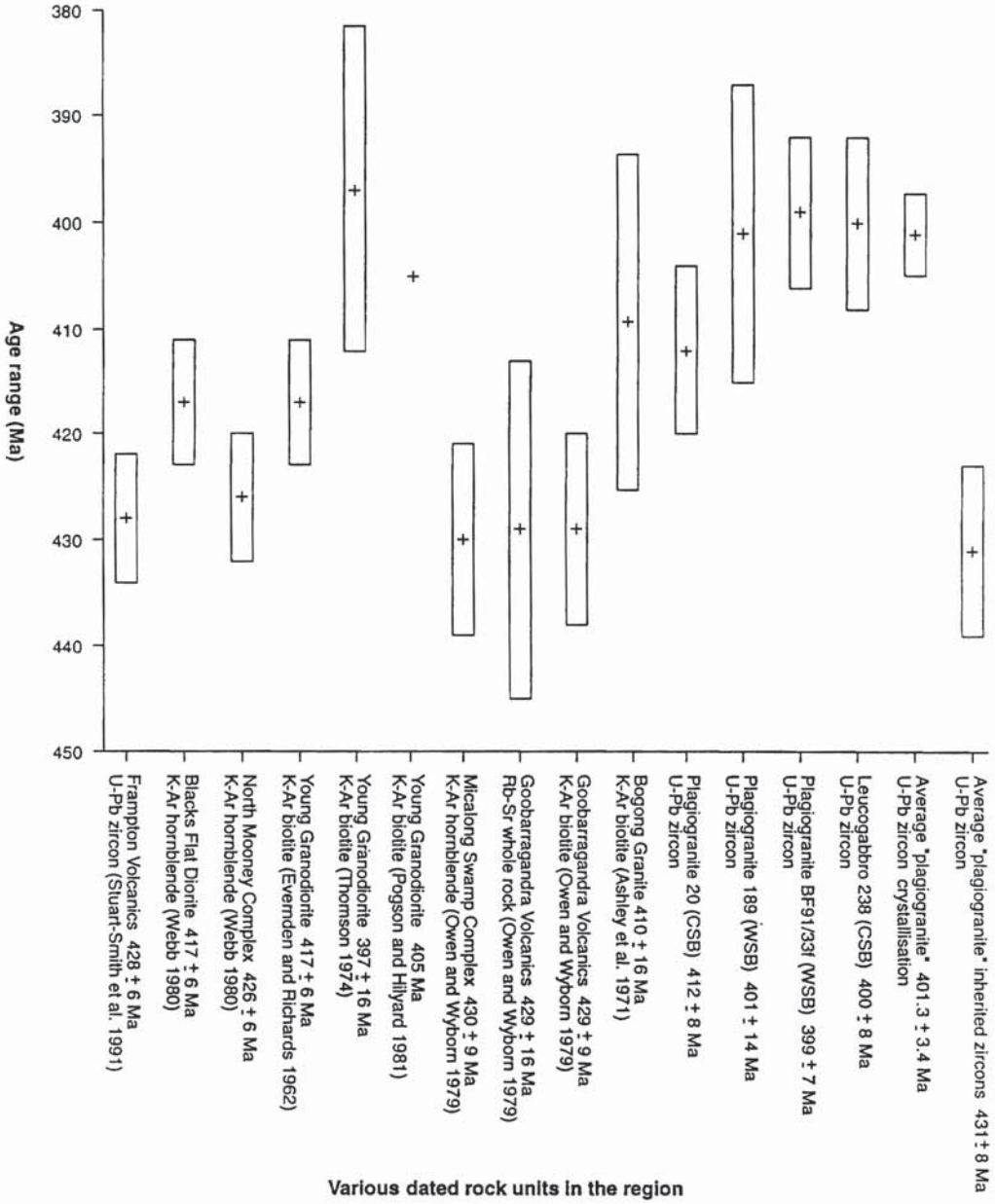

Figure 10.9 Published age data for rock units from the Tumut region.

10.5 CONCLUSIONS

The zircon U-Pb ages indicate that the rocks of the Tumut Serpentinite Province are younger than previously thought. Scheibner (1985) and Basden (1990) suggested that the Gundagai Serpentinite Belt and Wambidgee Serpentinite Belt were Cambrian-Ordovician in age and the Coolac Serpentinite Belt was at least as old as Early Silurian, whereas Stuart-Smith (1990a; 1990b) suggested that all of the Tumut Serpentinite Province was Cambro-Ordovician and represented the basement rocks of the region. A similar "basement" implication is built into tectonic interpretations by Glen (1992) and Gray (1997).

The zircon data show that the plagiogranites were contaminated by older zircons, with an age of approximately 431 ± 8 Ma, an age very similar to a U-Pb age (428 ± 6 Ma) reported by Stuart-Smith (1990) for the Frampton Volcanics. The approximate age of crystallisation of the plagiogranites and, by implication, the Tumut Serpentinite Province, fall within the age range (420-390 Ma - Chappell & Stephens 1988; Chappell 1994) of the principal granite-forming events in the Lachlan Fold Belt.

If the data from the SHRIMP zircon U-Pb investigations are taken into account (i.e the approximate age of crystallisation of the plagiogranites at 400 Ma and the crustal contamination component of approximately 430 Ma), the Sm-Nd whole rock data for all rock types (disregarding the 3 "outlier" points) yield an errochron with an approximate age of crystallisation of 406 Ma. When only the intrusive rocks are taken into account, this results in an age of crystallisation of 399 Ma. Bearing in mind the uncertainty attached to the Nd/Sm data, the result could be fortuitous.

The inescapable overall conclusion is that rocks of the Tumut Serpentinite Province are not Cambro-Ordovician basement as suggested by Stuart-Smith (1990), but are much younger and post-date the Frampton Volcanics and perhaps the other Silurian felsic volcanics (e.g. the Goobarragandra Volcanics) of the region.

CHAPTER 11: DISCUSSION, INTERPRETATION AND CONCLUSIONS

11.1 THE SERPENTINITE BELTS: A Summary

A comparative summary of the serpentinite belts (Tables 11.1 to 11.7) (and Chapters 3-8) allows the following points to be made:

(a) The gross shape, structure at margins, and gross internal structure are consistent with slices of dominantly harzburgitic upper mantle being tectonically emplaced within a convergent plate tectonic setting. The main foliation in each of the serpentinite belts has a consistent NNW-SSE trend; it has affected the serpentinite belts and adjacent rocks, and must have developed during or after the emplacement process.

(b) The similar range of lithologies and immobile trace element compositions are consistent with the belts forming within a similar geotectonic environment.

(c) Mafic rocks in the serpentinite belts, Honeysuckle Beds and North Mooney Complex are geochemically the same, whereas plagiogranites from the serpentinite belts are geochemically different from the Young Granodiorite and felsic parts of the Micalong Swamp Complex.

(d) The main mineral deposits differ between the belts. In the case of podiform chromitites, this could reflect the belts coming from different depths within the upper mantle sequence.

(e) U-Pb SHRIMP ion probe geochronology of zircons from plagiogranites and leucogabbros of the Coolac and Wambidgee serpentinite belts shows that crystallisation ages are the same in both belts and that an inherited zircon age has been derived from Early Silurian felsic volcanic rocks.

Maximum length: 63km
Maximum width: 3.5km
Gross internal structure: main harzburgite mass, Western Tectonic Melange Zone, internal shear zones
E-contact: intuded by / faulted against the Late Silurian Young Granodiorite
W-contact: tectonic melange against the Mid-Late Silurian Honeysuckle Beds
S-contact: intruded by the Early Devonian Bogong Granite
Primary ultramafic rocks: harzburgite, dunite, pyroxenite, wehrlite, hornblendite
Tectonic inclusions: granodiorite, basalt, dolerite, rhyodacite, metasediments
Nature of dykes: pyx gabbro, plagiogranite, albitite, rodingite, chlorite rock
Primary igneous layering: present
Chromitite pods: abundant
Mineral deposits: podiform chromite, Cu-Zn-Pb sulfides
Serpentinisation: lizardite+chrysotile
Peak metamorphism: lower greenschist (T~300°C)
U-Pb zircon geochronology: 412-400 Ma

Table 11.1 General features of the Coolac Serpentinite Belt.

Maximum length: 110km
Maximum width: 1.9km
Gross structure: main serpentinite mass, internal shear zones
E-contact: intruded by / faulted against the Late Silurian Young Granodiorite
W-contact: faulted against the Cambro-Ordovician Jindalee Beds
Primary ultramafic rocks: harzburgite, dunite, hornblende clinopyroxenite, hornblendite, peridotite
Tectonic inclusions: quartzite, marble
Nature of dykes: plagiogranite, chlorite rock, amphibolite, gabbro, rodingite
Primary igneous layering: present
Chromitite pods: rare
Mineral deposits: magnesite, talc
Serpentinisation: antigorite+chrysotile
Peak metamorphism: upper greenschist to middle amphibolite (400-700°C)
U-Pb zircon geochronology: 400 Ma

Table 11.2 General features of the Wambidgee Serpentinite Belt.

Maximum length: 23km
Maximum width: 1.8km
Gross structure: mixed massive/schistose serpentinite
E-contact: faulted against the Silurian Jackalass Slate
W-contact: faulted against the Cambro-Ordovician Jindalee Beds and Early Silurian Wandeen Formation
Primary ultramafic rocks: harzburgite, pyroxenite, peridotite
Tectonic inclusions: tonalite, tuff, hybrid felsic/mafic rock
Nature of dykes: gabbro, basalt, plagiogranite, chlorite rock
Primary igneous layering: absent
Chromitite pods: absent
Mineral deposits: talc
Serpentinisation: antigorite+chrysotile
Peak metamorphism: upper greenschist to lower amphibolite
U-Pb zircon geochronology: not determined

Table 11.3 General features of the Gundagai Serpentinite Belt.

Maximum length: 43km
Maximum width: 1.25km
Gross structure: main serpentinite mass, internal shear zones
E-contact: faulted against the Silurian Tumut Pond Group and O'Hares Beds
W-contact: faulted against the Silurian Tumut Pond Group and O'Hares Beds
Primary ultramafic rocks: hornblende clinopyroxenite
Tectonic inclusions: gabbro, basalt, andesitic tuff
Nature of dykes: rodingite, chlorite rock
Primary igneous layering: absent
Chromitite pods: absent
Mineral deposits: none known
Serpentinisation: lizardite+chrysotile
Peak metamorphism: lower greenschist (~300°C)
U-Pb zircon geochronology: not determined

Table 11.4 General features of the Tumut Ponds Serpentinite Belt.

Maximum length: 6km
Maximum width: 0.5km
Gross structure: main lherzolitic mass, internal shear zones
E-contact: faulted against the Ordovician Wagga Group
W-contact: faulted against the Ordovician Wagga Group
Primary ultramafic rocks: lherzolite, pyroxene hornblendite, hornblende peridotite
Tectonic inclusions: none known
Nature of dykes: none known
Primary igneous layering: absent
Chromitite pods: absent
Mineral deposits: none known
Serpentinisation: antigorite+chrysotile
Peak metamorphism: upper greenschist to middle amphibolite (400-700°C)
U-Pb zircon geochronology: not determined

Table 11.5 General features of the Eurongilly Serpentinite Belt.

Maximum length: 1.5km
Maximum width: 0.1km
Gross structure: main serpentinite mass, internal shear zones
E-contact: faulted against the Cambro-Ordovician Jindalee Beds
W-contact: faulted against the Cambro-Ordovician Jindalee Beds
Primary ultramafic rocks: hornblendite
Tectonic inclusions: none known
Nature of dykes: none known
Primary igneous layering: absent
Chromitite pods: absent
Mineral deposits: none known
Serpentinisation: antigorite+chrysotile
Peak metamorphism: upper greenschist (~350°C)
U-Pb zircon geochronology: not determined

Table 11.6 General features of the Darbalara Serpentinite Belt.

Maximum length: 3.8km Maximum width: 1.1km Gross structure: tectonic melange E-contact: faulted against the Late Silurian Blowering Formation W-contact: faulted against the Early Silurian Frampton Volcanics Primary ultramafic rocks: clinopyroxenite, lherzolite Tectonic inclusions: plagiogranite, amphibolite, basalt, gabbro Nature of dykes: none known Primary igneous layering: absent Chromitite pods: absent Mineral deposits: none known Serpentinisation: lizardite+chrysotile Peak metamorphism: lower greenschist (~300°C) U-Pb zircon geochronology: 400 Ma

Table 11.7 General features of the Western Wambidgee Serpentinite Melange.

11.2 ARE THE SERPENTINITE BELTS OPHIOLITIC FRAGMENTS?

The Penrose Conference (1972) defined an ophiolite as a fully-preserved layered sequence with mantle peridotite at its base, followed by crustal plutonic rocks, sheeted dykes, pillow lavas, and pelagic sediments (Figure 11.1). Although ophiolites were classically thought to have formed at mid-ocean ridges, modern concensus is that a significant proportion of them formed above subduction zones, at small ridges in small basins around volcanic arcs (Pearce *et al.* 1984; Pearce 1991). However, most ophiolite sequences are tectonically disrupted and incompletely preserved. Such dismembered sequences are widespread both in space and time, and include the Coast Range Ophiolite of western California (U-Pb zircon crystallisation ages of 170 to 160 Ma - Hopson *et al.* 1981; Shervais & Kimbrough 1985), the Xainxa ultramafic rocks of Tibet (Girardeau *et al.* 1985), the Chamrousse Ophiolite of the Western Alps France (U-Pb zircon crystallisation ages of 497 Ma - Pin & Carme 1987) and the Mesozoic ophiolites of Central Anatolia Turkey (Yaliniz *et al.* 1996).

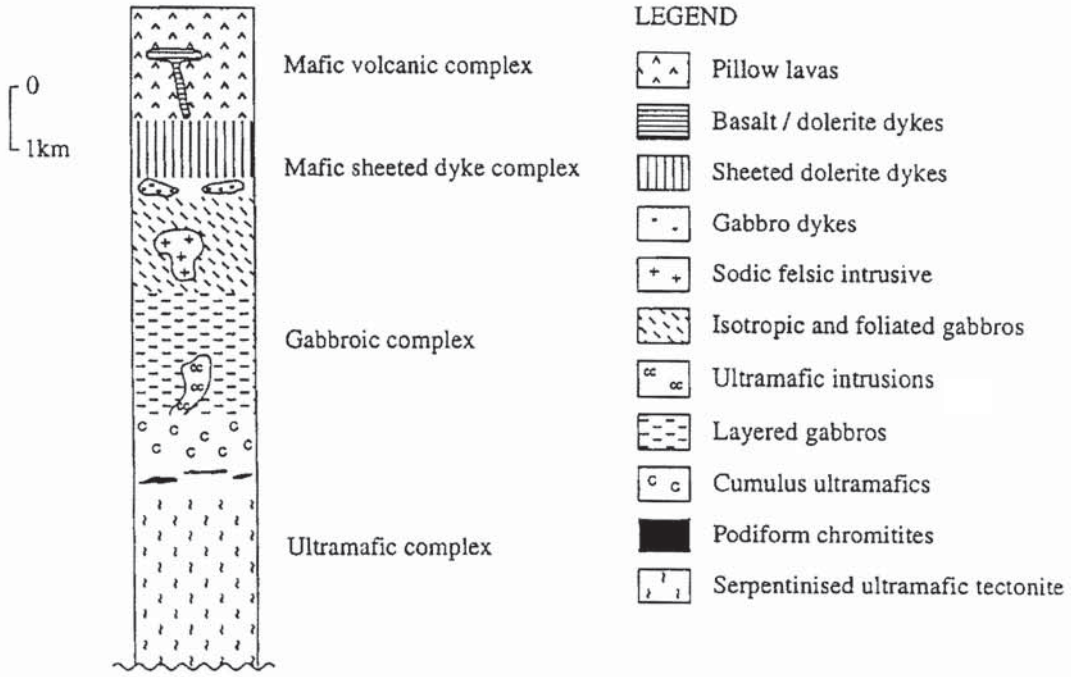

Figure 11.1 Penrose conference defined ophiolite (adapted from Coleman 1977).

According to Boudier & Nicolas (1985), spreading rates are the most influential parameter in the diversity of oceanic lithosphere and ophiolites. Nicolas (1989) subdivided ophiolites into two main types (Table 11.8 and Figure 11.2). The harzburgite (HOT) type reflects a high degree of partial melting, fast spreading, and a harzburgitic upper mantle (e.g. the Oman Ophiolite). The lherzolite (LOT) type reflects a low degree of partial melting, slow spreading, and an upper mantle dominated by plagioclase lherzolites (e.g. the Trinity Ophiolite). He also recognised intermediate types with a clinopyroxene-harzburgite to lherzolite upper mantle Section (e.g. the Xigaze Ophiolite).

	Harzburgite ophiolite type (HOT)	Lherzolite ophiolite type type (LOT)
Environmental formations		
cover	marine sediments and volcanics	marine sediments and volcanics breccias
sole	sole of metamorphic oceanic crust	sole of metamorphic continental oceanic crust
Mafic section		
thickness	2-3 km ~7 km	0-1 km 2-3 km
layered gabbros	thick and usually continuous	thin, absent or in restricted areas
nature of intrusives	rare diabase dikes wehrlite bodies	numerous diabase dikes and sills
nature of basalt directly associated with the ophiolite	tholeiitic	tholeiitic alkaline
Fe-Ti-gabbros/ Mg-gabbros	small	large
LT plastic deformation	absent, except local shear zones	very common (flaser gabbros)
Ultramafic section		
nature of mantle rocks	harzburgites and abundant dunites down to about 10 km below Moho	plagioclase lherzolites and abundant dunites within ≤ 2 km below Moho
HT plastic flow structures	flat foliation locally vertical with vertical lineation	usually steep foliation and moderately plunging lineation
neoblast grain size	large (~4mm)	small (~0.5mm)
chromite pods	present	absent
diabase occurrence	uncommon	common in top of section
serpentinization	lizardite	lizardite and antigorite ophicalcites

Table 11.8 Characteristics of Harzburgite (HOT) and Lherzolite (LOT) ophiolite types (adapted from Nicolas 1989).

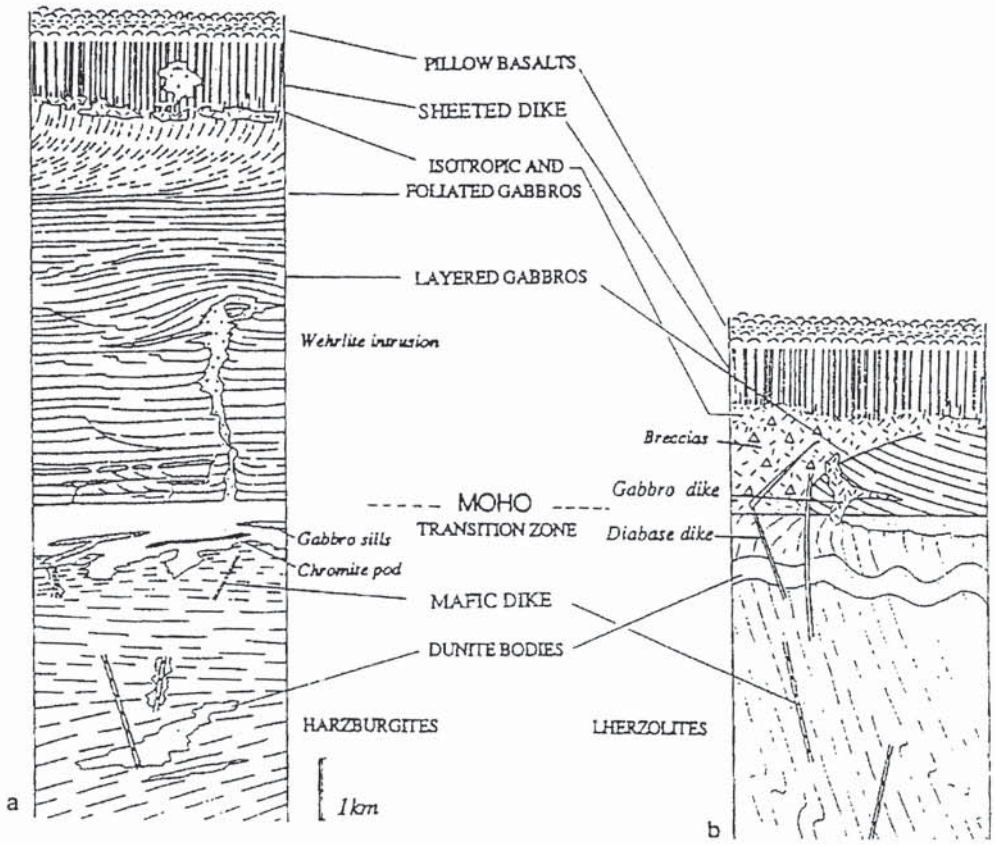

Figure 11.2 Vertical Sections through Harzburgite (HOT) and Lherzolite (LOT) ophiolite types. Internal structures and relative thicknesses are approximate (from Nicolas 1989).

Back-arc basins are common sites for the generation of ophiolites whereas island-arc ophiolites (e.g. Canyon Mountain Ophiolite) are rare (Nicolas 1989). Ophiolites form at either a mid-ocean ridge or supra-subduction zone environment, and are emplaced onto the continental margin by convergent plate movement (Cawood & Suhr 1992). However, Moores *et al.* (1984) stated that ophiolites are not 'typical' oceanic crust, as formed at mid-oceanic spreading centres, and that 'typical' oceanic crust may not be preserved on land. No single model adequately explains all ophiolite occurrences (Dickinson *et al.*1996); this is largely due to various types of data (e.g. geochemistry and structural analysis)

commonly being contradictory (Cawood & Suhr 1992), but could also reflect the possibility that the wide variety in orogenic belts preserve the range of geological environments in which present-day oceanic lithosphere is formed (Cawood & Suhr 1992). A recent study of the Coast Range Ophiolite of California (Dickinson *et al.* 1996) found that three mutually exclusive tectonic models could explain its development and that each model required different regional tectonic interpretation.

Den Tex (1969) first proposed the term 'alpine-type' for orogenic peridotites. He subdivided them into ophiolitic (or true alpine-type peridotites) and orogenic root-zone peridotites, the latter subsequently being named the lherzolitic subtype (Jackson & Thayer 1972) and the former, the harzburgite subtype (Nicolas & Jackson 1972). The harzburgite subtype occupies the basal portion of ophiolite sequences (Coleman 1977) and is the most abundant rock type within alpine-type peridotites. Tectonic dismembering leads to underlying basal peridotite separating from once overlying cumulate ultramafic sequences, gabbro and basalt (Coleman 1977). In orogenic zones, the peridotites may form completely serpentinised tectonic lenses that have separated from their mafic sequences and are termed alpine-type serpentinite belts (Coleman 1977). Thus, alpine-type serpentinite belts are essentially serpentinised harzburgitic massifs that once formed the basal part of an ophiolite.

Ophiolites vary in metamorphic grade from relatively pristine igneous assemblages (e.g. the Semail Ophiolite - Lippard *et al.* 1986) to amphibolite facies assemblages (e.g. the Chamrousse Ophiolite - Pin & Carme 1987). The Jurassic ophiolites of northern Italy and southern Switzerland have reached either eclogite or blueschist facies metamorphism (Lagabrielle & Cannat 1990).

The serpentinite belts of the Tumut Serpentinite Province are interpreted as dismembered ophiolites. Although lacking a cover sequence, mafic section, and metamorphic sole, they consist of ultramafic sections with intrusions that petrographically and geochemically typify the volcanic cover sequence and mafic section of harzburgite-type ophiolites (Chapters 3 to 8). A similar assemblage occurs within the Ligurian ophiolites of the Apennines where gabbros form small intrusive pockets within the peridotites (Lagabrielle *et al.* 1984). Such assemblages also occur on the Mid-Atlantic ridge where serpentinised peridotites and gabbros crop out on the sea-floor or are overlain by only a thin cover of basalt and deep-

sea sediments (Lagabrielle & Cannat 1990). In the ophiolite complexes of the deep-sea trenches of the Western Pacific, the dominant ultramafic rock type is serpentinised (chrysotile+antigorite) harzburgite; and both the gabbros and basalts have been metamorphosed to greenschist facies assemblages (Govorov *et al.* 1989).

The Coolac and Wambidgee serpentinite belts represent the basal section of harzburgite-type ophiolites (after Nicolas 1989), dominated by harzburgite, and with podiform chromitite pods; the dominant retrogressive serpentine group mineral is lizardite (although the Wambidgee Serpentinite Belt underwent higher T serpentinisation leading to the direct formation of antigorite - Section 4.5.2). The Gundagai and Tumut Ponds serpentinite belts lack known podiform chromitites (Section 9.1), and, like the Wambidgee Serpentinite Belt, underwent higher T serpentinisation leading to the direct formation of antigorite (Sections 5.5.2 and 6.3.2). The Eurongilly Serpentinite Belt differs from the other belts, in that the dominant ultramafic rock type is lherzolite and there are no reported podiform chromitite pods (Section 7.1). The belt probably represents the basal section of a lherzolite-type ophiolite (after Nicolas 1989).

The size and shape of the serpentinite belts is similar to those of the Northern Sierra Nevada region of California (Saleeby *et al.* 1989). The primary lithologies and geochemistry (Sections 3.5.1 - 3.5.3, 4.5.1, 5.5.1, 6.3.1; Chapters 7 and 8) are akin to those in most ophiolite belts, the metamorphism has parallels in many other ophiolites (Sections 3.5, 4.5, 5.5, 6.3; Chapter 7), and the podiform chromitites are characteristic of ophiolitic deposits from upper mantle harzburgite near the palaeo-Moho (Section 9.10.1). Thus, all bar one (the Eurongilly Serpentinite Belt) of the serpentinite belts of the Tumut Serpentinite Province are typical alpine-type serpentinites. They differ from more established ophiolites by lacking an upper mantle cumulate ultramafic sequence and overlying gabbroic and basaltic sequences; instead, these missing sequences are represented by small, isolated bodies within the main harzburgite mass (Sections 3.4.2, 3.5, 4.4.2, 4.5, 5.5, 6.3; Chapter 7). The Eurongilly Serpentinite Belt is petrologically and geochemically similar to the lherzolite massifs of southern Spain and Morocco (Van der Wal & Vissers 1993)(Sections 7.1 and 8.1) and, like them (Bodinier *et al.* 1987), could represent upper mantle from a transitional continental-oceanic environment.

The geochemical similarity of serpentinites from the Tumut Serpentinite Province suggests that they derived from harzburgite, in that the geochemistry matches that from the fresh harzburgite (Section 8.2). Gabbros within the serpentinite belts are geochemically similar, and to those of the North Mooney Complex and Honeysuckle Beds (Section 8.4). They differ from those of the Micalong Swamp Complex. It follows that the gabbros of the serpentinite bodies, the North Mooney Complex, and the Honeysuckle Beds are genetically related and have a common parental magma (Section 8.4.4). Comparison of the CN REE patterns with those for cumulus and high level gabbros from various ophiolite complexes (e.g. the Semail Ophiolite - Pallister & Knight 1981; the Troodos Ophiolite - Kay & Senechal 1976)(Section 8.4.4) shows that they are similar and suggests that they formed in an oceanic crustal environment.

Metabasalts from the serpentinite belts and Honeysuckle Beds are geochemically similar ocean floor tholeiitic MORB basalts, relatively enriched in Na_2O and depleted in K_2O (Jacques & Chappell 1980). They differ from those of the Micalong Swamp Complex (Section 8.5). Immobile trace element discrimination diagrams clearly show that they are back-arc basin basalts.

Plagiogranites from the various serpentinite belts are enriched in Na_2O and MgO relative to felsic portions of the Young Granodiorite and Micalong Swamp Complex (Section 8.7.2). Their major element and REE geochemistry is similar to plagiogranites from the Volti Group of the Ligurian Alps, the Sestri-Voltaggio Zone of Italy (Borsi *et al.* 1996), the Canyon Mountain Ophiolite (Gerlach *et al.* 1981) and the Josephine Ophiolite (Barnes *et al.* 1996)(Section 8.7.4). They therefore formed in an oceanic rather than crustal environment.

The tabular chromitite bodies from the Tumut Serpentinite Province (Section 9.2) are typical of those in the mantle sequence of most ophiolites (e.g. Leblanc & Violette 1983; Auge 1987). The presence of an unfoliated chromite-bearing dunitic envelope is common in ophiolites (e.g. Whittaker & Watkinson 1984; Johan 1986)(Section 9.10.1). High Cr and/or Al concentrations confirm that the chromitites are of podiform type (Dickey 1975); this also applies to the reciprocal variations of Cr_2O_3 and Al_2O_3, and the small variation and low values of Fe^{+2}/Mg (Thayer 1964; Leblanc & Violette 1983) (Section 9.4).

Chromitites from both the Coolac and Wambidgee serpentinite belts fall well within the ophiolitic chromitite field (Leblanc 1985) and are low in TiO_2 as generally found within podiform chromitites (Leblanc & Ceuleneer 1992; Leblanc 1995)(Section 9.4). The chromitites are enriched in Os, Ir and Ru, relative to Pt and Pd, this typifying ophiolitic chromitites (Auge 1988; Leblanc 1995)(Section 9.4). Also typical of ophiolitic chromitites are the CN PGE diagrams with positive slopes to Ru followed by negative slopes to Pt (Barnes *et al.* 1985)(Section 9.4).

Although the complete stratigraphic sequence of a 'typical' ophiolite is not developed within the serpentinite belts of the Tumut Serpentinite Province, all ophiolite lithologies are present. It is therefore proposed that the serpentinite belts of the Tumut Serpentinite Province could only have formed within an oceanic environment. Unlike most ophiolites however, a crustal sequence was not developed, perhaps because the ocean basin was very short-lived and narrow.

11.3 HOW MAY THE U-Pb SHRIMP DATA BE INTERPRETED?

The U-Pb SHRIMP data from the plagiogranites and leucogabbros of the Coolac and Wambidgee serpentinite belts constrain the time of formation of ophiolitic rocks within this region of the Lachlan Fold Belt (Graham *et al.* 1996). They show that the crystallisation ages overlap at approximately 400 Ma (Section 10.2.6) placing them in the Late Silurian-Early Devonian. Sm-Nd isotopic data on intrusive rocks of the serpentinite belts are similarly consistent with a crystallisation age of approximately 400 Ma. The host rocks, that is the main harzburgite mass and associated chromitite and dunite bodies, must be older than 400 Ma. However, as the chromitite and associated dunite bodies have undergone a similar deformational and metamorphic history to the plagiogranites (Chapters 3 - 9), they are unlikely to be more than a few million years older placing them within the Late Silurian. The age of the main harzburgite mass cannot be determined, but much of the eastern half of the Coolac Serpentinite Belt consists of relatively pristine harzburgite, and this is consistent with the harzburgite being little older than the rocks that have intruded it. More complex histories characterise older units in the region (e.g. Jindalee Beds, Frampton Volcanics). The 427 Ma age of crystallisation of the Frampton

Volcanics and inherited zircon age of 431 Ma within the plagiogranites, suggests that the main harzburgite mass of the serpentinite belts is younger than 427 Ma but older than 400 Ma.

The Young Granodiorite intrudes portions of the Coolac and Wambidgee serpentinite belts; the Masirah Ophiolite of Oman was similarly intruded by a potassic granite soon after it formed. Based on a K-Ar study of hornblende from gabbros and cross-cutting potassic granites, Smewing *et al.* (1991) obtained a gabbro age of 126-158 Ma interpreted as the formational age of the Masirah Ophiolite and a potassic granite age of 124-146 Ma equated with emplacement of the ophiolite; Smewing *et al.* (1991) concluded that the Masirah Ophiolite was emplaced soon after it had formed. It would also seem that the serpentinite belts of the Tumut Serpentinite Province were emplaced shortly after intrusion of the MORB magmas, which crystallised as cumulate ultramafic rocks, gabbro, basalt and plagiogranite.

Inherited zircons from the plagiogranites in the Coolac and Wambidgee serpentinite belts have a consistent age of approximately 430 Ma (Section 10.2.6), akin to that from felsic volcanic rocks (e.g. Frampton Volcanics) in the region (Section 10.4). This suggests that the intrusive MORB sequence formed in a rifting older (`430 Ma) volcanic arc, and that the serpentinite belts were the substrate to an oceanic basin (a back arc basin as suggested by Ashley *et al.* 1979) in which the Blowering Formation and Honeysuckle Beds were deposited in the Late Silurian-Early Devonian.

The plagiogranites and leucogabbros underwent the same sequences of deformation and metamorphism as most other rock types within the serpentinite belts (Chapters 3 to 8), so that their age of crystallisation places restrictions on the ages of deformation and metamorphism of the serpentinite belts. Fracturing and serpentinisation of the harzburgite massif (and Mg-metasomatism of the plagiogranites and gabbros) (Chapters 3 to 8) must have occurred sometime after 400 Ma but before intrusion of the Young Granodiorite and Bogong Granite. The main brittle-ductile deformational event and accompanying greenschist facies regional metamorphism, which affected the serpentinite belts and the Late Silurian rocks (including the margins of the Young Granodiorite), must have post-dated or accompanied ductilely deformed emplacement of the Young Granodiorite.

In summary, the U-Pb zircon geochronological data constrain the primary crystallisation and main periods of serpentinisation and pre-emplacement deformation of the serpentinite belts. They also constrain events from crystallisation of the MORB sequence (~ 400 Ma), through to emplacement of the serpentinite belts and accompanying regional metamorphism/deformation at their present sites.

11.4 HOW ELSE CAN THE SERPENTINISATION, METAMORPHISM AND DEFORMATION OF THE SERPENTINITE BELTS AND ASSOCIATED ROCK UNITS BE CONSTRAINED ?

Serpentinisation of the ultramafic rocks within the Tumut Serpentinite Province requires pervasive fracturing to create permeability pathways for the downward infiltration of serpentinising fluids (Chapter 3). Ingress of these fluids then promotes hydraulic fracturing so that, following initial fracturing, serpentinisation and fracturing are complementary, and occur over a protracted period. Serpentinisation followed crystallisation of the dykes (many of which underwent calcic metasomatism associated with the serpentinisation process) (Sections 3.5.8, 4.5.10, 6.3.5, 8.9) and preceded and/or was synchronous with emplacement of the ophiolite into continental crust. Initial cracking, due to cooling of the igneous rocks, is believed to have occurred during an extensional phase, this creating permeability pathways for the inflow of fluids. Then, when extension changed to shortening, hydraulic fracturing became the dominant process.

The primary ultramafic rocks first underwent a period of high temperature (1000-1100°C) recrystallisation (Section 3.5.1). Then, under conditions of falling temperature (to <300°C), rodingitisation and related serpentinisation developed. Rodingitisation resulted from calcic metasomatism of gabbroic and, to a lesser extent, basaltic dyke rocks (Sections 3.5.8, 4.5.10, 6.3.5, 8.9) (Figure 11.3), while serpentinisation released calcium and developed lizardite+chrysotile+magnetite assemblages within the Coolac and Tumut Ponds serpentinite belts and Western Wambidgee Serpentinite Melange, and antigorite within the other serpentinite belts.

After serpentinisation, intense ductile-brittle deformation affected the Tumut Serpentinite Province. Effects vary within and between belts (Chapters 3 to 7), but are particularly intense at the contacts with adjoining rock units and within discrete shear zones (Chapters 3 to 8). Because orientation data are consistent within the belts and intervening rock units, deformation must have accompanied and/or post-dated emplacement of the serpentinite belts at their present sites. The development of schistose serpentinite within the belts (Chapters 3 to 7) and the formation of the Western Tectonic Melange Zone are assigned to this deformational event.

The Coolac and Tumut Ponds serpentinite belts and the Western Wambidgee Serpentinite Melange experienced lower greenschist facies metamorphism (<260°C), whereas the other belts underwent the higher temperature conditions of the upper greenschist to middle amphibolite facies. There is no evidence for prograde metamorphism subsequent to serpentinisation, so the higher temperatures are ascribed to a higher geothermal gradient during serpentinisation. After serpentinisation and related metasomatic alteration, a period of retrogressive lower greenschist facies metamorphism overprinted the amphibolite facies metamorphism in some places. This event is equated with Late Silurian-Early Devonian regional-wide deformation that affected the low grade metamorphic of rock units throughout the Tumut region.

In summary, the serpentinite belts of the Tumut Serpentinite Province crystallised in the Late Silurian, and the MORB sequence (gabbro, basalt and plagiogranite) intruded and crystallised in the latest Silurian to Early Devonian. The serpentinite belts subsequently underwent progressive serpentinisation, and emplacement and deformation within continental crust. The majority of the slices experienced upper greenschist to middle amphibolite facies conditions during serpentinisation, whereas the Coolac and Tumut Ponds serpentinite belts, and the Western Wambidgee Serpentinite Melange experienced lower temperature greenschist facies conditions. Serpentinisation was initiated by cooling of the ultramafic and associated rocks within the oceanic environment and most probably facilitated detachment and subsequent emplacement in the continental environment. It seems likely that initial crystallisation through to emplacement, may have only spanned some 20 Ma (see also Warner *et al.* 1992).

SERPENTINITE BELT	FORMATION	OCEANIC SETTING			CONTINENTAL SETTING		
Coolac	crystallisation as harzburgite ~1300°C	high T metamorphism ~1000°C	——	serpentinisation and rodingitisation < 260°C	lower greenschist facies metamorphism < 300°C	early Devonian contact hornblende hornfels facies metamorphism by Bogong Granite	low T alteration < 100°C
Wambidgee	crystallisation as harzburgite ~1300°C	high T metamorphism ~1000°C	——	serpentinisation and rodingitisation 260-450°C	lower greenschist facies metamorphism < 300°C		low T alteration < 100°C
Gundagai	crystallisation as harzburgite ~1300°C	high T metamorphism ~1000°C	——	serpentinisation and rodingitisation 260-450°C	lower greenschist facies metamorphism < 300°C		low T alteration < 100°C
Tumut Ponds	crystallisation as harzburgite ~1300°C	high T metamorphism ~1000°C	——	serpentinisation and rodingitisation < 260°C	lower greenschist facies metamorphism < 300°C		low T alteration < 100°C
Eurongilly	crystallisation as lherzolite ~1300°C	high T metamorphism ~1000°C	——	serpentinisation and rodingitisation 260-450°C	lower greenschist facies metamorphism < 300°C		low T alteration < 100°C
Darbalara	crystallisation as harzburgite ~1300°C	high T metamorphism ~1000°C	——	serpentinisation and rodingitisation 260-450°C	lower greenschist facies metamorphism < 300°C		low T alteration < 100°C
Western Wambidgee Serpentinite Melange	crystallisation as harzburgite ~1300°C	high T metamorphism ~1000°C	——	serpentinisation and rodingitisation < 260°C	lower greenschist facies metamorphism < 300°C		low T alteration < 100°C

Figure 11.3 Summary of the tectonothermal history of the serpentinite belts.

11.5 GENESIS AND EVOLUTION OF THE SERPENTINITE BELTS WITHIN THE TUMUT SERPENTINITE PROVINCE

In this section, geochronological constraints taken from other rocks within the region will be combined with other parts of this thesis, in order to derive a tectonic model for the genesis and subsequent evolution of the serpentinite belts of the Tumut Serpentinite Province. Analogues are drawn with ancient and modern tectonic environments, and the significance of the derived model with respect to geological development of the Lachlan Fold Belt is examined.

Published geochronological data from the region, including the plagiogranite U-Pb zircon ages obtained during the current research, are presented in Figure 11.4. Rather than representing the oldest rock units (e.g. Stuart-Smith 1990), the intrusive mafic and felsic rocks of the serpentinite belts are amongst the youngest Late Silurian to Early Devonian sequences. They are younger than the Frampton Volcanics,

North Mooney Complex, Micalong Swamp Complex and Goobarragandra Volcanics. However, the gabbroic and basaltic bodies of the North Mooney Complex are akin to and, in all probability, approximately the same age (i.e. 400 Ma) as those from the serpentinite belts (Chapter 8), so new age determinations are needed on the North Mooney Complex. This also applies to the Bogong Granite, Blacks Flat Diorite and Young Granodiorite, as their age dates suggest that the intrusions are coeval with the serpentinite belts, whereas the Young Granodiorite intrudes the Coolac and Wambidgee serpentinite belts and is most probably younger than the crystallisation ages of the MORB sequence.

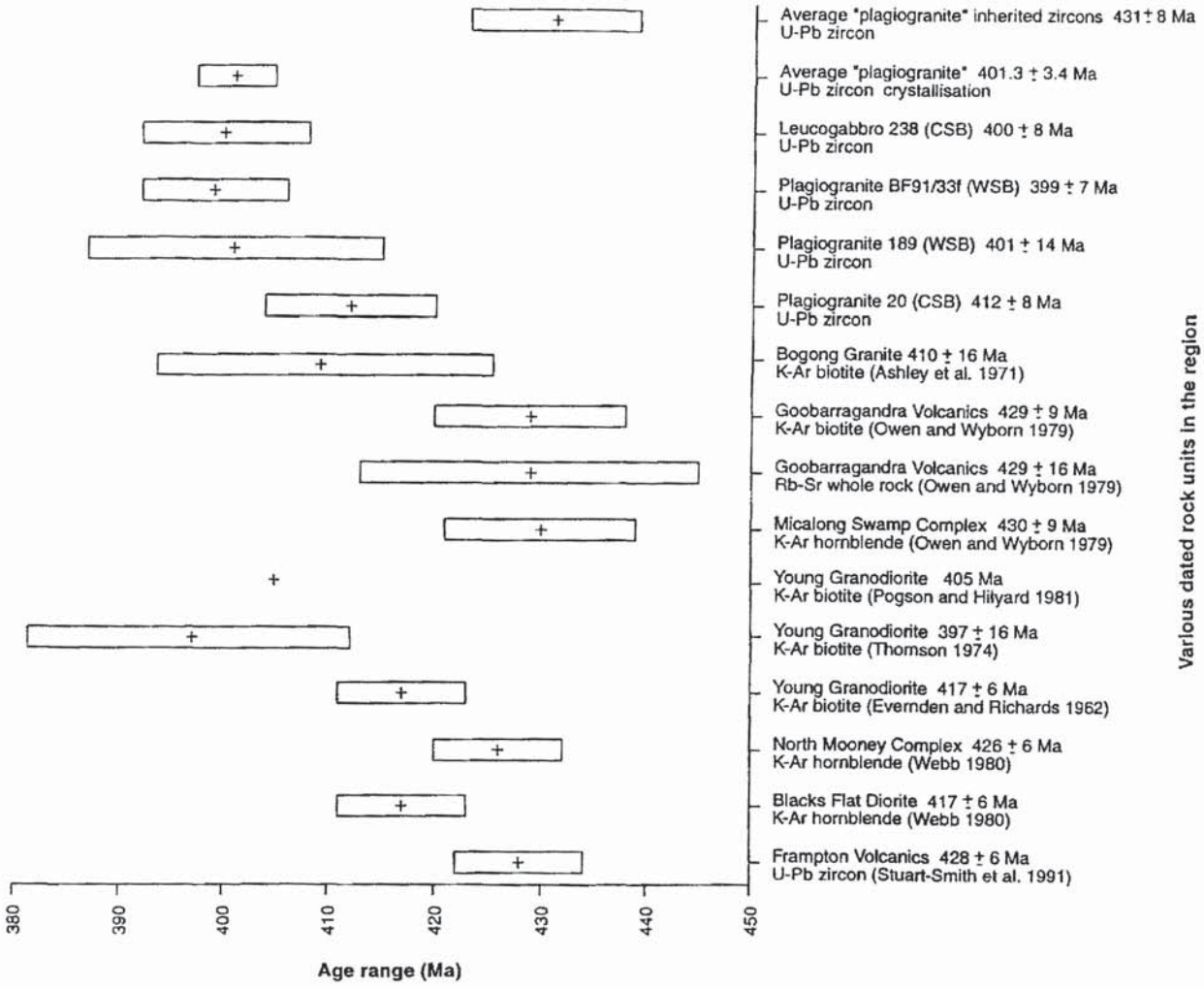

Figure 11.4 Summary of geochronological data from the rock units of the region.

The 'inherited zircon age' spans the same time period as the Goobarragandra Volcanics, Micalong Swamp Complex and Frampton Volcanics (Figure 11.4), thereby suggesting that one or more of these was responsible for the contamination of the MORB magmas prior to obduction.

The various geochronological constraints are consistent with a model in which, prior to development of the serpentinite belts, the region experienced widespread arc-related volcanic activity and was underlain by continental crust (possibly represented by the Jindalee Beds). Partial melting of the upper mantle region beneath the volcanic arc generated depleted harzburgite, but, in the far western section, a lesser degree of partial melting generated lherzolite. The latter could reflect melting at greater depth (presumably beneath thicker continental crust - e.g. Nicolas 1989), perhaps related to a melting front that migrated from deeper in the west to shallower in the east. Thus, in the most easterly region, partial melting up to the level of the Moho resulted in the dunite- and chromitite-forming MORB magmas (e.g. Nicolas 1989), and was accompanied by high T recrystallisation and plastic deformation of the harzburgite. Conversely, in the western region, partial melting was restricted to deeper within the upper mantle and conditions for producing the dunite- and chromitite-forming MORB magmas were not attained. This is consistent with the distribution of podiform chromitite deposits within the region; they increase in number and size towards the east and are absent from the most westerly belts. It is also consistent with the absence of gabbroic and basaltic rocks in the far western region.

The diapiric rise of the upper mantle derived MORB magma presumably induced rupturing of the overlying volcanic arc and enabled ascent of the magma through conduits within the upper mantle harzburgite. Dunite and chromitite crystallised first; then, as the magma ascended into higher crustal levels, it gave rise to cumulate ultramafic rocks, cumulate and non-cumulate gabbros and, on eruption MORB-type basalts. The diapiric rise may also have initiated rapid sea-floor spreading, this being deduced from the lack of well established cumulate ultramafic and mafic layered sequences and the poorly developed sheeted dyke complex (Brown 1980). Sea-floor spreading ceased because regional compression closed the basin and cut-off the magma supply. Lack of ophiolitic detritus (e.g. chromite grains, ultramafic rock fragments) in metasedimentary sequences in the region (Basden 1990) could imply that the basin was too short-lived for typical sedimentary cover sequences to form.

The most likely setting for the ophiolitic assemblages is a back-arc basin environment (e.g. the ophiolites of the Southern Andes, Chile - Dalziel *et al.* 1974). The serpentinite belts formed and were rapidly obducted following crystallisation of the plagiogranite and leucogabbro bodies. In essence, the serpentinite belts of the Tumut Serpentinite Province represent 'embryonic' ophiolites in that there was insufficient time (= spreading) for a 'typical' ophiolite to develop, but components of such an assemblage exist as commonly tectonised dyke-like bodies within and adjacent to the main harzburgite mass. Whether or not the individual belts represent a number of basins or a single basin is uncertain. However, the trace-element geochemical similarity of the same rock types from the different serpentinite belts is consistent with different slices from beneath a single basin. Circumstantial support is provided by the occurrence of the serpentinite belts occurring as parallel strips within a narrow tract. The Eurongilly Serpentinite Belt is distinctly different and is excluded from this interpretation. The slices were apparently emplaced at different levels within the continental crust, as evidenced by the different age of the host rocks.

Whilst still within an oceanic environment, solidification of the MORB intrusions induced a volume change that is expressed as a fracture network (e.g. Fyfe 1987). Downward infiltration of fluids is an inevitable consequence, particularly within an extensional tectonic regime (Nesbitt 1996). As extension changed to shortening, the fracture network selectively propagated by hydraulic processes and allowed pervasive infiltration of sea-water into the tracery of microfractures via deep master fractures. This initiated the retrogressive serpentinisation of the ultramafic rocks and concurrent metamorphism of the mafic and felsic rocks. Ongoing volume changes from progressive serpentinisation, coupled with iterative hydraulic fracture, synergistically created enhanced permeability and accompanying grain-scale alteration. As the rocks of these belts solidified only shortly before becoming emplaced into continental crust, the residual heat was an essential factor in the rodingitisation and serpentinisation of the gabbros, basalts and ultramafic rocks respectively. In order to explain some western belts experiencing serpentinisation at higher temperatures than the Coolac Serpentinite Belt, one may variously invoke a higher geothermal gradient, higher levels of residual heat, and slices derived from deeper in the mantle.

Following emplacement of the belts along the reactivated major basin-bounding faults of the region (e.g. the Mooney Mooney Fault System and Gilmore Fault Zone) the Bogong Granite intruded the southern part of the Coolac Serpentinite Belt and the Young Granodiorite intruded the Coolac and Wambidgee serpentinite belts and underwent mylonitisation along its upthrust western margin. Broadly concurrent with this, regional-scale deformation and low greenschist facies metamorphism were taking place as part of a large-scale tectonic event (the Bowning-Bindi Orogeny), that produced the NNW-SSE trending cleavage.

The ultramafic sequence of the North Mooney Complex most probably correlates with the upper mantle ultramafic serpentinite belts, whilst the North Mooney Complex gabbros and basalts are equated with the MORB components of the serpentinite belts. The Honeysuckle Beds are similarly equated with the basaltic and gabbroic rocks of the serpentinite belts and are interpreted as the top of the 'embryonic ophiolite' sequence. Thus, the mafic rocks of the North Mooney Complex and Honeysuckle Beds are equated with the mafic rocks of the serpentinite belts and represent the youngest igneous event, which, in terms of the Honeysuckle Beds, is also the youngest stratigraphic unit. The metasedimentary rocks of the Jindalee Beds are not genetically related to the serpentinite belts. They are interpreted as folded and metamorphosed pre-arc basinal sequences into which many of the serpentinite belts were emplaced.

Crystallisation of the MORB mafic and felsic intrusive rocks of the serpentinite belts occurred at approximately 412-400 Ma. Emplacement of the belts, serpentinisation of the ultramafic rocks and metamorphism/metasomatism of the mafic and felsic rocks, intrusion of the Young Granodiorite and Bogong Granite, and regional-scale deformation and greenschist facies metamorphism, all occurred within the next few million years. The collective thermotectonic event, as outlined, can be equated with the Bowning-Bindi Orogeny of the Lachlan Fold Belt.

Ophiolite generation in a region of continental crust after a relatively long period (approximately 20 m.y.) of calc-alkaline volcanism strongly suggests rifting within a magmatic arc environment. The close association of ophiolite formation and magmatic arc activity is similar to the Cretaceous tectonic setting of the southern Chilean Andes (Figure 11.5). During this period, elongate narrow basins, some 5-50 km

in width, (Dalziel 1981) opened concurrent with the generation of varying amounts of mafic crust (e.g. de Wit & Stern 1981; Bartholomew & Tarney 1984). Bruhn *et al.* (1978) and de Wit & Stern (1981) suggested that the basins resulted from mantle diapirism thinning and locally disrupting the crust. Basin opening was preceded and followed by voluminous silicic magmatism derived from the melting of deep crustal metasedimentary rocks by the rising diapir. Pillow lava and breccia grade downward into a sheeted dyke complex, in turn, underlain by locally layered gabbros; ultramafic rocks have not been observed, but this could be due to incomplete exposure as the lowermost gabbros are below sea level (Dalziel *et al.* 1974). For the basaltic rocks of these ophiolites, the concentrations of K, Sr, Ba and Rb have been affected by sea-water hydrothermal metamorphism, though other geochemical features show that they span the range from mid-oceanic basalts to the calc-alkaline field (Keller & Fisk 1992).

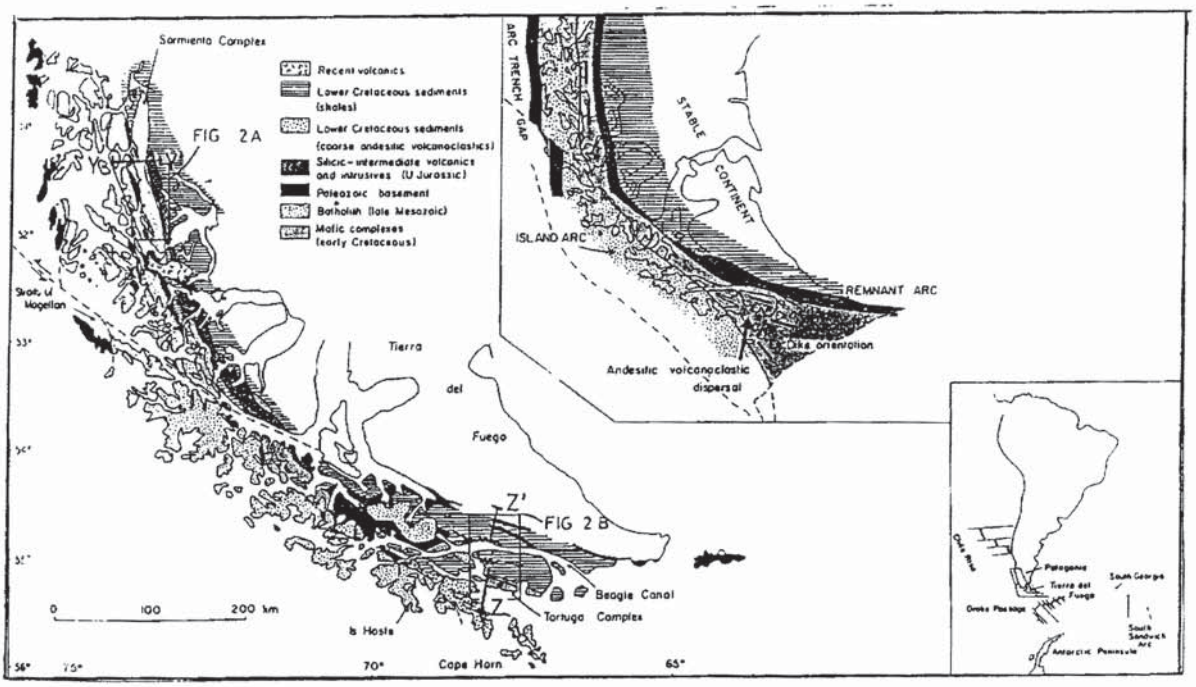

Figure 11.5 Simplified geological map of southern Chile showing the distribution of the major mafic complexes (ophiolites). Inset is a reconstruction of the major Early Cretaceous igneous-tectonic provinces (adapted from De Wit & Stern 1981).

Where the basin was sufficiently wide, ocean-floor basalts were generated, whereas within the narrower basins, transitional calc-alkaline volcanic rocks formed. According to Bartholomew and Tarney (1984), compressional periods were marked by calc-alkaline volcanism, whereas extensional periods resulted in either basaltic or bimodal silicic-basic volcanism and the high level emplacement of granitic magmas. These ophiolites are not dismembered crustal portions of a large oceanic basin but represent autochthonous mafic crust which was uplifted during closure of their respective marginal basins (Bruhn & Dalziel 1977). Their autochthonous nature requires formation in basins located on the continental margin (Keller & Fisk 1992), while tuffs and volcaniclastic sedimentary rocks overlying pillow basalts requires close proximity to an active volcanic arc (Dalziel *et al.* 1974). The present width of the Chilean ophiolites ranges from 5 km in the north to 50km in the south. However, as there is evidence of considerable shortening within the Cretaceous basin-fill, the original basins may have been as wide as 50-100 km (de Wit 1977). Warner *et al.* (1992) made similar calculations for the Tumut Trough and concluded that the trough was originally less than 100km wide.

Another possible analogue for the Tumut Serpentinite Province is the Late Tertiary to Quaternary marginal basin of Bransfield Strait (Figure 11.6). This narrow rift-basin, within the Jurassic to Tertiary Antarctic Peninsula magmatic arc, is floored by ensialic basement (Dalziel *et al.* 1974) (Figure 11.7). Some (e.g. Alabaster & Storey 1990) regard it as a back-arc basin, while others (e.g. Keller & Fisk 1992) call it a marginal basin. Arc magmatism within the South Shetland Islands mainly consists of extrusive low-K, high-alumina basalts, basaltic andesites and low-silica andesites; and intrusive gabbros, tonalites and granodiorite. The basaltic rocks of the marginal basin consist of subalkaline basalts and basaltic andesites (Keller & Fisk 1992). On the Y-Cr discrimination diagram of Pearce (1982) they straddle the mid-oceanic ridge and volcanic arc fields, whilst on CN-REE plots they have relatively flat, slightly downward curves (Keller & Fisk 1992). The basalts are also enriched in LILE relative to HFSE, this typifying arc volcanic rocks and, to a lesser extent, marginal basin basalts (Saunders & Tarney 1984; Hawkins *et al.* 1990); it is evidence for a subduction zone influence on the magmatic source of the basalts (Keller & Fisk 1992). The transition from arc-type basalts to ocean-ridge basalts requires a combination of changing sources and/or processes, as the rift propagates and widens (Keller & Fisk 1992).

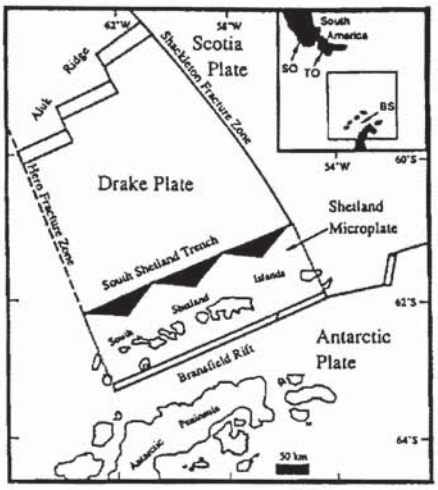

Figure 11.6 Present-day plate tectonic configuration near the Bransfield Strait. Double lines denote spreading centres, aligned triangles denote a subduction zone with the triangles pointing to the overriding plate. Abbreviations on inset map are: BS - Bransfield Strait; TO - Tortuga ophiolite; SO - Sarmiento ophiolite (adapted from Keller & Fisk 1992).

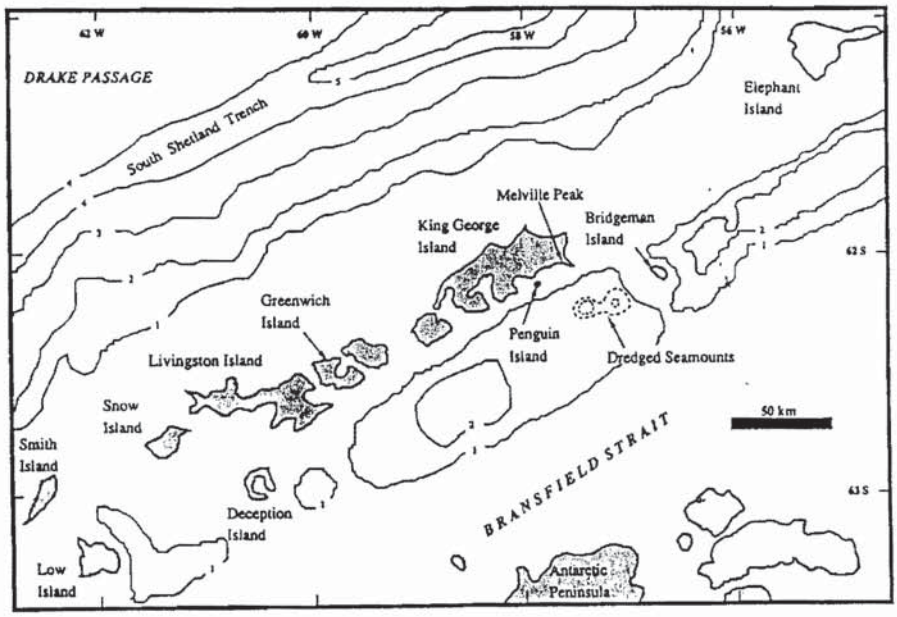

Figure 11.7 Bathymetry and relevant geography of the Bransfield Strait and South Shetland Islands. Bathymetry is contoured in km, with exception of the dredged seamounts which are contoured at 200m intervals (adapted from Keller & Fisk 1992).

In the Late Silurian and Early Devonian, the central part of the Lachlan Fold Belt was the site of rapid opening and closing of basins and regional-scale deformation (the Bowning-Bindi Orogeny - Graham *et al.* 1996). The development of these basins was controlled by basin-bounding and intrabasinal faults (e.g. Powell 1983) and their localised nature and movement directions suggest that they formed by oblique divergence and convergence (Smith & Marshall 1992). Many strike-slip faults were active during this time period within the Lachlan Fold Belt (e.g. Glen 1990; Stuart-Smith 1990; Morand & Gray 1991), so the serpentinite belts of the Tumut Serpentinite Province possibly formed in a transfer zone (a zone of crustal weakness) between the Mooney Mooney Fault System and Gilmore Fault. However, unlike other basins that formed at this time, mantle-derived magmas penetrated through deep crustal fractures leading to the development of a highly localised narrow elongate oceanic back-arc basin confined on both sides by volcanic arc rocks. After the closure of this basin at approximately 400-395 Ma, the region underwent a similar Late Palaeozoic geological history to the rest of the Lachlan Fold Belt.

The approximate age of crystallisation for the plagiogranites and leucogabbro of 412-400 Ma lies within the age range of 420-390 Ma for most of the granite bodies within the central and eastern parts of the Lachlan Fold Belt (Chappell & Stephens 1988; Chappell 1994). The crustal instability at this time most likely reflects the major thermal event that was expressed by the emplacement of voluminous I- and S-type granitic rocks throughout the fold belt. Thus, the development of both the oceanic crust of the Tumut Serpentinite Province and the generation of granitic magmas within the central and eastern parts of the Lachlan Fold Belt are symptomatic of the same Late Silurian to Early Devonian tectonothermal event. An important aspect of this is that oceanic and crustal rocks can form from complementary coeval processes within the same broad tectonic setting. The implication of this for tectonic and palaeogeographic interpretations in fold mountain belts are profound.

11.6 CONCLUSIONS

The principal objectives of this study were:

(a) To describe the geology of the serpentinite belts and then, using this information, construct a tectonic model for the relevant portion of the Lachlan Fold Belt.

(b) To determine the origin of the podiform chromitite bodies found within the serpentinite belts.

These objectives are satisfied by the following conclusions:

(a) On their eastern margins, the Coolac and Wambidgee serpentinite belts have a complex variously intruded/faulted contact with the Young Granodiorite; aplitic dykes from the granodiorite intrude both belts. On its western margin, the Coolac Serpentinite Belt has been intruded by mafic rocks of the North Mooney Complex. The Gundagai Serpentinite Belt has been intruded by the volcanic breccia phase of the Jones Creek Diorite. All other contacts for the serpentinite belts are faulted.

(b) The serpentinite bodies predominantly have the same geometry, orientation, serpentinised harzburgitic composition and geochemistry; the barely serpentinised portions of the Coolac Serpentinite Belt and lherzolitic Eurongilly Serpentinite Belt constitute compositional exceptions.

(c) Dunites and other ultramafic rocks, and gabbros and mafic volcanic rocks of the serpentinite belts, North Mooney Complex, and Honeysuckle Beds, are petrographically similar, have MORB geochemical affinities. They are unrelated to the Micalong Swamp Complex.

(d) Plagiogranites of the serpentinite belts are geochemically akin to plagiogranites from ophiolite complexes, but they differ from granitic rocks of the Young Granodiorite and tonalites of the Micalong Swamp Complex.

(e) Layering in the Coolac and Wambidgee serpentinite belts is ascribed to primary magmatic processes. Foliations within the serpentinite belts have broadly similar orientations and are ascribed to the one major ductile-brittle deformational event subsequent to serpentinisation. The Coolac and Tumut Ponds serpentinite belts, and the Western Wambidgee Serpentinite Melange, underwent serpentinisation during low greenschist facies conditions, whereas the other serpentinite were serpentinised under upper greenschist to middle amphibolite facies conditions.

(f) Geochronological investigation have shown that the intrusive MORB sequence of the serpentinite belts crystallised at 412-400 Ma. A 430 Ma age from inherited zircons lies within the age limit of volcanic arc sequences within the region. Plagiogranites and leucogabbros just overlap published ages for the Young Granodiorite and Bogong Granite, thereby requiring the former to have been emplaced shortly after crystallisation. Provisional Sm-Nd isotope studies support the zircon data.

(g) The chromitites range from Al-rich to Al-poor and are akin to podiform chromitites from the upper mantle Section of ophiolite complexes from around the world. They crystallised from a MORB-type magma due to changing conditions (e.g. oxygen fugacity, magmatic pressure) within narrow cavities in upper mantle harzburgite just below the Moho. The present distribution of chromitite types reflects the space/time distribution of progressive fractionation (Al increases with fractionation) of the MORB-type source. There is no evidence for the chromitite types deriving from different source magmas.

(h) The serpentinite belts are here interpreted as ophiolites of 'embryonic' type that formed within a back arc basin in the Late Silurian-Early Devonian. Typical 'ophiolite' stratigraphy did not develop as the back arc basin was very short-lived. Crystallisation of the MORB sequence and emplacement onto continental crust with accompanying metamorphism and deformation spanned some 20 Ma.

(i) In the Late Silurian to Early Devonian, the Tumut Serpentinite Province differed from similarly aged basins elsewhere in the Lachlan Fold Belt. A volcanic arc was ruptured by ascending mantle-derived MORB magmas and gave rise to the Tumut back-arc basin. This event was short lived and, after the Early Devonian, the Tumut region behaved like other parts of the Lachlan Fold Belt.

(j) Podiform chromitites of the Tumut Serpentinite Province have been used to restrict the tectonic environment of formation of the serpentinite belts. Their fracture-fill assemblages record the mineralogical evolution and constrain the environmental conditions within the belts. Other rocktypes similarly provide data on the crystallisation and evolving nature of the serpentinite belts.

(k) The Tumut Serpentinite Province is the tract between the Gilmore Fault Zone and Mooney Mooney Fault System that embraces the serpentinite belts and affiliated rock units. The belts and intrusive MORB sequences collectively comprise the Tumut Ophiolite Belts.

LIST OF REFERENCES

ADAMSON, C.L., 1953. Reconnaissance geology of the Snowy Mountains area. Progress Report No.7 - Tumut valley near Talbingo. *New South Wales Department of Mines Technical Report* **1**.

ADAMSON, C.L., 1954. Reconnaissance geology of the Snowy Mountains area. Progress Report No.11 - Yarrangobilly. *New South Wales Department of Mines Technical Report* **3**.

ADAMSON, C.L., 1960. Reconnaissance geology of the Snowy Mountains area. Progress Report No.16 - Tumut. *New South Wales Department of Mines - Technical Report* **5**, for 1957, 138-154.

ADAMSON C.L. & LOUDON A.G., 1966. *Wagga Wagga 1:250,000 Geological Sheet SI 55-15.* Geological Survey of New South Wales, Sydney.

AGAR, S.M., 1994. Rheological evolution of the ocean crust: a microstructural review. *Journal of Geophysical Research* **99(B2)**, 3175-3200.

AHMED, Z., 1984. Stratigraphic and textural variations in the chromite composition of the ophiolitic Sakhakot-Qila Complex, Pakistan. *Economic Geology* **79**, 1334-1359.

AITCHISON, J.C., BLAKE, M.C. (Jr), FLOOD, P.G. & JAYKO, A.S., 1994. Palaeozoic ophiolitic assemblages within the southern New England orogen of eastern Australia: implications for growth of the Gondwana margin. *Tectonics* **13(5)**, 1135-1149.

AITCHISON, J.C. & IRELAND, T.R., 1995. Age profile of ophiolitic rocks across the late Paleozoic New England Orogen, New South Wales: implications for tectonic models. *Australian Journal of Earth Sciences* **42,** 11-23.

AITCHISON, J.C., IRELAND, T.R., BLAKE, M.C. (Jr) & FLOOD, P.G., 1992. 530 Ma zircon age of ophiolite from the New England orogen: oldest rocks known from eastern Australia. *Geology* **20,** 125-128.

ALABASTER, T. & STOREY, D.C., 1990. Modified Gulf of California model for South Georgia, north Scotia Ridge and implications for the Rocas Verdes back-arc basin, southern Andes. *Geology* **18,** 497-500.

ARAI, S. & ABE, N., 1994. Podiform chromitite in the arc mantle: chromitite xenoliths from the Takashima alkali basalt, southwest Japan arc. *Mineralium Deposita* **29,** 434-438.

ARAI, S. & YURIMOTO, H., 1994. Podiform chromitites of the Tari-Misaka ultramafic complex, southwestern Japan, as mantle-melt interaction products. *Economic Geology* **89,** 1279-1288.

ARAI, S. & YURIMOTO, H., 1995. Possible sub-arc origin of podiform chromitites. *The Island Arc* **4,** 104-111.

ASHLEY, P.M., 1967. *The geology of the Red Hill - Brungle Creek district, Tumut, NSW.* BSc (Hons) Thesis, University of Sydney, Sydney (unpublished).

ASHLEY, P.M., 1968. Bogong copper mine, Tumut. *Geological Survey of New South Wales, Report GS 1968/274* (unpublished).

ASHLEY, P.M., 1969a. The petrology and mineralisation of the Coolac Serpentine Belt east of Brungle, NSW. *Proceedings of the Australasian Institute of Mining and Metallurgy* **230**, 19-27.

ASHLEY, P.M., 1969b. Pine Mountain Mine Tumut, NSW. *Geological Survey of New South Wales, Report GS 1969/048* (unpublished).

ASHLEY, P.M., 1970. Discussion and contributions: The petrology and mineralisation of the Coolac Serpentine Belt east of Brungle, NSW. *Proceedings of the Australasian Institute of Mining and Metallurgy* **234,** 81-82.

ASHLEY, P.M., 1973a. *Ultramafic and associated rocks near Tumut, NSW.* PhD Thesis, Macquarie University, Sydney (unpublished).

ASHLEY, P.M., 1973b. Petrogenesis of sulphide-bearing reaction zones in the Coolac ultramafic belt, NSW, Australia. *Mineralium Deposita* **8**, 370-378.

ASHLEY, P.M., 1974. Stratabound pyritic sulphide occurrences in an ophiolite rock assemblage near Tumut, NSW. *Journal of the Geological Society of Australia* **21(1),** 53-62.

ASHLEY, P.M., 1975a. Opaque mineral assemblage formed during serpentinisation in the Coolac ultramafic belt, NSW. *Journal of the Geological Society of Australia* **22(1),** 91-102.

ASHLEY, P.M., 1975b. Southern serpentinite belts, *In*: Markham N.L. & Basden H. (eds), *The Mineral Deposits of New South Wales,* p.184-194. Geological Survey of New South Wales, Sydney.

ASHLEY, P.M., 1997. Silicate-carbonate alteration zones and gold mineralisation in the Great Serpentinite Belt, New England Orogen, New South Wales. *In*: Ashley, P.M., and Flood, P.G.

(eds), *Tectonics and Metallogenesis of the New England Orogen*. Geological Society of Australia Special Publication 19, 212-225.

ASHLEY, P.M. & BASDEN, B., 1973. Revision of nomenclature of granitic intrusions at Burrinjuck, Young and Cowra. *Records of the Geological Survey of New South Wales* **15,** 213-220.

ASHLEY, P.M., BROWN, P.F., FRANKLIN, B.J., RAY, A.S. & SCHEIBNER, E., 1979. Field and geochemical characteristics of the Coolac ophiolite suite and its possible origin in a marginal sea. *Journal of the Geological Society of Australia* **26(1),** 45-60.

ASHLEY, P.M. & CHENHALL, B.E., 1976. Mylonitic rocks in the Young Granodiorite, southern NSW. *Journal and Proceedings of the Royal Society of New South Wales* **109(1-2),** 25-33.

ASHLEY, P.M., CHENHALL, B.E., CREMER, P.L. & IRVING, A.J., 1971. The geology of the Coolac Serpentinite and adjacent rocks east of Tumut, NSW. *Journal and Proceedings of the Royal Society of New South Wales* **104,** 11-29.

ASHLEY, P.M., FRANKLIN, B.J. & RAY, A.S., 1983. Plagiogranites in the Coolac ophiolite suite, New South Wales, Australia. *Geological Magazine* **120(1),** 1-20.

AUCLAIR, M., GAUTHIER, M., TROTTIER, J., JEBRAK, M. & CHARTRAND, F., 1993. Mineralogy, geochemistry, and paragenesis of the Eastern Metals serpentinite-associated Ni-Cu-Zn deposit, Quebec Appalachians. *Economic Geology* **88,** 123-138.

AUGE, T. 1987. Chromite deposits in the northern Oman ophiolite: mineralogical constraints. *Mineralium Deposita* **22,** 1-10.

AUGE, T. 1988. Platinum group minerals in the Tiebaghi and Vourinos ophiolitic complexes: genetic implications. *Canadian Mineralogist* **26,** 177-192.

BACUTA, G.C. (Jr), KAY, R.W., GIBBS, A.K. & LIPIN, B.R., 1990. Platinum-group element abundance and distribution in chromite deposits of the Acoje Block, Zambales Ophiolite Complex, Phillipines. *Journal of Geochemical Exploration* **37,** 113-145.

BALLANTYNE, P., 1992. Petrology and geochemistry of the plutonic rocks of the Halmahera ophiolite, Eastern Indonesia, an analogue of modern oceanic forearcs. *In*: Parson, L.M., Murton, B.J. & Browning, P. (eds), *Ophiolites and their Modern Oceanic Analogues,* p.179-202. The Geological Society, London.

BARNES, S.J., NALDRETT, A. & GORDON, M.P., 1985. The origin of the fractionation of platinum-group elements in terrestrial magmas. *Chemical Geology* **53,** 303-323.

BARNES, C.G., PETERSEN, S.W., KISTLER, R.W., MURRAY, R. & KAYS, A.M., 1996. Source and tectonic implications of tonalite-trondhjemite magmatism in the Klamath Mountains. *Contributions to Mineralogy and Petrology* **123,** 40-60.

BARRON, L.M., 1972. Basaltic and nepheline olivine lamprophyric rocks from the Cootamundra area. *Petrological Report 1972/52. Geological Survey of New South Wales Report GS1972/443* (unpublished).

BARRON, L.M., 1994. Ultramafics and faulted Clifton Grove Formation siltstones and felsic volcanics. *In*: Pogson, D. & Wyborn, D. (eds), *Excursion Guide Bathurst 1: 250 000 Geological Sheet,* p.98-100. Geological Survey of New South Wales Report GS 1994/139.

BARRON, L.M., SUPPEL, D., SLANSKY, E., JOHAN, Z., OHNENSTETTER, M. & SPENCER, R., 1991. The Fifield Platinum Province. Tectonics and Metallogenesis of the Lachlan Fold Belt. *Geological Society of Australia, Abstracts and Field Trip Guide* **29**, 3.

BARTHOLOMEW, D.S. & TARNEY, J., 1984. Crustal extension in the Southern Andes (45-46°S), *In*: Kokelaar, B.P. & Howells, M.F. (eds), *Marginal Basin Geology,* p.195-205. Geological Society Special Publication **16**, Blackwell Scientific Publications, UK.

BARTHOLOMEW, I.D., 1993. The interaction and geometries of diapiric uprise centres along mid-ocean ridges - evidence from mantle fabric studies of ophiolite complexes. *In*: Prichard, H.M., Alabaster, T., Harris, N.B.W. & Neary, C.R. (eds), *Magmatic Processes and Plate Tectonics,* p.245-256. Geological Society Special Publication **76**, Geological Society Publications, UK.

BASDEN, H., 1974. Preliminary report on the geology of the Cootamundra 1: 100 000 sheet. *Geological Survey of New South Wales, Quarterly Notes* **15,** 7-18.

BASDEN, H., 1978. Preliminary report on the geology of the Tumut 1: 100 000 sheet. *Geological Survey of New South Wales Report GS 1978/322* (unpublished).

BASDEN, H., 1980. A model for the development and destruction of the Tumut trough in southern New South Wales. *Geological Survey of New South Wales Report GS 1980/212* (unpublished).

BASDEN, H., 1982. Preliminary report on the geology of the Tumut 1: 100 000 sheet area, southern New South Wales. *Geological Survey of New South Wales, Quarterly Notes* **46,** 1-18.

BASDEN, H., 1986. *Tectonostratigraphic and geochemical development of the Tumut area, southeastern New South Wales.* MSc Thesis, New South Wales Institute of Technology, Sydney (unpublished), 411p.

BASDEN, H., 1990. *Geology of the Tumut 1: 100 000 geological sheet 8527.* Geological Survey of New South Wales, Sydney.

BASDEN, H., 1990. *Tumut 1:100,000 Geological Sheet 8527.* Geological Survey of New South Wales, Sydney.

BASDEN, H., ADRIAN, J., CLIFT, D.S.L. & WINCHESTER, R.E., 1975. *Cootamundra 1:100,000 Geological Sheet 8528.* Geological Survey of New South Wales, Sydney.

BASDEN, H., ADRIAN, J., CLIFT, D.S.L. & WINCHESTER, R.E., 1978. *Geology of the Cootamundra 1:100,000 Geological Sheet 8528.* Geological Survey of New South Wales, Sydney.

BASDEN, H., FRANKLIN, B.J., MARSHALL, B. & WALTHO, A.E., 1985. Tectonostratigraphy of the Tumut trough and adjacent terranes. *In*: Leitch, E.C. & Scheibner, E. (eds), *3rd Circum-Pacific Terrane Conference, Sydney, Extended Abstracts,* p.16-21. Geological Society of Australia Abstracts **14**.

BASDEN, H., FRANKLIN, B.J., MARSHALL, B. & WALTHO, A.E., 1987. Terranes of the Tumut District, Southeastern New South Wales, Australia. *In*: Leitch, E.C. & Scheibner, E., (eds), *Terrane Accretion and Orogenic Belts*, p.57-66. American Geophysical Union Geodynamic Series **19**, American Geophysical Union.

BATES, R.L. & JACKSON, J.A. (eds), 1980. *Glossary of Geology* (2nd edition). American Geological Institute, Virginia, 640p.

BELL, J.M., CLARKE, E.C. & MARSHALL, P., 1911. The geology of the Dun Mountain subdivision, Nelson. *New Zealand Geological Survey Bulletin* **12,** 1-71.

BENSON, W.N., 1926. The tectonic conditions accompanying the intrusion of basic and ultrabasic igneous rocks. *United States National Academy of Science, Memoir* **19,** 90p.

BERTHE, D., CHOUKROUNE, P. & JEGOUZO, P., 1979. Orthogneiss, mylonite and non-coaxial deformation of granites: the example of the South Armorican shear zone. *Journal of Structural Geology* **1,** 31-42.

BISCHOFF, G.C.O. & PRENDERGAST, E.I., 1987. Newly discovered Middle and Late Cambrian fossils from the Wagonga Beds of NSW, Australia. *Neues Jahrbuch für Geologie und Palaontologie* **175,** 39-64.

BODINIER, J.L., DUPUY, C. & DOSTAL, J., 1984. Geochemistry of Precambrian ophiolites from Bou Azzer, Morocco. *Contributions to Mineralogy and Petrology* **87,** 43-50.

BODINIER, J.L., MORTEN, L., PUGA, E. & DIAZ DE FEDERICO, A., 1987. Geochemistry of ultrabasites from the Nevado-Filabride complex, Betic Cordilleras, Spain: relicts of a dismembered ophiolite sequence. *Lithos* **20,** 235-245.

BORSI, L., SCHARER, U., GOGGERO, L. & CRISPINI, L., 1996. Age, origin and geodynamic significance of plagiogranites in lherzolites and gabbros of the Piedmont-Ligurian ocean basin. *Earth and Planetary Science Letters* **140,** 227-241.

BOUDIER, F., CEULENEER, G. & NICOLAS, A., 1988. Shear zones, thrusts and related magmatism in the Oman ophiolite: initiation of thrusting on an oceanic ridge. *Tectonophysics* **151,** 275-296.

BOUDIER, F. & NICOLAS, A., 1985. Harzburgite and lherzolite subtypes in ophiolite and oceanic environments. *Earth and Planetary Science Letters* **75,** 215-222.

BOUDIER, F. & NICOLAS, A., 1995. Nature of the Moho transition zone in the Oman Ophiolite. *Journal of Petrology* **36(3),** 777-796.

BOYNTON, W.V., 1984. Geochemistry of the rare earth elements: meteorite studies. *In*: Henderson, P. (ed), *Rare Earth Element Geochemistry*, p.63-114. Elsevier, New York.

BRADLEY, G.M., 1968. *The Geology of the upper Gilmore Creek district, northeast of Batlow, N.S.W.* BSc (Hons) Thesis, University of Sydney (unpublished).

BROWN, M., 1982. *Chromite deposits and their ultramafic host rocks in the Oman ophiolite.* PhD Thesis, The Open University, London England, 264p. (unpublished).

BROWN, P.F., 1973. *Ophiolites of the central Mooney Mooney Range, a portion of the Coolac-Goobarragandra ultramafic belt, NSW.* BSc (Hons) Thesis, University of New South Wales, Sydney (unpublished).

BROWN, P.F., 1979. A sheeted dyke complex within the Coolac Ophiolite, southeastern NSW. *Journal of the Geological Society of Australia* **26,** 411-417.

BROWN, P.F., 1980. *The petrogenesis and geochemistry of an ophiolite sequence, Coolac, NSW.* PhD Thesis, University of New South Wales, Sydney (unpublished).

BRUHN, R.L. & DALZIEL, I.W.D., 1977. Destruction of the Early Cretaceous marginal basin in the Andes of Tierra del Fuego. *In*: Talwani, M. & Pitman III, W.C. (eds), *Island-Arcs, Back-Arc Basins and Deep Sea Trenches,* p.395. American Geophysical Union, Maurice Ewing Ser.**1**.

BRUHN, R.L., STERN, C.R. & DE WIT, M.J., 1978. The bearing of new field and geochemical data on the origin and development of a Mesozoic volcano-tectonic rift zone and back-arc basin in southernmost South America. *Earth and Planetary Science Letters* **41,** 32-46.

BRUNKER, R.L., OFFENBERG, A.C. & WEST, J.L., 1970. *Macquarie 1:500,000 Geological Sheet.* Geological Survey of New South Wales, Sydney.

CALLAN, T., 1984. *The geology of the Micalong Swamp Basic Igneous Complex near Wee Jasper NSW.* BAppSci (Hons) Thesis, New South Wales Institute of Technology, Sydney (unpublished).

CAMPBELL, I.H. & MURCK, B.W., 1993. Petrology of the G and H chromitite zones in the Mountain View Area of the Stillwater Complex, Montana. *Journal of Petrology* **34(2),** 291-316.

CARD, G.W., 1896. A peridotite from Gundagai. *In*: *Mineralogical and Petrological Notes, No.4,* 11-12. Records of the Geological Survey of New South Wales **5(1)**.

CARNE, J.E., 1893. Report on the chrome iron ore deposits near Coolac, in the Parish of Gobarralong, County Harden and Darbalara, County Buccleugh. *Annual Report, New South Wales Department Mines for 1892, Appendix* **5B**, 153-159.

CARNE, J.E., 1896. Further report on the chrome deposits of the Gundagai and Tumut districts. *Annual Report, New South Wales Department Mines for 1895, Appendix* **7,** 125-128.

CARNE, J.E., 1898. Notes on chromic iron ore: Its modes of occurrence, mining, dressing, uses and value; with a register of NSW localities. *Annual Report, New South Wales Department of Mines for 1897, Appendix* **5**, 143-150.

CARTER, N.L. & AVE LALLEMENT, H.G., 1970. High temperature flow of dunite and peridotite. *Geological Society of America Bulletin* **81,** 2181-2202.

CAS, R.A.F., 1983. Paleogeographic and tectonic development of the Lachlan Fold Belt of southeastern Australia. *Geological Society of Australia, Special Publication* **10,** 104p.

CAS, R.A.F., POWELL, C.Mc.A. & CROOK, K.A.W., 1980. Ordovician paleogeography of the Lachlan Fold Belt: a modern analogue and tectonic constraints. *Journal of the Geological Society of Australia* **27,** 19-32.

CAWOOD, P.A. & SUHR, G., 1992. Generation and obduction of ophiolites: constraints from the Bay of Islands Complex, western Newfoundland. *Tectonics* **11(4)**, 884-897.

CEULENEER, G., NICOLAS, A. & BOUDIER, F., 1988. Mantle flow patterns at an oceanic spreading centre: the Oman peridotite record. *Tectonophysics* **151,** 1-26.

CHAPPELL, B.W., 1994. Lachlan and New England: Fold Belts of contrasting magmatic and tectonic development. *Journal and Proceedings of the Royal Society of New South Wales* **127,** 47-59.

CHAPPELL, B.W. & STEPHENS, W.E., 1988. Origin of infracrustal (I-type) granite magmas. *Royal Society of Edinburgh Transactions, Earth Sciences* **79,** 71-86.

CHAPPELL, B.W., WHITE, A.J.R. & HINE, R., 1988. Granite provinces and basement terranes in the Lachlan Fold Belt, southeastern Australia. *Australian Journal of Earth Sciences* **35,** 505-524.

CHEADLE, P., 1993. *A mapping and petrological study of an area of the Wambidgee Serpentinite Belt in the Cootamundra region, NSW.* BAppSci (Hons) Thesis, University of Technology, Sydney (unpublished).

CHRISTIANSEN, F.G., 1985. Deformation fabric and microstructures in ophiolitic chromitites and host ultramafics, Sultanate of Oman. *Geologische Rundschau* **74,** 61-76.

CHRISTIANSEN, F.G., 1986. Deformation of chromite: SEM investigations. *Tectonophysics* **121,** 175-196.

CLARKE, D.B. & CARSWELL, D.A., 1977. Green garnets from the Newlands Kimberlite, Cape Province, South Africa. *Earth and Planetary Science Letters* **34,** 30-38.

CLIFT, D.S.L., 1967. *Geology of the Coolac-Wambidgee area.* BSc (Hons) Thesis, University of New South Wales, Sydney (unpublished).

CLOOS, M., 1984. Flow melanges and the structural evolution of accretionary melanges. *In*: Raymond, L.A. (ed), *Melanges: Their Nature, Origin and Significance*, p.71-80. Geological Society of America, Special Paper **198**.

COLEMAN, R.G., 1967. Low-temperature reaction zones and alpine ultramafic rocks of California, Oregon and Washington. *United States Geological Survey Bulletin 1247.*

COLEMAN, R.G., 1971. Petrologic and geophysical nature of serpentinites. *Bulletin of the Geological Society of America* **82,** 897-918.

COLEMAN, R.G., 1977. *Ophiolites*. Springer-Verlag, Berlin, 231p.

COLEMAN, R.G. & DONATO, M.M., 1979. Oceanic plagiogranite revisited. *In*: Barker, F., (ed), *Trondhjemites, Dacites & Related Rocks,* p.149-167. Elsevier Publishing Company, New York.

COLLINS, W.J. & VERNON, R.H., 1992. Palaeozoic arc growth, deformation and migration across the Lachlan Fold Belt, southeastern Australia. *Tectonophysics* **214,** 381-400.

COMPSTON, W., WILLIAMS, I.S., KIRSCHVINK, J.L., ZHANG, Z. & MA, G., 1992. Zircon U-Pb ages for the Early Cambrian time-scale: *Journal of the Geological Society of London* **149,** 171-184.

CONEY, P.J., 1992. The Lachlan belt of eastern Australia and Circum-Pacific tectonic evolution. *Tectonophysics* **214,** 1-25.

CONEY, P.J., EDWARDS, A., HINE, R., MORRISON, F. & WINDRIM, D., 1990. The regional tectonics of the Tasman orogenic system, eastern Australia. *Journal of Structural Geology* **2,** 289-303.

COOPER, I.B., 1985. *The geology of the Wallendbeen-Fontenoy District, NSW*. BSc (Hons) Thesis, University of Sydney, Sydney (unpublished).

COX, K.G., BELL, J.D. & PANKHURST, R.J., 1979. *The Interpretation of Igneous Rocks*. George, Allen and Unwin, London, 450p.

CRAWFORD, A.J., 1988. Cambrian. *In*:, Douglas, J.G. & Ferguson, J.A., (eds), *Geology of Victoria,* p.37-62. Geological Society of Australia, Melbourne.

CRAWFORD, A.J., CAMERON, W.E. & KEAYS, R.R., 1984. The association boninite-low-Ti andesite-tholeiite in the Heathcote Greenstone Belt, Victoria: ensimatic setting for the early Lachlan Fold Belt. *Australian Journal of Earth Sciences* **31,** 161-175.

CRAWFORD, A.J. & KEAYS, R.R., 1978. Cambrian greenstone belts in Victoria: marginal sea-crust slices in the Lachlan Fold Belt of southeastern Australia. *Earth and Planetary Science Letters* **41,** 197-208.

CROCKET, J.H., 1981. Geochemistry of the platinum-group elements. *In*: *Platinum-Group Elements: Mineralogy, Geology, Recovery*, p.47-64. Canadian Institute of Mining and Metallurgy, Special Publication **23**.

CROOK, K.A.W., 1980. Fore-arc evolution in the Tasman Geosyncline: the origin of the southeast Australian continental crust. *Journal of the Geological Society of Australia* **27,** 215-232.

CROOK, K.A.W. & FELTON, E.A., 1975. Tasman Geosyncline greenstones and ophiolites. *Journal of the Geological Society of Australia* **22(1),** 117-131.

CROOK, K.A.W. & POWELL, C.Mc.A., 1976. The evolution of the southeastern part of the Tasman Geosyncline. *25th International Geological Conference Field Guide* **17A**.

CURTIS, C.D. & BROWN, P.E., 1969. The metasomatic development of zoned ultrabasic bodies in Unst, Scotland. *Contributions to Mineralogy and Petrology* **24,** 275-292.

DADD, K.A., 1998. Incipient backarc magmatism in the Silurian Tumut Trough, New South Wales: an ancient analogue of the early Lau Basin. *Australian Journal of Earth Sciences* **45,** 109-121.

DALZIEL, I.W.D., 1981. Back-arc extension in the Southern Andes: a review and initial appraisal. *Royal Society of London Philosophical Transactions, Ser. A***300,** 319-335.

DALZIEL, I.W.D., DE WIT, M.J. & PALMER, K.F., 1974. Fossil marginal basin in the southern Andes. *Nature* **250,** 291-294.

DEER, W.A., HOWIE, R.A. & ZUSSMAN, J., 1985. *An Introduction to the Rock Forming Minerals.* 15th impression, Longman Publishing, London and New York, 528p.

DEGELING, P.R., 1977. *Wagga Wagga 1:250,000 Metallogenic Map SI 55-15.* Geological Survey of New South Wales, Sydney.

DEGELING, P.R., 1982. *Wagga Wagga 1:250,000 Metallogenic Map SI 55-15- Mine Data Sheets and Metallogenic Study.* Geological Survey of New South Wales, Sydney, 451p.

DE LA ROCHE, H., LETERRIER, J., GRANDCLAUDE, P. & MARCHAL, M., 1980. A classification of volcanic and plutonic rocks using R_1R_2 diagram and major-element analysis - its relationships with current nomenclature. *Chemical Geology* **29,** 183-210.

DEN TEX, E., 1969. Origin of ultramafic rocks, their tectonic setting and history: a contribution to the discussion of the paper "The origin of basic and ultrabasic rocks" by P.J. Wyllie. *Tectonophysics* **7,** 457-488.

DEPAOLO, D.J. & WASSERBURG, G.J., 1976. Nd isotopic variations and petrogenetic models. *Geophysical Research Letters* **3,** 249-252.

DE WIT, M.J., 1977. The evolution of the Scotia Arc as a key to the reconstruction of southwestern Gondwanaland. *Tectonophysics* **37,** 53-81.

DE WIT, M.J. & STERN, C.R., 1981. Variation in the degree of crustal extension during formation of a back-arc basin. *Tectonophysics* **72,** 229-260.

DICK, H.J.B. & SINTON, J.M., 1979. Compositional layering in alpine peridotites: evidence for pressure solution creep in the mantle. *Journal of Geology* **87,** 403-416.

DICKEY, J.S. (Jr), 1975. A hypothesis of origin for podiform chromite deposits. *Geochimica et Cosmochimica Acta* **39,** 1061-1074.

DICKINSON, W.R., HOPSON, C.A. & SALEEBY, J.B., 1996. Alternate origins of the Coast Range Ophiolite (California): introduction and implications. *GSA Today* **6(2),** 1-10.

DIEMAR, V.A., 1998. Thuddungra magnesite deposits. *In*: Berkman, D.A. & Mackenzie, D.H. (eds), *Geology of Australian and Papua New Guinea Mineral Deposits*. The Australasian Institute of Mining and Metallurgy, Melbourne, 655-660.

DIPPLE, G.M. & FERRY, J.M., 1992. Metasomatism and fluid flow in ductile fault zones. *Contributions to Mineralogy and Petrology* **112,** 149-164.

DOBBE, R.T.M., 1994. Geochemistry of cordierite-anthophyllite rocks, Tunaberg, Bergslagen Sweden. *Economic Geology* **89,** 919-930.

DUBINSKA, E., 1995. Rodingites of the eastern part of the Jordanow-Gogolow serpentinite massif, lower Silesia, Poland. *Canadian Mineralogist* **33,** 585-608.

DUPEN, P., 1986. *A study on a mylonite belt in the Mooney Mooney Thrust System near Tumut, south-eastern New South Wales*. BAppSci (Hons) Thesis, New South Wales Institute of Technology, Sydney (unpublished).

EKERS, B., 1992. *Geology of the Frampton Volcanics near the "Kerry" property, northwest of Gundagai, NSW*. BAppSci (Hons) Thesis, University of Technology, Sydney, 76p, (unpublished).

ELLIOTT, S.J., MARTIN, A.R., JONES, G.J. & DERRICK, G.M., 1991. *Geology and mineralisation of the Fifield Platinum Province, New South Wales.* 6th International Platinum Symposium Guidebook for the Pre-Symposium Excursion. Geological Society of Australia.

ENCARNACION, J.P. & MUKASA, S.B., 1993. Zircon U-Pb geochronology of the Zambales and Angat Ophiolites, Luzon, Phillipines: evidence for an Eocene arc-back arc pair. *Journal of Geophysical Research* **98(B11)**, 19,991-20,004.

EVANS, B.W., 1977. Metamorphism of alpine peridotite and serpentinites. *Annual Reviews of Earth and Planetary Science* **5,** 397-447.

EVERNDEN, J.E. & RICHARDS, J.R., 1962. Potassium-argon ages in eastern Australia. *Journal of the Geological Society of Australia* **9,** 1-49.

FERGUSSON, C.L. & CONEY, P.J., 1992. Convergence and intraplate deformation in the Lachlan Fold Belt of southeastern Australia. *Tectonophysics* **214,** 417-439.

FERGUSSON, C.L. & VANDENBERG, A.H.M., 1990. Middle Palaeozoic thrusting in the eastern Lachlan Fold Belt, southeastern Australia. *In*: Grady, A.E., James, P.R., Parker, A.J. & Platt, J.P. (eds), *Australasian Tectonics*, p.577-589. Journal of Structural Geology, **12.**

FERRY, J.M. & DIPPLE, G.M., 1991. Fluid flow, mineral reactions and metasomatism. *Geology* **19,** 211-214.

FITZPATRICK, K.R., 1976. *Cootamundra 1: 250 000 Metallogenic Map.* Geological Survey of New South Wales, Sydney.

FORTOWSKI, D., 1981. Exploration Licence No 1285. Final Report to the Department of Mineral Resources. Jododex Australia Pty Ltd. Report (GS1980/296) (unpublished).

FRANKLIN, B.J., 1975. *The geology of the North Mooney Complex- a zoned and layered mafic to ultramafic body associated with the Coolac Serpentinite Belt.* PhD Thesis, University of New South Wales, Sydney, 305p, (unpublished).

FRANKLIN, B.J., GRAHAM, I.T. & MARSHALL, B., 1992. The serpentinite belts of southern NSW- slices of Palaeozoic upper mantle? *Geological Society of Australia, Abstracts* **32,** 31.

FRANKLIN, B.J., GRAHAM, I.T. & MARSHALL, B., 1993. The genesis and evolution of podiform chromitites from southeastern Australia. *IAVCEI General Assembly, Canberra 1993 Abstracts,* 35.

FRANKLIN, B.J., MARSHALL, B., GRAHAM, I.T. & MCANDREW, J., 1992. Remobilization of PGE in podiform chromitite in the Coolac Serpentinite Belt, Southeastern Australia. *Australian Journal of Earth Sciences* **39,** 365-371.

FREY, F.A., SUEN, C-Y.J. & STOCKMAN, H.W., 1985. The Ronda high temperature peridotite: geochemistry and petrogenesis. *Geochimica et Cosmochimica Acta* **49,** 2469-2491.

FYFE, W.S., 1987. Granites and thermal structures in the lithosphere. *Geologische Rundschau* **76(1),** 15-22.

GAMBLE, J.A., SMITH, I.E.M., McCULLOCH, M.T., GRAHAM, I.J. & KOKELAAR, B.P., 1993. The geochemistry and petrogenesis of basalts from the Taupo Volcanic Zone and Kermadec Island Arc, S.W. Pacific. *Journal of Volcanology and Geothermal Research* **54,** 265-290.

GARMANN, L.B., BRUNFELT, A.O., FINSTAD, K.G. & HEIER, K.S., 1975. Rare earth element distribution in basic and ultrabasic rocks from west Norway. *Chemical Geology* **15,** 103-116.

GATES, A.E., 1991. Shear zone control on mineral deposits in the State-Line serpentinite, Pennsylvania Piedmont. *Ore Geology Reviews* **6,** 171-184.

GERLACH, D.C., LEEMAN, W.P. & AVE LALLEMANT, H.G., 1981. Petrology and geochemistry of plagiogranite in the Canyon Mountain Ophiolite, Oregon. *Contributions to Mineralogy and Petrology* **77,** 82-92.

GIBBONS, G.S., 1963. Potential of Wallendbeen talc deposits. *Geological Survey of New South Wales, Report GS1963/071* (unpublished).

GIDDEY, J.K., 1995. *The petrology of the Gundagai Serpentinite Belt, southeastern New South Wales.* BAppSci (Hons) Thesis, University of Technology, Sydney (unpublished).

GIRARDEAU, J., MARCOUX, J., FOURCADE, E., BASSOULLET, J.P. & YOUKING, T., 1985. Xainxa ultramafic rocks, central Tibet, China: tectonic environment and geodynamic significance. *Geology* **13,** 330-333.

GLEN, R.A., 1990. Formation and inversion of transtensional basins in the western part of the Lachlan Fold Belt, Australia, with emphasis on the Cobar Basin. *Journal of Structural Geology* **12,** 601-620.

GLEN, R.A., 1992. Thrust, extensional and strike-slip tectonics in an evolving Palaeozoic orogen: a structural synthesis of the Lachlan Orogen of southeastern Australia. *In*: Fergusson, C.L. & Glen, R.A. (eds), *The Palaeozoic eastern margin of Gondwanaland: Tectonics of the Lachlan Fold Belt, southeastern Australia and related orogens,* p.341-380. Tectonophysics **214**.

GOLDING, H.G., 1961. *In*: *Section of Geology. Abstract of Proceedings 1961,* p.175. Journal and Proceedings of the Royal Society of New South Wales **96**.

GOLDING, H.G., 1962. Rodingitic and aplitic inclusions in the Coolac-Goobarragandra Serpentine Belt. *Australian Journal of Science* **25,** 63.

GOLDING, H.G., 1963a. The Coolac-Goobarragandra Serpentine Belt- Preliminary Findings. (unpublished) *See*: Vallance, T.G. *In*: Packham, G.H. (ed) *Geology of New South Wales,* p.190. Journal of the Geological Society of Australia **16** (1969).

GOLDING, H.G., 1963b. The occurrence of terrestrial nickel-iron in serpentinite near Coolac, NSW. *Australian Journal of Science* **26,** 152-153.

GOLDING, H.G., 1966. *The constitution and genesis of the chrome ores in the Coolac Serpentine Belt, NSW, Australia.* PhD Thesis, University of New South Wales, Sydney (unpublished).

GOLDING, H.G., 1967. Variolitic spilite and derived metasomatites from Mt.Lightning, *In*: *Section of Geology. Abstract of Proceedings, 1966,* p.46. Journal and Proceedings of the Royal Society of NSW, **101(1)**.

GOLDING, H.G., 1969. The Coolac-Goobarragandra ultramafic belt, NSW. *Journal and Proceedings of the Royal Society of New South Wales* **102,** 173-187.

GOLDING, H.G., 1971. Local and regional trends of serpentinisation and metaserpentinisation in the Coolac-Goobarragandra ultramafic mass, NSW. *Geological Society of Australia, Special Publication* **3,** 321-329.

GOLDING, H.G., 1975. Relict textures of chromitites from NSW. *Journal of the Geological Society of Australia* **22,** 397-412.

GOLDING, H.G. & BAYLISS, P., 1968. Altered chrome ores from the Coolac Serpentine Belt, NSW, Australia. *American Mineralogist* **53,** 162-183.

GOLDING, H.G. & JOHNSON, K.R., 1971. Variation in gross chemical composition and related physical properties of podiform chromite in the Coolac District, NSW, Australia. *Economic Geology* **66,** 1017-1027.

GOLDING, H.G. & RAY, A.S., 1975a. Epidote minerals from Coolac, NSW. *Mineralogical Magazine* **40,** 205-208.

GOLDING, H.G. & RAY, A.S., 1975b. Hydrothermal Ca-Al silicates in ophiolitic rocks near Coolac, NSW. *Journal and Proceedings of the Royal Society of New South Wales* **108,** 119-130.

GOVOROV, I.N., TARARIN, I.A. & CHUDNEV, O.V., 1989. Ophiolite complexes of deep-sea trenches of the western Pacific. *Ofioliti* **14(3)**, 119-133.

GRAFENAUER, S., 1977. Genesis of chromite in Yugoslavian peridotites. *In*: Klem and Schneider.

GRAHAM, I.T., 1990. *The search for platinum-group elements and a possible genetic model for the formation and emplacement of the chromitite bodies at Mount Lightning, near Coolac, southwestern NSW.* BAppSci (Hons) Thesis, University of Technology, Sydney (unpublished).

GRAHAM, I.T. & COLCHESTER, D.M., 1995. The occurrence and origin of well-crystallised uvarovite garnet from the podiform chromitite deposits of south-eastern New South Wales. *Journal and Proceedings of the Royal Society of New South Wales* **128,** 79-88.

GRAHAM, I.T., FRANKLIN, B.J. & MARSHALL, B., 1993. Chemistry of podiform chromitite deposits, southeastern Australia. *Terra Nova, Abstract Supplement* **2,** 18.

GRAHAM, I.T., FRANKLIN, B.J. & MARSHALL, B., 1994. Evidence and timing of remobilisation in upper mantle peridotite. *Geological Society of Australia, Abstracts* **37.**

GRAHAM, I.T., FRANKLIN, B.J. & MARSHALL, B., 1996. Chemistry and mineralogy of podiform chromitite deposits, southern NSW, Australia: a guide to their origin and evolution. *Mineralogy and Petrology* **57,** 129-150

GRAHAM, I.T., FRANKLIN, B.J., MARSHALL, B., LEITCH, E.C. & FANNING, M., 1996a. Age and tectonic significance of ophiolitic rocks from the Tumut-Gundagai region of New South Wales. *Geological Society of Australia, Abstracts* **41,** 161.

GRAHAM, I.T., FRANKLIN, B.J., MARSHALL, B., LEITCH, E.C. & FANNING, M., 1996b. Tectonic significance of 400 Ma zircon ages for ophiolitic rocks from the Lachlan Fold Belt, eastern Australia. *Geology* **24**(12), 1111-1114.

GRAHAM, I.T., MARSHALL, B. & FRANKLIN, B.J., 1991a. Fluid-controlled formation and evolution of chromite, sulphides and PGE's in podiform chromitite in the Coolac Serpentinite Belt, NSW. *In: SGEG Ore Fluids Conference*, p.25.BMR Record No. 1990/95.

GRAHAM, I.T., MARSHALL, B. & FRANKLIN, B.J., 1991b. PGE remobilization, Coolac serpentinite, Australia. *In:* Pagel, M. and Leroy, J.L. (eds), *Source, Transport and Deposition of Metals*, p.619-622. Balkema, Rotterdam.

GRAHAM, I.T., MARSHALL, B. & FRANKLIN, B.J., 1993. Textures of podiform chromitite, southeastern Australia. *In:* Hach-Ali, F., Torres-Ruiz and Gervilla (eds), *Current Research in Geology Applied to Ore Deposits*, p.117-120. University of Granada, Spain.

GRAY, C.M., 1990. A strontium isotopic traverse across the granitic rocks of southeastern Australia: Petrogenetic and tectonic implications. *Australian Journal of Earth Sciences* **37,** 331-349.

GRAY, C.M. & WEBB, J.A., 1995. Provenance of Palaeozoic turbidites in the Lachlan Orogenic Belt: strontium isotope evidence. *Australian Journal of Earth Sciences* **42(1)**, 95-105.

GRAY, D.R., 1988. Structure and Tectonics. *In:* Douglas, J.G. & Ferguson, J.A., (eds), *Geology of Victoria* (2nd edition), p.1-36. Victorian Division, Geological Society of Australia, Melbourne.

GRAY, D.R., 1997. Tectonics of the southeastern Australia Lachlan Fold Belt: structural and thermal aspects. *In:* Burg, J-P & Ford, M. (eds), *Orogeny Through Time*, p.149-177. Geological Society Special Publication **121.**

GRAY, D.R. & WILLMAN, C.E., 1991. Deformation in the Ballarat slate belt, central Victoria and implications for the crustal structure across eastern Australia. *Australian Journal of Earth Sciences* **38,** 171-201.

GRAY, D.R., WILSON, C.J.L. & BARTON, T.J., 1991. Intracrustal detachments and implications for crustal evolution within the Lachlan Fold Belt, southeastern Australia. *Geology* **19,** 574-577.

GREENLY, E., 1919. The geology of Anglesey. *Great Britain Geological Survey Memoir* **1,** 980p.

HALL, L.R. & RELPH, R.E., 1957. Reconnaissance geology of the Snowy Mountains area. Progress Report No. 9. Talbingo-Tumut. *New South Wales Department of Mines Technical Report* **1**, for 1953, 9-13.

HARRIS, P.E., 1987. *A study on the Mooney Mooney Thrust System in the vicinity of Coolac, southeastern NSW.* BAppSci (Hons) Thesis, New South Wales Institute of Technology, Sydney (unpublished).

HATCHER, R.D.Jr., 1987. Tectonics of the southern and central Appalachian Internides. *Annual Review of Earth and Planetary Science* **15,** 337-362.

HAWKINS, J.W., LONDSALE, P.F., MACDOUGALL, J.D. & VOLPE, A.M., 1990. Petrology of the axial ridge of the Mariana Trough back-arc spreading center. *Earth and Planetary Science Letters* **100,** 226-250.

HELLMAN, P.L. & HENDERSON, P., 1977. Are rare earth elements mobile during spilitization? *Nature* **267,** 38-40.

HENRY, D.A. & BIRCH, W.D., 1992. Cambrian greenstone on Phillip Island, Victoria. *Australian Journal of Earth Sciences* **39,** 567-575.

HOBBS, B.E., MEANS, W.D. & WILLIAMS, P.F., 1976. *An Outline of Structural Geology.* John Wiley and Sons. 571p.

HOBBS, B.E. & ORD, A., 1987. Crustal modelling. International conference on deformation of crustal rocks. *Geological Society of Australia, Abstracts* **19,** 77.

HOLLISTER, L.S. & CRAWFORD, M.L., 1986. Melt-enhanced deformation: A major tectonic process. *Geology* **14,** 558-561.

HONNOREZ, J. & KIRST, P., 1975. Petrology of rodingites from the Equatorial Mid-Atlantic fracture zones and their geotectonic significance. *Contributions to Mineralogy and Petrology* **49,** 233-257.

HOPSON, C.A., MATTINSON, J.M. & PESSAGNO, E.A.Jr., 1981. Coast Range Ophiolite, western California. *In:* Ernst, W.G. (ed), *The Geotectonic Development of California.* Prentice-Hall, New Jersey, 418-510.

HORTON, J.W., DRAKE, A.A. & RANKIN, D.W., 1989. Tectonostratigraphic terranes and their Palaeozoic boundaries in the central and southern Appalachians. *Geological Society of America, Special Paper* **230,** 213-246.

HUCKENHOLZ, H.G., 1975. Uvarovite stability in the $CaSiO_3$-Cr_2O_3 join. *Neues Jahrbuch für Mineralogie Monatschefte,* 337-360.

HUCKENHOLZ, H.G. & KNITTEL, D., 1975. Uvarovite: Stability of Uvarovite-Grossularite Solid Solution at low pressure. *Contributions to Mineralogy and Petrology* **49,** 211-231.

HULBERT, L.J. & VON GRUENEWALDT, G., 1985. Textural and compositional features of chromite in the lower and critical zones of the Bushveld Complex south of Potgietersrus. *Economic Geology* **80,** 872-895.

IRVINE, T.N., 1967. Chromian spinel as a petrogenetic indicator. Part II: Petrologic applications. *Canadian Journal of Earth Sciences* **4,** 71-103.

IRVINE, T.N., 1982. Terminology for layered intrusions. *Journal of Petrology* **23,** 127-162.

IRVING, A.J. & ASHLEY, P.M., 1976. Amphibole-olivine-spinel, cordierite-anthophyllite and related hornfelses associated with metamorphosed serpentinites in the Goobarragandra district, near Tumut, New South Wales. *Journal of the Geological Society of Australia* **23(1),** 19-43.

JACKSON, E.D., 1967. Ultramafic cumulates in the Stillwater, Great Dyke and Bushveld intrusions. *In:* Wyllie, P.J. (ed), *Ultramafic and Related Rocks*, p.20-38. JohnWiley and Sons Inc. New York.

JACKSON, E.D. & THAYER, T.P., 1972. Some criteria for distinguishing between stratiform, concentric and alpine peridotite-gabbro complexes. *Proceedings of the 24th International Geological Congress (Montreal, Canada) Part* **2**, 289-302.

JACQUES, A.L. & CHAPPELL, B.W., 1980. Petrology and trace element geochemistry of the Papuan ultramafic belt. *Contributions to Mineralogy and Petrology* **75,** 55-70.

JACQUET, J.B., 1896a. Geological report on the Berthong Estate, near Wallendbeen. *New South Wales Department of Mines, Annual Report for 1895, Appendix* **29**, 179-180.

JACQUET, J.B., 1896b. The intrusive and metamorphic rocks of Berthong, Co. Bland, NSW, with especial reference to the occurrence of serpentine after amphibolite. *Geological Survey of New South Wales Records* **5(1)**, 18-25.

JEFFRESON, H., 1982. *The structure and emplacement of a portion of the Coolac ophiolite in the northern Mooney Mooney Range, southern NSW.* BAppSci (Hons) Thesis, New South Wales Institute of Technology, Sydney (unpublished).

JOHAN, Z., 1986. Chromite deposits in the Massif Du Sud ophiolite, New Caledonia: genetic considerations. *In:* Stowe, C.W. (ed), *Evolution of Chromium Ore Fields,* p.311-339. Van Nostrand Rheinhold, New York.

JOHAN, Z., DUNLOP, H., LE BEL, L., ROBERTS, J.L. & VOLFINGER, M., 1983. Origin of chromite deposits in ophiolitic complexes: evidence for a volatile- and sodium-rich reducing fluid phase. *Forstschrifte Mineralogische* **61**, 105-107.

JOHAN, Z., OHENSTETTER, M., SLANSKY, E., BARRON, L.M. & SUPPEL, D., 1989. Platinum mineralisation in the Alaskan-type intrusive complexes near Fifield, New South Wales, Australia. Part 1: Platinum-group minerals in clinopyroxenites of the Kelvin Grove Prospect, Owendale Intrusion. *Geological Survey of New South Wales, unpublished Report No 89/14.*

JOHNSON, S.E., VERNON, R.H. & HOBBS, B.E., 1994. Deformation and metamorphism of the Cooma Complex, southeastern Australia. *Geological Society of Australia Specialist Group in Tectonics and Structural Geology, Field Guide* **4,** 89p.

JONES, P.A., 1991. *The geology of the Rosevilla Area, north of Coolac in southern NSW.* BAppSci (Hons) Thesis, University of Technology, Sydney (unpublished).

KAY, R.W. & SENECHAL, R.G., 1976. The rare earth geochemistry of the Troodos Ophiolite Complex. *Journal of Geophysical Research* **81(5)**, 964-970

KELLER, R.A. & FISK, M.R., 1992. Quaternary marginal basin volcanism in the Bransfield Strait as a modern analogue of the Southern Chilean Ophiolites. *In:* Parson, L.M., Murton, B.J. & Browning, P. (eds), *Ophiolites and their Modern Oceanic Analogues,* p.155-169. The Geological Society, London.

KELLEY, D.S., GILLIS, K.M. & THOMPSON, G., 1993. Fluid evolution in submarine magma-hydrothermal systems at the Mid-Atlantic Ridge. *Journal of Geophysical Research* **98(B11)**, 19,579-19,596.

KELLEY, D.S., ROBINSON, P.T. & MALPAS, J.M., 1993. Processes of brine generation and evolution in the oceanic crust: fluid inclusion evidence from the Troodos ophiolite, Cyprus. *Journal of Geophysical Research* **97,** 9307-9322.

KEUSEN, H.R., 1972. Mineralogie und Petrographie des metamorphen ultramafitit-komplexes vom Geisspfad (Penninische Alpen). *Schweizer Mineralogie Petrographische Mitteilungen* **52**, 385-478.

KIMBROUGH, D.L., MATTINSON, J.M., COOMBS, D.S., LANDIS, C.A. & JOHNSTON, M.R., 1992. Uranium-lead ages from the Dun Mountain ophiolite belt and Brook Street terrane, South Island, New Zealand. *Bulletin of the Geological Society of America* **104,** 429-443.

KORSCH, R.J. & HARRINGTON, H.G., 1981. Stratigraphic and structural synthesis of the New England Orogen. *Journal of the Geological Society of Australia* **28,** 205-226.

LAGABRIELLE, Y. & CANAT, M., 1990. Alpine Jurassic ophiolites resemble the modern Central Atlantic basement. *Geology* **18,** 319-322.

LAGABRIELLE, Y., POLINO, R., AUZENDE, J.M., BLANCHET, R., CABY, R., FUDRAL, S., LEMOINE, M., MEUEL, C., OHNENSTETTER, M., ROBERT, D. & TRICART, P., 1984. Les temoins d'une tectonique intraoceanique dans le domaine Tethysien: Analyse des rapports entre les ophiolites et leurs couvertures metasedimentaires dans la zone piemontaise des Alpes franco-italiennes. *Ofioliti* **9,** 67-88.

LAGO, B.L., RABINOWICZ, M. & NICOLAS, A., 1982. Podiform chromite orebodies: a genetic model. *Journal of Petrology* **23,** 103-125.

LAROCQUE, A.C.L. & HODGSON, C.J., 1995. Effects of greenschist-facies metamorphism and related deformation on the Mobrun massive sulfide deposit, Quebec, Canada. *Mineralium Deposita* **30(6),** 439-448.

LAURENT, R. & HEBERT, Y., 1979. Paragenesis of serpentine assemblages in harzburgite tectonite and dunite cumulate from the Quebec Appalachians. *Canadian Mineralogist* **17(4)**, 857-869.

LAWRENCE, L.J. & GOLDING, H.G., 1970. A cubanite-rich sulphide ore associated with ultramafic rocks near Tumut, NSW. *Proceedings of the Australasian Institute of Mining and Metallurgy* **231,** 33-39.

LEACH, T.M. & RODGERS, K.A., 1978. Metasomatism in the Wairere Serpentinite, King Country, New Zealand. *Mineralogical Magazine* **42,** 45-62.

LEBLANC, M., 1980. Chromite growth, dissolution and deformation from a morphological view point: SEM investigations. *Mineralium Deposita* **16,** 269-282.

LEBLANC, M., 1985. Les gisements de spinelles chromiferes. *Bulletin Mineralogie* **108,** 587-602.

LEBLANC, M., 1986. Chromite in ocean arc environments: New Caledonia. *In:* Stowe, C.W. (ed), *Evolution of Chromium Ore Fields,* p.265-296. Van Nostrand Rheinhold, New York.

LEBLANC, M., 1995. Chromitite and ultramafic rock compositional zoning through a palaeotransform fault, Poum, New Caledonia. *Economic Geology* **90,** 2028-2039.

LEBLANC, M., CASSARD, D. & JUTEAU, T., 1981. Cristallisation et deformation des orbicules de chromite. *Mineralium Deposita* **16,** 269-282.

LEBLANC, M. & VIOLETTE, J-F., 1983. Distribution of aluminium-rich and chromium-rich chromite pods in ophiolitic peridotites. *Economic Geology* **78,** 293-301.

LEBLANC, M. & CEULENEER, G., 1992. Chromite crystallisation in a multicellular magma flow: evidence from a chromitite dike in the Oman ophiolite. *Lithos* **27,** 231-257.

LEITCH, E.C., 1982. Crustal development in New England. *In:* Flood, P.G. & Runnegar, B. (eds), *New England Geology, Voisey Symposium Volume,* p.9-16. University of New England , Armidale, New South Wales.

LEITCH, E.C., 1984. Island arc elements and arc-related ophiolites. *Tectonophysics* **106,** 177-203.

LE MAITRE, R.W., 1989. *A Classification of Igneous Rocks and Glossary of Terms.* Blackwell Scientific Publications. 193p.

LEVEN, J., STUART-SMITH, P.G., MUSGROVE, B., RICKARD, M. & CROOK, K.A.W., 1991. A geophysical survey across the Tumut Synclinorial Zone, NSW. *Geological Society of Australia Abstracts* **29,** 31.

LIGHTNER, J.D., 1977. *The stratigraphy, structure and depositional history of the Tumut region, New South Wales.* MSc Thesis, Australian National University, Canberra (unpublished).

LINDER, D.E., WYLIE, A.G. & CANDELA, P.A., 1992. Mineralogy and origin of the State Line talc deposit, Pennsylvania. *Economic Geology* **87,** 1607-1615.

LIPPARD, S.J., SHELTON, A.W. & GASS, I.G., 1986. (eds). *The Ophiolite of Northern Oman.* Geological Society Memoir No. **11.**

LISTER, G.S., 1998. What is a metamorphic core complex and how does it form? *Geological Association of Canada, Canadian Tectonics Group 18th Annual Meeting 'Evolution of Structures in Deforming Rocks'. September 26-28, 1998.*

LISTER, G.S. & SNOKE, A.W., 1984. S-C Mylonites. *Journal of Structural Geology* **6(6),** 617-638.

LLOYD, J.C., 1942. Wallendbeen chromite deposits. *Geological Survey of New South Wales Report GS1942/037* (unpublished).

LOHAN, A.J., 1982. *Fabrics in and adjacent to chromite bodies in the Coolac Serpentinite Belt, near Coolac, NSW.* BAppSci (Hons) Thesis, New South Wales Institute of Technology, Sydney (unpublished).

LORAND, J.P. & CEULENEER, G., 1989. Silicate and base-metal sulfide inclusions in chromites from the Maqsad area (Oman ophiolite, Gulf of Oman): a model for entrapment. *Lithos* **22,** 173-190.

LOUBET, M., SHIMIZU, N. & ALLEGRE, C.J., 1975. Rare earth elements in alpine peridotites. *Contributions to Mineralogy and Petrology* **53,** 1-12.

LYONS, M.T., BROOKS, R.R. & CRAIG, D.C., 1975. The influence of soil composition on the vegetation of the Coolac Serpentinite Belt in NSW. *Journal and Proceedings of the Royal Society of New South Wales* **107(3-4),** 67-75.

MACKLIN, S., 1985. *The geology of an area east of Cootamundra, NSW, in the Bogan Gate Synclinorial Zone*. BAppSci (Hons) Thesis, New South Wales Institute of Technology, Sydney (unpublished).

MARSHALL, B. & FRANKLIN, B.J., 1992. Structural, igneous and tectonic implications of the Coolac Serpentinite/Young Granodiorite boundary, southeastern NSW. *Geological Society of Australia Abstracts* **32,** 235-236.

McANDREW, J., 1989. The mineralogy of platinum group elements in ophiolite peridotite, New Caledonia. *In: Mineralogy-Petrology Symposium, Sydney* p.37-43. Australasian Institute of Mining & Metallurgy, Sydney Branch.

McANDREW, J., SIE, S.H. & FINLAY, C.J., 1987. Platinum-group elements and their mineralogical occurrence in podiform chromitite, New Caledonia. *CSIRO Division of Mineral Physics and Mineralogy. Restricted Investigation Report.*

McBIRNEY, A. & NOYES, R.M., 1979. Crystallisation and layering of the Skaergaard intrusion. *Journal of Petrology* **20,** 487-554.

MENZIES, M., 1976. Rare earth geochemistry of fused ophiolitic and alpine lherzolites- I. Othris, Lanzo and Troodos. *Geochimica et Cosmochimica Acta* **40,** 645-656.

MENZIES, M., BLANCHARD, D., BRANNON, J. & KOROTEV, R., 1977. Rare earth and trace element geochemistry of a fragment of Jurassic seafloor, Point Sal, California. *Geochimica et Cosmochimica Acta* **41,** 1419-1430.

MENZIES, M., BLANCHARD, D. & XENOPHONTOS, C., 1980. Genesis of the Smartville arc-ophiolite, Sierra Nevada foothills, California. *American Journal of Science* **280-A,** 329-344.

MESCHEDE, M., 1986. A method of discriminating between different types of mid-ocean ridge basalts and continental tholeiites with the Nb-Zr-Y diagram. *Chemical Geology* **56,** 207-218.

MIYASHIRO, A., 1978. *Metamorphism and Metamorphic Belts.* 3rd impression. Unwin Brothers Limited, Surrey England. 492p.

MIYASHIRO, A., 1994. *Metamorphic Petrology.* UCL Press, London, 404p.

MOODY, J.B., 1979. Serpentinites, spilites and ophiolite metamorphism. *Canadian Mineralogist* **17(4),** 871-888.

MOORES, E.M., ROBINSON, P.T., MALPAS, J. & XENOPHONTOS, C., 1984. Model for the origin of the Troodos Massif, Cyprus and other mideast ophiolites. *Geology* **12,** 500-503.

MORAND, V.J., 1990. Low-pressure regional metamorphism in the Omeo Metamorphic Complex, Victoria, Australia. *Journal of Metamorphic Geology* **8,** 1-12.

MORAND, V.J. & GRAY, D.R., 1991. Major fault zones related to the Omeo Metamorphic Complex, northeastern Victoria. *Australian Journal of Earth Sciences* **38,** 203-221.

MORLEY, C.K., 1986. A classification of thrust fronts. *Bulletin of the American Association of Petroleum Geologists* **70,** 12-25.

NALDRETT, A.J. & DUKE, J.M., 1980. Platinum metals in magmatic sulfide ores. *Science* **208,** 1417-1428.

NEAL, C.R. & TAYLOR, L.A., 1989. A negative Ce anomaly in a peridotite xenolith: evidence for crustal recycling into the mantle or mantle metasomatism? *Geochimica et Cosmochimica Acta* **53,** 1035-1040.

NESBITT, B.E., 1996. Fluid inclusions in the study of crustal scale Paleo-fluid regimes. *In:* Brown, P.E. & Hagemann, S.G. (eds), *Program and Abstracts, PACROFI VI*, p.99-101. Madison WI USA.

NETHERY, J.E., 1975. Tumut E.L 200. Final report on exploration in the five year period to August 14, 1974. *A.O.G Minerals Pty Ltd. Report (GS1975/123)* (unpublished).

NGUYEN, V.V., 1977. Some sediments from the Gundagai district. *Geological Survey of New South Wales. Petrological Report 1977/28 (GS1977/226)* (unpublished).

NICKEL, E.H. & NICHOLS, M.C., 1991. *Mineral Reference Manual.* Van Nostrand Reinhold, New York. 250p.

NICOLAS, A., 1986. A melt extraction model based on structural studies in mantle peridotites. *Journal of Petrology* **27(4)**, 999-1022.

NICOLAS, A., 1989. *Structures of Ophiolites and Dynamics of Oceanic Lithosphere*. Kluwer Academic Publishers, Dordrecht/Boston/London. 367p.

NICOLAS, A., 1995. *The Mid-Oceanic Ridges*. Springer-Verlag, Berlin Heidelberg. 200p.

NICOLAS, A. & JACKSON, E.D, 1972. Repentition en deux provinces des peridotites des chaines alpines logeant la Mediterranee: implications geotectonique. *Schweizer Mineralogie Petrographisches Mitteilungen* **52,** 479-495.

NICOLAS, A., BOUDIER, F. & BOUCHEZ, J-C., 1980. Interpretation of peridotite structures from ophiolite and oceanic environments. *American Journal of Science* **280A,** 192-210.

NICOLAS, A. & LE PICHON, X., 1980. Structures of ophiolitic and oceanic peridotites and deformation in oceanic lithosphere. *Earth and Planetary Science Letters.*

NICOLAS, A. & CHRISTIENSEN, N.I., 1987. Formation of anisotropy in upper mantle peridotites - a review. *In:* Fuchs, K. & Froidevaux, C. (eds), *Composition, Structure and Dynamics of the Lithosphere-Asthenosphere System*, p.111-123. American Geophysical Union Geodynamic Series **16**.

NORRISH, K. & CHAPPELL, B.W., 1975. X-ray fluorescence spectrometry. *In:* Zussman, J., (ed), *Physical Methods in Determinative Mineralogy*, p.201-272. Academic Press, London.

NORRISH, K. & HUTTON, J.T., 1969. An accurate X-ray spectrographic method for the analysis of a wide range of geological samples. *Geochimica et Cosmochimica Acta* **33,** 431-453.

OFFLER, R. & WILLIAMS, A., 1987. Evidence for sinistral movement on the Peel Fault System in serpentinites, Glenrock Station, New South Wales. *In*: Leitch, E.C. & Scheibner, E. *Terrane accretion and orogenic belts*. American Geophysical Union and the Geological Society of America, Geophysical Series 19, 141-151.

OFFLER, R., McKNIGHT, S. & MORAND, V., 1998. Tectonothermal history of the Western Lachlan Fold Belt, Australia: insights from white mica studies. *Journal of Metamorphic Geology* **16**, 531-540.

OFFLER, R., MC.L MILLER, J., GRAY, D.R., FOSTER, D.A. & BALE, R., 1998. Crystallinity and b_o spacing of K-white micas in a Palaeozoic Accretionary Complex, Eastern Australia: metamorphism, palaeogeotherms, and structural style of an underplated sequence. *Journal of Geology* **106,** 495-509.

O'HANLEY, D.S., 1996. Serpentinites: records of tectonic and petrological history. *Oxford Monographs on Geology and Geophysics* **34**. Oxford University Press Inc. 277p.

O'HANLEY, D.S., SCHANDL, E.S. & WICKS, F.J., 1992. The origin of rodingites from Cassiar, British Columbia and their use to estimate T and P (H_2O) during serpentinisation. *Geochimica et Cosmochimica Acta* **56,** 97-108.

O'HANLEY, D.S. & WICKS, F.D., 1995. Conditions of formation of lizardite, chrysotile and antigorite, Cassiar, British Columbia. *The Canadian Mineralogist* **33,** 753-773.

OWEN, M. & WYBORN, D., 1979. Geology and Geochemistry of the Tantangara and Brindabella Area. *Bureau of Mineral Resources, Geology and Geophysics, Bulletin* **204**.

PAGE, N.J., CASSARD, D. & HAFTY, J., 1982. Palladium, platinum, rhodium, ruthenium and iridium in chromitites from the Massif Du Sud and Tiebaghi Massif, New Caledonia. *Economic Geology* **77,** 1571-1577.

PAGE, N.J., SINGER, D.A., MORING, B.C., CARLSON, C.A, MCDADE, J.M. & WILSON, S.A., 1986. Platinum-group element resources in podiform chromitites from California and Oregon. *Economic Geology* **81,** 1261-1271.

PAKTUNC, A.D., 1990. Origin of podiform chromitite deposits by multistage melting, melt segregation and magma mixing in the upper mantle. *Ore Geology Reviews* **5,** 211-222.

PALLISTER, J.S. & KNIGHT, R.J., 1981. Rare-earth element geochemistry of the Semail Ophiolite near Ibra, Oman. *Journal of Geophysical Research* **86(B4)**, 2673-2697.

PARK, A.F., 1989. Intrusion-layered. *In:* Bowes, D.R. (ed), *The Encyclopedia of Igneous and Metamorphic Petrology*, 253-256. Van Nostrand Rheinhold, New York.

PARKER, R., 1993. *Geology of the "Warralong" and "the Hill" properties Coolac, NSW.* BAppSci (Hons) Thesis, University of Technology, Sydney (unpublished).

PEARCE, J.A., 1975. Basalt geochemistry used to investigate past tectonic environments on Cyprus. *Tectonophysics* **25,** 41-67.

PEARCE, J.A., 1976. Statistical analysis of major element patterns in basalt. *Journal of Petrology* **17,** 15-43.

PEARCE, J.A., 1982. Trace element characteristics of lavas from destructive plate boundaries. *In:* Thorpe, R.S. (ed), *Andesites*, p.525-548. Wiley, Chichester.

PEARCE, J.A., 1983. Role of sub-continental lithosphere in magma genesis at active continental margin. *In:* Hawkesworth, C.J. & Norry, M.J. (eds), *Continental Basalts and Mantle Xenoliths* p.230-249. Shira Publishing, Nantwich.

PEARCE, J.A., 1991. Ocean floor comes ashore. *Nature* **354,** 110-111.

PEARCE, J.A. & CANN, J.R., 1973. Tectonic setting of basic volcanic rocks determined using trace element analysis. *Earth and Planetary Science Letters* **19,** 290-300.

PEARCE, J.A. & NORRY, M.J., 1979. Petrogenetic implications of Ti, Zr, Y and Nb variations in volcanic rocks. *Contributions to Mineralogy and Petrology* **69,** 33-47.

PEARCE, J.A., LIPPARD, S.J. & ROBERTS, S., 1984. Characteristics and tectonic significance of supra-subduction zone ophiolites. *In:* Kokelaar, B.P. & Howells, M.F. (eds), *Marginal Basin Geology (Volcanic and associated sedimentary and tectonic processes in modern and ancient marginal basins)*, p.77-94. Geological Society Special Publication **16**. Blackwell Scientific Publications, London.

PFEIFER, H-R., 1987. A model for fluids in metamorphosed ultramafic rocks: IV. Metasomatic veins in metaharzburgites of Cima di Gagnone, Valle Verzasca, Switzerland. *In:* Helgeson, H.C. (ed), *Chemical Transport in Metasomatic Processes*, p.591-632. D. Reidel Publishing.

PHILLIPS, W.J., 1972. The role of differential stress in the formation and migration of hydrothermal fluids. *International Geological Congress, Abstracts* **24,** 143.

PIN, C. & CARME, F., 1987. A Sm-Nd isotopic study of 500 Ma old oceanic crust in the Variscan Belt of Western Europe: the Chamrousse ophiolite complex, western Alps (France). *Contributions to Mineralogy and Petrology* **96,** 406-413.

PITTMAN, E.F., 1882. Progress Report for 1881. *New South Wales Department of Mines, Annual Report for 1881, Appendix* **C,** 139-141.

PLATT, J.P. & VISSERS, R.L.M., 1989. Extensional collapse of thickened continental lithosphere: A working hypothesis for the Alboran Sea and Gilbraltar arc. *Geology* **17,** 540-543.

POGSON, D.J. & HILYARD, D., 1981. Results of isotopic age dating related to Geological Survey of New South Wales investigations, 1974-1978. *Geological Survey of New South Wales, Records* **20(2),** 251-273.

POWELL, C.Mc.A., 1983. Tectonic relationships between the Late Ordovician and Late Silurian palaeogeographies of southeastern Australia. *Australian Journal of Earth Sciences* **30,** 353-373.

POWELL, C.Mc.A., 1984. Uluru regime. *In:* Veevers, J.J. (ed), *Phanerozoic Earth History of Australia,* p.290-337, Oxford Geological Sciences Series **2.**

POWELL, C.Mc.A. & EDGECOMBE, D.R., 1978. Mid-Devonian movements in the northeastern Lachlan Fold Belt. *Journal of the Geological Society of Australia* **25,** 165-184.

PRICE, R.A. & HATCHER, R.D., 1983. Tectonic significance of similarities in the evolution of the Alabama Pennsylvania Appalachians and the Alberta-British Columbia Canadian Cordillera. *In:* Hatcher, R.D., Williams, H. & Zietz, I. (eds), *The Tectonics and Geophysics of Mountain Chains,* p.149-160. Geological Society of America, Memoir **158.**

PRICHARD, H.M., 1985. The Shetland Ophiolite. *In:* Gee, D.G. & Sturt, B.A. (eds), *The Caledonide Orogen- Scandinavia and Related Areas,* p.1173-1184. John Wiley and Sons Ltd.

PRICHARD, H.M. & LORD, R.A., 1990. Platinum and palladium in the Troodos Ophiolite Complex, Cyprus. *Canadian Mineralogist* **28,** 607-617.

PRICHARD, H.M. & NEARY, C.R., 1982. Some observations on the chromite in the Shetland ophiolite complex. *Ofioliti* **2/3,** 455-466.

RAMSAY, J.G. & HUBER, M.I., 1983. *The Techniques of Modern Structural Geology, Volume 1: Strain Analysis.* Academic Press, London, 1-306.

RAMSAY, J.G. & HUBER, M.I., 1987. *The Techniques of Modern Structural Geology, Volume 2: Folds and Fractures.* Academic Press, New York, 307-700.

RAY, A.S., 1977. *Petrology of ultramafic and related rocks at Mount Lightning near Coolac, NSW.* PhD Thesis, University of New South Wales, Sydney (unpublished).

RAYMOND, L.A., 1975. Tectonite and melange - a distinction. *Geology* **3,** 7-9.

RAYMOND, L.A., 1984. Melanges: Their nature, origin and significance. *In*: Raymond, L.A. (ed), *The Geological Society of America, Special Paper* **198,** 170p.

REYNOLDS, P., 1993. *Genesis of the Thuddungra magnesite deposit and serpentinisation of the Thuddungra area, near Young, NSW.* BAppSci (Hons) Thesis, University of Technology, Sydney (unpublished).

RICHARD, P., SHIMIZU, N. & ALLEGRE, C.J., 1976. $^{143}Nd/^{146}Nd$, a natural tracer: an application to oceanic basalts. *Earth and Planetary Science Letters* **31,** 269-278.

ROBERTS, S., 1988. Ophiolitic chromitite formation: a marginal basin phenomenon? *Economic Geology* **83,** 1034-1036.

ROCK, N.M.S., 1991. *Lamprophyres.* Blackie and Son Ltd, London.

ROLLINSON, H.R., 1993. *Using Geochemical Data: Evaluation, Presentation, Interpretation.* Longman Scientific and Technical, England, 352p.

ROSE, G., 1967. *Cootamundra 1:250 000 Geological Sheet.* Geological Survey of New South Wales, Sydney.

SALEEBY, J.B., SHAW, H.F., NIEMEYER, S., MOORES, E.M. & EDELMAN, S.H., 1989. U/Pb, Sm/Nd & Rb/Sr geochronological and isotopic study of northern Sierra Nevada ophiolitic assemblages, California. *Contributions to Mineralogy and Petrology* **102,** 205-220.

SAUNDERS, A.D. & TARNEY, J., 1984. Geochemical characteristics of basaltic volcanism within back-arc basins. *In:* Kokelaar, B.P. & Howells, M.F. (eds), *Marginal Basin Geology,* p.59-76. Geological Society, London Special Publication **16**.

SCHANDL, E.S., O'HANLEY, D.S. & WICKS, F.J., 1989. Rodingites in serpentinised ultramafic rocks of the Abitibi greenstone belt, Ontario. *Canadian Mineralogist* **27,** 579-591.

SCHANDL, E.S., O'HANLEY, D.S. & WICKS, F.J., 1990. Fluid inclusions in rodingite: a geothermometer for serpentinisation. *Economic Geology* **85,** 1273-1276.

SCHEIBNER, E., 1972. The Kanmantoo Pre-Cratonic Province in New South Wales. *Geological Survey of New South Wales Quarterly Notes* **7,** 1-10.

SCHEIBNER, E., 1985. Suspect terranes in the Tasman Fold Belt System, eastern Australia. *In:* Howell, D.G. (ed), *Tectonostratigraphic Terranes in the Circum-Pacific Region,* p.493-514. Circum-Pacific Council for Energy and Mineral Resources, American Association of Petroleum Geologists, Earth Science Series 1.

SCHEIBNER, E., 1987. Palaeozoic tectonic development of eastern Australia in relation to the Pacific region. *In: Circum-Pacific Orogenic Belts and the Evolution of the Pacific Basin,* p.133-165. American Geophysical Union Geodynamic Series **18**.

SCHEIBNER, E., 1989. The tectonics of New South Wales in the second decade of application of the plate tectonic paradigm. *Journal and Proceedings, Royal Society of New South Wales* **122,** 35-74.

SCHEIBNER, E., 1993. Structural framework of New South Wales. *Geological Survey of New South Wales, Quarterly Notes* **93,** 1-35.

SHERVAIS, J.W., 1982. Ti-V plots and the petrogenesis of modern and ophiolitic lavas. *Earth and Planetary Science Letters* **59,** 101-118.

SHERVAIS, J.W. & KIMBROUGH, D.L., 1985. Geochemical evidence for the tectonic setting of the Coast Range Ophiolite: a composite island arc-oceanic crust terrane in western California. *Geology* **13,** 35-38.

SIBSON, R.H., 1977. Fault rocks and fault mechanisms. *Journal of the Geological Society, London* **133,** 191-213.

SIBSON, R.H., 1996. Structural permeability of fluid-driven fault-fracture meshes. *Journal of Structural Geology* **18(8)**, 1031-1042.

SKILBECK, C.G., FRANKEL, E., DADD, K.A. & LEITCH, E.C., 1992. Polymictic conglomerates of the Frampton Volcanics: pre-Benambran volcanic arc derivatives or the products of post-Benambran uplift? *Geological Society of Australia, Abstracts* **32,** 36.

SLEE, W.H.J., 1895. Report by Mr. W.H.J. Slee, F.G.S., Chief Inspector of Mines, on the Tumut district. *New South Wales Department of Mines, Annual Report for 1894,* 74-75.

SMEWING, J.D. & POTTS, P.J., 1976. Rare-earth abundances in basalts and metabasalts from the Troodos Massif, Cyprus. *Contributions to Mineralogy and Petrology* **57,** 245-258.

SMEWING, J.D., ABBOTTS, I.L., DUNNE, L.A. & REX, D.C., 1991. Formation and emplacement ages of the Masirah ophiolite, Sultanate of Oman. *Geology* **19,** 453-456.

SMITH, J.V. & MARSHALL, B., 1992. Strain distribution and fold interference in oblique contraction: Cobar Basin. *Geological Society of Australia, Abstracts* **32,** 228.

STEVENS, B.P.J. & STROUD, W.J., (eds), 1983. Rocks of the Broken Hill Block: their classification, nature, stratigraphic distribution and origin. *Records of the Geological Survey of New South Wales* **21(1)**, 1-323.

STEVENS, M.K., 1975. *The geology of the South Gundagai district.* BSc (Hons) Thesis, Australian National University, Canberra (unpublished).

STEVENS, N.C., 1952. The petrology of the Cowra intrusion and associated xenoliths. *Proceedings of the Linnean Society of New South Wales* **77(3,4),** 132-141.

STUART-SMITH, P.G., 1988. Surface geology and structure of the Tumut seismic traverse, Lachlan Fold Belt, New South Wales. *Bureau of Mineral Resources, Geology and Geophysics, Record* **1988/27**, 1-62.

STUART-SMITH, P.G., 1989. The fault history and emplacement of the Coolac Serpentinite, Lachlan Fold Belt, NSW. *Geological Society of Australia, Abstracts* **24,** 138.

STUART-SMITH, P.G., 1990a. Evidence for extensional tectonics in the Tumut Trough, Lachlan Fold Belt, NSW. *Australian Journal of Earth Sciences* **37,** 147-167.

STUART-SMITH, P.G., 1990b. The emplacement and fault history of the Coolac Serpentinite, Lachlan Fold Belt, southeastern Australia. *Journal of Structural Geology* **12,** 621-638.

STUART-SMITH, P.G., 1991a. The 'Tumut Trough' is no more. *BMR Research Newsletter* **14,** 2-3.

STUART-SMITH, P.G., 1991b. The Gilmore Fault Zone- the deformational history of a possible terrane boundary within the Lachlan Fold Belt, New South Wales. *BMR Journal of Australian Geology and Geophysics* **12,** 35-50.

STUART-SMITH, P.G., HILL, R.I., RICKARD, M.J. & ETHERIDGE, M.A., 1992. The stratigraphy and deformation history of the Tumut region: implications for the development of the Lachlan Fold Belt. *In:* Ferguson, C.L. & Glen, R.A. (eds), *The Palaeozoic Eastern Margin of Gondwanaland: Tectonics of the Lachlan Fold Belt, Southeastern Australia and Related Orogens,* p.211-237. Tectonophysics, **214**.

STUART-SMITH, P.G. & DADD, K.A., 1993. Tumut Region. IAVCEI General Assembly Excursion Guide B2. *Australian Geological Survey Organisation, Record* **1993/60,** 21p.

SUHR, G., 1993. Evaluation of upper mantle microstructures in the Table Mountain Massif (Bay of Islands ophiolite). *Journal of Structural Geology* **15,** 1273-1292.

SUPPEL, D.W., WARREN, A.Y.E., WATKINS, J.J., CHAPMAN, J., TENISON WOODS, K. & BARRON, L., 1986. A reconnaissance study of the geology and gold deposits of the West Wyalong-Temora-Adelong District. *Geological Survey of New South Wales, Quarterly Notes* **64,** 1-30.

TAKAHASHI, E. & KUSHIRO, I., 1983. Melting of a dry peridotite at high pressures and basalt magma genesis. *American Mineralogist* **68,** 859-879.

TALKINGTON, R.W., WATKINSON, D.H., WHITTAKER, P.J. & JONES, P.C., 1984. Platinum-group element-bearing minerals and other solid inclusions in chromite of ophiolitic complexes: occurrences and petrological significance. *Tschermaks Mineralogie Petrographisches Mitteilungen* **32,** 285-301.

THAYER, T.P., 1964. Principal features and origin of podiform chromite deposits and some observations in the Guleman-Soridag district, Turkey. *Economic Geology* **59,** 1497-1524.

THOMSON, J., 1974. Results of radiometric dating programme, 1971-1973. *Geological Survey of New South Wales, Record* **16(3),** 239-244.

VANDENBERG, A.H.M. & STEWART, I.R., 1992. Ordovician terranes of the southeastern Lachlan Fold Belt: Stratigraphy, structure and paleogeographic reconstruction. *Tectonophysics* **214,** 159-176.

VAN DER WAAL, D. & VISSERS, R.L.M., 1993. Uplift and emplacement of upper mantle rocks in the western Meditterranean. *Geology* **21,** 1119-1122.

VERNON, R.H., 1983. Clarke Memorial Lecture. Restite, xenoliths and microgranitoid enclaves in granites. *Journal and Proceedings, Royal Society of New South Wales* **116(3,4),** 77-103.

VERNON, R.H. & FLOOD, R.H., 1982. Some problems in the interpretation of microstructures in granitoid rocks, *In,* Flood, P.G. & Runnegar, B. (eds), *New England Geology*, p.201-210. Department of Geology, University of New England and AHV Club, Armidale NSW.

VOLLMER, F.W. & BOSWORTH, W., 1984. Formation of melange in a foreland basin overthrust setting: example from the Taconic orogen. *In:* Raymond, L.A. (ed), *Melanges: Their Nature, Origin and Significance*, p.53-70. Geological Society of America, Special Paper **198**.

WANG, P. & GLOVER III, L., 1992. A tectonics test of the most commonly used geochemical discriminant diagrams and patterns. *Earth Science Reviews* **33,** 111-131.

WARNER, P.J., 1988. *A regional study of the Mooney Mooney fault system and associated rocks in southeastern NSW.* BAppSci Thesis, New South Wales Institute of Technology, Sydney (unpublished).

WARNER, P.J., MARSHALL, B. & FRANKLIN, B.J., 1992. The Mooney Mooney Fault System and Coolac ophiolite suite in the tectonics of the Tumut Trough, southeastern Australia. *Australian Journal of Earth Sciences* **39,** 127-140.

WARREN, A.Y.E., GILLIGAN, L.B. & RAPHAEL, N.M., 1995. *Explanatory notes for the Cootamundra 1: 250 000 geological sheet SI/55-11.* Geological Society of New South Wales, Sydney.

WEBB, A.W., 1980. K-Ar analyses (Tumut area). Unpublished report, the Australian Mineral Development Laboratories, AC 5446/80.

WHITE, A.J.R. & CHAPPELL, B.W., 1983. Granitoid types and their distribution in the Lachlan Fold Belt, southeastern Australia. *Geological Society of America, Memoir* **159,** 21-34.

WHITTAKER, P.J. & WATKINSON, D.H., 1984. Genesis of chromite from the Mitchell Range, central British Columbia. *Canadian Mineralogist* **22,** 161-172.

WHITWORTH, H.F., 1942. Mineralogical note on chromite from the Wallendbeen district. *Geological Survey of New South Wales, Report GS942/039* (unpublished).

WICKS, F.J., 1984. Deformational histories as recorded by serpentinites. I. Deformation prior to serpentinisation. *Canadian Mineralogist* **22,** 185-195.

WICKS, F.J. & WHITTAKER, E.J.W., 1977. Serpentine textures and serpentinisation. *Canadian Mineralogist* **15,** 459-488.

WICKS, F.J. & PLANT, G., 1979. Electron microprobe and X-ray microbeam studies of serpentinite textures. *Canadian Mineralogist* **17,** 785-830.

WILLIAMS, I.S. & CLAESSON, S., 1987. Isotopic evidence for the Precambrian province and Caledonian metamorphism of high grade paragneisses from the Seve Nappes, Scandinavian Caledonides. II. Ion microprobe zircon U-Th-Pb. *Contributions to Mineralogy and Petrology* **97,** 205-217.

WILSHIRE, H.G. & KIRBY, S.H., 1989. Dikes, joints and faults in the upper mantle. *Tectonophysics* **161,** 23-31.

WILSON, J.M., 1993. *The geology of the "Wambidgee-Weatherall" properties, northwest of Coolac, NSW.* BAppSci (Hons) Thesis, University of Technology, Sydney (unpublished).

WINCHESTER, J.A. & FLOYD, P.A., 1977. Geochemical discrimination of different magma series and their differentiation products using immobile elements. *Chemical Geology* **20,** 325-343.

WINWARD, K., 1972. *The geology of the Gundagai district.* BSc (Hons) Thesis, University of Sydney (unpublished).

WOOD, D.S., 1974. Ophiolites, melanges, blueschists and ignimbrites: early Caledonian subduction in Wales? *In:* Dott, R.H. & Shaver, R.H. (eds), *Modern and Ancient Geosynclinal Sedimentation,* p.334-344. Tulsa, Society of Economic Palaeontologists and Mineralogists, Special Publication **19**.

WYATT, B.W., YEATES, A.M. & TUCKER, D.H., 1980. A regional review of the geological sources of magnetic and gravity anomaly fields in the Lachlan Fold Belt of New South Wales. *BMR Journal of Australian Geology and Geophysics* **5,** 289-300.

WYBORN, D., 1992. The tectonic significance of Ordovician magmatism in the eastern Lachlan Fold belt. *Tectonophysics* **214,** 177-192.

WYBORN, L.A.I, 1977. *Aspects of the geology of the Snowy Mountains region and their implications for the tectonic evolution of the Lachlan Fold Belt.* PhD Thesis, Australian National University, Canberra (unpublished).

WYLLIE, P.J., 1967. *Ultramafic and Related Rocks.* John Wiley and Sons, Inc. 464p.

YALINIZ, M.K., FLOYD, P.A. & GONCUOGLU, M.C., 1996. Supra-subduction zone ophiolites of the Central Anatolia: geochemical evidence from the Sarikaraman Ophiolite, Aksaray, Turkey. *Mineralogical Magazine* **60(402),** 697-710.

YANG, K. & SECCOMBE, P.K., 1993. Platinum-group minerals in the chromitites from the Great Serpentinite Belt, NSW, Australia. *Mineralogy and Petrology* **47,** 263-286.

ZHOU, M-F, ROBINSON, P.T., MALPAS, J. & LI, Z., 1996. Podiform chromitites in the Luobusa ophiolite (southern Tibet): implications for melt-rock interaction and chromite segregation in the upper mantle. *Journal of Petrology* **37(1),** 3-21.

APPENDIX A1

WHOLE-ROCK CHROMITITE ANALYSIS

Bulk samples of the chromitites and associated dunitic host rocks were analysed for their major elements by SHEEN Analytical Laboratories, Western Australia, and for their trace elements by Macquarie University, Sydney.

Samples were initially crushed to a grainsize of less than 10mm, and then to a grainsize of less than 200um at the mineral preparation laboratories, CSIRO Division of Exploration and Mining, North Ryde, Sydney.

The samples were then sent to SHEEN Analytical Laboratories, Western Australia. 0.4g of each sample were fused with sodium peroxide and made up to 500ml with deionised water. After sodium peroxide fusion, the samples were analysed by Inductively Coupled Plasma Optical Emission Spectrometry. The detection limits were as follows: Fe, Al_2O_3, MgO, TiO_2, Cr_2O_3, MnO, V_2O_3 ZnO and NiO 100ppm.

For the trace elements, the samples were sent to Macquarie University and analysed by X-Ray Fluoresence. Due to the high Cr concentrations in these rocks, routine analytical methods could not be used. The samples were firstly analysed for volatiles (H_2O^-, H_2O^+ and CO_2^-), the values of which varied from 1.60 to 16.5 wt%, the remainder was then assumed to be silica. Estimates of precision (1a) based on USGS standards BCR-1 and GSP-1, and NIM standard NIM-G are:

Trace elements < ±1% relative; V ±2% relative.

APPENDIX A2

Nd-Sm ISOTOPIC ANALYSIS

Nd-Sm isotopic analyses were performed on selected samples from a number of the different serpentinite belts using isotope dilution mass spectrometry by Dr Brian Cousens of Carleton University, Ottawa Canada.

Initially, samples were examined in thin-section in order to evaluate the degree and intensity of alteration. Selected samples were then crushed with a jaw crusher, then washed thoroughly and cleaned in distilled water and acetone, before being reduced to an average grainsize of 150um with the aid of a ring grinder at the University of Technology, Sydney. Samples were sent to Becquerel Laboratories (Lucas Heights, Sydney) in order to obtain the concentrations of Nd and Sm (in each sample) by neutron activation analysis.

The samples were then sent to the Department of Earth Sciences at Carleton University, Ottawa Canada for isotopic analysis. Samples which gave "odd" or "unusual" results during a first isotopic analysis were re-run in order to check the initial results. For samples with low concentrations, the precision of the concentration data is approximately ±1%. However, because a mixed Sm-Nd spike was used, the precision of the $^{147}Sm/^{144}Nd$ ratio is approximately 0.5%.

APPENDIX A3

PLATINUM-GROUP ELEMENT ANALYSIS

Some of the chromitites and associated dunitic and harzburgitic host rocks were analysed for their Platinum-Group Elements and gold by SHEEN Analytical Laboratories, Western Australia.

Samples were initially crushed to a grainsize of less than 200um at the University of Technology, Sydney. For the chromitites, a chromite concentrate was then obtained using gravity methods of the crushed samples at the University of Technology, Sydney. The samples were then sent to SHEEN analytical laboratories.

The Platinum-Group Elements and gold were determined by Fire Assay (in new pots) using nickel sulfide as the collection media. The platinoids were recovered from the nickel sulfide and analysed by Inductively Coupled Plasma Mass Spectrometry. Detection limits for the samples were as follows: Au 2ppb; Pt, Pd, Ru, Rh and Ir 0.5ppb; and Os 2ppb.

APPENDIX A4

RARE EARTH AND TRACE ELEMENT ANALYSIS

The rare earth elements and selected trace elements were analysed using Neutron Activation Analysis by Becquerel Laboratories, Lucas Heights Sydney.

Initially, samples were crushed to a grainsize of less than 200um at the University of Technology, Sydney. They were then sent to Becquerel Laboratories where they were analysed using Neutron Activation Analysis. Two different types of samples were sent, chromitites and their associated dunitic host rocks, and general petrological samples.

For the chromitites and associated dunitic host rocks, the detection limits were as follows: Lanthanum 0.1ppm; Cerium 1.0ppm; Neodymium 2.0ppm; Samarium 0.05ppm; Europium 0.1ppm; Terbium 0.2ppm; Holmium 0.2ppm; Ytterbium 0.1ppm; Lutetium 0.05ppm; Antimony 0.2ppm; Arsenic 1.0ppm; Chromium 5.0ppm; Cobalt 1.0ppm; Gold 5.0ppb; Hafnium 0.5ppm; Iridium 20.0ppb; Iron 0.05 Wt%; Scandium 0.05ppm; Tantalum 0.5ppm and Thorium 0.5ppm.

For the general petrological samples, the detection limits were as follows: Lanthanum 0.05ppm; Cerium 0.5ppm; Neodymium 1.0ppm; Samarium 0.01ppm; Europium 0.05ppm; Terbium 0.2ppm; Holmium 0.2ppm; Ytterbium 0.03ppm; Lutetium 0.01ppm; Antimony 0.1ppm; Arsenic 0.5ppm; Chromium 2.0ppm; Cobalt 0.5ppm; Gold 5.0ppb; Hafnium 0.2ppm; Iridium 10ppb; Iron 0.02 Wt%; Scandium 0.05ppm; Tantalum 0.5ppm and Thorium 0.2ppm.

Chondrite-Normalised patterns were also produced for each sample by Becquerel Laboratories using the chondrite values of Boynton (1984).

APPENDIX A5

XRF ANALYSIS

The XRF analyses were determined at Macquarie University using a Siemens SRS-1 instrument, following the method of Norrish and Chappell (1977). All samples were analysed in duplicate.

Major elements, except for FeO, H_2O^-, H_2O^+ and CO_2, were determined using glass fusion discs (Norrish and Hutton 1969). Trace elements were analysed using pressed powder pellets and corrected using mass absorption coefficients calculated from major element analyses (Norrish and Chappell 1977). Calibration for both major and trace elements was by means of international rock standards, and appropriate international rock standards or well-calibrated internal standards were included as unknowns in each run.

Estimates of precision (1a) based on USGS standards BCR-1 and GSP-1, and NIM standard NIM-G were as follows:

Major elements $<\pm 1\%$ relative at >10wt% levels; Mn, P, Mg, Na, $<\pm 4\%$ relative at <4wt%

Trace elements $<\pm 1\%$ relative; V $\pm 2\%$ relative

FeO (ferrous iron) was determined by HF digestion and titration with ceric sulphate

H_2O^+ and CO_2 were analysed using a LECO^k induction furnace, with magnesium perchlorate (H_2O) and Lecosorb (CO_2) "collectors". H_2O^- was determined separately by drying at 110°C.

Estimates of precision (1a) based on an internal standard are for H_2O^-, 36% relative; H_2O^+, 7% relative; CO_2, 50% relative; FeO, <2% relative.

APPENDIX A6

U-Pb ZIRCON SHRIMP ANALYSES

U-Pb isotopes were determined on magmatic zircon grains from selected plagiogranite and leucogabbro samples by Mark Fanning of the Precise Radiogenic Isotope Services (PRISE) laboratories at the Research School of Earth Sciences, Australia National University (ANU), Canberra.

Initially, samples were sliced on a diamond saw in order to remove any metabasaltic enclaves and then crushed to a grainsize of less than 10mm at the University of Technology, Sydney (UTS). The grainsize was then reduced to less than 200um and zircon concentrates obtained by heavy liquid separation techniques at the mineral preparation laboratories, CSIRO Division of Exploration and Mining, North Ryde Sydney.

The concentrates were then sent to the PRISE laboratories. Zircons were hand-picked under a binocular microscope and mounted in epoxy along with a chip of the RSES standard zircon SL13. They were then sectioned and polished.

The zircons were analysed using both SHRIMP I and SHRIMP II. Analyses consisted of 6 scans through the mass range. The SHRIMP data were reduced in a manner similar to that described by Compston *et al.* (1992) and Williams and Claesson (1987). Augmented uncertainties for the isotope ratios were calculated by Mark Fanning using software of T.R. Ireland (RSES)(pers.comm). The observed coefficient of variation in the Pb/U ratio measured for the SL13 standard was 2.37% and 2.36%. Pb/U ratios were normalised to a value of 0.09279 for the $^{206}Pb/^{238}U$ ratio of this standard, equivalent to an age of 572 Ma for the standard. Uncertainties given for the individual analyses (both ratios and ages) are at the one sigma level, whereas uncertainties in the weighted mean ages are at 95% confidence limits.

APPENDIX A7

PROTON MICROPROBE TRACE ELEMENT ANALYSIS

The proton microprobe analyses were carried-out at the Heavy Ion Analytical Facility, Division of Exploration Geoscience, CSIRO, North Ryde NSW.

The detection limits for the proton microprobe analyses (ppm) were as follows:

Mn 58-68	Ni 10.0	Zn 4
Ga 3	Ge 2.5	As 2.5
Au 5.0-5.5	Ru 3	Cu 5.5
Rh 3		

APPENDIX LOC

SAMPLE LOCALITY DATA AND GRID REFERENCES

Number	Locality	Map	Grid Ref
BF91/20	Wee Jasper Rd	Tumorrama	225 032
BF91/21	Wee Jasper Rd	Tumorrama	226 034
BF91/22	Red Hill Quarry	Tumorrama	230 112
BF91/23	McAlpine Cu Mine	Tumorrama	190 120
BF91/24	Cr-prospect 75	Adjungbilly	185 152
BF91/25	Cr-prospect 74	Adjungbilly	185 158
BF91/26	Sunnybrae Hom.	Coolac	037 398
BF91/27	Caulderwood Rd	Coolac	085 444
BF91/28	Muttama talc mine	Coolac	025 508
BF91/29	N of Cootamundra	Cootamundra	026 745
BF91/30	E of Cootamundra	Cootamundra	062 590
BF91/31	E of Cootamundra	Coolac	106 536
BF91/32	Thuddungra Mg mine	Bendick Murrell	970 186
BF91/33	Jacks Hill	Bendick Murrell	972 186
BF91/34	Fontenoy Cr mine	Young	035 883
BF91/35	McInerys Cr mine	Lacmalac	230 960
BF91/36	Mingay Cr-prospect 1	Coolac	066 291
BF91/37	Mingay Cr-prospect 2	Coolac	065 294
BF91/38	N Gundagai quarry	Gundagai	007 198
BF91/39	Mungi Mungi	Coolac	088 377
BF91/41	Wantabadgery Rd	Junee	692 310
BF91/42	W-J-E Triangle	Junee	686 306
BF91/43	Junee 20km T-junct	Junee	694 330
BF91/44	Kurrajong trees	Junee	688 332
BF91/45	E of Muttama talc mine	Coolac	058 507
46	South Gundagai	Gundagai	015 175
47	South Gundagai	Gundagai	012 176
48/39	Mt. Mary Cr mines	Coolac	139 269
49	Darbalara	Gundagai	108 238
50	Arbalara	Gundagai	119 230
51	Arbalara	Gundagai	117 230
52	Arbalara	Gundagai	112 237
53	Darbalara	Gundagai	210 098
54	Sunnybrae lim/quarry	Coolac	037 417
55	Sunnybrae	Coolac	040 407
56	Sunnybrae	Coolac	042 410
57	Sunnybrae	Coolac	047 428
58	Booths Reward Au mine	Coolac	050 400
59	Booths Reward Au mine	Coolac	056 401
60	Coolac West	Coolac	969 363
61	Coolac West	Coolac	990 337

62	Coolac West	Coolac	996 384
63	Warrenoy	Young	055 892
64	Warrenoy/Fontenoy	Young	044 892
65	Fontenoy	Young	039 891
67	Mt Lightning E	Adjungbilly	152 260
68	Mt Lightning E	Adjungbilly	152 260
69	Mt Lightning SE	Adjungbilly	154 255
70	Mt Lightning SE	Adjungbilly	154 255
71	Gobbaralong	Coolac	124 312
72	Gobbaralong	Coolac	124 312
73	Gobbaralong	Coolac	124 312
74	Gobbaralong	Coolac	124 312
75	Mt Lightning Crest	Adjungbilly	146 261
76	Mt Lightning W	Gundagai	138 253
77	Mt Lightning W	Gundagai	138 253
78	Mt Lightning W	Gundagai	138 253
79	Mt Lightning W	Gundagai	138 253
80	Mt Lightning W	Gundagai	138 253
81	Mt Lighnting W	Gundagai	138 253
82	Mt Lighnting W	Gundagai	138 253
83	Muttama talc mine	Coolac	024 516
84	Mt Lightning SE	Adjungbilly	154 255
85	Mt Lightning SE	Adjungbilly	154 255
86	Mt Lightning SE	Adjungbilly	154 255
87	Mt Lightning SE	Adjungbilly	154 255
88	Mt Lightning E	Adjungbilly	152 260
89	Mt Lightning Crest	Adjungbilly	146 261
90	Mt Lightning Crest	Adjungbilly	146 261
91	Mt Lightning SE	Adjungbilly	154 255
92	Mt Lightning SE	Adjungbilly	154 255
93	Mt Lightning SE	Adjungbilly	154 255
94	Mt Lightning NW	Coolac	138 350
95	Mt Lightning W	Gundagai	138 253
96	Mt Lightning W	Gundagai	138 253
97	Mt Lightning W	Gundagai	138 253
98	Mt Lightning W	Gundagai	138 253
99	Mt Lightning W	Gundagai	138 253
100	Mt Lightning W	Gundagai	138 253
101	Mt Lightning W	Gundagai	138 253
102	Long Tunnel mine	Gundagai	925 224
103	Mt Lightning S	Adjungbilly	145 255
104	Arctic Cr mine	Adjungbilly	254 146
105	Mt Lightning S	Adjungbilly	145 255
106	Mt Lightning S	Adjungbilly	145 255
107	Mt Lightning S	Adjungbilly	145 255
108	Mt Lightning S	Adjungbilly	145 255
109	Mt Lightning S	Adjungbilly	145 255
110	Mt Lightning S	Adjungbilly	145 255

111	Mt Lightning S	Adjungbilly	145 255
112	Mt Lightning S	Adjungbilly	145 255
113	Mt Lightning S	Adjungbilly	145 255
114	Mt Lightning S	Adjungbilly	145 255
115	Mt Lightning S	Adjungbilly	145 255
116	Mt Lightning S	Adjungbilly	145 255
117	Mt Lightning S	Adjungbilly	145 255
118	Mt Lighting S	Adjungbilly	145 255
119	Mt Lightning S	Adjungbilly	145 255
120	Mt Lightning S	Adjungbilly	145 255
121	Mt Lightning S	Adjungbilly	145 255
122	Mt Lightning S	Adjungbilly	145 255
123	Mt Lightning SW	Adjungbilly	141 255
124	Mt Lightning W	Gundagai	138 253
125	Mt Lightning W	Gundagai	138 253
126	Mt Lightning W	Gundagai	138 253
127	Mt Lightning W	Gundagai	138 253
128	Mt Lightning W	Gundagai	138 253
129	Mt Lightning NW	Coolac	138 350
130	Mundongo Trig	Lacmalac	238 917
131	Mundongo W	Lacmalac	235 917
132	Mundongo W	Lacmalac	234 917
133	Mundongo Cr mine	Lacmalac	233 911
134	Mundongo Mg mine	Lacmalac	236 898
135	Mt Miller Cr mine	Tumorrama	232 038
136	Cu Prospect 140	Tumorrama	233 037
137	Emu Cr mine	Tumorrama	240 039
BF92/1	Warrenoy	Young	058 896
BF92/2	Warrenoy	Young	058 896
BF92/3	Warrenoy	Young	058 896
BF92/4	Warrenoy	Young	058 896
BF92/5	Warrenoy	Young	058 896
BF92/6	Warrenoy	Young	058 896
BF92/7	Warrenoy	Young	058 896
BF92/8	Moonbilen	Young	050 880
BF92/9	Moonbilen	Young	050 880
BF92/10	Moonbilen	Young	050 880
BF92/11	Moonbilen	Young	050 880
138	Kang/W Cr mine	Adjungbilly	182 172
139	Kang/E Cr mine	Adjungbilly	191 168
140/BF92/28	North/Mooney Comp.	Coolac	098 353
(Includes sample BF92/29)			
141/BF92/30	North/Mooney Comp.	Coolac	112 336
142/BF92/31	North/Mooney Comp.	Coolac	112 364
143/BF92/32	North/Mooney Comp.	Coolac	112 363
144/BF92/33	North/Mooney Comp.	Coolac	110 362
145/BF92/34	North/Mooney Comp.	Coolac	107 360
146/BF92/35	North/Mooney Comp.	Coolac	104 358

147/BF92/36	Goobarragandra	Lacmalac	262 871
148	Goobarragandra	Lacmalac	265 869
149/BF92/37	Goobarragandra	Lacmalac	267 865
150/BF92/38	Goobarragandra	Lacmalac	267 864
(Includes samples BF92/39, BF92/40)			
151/BF92/41	Goobarragandra	Lacmalac	268 864
152/BF92/42	Goobarragandra	Lacmalac	269 865
(Includes sample BF92/43)			
153/BF92/44	Goobarragandra	Lacmalac	269 867
154/BF92/45	Goobarragandra	Lacmalac	269 870
155/BF92/46	Mund/Peak quarry	Lacmalac	229 931
(Includes samples BF92/47 - BF92/51)			
156/BF92/52	Bombowlee Creek	Lacmalac	234 965
(Includes samples BF92/53 - BF92/56)			
157/BF92/23	Tumut Ponds A	Yarrangobilly	143 545
(Includes samples BF92/24, BF92/25)			
158/BF92/26	Tumut Ponds A	Yarrangobilly	143 545
159/BF92/27	Tumut Ponds A	Yarrangobilly	139 545
160/BF92/57	Hume Hwy 1	Gundagai	004 207
(Includes samples BF92/58, BF92/59)			
161/BF92/60	Hume Hwy 2	Gundagai	001 205
(Includes samples BF92/61, BF92/62)			
162/BF92/63	South Gundagai	Gundagai	031 147
(Includes samples BF92/64 - BF92/67)			
163/BF92/68	NE of Muttama talc mine	Coolac	030 512
164/BF92/69	Avoca	Coolac	040 467
165/BF92/70	Avoca	Coolac	050 460
(Includes sample BF92/71)			
166/BF92/72	Avoca	Coolac	045 460
167/BF92/73	Avoca	Coolac	043 460
(Includes sample BF92/74)			
BF92/12	Wheatley Hom.	Cootamundra	078 758
BF92/13	Wallendbeen	Cootamundra	070 781
BF92/14	Thuddungra Mg mine	Bendick Murrell	970 174
BF92/15	Coolac West	Coolac	990 356
BF92/16	Pettits	Coolac	059 310
BF92/17	Coolac West	Coolac	987 350
BF92/18	E of Coolac	Coolac	113 284
168	Red Hill	Adjungbilly	188 156
WW1	Wamb West	Coolac	990 337
WW2	Wamb West	Coolac	990 337
WW3	Wamb West	Coolac	990337
WW4	Wamb West	Coolac	990 337
WW5	Wamb West	Coolac	990 337
169	Wamb West	Coolac	990 337
170	Wamb West	Coolac	990 337
171	Wamb West	Coolac	990 337
172	Wamb West	Coolac	990 337

173	Wamb West	Coolac	990 337
174	Wamb West	Coolac	990 337
175	Wamb West	Coolac	990 337
176	Wamb West	Coolac	990 337
177	Coolac Ridge	Coolac	045 337
178	Coolac West	Coolac	969 363
179	Coolac West	Coolac	969 363
180	Jacks Hill	Bendick Murrell	977 185
181	Jacks Hill	Bendick Murrell	977 188
182	Jacks Hill	Bendick Murrell	977 198
183	Jacks Hill	Bendick Murrell	977 198
184	Jacks Hill	Bendick Murrell	977 201
185	Jacks Hill	Bendick Murrell	977 201
186	Jacks Hill	Bendick Murrell	970 204
187	Jacks Hill	Bendick Murrell	970 202
188	Jacks Hill	Bendick Murrell	972 198
189	Jacks Hill	Bendick Murrell	972 194
190	Jacks Hill	Bendick Murrell	970 190
191	Ardnaree	Bendick Murrell	953 117
192	Memagong Hill	Bendick Murrell	956 130
193	Memagong Hill	Bendick Murrell	956 132
194	Memagong Hill	Bendick Murrell	956 134
195	Quartz Hill	Bendick Murrell	953 100
196	Quartz Hill	Bendick Murrell	958 101
197	Quartz Hill	Bendick Murrell	963 100
198	Quartz Hill	Bendick Murrell	950 101
199	Quartz Hill	Bendick Murrell	950 098
200	Quartz Hill	Bendick Murrell	953 098
201	North Gundagai	Coolac	971 270
202	North Gundagai	Coolac	974 270
203	North Gundagai	Gundagai	992 218
204	Gundagai Limestone	Gundagai	959 239
205	Mount Lightning	Coolac	108 261
206	Darbalara	Gundagai	098 240
207	Darbalara	Gundagai	108 231
208	Adjunbilly	Gundagai	134 239
209	Adjunbilly	Gundagai	141 240
210	Adjunbilly	Adjunbilly	155 243
211	Adjunbilly Cr mine	Adjunbilly	157 244
212	Young Incl	Tumorrama	234 041
213	Creek Bed	Tumorrama	236 047
214	Rd-cutting contact	Tumorrama	223 030
215	Gundagai South	Gundagai	015 175
216	Gundagai South	Gundagai	016 174
217	Gundagai South	Gundagai	016 173
218	Gundagai South	Gundagai	015 173
219	Gun serp quarries	Gundagai	015 176
220	Gundagai South	Gundagai	015 169

221	Gundagai South	Gundagai	014 167
222	Blacks Flat	Gundagai	118 168
223	Warrenoy	Young	058 896
224	Warrenoy	Young	058 896
225	Warrenoy	Young	058 896
226	Warrenoy	Young	058 896
227	Warrenoy	Young	058 896
228	T25	Adjungbilly	183 158
229	T25	Adjungbilly	183 158
230	T25	Adjungbilly	184 158
231	T25	Adjungbilly	184 158
232	Cr-deposit 74	Adjungbilly	185 158
233		Coolac	099 368
234	up the creek	Coolac	105 365
235	lower creek bed	Coolac	100 365
236	Layer 1 of sequence	Coolac	096 365
237	Wee Jasper Rd	Tumorrama	227 030
238	Bombowlee Creek Bed	Lacmalac	230 964
239	Mount Selwyn	Cabramurra	291 234
240	Mount Selwyn	Cabramurra	287 233
241	Quarry	Cabramurra	290 227
242	silt/serp contact	Cabramurra	279 224
243	siltstone	Cabramurra	276 223
244	Tertiary basalt	Cabramurra	275 225
245	Link road area	Cabramurra	264 273
246	Down the hill	Cabramurra	266 274
247	Metaserp	Cabramurra	265 270
248	Laterite	Cabramurra	267 268
249	E contact	Cabramurra	274 264
250	Schist serp	Cabramurra	269 267
251	Columnar jointing	Cabramurra	262 272
252	Buddong Falls area	Yarrangobilly	148 546
253	Buddong Falls area	Yarrangobilly	150 548
254	Buddong Falls area	Yarrangobilly	147 545
255	Buddong Falls area	Yarrangobilly	142 545
256	Buddong Falls area	Yarrangobilly	142 544
257	Buddong Falls area	Yarrangobilly	141 545
258	Small serp body	Yarrangobilly	148 559
MLV	Mt Lightning N	Adjungbilly	147 262
270	Gundagai N	Gundagai	002 245
271	Gundagai N	Gundagai	999 245
272	Gundagai N	Gundagai	998 244
273	Gundagai N	Gundagai	000 232
274	Gundagai N	Gundagai	001 233
275	Gundagai N	Gundagai	000 235
276	Gundagai N	Gundagai	002 235
277	Gundagai N	Gundagai	002 218
278	Gundagai N	Gundagai	003 215

279	Gundagai S	Gundagai	032 141
280	Gundagai S	Gundagai	036 131
281	Gundagai S	Gundagai	033 141
282	Gundagai S	Gundagai	030 146
283	Gundagai S	Gundagai	028 156
284	Bombowlee Ck section	Lacmalac	230 964
285	Bombowlee Ck section	Lacmalac	234 963
286	Bombowlee Ck section	Lacmalac	235 963
287	Bombowlee Ck section	Lacmalac	235 963
MLA	Mount Lightning Adit	Adjungbilly	146 261
QOC	Quilters O/C	Adjungbilly	146 261
MM	Mount Miller	Tumorrama	232 038
ML	Mount Lightning	Adjungbilly	146 261

APPENDIX 3PD

PETROGRAPHIC DESCRIPTIONS OF ROCK TYPES FROM THE COOLAC SERPENTINITE BELT AND ABUTTING UNITS

The Honeysuckle Beds

The metasedimentary component of the Honeysuckle Beds generally comprise phyllite, chert and well-laminated siltstone, with minor components including intermediate tuffs and quartzite (Ray 1977). During the present study, the following metasedimentary assemblages were found to occur within the Honeysuckle Beds:

1. Highly cleaved, light brown well-bedded metapelite/metapsammite (G.R. 138 253).
2. Well-laminated metasiltstone with well-developed graded bedding (including a small cross-bedded layer within a rare psammitic bed) and prominent cleavage (G.R. 145 255).
3. Massive fine-grained siliceous chert (G.R. 141 240).

Most of the metavolcanic rocks of the Honeysuckle Beds are spilitic metabasalts. Variolitic varieties (with the variolites defined by slender quenched plagioclase and augite) are of minor occurrence whereas pillow basalts are common.

During the present study, the following metavolcanic assemblages were found to occur within the Honeysuckle Beds:

1. Relatively unfoliated, medium-grained hornblende gabbro. In thin-section, this gabbro exhibits a hypidiomorphic granular texture defined by interlocking grains of prismatic hornblende, plagioclase and tremolite, along with minor finer-grained chlorite and clinozoisite. The modal composition of this gabbro is plagioclase (50%), hornblende (40%), tremolite (7%), Mg-chlorite (3%) and minor clinozoisite and accessory opaques. The hornblende grains are complexly zoned, have ragged edges and are commonly rimmed and replaced by secondary tremolite and chlorite. Plagioclase lacks any compositional zoning and the clinozoisite occurs as rare replacements of some of the plagioclase (G.R. 145 255).
2. Massive, fine-grained quench-textured metabasalt. In thin-section, this basalt has a well-developed quench texture defined by prismatic elongate phenocrysts of plagioclase in a finer-grained matrix of epidote, clinoclinozoisite and quartz. The modal composition is albite (60%), epidote (30%), clinoclinozoisite (10%), along with minor quartz and cross-cutting veinlets of quartz/epidote/clinozoisite. (G.R. 145 255).
3. Massive, fine-grained amygdaloidal metabasalts. In thin-section, these basalts have i) a granoblastic texture (G.R. 262 871) defined by interlocking grains of albite, green/brown hornblende, epidote, quartz, apatite and rare epidote-filled amygdaloids; or, ii) a glomeroporphyritic texture (G.R. 134 239) defined by either phenocrysts of albite, composite amygdaloids of epidote/Mg-chlorite and Mg-chlorite amygdaloids in a fine-grained matrix of interlocking albite, epidote, chlorite, quartz and clinoclinozoisite; or, iii) interlocking aggregates of lath-shaped albite and irregularly-shaped amygdaloids of epidote/clinoclinozoisite/chlorite in a fine-grained matrix of needle-like albite and interlocking granular epidote and chlorite. The modal composition of the granoblastic type is green/brown hornblende (50%), albite (20%), quartz (20%), epidote (10%) and minor apatite and opaques.
4. Hornfelsed metabasalt. In thin-section, this basalt has a porphyroblastic decussate texture defined by elongate bladed sub-prismatic porphyroblasts of actinolite in a groundmass of long

prismatic albite grains and very fine-grained needle-like bunches of actinolite grains. The modal composition is actinolite (70%), albite (25%), and chlorite (5%), along with rare epidote and opaques, and cross-cutting veinlets of epidote and quartz/clinoclinozoisite. The chlorite occurs as pseudomorphous grains after some of the larger actinolite grains (G.R. 267 864).

5. Altered fragmental metabasalt. In thin-section, this rock has a decussate-granoblastic metamorphic texture defined by interlocking grains of albite, epidote, clinozoisite, quartz and rare lithic fragments. The modal composition is epidote (60%), albite (26%), clinozoisite (5%), quartz (5%), carbonate (2%) and relict calcic plagioclase (2%). The albite grains are commonly moderately bent and much of the albite is altered to very fine-grained mixtures of carbonate, epidote and quartz. The lithic fragments are rare and consist of very elongate and thin non-aligned albite laths in a very fine-grained groundmass (G.R. 113 284).
6. Once-glassy fractured metabasalt. This basalt is atypical of the Honeysuckle Beds as it has intense pervasive fracturing throughout. Many of these fracture are curved, no displacement is observable on either side of the fractures and they appear to represent a preserved perlitic cracking texture. In thin-section, the rock has a porphyritic intergranular texture defined by phenocrysts of albite pseudomorphous after calcic plagioclase and pseudomorphs of tremolite/actinolite after pyroxene in an even-grained, fine-grained groundmass of interlocking, non-aligned grains of epidote, albite, quartz, clinoclinozoisite and rare Mg-chlorite (G.R. 108 261).
7. Layered, altered metabasalt. The two dominant textures of this unusual metasommatically altered metabasalt are pseudosedimentary layering and a decussate-granoblastic metamorphic texture. The granoblastic texture is defined by interlocking grains of epidote, clinoclinozoisite, Mg-chlorite, hydrogrossular and albite. The pseudosedimentary texture is defined by varying proportions of epidote (50-10 modal%) and Mg-chlorite (50-90%) in thin bands throughout the rock. The overall modal composition of this metabasalt is epidote (50%), Mg-chlorite (25%), hydrogrossular (20%), clinoclinozoisite (4%) and relict albite (1%) (G.R. 134 239).

The Blowering Formation

The Blowering Formation dominantly comprises porphyritic dacites and rhyodacites, dacitic and rhyodacitic tuffs, conglomerates, abundant arenites of variable composition, siltstones, mudstones, and minor basalt (Basden 1990). The felsic volcanics are typically massive and largely consist of large phenocrysts of quartz, plagioclase and rarely potassic feldspar and hornblende (Franklin 1975) along with lithic clasts and minor biotite in a fine-grained light gray groundmass. Numerous xenoliths and rare fragmented garnet phenocrysts also occur (Basden 1990). Basalts are rare, and when found they are completely enclosed within the dacitic porphyries. Lithic clasts include micro-graphic tonalite, plagioclase-biotite-chlorite hornfels, rare metaquartzite and quartz fragments up to 15cm in maximum dimension (Stuart-Smith & Dadd 1993).

The porphyries are non-welded to completely welded ash flow tuffs and/or lavas in which the original texture is no longer discernible (Basden 1990). They are composed of phenocrysts of quartz, plagioclase (with the plagioclase being partly to completely sericitised), and strongly corroded chloritised biotite in a finer-grained groundmass of elongate devitrified glass shards and ash material interspersed with grains of chlorite, biotite, muscovite and opaques. Apatite, zircon and garnet are rare accessories and alteration minerals include chlorite, epidote, calcite and prehnite (Basden 1990).

The Blowering Formation was not intentionally looked at during the course of this present study, however, two occurrences completely enclosed within the Coolac Serpentinite Belt were found and are briefly described below.

G.R. 146 261. Very sparse outcrop on the western-side of the crest of Mount Lightning consisting of moderately foliated feldspar-rich dacite. In thin-section, it has a mylonitic or porphyroclastic texture defined by moderately aligned (with the longest dimension of the grains parallel to the foliation in the rock) phenocrysts of altered plagioclase and quartz in a fine-grained, decussate-like groundmass of actinolite, chlorite, quartz and rare equant-shaped plagioclase grains. It has a modal composition of altered plagioclase (50%), quartz (30%), actinolite (5%), chlorite (5%) and clay minerals+fine-grained micas (10%). Most of the plagioclase occurs as highly altered grains (i.e. a mixture of fine-grained clays, micas and quartz), which in places, enclose strongly embayed quartz grains. A few of the unaltered grains retain their original compositional zonation and have rare inclusions of altered hornblende. They are also strongly bent with strongly kinked multiple twin lamellae. The quartz occurs as polygonal-shaped subgrains and much of it appears to replace the altered plagioclase phenocrysts.

G.R. 185 158. A moderate-sized (at least 5x5m) body of relatively unfoliated, medium-grained biotite-rich dacite completely enclosed within massive porphyroclastic harzburgite. In hand-specimen, this rock is composed of phenocrysts of plagioclase along with fine-grained intergranular biotite, micas and clays. No visible quartz is present.

The North Mooney Complex

(Largely taken from Franklin 1975)

The North Mooney Complex has been subdivided into two main zones, a cumulus dominantly ultramafic zone termed "the layered series" and a massive, dominantly gabbroic zone termed "the marginal series" (Franklin 1975). Within the layered series, mineral-graded layers occur within the wehrlites and gabbros, which are commonly repeated a number of times (i.e. rhythmic layering). Size-graded layering occurs within the gabbros and clinopyroxenites but is more irregular and discontinuous than the mineral-graded layering (Franklin 1975). Within the marginal series, layering is uncommon, weakly developed and discontinuous.

The Layered Series

The layered series itself has been subdivided into a main layered series consisting of well-layered, relatively unaltered massive rock types, and a western layered series consisting of an incomplete section with alteration becoming intense near its western margin (Franklin 1975).

Dunites: are of minor occurrence as discontinuous pods and lenses in the lower portions of the main layered series and as pods in shear zones in the western layered series. They vary from partially to completely serpentinised with the main serpentine assemblage being antigorite+clinochrysotile. They usually contain minor amounts of diopside (2-8 modal%) and bastitised orthopyroxene (up to 3 modal%), rare chrome spinel and abundant accessory secondary magnetite. Chlorite and clinoclinozoisite occur as cross-cutting veinlets and patches. Olivine within the dunites of the main layered series is relatively undeformed whereas olivine within the western layered series contains abundant evidence of strain and recrystallisation.

Wehrlites: are the most extensive ultramafic rock type within the North Mooney Complex. They occur as mappable layers within the main layered series and as three narrow bands within the western layered series. There is a 3-5m wide metasommatic reaction zone between the lowest wehrlite band in the main layered series and the underlying harzburgite of the Coolac Serpentinite Belt. Layering within the wehrlites is well-developed, straight and continuous. The wehrlites vary from being fresh (with no serpentine minerals) to completely serpentinised (with no fresh olivine). They have a modal composition of olivine+its serpentine alteration products (21-75%), diopside (22-78%), minor brown hornblende (up to 7%), rare orthopyroxene (6%) and rare magnetite, chlorite and talc. Within the uppermost wehrlite layer, olivine has been replaced by fibrous tremolite, serpentine has been altered to chlorite, tremolite occurs around the rims and along cleavage planes of the diopside grains, and the orthopyroxene grains have been completely replaced by chlorite.

Clinopyroxenites: are half as abundant as the wehrlites and are more discontinuous and irregular than the wehrlite layers. Many of them are extremely coarse-grained, with xls as large as 200mm. They have a modal composition of diopside (93-98%), variably serpentinised olivine (up to 5%), postcumulus hornblende (up to 3%) and plagioclase (up to 3%). The plagioclase is often strongly saussuritised to a mixture of epidote/chlorite/albite and tremolite fringes occur around some the diopside grains.

Gabbros and Gabbro Pegmatites: are of rare occurrence within the main layered series and occur either at the junction between two of the ultramafic units or wholly enclosed within the clinopyroxenites. The gabbros are usually well-layered (exhibiting both mineral- and size-graded layers) often exhibiting rhythmic layering. The gabbro pegmatites are all hornblende-bearing and occur as either small patches, small dykes, or veinlets. The contacts with the surrounding rock types are sharp. They have a modal composition of diopside (up to 50%), calcic plagioclase (up to 47%), minor cumulus olivine (up to 5%) and postcumulus green/brown hornblende (up to 30%). In half of the gabbros, the diopside grains are mantled by pleochroic green/brown hornblende. Tremolite is a minor phase, occurring as fringes on some of the diopside grains and replacement patches within the hornblende grains. The gabbro pegmatites have a modal composition of green/brown hornblende (up to 60%), calcic plagioclase (up to 45%), diopside (up to 18%), epidote (up to 3%) and rare magnetite.

The Marginal Series

The marginal series is dominantly composed of textural varieties of gabbro, along with smaller proportions of hornblende gabbro pegmatites, diorites and rare albitites and plagiogranites. They all have mineral assemblages indicative of low grade greenschist facies metamorphism. In general, plagioclase within the marginal series is not saussuritised, except within shear zones. Dykes and angular xenoliths of metabasaltic rocks occur in all of the members of the marginal series.

Gabbros: although they vary considerably in texture and grain-size, the gabbros of the marginal series are all chemically and mineralogically similar. They dominantly consist of assemblages of diopside (10-60%) and calcic plagioclase (25-50%). Olivine (0-12%) is confined to the more mafic varieties and green/brown hornblende (0-35%) may be present or absent. The accessory minerals magnetite, sulfides and sphene are rare or absent while secondary tremolite (1-10%), chlorite (trace-5%), epidote and clinoclinozoisite (trace-8%) are common. The hornblende commonly replaces the diopside grains, which are also fringed by and altered to tremolite. Blue/green

hornblende (sodium-rich pargasitic hornblende) is rare as small patches within the green/brown hornblende.

Hornblende gabbro pegmatites: occur spasmodically as isolated patches and dykes. They are dominantly composed of hornblende (45-65%) and calcic plagioclase (27-34%), while some are also diopside-rich (up to 20%). The secondary minerals include tremolite (1%), chlorite (3%) and epidote (up to 9%) while accessory apatite and magnetite occur in some of the rocks. When present, the diopside generally occurs as cores to the hornblende grains and are usually altered along fractures to mixtures of tremolite and chlorite.

Diorites, albitites and plagiogranites: these comprise only some 5 vol% of the marginal series and are concentrated towards the western margin close to the contact with the Honeysuckle Beds. The diorites generally occur as irregular-shaped masses within the gabbros whereas the albitites and plagiogranites are confined to small plug-like masses, segregations and dykes. Diopside (up to 8 modal%) occurs within the more mafic types whereas hornblende varies from 30 to 58% in the diorites but is as low as 6% in the plagiogranites. Plagioclase ranges from 30 to 56% in the diorites up to 80% in the plagiogranites. Quartz is absent in most of the diorites and albitites but varies between 10 and 23% within the plagiogranites. Chlorite (up to 5% in the diorites) and tremolite (up to 11% in the diorites and 5% in the plagiogranites) are the most abundant secondary phases while epidote group minerals generally occur in cross-cutting veins and patches. Biotite occurs as a rare primary phase in the plagiogranites. Magnetite, sphene and apatite are common accessory minerals in all of the rock types whereas zircon is restricted to the plagiogranites.

Although the contacts of the North Mooney Complex rocks with surrounding rock units were not looked at during this study, a number of petrological observations were made (see below) along with new geochemical and geochronological data.

G.R. 098 353. Outcrop of fine-grained pillow basalts and micro-gabbro.

Metabasalt: exhibits a porphyritic intersertal texture defined by occasional phenocrysts of albite and relatively large grains of actinolite in a fine-grained groundmass of albite, actinolite, epidote, chlorite and minor opaques. The modal composition is albite (50%), actinolite (40%), chlorite (7%) and epidote (3%). The albite occurs as lath-shaped grains, intimately associated with both the actinolite and chlorite grains. Epidote is restricted to clots (amygdules) within the basalt while chlorite occurs as a replacement of some of the actinolite grains.

Meta micro-gabbro: exhibits a hypidiomorphic granular texture defined by interlocking grains of plagioclase, hornblende, quartz, actinolite/tremolite, epidote, chlorite, clinozoisite and rare accessory ilmenite. It has a modal composition of plagioclase (70%), pale green hornblende (18%), actinolite/tremolite (5%), epidote (3%), quartz (2%), chlorite (2%), rare clinozoisite and very rare accessory ilmenite. The plagioclase is strongly saussuritised while the actinolite/tremolite occurs as fringes around and replacements of the hornblende grains. Chlorite occurs as replacements of some of the hornblende grains and is commonly associated with both epidote and clinoclinozoisite.

G.R. 107 360. Dyke-like body of massive pyroxene gabbro. In thin-section, this gabbro has a pseudoporphyritic allotriomorphic granular post-cumulus space-filling texture defined by relatively large subprismatic grains of diopside and minor orthopyroxene in a matrix of highly saussuritised

plagioclase, clinoclinozoisite, chlorite and tremolite. It has a modal composition of diopside (40-42%), orthopyroxene (2-5%), saussuritised plagioclase (10-45%), clinoclinozoisite (3-15%), pleochroic green/brown hornblende (0-5%), tremolite (2-10%) and chlorite (0-33%) along with rare accessory apatite. Many of the diopside grains strongly impinge on each other. Rim replacement of the diopside grains by tremolite and green/brown hornblende is common, as are tremolite fringes around the diopside grains. Tremolite also occurs as needle-like grains within the saussuritised plagioclase. The plagioclase is completely saussuritised to a mixture of clinoclinozoisite, tremolite, quartz and chlorite.

G.R. 104 358. Small outcrop of relatively massive (but with highly localised shear zones), medium-grained hornblende gabbro. In thin-section, it has a post-cumulus space-filling and post-cumulus overgrowth texture defined by relatively large diopside grains, the spaces between which are filled by smaller hornblende grains enclosed within large plagioclase grains. It has a modal composition of plagioclase (40%), hornblende (30%), diopside (8%), tremolite (12%), chlorite (7%), quartz (2%), epidote (<1%) and accessory apatite and opaques. In places, the plagioclase has been replaced by mixtures of quartz and epidote, but it largely occurs as fresh multiply twinned grains. The hornblende is of two generations with the earlier generation occurring as khaki-brown angular grains between the pyroxene grains (enclosed within plagioclase) and as overgrowths on the diopside grains. The later generation of hornblende occurs as large pale green grains that replace the earlier hornblende grains and commonly occur as overgrowths on the diopside grains. This later generation is itself replaced by later fibrous tremolite and chlorite. The tremolite also occurs as rims around the diopside and hornblende grains and as matted groups of acicular xls within the plagioclase grains.

G.R. 099 368. A fairly large body (i.e. at least some 80X5m) of moderately foliated pyroxene gabbro with cross-cutting veins of pegmatitic hornblende gabbro containing rare enclaves of metabasalt.

Pyroxene gabbro: in thin-section, these gabbros have a hypidiomorphic to allotriomorphic granular texture with postcumulus overgrowth defined by relatively large anhedral strongly embayed cumulus diopside grains with the interstices filled by post-cumulus space-filling plagioclase and secondary, cross-cutting grains of tremolite/actinolite. The modal composition is plagioclase (40-60%), diopside (30-40%), pleochroic brown hornblende (3-9%), epidote (0-5%), clinoclinozoisite (<1 to 5%), actinolite (0-7%), tremolite (0-3%) and rare accessory corroded sulfides. The diopside grains are strongly embayed by the plagioclase grains and primary diopside is restricted to remnant patches and cores. Most of the plagioclase occurs as fresh unaltered interstitial grains. Altered plagioclase occurs as either relatively fine-grained aggregates of clinoclinozoisite, fibrous tremolite, quartz and albite, or as very fine-grained aggregates of albite and quartz with cross-cutting fibrous tremolite. Hornblende occurs as rims around the diopside grains and rarely as a post-cumulus phase between the diopside and plagioclase grains. In some instances, it occurs as zoned grains with an inner core of pleochroic brown hornblende and an outer zone of pleochroic (light to dark green) green hornblende. The outer zone is commonly fringed by tremolite/actinolite grains, which also cut-across the adjacent plagioclase grains. Within the post-cumulus space-fill, the khaki brown hornblende has impinged on the growth of plagioclase suggesting that it formed between the plagioclase grains and is therefore a magmatic rather than secondary alteration phase. Both the tremolite and actinolite occur as replacements of the diopside grains and as cross-cutting fracture-fill phases.

Pegmatitic hornblende gabbro veins: in thin-section, these gabbros exhibit an allotriomorphic granular texture defined by interlocking hornblende and plagioclase grains. They have a modal composition of hornblende (30-90%) and plagioclase (10-70%), along with minor diopside, clinoclinozoisite, epidote and abundant accessory zircon. The hornblende generally occurs as strongly pleochroic zoned grains with a brown core and green outer rim. Triple-junction grain boundaries are common between the hornblende grains and they contain common inclusions of opaques and zircon. Plagioclase occurs as interlocking grains with the hornblende and exhibits strong compositional (sector) zoning. The boundary between these veins and pyroxene gabbro host rock is sharp with abundant cross-cutting tremolite on the boundary. On the contact, the hornblende of the vein is in direct contact with the diopside of the host, with the diopside being rimmed and partially replaced by the hornblende.

G.R. 105 365. A large mass of relatively fresh, extremely coarse-grained (with individual grains up to 150mm in length) clinopyroxenite with abundant veins of pegmatitic hornblende gabbro (with individual hornblende xls up to 20mm in length). The diopside grains within this clinopyroxenite are euhedral in shape, interlocking with each other and have interstitial hornblende between them.

G.R. 100 365. Relatively unfoliated basaltic dyke intruding into hornblende gabbro. In thin-section, the metabasalt exhibits a porphyritic intergranular decussate texture defined by non-aligned phenocrysts of plagioclase and resorbed diopside grains in a non-aligned groundmass of albite, actinolite, chlorite and rare epidote. The diopside grains are strongly resorbed and have an alteration rim of actinolite.

G.R. 096 365. Interbedded, fine-grained metabasalts, meta-andesites, albitites and cherts.
Amygdaloidal basalts: in thin-section, these metabasalts exhibit a porphyritic intergranular and decussate texture defined by occasional phenocrysts of albitic plagioclase and amydaloids of epidote in a fine-grained groundmass of non-aligned albite, epidote, chlorite and rare biotite. The modal composition is albite (65%), epidote (15%), clinoclinozoisite (5%), chlorite (5%), quartz (5%) and biotite (<1%) with accessory apatite. The albitic plagioclase phenocrysts commonly occur as aggregates defining a glomeroporphyritic texture. Biotite is of rare occurrence, enclosed within chlorite.

Basalt breccia: consists of two components:
i) breccia fragments exhibiting a hypidiomorphic granular texture defined by interlocking plagioclase grains, between which occur interstitial hornblende and actinolite. The plagioclase occurs as only weakly altered multiply twinned grains. Hornblende occurs as moderately pleochroic (pale to olive green) irregular-shaped platy grains. The actinolite occurs as masses of tiny fibrous grains which fill-up the interstices between the plagioclase and hornblende grains, and, in places, as replacements of the hornblende grains.
ii) a granoblastic-textured matrix consisting of non-aligned aggregates of epidote, clinoclinozoisite, fibrous green-brown chlorite, highly strained quartz and albite, and rare platy hornblende/actinolite.

The Young Granodiorite

The massive granodiorite has an even hypidiomorphic granular texture (Franklin 1975) and is composed of quartz (30-50%), plagioclase (25-50%), biotite (10-20%) and K-feldspar (5-15%), along with minor amounts of epidote, green hornblende, magnetite, apatite, ilmenite, zircon and

sphene. Alteration phases include sericite, muscovite, epidote and albite (Basden 1990). The plagioclase is oligoclase-andesine (An_{28-32}) with albite rims (An_8) (Franklin 1975). The quartz almost always exhibits moderate undulose extinction and the biotite is often altered to chlorite (Basden 1990). Nearly every thin-section of the Young Granodiorite exhibits some sign of deformation (Basden 1990). The quartz has sutured grain boundaries, recrystallisation is common and both biotite and plagioclase are commonly bent.

Within the foliated varieties of the Young Granodiorite, quartz either occurs in single grains exhibiting strong undulose extinction or in polygonal aggregates; the plagioclase is often fractured and exhibits bent and/or microfaulted twin lamellae; and the biotite occurs as bent and kinked grains (Basden 1990). The foliation is macroscopically defined by the preferred orientation of biotite grains and lenticular quartz aggregates (Franklin 1975). Towards both internal and marginal shear zones, the granodiorite has been intensely sheared and mylonitised. This deformation has affected the different constituent minerals to differing degrees with the plagioclase occurring as fractured and microfaulted porphyroclasts exhibiting weak undulose extinction. With increasing intensity of deformation, these grains become smaller and more rounded (Basden 1990). In the most intensely deformed varieties, the quartz occurs as very small elongate grains with intensely crenulated and granulated margins (Franklin 1975).

Enclaves occur in almost every outcrop of the granodiorite, the most common being composed of fine-grained biotite and feldspar with minor quartz (Basden 1990). The contact with the enclosing granodiorite can be either sharp or gradational. In thin-section, they exhibit a hypidiomorphic granular texture and have a modal composition of plagioclase (65%), biotite (25%) and quartz (10%), along with minor epidote, chlorite and sericitic alteration (Basden 1990). Areas of porphyritic granodiorite, along with volcanic inclusions and aplitic dykes, occur in the central parts of the main mass which suggests that it has only just been unroofed (Basden 1990).

During the present study, only the contacts between the Young Granodiorite and Coolac Serpentinite Belt were looked at in detail. These observations are presented below.

G.R. 152 260. Outcrop of relatively fresh, unfoliated granodiorite within 100m of the eastern contact with the Coolac Serpentinite Belt. In thin-section, this rock exhibits a hypidiomorphic granular texture defined by an interlocking mosaic of non-aligned plagioclase, quartz, biotite, chlorite and muscovite. The modal composition is quartz (40%), plagioclase (35%), alkali feldspar (10%), biotite (10%), muscovite (2%), chlorite (2%) and kaolinite (<1%), along with accessory apatite and zircon. The plagioclase exhibits well-defined internal compositional zoning and multiple twinning, and many of the grains are partially altered to sericite and clay. Quartz generally occurs as aggregates of ribbon-like subgrains exhibiting strong undulose extinction. All of the quartz is strongly recrystallised, triple-junction grain boundaries are common, as are graphic-like intergrowths with alkali feldspar. Biotite occurs as strongly pleochroic grain aggregates, with minor cleavage replacement by chlorite. Muscovite is of rare occurrence, commonly as fringes around the biotite grains.

G.R. 152 260. Sparse outcrop of micro-granodiorite (i.e. chilled granodiorite) on the contact with the Coolac Serpentinite Belt. In thin-section, it exhibits a hypidiomorphic granular texture defined by large equant to quite elongate aggregates of quartz subgrains, separated from each other by irregularly-shaped large anhedral altered plagioclase grains. The modal composition is quartz

(35%), plagioclase (30%), chlorite (25%), epidote (10%) and hornblende (<1%), along with rare accessory opaques. The quartz grains are generally composed of many subgrains. All of the quartz exhibits very strong undulose extinction and many of the subgrains have well-developed sharp triple junction subgrain boundaries. No fresh plagioclase occurs, all of it has been altered to fine-grained aggregates of epidote, quartz, chlorite and clay minerals. Chlorite also occurs in the form of continuous veins which cut-across both the quartz and altered plagioclase grains. Accessories are rare and consist of fine-grained aggregates of opaque minerals within the chlorite grains and euhedral apatite and zircon grains within the altered plagioclase grains.

G.R. 124 312. Moderate-sized dyke-like outcrop of a highly silicified granite completely enclosed within partially serpentinised, massive harzburgite. In thin-section, it exhibits a granoblastic cuneiform texture defined by ribbon-like grains of quartz and minor plagioclase which exhibit a strong preferred crystallographic orientation, and between which occur very fine-grained quartz, tremolite and kaolinite. The modal composition is quartz (82%), plagioclase (10%), alkali feldspar (4%), kaolinite (2%), tremolite (1%) and secondary goethite (<1%).

Quartz occurs in three main forms:
i) single anhedral grains exhibiting very strong undulose extinction and subgrain development.
ii) ribbon-like elongate grains which exhibit moderate undulose extinction.
iii) extremely fine-grained aggregates of equant-shaped grains which exhibit strong undulose extinction and occur as a matrix to the other forms of quartz.

The plagioclase occurs as fresh strongly deformed grains that are commonly elongate in shape, exhibit strong undulose extinction, and have undergone minor subgrain development. Alkali feldspar occurs as rare graphic intergrowths with the larger quartz grains. Tremolite occurs as very fine-grained colourless fibrous grains within the matrix.

G.R. 124 312. Fairly large dyke-like outcrop of silicified granite enclosed within schistose serpentinite. In thin-section, it exhibits a hypidiomorphic granular texture defined by granular aggregates (of highly variable grain-size) of quartz, plagioclase, and alkali feldspar along with very fine-grained tremolite.

Quartz occurs in two main forms:
i) extremely fine-grained grains which exhibit moderate undulose extinction and are commonly polygonal in shape.
ii) fairly large aggregates of subgrains which exhibit very strong undulose extinction and have highly serrated grain boundaries. Triple junctions are common.

Plagioclase also occurs in two main forms:
i) fresh plagioclase occurring as subequant to prismatic grains which exhibit well-developed multiple twinning and moderate undulose extinction.
ii) altered plagioclase which occurs as much larger grains that are anhedral in shape and have ragged grain boundaries. The plagioclase within these grains has been altered to mixtures of sericite, quartz subgrains and calcite.

Tremolite occurs as extremely fine-grained fibrous aggregates which cross-cut all of the other phases present. Alkali feldspar is of rare occurrence as subprismatic grains which exhibit moderate undulose extinction and have ragged grain boundaries.

G.R. 154 255. Small outcrop of fine-grained quartz-plagioclase-biotite aplite within partially serpentinised porphyroclastic harzburgite.

G.R. 146 261. Small intrusive-like body of massive granite within massive, porphyroclastic harzburgite. In thin-section, it exhibits a hypidiomorphic granular texture defined by relatively even-grained, interlocking grains of plagioclase, quartz, K-feldspar and rare biotite, along with cross-cutting tremolite/actinolite and chlorite. All of the grains are commonly embayed into each other and triple junction grain boundaries are common for the plagioclase, quartz, K-feldspar and biotite. The plagioclase has sharp grain boundaries, moderately developed multiple twin lamellae, strong compositional zoning, and weak undulose extinction.

Quart occurs in two main forms:
i) discrete grains with sharp grain boundaries which exhibit strong undulose extinction and strongly embay into each other.
ii) graphic intergrowths with K-feldspar.

The K-feldspar also occurs in two main forms:
i) discrete grains which have well-developed stringy perthites and very ragged grain boundaries.
ii) graphic intergrowths with quartz grains.

Biotite generally occurs as very elongate prismatic grains. Many of the biotite grains have ragged grain boundaries and some of them are completely replaced by fibrous tremolite/actinolite. The tremolite/actinolite occurs as colourless to light green aggregates of tiny prismatic acicular grains that both replace some of the biotite grains and occur as cross-cutting grains throughout the rock.

G.R. 235 917. A fairly large mass of fine-grained aplite completely enclosed within moderately sheared harzburgite. The aplite is very fine-grained, quartz-rich, biotite-free, and contains discrete zones of foliation. In thin-section, there are two distinctly different types of granodiorite at this locality:

Type 1: this variety exhibits a hypidiomorphic granular texture defined by relatively large interlocking subhedral ragged grains of plagioclase between which are smaller equant-shaped grains of quartz and fibrous tremolite which cross-cuts all of the other phases. The modal composition is plagioclase (determined by XRD to be low albite) (75%), quartz (10%), alkali feldspar (<5%) and tremolite (5-10%). The plagioclase occurs as interlocking grains with very ragged edges, well-developed antiperthites, bent twin lamellae and moderate undulose extinction. A rarer form of plagioclase occurs interstitial to these grains and is associated with quartz and tremolite. It occurs as small equant-shaped anhedral grains with well-developed thick twin lamellae, strong undulose extinction and sharp grain boundaries. Quartz occurs as both small grains and aggregates of sub-grains which exhibit strong undulose extinction and are commonly polygonal in shape. The tremolite occurs as abundant extremely fine-grained aggregates of colourless fibrous grains which are both interstitial to and cross-cut the other phases. Alkali feldspar is of minor

occurrence as small subprismatic untwinned grains associated with the interstitial quartz, plagioclase and tremolite.

Type 2: exhibits an allotriomorphic granular texture defined by large porphyroclasts of ragged-edged plagioclase and alkali feldspar between which are smaller grains of plagioclase, alkali feldspar and tiny fibrous masses of tremolite which cross-cut all of the other phases present. The modal composition is plagioclase (45%), alkali feldspar (45%), quartz (8%), tremolite (2%) along with rare opaques, remnant biotite, tourmaline and zircon. The plagioclase grains have ragged edges and exhibit partial alteration to mixtures of quartz, albite and carbonate. Some of the grains exhibit minor micro-faulting (with offset twin lamellae), and moderate undulose extinction is common. The alkali feldspar occurs as quite large equant-shaped anhedral grains which have very ragged edges and well-developed stringy perthites. They exhibit moderate undulose extinction, are commonly highly fractured (with the fractures being filled by tiny grains of equant-shaped granular quartz and plagioclase) and moderately embayed. Quartz occurs as small masses of subgrains which commonly surround the feldspar grains. They exhibit moderate undulose extinction and have sharp grain boundaries. Tremolite is common as tiny bunches of elongate prismatic grains which cross-cut all of the other phases present.

G.R. 234 041. Inclusion of mylonitic (S-C fabric) granodiorite within schistose serpentinite. In thin-section, it has a cataclastic, mylonitic texture defined by porphyroclastic equant to subprismatic grains of quartz and plagioclase between which are very fine-grained granular grains of quartz and feldspar. The modal composition is quartz (60%), plagioclase (35%), alkali feldspar (5%), phengite (3%) and clay minerals (<2%).

Quartz occurs in two main forms:

i) porphyroclasts: occur as anhedral equant to elongate ribbon-like grains which exhibit strong undulose extinction and have very ragged edges. Subgrains are commonly developed in the larger grains and consist of equant-shaped, generally unstrained quartz. The ribbon-like grains consist of many subgrains which are strongly embayed into each other, anhedral in shape, and exhibit strong to extreme undulose extinction. These grains define the dominant foliation within the granodiorite and wrap-around the porphyroclasts.
ii) granular matrix: these grains occur as tiny equant-shaped anhedral grains which have strongly sutured grain boundaries and exhibit moderate undulose extinction.

Like the quartz, the plagioclase also occur in two main forms:

i) porphyroclasts: these grains occur as equant to prismatic subhedral grains which are moderately embayed and exhibit minor subgrain development. The larger grains are commonly altered to sericite while the smaller grains are unaltered. Many of the grains have quite strongly bent multiple twin lamellae and exhibit moderate undulose extinction.
ii) fine-grained plagioclase: these grains are equant-shaped and subhedral and occur within the finer-grained granular quartz grains. They do not exhibit any subgrain development and are commonly embayed by the finer-grained quartz.

Alkali feldspar is of minor occurrence as subprismatic subhedral untwinned grains which are commonly altered to sericite. They have extremely ragged grain boundaries and exhibit moderate undulose extinction.

The Coolac Serpentinite Belt

Harzburgites

The harzburgites comprise fresh harzburgite, moderately serpentinised harzburgite, and completely serpentinised harzburgite.

Fresh harzburgites are defined as those with greater than 30 modal% fresh olivine. They exhibit a pseudoporphyritic porphyroclastic texture in which relatively large porphyroclasts of orthopyroxene are separated from each other by, and interlock with, relatively finer-grained olivine and chromite grains, all three minerals being cross-cut by fracture-fill veinlets of chrysotile and/or magnetite. The modal composition (visually determined) is fresh olivine (30-75%), orthopyroxene (10-20%), clinopyroxene (0-5%), chromite (0-2%), serpentine (8-50%), along with minor magnetite and chlorite.

Away from micro shear zones, the olivine occurs as equant to subprismatic, anhedral, generally ovoid-shaped grains whereas close to these shear zones, it occurs as more elongate and shard-like grains which exhibit a strong preferred crystallographic orientation. All of the olivine grains are strongly fractured with the fractures being filled by chrysotile, linear aggregates of tiny particles of magnetite, or various combinations of both. The olivine grain boundaries are very ragged in places, with many grains impinging on each other. Some of the olivine grains (particularly the larger ones) exhibit weak to moderate undulose extinction. The olivine grains commonly strongly embay the orthopyroxene grains and in places, appear to replace them. Within the micro shear zones, the olivine grains occur as elongate boudins which are strongly aligned in the shear direction and are separated from each other by chrysotile veinlets (with the long axis of the chrysotile fibres being oriented perpendicular to the shear direction).

The orthopyroxene generally occurs as porphyroclasts of variable grain size. They are generally subhedral in shape, strongly embayed (with the embayments being filled by either fresh olivine or serpentine pseudomorphs after olivine), and most exhibit moderate to strong undulose extinction. Some of the grains exhibit subgrain development. The more elongate grains generally have very ragged edges and some have been replaced by olivine either along their cleavage planes or around the grain margins (i.e. rim replacement). Some of the orthopyroxene grains contain inclusions of very finely banded pervasive exsolution lamellae of diopside, ovoid-shaped olivine grains, and rarely, small subhedral grains of chromite. Some of the orthopyroxene grains have been completely replaced by chrysotile and these exhibit extreme undulose extinction. Many of the orthopyroxene grains are cut-across by late-stage chrysotile veinlets and are essentially free of secondary magnetite which instead occurs in the late-stage cross-cutting chrysotile veinlets.

Discrete grains of diopside are rare, and occur as equant-shaped grains which exhibit strong diallage parting. Some of them exhibit a well-developed parting perpendicular to the trend of the diallage parting and this can be termed a kink band. They are commonly embayed by the olivine grains and have moderately ragged edges (though not as ragged as those of the orthopyroxene grains).

Chrome spinel generally occurs as very small anhedral strongly embayed, amoeboid-shaped grains scattered throughout the harzburgite. It rarely occurs as elongate inclusions within the diopside grains, with the elongation direction of these spinel grains paralleling the trend of the diallage

parting of the host. It also occurs as anhedral-shaped masses of equant-shaped grains which, in places, are partially replaced by secondary magnetite grains. The individual spinel grains within these masses are generally amoeboid-shaped, irregular grains which appear to have intergrown with the surrounding olivine grains.

Within the micro shear zones, the C-surface foliation is defined by the elongation direction of the olivine grains, the alignment direction of linear aggregates of the olivine grains, and the dominant trend of the chrysotile/magnetite veinlets (with the long axis of the chrysotile fibres within these veins being oriented at approximately 70° to 90° to this plane). In contrast, the S-surface foliation is defined by the lesser dominant trend of the chrysotile/magnetite veinlets (with the long axis of these chrysotile fibres oriented at approximately 30° to 40° to the C-surface foliation).

Moderately serpentinised harzburgites are defined as those harzburgites which have less than 30 modal% fresh olivine. They exhibit a pseudoporphyritic porphyroclastic texture in which relatively large porphyroclasts of bastitised orthopyroxene are encompassed by a groundmass of mesh textured lizardite/chrysotile, minor relict olivine and cross-cutting chrysotile/magnetite veinlets. The modal composition (visually determined) is fresh olivine (3-20%), orthopyroxene (10-15%), clinopyroxene (0-2%), chromite (1-3%) and serpentine (63-85%), along with minor magnetite and magnesian chlorite.

Minor fresh olivine occurs in patches throughout these harzburgites, generally as grain aggregates.

The orthopyroxene grains are strongly bastitised and replaced by fibrous chrysotile. They generally occur as subequant to elongate prismatic, anhedral to subhedral, moderately embayed grains (with the embayments being filled by either relict olivine grains or serpentine pseudomorphs after olivine). They have very ragged edges and exhibit moderate undulose extinction. Olivine inclusions are common, as are very finely-spaced cleavage parallel exsolution lamellae of diopside and linear aggregates of tiny magnetite grains along cleavage planes. The pseudomorphic chrysotile fibres have replaced the orthopyroxene grains along their cleavage planes. Some of the orthopyroxene grains are quite strongly bent, while others are strongly fractured with the dominant fracture set being oriented perpendicular to the long axis of the orthopyroxene grains.

Diopside is of rare occurrence as small, equant-shaped grains which exhibit very closely-spaced fine diallage parting.

The chrome spinel occurs as anhedral, subprismatic strongly fractured grains. Two dominant fracture sets occur with the more weakly developed fracture set paralleling the long axis of the grains and the more pronounced fracture set perpendicular to this elongation direction. Chrome spinel also rarely occurs as amoeboid-shaped grains within serpentine embayments (originally olivine grains) in cuspate-shaped orthopyroxene grains. The chrome spinel grains are commonly rimmed by Mg-chlorite.

The mesh texture in these harzburgites consists of lizardite (and in rarer cases, relict olivine) cores surrounded by a narrow rim of chrysotile. The cores vary in shape from equant ovoid grains to elongate ovoid grains with the long axis being parallel to the dominant late-stage chrysotile veinlet direction. The rims consist of fibrous chrysotile grains with the individual grains being oriented between 60° to 90° to the rim walls.

The orientation of the chrysotile/magnetite veinlets is strongly controlled by the mesh texture serpentine as these veinlets occur as inter mesh texture space-filling and are aligned parallel to the long axis of the mesh texture cores. Within these veinlets, the magnetite occurs as linear aggregates of tiny grains at the centre of the veinlets while the chrysotile fibres are oriented approximately perpendicular to the vein margins.

Completely serpentinised harzburgites are here defined as those which lack relict olivine. They exhibit a "classic" mesh texture defined by ovoid lizardite cores with chrysotile rims, or a sub-mesh texture, or a feathery decussate texture, but porphyroclastic orthopyroxene (or its pseudomorphs) is always present. The modal composition (visually determined) is orthopyroxene (10-20%), chromite (1-3%), and serpentine (80-90%), along with minor magnetite.

The orthopyroxene grains are completely bastitised, elongate prismatic, and subhedral in shape. Schiller structure (i.e. fine exsolution lamellae of diopside) is extremely finely-spaced and well-developed along the dominant longitudinal cleavage. The orthopyroxene grains commonly exhibit strong undulose extinction and are cut-across by chrysotile veinlets.

Chrome spinel occurs as cores to some of the larger magnetite aggregates and as heavily embayed amoeboid-shaped grains rimmed by secondary magnetite.

The 'classic' mesh texture is defined by complete lizardite pseudomorphs after ovoid-shaped former olivine grains and narrow outer rims of chrysotile veinlets which exhibit moderate undulose extinction. The mesh texture consists of two distinct parts:

i) a core of sub-isotropic featureless lizardite which is in places, partially replaced by magnetite.
ii) an outer rim consisting of fibrous chrysotile grains which exhibit moderate to strong undulose extinction. These fibres are oriented at an oblique angle (which is highly variable from 30° to 90°) to the outer rim.

The serpentine shear bands are defined by 'boudinaged' (i.e. flattened) mesh texture cores with the outer chrysotile rims coalescing into discrete, continuous C-surface chrysotile vein fibres which are parallel to the long axis of the lizardite cores. The S-surface is defined by cross-cutting chrysotile fibres that are at an angle of 30° to 60° to the C-surface foliation. These shear bands are of restricted occurrence and continuous for only some 1.8mm. Magnetite occurs within the cross-cutting veinlets as linear aggregates of tiny equant-shaped grains.

Dunites

The Coolac Serpentinite Belt dunites can be subdivided into relatively fresh and completely serpentinised groups. Unlike the harzburgites, transitional types seem not to exist.

Fresh dunites are defined as having more than 85 modal% fresh olivine. They are granoblastic to subporphyroclastic, the later texture comprising interlocking highly fractured olivine grains with minor orthopyroxene, clinopyroxene, chromite, space-fill serpentine and magnetite. The modal composition of these dunites (visually determined) is fresh olivine (85-90%), orthopyroxene (2-5%), clinopyroxene (2%), chromite (0-3%), serpentine (5-6%) along with minor magnetite.

Olivine occurs as subprismatic, anhedral grains with strongly sutured grain boundaries. They are highly fractured, with the fractures being filled by either:

i) linear aggregates of tiny equant-shaped magnetite grains.
ii) veinlets of fibrous chrysotile.
iii) composite veinlets of chrysotile/magnetite.

The veinlets are very discontinuous and commonly anastomose into each other. Early chrysotile veinlets are cross-cut by later veinlets and three distinct generations of veinlets can be recognised.

Orthopyroxene occurs as relatively small subprismatic, subhedral grains which are highly embayed by the olivine grains and moderately fractured.

Clinopyroxene occurs as composite grain aggregates with the individual grains being subprismatic and subhedral in shape and exhibiting weak undulose extinction. They exhibit very fine diallage parting and are moderately embayed by the olivine grains.

The chrysotile/magnetite veinlets occur as intergranular space-filling veinlets between the olivine grains.

Completely serpentinised dunites lack fresh olivine grains and have well-developed mesh texture defined by lizardite cores and fibrous chrysotile rims, and minor cross-cutting chrysotile veinlets. Their modal composition (visually determined) is chromite (0-10%) and serpentine (90-100%) with minor chlorite and magnetite.

The mesh texture within these dunites consists of sub-isotropic cores of lizardite surrounded by rims of fibrous chrysotile. The cores are generally equant and ovoid in shape and the outer rims consist of very fine-grained fibrous aggregates of chrysotile which exhibit strong undulose extinction. Individual chrysotile grains are oriented at near right-angles to the rim margins.

The cross-cutting chrysotile veinlets are of minor occurrence and have variable continuity (300um to 12mm). They have a very consistent orientation with most of the veinlets paralleling one another. The veinlets are strongly sigmoidal in shape with the long axis of the individual chrysotile fibres being oriented perpendicular to the veinlet walls.

Magnetite is ubiquitous throughout all of the completely serpentinised dunites as either single isolated aggregates of tiny equant-shaped grains (possibly replacing primary chrome spinel) or as linear aggregates of tiny equant-shaped grains which also help to define the mesh texture.

Chrome spinel occurs as anhedral to subhedral isolated grains that are generally amoeboid in shape. Colour zoning occurs in some of the larger grains with black cores and pale brown rims. Many of the chrome spinel grains are intensely fractured and brecciated with fracture- and breccia-fill by chrysotile veinlets, talc and Mg-chlorite. Also, many of the chrome spinel grains exhibit a weak to moderately defined extension direction and bent chrome spinel grains are very rare. Within these dunites, it is often hard to distinguish between the chrome spinel and magnetite due to partial rim and fracture-related replacement of the chrome spinel by secondary magnetite. Many of the chrome spinel grains are moderately embayed, with the embayments being filled by lizardite/chrysotile after olivine.

Mg-chlorite is restricted to narrow zones surrounding the larger chrome spinel grains and as fracture-fill between them.

Talc/magnesite occur as patchy replacement of lizardite/chrysotile, replacements of chrysotile veinlets, and as fracture-fill within chromite.

Pyroxenites and Hornblendites

The pyroxenites are generally clinopyroxene-rich (with >70 modal% clinopyroxene) and rarely olivine-rich (up to 80 modal% olivine), clinopyroxene-bearing (up to 10 modal% clinopyroxene) and amphibole-bearing (up to 15 modal% amphibole) (Basden 1990). The wehrlites are medium-grained (approx. 2mm) with a xenoblastic granular texture and the amphibole-bearing varieties display an intercumulus texture (Basden 1990). True pyroxenites were not found within the Coolac Serpentinite Belt during the present study. The hornblendites display a porphyroclastic pseudoporphyritic texture defined by large grains of hornblende (fringed by tremolite) in a relatively fine-grained serpentine groundmass. The modal composition of these hornblendites (visually determined) is hornblende (50-70%), serpentine (0-45%), tremolite (5-50%), actinolite (0-5%), chlorite (0-7%) and epidote (0-3%) along with minor chromite and magnetite.

Hornblende occurs as relatively large euhedral to subhedral, prismatic to elongate prismatic grains which generally have a pale green core and dark brown rim. They do not exhibit any preferred crystallographic orientation and all of the hornblende grains have well-developed ragged edges and tremolite fringes. Some of the hornblende grains are completely replaced by mixtures of tremolite, actinolite and chlorite. The centre of some of the hornblende grains are hollow and filled with serpentine (perhaps after original magmatic olivine of pyroxene) and some of the grains exhibit moderate undulose extinction.

Serpentine dominates the groundmass of the hornblendites and occurs as colourless cross-cutting masses of small fibrous grains. Tremolite occurs as parallel groups of colourless elongate prismatic grains both as fringes around the hornblende grains and as replacements of them. Actinolite occurs as bright green, elongate prismatic diamond-shaped grains either on the rims of hornblende grains or as a constituent phase within the groundmass between the hornblende grains. They exhibit no preferred crystallographic orientation. Chlorite occurs as non-descript looking pale green replacements of both hornblende and actinolite. Epidote is of minor occurrence within the groundmass between the hornblende grains as clusters of anhedral, equant-shaped pale yellow grains.

Serpentinites

According to Ashley (1973), the massive serpentinites exhibit a well-developed "mesh texture" which is preserved in the schistose serpentinites as lenticular relicts but completely destroyed in the highly schistose varieties where the foliation is defined by the preferred crystallographic orientation of sub-fibrous serpentine and linear aggregates of magnetite grains.

The modal composition of both massive and schistose varieties (visually determined) is serpentine (80-99%), relict chrome spinel (0-5%), relict completely bastitised orthopyroxene (0-10%), talc (0-5%), chlorite (0-7%) and tremolite (0-5%), along with minor secondary magnetite. The massive varieties generally exhibit a pseudoporphyroclastic texture defined by relatively large pseudoporphyroclasts of completely bastitised orthopyroxene grains in a matrix of mesh-textured

serpentine, along with minor chrome spinel. They also exhibit a sub mesh-texture defined by lizardite cores surrounded by chrysotile rims (just like those in the completely serpentinised harzburgites). The schistose varieties generally exhibit a well-developed S-C fabric defined by the alignment of subparallel continuous chrysotile veinlets, linear aggregates of magnetite grains, the elongation direction of chrome spinel grains and cross-cutting discontinuous chrysotile/magnetite veinlets. In both varieties, cross-cutting veinlets of chrysotile/magnetite occur, as do decussate and feathery non-oriented serpentine grains.

Within the massive varieties, chrome spinel occurs as subhedral, equant-shaped moderately fractured grains which have undergone intense rim replacement by tiny magnetite grains. Within the schistose varieties, the chrome spinel grains are generally elongate and anhedral in shape. Many of them have been completely replaced by magnetite and they are commonly surrounded by narrow rims of colourless Mg-chlorite. "dust-like" linear aggregates of tiny equant-shaped magnetite grains trail-off the chrome spinel grains.

Remnant orthopyroxene grains are rare and are completely bastitised and pseudomorphed by fibrous chrysotile. They are subprismatic and subhedral in shape, exhibit extreme undulose extinction, possess rounded grain boundaries and are commonly embayed by the matrix serpentine (after former olivine grains). Within the schistose varieties, the orthopyroxene grains are elongate in the dominant shear direction (i.e. the long axis of the orthopyroxene grains parallels the dominant linear direction of the chrysotile veinlets). Within the massive varieties, the chrysotile that has replaced the orthopyroxene is of a different crystallographic orientation than that in the groundmass.

Tremolite is of rare occurrence as colourless subprismatic, diamond-shaped grains which are commonly moderately bent and exhibit weak to moderate undulose extinction. Within the schistose varieties, linear aggregates of tiny magnetite grains (which help to define the prominent C-surface foliation in these rocks) cut-across the tremolite grains.

Magnetite occurs in a number of different forms:
i) as tiny subhedral, equant-shaped isolated grains.
ii) as aggregates of these tiny grains. These aggregates are elongate in the schistose varieties and help to define the prominent C-surface foliation.
iii) as discontinuous veinlets which help to define both the C- and S-surface foliations.

Matrix chrysotile generally occurs within the more massive varieties as abundant kinked veinlets interspersed between much finer-grained serpentine. Both the veinlets and finer-grained serpentine do not exhibit any preferred orientation.

Mesh-textured serpentine is of minor occurrence, and is generally confined to the more massive varieties. It is defined by equant, ovoid-shaped cores of lizardite surrounded by chrysotile rims with the individual chrysotile fibres within the rims being oriented approximately perpendicular to the rim margins.

Cross-cutting chrysotile veinlets are generally only continuous for some 1mm. The fibres within these veinlets exhibit extreme undulose extinction which is oblique to the long axis of the veinlets. These veinlets commonly anastomose into each other and also enclose the magnetite veinlets.

The S-C foliation within the serpentinites is of a strongly linear character and is dominated by the C-surface foliation which is defined by the dominant orientation of continuous, subparallel large chrysotile veinlets and linear aggregates of tiny subhedral equant-shaped magnetite grains. The C-surface defining chrysotile veinlets are often en echelon in character and the larger veinlets exhibit extreme undulose extinction. The S-surface foliation is defined by less continuous chrysotile veinlets which are oriented approximately 30-45° to the C-surface orientation and also by linear aggregates of the same orientation comprising tiny magnetite grains. The S-surface defining veinlets merge into the C-surface defining veinlets when they approach them.

Talc-carbonate rocks

Ashley (1969) recognised talc-antigorite-chromite schists, talc-bearing metaserpentinites, magnesite-bearing metaserpentinites and talc-tremolite-magnetite-chromite schists. In this present study, two distinct assemblages are recognised and will be referred to as talc-rich metaserpentinites (with >75 modal% talc) and magnesite-rich metaserpentinites (with >40 modal% magnesite).

The talc-rich metaserpentinites are generally fine to very fine-grained and exhibit either a granoblastic hornfelsic texture (i.e. non-aligned mineral components) or a decussate schistose texture (i.e. with aligned mineral components). The modal composition of these rocks (visually determined) is talc (75-90%), serpentine (0-23%), chlorite (0-3%), tremolite (0-5%) and anthophyllite (0-5%) along with minor primary chrome spinel and secondary magnetite. The granoblastic hornfelsic texture is defined by pseudoporphyroblasts (up to 0.75x0.75mm in maximum dimension) of talc and magnesite in a much finer-grained groundmass of chlorite. In contrast, the decussate schistose texture is defined by aligned subparallel grains of prismatic talc, serpentine, tremolite and anthophyllite.

Talc occurs in a number of different forms:

i) non-descript, equant to subprismatic, subhedral grains which exhibit weak to moderate undulose extinction.
ii) very fine-grained strongly interlocking prismatic bladed grains.
iii) tiny prismatic feathery grains pseudomorphous after serpentine.

Serpentine occurs as tiny prismatic interlocking grains. Chlorite occurs as colourless aggregates of tiny, elongate prismatic non-aligned grains which are cut-across by the talc grains. Tremolite occurs as colourless, elongate prismatic grains which are preferentially confined to discrete zones and are intimately associated with anthophyllite. Anthophyllite occurs as colourless, prismatic diamond-shaped grains which, like the tremolite are confined to discrete zones. Chrome spinel occurs as anhedral to subhedral, equant-shaped grains, commonly with magnetite "stringers" tailing off them which are similar in appearance to pressure shadows around porphyroblasts in regionally metamorphosed rocks.

Magnesite-rich metaserpentinites are of very rare occurrence within the Coolac Serpentinite Belt (with only one being found in the course of the present study) and exhibit a pseudoporphyritic texture defined by pseudoporphyroblasts of magnesite in a finer-grained matrix of serpentine. The modal composition of these rocks (visually determined) is magnesite (40%) and serpentine matrix (60%), along with minor primary chrome spinel and secondary magnetite. Magnesite occurs as subhedral to euhedral, rhombic subprismatic grains which appear to be pseudomorphous after original olivine grains. Serpentine generally consists of equant, ovoid-shaped lizardite cores

surrounded by thin outer rims of chrysotile. Chrysotile veinlets occur as relatively continuous thin veinlets which commonly enclose magnetite veinlets.

Gabbros

Texturally, the gabbros of the Coolac Serpentinite Belt are of two main types, those which exhibit dominantly cumulus textures and those which exhibit dominantly granular textures. Mineralogically, they are mostly hornblende gabbros with clinopyroxene gabbros being the second most dominant type and orthopyroxene- and olivine-bearing types being of rare occurrence. The gabbros have experienced varying degrees of intensity of metamorphism and alteration which may have affected the original cumulus texture and led to the development of a more granular texture. Both gabbros types commonly occur together in the same outcrop (i.e. G.R. 234 965).

The **cumulus gabbros** dominantly exhibit a post-cumulus space-fill texture defined by the following:

i) large platy grains of clinopyroxene between which occur postcumulus space-fill grains of plagioclase.
ii) interlocking grains of hornblende (with rare clinopyroxene cores) with the spaces between these grains being completely filled by saussuritised plagioclase and abundant cross-cutting fibrous tremolite.
iii) strongly interlocking moderately embayed grains of plagioclase and tremolite pseudomorphs after hornblende with intergranular alteration assemblages of tremolite and chlorite, and minor cross-cutting veinlets of albite/epidote/quartz, chlorite/tremolite and clinoclinozoisite.

In these gabbros, the hornblende clearly postdates the clinopyroxene which it commonly encloses and a complete spectrum exists from leucogabbros (with >85 modal% plagioclase) to clinopyroxene gabbros (with Cpx>Hrbl) and hornblende gabbros (with Hrbl>Cpx). Thus, these gabbros can be subdivided into leucogabbros, clinopyroxene-dominant gabbros and hornblende-dominant gabbros.

The only "true" **leucogabbros** were found at Bombowlee Creek (G.R. 234 965) and these have a modal composition (visually determined) of plagioclase (85%), clinopyroxene (0-5%), hornblende (3-5%), tremolite (5-7%) and chlorite (0-5%), along with cross-cutting veinlets of albite/epidote/quartz, chlorite/tremolite and clinoclinozoisite.

Plagioclase occurs in two main forms:

i) fresh plagioclase occurs as subhedral equant to subprismatic grains which exhibit well-developed multiple twin lamellae with most lamellae exhibiting strong micro-faulting (i.e. shear displacement of the lamellae). These grains strongly embay into each other and some of them are strongly bent and exhibit moderate undulose extinction.
ii) altered plagioclase occurs as mixtures of fine-grained epidote, albite and quartz that completely replace the plagioclase grains though retaining the original plagioclase shape, and in some cases, some of the multiple twin lamellae. Discrete grain boundaries of these grains do not occur as they merge into each other.

Brown/green hornblende occurs as rare tiny cores within tremolite pseudomorphs after these grains. The pseudomorphs have retained the original hornblende shape but now consist of colourless, fibrous tremolite grains and minor, colourless chlorite. The cross-cutting veinlets are continuous for

only some 8mm and have highly variable widths along their length. They cut-across both the plagioclase and tremolite pseudomorphs after hornblende.

"True" **clinopyroxene gabbros** with cumulus textures were also only found to occur along Bombowlee Creek (G.R. 234 965). These have a modal composition (visually determined) of plagioclase (45-70%), clinopyroxene (25-40%), hornblende (0-15%), olivine (0-5%), Mg-chlorite (<1-5%), tremolite (0-5%), clinoclinozoisite (0-4%) and quartz (0-3%), along with minor talc, cross-cutting veinlets of prehnite, and rare accessory opaques and apatite.

Plagioclase occurs as subhedral, subprismatic to elongate prismatic grains which exhibit well-developed multiple twin lamellae. They strongly embay into both each other and the diopside grains. They commonly exhibit moderate undulose extinction, and in some cases, are highly fractured and completely saussuritised.

Diopside occurs as colourless, anhedral to subhedral, equant to prismatic strongly embayed grains. Both hornblende and tremolite commonly occur as narrow fringes around the diopside grains. The diopside grains are commonly moderately fractured (with chlorite fracture-fill) and rarely brecciated (but with negligible rotation of the diopside fragments).

Hornblende occurs as strongly pleochroic brown and rarely weakly pleochroic green subhedral angular prismatic grains. It occurs as either narrow fringes around the diopside grains or as discrete grains enclosed within plagioclase. Olivine is of rare occurrence as small equant-shaped ovoid grains which occur between the diopside grains. Mg-chlorite occurs as colourless masses of platy grains within space-filling between the diopside and plagioclase grains, and as fracture-fill between the diopside grains. Tremolite occurs as colourless bladed prismatic grains, commonly fringing diopside grains. Clinoclinozoisite occurs as moderately large subhedral prismatic grains between the plagioclase. Talc occurs as fine-grained replacements of some of the olivine.

Cross-cutting prehnite veinlets occur throughout these gabbros and cut-across all of the other phases present. They consist of colourless prismatic elongate subhedral prehnite grains which exhibit well-developed intense undulose extinction and are commonly fractured.

Hornblende gabbros occur throughout the Coolac Serpentinite Belt although those with cumulus textures are much rarer than those with granular textures. They have a modal composition (visually determined) of plagioclase (40-50%), hornblende (30-50%), diopside (0-3%), tremolite (0-27%), epidote (0-1%) and chlorite (0-1%), along with rare clinoclinozoisite. At G.R. 234 917, such a hornblende gabbro has been intruded by an aplitic granite.

Plagioclase has almost been completely saussuritised (with rare fresh plagioclase cores) to a fine-grained mixture of non-descript albite/quartz/epidote. It occurs as space-filling between the hornblende grains.

Hornblende generally occurs as highly ragged subhedral subprismatic angular grains. They contain rare inclusions of colourless diopside and are commonly replaced by fibrous tremolite. They commonly interlock with each other (very similar to a postcumulus overgrowth texture) and are generally completely replaced by tremolite.

Tremolite occurs as colourless, elongate prismatic angular grains which cut-across all of the other phases present and commonly replace the hornblende grains.
Chlorite occurs as non-descript fine-grained fan-like masses within saussuritised plagioclase.
Epidote/clinoclinozoisite occur as small granular masses within saussuritised plagioclase.

The **granular-textured gabbros** exhibit either an allotriomorphic granular or hypidiomorphic granular texture defined by the following:

i) strongly interlocking anhedral to subhedral grains of plagioclase, clinopyroxene and hornblende, along with cross-cutting alteration assemblages of chlorite, epidote, tremolite/actinolite, carbonate and clinoclinozoisite.
ii) interlocking grains of hornblende, plagioclase, clinopyroxene, prehnite and rare grossular garnet.
iii) interlocking, fairly even-grained hornblende and plagioclase, along with minor quartz and chlorite, and cross-cutting fibrous tremolite.
iv) interlocking grains of highly saussuritised plagioclase (and its alteration products including epidote, clinoclinozoisite, pale green amphibole, chlorite, tremolite and quartz).
v) interlocking subhedral angular grains of hornblende and plagioclase, along with cross-cutting veinlets of grossular and decussate aggregates of prehnite.

Mineralogically, the granular-textured gabbros can be subdivided into leucogabbros, hornblende gabbros, clinopyroxene gabbros and completely altered gabbros.

Leucogabbros are of common occurrence in the central part of the Coolac Serpentinite Belt but are rare elsewhere. All of the leucogabbros exhibit an allotriomorphic granular texture and have a modal composition (visually determined) of plagioclase (60-85%), hornblende (0-15%), clinopyroxene (0-10%), alkali feldspar (0-5%), quartz (0-20%), chlorite (0-3%), tremolite/actinolite (2-15%), epidote (0-5%) and clinoclinozoisite (0-1%), along with minor carbonate alteration, accessory apatite and opaques, and cross-cutting veinlets and patches of epidote/clinoclinozoisite.

Plagioclase is of large grain-size variation and generally occurs as subhedral subprismatic grains which strongly embay into each other, exhibit well-developed multiple twin lamellae and appear to lack any compositional zoning. Many of the plagioclase grains are completely altered to mixtures of albite/quartz/epidote/clinoclinozoisite/carbonate. Some of the grains and twin lamellae are moderately bent and many of the grains are moderately fractured, with fracture-fill by clinoclinozoisite, epidote, tremolite/actinolite and carbonate.

Hornblende generally occurs as quite large strongly pleochroic green/brown subhedral subprismatic grains with rare strongly pleochroic blue-green outer rims. They exhibit moderate undulose extinction and partial tremolite replacement.

Diopside occurs as colourless anhedral subprismatic strongly embayed grains. Some have narrow pleochroic brown hornblende rims whereas others are completely replaced by fibrous mixtures of tremolite/actinolite.

Alkali feldspar occurs as untwinned or moderately perthitic anhedral equant-shaped grains which have strongly sutured grain boundaries with adjacent plagioclase and quartz. They exhibit quite intense sericitic alteration.

Quartz occurs as an alteration product of both plagioclase and alkali feldspar or as small anhedral equant-shaped discrete grains which exhibit strong undulose extinction. Chlorite occurs as colourless, non-descript patches of tiny grains throughout the gabbros and as a fracture-fill phase. Tremolite/actinolite occurs as replacements of both diopside and hornblende grains which consist of tiny subhedral prismatic grains. It also occurs as fibrous aggregates of tiny elongate prismatic grains which cross-cut the diopside, hornblende and plagioclase grains. Epidote/clinoclinozoisite occur as non-descript small alteration patches and as cross-cutting veinlets.

Hornblende gabbros are the most common gabbro type within the Coolac Serpentinite Belt and are widespread in occurrence. They exhibit either hypidiomorphic granular or allotriomorphic granular textures and have a modal composition (visually determined) of plagioclase (5-50%), hornblende (5-50%), chlorite (0-15%), epidote (0-40%), tremolite/actinolite (0-4%), prehnite (0-70%), quartz (0-3%), grossular (0-2%), clinopyroxene (0-1%) and clinoclinozoisite (0-0.5%), along with accessory zircon, apatite, allanite and opaques, and with cross-cutting veinlets of clinoclinozoisite and grossular.

Plagioclase occurs in two main forms:

i) rarely as fresh plagioclase grains which exhibit well-developed multiple twin lamellae (which is often slightly bent) and have weak to absent compositional zoning. These grains occur as relatively small, anhedral subprismatic grains which have moderately sutured grain boundaries. They either poikilitically enclose the hornblende grains or occur interstitial to them.
ii) most commonly as completely altered anhedral to subhedral, subprismatic grains. They sometimes retain well-defined multiple twin lamellae but in most cases, occur as non-descript aggregates of albite-epidote-quartz or prehnite-grossular.

Hornblende contains rare cores of diopside and occurs as moderately pleochroic green/brown grains, generally with brown cores and green rims. They are generally subhedral and prismatic in shape and have ragged edges. They exhibit no preferred crystallographic orientation and in places, contain tremolite/actinolite fringes and rare chlorite alteration. Some of the grains are moderately bent and exhibit moderate undulose extinction while others are unbent and lack any undulose extinction.

Chlorite occurs as either colourless non-descript aggregates or as replacements of hornblende. Epidote occurs as small anhedral equant-shaped pale yellow grain aggregates or as a replacement of plagioclase. Tremolite/actinolite occurs as thin needle-like elongate prismatic grains, fringes on hornblende grains, and as a complete replacement of hornblende. Prehnite occurs as abundant subhedral prismatic grains commonly in the form of fan-shaped aggregates, generally replacing former plagioclase grains. Grossular occurs as either colourless fine-grained aggregates commonly associated with prehnite, or as moderately continuous sinuous veinlets. Clinoclinozoisite occurs as aggregates within altered plagioclase or as elongate sinuous veinlets. Allanite occurs as strongly pleochroic (pale to dark brown) anhedral to subhedral, equant to prismatic grains (often in the form of grain aggregates) which are commonly embayed by plagioclase and hornblende. Zircon occurs as aggregates of anhedral equant-shaped grains and more rarely, as quite large subhedral prismatic angular grains.

Clinopyroxene gabbros are of extremely rare occurrence with only one granular-textured type being found during the present study (G.R. 234 965). This gabbro exhibits a porphyritic allotriomorphic granular texture defined by relatively large grains of strongly embayed anhedral subequant clinopyroxene within a finer-grained matrix of fresh multiply twinned plagioclase grains and minor cross-cutting grains of chlorite and clinoclinozoisite. The modal composition of this gabbro (visually determined) is clinopyroxene (40%), saussuritised plagioclase (50%), Mg-chlorite (9%) and clinoclinozoisite (1%), along with accessory apatite.

In hand-specimen, the completely altered gabbros have the appearance of the granular-textured hornblende gabbros but in thin-section, they are almost completely altered and are strongly veined. They are of very rare occurrence though widely distributed throughout the Coolac Serpentinite Belt and are most common in the central part of the belt. They have a modal composition (visually determined) of hornblende (0-45%), epidote (0-45%), clinoclinozoisite (2-40%), chlorite (5-30%) and tremolite (3-30%), along with accessory apatite and opaques.

Hornblende occurs as subhedral subprismatic non-aligned grains which are moderately pleochroic green in colour. Much of it occurs in the form of strongly interlocking grains. Epidote occurs as colourless, subhedral equant-shaped grains which are interstitial to the hornblende grains and appear to be replacements of former plagioclase. Clinoclinozoisite occurs as either anhedral formless colourless grains associated with epidote, or as cross-cutting veinlets. Chlorite occurs as pale green non-descript replacements of hornblende. Tremolite occurs as elongate prismatic fibrous rims on hornblende, more rarely as complete replacements of hornblende grains, and as cross-cutting discrete fibrous grains.

Plagiogranites

All of the plagiogranites exhibit an allotriomorphic granular texture defined by strongly interlocking grains (of variable grain-size) of quartz, plagioclase, hornblende and rare microcline, along with cross-cutting fibrous Mg-chlorite. The modal composition of the plagiogranites (visually determined) is quartz (40-60%), albitic plagioclase (30-55%), hornblende (0-3%), microcline (0-10%), sodic muscovite (0-<0.5%), Mg-chlorite (<1-2%) and epidote (0-<1%), along with accessory apatite, zircon and opaques. Ashley *et al.* (1983) report that alkali feldspar is typically absent and rarely up to 4% biotite occurs in these rocks.

Quartz occurs as anhedral to subhedral, equant to subprismatic grains of highly variable grain-size. They have moderate to strongly sutured grain boundaries, common subgrain development, and strong undulose extinction. The subgrains tend to occur as "ribbon-like" lenticular grains.

Plagioclase occurs as subhedral subequant to prismatic grains with moderately sutured grain boundaries. They exhibit well-developed multiple twinning (often with strongly bent and kinked twin lamellae) and weak undulose extinction. Alkali feldspar occurs as untwinned, relatively large subhedral equant-shaped grains. They have strongly sutured grain boundaries and have weak sericitic alteration. Hornblende is of rare occurrence as subhedral, subprismatic pale green grains which are partially replaced by tremolite. Sodic muscovite occurs completely enclosed within the alkali feldspar and plagioclase grains as colourless, tiny platy grains with strongly sutured grain boundaries. Chlorite is common as non-descript, elongate platy pale green grain aggregates which occur as fracture-fill between the other phases.

Albitites

The albitites exhibit a hypidiomorphic granular to allotriomorphic granular texture defined by interlocking grains (of variable grain-size) of albitic plagioclase, quartz, hornblende and rare microcline, along with cross-cutting tremolite, chlorite and clinoclinozoisite. They have a modal composition (visually determined) of albitic plagioclase (77-90%), quartz (5-10%), hornblende (3-7%), microcline (0-3%), tremolite (0-<1%), Mg-chlorite (<1-3%) and clinoclinozoisite (0-5%), along with accessory apatite, zircon, sphene and opaques.

Plagioclase occurs as subhedral, subequant to prismatic grains of highly variable grain-size. They generally exhibit well-developed multiple twinning and lack compositional zoning. Most of the grains have strongly sutured grain boundaries and some of the plagioclase is strongly saussuritised. Quartz occurs as anhedral, equant to subprismatic grains which have strongly sutured grain boundaries but exhibit only weak undulose extinction. Hornblende occurs as subhedral subprismatic olive-green grains which are commonly altered to fibrous tremolite and chlorite. Microcline is of rare occurrence as subhedral, equant-shaped polysynthetically twinned grains. Tremolite generally occurs as aggregates of tiny acicular colourless grains which cross-cut the other phases present and less commonly, as discontinuous narrow veinlets. Chlorite occurs as small aggregates of pale green grains which cut-across the other phases present, and as replacements of some of the hornblende grains. Clinoclinozoisite occurs as narrow discontinuous cross-cutting veinlets. Zircon occurs as subhedral, subprismatic grains with slightly rounded edges and abundant fractures.

Rodingites

For all of the rodingites of the Coolac Serpentinite Belt, clinopyroxenes are the only phases which can be easily recognised in hand-specimen. The following is largely summarised from Ray (1977). Group one rodingites have a relatively simple mineralogy of garnet and/or vesuvianite, clinopyroxene, minor tremolite, chlorite and magnetite, along with very rare zoisite and chromite. The relative proportions of these minerals varies enormously; garnet (0-35.6%), vesuvianite (0-86.6%) and chlorite (13.4-37.3%). There is a systematic variation from the margins of the dykes towards their centres as follows:

i) heterogeneous margins become monominerallic at the centres.
ii) vesuvianite increases in abundance relative to garnet towards the centres.
iii) relict clinopyroxene decreases in abundance towards the centres.

Relict textures occur with gabbroic, doleritic and basaltic parents for different samples being recognised and with garnet and/or vesuvianite occurring as subhedral pseudomorphous grains after plagioclase with unaltered clinopyroxene. When this relict texture is absent, the group one rodingites exhibit a porphyroclastic texture which is defined by relatively large grains of clinopyroxene in a finer-grained groundmass of garnet and/or vesuvianite.

For the group two rodingites, none of the constituent minerals can be easily recognised in hand-specimen. They have a simple mineralogy of zoisite and/or prehnite with or without garnet, chlorite, tremolite/actinolite and sphene. Most of the group two rodingites are monominerallic and have variable compositions; zoisite (0-90.1%), prehnite (0-91.8%), garnet (0-87%), chlorite (1.3-13.9%), sphene (0-3.6%), tremolite/actinolite (0-4.8%) and albite (0-14%).

During the present study, the Coolac Serpentinite Belt rodingites were found to exhibit granoblastic (defined by interlocking grains of the constituent phases), decussate (defined by interlocking

elongate grains of zoisite and/or talc and chlorite), domainal (defined by interlocking grains of chlorite-zoisite-grossular in discrete bands between bands dominated by clinopyroxene) and banded (defined by variation in grain-size within discrete bands, of the various constituent minerals present) textures. The rodingites can be subdivided into zoisite dominant, diopside-grossular dominant, chlorite-rich, grossular-zoisite and grossular types.

Zoisite dominant rodingites are of common occurrence throughout the Coolac Serpentinite Belt and exhibit either a decussate or granoblastic texture. They have a modal composition (visually determined) of zoisite (60-80%), chlorite (10-15%), serpentine (0-40%), diopside (0-5%) and altered plagioclase (0-10%), along with minor secondary magnetite.

Diopside-grossular dominant rodingites are also of common occurrence throughout the Coolac Serpentinite Belt and generally exhibit a granoblastic texture or rarely, a banded texture. They have a modal composition (visually determined) of diopside (20-70%), grossular (15-60%), chlorite (10-30%), along with rare clinoclinozoisite, orthopyroxene and accessory opaques.

Diopside occurs as colourless, anhedral to subhedral, equant to subprismatic grains which commonly exhibit well-developed closely-spaced diallage parting and have ragged edges. Some of the diopside occurs in the form of clusters of small grains. The diopside is moderately embayed, commonly fractured and fragmented. Many of the grains exhibit strong undulose extinction and triple junction grain boundaries are common.

Grossular occurs as colourless, non-descript aggregates of small anhedral equant-shaped grains. Chlorite generally occurs as colourless, feathery clusters of fibrous prismatic small grains and more rarely as a fracture-fill phase within the grossular aggregates. Clinoclinozoisite occurs as colourless, subhedral equant-shaped grains which are commonly associated with the diopside. Orthopyroxene is of extremely rare occurrence as colourless, subhedral equant-shaped grains which often occur as clusters of grains and as cores to the diopside grains. Opaques are of very rare occurrence as angular, fractured elongate grains.

Chlorite-rich rodingites are of moderately rare occurrence throughout the Coolac Serpentinite Belt and exhibit either a granoblastic domainal or decussate texture. They have a modal composition (visually determined) of chlorite (40-60%), zoisite (30-50%), grossular (0-5%), diopside (0-5%) and talc (0-10%), along with minor secondary magnetite.

Chlorite generally occurs as veinlets and radial aggregates of colourless grains which exhibit moderate undulose extinction. The vein-related chlorite grains are much coarser-grained and exhibit a strong basal cleavage whereas the chlorite within the radial aggregates is much finer-grained and does not exhibit any well-developed basal cleavage. All of the chlorite grains do not exhibit any preferred crystallographic orientation.

Zoisite and grossular both occur as non-descript colourless aggregates of tiny grains and cross-cutting veinlets. Diopside generally occurs as anhedral to subhedral, subprismatic subangular grains which exhibit very closely-spaced diallage parting and up to moderate undulose extinction. They have undergone minor cataclasis and have been partially replaced (rim replacement) by grossular-zoisite mixtures. Talc occurs as non-descript very fine-grained aggregates intimately associated with chlorite.

Grossular-zoisite rodingites are of very rare occurrence in the Coolac Serpentinite Belt and generally consist of interlocking grains of elongate zoisite and aggregates of grossular. They have a modal composition (visually determined) of grossular (50%) and zoisite (50%), along with rare Mg-chlorite.

Grossular generally occurs as colourless, anhedral grains which occur in the form of grain aggregates. The aggregate are very irregular in shape and commonly contain inclusions of zoisite, thus defining a poikiloblastic texture. Zoisite occurs as colourless (though commonly "clouded") subhedral tiny elongate prismatic grains, or as much larger subhedral equant to subprismatic grains. Both types have very ragged edges.

Grossular rodingites are of extremely rare occurrence and have only been found at the one site on Mount Lightning (G.R. 138 253) (though a similar grossular-goethite rodingite also occurs on Mount Lightning at the MLA deposit, see Chapter 9). This rodingite is entirely composed of grossular and occurs as vein fillings in between schistosity planes within highly schistose metaserpentinite which has a modal composition (visually determined) of serpentine (80%) and talc (20%). The contact between the grossular veinlets and serpentinite is extremely sharp and the rodingite is massive and unfoliated.

Mafic amphibolites

The mafic amphibolites display either a lepidoblastic texture (defined by the strong preferred crystallographic orientation of hornblende grains) or a pseudo-gneissic domainal texture (defined by alternating hornblende-rich and plagioclase-epidote rich bands). They have a modal composition (visually determined) of hornblende (20-40%), plagioclase (30%), quartz (10-25%), diopside (0-20%), epidote (0-20%) and tremolite (0-5%), along with minor accessory apatite, sulfides and sphene.

Hornblende occurs a strongly pleochroic brown and green grains, with the brown variety being the most common. These grains are anhedral to subhedral, angular and elongate prismatic in shape. They are quite strongly aligned and define a well-defined mineral elongation lineation. They commonly contain fairly large euhedral prismatic inclusions of apatite. Plagioclase generally occurs as subhedral, equant-shaped angular grains which exhibit extreme undulose extinction and multiple twin lamellae. Many of the grains are quite turbid in appearance (due to clay alteration) and they commonly contain inclusions of tiny apatite needles.

Quartz occurs as small subhedral equant-shaped polygonal-shaped grains with well-developed triple junction grain boundaries. A rarer occurrence is as larger elongate anhedral grains. Both types exhibit moderate to strong undulose extinction and commonly contain small euhedral apatite inclusions. Diopside occurs as colourless subhedral equant-shaped grains which exhibit well-developed diallage parting and contain sulfides at their interstices. It appears to be intimately associated with both plagioclase and epidote. Epidote occurs as colourless to pale straw yellow non-descript aggregates of anhedral subprismatic grains associated with plagioclase, quartz and diopside. Tremolite occurs as fringes of very small needle-like grains on the edges of some of the hornblende grains and more rarely as complete replacements of some of the hornblende grains.

Mafic hornfelses

The mafic hornfelses exhibit a decussate feathery pseudoporphyritic texture defined by elongate bladed feathery clusters of cross-cutting anthophyllite and tremolite within a finer-grained matrix of olivine, green spinel and talc. These rocks have a modal composition (visually determined) of olivine (3-25%), green spinel (5-17%), anthophyllite (0-80%) and tremolite (0-70%), along with minor accessory magnetite and sulfides.

Olivine occurs as small anhedral equant rounded inclusions within the green spinel grains, and as anhedral moderately fractured (with fracture-fill by secondary goethite) colourless elongate grains. Green spinel occurs as clusters of bright emerald green, tiny subhedral equant-shaped angular grains. They are full of inclusions of opaques (magnetite?) and olivine. The clusters are cut-across by both the anthophyllite and tremolite grains.

Anthophyllite occurs as subhedral, elongate prismatic grains which have a bladed feathery habit and usually occur in grain clusters. They appear to have no preferred crystallographic orientation and commonly cross-cut each other. They also cut-across both the green spinel and olivine grains, the later of which they commonly form fringes to. They commonly contain abundant inclusions of opaque (sulfide?) minerals. Tremolite occurs as subhedral, prismatic lath-like "stubby" grains which do not appear to exhibit any preferred crystallographic orientation and commonly cross-cut each other. They commonly contain abundant inclusions of opaque minerals (sulfides?). Talc occurs as tiny colourless grains on the rims of the olivine grains.

Metabasalts

The metabasalts of the Coolac Serpentinite Belt are either epidosites or low greenschist facies amygdaloidal metabasalts. They exhibit either a porphyritic intergranular quench texture (defined by elongate spindle-like phenocrysts of relict plagioclase and albite along with equant-shaped phenocrysts of diopside and epidote-filled amygdules, within a finer-grained groundmass of albite, actinolite and chlorite, and with cross-cutting quartz-albite veinlets) or a domainal granoblastic texture (defined by epidote-rich zones and chlorite-rich bands throughout the rock along with cross-cutting veinlets of albite). They have a modal composition (visually determined) of diopside (0-2%), relict plagioclase (0-3%), epidote (40-70%), albite (5-22%), chlorite (3-25%) and actinolite (0-30%), along with minor accessory opaques. Scanning Electron Microscopy investigations reveal that the epidote in the epidosites contains fine inclusions of sphene.

Diopside is of rare occurrence as euhedral, equant-shaped "blocky" pale green grains with well-developed crystal faces. Relict plagioclase is of rare occurrence as subhedral subprismatic to elongate prismatic grains. Some of the phenocrysts are moderately bent but only rarely fragmented and broken. They have largely been altered to a mixture of epidote-chlorite-quartz.

Epidote occurs in two main forms:
i) as radial aggregates of pale yellow subhedral, prismatic grains which fill amygdules.
ii) as pale yellow subhedral prismatic grains of large grain-size.

Albite occurs in three different forms:
i) as very thin, elongate spindle-like grains throughout the groundmass.
ii) as very rare phenocrysts of subhedral "blocky" prismatic grains.

iii) as veinlets of blocky subhedral prismatic grains. These grains exhibit well-developed multiple twin lamellae.

Chlorite occurs in two different forms:
i) as a pale green replacement of actinolite (and possibly hornblende) whose form it takes.
ii) as pale green radial masses which occur in discrete bands.

Actinolite occurs as emerald green subhedral prismatic acicular grains which occur throughout the groundmass.

Chlorite-rich rocks
The chlorite-rich rocks of the Coolac Serpentinite Belt exhibit a strong decussate feathery texture defined by interlocking fibrous grains of chlorite with or without cross-cutting veinlets of clinozoisite. They have a modal composition (visually determined) of chlorite (50-100%) and clinozoisite (0-50%), along with rare accessory Al-rich chromite (confirmed by XRD methods).

Chlorite occurs as moderately pleochroic green-brown subhedral to euhedral, equant to prismatic grains which are strongly interlocking with each other and exhibit strong undulose extinction. They commonly contain small subhedral to euhedral, equant to prismatic opaque inclusions. Mg-chlorite occurs as colourless sinuous veinlets which are composed of tiny radiating masses of grains and cut-across all of the other phases present. Clinozoisite occurs as irregularly distributed, pervasive veinlets throughout the rock which consist of colourless, subhedral elongate prismatic grains.

Granitoids
The granitoids display a hypidiomorphic granular texture defined by anhedral to euhedral grains (of highly variable grain-size) of plagioclase, alkali feldspar, quartz, chlorite and tremolite.

The intrusive granitoids from the vicinity of the Goobarragandra Copper Mine also exhibit a myrmekitic graphic texture defined by strongly interlocking grains of quartz and alkali feldspar. They have a modal composition (visually determined) of quartz (35%), plagioclase (40%), alkali feldspar (23%) and chlorite (2%), along with accessory apatite and zircon. Quartz occurs as myrmekitic and graphic intergrowths with alkali feldspar and as anhedral equant-shaped grains which exhibit moderate undulose extinction. Plagioclase occurs as lath-like elongate prismatic grains, commonly as grain aggregates. It exhibits well-developed multiple twin lamellae and strong undulose extinction. Alkali feldspar occurs as myrmekitic and graphic intergrowths with quartz. Chlorite occurs as green-brown thin veinlets and as fracture-fill.

The tectonic felsic granitoid inclusion from the vicinity of McAlpines Copper Mine also exhibits a cataclastic texture defined by strongly fractured and bent plagioclase and alkali feldspar grains of highly variable grain-size. It has a modal composition (visually determined) of plagioclase (65%), alkali feldspar (20%), chlorite (10%), tremolite (3%) and cordierite (2%), along with minor epidote.

Plagioclase is of highly variable grain-size and occurs as anhedral to euhedral, equant to subprismatic grains which exhibit well-developed multiple twin lamellae (which is strongly bent in places), moderate compositional zoning and moderate undulose extinction. Grain boundaries are extremely ragged and much of the plagioclase has been altered to mixtures of albite-quartz-epidote-

carbonate. Alkali feldspar occurs as anhedral, equant to subprismatic grains which are strongly sericitised and untwinned. Many of the grains are fragmented and have extremely ragged edges.

Chlorite occurs in two main forms:
i) as replacements after subhedral, subprismatic biotite grains.
ii) most commonly as green-brown non-descript fibrous intergranular space-fillings.

Tremolite is of rare occurrence as colourless cross-cutting subhedral elongate prismatic grains.
Cordierite is of rare occurrence as very small anhedral elongate grains which exhibit moderate undulose extinction.

APPENDIX 4PD

PETROGRAPHIC DESCRIPTIONS OF ROCK TYPES FROM THE WAMBIDGEE SERPENTINITE BELT AND ABUTTING UNITS

The Jindalee Beds

The Jindalee Beds comprise a large variety of metasedimentary and metavolcanic rocks and can be subdivided into the following sub-units:

Quartzite

Quartzites of the Jindalee Beds are here defined as those quartz-dominant rocks with less than 10modal% opaques and/or micaceous minerals. They are widespread throughout the Jindalee Beds and have a very simple mineralogy consisting dominantly of recrystallised quartz with minor graphite and magnetite and/or hematite. Clift (1967) also recorded illite, metamorphic biotite and stilpnomelane within banded quartzite north of Coolac, and Cheadle (1993) recorded chlorite within quartzites in the Muttama area. During the course of the present study, muscovite, phengitic muscovite and chlorite were all found to occur. Grain-size variation within the quartzites ranges from <0.05 to 0.5mm. Most of the quartzites exhibit a polygonal mosaic texture defined by strongly interlocking polygonal-shaped quartz grains which are cross-cut by strongly aligned grains of elongate prismatic muscovite/phengite and/or muscovite/chlorite. Depending on the intensity of deformation and extent of recovery, the quartz grains vary considerably in shape from strongly polygonal-shaped grains with well-developed triple junction sutured grain boundaries with weak undulose extinction, to elongate prismatic grains which exhibit strong undulose extinction and have well-developed subgrains. The micaceous minerals wrap-around the quartz grains and chlorite occurs as a partial replacement of some of the muscovite grains. Accessory minerals include magnetite and apatite. Relict bedding within the quartzites is defined by either varying grain-size or the preferred distribution of either mica (M domains), quartz (Q domains) or opaques (O domains). Foliations within the quartzites are defined by either the long axis of the quartz grains and/or micaceous grains aligned parallel to the long axis of the quartz grains. Metamorphic layering is most commonly developed where folding is intense and is defined by recrystallised quartz separated by layers of opaques and/or micaceous minerals. Within these strongly folded quartzites, the overall texture is defined by strongly folded mica-rich and quartz-rich layers. The main folded layers are themselves folded, thus defining a crenulated schistosity. Many of the mica-rich bands consist of 100% mica and generally occur as thin and continuous layers. These layers define a strong penetrative foliation defined by the preferred alignment of the mica grains which strongly overprint the quartz grains.

Quartz-magnetite rock

Are here defined as those quartz-rich rocks of the Jindalee Beds which contain greater than 10 modal% magnetite. They are composed of fine-grained granoblastic quartz, magnetite and/or hematite, along with minor biotite, stilpnomelane and fibrous amphibole (Basden *et al.* 1974). Barron (1972) also reported grunerite, Cooper (1985) reported tremolite and Reynolds (1993) reported brown/green mica. In both outcrop and hand-specimen, these rocks have a similar appearance to the banded iron formations of the Broken Hill region.

Chert

Cherts are of minor occurrence and have been described by both Macklin (1985) and Jones (1991). According to Macklin (1985), carbonaceous cherts grade into the massive sugary quartzites of the Jindalee Beds. Jones (1991) recorded that the cherts are commonly laminated with these laminations being cross-cut by thin quartz veinlets. The cherts are generally composed of equigranular recrystallised chalcedonic quartz and pervasive opaque minerals (Basden *et al.* 1974; Jones 1991).

Limestone

Basden *et al.* (1974) recorded the occurrence of a lenticular limestone body within metabasites of the Jindalee Beds near Coolac. However, this body is more correctly termed a dolomitic marble as it dominantly consists of recrystallised calcite/dolomite in a granoblastic fabric along with intergranular diopside, quartz, tremolite and minor talc.

Metapelite/Metapsammite

The metapelite/metapsammite sub-units of the Jindalee Beds are almost as common and widespread as the quartzite sub-units to the north and west of Coolac. In fact, this can probably be said for all areas where the Jindalee Beds occur as these sub-units outcrop poorly and are generally interbedded with the quartzite sub-units. In the south, Wilson (1993) recorded the occurrence of phyllites, further north in the Fontenoy area, Cooper (1985) recorded the occurrence of quartz-muscovite schists and during the course of this present study, the author found knotted quartz-muscovite-chlorite schists in the Fontenoy area. Mineralogically, the metapelite/metapsammite rocks of the Jindalee Beds are composed of varying amounts of quartz, biotite, muscovite, almandine garnet, chlorite and minor opaques. Macklin (1985) also recorded cordierite retrogressed to chlorite in the central part of the belt, and Parker (1993) recorded both sillimanite and andalusite in the southern part of the belt. The overall texture of the knotted quartz-muscovite-chlorite schists is defined by strongly folded boudins and lenticles of strongly polygonal-shaped quartz grains in a fine-grained matrix of strongly aligned phengitic muscovite and rare ferroan chlorite. A minnesotaite-magnetite (determined by XRD methods) rock was found during the present study in the northern part of the belt. At meso-scale, it has the appearance of a very fine-grained, moderately folded (with what appears to be primary sedimentary slump folds) well-cleaved metapelitic rock. It consists of quartz (20 modal%), minnesotaite (an Fe analog of talc, 50 modal%), and phengitic muscovite (30 modal%), along with minor opaques and apatite. In thin-section, the overall texture is defined by moderately well-aligned subprismatic grains of minnesotaite and phengitic muscovite along with lenticles of quartz. Pseudo-sedimentary layering (i.e. the apparent primary sedimentary layering visible at meso-scale) is defined by varying proportions of the opaque grains within individual layers.

Metabasite

Metabasites of the Jindalee Beds can be genetically sub-divided into intrusive and extrusive types. The intrusive types are dominated by pyroxene metagabbros and metadolerites while the extrusive types are mainly metabasalts and rare meta-andesites. The metabasalts themselves can be further sub-divided into actinolite schists, actinolite-albite-epidote schists, amphibole-albite rocks, chlorite-epidote-albite schists and chlorite-epidote-clinozoisite rocks (Macklin 1985; Jones 1991). The metabasalts are fine to very fine-grained slightly porphyritic rocks (Basden *et al.* 1974). Massive, foliated and amygdaloidal types occur with the amygdules filled by varying amounts of epidote, clinozoisite, quartz, albite and chlorite. The metabasalts are composed of varying proportions of

albitic plagioclase, actinolite, epidote, quartz, clinozoisite, chlorite and secondary carbonates. Rare primary phenocrysts include andesine, diopsidic augite and hornblende, and accessory phases include magnetite, sulfides, apatite, sphene, zircon and almandine garnet. Cross-cutting veinlets composed of varying proportions of quartz, epidote, chlorite, calcite and albite are common. In thin-section, these metabasalts exhibit a decussate granoblastic texture.

Amphibolites are rare in the southern portion of the Jindalee Beds but common in the far north of the belt, in the Thuddungra area. They are diverse in character, fine- to coarse-grained, massive to strongly foliated and are commonly banded. The primary mineralogy of the amphibolites is dominated by hornblende and calcic plagioclase along with accessory sphene and ilmenite. Relict textures within some of the amphibolites suggests hat they were once basalts, porphyritic mafic tuffs and dolerites (Cooper 1985) or gabbros. Retrogressive metamorphic phases include abundant actinolite and albitic plagioclase, along with lesser amounts of quartz, chlorite, dolomite, calcite and clinoclinozoisite.

Metagabbros are of minor occurrence within the Jindalee Beds. Away from contacts, they are massive, but along contacts they are strongly sheared. The primary assemblage of the metagabbros is diopside-augite, hypersthene, plagioclase, rare hornblende and accessory ilmenite. Most of the plagioclase has been completely saussuritised and other pervasive metamorphic phases include actinolite, clinozoisite, chlorite and quartz. All of the metagabbros exhibit a pseudoporphyritic granular texture defined by large grains of pyroxene and rare hornblende in a fine-grained matrix.

The Frampton Volcanics

The Frampton Volcanics are mainly a silicic volcanic sequence along with minor intercalated conglomerate and fine-grained sedimentary rocks which are restricted to their southern limit of exposure (Stuart-Smith & Dadd 1993). The volcanic rocks are dominated by rhyolitic to rhyodacitic crystal-rich vitric tuff with minor dacitic tuff and rare andesite and basalt (Stuart-Smith & Dadd 1993). These volcanic rocks contain phenocrysts of partially resorbed quartz, K-feldspar, plagioclase, biotite, muscovite, sericite and chlorite (Basden *et al.* 1974). The matrix may be recrystallised, flow banded or foliated, and consists of fine-grained quartz, K-feldspar, plagioclase, biotite and sericite (Basden *et al.* 1974). The conglomerates within the Frampton Volcanics range from oligomictic (with locally-derived volcanic clasts) to polymictic (with clasts of arenite, siltstone, volcanic rocks, limestone and rare granite) and siltstones are rare. The occurrence of metamorphic biotite and sericitic alteration within the volcanic rocks of the Frampton Volcanics suggests that they have only undergone low grade regional metamorphism reaching the biotite zone of the greenschist facies (Basden *et al.* 1974).

The rocks vary from being weakly to strongly foliated. Within the volcanic rocks, this foliation is defined by the preferred alignment of micaceous minerals which wrap-around the phenocrysts and define a spaced schistosity. Within the sedimentary rocks, this foliation occurs as a slaty cleavage.

The Young Granodiorite

Small, isolated intrusive dyke-like bodies of felsic rocks of the Young Granodiorite and mafic rocks of unknown affinity occur far to the west of the main mass (some 3-8km) and have clearly intruded into the Wambidgee Serpentinite Belt, Jindalee Beds and Blowering Formation. These intrusive

bodies occur both in the south (to the north of Coolac and east of Cootamundra) and far in the north (to the south of Thuddungra).

From south to north, the petrography of the Young Granodiorite along the contact with the Wambidgee Serpentinite Belt can be summarised as follows:

North of Coolac

A small intrusive granodioritic body occurs within metapelitic and metapsammitic rocks of the Jindalee Beds to the north of Coolac. This granodiorite exhibits a hypidiomorphic granular texture and has a modal composition of quartz (40%), plagioclase (30%), K-feldspar (15%), biotite (10%) and muscovite (5%), along with minor sericite and chlorite after biotite, and accessory ilmenite, almandine garnet and zircon (Jones 1991). Within the same general area (at the Booths Reward gold mine), intrusive aplitic dykes of the Young Granodiorite and mafic dykes of unknown affinity occur within metapelitic rocks of the Jindalee Beds. The mafic dyke has sheared intrusive margins with the Jindalee host rocks and the felsic aplitic dykes have themselves intruded the mafic dyke. The mafic dyke is coarse-grained (with individual hornblende grains up to 50mm in length) and has a modal composition of hastingsite (75%, determined by XRD methods), biotite (15%), intergranular quartz+feldspar (5%), magnetite (4%) and almandine garnet (1%) (Jones 1991). The aplitic dykes were looked at during the present study and were found to have a modal composition of plagioclase (45%), quartz (42%), and K-feldspar (10%), along with minor actinolite, epidote, clay minerals, and chlorite, and accessory opaques and apatite. They exhibit an aplitic texture defined by strongly interlocking equant to subprismatic grains of quartz, plagioclase and K-feldspar, along with cross-cutting secondary actinolite, chlorite, epidote and clay minerals.

East of Muttama

Intrusive aplitic dykes of the Young Granodiorite and mafic dykes of unknown affinity occur within metasedimentary rocks of the Blowering Formation some 1km east of the Wambidgee Serpentinite Belt. The mafic dykes are medium- to coarse-grained, have a modal composition of augite (65-75%), plagioclase (25-30%), quartz (15-25%), chlorite (0-5%) and opaques (0-5%) and contain enclaves of both siltstone and quartzite (Cheadle 1993). In contrast, the aplitic dykes are devoid of xenoliths and are massive. They have a modal composition of quartz (60-80%), K-feldspar (20-25%), muscovite (0-15%) and biotite (0-5%) (Cheadle 1993). Other intrusive rocks were also found in this area during the course of the present study and according to the IUGS classification of plutonic rocks, they are quartz monzodiorites. These have a modal composition of plagioclase (40%), hornblende (15-32%), quartz (10-12%), K-feldspar (5-7%) and biotite (10%), along with minor epidote, actinolite and clinoclinozoisite, and accessory apatite, zircon, rutile and opaques. They exhibit a hypidiomorphic granular texture defined by strongly interlocking grains of the constituent phases of highly variable grain-size and euhedralcy.

Fontenoy area

The Young Granodiorite in the Fontenoy area varies from massive to gneissic and mylonitic varieties (Cooper 1985). Within the massive varieties, the plagioclase and K-feldspar exhibit patchy alteration to sericitic mica, biotite is partially altered to chlorite along with minor amounts of epidote, quartz exhibits undulose extinction and minor muscovite and accessory magnetite, ilmenite and zircon occur (Cooper 1985). The foliated varieties exhibit a well-developed gneissosity defined by the preferred alignment and distribution of biotite which wraps-around the quartz and feldspar augen. They have an identical mineralogy to the more massive varieties but contain more abundant

alteration phases (Cooper 1985). Mylonitised granodiorite occurs at the margins of the intrusion in zones some 15-50m in width. Xenoliths are abundant in almost every outcrop and comprise biotite and biotite-quartz segregations, small quartz vein blebs and tonalitic xenoliths (Cooper 1985). In the course of this present study, quite large (up to 0.4m in length) rounded elongate enclaves of banded Jindalee Beds quartzite were found to occur completely enclosed within protomylonitic granodiorite within this area. Two aplitic dykes of the Young Granodiorite were also found in this area by Cooper (1985). Metasomatised aplites also occur, range in composition from unaltered granite aplites to quartz-oligoclase-actinolite rocks, and occur as dyke-like bodies completely enclosed within talcosic metaserpentinite (Cooper 1985).

Quartz Hill, south of Thuddungra

Along the main contact between the Young Granodiorite and Wambidgee Serpentinite Belt in this area, the granodiorite occurs as a medium-grained, biotite-rich mylonitic variety with a hypidiomorphic granular texture and modal composition of quartz (35-60%), plagioclase (25-40%), biotite (10-20%), K-feldspar (0-8%) and muscovite (0-5%) along with minor secondary chlorite and fine-grained muscovite (Reynolds 1993). Away from the main contact, the granodiorite is weakly foliated and relatively even-grained whereas in a zone some 200-300m in width along its western margin, the granodiorite is porphyroclastic and strongly foliated. It has the same mineralogy as the more massive variety, but with strongly recrystallised quartz and strongly aligned grains of biotite.

Reynolds (1993) classified microgranites which occur completely enclosed within the Wambidgee Serpentinite Belt in this area as an integral part of the serpentinite belt itself. However, their mineralogy, mode of occurrence and lack of any other large granitic bodies in this area suggests that they are in fact aplitic dykes of the Young Granodiorite. In this general area, during the present study, at least two weakly foliated muscovite-bearing granite aplites were found to occur completely enclosed within metaserpentinites and are associated with extensive quartz veining and talc mineralisation. In thin-section, these aplites exhibit a porphyritic granular texture defined by relatively large grains of microcline, plagioclase, quartz and muscovite in a finer-grained granular matrix of biotite, quartz and plagioclase. They have a modal composition of plagioclase (41%), quartz (30%), microcline (15%), muscovite (3%) and biotite (1%), along with minor chlorite and sericitic mica, and accessory tourmaline and opaques.

The Wambidgee Serpentinite Belt

Dunites

To date, only completely serpentinised dunites have been found within the Wambidgee Serpentinite Belt and are recognised by their well-developed mesh texture and absence of any pyroxene grains. The mesh texture is defined by narrow discontinuous veinlets of fibrous chrysotile around ovoid-shaped replacements of lizardite 6T (determined by XRD methods) after olivine.

The mesh texture consists of two distinct parts:

i) a core consisting of subrounded ovoid-shaped lizardite replacements after olivine. Many of these grains are quite elongate, though with no preferred plane of flattening, and they contain abundant inclusions of fine-grained magnetite at their outer margin.
ii) a rim consisting of discontinuous veinlets of fibrous chrysotile around the lizardite cores. These veinlets are only as continuous as the maximum dimension of the cores and commonly merge into each other at the core margins. The veinlets consist of fine-grained prismatic fibrous

chrysotile with the long axis of the individual fibres generally oriented perpendicular to the core walls.

Chrome spinel is a common primary mineral within these dunites and occurs as relatively large anhedral to subhedral, equant-shaped grains. Many of these grains have been replaced by aggregates of fine-grained magnetite with remnant chrome spinel occurring as small central cores.

Cross-cutting serpentine veinlets are ubiquitous in the dunites. They are generally continuous for only a few mm, have highly variable widths along their length and cross-cut all of the other phases present. The individual grains within these veinlets exhibit no preferred orientation though the dominant orientation of these grains appears to be parallel to the vein walls. The veinlets are composed of very fibrous elongate, commonly bent serpentine grains, commonly with linear aggregates of very fine-grained magnetite grains at their centre.

Mg-chlorite also commonly occurs within these dunites as colourless non-descript fan-shaped aggregates of fibrous grains surrounding the chrome spinel grains.

Metaharzburgites

Like the dunites, only completely serpentinised harzburgites have been found within the Wambidgee Serpentinite Belt. They are far more common in the south of the belt and are here defined as those completely serpentinised ultramafic rocks of the Wambidgee Serpentinite Belt which have > 10modal% bastite pseudomorphs after orthopyroxene in a matrix of serpentine. In general, the harzburgites exhibit a pseudoporphyritic decussate feathery texture defined by relatively large, completely bastitised orthopyroxene grains in a fine-grained non-aligned matrix of feathery decussate antigorite along with cross-cutting veinlets of tremolite and chrysotile. They have a modal composition of relict orthopyroxene (10-15%), antigorite+chrysotile (80-95%, identified by XRD methods), rare chromian spinel (0-2%), rare ferroan chlorite (0-3%), along with accessory secondary magnetite and cross-cutting tremolite.

Orthopyroxene within the harzburgites is often hard to distinguish due to it having been completely replaced by chrysotile. Orthopyroxene is randomly distributed throughout these harzburgites and the chrysotile is itself in places completely replaced by fibrous antigorite, making it hard to distinguish from the surrounding antigorite matrix. The orthopyroxene grains are usually strongly embayed, with the embayments being filled by the matrix antigorite, and although they have been completely replaced by fibrous chrysotile, they still retain their original well-developed finely-parted cleavage. The chrysotile fibres within these grains are quite strongly bent and exhibit strong undulose extinction. They have very ragged edges, are strongly fractured and commonly brecciated (with fracture- and breccia-fill by feathery antigorite). Cross-cutting, narrow chrysotile veinlets occur throughout the orthopyroxene grains and aggregates of fine-grained magnetite overprint the orthopyroxene grains. The orthopyroxene grains are also cross-cut by the matrix antigorite, tremolite veinlets and magnetite veinlets.

The antigorite matrix generally consists of very fine to fine-grained feathery decussate, non-aligned plumose aggregates of antigorite. There is extreme variability in grain-size for the individual fibres though there is no spatial distribution of the various grain-sizes except where the antigorite occurs in veinlets, in which case it is either of the most coarse or fine-grained type. Chrome spinel is of

rare occurrence as anhedral elongate prismatic, highly fractured grains which exhibit strong rim- and fractured-related replacement by fine-grained secondary magnetite.

Chrysotile veinlets cross-cut all of the other phases present and are of a number of different generations. The earliest generation occurs as narrow discontinuous (some 0.5-1mm) veinlets which cross-cut the orthopyroxene grains. Later generations are wider and more continuous (up to 15mm) and the individual fibres within these later generations are generally oriented either parallel or perpendicular to the veinlets walls and exhibit strong undulose extinction.

Tremolite occurs in two main forms within the metaharzburgites:

i) as rare subhedral to euhedral, diamond-shaped angular grains which strongly overprint the antigorite matrix. These grains generally occur in the form of plumose aggregates and exhibit weak to moderate undulose extinction.
ii) more commonly, tremolite occurs in the form of discontinuous (up to 3mm) strongly sigmoidal-shaped, often en-echelon, veinlets of colourless grains. The individual fibres within these veins are generally oriented at 70-90° to the veinlets walls and exhibit moderate undulose extinction.

Magnetite occurs in the following forms:

i) as randomly distributed, non-aligned equant-shaped aggregates of tiny grains.
ii) as discontinuous (up to 1mm) linear aggregates of fine-grained magnetite which in places defines former olivine grain boundaries.
iii) as linear aggregates of fine-grained equant-shaped subhedral grains which define former cleavage planes within the bastitised orthopyroxene grains and also cross-cut the orthopyroxene grain boundaries.

Hornblende clinopyroxenites

Are of extremely rare occurrence and have only been found at Jack's Hill, north of Thuddungra. They exhibit either a fine-grained granoblastic or porphyroblastic decussate texture. The granoblastic texture is defined by strongly interlocking moderately aligned grains of diopside and hornblende with cross-cutting grains of fibrous tremolite. In contrast, the porphyroblastic decussate texture is defined by relatively large porphyroblasts of diopside (many of which have been replaced by secondary fibrous tremolite) in a strongly interlocking granular matrix of moderately aligned hornblende and smaller diopside grains, along with cross-cutting secondary fibrous tremolite. These rocks have a modal composition of diopside (40%), hornblende (40-50%), tremolite/actinolite (10%), serpentine (0-10%) and minor opaques.

Diopside occurs in two main forms:

i) as relatively large porphyroblasts of colourless subhedral equant-shaped angular grains. These grains exhibit quite strong undulose extinction, and in places, micro-faulting and subgrain development. In most instances, they exhibit either rim or complete replacement by secondary fibrous tremolite.
ii) as relatively fine-grained colourless, anhedral to subhedral, equant-shaped grains which are commonly rimmed by secondary fibrous tremolite. These grains occur in the matrix associated with hornblende, are moderately polygonal in shape, exhibit moderate undulose extinction, have sharp to diffuse grain boundaries, and commonly exhibit well-developed triple-junction grain boundaries.

Hornblende occurs as weakly to moderately pleochroic (pale green to pale tan brown) subhedral, equant to subprismatic grains which are commonly polygonal in shape. They are relatively fine-grained and are associated with the fine-grained diopside. They commonly have strongly sutured grain boundaries with both each other and the fine-grained diopside, and exhibit moderate undulose extinction. They are commonly zoned with pleochroic cores and colourless rims which have undergone replacement by secondary fibrous tremolite.

Tremolite occurs in two main forms:

i) as relatively small plumose aggregates of fibrous elongate prismatic grains which occur within the matrix, cross-cut both the diopside and hornblende grains, and exhibit very strong undulose extinction.

ii) as subhedral, fibrous elongate prismatic grains which occur as rim to complete replacements of both the diopside (particularly the porphyroblasts) and hornblende grains. These grains also exhibit quite strong undulose extinction, are of random orientation and are commonly moderately bent.

Hornblendites

Are of rare occurrence but have been found in both the central and northern parts of the belt. Those in the central part of the belt tend to be coarse-grained whereas those in the north of the belt are fine-grained. The fine-grained hornblendites exhibit an equigranular strongly granoblastic texture defined by strongly interlocking equant- shaped polygonal grains of hornblende, diopside and rare orthopyroxene. The coarse-grained hornblendites exhibit a cumulus texture defined by relatively large (up to 60mm) subprismatic hornblende grains and rarer diopside along with interstitial and fracture-fill tremolite and actinolite. The modal composition of both hornblendite types is hornblende (60-80%), diopside (0-35%), orthopyroxene (0-5%), tremolite (0-30%), actinolite (0-1%), chlorite (0-5%), talc (0-5%) and rare secondary magnetite.

The hornblende generally occurs as strongly pleochroic (either green/brown to tan brown or pale to dark brown) subhedral, angular subprismatic grains which exhibit weak to moderate undulose extinction. Those in the finer-grained hornblendites exhibit well-developed triple-junction sharp grain boundaries while those in the coarse-grained variety are heavily embayed with the embayments being filled with secondary fibrous tremolite. Many of the grains exhibit a well-developed and consistently oriented fracture parting oriented at 90° to the long axis of the hornblende grains. Most of the larger grains have a well-developed though narrow fringe of secondary fibrous tremolite. Some of the hornblende grains have hollow cores, now filled by fibrous tremolite. The intergranular spaces between the larger hornblende grains consists of much smaller subhedral subequant hornblende grains which exhibit weak to moderate undulose extinction. There is strong evidence to suggest that these smaller interstitial hornblende grains were derived by the fragmentation of the larger hornblende grains as in places (where secondary tremolite alteration is weak), the smaller grains can easily be fitted together and no rotation of these fragments appears to have occurred. Some of the hornblende grains contain ovoid to cuspate-lobate shaped inclusions which now consist of mixtures of talc and chlorite but were most likely once primary olivine grains. These grains also occur interstitial to the larger hornblende grains. Many of the hornblende grains have ragged grain boundaries (particularly between adjoining hornblende grains) and common fracture-fill by both fibrous tremolite and actinolite.

Diopside is of minor occurrence as anhedral to subhedral, angular equant-shaped grains, commonly with cuspate-lobate shapes, and occur interstitial to the larger hornblende grains. Within the coarse-grained hornblendites, they have very ragged grain boundaries and the central parts of these grains exhibit moderate undulose extinction, whereas in the fine-grained hornblendites, they commonly have well-developed triple-junction grain boundaries with the surrounding hornblende grains, have sharp grain boundaries, and exhibit moderate undulose extinction. Many of the diopside grains have been replaced by secondary fibrous tremolite.

Orthopyroxene is of extremely rare occurrence and has only been found within the fine-grained variety. It occurs interstitial to the hornblende as subhedral, angular equant-shaped grains. They have well-developed triple-junction grain boundaries with the surrounding grains, very sharp grain boundaries, and exhibit moderate undulose extinction.

Tremolite occurs in the following forms:
i) interstitial replacements after former diopside.
ii) narrow fringes on the edges of the hornblende grains.
iii) pseudomorphous cores after diopside in the centre of some of the hornblende grains.
In all occurrences, the tremolite is of the one form existing as very fibrous interweaving mats of subhedral elongate prismatic grains. They are of no preferred crystallographic orientation and cut-across both the hornblende and diopside grains.

Actinolite occurs as fine-grained cross-cutting fibrous grains either interstitial to the hornblende grains, as rims around the hornblende grains, pseudomorphous grains after diopside, or as fracture-fill within the hornblende grains. Talc is restricted to the fine-grained variety as colourless, cross-cutting elongate prismatic needle-like fracture-fill grains interstitial to the other phases. Magnetite occurs as rare aggregates of fine-grained equant-shaped grains within the interstitial tremolite.

Layered peridotites
These have only been found to occur in two areas within the Fontenoy region of the central part of the belt, where they are relatively common. The largest outcrop consists of completely serpentinised rhythmically layered peridotite surrounded by schistose and massive serpentinite while the smaller consists of weakly serpentinised, simply layered peridotite which itself occurs as a layer within a hornblendite unit.

The relatively fresh weakly serpentinised layered peridotite exhibits a cumulate texture defined by relatively large strongly embayed orthopyroxene grains (now mostly replaced by secondary tremolite) intergrown with highly fractured olivine grains of the same general size, thus defining a postcumulus overgrowth texture. They have a modal composition of olivine (80%, partially altered to a structureless chlorite) and orthopyroxene (20%, mostly replaced by secondary fibrous tremolite) along with accessory magnetite, and an amphibole-rich layer which largely consists of tremolite pseudomorphous after orthopyroxene grains with minor interstitial chloritised olivine.

Within this variety, olivine occurs as highly fractured and partially altered (with fracture-related alteration by pale green chlorite) subgrains. The fractures between these subgrains and parental grains are filled by both fine-grained magnetite and pale green chlorite. The olivine exhibits both differential extinction and well-developed parting.

Orthopyroxene occurs as heavily embayed grains and contain abundant inclusions of ovoid-shaped former olivine grains (now Mg-chlorite). Most of them have been completely replaced by fibrous secondary tremolite though they still retain their original precursor orthopyroxene shape. Rare complex grains occur which have a core of once olivine (now Mg-chlorite) with a narrow rim of once orthopyroxene (now tremolite).

The amphibole layer consists largely of tremolite pseudomorphs after subhedral, subprismatic orthopyroxene grains with minor smaller interstitial chloritised olivine grains. The tremolite pseudomorphs strongly impinge on each other and therefore exhibit a pseudo postcumulus overgrowth texture with the once interstitial olivine representing postcumulus space-filling.

The completely serpentinised layered peridotites generally exhibit a domainal decussate pseudoporphyritic feathery texture defined by completely bastitised orthopyroxene-dominant layers within non-aligned plumose aggregates of feathery antigorite interspersed with layers consisting solely of feathery antigorite. They largely consist of relict orthopyroxene grains (up to 15 modal% and completely bastitised), rare relict diopside grains, feathery antigorite (up to 99 modal%), rare talc and ferroan chlorite, and common secondary tremolite which occurs both pseudomorphic (after orthopyroxene and diopside grains) and cross-cutting non-aligned grains. They exhibit a number of distinct layer types:

i) orthopyroxene-rich layers: within these layers, the orthopyroxene grains occur as poorly defined (due to them being completely replaced by fibrous chrysotile which, except that it is of the one orientation with the long axis of the grains parallel to the dominant cleavage within the orthopyroxene grains, looks very similar to the surrounding antigorite groundmass) grains. They occur as relatively large (up to 4mm), strongly embayed (with the embayments being filled by the matrix antigorite) subhedral platy grains which exhibit both extreme undulose extinction and well-developed subgrains. These grains are strongly fractured and brecciated and tend to be concentrated in discrete layers associated with minor interstitial feathery plumose aggregates of non-aligned antigorite grains. The orthopyroxene grains also contain abundant inclusions of fine-grained magnetite which both define former cleavage planes within the orthopyroxene grains and occur as cross-cutting narrow veinlets. Many of these orthopyroxene grains have been replaced by secondary fibrous tremolite after firstly being replaced by chrysotile.

ii) antigorite-rich layers: these layers largely consist of very fine-grained plumose aggregates of fibrous elongate prismatic antigorite grains. The boundary between these layers and the orthopyroxene-rich layers is either very sharp or diffuse with isolated bastitised orthopyroxene grains occurring completely surrounded by the antigorite matrix.

iii) amphibole-rich layers: consist of rare cores of moderately pleochroic (pink to tan brown) subhedral equant to subprismatic, amphiboles surrounded by colourless fringes (and in places, completely replaced by them) of elongate prismatic tremolite grains, intergranular tremolite, and fine-grained plumose aggregates of antigorite. The modal composition of these layers is primary amphibole (20-40%), tremolite (40-50%) and antigorite (30-40%). The distribution of the various phases varies along the length of the layer. The intergranular tremolite occurs as colourless subhedral subprismatic grains which exhibit moderate undulose extinction and commonly take the form of plumose aggregates. The primary amphiboles occur as strongly interlocking grains with well-developed triple-junction grain boundaries, subgrain development,

and minor polygonal-shaped grains. Also, relatively large (up to 2mm) patches of feathery antigorite occur completely enclosed within these layers. The contact between these amphibole-rich layers and the antigorite-rich layers is diffuse with aggregates of the primary amphibole grains occurring within some of the antigorite-rich layers.

iv) tremolite+Mg-chlorite layers: these consist of relatively fine-grained subhedral, equant to elongate prismatic tremolite grains and plumose aggregates of very fine-grained Mg-chlorite. This layer has a very diffuse contact with the above lying amphibole-rich layer and has a modal composition of tremolite (50%) and Mg-chlorite (50%). Also, there is no consistent distribution of the two constituent phases along the strike of this layer.

Within all of these layers, accessory secondary magnetite occurs in the following forms:
i) as discontinuous (up to 0.5mm) linear aggregates of tiny grains.
ii) as randomly distributed subhedral equant-shaped aggregates of very fine-grained magnetite.
iii) as very fine-grained linear aggregates of tiny grains which help to define the cleavage planes within the primary amphibole grains.

Serpentinites
Primary phases are rare within the serpentinites of this belt and comprise olivine, chrome spinel and completely bastitised orthopyroxene grains. Secondary metamorphic phases are almost ubiquitous at every outcrop and include tremolite, talc, Mg-chlorite and rare magnesite. Texturally, the serpentinites can be subdivided into massive and schistose types.

The **massive serpentinites** have a modal composition of chrome spinel (0-2%), serpentine (90-100%), tremolite (0-5%) and Mg chlorite (0-2%), along with cross-cutting veinlets of tremolite and chrysotile and accessory secondary magnetite. In general, the massive serpentinites exhibit a decussate feathery texture defined by non-aligned plumose aggregates of fibrous antigorite grains. They are commonly veined, with chrysotile and tremolite veinlets cross-cutting the antigorite matrix. At one locality, G.R. 970 186, the massive serpentinite has a pseudo-layered texture consisting of alternating layers of magnetite-poor (<1 modal%) and magnetite-rich (>5 modal%) bands in a matrix of non-aligned feathery decussate serpentine.

Chrome spinel occurs as randomly distributed, non-aligned fragments of anhedral to subhedral, generally angular, equant to subprismatic grains which are intensely fractured and are commonly rimmed and replaced by secondary fine-grained magnetite. Rare grains exist which have the form of symplectic intergrowths with once pre-existing olivine (now, non-aligned feathery fine-grained serpentine).

The serpentine matrix consists of non-aligned plumose aggregates of generally fine-grained fibrous prismatic grains. Individual grains are commonly bent and exhibit moderate to extreme undulose extinction.

Magnetite occurs in the following forms:
i) as randomly distributed aggregates which consist of tiny equant-shaped grains.
ii) as strongly aligned discontinuous (up to 4mm) linear aggregates of tiny equant subhedral grains which are of two distinct orientations subperpendicular to each other.

iii) as non-aligned fracture-fill veinlets of tiny grains between the serpentine matrix grains defining former olivine subgrain boundaries.
iv) as partial to complete replacements of chrome spinel grains.

Tremolite occurs in the following forms:
i) as cross-cutting patches composed of aggregates of fibrous prismatic elongate subhedral grains with the individual grains exhibiting weak to moderate undulose extinction.
ii) as cross-cutting veinlets which are elongate and linear in character. These veinlets are of two dominant orientations at 45° to each other. The long axis of the individual tremolite grains within these veinlets is oriented either parallel or subperpendicular to the veinlet walls.

Cross-cutting chrysotile veinlets are generally discontinuous (up to 30mm), very narrow, and consist of fibrous chrysotile grains with the long axis of these grains being oriented either parallel or subperpendicular to the veinlet walls. In some cases, the chrysotile fibres which are oriented at a high angle to the veinlet walls appear to be of a later generation and clearly cross-cut those oriented parallel to the veinlet walls. The veinlets are of a very sinuous nature, commonly have highly variable widths along their length, and are commonly micro-faulted. The chrysotile within these veinlets exhibits moderate undulose extinction.

Cross-cutting chrysotile/magnetite veinlets contain highly variable modal proportions of chrysotile and magnetite, are generally discontinuous (up to 30mm) and are of two dominant orientations with the less continuous veinlets being oriented at 45° to the more continuous veinlets. They commonly anastomise into each other with the less continuous veinlets being micro-faulted and offset by the more continuous veinlets. The long axis of the chrysotile fibres within these veinlets is usually oriented perpendicular to the veinlet walls.

Talc occurs as very fine-grained non-descript aggregates of grains throughout the massive serpentinites and cross-cut the serpentine matrix, tremolite grains and chrysotile veinlets. It also occurs more rarely as cross-cutting discontinuous veinlets consisting of fan-shaped aggregates which cross-cut the other phases present and exhibit strong undulose extinction.

The **schistose serpentinites** have a modal composition of relict olivine (0-15%), chrome spinel (0-2%), serpentine (85-100%), rare talc and secondary accessory magnetite. They generally exhibit a feathery decussate texture defined by either strongly aligned elongate serpentine grains or continuous aligned linear veinlets of chrysotile alternating with bands of non-aligned plumose aggregates of fine-grained serpentine.

Olivine has only been found at G.R. 085 444 where it occurs as relatively discontinuous (up to 20mm) lenticular-shaped patches (which resemble boudins) with their long axes generally oriented parallel to the dominant shear direction (marked by the dominant trend of chrysotile veinlets). They consist of strongly fractured (with the fractures being mostly filled by fine-grained magnetite) generally elongate ovoid-shaped olivine grains. Although forming quite coherent lenticular fragments, individual grains go into extinction at distinctly different angles. These olivine grains are rarely intergrown with small subhedral equant-shaped orthopyroxene grains and are cross-cut by both the feathery serpentine groundmass and chrysotile veinlets.

Chrome spinel is of rare occurrence as anhedral amoeboid-shaped strongly fractured and brecciated grains. These grains now comprise a core of chrome spinel and a wider rim of fine-grained secondary magnetite. They are strongly embayed with the embayments being filled by the serpentine groundmass.

The serpentine matrix is fairly even-grained throughout and consists of plumose aggregates of subhedral prismatic grains which exhibit moderate undulose extinction. At one locality, G.R. 037 398, the serpentine matrix consists of alternating very fine-grained and fine-grained non-aligned serpentine grains.

Within the S-C fabric defining serpentine, the S-surface is defined by "boudins" of subparallel serpentine grains which are cross-cut by the C-surface serpentine grains. The long axis of the serpentine grains within these "boudins" is oriented 30-45° to the long axis of the serpentine grains which define the C-surfaces. The C-surface is defined by regularly spaced and continuous aligned elongate serpentine grains which are subparallel to each other.

The chrysotile veinlets are generally narrow and with variable (1-12mm) continuity. The individual fibres within these veinlets are generally oriented perpendicular to the veinlet walls and exhibit moderate undulose extinction. These veinlets are of a sinuous nature and are of two main orientations subperpendicular to each other.

Chrysotile/magnetite veinlets occur as very linear elongate strongly oriented veinlets of two dominant orientations, both of which are equally developed, defining both S- and C-surface foliations within the schistose serpentinites, and are generally oriented at 30-45° to each other. The long axis of the chrysotile fibres within these veinlets are generally oriented perpendicular to the veinlet walls. Many different vein generations are present with earlier veinlets being cross-cut by later veinlets. The different generations of these veinlets are observable due to their differing orientation and grainsize of the chrysotile fibres.

Talc occurs as extremely fine-grained vein-like aggregates which cross-cut the other phases present. Magnesite is of rare occurrence as cross-cutting patches within the chrysotile veinlets.

Magnetite occurs in the following forms:
i) as randomly distributed, generally equant-shaped aggregates of fine-grained magnetite.
ii) as rim replacements of chrome spinel grains.
iii) as linear aggregates (of two distinct orientations perpendicular to each other) of fine-grained equant-shaped grains. The long axis of these aggregates tends to parallel the C-surface foliation within these rocks.

Talc-carbonate rocks
The talc-carbonate rocks of this belt can be subdivided into the following three groups:

talc+magnesite rich metaserpentinites
These rocks have a modal composition of serpentine (5-50%), talc (17-60%) and magnesite (15-45%) along with rare chrome spinel (up to 3%) and common accessory secondary magnetite. They are by far the most common variety of talc-carbonate rocks within this belt. They generally exhibit a pseudoporphyritic feathery decussate texture defined by randomly distributed patches of non-

aligned feathery antigorite grains which in places are partially replaced and cross-cut by very fine-grained fibrous talc and equant to subprismatic grains of magnesite.

Chrome spinel occurs as isolated highly fractured and brecciated, stretched (i.e. elongate) anhedral grains which consist of a core of chrome spinel which is completely rim-replaced by very fine-grained magnetite. Although these grains have been quite highly brecciated, there appears to have been no rotation of the chromite fragments. The elongation direction of these chrome spinel grains cannot be correlated with any preferred fabric orientation within the rest of the rock and was therefore most likely a pre-serpentinisation feature. Also within these elongate grains, two distinct fracture orientations occur with the more dominant orientation being subperpendicular to the elongation direction and the other at 45° to this. Magnetite may now constitute up to 75% of the original chrome spinel.

Antigorite occurs as randomly distributed patches of varying size and shape. These patches consist of non-aligned, cross-cutting feathery prismatic elongate antigorite grains which occur in the form of fan-shaped aggregates and exhibit moderate to strong undulose extinction. In some cases, the serpentine occurs as fractured and brecciated subrounded clasts which are randomly distributed throughout these rocks and the serpentine within these clasts has been partially replaced, firstly by very fine-grained talc and then by much coarser-grained magnesite.

Talc occurs as non-aligned very fine-grained non-descript patches throughout the rock which have replaced pre-existing antigorite grains. The talc appears to have initially replaced the antigorite by rim replacement. Where both talc and magnesite co-exist in the same area, the talc appears to be replaced by the magnesite and it occurs as small patches completely enclosed within the magnesite grains.

Magnesite generally occurs as either randomly distributed single euhedral subequant grains within a matrix of either talc and/or antigorite, or as granular aggregates of varying shape and size which generally consist of subhedral subequant grains. The magnesite grains cross-cut both the talc and antigorite grains and do not exhibit any preferred orientation or distribution. Continuous veinlets (at least for 30mm) of magnesite aggregates also occur with the magnesite within these veinlets exhibiting no preferred orientation or elongation. The large isolated magnesite grains contain inclusions of both antigorite and talc.

Magnetite occurs in the following forms:
i) as randomly distributed anhedral amoeboid-shaped aggregates of tiny equant grains.
ii) as very linear-shaped aligned veinlets (of two dominant preferred orientations which are at approx. 60° to each other) which consist of very fine-grained subhedral equant-shaped magnetite grains. Although the grains do not exhibit any preferred elongation, they are aligned as such that the aggregates exhibit a very strong linear fabric. Some of these veinlets exhibit micro-faulting (with lateral displacements in the order of 0.25mm).

talc-rich metaserpentinites
These are of minor occurrence though common within the vicinity of the Muttama talc mine. They have a modal composition of talc (70-100%), antigorite (0-30%) along with rare chrome spinel (<1%) and common accessory secondary magnetite. They generally exhibit a schistose pseudoporphyritic decussate texture defined by either randomly distributed anhedral masses of

feathery antigorite within a matrix of strongly aligned very fine-grained talc, or by narrow (0.7mm) linear bands of opaque-rich zones within much wider (1-3mm) opaque-poor bands.

Talc occurs as very fine-grained non-aligned to strongly aligned fibrous masses which has replaced former antigorite grains. Antigorite occurs as fine-grained non-aligned fibrous masses of elongate prismatic grains randomly distributed. Chrome spinel occurs as very rare amoeboid-shaped anhedral strongly fractured and brecciated grains an have largely been replaced by aggregates of very fine-grained magnetite.

The opaque-rich zones consist of equant to elongate ovoid (with the elongation direction being parallel to the strike of the zone) pre-kinematic opaque minerals (approx. 10 modal% of these zones) which occur within a matrix of post to syn-kinematic very fine-grained talc which wraps-around the opaque grains. These bands are relatively continuous (at least 30mm), of a very strong preferred orientation and do not appear to merge into each other. Although the talc grains quite clearly wrap-around the opaque grains, most of the talc appears to occur as non-aligned plumose aggregates. The opaques are neither fractured or brecciated. The opaque-poor zones generally consist of non-aligned very fine-grained plumose aggregates of fibrous talc grains with trace amounts of very fine-grained equant-shaped opaque minerals.

magnesite-rich metaserpentinites

These have only been found to occur within the southern part of the belt at G.R. 040 407. They have a modal composition of antigorite (50-75%), magnesite (24-50%) along with rare chrome spinel and common accessory secondary magnetite. They are schistose at meso-scale and exhibit a feathery decussate lepidoblastic texture at micro-scale defined by vein-like linear aggregates of equant-shaped magnesite grains within a non-aligned matrix of fibrous antigorite.

Antigorite occurs as non-aligned feathery elongate prismatic grains and patches of equigranular grains which appear to be strongly preferentially distributed. The antigorite grains commonly occur in the form of fibrous bunches and exhibit moderate to strong undulose extinction. Chrysotile veinlets are of minor occurrence as strongly aligned (all being parallel to each other) continuous (up to 50mm) veinlets which consist of fibrous chrysotile and elongate linear aggregates of very fine-grained magnetite. The chrysotile exhibits moderate undulose extinction and the long axis of the fibres are oriented at 60° to the main schistosity plane within these rocks. Magnesite occurs as cross-cutting vein-like aggregates of subhedral equant-shaped grains. They strongly cross-cut the antigorite within the groundmass.

Magnetite occurs in the following forms:

i) as narrow linear aggregates of very fine-grained magnetite. These aggregates are generally of two dominant preferred orientations which are at an angle of 30-45° to each other and generally parallel the trend of the magnesite veinlets.
ii) as unusual dense aggregates (with these aggregates appearing to define former subhedral subprismatic pyroxene grains).
iii) as randomly distributed aggregates of tiny grains which are equant to subelongate in shape.

Tremolite-rich metaserpentinites

These rocks are defined as those metaserpentinites of the Wambidgee Serpentinite Belt which contain > 30modal% tremolite. The tremolite within these rocks is of a metamorphic origin and

clearly cross-cuts the matrix serpentine. These rocks have only been found to occur in the far north of the belt where they are common and are confined to narrow lenses enclosed within either metaserpentinite or amphibolite. They have a modal composition of serpentine (40-58%, identified by XRD methods as antigorite), tremolite (40-58%), talc (0-10%) and chlorite (<1-5%), along with common secondary accessory magnetite and rare accessory ilmenite. They generally exhibit either a decussate lepidoblastic texture defined by cross-cutting elongate prismatic bladed tremolite within a fine-grained non-aligned feathery antigorite matrix or a pseudoporphyritic texture defined by pseudoporphyroblasts of tremolite in a fine-grained groundmass of antigorite and talc.

Antigorite occurs in the groundmass as non-aligned very fine-grained strongly interlocking feathery aggregates of prismatic elongate grains which exhibit strong undulose extinction.

Tremolite occurs in the following forms:

i) as cross-cutting pseudoporphyroblasts within the antigorite matrix. These occur as relatively large (up to 1mm) subprismatic angular grains which appear to be replacements of former primary amphibole grains. They are strongly interlocking, and, in places, have well-developed triple-junction grain boundaries.
ii) as strongly cross-cutting fibrous elongate prismatic subhedral grains of varying dimensions. These commonly occur as non-aligned plumose aggregates and tremolite-rich zones (with up to 75 modal% tremolite) are common. The tremolite exhibits weak to moderate undulose extinction and bent broken grains are rare.
iii) as quite wide (up to 2mm) relatively continuous (up to 30mm) veinlets in which the tremolite grains are strongly oriented perpendicular to the vein walls. These veinlets tend to have variable widths along their length, are sinuous in nature, and cross-cut all of the other phases present. The tremolite grains within these veinlets generally exhibit moderate to strong undulose extinction.

Magnetite occurs in the following forms:

i) as linear aggregates of tiny grains which define former olivine (now antigorite) and hornblende grain boundaries. These aggregates appear to be of two dominant preferred orientations at an angle of 70° to each other.
ii) as randomly distributed, equant-shaped aggregates of tiny grains.
iii) as strongly aligned linear aggregates of tiny grains. When these aggregates approach the tremolite veinlets, their orientation changes abruptly and they then follow the orientation of the tremolite veinlets.

Fe-chlorite is of very rare occurrence and is confined to narrow rims around some of the magnetite grains.

Gabbros

The gabbros of this belt can be subdivided into clinopyroxene-rich and hornblende-rich types. Both types have been affected by metamorphism to some degree and in some cases, this has been so intense that the pre-cursor gabbro type cannot be determined.

Clinopyroxene-rich gabbros: these gabbros generally exhibit a pseudoporphyritic intergranular texture defined by relatively large diopside grains in a "matrix" of non-aligned plagioclase and minor quartz, along with strongly cross-cutting grains of fibrous tremolite/actinolite. They have a

nodal composition of diopside (10-25%), plagioclase (30-40%), quartz (0-10%), remolite/actinolite (30-60%) and epidote/clinozoisite (0-5%), along with accessory apatite and sulfides.

Diopside generally occurs as relatively large (up to 4mm) subhedral equant to subprismatic, strongly embayed grains. They are strongly bent in places (up to 45°), exhibit weak to intense undulose extinction and have ragged grain boundaries. Most of the grain are partially to completely replaced by secondary tremolite/actinolite. The grains commonly have a narrow rim (0.05 -0.1mm) of fibrous tremolite and exhibit well-developed, closely-spaced cleavage planes. The embayments are filled by either plagioclase or secondary tremolite.

Plagioclase occurs as both relatively fresh and completely saussuritised grains. The relatively fresh grains occur as subhedral subequant grains with well-developed multiple twin lamellae. They exhibit moderate to strong undulose extinction, have strongly sutured grain boundaries, well-developed triple-junction grain boundaries, and commonly occur in the form of subpolygonal to polygonal grains with rare subgrain development. They are cross-cut by both the tremolite/actinolite and epidote/clinozoisite grains. The completely saussuritised grains occur as non-descript fine-grained mixtures of albite, quartz and epidote. The pre-cursor plagioclase occurred as common rounded embayments within the diopside grains and most probably represented a post-cumulus space-filling phase.

Quartz is of minor occurrence as relatively fine-grained subhedral, equant to subprismatic grains. They exhibit moderate to strong undulose extinction, have moderately sutured grain boundaries, often with well-developed triple-junction grain boundaries and common subgrain development. They are also commonly polygonal in shape.

Tremolite/actinolite occur as colourless to pale green, subhedral, subprismatic to elongate prismatic grains which commonly occur in the form of plumose aggregates and do not exhibit any preferred orientation or distribution. They exhibit weak to strong undulose extinction, are commonly bent, and cross-cut all of the other phases present. Tremolite/actinolite occur in the following forms in these gabbros:
i) as partial to complete replacements of the diopside grains.
ii) as poor to well-defined narrow fringes (0.05-0.2mm) around the diopside grains.
iii) as patches of cross-cutting fibrous prismatic grains.
In all cases, the tremolite/actinolite cross-cuts all of the other phases in these gabbros and the cross-cutting tremolite/actinolite in the "matrix" cross-cuts the tremolite/actinolite pseudomorphs after diopside, suggesting at least two generations of tremolite/actinolite in these gabbros.

Epidote is of minor occurrence as widely-spaced aggregates of subhedral, subprismatic grains within plagioclase. Clinozoisite is of minor occurrence as anhedral to subhedral, equant to subprismatic grains which occur in the form of granular aggregates as fracture-fill between the plagioclase grains.

Hornblende-rich gabbros: generally exhibit an allotriomorphic granular texture defined by either non-aligned or more rarely, moderately aligned, strongly interlocking grains of hornblende, plagioclase and quartz, along with cross-cutting grains and veinlets of actinolite, epidote/clinozoisite and chlorite. They have a modal composition of hornblende (5-25%),

plagioclase (50-70%), quartz (0-20%), actinolite (5-18%), epidote/clinozoisite (<1-10%), rare chlorite (0-5%) and phlogopite mica (0-2%) along with accessory apatite, zircon, sphene and almandine garnet.

Hornblende generally occurs as moderately pleochroic (either pale to dark green or green-brown to tan-brown) subhedral short to elongate prismatic grains. They are commonly simply twinned, rarely bent (up to 60°), and contain rare inclusions of plagioclase grains. They commonly occur in the form of granular aggregates and have well-developed fringes of fibrous cross-cutting actinolite. Many of them are partially to completely replaced by secondary fibrous actinolite. Inclusions of anhedral to subhedral sphene are common. The hornblende grains do not exhibit any preferred crystallographic orientation or distribution. The elongate prismatic hornblende grains generally exhibit strong undulose extinction whereas the more equant-shaped hornblende grains exhibit weak to moderate undulose extinction.

Plagioclase generally occurs as relatively large (up to 3mm) anhedral to subhedral, equant to short prismatic grains which have strongly sutured grain boundaries and commonly exhibit well-developed subgrains at these grain boundaries consisting of
mixtures of albite and quartz. These subgrains have strongly sutured grain boundaries and exhibit moderate undulose extinction. Multiple twinning is commonly well-developed within the larger plagioclase grains which also exhibit moderate undulose extinction. The plagioclase grains strongly impinge on each other and are cross-cut by grain aggregates and veinlets of actinolite, epidote and clinozoisite.

Quartz is of minor though common occurrence as relatively small (generally <0.1mm) anhedral to subhedral, equant to subprismatic grains which are intimately associated with the plagioclase grains. They have moderately to strongly sutured grain boundaries, exhibit moderate to intense undulose extinction, and commonly have well-developed subgrains. The subgrains are more equant-shaped (commonly polygonal) than their parent host grains and triple junction grain boundaries are commonly developed in the smaller grains.

Actinolite is of common occurrence as moderate to strongly pleochroic (olive-green to blue-green) subhedral, generally elongate prismatic needle-like grains which are often in the form of stellate aggregates. They cross-cut all of the other phases present, exhibit moderate undulose extinction and do not exhibit any preferred orientation. The actinolite grains occur in the following forms:
i) as narrow (up to 0.3mm) rims around the hornblende grains.
ii) as partial to complete replacements of the hornblende grains.
iii) as cross-cutting aggregates.

Epidote cross-cuts both the hornblende and plagioclase grains and occurs in the following forms:
i) as relatively continuous (up to 10mm) but narrow (0.1-0.5mm) veinlets which consist of subhedral, equant to subprismatic grains which are strongly interlocking with each other and of variable grainsize.
ii) as both single and aggregates of cross-cutting subhedral, equant to subprismatic, grains.

Clinozoisite occurs as relatively common cross-cutting aggregates (which themselves are cross-cut by the secondary actinolite grains) of small subhedral, equant to subprismatic grains and relatively narrow (0.1-0.3mm) continuous (up to 16mm) veinlets.

Clinozoisite/epidote/actinolite veinlets are of minor occurrence and consist of non-aligned aggregates of subhedral, equant to subprismatic grains of clinozoisite and epidote (both of which exhibit moderate undulose extinction) along with fine-grained acicular needle-like cross-cutting aggregates of actinolite.

Phlogopite mica is of extremely rare occurrence as quite strongly pleochroic (pale orange to dark orange-brown) generally anhedral platy subequant grains which commonly contain inclusions of elongate rod-shaped opaques (possible ilmenite?). These grains appear to cross-cut both the plagioclase and quartz grains but are themselves cross-cut by the actinolite grains.

Sphene generally occurs as euhedral diamond-shaped grains enclosed within hornblende and plagioclase. Zircon is generally associated with the hornblende grains and occurs as aggregates of anhedral to subhedral, equant to subprismatic grains.

Completely altered gabbros: these are more correctly termed metagabbros and exhibit a granoblastic decussate texture defined by strongly cross-cutting patches of fibrous tremolite in a fine-grained matrix of completely saussuritised plagioclase. They have a modal composition of saussuritised plagioclase (40%) and tremolite (60%) along with rare accessory opaques.

Saussuritised plagioclase occurs as completely non-descript very fine-grained mixtures of albite, quartz, epidote and grossular garnet. These grains are strongly cross-cut by the tremolite grains.

Tremolite occurs as subhedral, angular short prismatic to elongate prismatic grains, commonly in the form of plumose aggregates. All of the tremolite grains exhibit weak to moderate undulose extinction. Although most of these grains do not exhibit any preferred crystallographic orientation, some of the patches occur in the form of subparallel fibrous grains which may represent complete replacements of former diopside or hornblende grains.

Plagiogranites

The plagiogranites of this belt are here defined as those felsic igneous intrusive rocks which are dominantly composed of quartz and albitised plagioclase (determined by XRD methods) and exhibit a strong granular texture. They commonly contain enclaves of amphibolite. The plagiogranites commonly exhibit an allotriomorphic granular texture defined by strongly interlocking non-aligned grains of quartz, plagioclase and minor alkali feldspar along with cross-cutting fibrous aggregates of tremolite and alteration grains of epidote. Very fine-grained cataclasite zones commonly cross-cut the plagiogranites. They have a modal composition of quartz (15-40%), albitised plagioclase (50-70%), minor alkali feldspar (0-10%), tremolite (8-10%), epidote (0-2%), chlorite (0-2%) and clinozoisite (0-1%) along with accessory apatite, zircon, almandine garnet and sphene.

Quartz occurs as subhedral, equant to subprismatic grains which generally exhibit moderate to strong undulose extinction and common subgrain development with sharp triple junction grain boundaries. The subgrains exhibit moderate to intense undulose extinction and commonly have very fine-grained quartz grains at their grain boundaries. All of the quartz grains have strongly sutured grain boundaries.

Plagioclase generally occurs as subhedral short prismatic grains which have well-developed multiple twinning with common strongly bent twin lamellae and rare micro-faulting. They have

strongly sutured grain boundaries and commonly exhibit subgrain development at the grain boundaries which consist of more equant-shaped and much finer-grained plagioclase. These grains exhibit moderate undulose extinction and in places, some of the finer-grained plagioclase have triple-junction grain boundaries.

Tremolite/actinolite cross-cut all of the other phases present and generally occur as pale green non-aligned plumose aggregates. The individual grains occur as elongate prismatic often needle-like grains which are commonly bent and exhibit moderate undulose extinction.

Epidote/clinozoisite occur as fine-grained subhedral equant to subprismatic grains which exhibit moderate undulose extinction and have strongly sutured grain boundaries. The epidote/clinozoisite occurs in the following forms:

i) as randomly distributed aggregates which occur as an alteration product of the plagioclase grains.
ii) as quite continuous (up to 20mm) narrow sinuous veinlets consisting of non-aligned grains.
iii) as fine granular aggregates at the plagioclase grain boundaries.

Alkali feldspar has only been found at G.R. 058 896, and occurs as relatively large short prismatic grains which exhibit well-developed simple twinning, moderate undulose extinction and moderately sutured grain boundaries.

Chlorite is of similar occurrence to the tremolite/actinolite grains but consist of coarser-grained plumose aggregates of grains. Garnet is of rare occurrence as small (0.2mm) euhedral equant-shaped grains enclosed within plagioclase.

The cross-cutting cataclasite zones occur as discontinuous (up to 15mm) generally narrow (0.01-0.5mm) zones throughout some of the plagiogranites. These zones are of a very sinuous nature and occur along grain boundaries in the plagioclase and quartz veins. They consist of relatively fine-grained subhedral equant-shaped grains of both quartz and plagioclase which have strongly sutured grain boundaries and exhibit intense undulose extinction.

The contact between the plagiogranites and contained amphibolite enclaves is generally very sharp and planar in character though isolated grain aggregates of hornblende (from the amphibolite enclaves) occur within the plagiogranites (these hornblende grains are of a completely different character to the tremolite/actinolite grains within the plagiogranites).

Amphibolites

The amphibolites of this belt can be subdivided into non-aligned, aligned and layered types. All types have been strongly metamorphosed and their pre-cursor igneous rock types cannot be determined.

Non-aligned types: generally exhibit a granoblastic decussate texture defined by strongly interlocking non-aligned grains of plagioclase, quartz, hornblende and epidote/clinozoisite which are cross-cut by non-aligned decussate actinolite. They have a modal composition of hornblende (0-50%), plagioclase (5-40%), very rare relict diopside (0-10%), quartz (0-30%), actinolite (0-60%), epidote/clinozoisite (0-10%), and chlorite (0-5%), along with accessory zircon, sphene, apatite, magnetite and ilmenite.

Hornblende occurs as strongly pleochroic (either pale to dark green or olive-green to green-brown) strongly interlocking grains which have ragged grain boundaries (commonly with fibrous fringes) and completely enclose the diopside grains. They are generally subhedral and prismatic in shape, are commonly bent (up to 45°) and generally exhibit moderate undulose extinction. They are strongly embayed and commonly consist of many fibrous subparallel grains. In places, they are quite strongly fractured (with fracture-fill by fibrous tremolite) and rimmed by fibrous actinolite. Diopside has been almost completely replaced by hornblende but still retain the original equant-shaped morphology with closely-spaced diallage parting.

Plagioclase occurs in the following forms:

i) as very small equant-shaped strongly interlocking polygonal-shaped grains which have well-developed triple-junction grain boundaries, exhibit moderate undulose extinction and have well-developed multiple twinning. They are commonly altered to epidote.
ii) as relatively small, strongly multiply twinned grains which are strongly intergrown with the quartz grains and are strongly cross-cut by the actinolite grains. They are generally subhedral, equant to subprismatic in shape and exhibit strong undulose extinction. They have moderately sutured grain boundaries and well-developed subgrains at the grain boundaries. These subgrains are generally equant and commonly polygonal in shape with well-developed triple-junction grain boundaries.
iii) as completely saussuritised non-descript very fine-grained mixtures of albite, quartz and epidote.

Quartz occurs in the following forms:

i) as very small equant-shaped, strongly interlocking, commonly polygonal-shaped grains which have well-developed triple-junction grain boundaries and exhibit moderate undulose extinction. These are strongly intergrown with the plagioclase grains and are cross-cut by the actinolite grains.
ii) as anhedral to subhedral, equant to subprismatic grains with strongly sutured grain boundaries. They commonly exhibit subgrain development and moderate to intense undulose extinction. Tiny equant polygonal-shaped grains commonly occur on the edges of the larger quartz grains and these have well-developed triple-junction grain boundaries.

Actinolite occurs as strongly pleochroic (green-brown to blue-green) non-aligned to weakly aligned aggregates of grains which cross-cut all of the other phases present. They have very ragged grain boundaries and occur in the form of subprismatic to elongate prismatic grains which exhibit moderate to intense undulose extinction. They commonly occur in the form of fibrous aggregates and are commonly strongly bent (up to 45°). Some of these grains appear to have completely replaced former primary hornblende grains whose form is largely retained.

Epidote is of minor occurrence as fine-grained equant to subprismatic grains which exhibit moderate undulose extinction and cross-cut the plagioclase grains. Clinozoisite occurs as strongly cross-cutting grains (though they are themselves cross-cut by the actinolite grains) which are in places, strongly bent (up to 30°). They occur as equant to subprismatic grains, which exhibit strong undulose extinction and have strongly sutured grain boundaries. They often occur in the form of narrow (<0.01mm) to relatively wide (0.5mm) generally discontinuous (2mm) veinlets.

Chlorite is of rare occurrence as non-pleochroic pale green aggregates which are composed of strongly interlocking fibrous prismatic grains. They are intimately associated with the actinolite grains and have partially replaced some of the hornblende grains. Zircon is of common occurrence as an accessory phase and occurs as relatively large aggregates which consist of anhedral subprismatic grains which are strongly embayed and are completely enclosed within the hornblende and plagioclase grains. Sphene is a relatively common accessory phase and occurs as relatively large generally subhedral equant-shaped grains enclosed within plagioclase. Opaques are moderately abundant accessory phases and occur as aggregates consisting of subhedral equant-shaped cubic grains.

Aligned types: these amphibolites generally exhibit a schistose texture defined by either moderate to well-aligned amphibole minerals or by well-aligned relatively large grains of hornblende and plagioclase in a very fine-grained granular matrix. They have a modal composition of hornblende (0-30%), plagioclase (0-37%), quartz (0-30%), epidote (0-20%), actinolite (0-50%), chlorite (0-5%), quartzofeldspathic groundmass (0-45%), along with accessory apatite and opaques.

Hornblende occurs as moderately pleochroic (olive-green to tan-brown) small (<0.2mm) to relatively large (1-2mm) grains. The larger grains are generally prismatic in shape and commonly contain inclusions of subhedral, equant-shaped colourless clinopyroxene grains in their cores. These hornblende grains have very ragged grain boundaries, are generally subhedral in shape, in places moderately bent (up to 30°), exhibit weak to moderate undulose extinction, and commonly have subgrains. The smaller hornblende grains are generally subhedral, equant to subprismatic in shape, and are strongly associated with the fine-grained plagioclase and quartz matrix. They exhibit only weak undulose extinction and commonly have well-developed triple-junction grain boundaries.

Plagioclase occurs as small (<0.2mm) to relatively large (1-2mm) grains. The large grains are commonly strongly deformed (i.e. with strongly bent twin lamellae and extreme undulose extinction), generally prismatic in shape, and exhibit well-developed multiple twin lamellae. They have intensely sutured grain boundaries, are highly embayed, and have well-developed subgrains at their grain boundaries. The smaller plagioclase grains are generally equant in shape, exhibit only weak undulose extinction and often have well-developed triple-junction grain boundaries.

Quartz generally occurs as relatively small (0.2-1mm) anhedral to subhedral, equant to subprismatic grains which exhibit moderate undulose extinction and occur within the fine-grained matrix. They have largely been transformed into subgrains which have strongly sutured subgrain boundaries with well-developed triple-junctions.

Actinolite cross-cuts all of the other phases present and occurs in two main forms:

i) as strongly aligned, relatively large (1-5mm) elongate prismatic grains which are commonly strongly bent (up to 80°) and broken and exhibit strong undulose extinction. They define a strong linear fabric in these amphibolites and are commonly cross-cut and fringed by smaller needle-like actinolite grains.
ii) as non-aligned, relatively small (<0.1-0.5mm) elongate prismatic needle-like grains which commonly occur in the form of stellate aggregates and cross-cut the larger actinolite grains.

Quartzofeldspathic matrix consists of very fine-grained strongly interlocking aggregates of polygonal-shaped quartz and plagioclase grains with well-developed triple-junction grain boundaries and moderate undulose extinction. Epidote generally occurs as small subhedral, equant to subprismatic grains which exhibit moderate undulose extinction and occur within the fine-grained matrix. Chlorite is of minor occurrence as pale green non-descript fibrous masses of grains intimately associated with the actinolite grains.

Layered types: are of very rare occurrence and have only been found at G.R. 970 190 associated with amphibolites of the non-aligned type. They exhibit a well-developed domainal texture defined by strongly alternating layers of differing composition. These layers are relatively continuous (at least for 50mm), of a planar character, and the contacts between the various layers are sharp.

Layer 1 has a modal composition of hornblende (50%), plagioclase (40%) and quartz (10%). It consists of strongly interlocking grains of plagioclase which have strongly sutured grain boundaries, along with minor fine-grained commonly polygonal-shaped quartz grains and cross-cutting aggregates of hornblende. The hornblende within this layer have pleochroic pale to dark brown cores and wider pleochroic pale to dark green rims of fibrous actinolite which cross-cuts the other phases within this layer.

Layer 2 has a modal composition of actinolite (50%), quartz (40%), plagioclase (8%) and clinozoisite (2%). It consists of very fine-grained equant to subprismatic strongly interlocking grains of quartz and minor relatively large grains of plagioclase with strongly sutured grain boundaries, and strongly cross-cutting elongate prismatic fibrous mats of pale green (often with tiny pleochroic brown cores) actinolite.

Layer 3 has a modal composition of hornblende (95%) and quartz (5%). It is of more limited occurrence than the other two layers and generally consists of moderately pleochroic (olive-green to tan-brown) strongly interlocking grains of hornblende which exhibit common subgrain development (consisting of strongly polygonal-shaped grains with well-developed triple-junction grain boundaries) along with minor interstitial quartz.

Tremolite/Actinolite rocks

These can be subdivided into tremolite-rich and actinolite-rich types and appear to be the products of metasomatism. They occur in discrete narrow zones at the contacts between plagiogranite, metagabbro and quartzite and the enclosing serpentinite.

Tremolite rocks: exhibit a very strong decussate texture defined by non-aligned plumose aggregates of tremolite which commonly cross-cut each other, and when present, fine-grained mixtures of quartz and plagioclase. They have a modal composition of tremolite (80-100%), quartzofeldspathic matrix (0-20%), chlorite (0-1%) and accessory opaques.

Tremolite generally occurs as colourless, subhedral to euhedral, elongate prismatic grains which are of a very fibrous nature. They exhibit moderate undulose extinction, are commonly strongly bent (up to 40°) and commonly cross-cut each other.

Quartzofeldspathic matrix has only been found at G.R. 970 186 and consists of very fine-grained equant-shaped grains of quartz and plagioclase which are strongly interlocking, commonly

polygonal in shape, and exhibit moderate undulose extinction. Chlorite is of rare occurrence as pale brown plumose aggregates of very fine-grained fibrous grains. Magnetite occurs as aggregates of tiny equant-shaped grains.

Actinolite rocks: exhibit a strong decussate texture defined by non-aligned plumose aggregates of actinolite along with rare cross-cutting veinlets of clinozoisite.

Actinolite occurs as strongly zoned (with pleochroic pale-brown to orange-brown cores and pale-green to olive-green rims), either short prismatic or tiny elongate prismatic needle-like grains. The larger grains are commonly twinned, cross-cut each other and have ragged grain boundaries.

Chlorite rocks

The chlorite rocks of the Wambidgee Serpentinite Belt are here defined as those metamorphic/metasommatic products which contain more than 80 modal% chlorite and exhibit a strong decussate texture. They generally exhibit a feathery decussate texture defined by non-aligned fine-grained plumose aggregates of Fe-chlorite along with randomly distributed equant-shaped grains of clinozoisite and opaques, and cross-cutting veinlets of Mg-chlorite+calcite. They have a modal composition of Fe-chlorite (95-100%), minor clinozoisite (0-5%), accessory opaques, and cross-cutting veinlets of calcite+Mg-chlorite.

Fe-chlorite generally occurs as pale green, non-descript non-aligned plumose aggregates of feathery decussate grains, often with a radial structure. These grains are often of a very fibrous nature. Clinozoisite is of minor occurrence as small subhedral, equant to subprismatic grains randomly distributed throughout the chlorite matrix.

Opaques occur in the following forms:

i) as relatively large (0.2-6mm) prismatic elongate often flattened diamond-shaped grains which consist of smaller, tiny equant-shaped grains. These may represent magnetite/ilmenite pseudomorphs after sphene.
ii) as subprismatic subrounded subhedral aggregates (up to 1mm) composed of tiny grains.

Cross-cutting calcite+Mg-chlorite veinlets have only been found at G.R. 050 880 and cross-cut all the other phases present. They are composed of strongly interlocking, subhedral sub-equant grains of calcite (commonly with triple-junction grain boundaries) along with relatively large (up to 4mm) platy grains of pale orange Mg-chlorite which appears to be cross-cut by the calcite grains in these veinlets. These veinlets are relatively continuous (up to 10mm) and wide (0.3-2mm).

Cross-cutting shear zones occur within the schistose chlorite rocks and are composed of parallel-aligned aggregates of the chlorite grains with the long axis of these grains oriented at 60° to the shear direction. These shear zones are narrow (with a maximum width of 0.5mm) and continuous for 8mm. The chlorite within these zones does not appear to be any different from that within the rest of the chlorite rocks.

Felsic volcanic tuffs

These rocks have only been found to occur at G.R. 058 896 in the central part of the belt. They exhibit a linear fabric defined by moderately aligned fibrous actinolite grains which wrap-around moderately aligned phenocrysts of plagioclase and quartz in a very fine-grained non-aligned matrix.

They have a modal composition of plagioclase (30-65%), quartz (10-35%), actinolite (10-30%) and clinozoisite (<1-3%), along with accessory apatite and zircon.

Plagioclase occurs in two main forms:

i) as relatively large (0.5-3mm) well-rounded phenocrysts which are moderately aligned (defined by the parallelism of the long axis of these grains), exhibit only weak multiple twinning and moderate undulose extinction. They have moderately sutured grain boundaries and commonly exhibit subgrain development at these grain boundaries which consist of very fine-grained (<0.05mm) subhedral equant polygonal-shaped grains. The plagioclase grains commonly have small clinozoisite grains at their cores and are strongly cross-cut by the actinolite grains. They are generally equant to subprismatic in shape, and in places are strongly broken and bent with moderately bent twin lamellae (up to 40°).
ii) as tiny granular grains (<0.05mm) which are equant and polygonal in shape with well-developed triple-junction grain boundaries.

Quartz also occurs in two main forms:

i) as relatively large (0.2-1mm) well-rounded phenocrysts which are moderately aligned (defined by the parallelism of the long axis of these grains), generally exhibit strong undulose extinction, are moderately embayed in places, and have moderately sutured grain boundaries. These grains have well-developed subgrain at their grain boundaries which consist of tiny (<0.05mm) equant polygonal-shaped grains with well-developed triple-junction subgrain boundaries.
ii) as tiny (<0.05mm) equant polygonal-shaped grains with well-developed triple-junction grain boundaries.

Actinolite generally occurs as moderately aligned (defined by the parallelism of the long axis of the relatively large actinolite grains) to non-aligned (generally fine-grained stellate masses) grains which cross-cut all of the other phases present. Two principal forms of actinolite occur:

i) moderately-aligned, relatively large (0.5-1mm), moderately pleochroic (olive-green to brown-green) prismatic grains which commonly occur as aggregates of needle-like grains. They commonly have very fibrous edges, exhibit moderate to strong undulose extinction, and are commonly moderately bent (up to 60°). Many are fringed by the more fibrous actinolite.
ii) as non-aligned very fibrous elongate prismatic grains (<0.1-1mm) which commonly occur in the form of stellate aggregates and cross-cut all of the other phases present, including the other actinolite grains. They are commonly moderately bent (up to 45°) and exhibit moderate to strong undulose extinction.

Clinozoisite occurs as small (<0.1mm) subhedral equant-shaped grains in the core of the plagioclase phenocrysts.

Metabasalts

Are of rare occurrence as small dyke-like bodies enclosed within either massive or schistose serpentinite. They have a pseudoporphyritic decussate texture defined by either non-aligned relatively large grains of hornblende (commonly with lenticular aggregates of quartz) in a fine-grained matrix of albite, chlorite and actinolite or by non-aligned plumose aggregates of actinolite with intergranular epidote, clinozoisite and almandine garnet. They have a modal composition of hornblende (0-64%), plagioclase (0-30%), actinolite (0-90%), chlorite (0-5%), epidote (<1-5%),

quartz (0-15%), clinozoisite (0-3%) and almandine garnet (0-2%), along with accessory sphene and apatite and cross-cutting veinlets of clinozoisite.

Hornblende occurs in two main forms:

i) as relatively large (0.5-1mm) subhedral, generally subprismatic grains which are moderately pleochroic (olive-green to tan-brown), strongly embayed by the matrix, and exhibit moderate undulose extinction. They occur as either single grains or strongly interlocking grain aggregates. They are commonly bent (up to 30°) and fractured, and cross-cut by grains of actinolite and epidote. They are often rimmed and partially replaced by secondary fibrous actinolite.
ii) as relatively fine-grained (0.1-0.2mm) strongly interlocking and commonly twinned grains. They are generally subhedral and prismatic in shape with ragged grain boundaries, and exhibit weak undulose extinction.

Plagioclase occurs as fine to very fine-grained (<0.05-0.5mm) subhedral short prismatic grains within the matrix. They generally lack well-developed multiple twin lamellae and are strongly saussuritised to fine-grained mixtures of albite, quartz and epidote.

Actinolite occurs in the following forms:

i) as moderately pleochroic (pale to dark green) generally elongate prismatic grains (0.2-1mm) which often occur in the form of stellate aggregates. They are commonly strongly bent (up to 60°) and exhibit strong undulose extinction. These grains are non-aligned and cross-cut all of the other phases present.
ii) as relatively small (0.1-0.5mm) subhedral prismatic grains which are moderately pleochroic (either pale brown or pale green to blue-green). They have ragged grain boundaries, cross-cut each other, and generally exhibit moderate undulose extinction.

Quartz lenticles: appear to be both randomly oriented and distributed within the metabasalts and occur as both ovoid-shaped (possibly former amygdules) and elongate prismatic vein-like aggregates of strongly polygonal-shaped quartz grains. They have well-developed triple-junction grain boundaries and exhibit only weak undulose extinction. They are strongly cross-cut by both the secondary fibrous actinolite and granular epidote/clinozoisite grains.

Clinozoisite occurs as strongly cross-cutting veinlets composed of non-aligned subhedral prismatic grains which exhibit moderate undulose extinction. Epidote is of common occurrence as very fine-grained (<0.05mm) subhedral, equant to subprismatic grains which exhibit moderate undulose extinction and occur within the matrix.

Almandine garnet is of rare occurrence, though abundant when present, as small (<0.1mm) subhedral to euhedral, moderately rounded grains which commonly occur in the form of granular aggregates. The almandine is interstitial to the actinolite grains and is associated with relatively small (<0.05-0.1mm) grains and aggregates of epidote and clinozoisite.

Actinolite hornfels

These rocks have only been found to occur at G.R. 039 891 in the central part of the belt. They exhibit a porphyroblastic decussate texture defined by large platy grains of poikiloblastic actinolite in a non-aligned much finer-grained matrix of actinolite and talc. They have a modal composition of

actinolite porphyroblasts (50%), fine-grained matrix actinolite (40%), talc (10%), minor clinozoisite (<1%) and accessory opaques.

Actinolite occurs in two main forms:

i) as relatively large (5-12mm) platy, generally equant-shaped grains which have very ragged grain boundaries. They are strongly poikiloblastic, containing abundant inclusions of the finer-grained actinolite, talc and clinozoisite. They are strongly pleochroic (colourless to olive-green) and commonly interlocking with each other, with well-developed triple-junction grain boundaries.
ii) as much finer-grained (0.1-0.7mm) elongate prismatic simply twinned grains. These are moderately pleochroic (brown-green to blue-green), non-aligned, and subhedral to euhedral.

Talc occurs as very fine-grained (<<005mm) non-descript non-aligned fibrous masses. Clinozoisite is restricted to the poikiloblastic actinolite grains where it occurs as subhedral, equant to subprismatic inclusions with sharp grain boundaries.

Actinolite-chlorite rocks

These rocks have only been found to occur at G.R. 970 186 in the northern part of the belt. They exhibit a feathery decussate texture defined by non-aligned prismatic grains of actinolite and minor clinozoisite in a much finer-grained matrix of chlorite. They have a modal composition of actinolite (48%), chlorite (48%) and clinozoisite (4%), along with accessory ilmenite.

Actinolite generally occurs as subhedral to euhedral, strongly pleochroic (either pale green to blue-green or olive-green to tan-brown) prismatic grains which are non-aligned and cross-cut the chlorite matrix. They are commonly twinned and are overprinted by the ilmenite grains.

Chlorite occurs as colourless to pale green aggregates of very fine-grained (<<0.05mm) non-aligned fibrous grains which are cross-cut by both the actinolite and ilmenite. Clinozoisite is of minor occurrence as subhedral, equant to subprismatic, grains (0.1-0.5mm) which cut-across the actinolite grains but are themselves cross-cut by the ilmenite grains. Ilmenite cross-cuts all of the other phases and occurs as non-aligned elongate prismatic euhedral grains (<0.1-0.6mm).

Chlorite-clinozoisite-talc rocks

These rocks are moderately common in the southern part of the belt as small lenses near the contacts with the Jindalee Beds quartzites. They are quite strongly layered, with this layering being defined by varying proportions of the constituent phases. They have a modal composition of chlorite (40-75%), clinozoisite (15-30%), talc (8-40%) and tremolite (0-3%), along with accessory opaques. Generally, three distinct types of layering occur within these rocks:
Layer 1: has a modal composition of chlorite (98-99%) and clinozoisite (1-2%)
Layer 2: has a modal composition of chlorite (60%) and clinozoisite (40%)
Layer 3 has a modal composition of talc (40%), chlorite (30%) and clinozoisite (30%)

Chlorite occurs in the following forms:

i) as pale green relatively fine-grained (<0.05-0.3mm) fibrous grains which commonly occur in the form of plumose aggregates. They exhibit no preferred crystallographic orientation and strongly cross-cut and replace the clinozoisite grains.

ii) as semi-continuous bands (0.1-0.5mm in width) of colourless platy, moderately aligned grains (with the long axis of these grains being parallel to the layering within these rocks). The individual chlorite grains are subhedral and prismatic in shape.

Clinozoisite is restricted to a discrete layer and occurs as relatively large (0.2-2mm) equant to prismatic, generally subhedral strongly embayed grains (with the embayments being filled by talc and chlorite). They commonly exhibit subgrain development with triple-junction grain boundaries. They have strongly sutured grain boundaries, and the larger grains are commonly fractured and brecciated (with fracture- and breccia- fill by chlorite and talc).

Talc occurs as colourless, extremely fine-grained (<<0.05m) fibrous grains which cross-cut all the other phases present. Opaques occur as either aggregates of tiny grains or elongate prismatic grains. The layering within these rocks is defined by varying modal proportions of opaques and clinozoisite. Cross-cutting veinlets consist of euhedral tremolite grains, subhedral muscovite/chlorite grains, and subhedral clinozoisite/vesuvianite grains.

Rodingites

Have only been found to occur at G.R. 037 398 in the southern part of the belt. They exhibit a pseudoporphyritic decussate texture defined by strongly deformed relatively large grains of diopside in a finer-grained matrix of zoisite, talc and Mg-chlorite. They have a modal composition of diopside (20%), zoisite (40%), Mg-chlorite (30%) and talc (10%), along with accessory opaques.

Diopside occurs as colourless, relatively large (1-5mm) equant to prismatic grains which are commonly bent in places (with bent exsolution lamellae up to 75°), and often quite strongly fractured and brecciated. Most of the grains exhibit intense undulose extinction, have ragged edges and are often embayed.

Zoisite occurs as colourless, non-aligned grains (0.1-1mm) which are generally subhedral and equant to prismatic in shape. They commonly occur in the form of stellate aggregates, cross-cut the diopside grains, but are themselves broken-up, cross-cut and partially replaced by talc. Talc occurs as very fine-grained (<<0.05mm) non-descript prismatic grains which cross-cut all of the other phases present. Mg-chlorite occurs as colourless, moderately large patches (up to 1mm) of non-oriented elongate prismatic fibrous grains which are cross-cut by the fine-grained talc.

Olivine-amphibole-chlorite hornfels

These rocks have only been found at G.R. 050 880 in the central part of the belt as small lenses within chlorite rocks. They exhibit a pseudoporphyritic decussate texture defined by relatively large highly fractured ovoid-shaped olivine grains in a fine-grained matrix of decussate amphiboles (Mn-bearing?), olivine fragments and fibrous chlorite. They have a modal composition of olivine (20%), pink amphibole (75%) and Mg-chlorite (5%), along with accessory opaques.

Olivine occurs as relatively large (1-8mm) well-rounded spherical to ovoid-shaped grains which are relatively fresh but invariably highly fractured (with both fracture-fill and rim replacement by Mg-chlorite). These fractures are of two dominant orientations perpendicular to each other. Some of the olivine exhibits subgrain development with these subgrains going into extinction at a different angle than that of the host grain. The olivine grains are strongly embayed and have ragged grain boundaries. Many of the olivine grains have been fragmented into much smaller (<0.1-0.4mm)

equant-shaped angular grains which have been displaced as much as 1mm from the parent grains. Many of the olivine grains are moderately aligned and the olivine fragments appear to be aligned parallel to the long axis of the parental grains.

Amphibole occurs as moderately pleochroic (colourless to orange-pink) grains with a large range in grain-size (<0.1-1mm). They generally occur as angular subprismatic grains with ragged grain boundaries and moderate undulose extinction. They are commonly fractured (with fracture-fill by fine-grained chlorite), do not exhibit any preferred crystallographic orientation, and are commonly simply twinned.

Mg-chlorite occurs as colourless, non-descript masses of very fine-grained (<0.05mm) fibrous elongate prismatic grains. They do not exhibit any preferred crystallographic orientation and cross-cut the other phases present. They commonly occur in the following forms:

i) as rim and fracture-related replacement of olivine.
ii) as complete pseudomorphs after the olivine grains, commonly with aggregates of fine-grained magnetite at their centre.
iii) as rim and fracture-related replacement of amphibole.

APPENDIX 5PD

PETROGRAPHIC DESCRIPTIONS OF ROCK TYPES FROM THE GUNDAGAI SERPENTINITE BELT AND ABUTTING UNITS

The Jones Creek diorite and breccia

The Jones Creek diorite comprises the following different rock types:

Massive hornblende diorite

This diorite has a modal composition (visually determined) of albitic plagioclase (47%), hornblende (45%), quartz (3%), actinolite (4%) and epidote (1%), along with minor chlorite and clinozoisite, and accessory sulfides, zircon, apatite, magnetite and sphene. It exhibits a hypidiomorphic granular texture defined by non-aligned strongly interlocking grains of plagioclase, hornblende and quartz, and cross-cutting grains of fibrous actinolite, epidote, chlorite, clinozoisite and sulfides, and minor cross-cutting veinlets of epidote.

Plagioclase occurs as subhedral to euhedral, lath-like short prismatic grains (1-3mm) which exhibit well-developed multiple twin lamellae, rarely with micro-faulted and bent twin lamellae (up to 30°). They commonly impinge upon each other and have strongly sutured grain boundaries though lack subgrain development.

Hornblende occurs as anhedral to subhedral, generally short prismatic moderately pleochroic (colourless to olive-green) grains (0.5-2mm). They exhibit moderate undulose extinction and are commonly simply twinned. The hornblende grains have very ragged grain boundaries, fibrous actinolite fringes, and are cross-cut and in places, completely replaced by fibrous actinolite or chlorite.

Quartz is of minor occurrence as anhedral-shaped, elongate grains (up to 1mm) which are intimately associated with the plagioclase grains and have strongly mutually sutured grain boundaries with them. They exhibit strong undulose extinction but appear to lack subgrain development.

Actinolite occurs as fringes and partial to complete replacements of the hornblende grains. It occurs as moderately pleochroic (colourless to olive-green) strongly fibrous grains which are commonly bent in places (up to 50°) and are cross-cut by the epidote, clinozoisite and sulfide grains. Epidote/clinozoisite cut-across all of the other phases present with the exception of the sulfide grains. They generally occur in the form of aggregates and veinlets of small (<0.05-0.1mm) anhedral to subhedral, equant to subprismatic grains. Sulfides cut-across all of the other phases present and occur as euhedral equant cubic grains (0.1-1mm) which are commonly altered to secondary goethite.

Metahornblendite

The metahornblendite (G.R. 999 245) occurs as segregations within the massive hornblende diorite mass, and has a modal composition (visually determined) of hornblende (45%), actinolite (50%), chlorite (2%), and epidote (3%), along with minor carbonate and quartz, and accessory opaque phases. The rock has a postcumulus overgrowth pseudoporphyritic texture defined by relatively

large grains and fragments of hornblende in a much finer-grained secondary matrix of actinolite, chlorite, epidote, carbonate and quartz.

Hornblende occurs as moderately pleochroic (olive-green to tan-brown) relatively large (0.5-3mm) anhedral to subhedral, equant to subprismatic grains. They are commonly simply twinned and exhibit weak to moderate undulose extinction. They are strongly embayed, have very ragged grain boundaries, and are commonly rimmed, and partially to completely replaced by secondary actinolite. Many of these hornblende grains appear to have been fractured and brecciated prior to the development of the actinolite.

Actinolite occurs as moderately pleochroic (pale olive-green to intense blue-green) very fine-grained (<0.05mm), commonly moderately bent (up to 45°) grains which generally occur in the form of plumose aggregates. They occur in the following forms:

i) as rim replacements around the hornblende grains.
ii) as partial to complete replacements of the hornblende grains.
iii) as plumose aggregates within the matrix where they cross-cut all of the other phases present with the exception of the sulfide grains.

Epidote occurs as amber yellow, anhedral to subhedral, equant to subprismatic grains throughout the matrix. They are fractured and cross-cut by the actinolite grains.

Diorite breccia

The best exposure of the Jones Creek Diorite breccia is on Flowers Hill at G.R. 002 218. It consists of angular to subrounded, relatively large (up to 15cm in maximum dimension) fragments of hornblende andesite, microgabbro, quartzite and metapelite, in a matrix of chlorite+epidote+actinolite+quartz. The hornblende andesite clasts have a modal composition (visually determined) of plagioclase phenocrysts (35-50%) and hornblende phenocrysts (3-5%) in a much finer-grained matrix of chlorite (30%), epidote (10%), actinolite (7%) and minor quartz. The rock has a porphyritic felty texture defined by strongly aligned phenocrysts of plagioclase and hornblende in a non-aligned fine-grained matrix.

The magmatic flow texture within this andesite is defined by the parallel alignment of the long axis of the plagioclase grains. These grains are generally subhedral and prismatic in shape, with sharp grain boundaries. Most of them are strongly altered though they retain their former well-developed multiple twin lamellae. They are cross-cut by the groundmass phases.

Hornblende phenocrysts are of minor occurrence and have generally been completely replaced by secondary fibrous blue-green actinolite. They occur as randomly distributed subhedral prismatic grains with their long axis paralleling the long axis of the plagioclase grains, thus helping define the magmatic flow texture. They exhibit well-developed twinning, have ragged grain boundaries, and have rim replacement by both actinolite and chlorite.

The groundmass generally consists of fine-grained (0.1-0.2mm) non-aligned actinolite, epidote, chlorite and patches of strongly recrystallised equant-shaped quartz grains. These patches may represent former devitrified glass fragments.

The matrix between these fragments is also of a volcanic nature and has a modal composition (visually determined) of phenocrysts [plagioclase (45%) and hornblende (5%)] and groundmass [chlorite (30%), epidote (15%), quartz (3%) and actinolite (2%), along with accessory opaques]. The overall texture of this matrix is defined by relatively large phenocrysts of plagioclase and hornblende in a much finer-grained matrix of chlorite, epidote, actinolite, quartz and opaques.

Plagioclase generally occurs as strongly altered, euhedral to subhedral, prismatic, commonly moderately rounded grains (0.3-1.5mm). They exhibit moderately developed multiple twin lamellae and compositional zoning. They are strongly embayed (with these embayments being filled by the groundmass epidote and chlorite) and cross-cut by the groundmass epidote.

Hornblende generally occurs as strongly pleochroic (olive-green to blue-green) subhedral prismatic grains (0.4-1mm) which are commonly simply twinned, have ragged grain boundaries, and are cross-cut by the groundmass epidote and actinolite.

The groundmass consists of relatively fine-grained (<0.05-0.2mm) mixtures of pale green-brown chlorite, subhedral equant-shaped epidote, fibrous actinolite, and aggregates of fine-grained quartz. These quartz aggregates consist of polygonal-mosaic grains with well-developed triple junction grain boundaries which may represent former devitrified glass.

The Wandeen Formation

The Wandeen Formation was investigated by the present author at G.R. 969 363. At this locality, talcosic metaserpentinite of the Gundagai Serpentinite Belt is faulted against mafic sandstone to the east and basaltic meta-andesite to the west. The basaltic meta-andesite has phenocrysts of hornblende (5-20 modal%), albitic plagioclase (5-10 modal%) and rare olivine (0-10 modal%) in a fine-grained groundmass of albitic plagioclase (up to 50 modal%), actinolite (10-28 modal%), chlorite (5-10 modal%), epidote (0-15 modal%), clinozoisite (2-15 modal%) and tremolite (0-1 modal%), along with accessory ilmenite, magnetite and zircon, and cross-cutting veinlets of clinozoisite. The texture is porphyritic intersertal (commonly with quench-textured plagioclase).

Hornblende occurs as relatively large (1-3mm), strongly pleochroic (either colourless to olive-green or pale olive-green to blue-green), subhedral to euhedral, short to elongate prismatic grains which exhibit weak undulose extinction. They are commonly simply twinned and have ragged gain boundaries. They are cross-cut, commonly rimmed, and partially to completely replaced by secondary actinolite. They are also cross-cut by epidote.

Olivine occurs as moderately altered (with both fracture-fill and rim replacement by pale green non-descript chlorite), subhedral subrounded short prismatic grains (0.5-1.5mm). They are strongly fractured and strongly rimmed by fibrous blue-green actinolite though have relatively sharp grain boundaries.

Plagioclase occurs in the following forms:

i) as relatively large (1-2mm) subhedral altered phenocrysts. These grains are angular, subprismatic to prismatic in shape, and have sharp grain boundaries. They commonly impinge on each other and are cross-cut by the secondary actinolite and epidote grains. They exhibit only weakly developed multiple twin lamellae and compositional zoning.

ii) as aggregates of non-aligned grains (1-3mm) which are commonly associated with both epidote and clinozoisite. The individual plagioclase grains are generally subhedral and equant to subprismatic in shape. They strongly impinge on each other and exhibit well-developed multiple twin lamellae and compositional zoning.
iii) as relatively small (0.2-0.5mm) anhedral to subhedral, short to elongate prismatic grains within the groundmass. They exhibit weak to well-developed multiple twin lamellae and compositional zoning. They generally have strongly sutured grain boundaries and are intimately associated with the groundmass quartz. They appear to be cross-cut by the other phases within the groundmass.

Actinolite occurs in the following forms:
i) as moderately pleochroic (colourless to blue-green) generally elongate prismatic non-aligned grains within the groundmass. These grains are generally subhedral in shape and have ragged grain boundaries.
ii) as narrow rims around olivine grains.
iii) as rims around, and partial to complete replacements of the hornblende grains.

Quartz is of minor occurrence within the groundmass and appears to be intimately associated with the groundmass albitic plagioclase.

Chlorite generally occurs as non-descript pale green masses of the following forms:
i) as fracture- and rim-replacement of the olivine grains.
ii) as masses of fibrous grains throughout the groundmass.

Epidote is evenly and widely distributed as anhedral to subhedral, equant to elongate prismatic grains (0.1-1mm) and grain aggregates. Clinozoisite is of similar occurrence to the epidote grains but also occurs as narrow to wide (up to 1.5mm) cross-cutting discontinuous veinlets.

The Jackalass Slate

The Jackalass Slate is dominated by slate and siltstone which are composed of recrystallised quartz, plagioclase, hornblende, magnetite, chlorite, biotite and sericite (Basden 1990; Giddey 1995) and are tuffaceous (Nguyen 1977). Sandstones are of minor occurrence, are also tuffaceous, and range in composition from andesitic to rhyodacitic. Phenocrysts of angular quartz and plagioclase, opaques, biotite and pyroxene? are set in a fine-grained foliated matrix of recrystallised quartz, sericite, biotite and epidote (Basden 1990).

A small pod of dolomitised marble was investigated during the course of the present study at G.R. 004 215. It occurs between serpentinite of the Gundagai Serpentinite Belt and the metapelitic rocks described above. In thin-section, this marble has a granoblastic linear fabric defined by strongly interlocking grains of dolomite, along with minor quartz, magnetite and rare phengitic muscovite. The linear fabric is defined by magnetite-rich and magnetite-poor bands and may define former bedding planes within the original marly limestone protolith.

The volcanic rocks of the Jackalass Slate include meta-andesite, quartz-feldspar porphyries and feldspar porphyries (Basden 1990). The andesitic rocks are porphyritic and contain phenocrysts of plagioclase and amphibole in a groundmass of plagioclase, hornblende, recrystallised quartz, epidote, opaques, chlorite and biotite (Basden 1990).

A small "pod-like" body of dacitic tuff within the metasedimentary sequence of the Gundagai Serpentinite Belt was investigated at G.R. 015 175. This rock has a porphyritic intersertal texture defined by non-aligned phenocrysts of quartz, hornblende and plagioclase within a fine-grained feldspathic groundmass. The quartz and hornblende phenocrysts are commonly embayed; quartz is well-rounded whereas the hornblende is euhedral and altered. Rare almandine garnet fragments are embayed and have groundmass as fracture-fill.

The Gundagai Serpentinite Belt

Primary ultramafic rocks

The following primary ultramafic rock types were identified within the Gundagai Serpentinite Belt during the course of the present study:

Metaharzburgites

The metaharzburgites generally exhibit a relict porphyroclastic texture and contain > 5 modal% visible bastitised orthopyroxene. They have all been altered to some degree. Most are relatively massive and unfoliated, though a few are schistose. These metaharzburgites have a modal composition (visually determined) of chrome spinel (1-2%), bastitised orthopyroxene (5-10%), antigorite (80-88%) and magnesite (0-15%), along with secondary accessory magnetite. In general, they exhibit a porphyroclastic texture defined by relatively large grains of completely bastitised orthopyroxene and chrome spinel in a matrix of non-aligned fibrous antigorite grains.

Orthopyroxene occurs as completely bastitised (i.e. replaced by fibrous chrysotile) relatively large (0.6-1.75mm) grains which are strongly embayed by the matrix. They are anhedral to subhedral, and equant to subprismatic in shape. The chrysotile fibres within these grains are generally oriented with their long axes perpendicular to the long axis of the parental orthopyroxene grains. They generally exhibit moderate to extreme undulose extinction, are commonly fractured, and are cross-cut by the matrix antigorite and chrysotile veinlets.

Chrome spinel generally occurs as quite angular, strongly embayed and fractured grains. They are commonly anhedral and elongate prismatic in shape (0.2-1mm), and are strongly rimmed and fracture-replaced by secondary fine-grained magnetite.

Mesh-textured serpentine consists of two main components:

i) structureless, generally elongate well-rounded ovoid-shaped cores (0.2-0.3mm) which exhibit moderate undulose extinction.
ii) narrow rims (<0.05-0.1mm) of fibrous chrysotile grains around these cores. The long axis of these grains are generally oriented perpendicular to the rim walls, and these grains also exhibit moderate undulose extinction.

The antigorite matrix is composed of fine-grained (<0.05-0.1mm) non-aligned elongate fibrous prismatic grains. They commonly occur in the form of plumose aggregates and exhibit moderate undulose extinction. These grains cross-cut the orthopyroxene grains but are themselves cross-cut by the magnesite grains.

Chrysotile veinlets are generally moderately continuous (4-8mm), sigmoidal-shaped, and narrow (<0.05-0.3mm). The chrysotile grains within these veinlets exhibit moderate undulose extinction and are generally oriented perpendicular to the veinlet walls.

Magnetite generally occurs in two main forms:

i) as very discontinuous (up to 1mm) narrow veinlets composed of tiny fine-grained equant-shaped grains. These veinlets appear to define former olivine subgrain boundaries.
ii) as rim- and fracture-related replacements of relatively large (0.2-1mm) chrome spinel grains.

Magnesite occurs as relatively large (0.1-4mm) patches composed of non-descript anhedral to subhedral, equant-shaped grains. They often contain inclusions of the matrix antigorite and occur in the form of randomly distributed patches throughout these rocks which cross-cut all of the other phases present.

Clinopyroxenites

The clinopyroxenites of the Gundagai Serpentinite Belt are here defined as those ultramafic rocks which contain >80 modal% clinopyroxene and <15 modal% olivine. To date, only one such outcrop has been found in the northern half of the belt at G.R. 992 218. This clinopyroxenite has a modal composition (visually determined) of clinopyroxene (85%), talc (10%) and serpentine (5%), along with accessory secondary magnetite. This rock exhibits a post-cumulus space-fill texture defined by strongly interlocking, relatively large grains of clinopyroxene and altered olivine (i.e. mixtures of talc+serpentine) in a fracture-fill matrix of relatively fine-grained serpentine and talc.

Clinopyroxene occurs as relatively large (1.5-3mm), generally subhedral equant to subprismatic grains which exhibit well-developed diallage parting. They are strongly interlocking with each other (and the altered olivine grains) with well-developed triple-junction grain boundaries. They exhibit moderate undulose extinction and are commonly highly fractured and brecciated (with fracture- and breccia-fill by fine-grained talc, serpentine and magnetite). They are commonly strongly embayed by the serpentine+talc matrix which appears to represent former intergranular olivine.

Olivine occurs as anhedral, moderately rounded, ovoid-shaped grains (1-1.5mm) which occur intergranular to the clinopyroxene grains. They have been completely altered to a mixture of fine-grained serpentine+talc.

Metapyroxenites

The metapyroxenites of the Gundagai Serpentinite Belt are here defined as those ultramafic rocks which are dominantly composed of clinopyroxene and orthopyroxene and exhibit a granoblastic to porphyroclastic texture. To date, metapyroxenites have only been found at the one locality (G.R. 016 174) in the southern half of the belt. They have a modal composition (visually determined) of diopside (58-70%), orthopyroxene (10-20%), serpentine (0-7%), tremolite (15%) and chlorite (0-5%), along with secondary accessory magnetite. The porphyroclastic texture of these rocks is defined by relatively large, commonly highly fractured grains of diopside and orthopyroxene between which occur both fracture- and breccia-fill of tremolite, serpentine, chlorite and talc.

Clinopyroxene occurs as relatively large (0.5-5mm), highly fractured, subhedral equant to prismatic grains which are also commonly highly brecciated (with fracture- and breccia-fill by serpentine, tremolite, chlorite and talc). They exhibit very finely-spaced diallage parting, weak to moderate undulose extinction, and some are moderately bent (up to 30°). These grains were once strongly

interlocking with both each other and the orthopyroxene grains, defining a postcumulus magmatic texture. They have ragged grain boundaries with partial rim replacement by secondary tremolite.

Orthopyroxene is of minor occurrence as relatively large (1-2mm) strongly bastitised grains which are subhedral and subprismatic in shape. They are commonly moderately embayed by the matrix tremolite and have crystallised synchronously with the clinopyroxene grains. They exhibit moderate undulose extinction, and, like the clinopyroxene grains, are strongly fractured and brecciated (with fracture- and breccia-fill by secondary tremolite).

Tremolite generally occurs as very fine-grained (<0.1mm) fibrous elongate prismatic grains. These grains are non-aligned and occur as fracture- and vein-fill between the pyroxene grains. They exhibit moderate undulose extinction, and in places, are commonly bent (up to 30°). They cross-cut the other phases present and commonly occur in the form of plumose aggregates.

Serpentine is of minor occurrence within the matrix where it occurs as randomly distributed patches (1-3mm) of very fine-grained (<0.05mm) fibrous elongate prismatic grains, and as intergranular fibrous masses between the pyroxene grains. They also occur as fracture- and breccia-fill within the pyroxene grains and are themselves cross-cut by the tremolite grains. Chlorite is of minor occurrence as randomly distributed patches (0.2-4mm) of pale green very fine-grained (<<0.05mm) fibrous grains which are cross-cut by the tremolite grains.

Magnetite occurs in the following forms:

i) as very fine-grained (<<0.05mm) equant-shaped grains which occur in the form of linear aggregates which help to define cleavage planes in the clinopyroxene grains.
ii) as very fine-grained (<<0.05mm) discontinuous intergranular aggregates which consist of tiny equant-shaped grains.
iii) as discontinuous linear aggregates which help to define former grain boundaries in the pyroxene grains and are composed of fine-grained (<0.05mm) equant-shaped grains.

Metaperidotites

The metaperidotites of the Gundagai Serpentinite Belt are here defined as those ultramafic rocks which were once dominantly composed of olivine and pyroxenes but are now dominantly composed of pseudomorphous serpentine and talc. To date, only one body of metaperidotite has been found within the southern half of the belt (G.R. 001 205). This rock is quite strongly sheared (with a well-developed S-C fabric) and has a modal composition (visually determined) of serpentine (60%) and talc (40%), along with minor secondary magnesite ad accessory magnetite.

Serpentine occurs in two main forms:

i) as typical 'mesh-textured' serpentine which consists of fibrous veinlets of chrysotile around a central core of structureless lizardite. Some of the larger chrysotile veinlets have been micro-faulted with lateral offsets of <0.1mm. The material between consists of fine-grained talc and magnetite. Magnetite also occurs around the chrysotile veinlets and helps to define the mesh texture.
ii) as pseudomorphic replacements of former subhedral prismatic angular pyroxene grains with very ragged grain boundaries. Magnetite veinlets define former cleavage planes within these grains which have been completely replaced by fibrous serpentine. Some are strongly embayed

by the groundmass serpentine. They are commonly cross-cut by chrysotile veinlets, and in places, are moderately fragmented.

Chrysotile veinlets are of minor occurrence, cross-cut the other serpentine grains, but are themselves cross-cut by the talc/magnesite veinlets. They are relatively continuous (up to 20mm) and of variable width (<0.05-0.5mm). They are also strongly sigmoidal in shape and the chrysotile fibres within these veinlets are generally oriented perpendicular to the veinlet walls. Talc/magnesite occur as cross-cutting veinlets throughout these rocks and have replaced former serpentine grains.

Magnetite occurs in the following forms:

i) as relatively continuous (up to 4mm) veinlets composed of very fine-grained (<0.05mm) equant-shaped grains which occur in the outer margins of the cross-cutting chrysotile and talc/magnesite veinlets.

ii) as highly discontinuous narrow veinlets composed of tiny equant-shaped magnetite grains which help to define former olivine and pyroxene grain boundaries.

Serpentinites

The serpentinites of the Gundagai Serpentinite Belt are here defined as those ultramafic rocks which are dominantly composed of serpentine-group minerals, contain < 15modal% talc+magnesite and exhibit a secondary texture. Using this definition, the serpentinites of this belt can be subdivided into three main groups:

Massive serpentinites

At meso-scale, these rocks are relatively unsheared and massive. At micro-scale, they commonly exhibit decussate, feathery and pseudoporphyritic textures. They have a modal composition (visually determined) of serpentine (80-100%), chrome spinel (0-1%), magnesite (3-15%) and talc (0-15%), along with secondary magnetite. They generally exhibit a pseudoporphyritic texture defined by relatively large grains and patches of secondary magnesite which strongly overprints a fine-grained matrix of non-aligned antigorite.

Antigorite occurs in two main forms:

i) as non-aligned plumose aggregates (0.05-0.5mm) of fibrous subhedral elongate prismatic grains which exhibit moderate undulose extinction. The individual antigorite is generally very fine-grained (<<0.05mm) and often needle-like in habit.

ii) as randomly distributed patches of coarser-grained (0.1-0.2mm) subhedral elongate prismatic grains which occur in the form of cross-cutting plumose aggregates. They cross-cut the finer-grained antigorite but are themselves cross-cut by magnesite and talc.

Chrysotile veinlets occur as relatively discontinuous (1-4mm), narrow (<0.05-0.2mm) sigmoidal-shaped veinlets. The chrysotile within these veinlets generally exhibits moderate undulose extinction.

Chrome spinel is of rare occurrence as relatively large (0.2-2mm), subhedral equant to elongate prismatic grains which are strongly embayed by the matrix antigorite and partially replaced (both rim- and fracture-replacement) by fine-grained secondary magnetite. They are strongly fractured (with one main fracture orientation perpendicular to the long axis of the grains) and brecciated, and are often rimmed by fine-grained magnetite.

Magnesite cross-cuts the other phases present and occurs in two main forms:

i) as relatively large (0.5-2mm) anhedral to subhedral, equant to subprismatic, generally moderately rounded porphyroblastic grains which overprint the antigorite matrix. It commonly occurs in the form of granular aggregates which commonly contain inclusions of the matrix antigorite and secondary magnetite.
ii) as discontinuous (up to 8mm) veinlets which have highly variable widths along their length (<0.05-5mm) and are sigmoidal in shape. These veinlets also cross-cut the secondary magnetite veinlets.

Talc occurs in the following forms:

i) as relatively continuous (up to 16mm), relatively narrow (<0.05-0.2mm) sigmoidal-shaped veinlets which cross-cut all of the other phases present.
ii) as randomly distributed patches of very fine-grained (<<0.05mm) talc which strongly overprint all of the other phases present.

Magnetite occurs in the following forms:

i) as fine-grained (<0.05mm) disseminated equant-shaped grains.
ii) as relatively large (0.1-1mm) aggregates of the disseminated grains described above.
iii) as partial replacements of the chrome spinel grains.
iv) as relatively discontinuous (1-4mm), generally narrow (<0.05-0.2mm) sigmoidal-shaped veinlets. These veinlets are composed of fine-grained (<0.05mm) equant-shaped grains.

Schistose serpentinites

At meso-scale, the schistose serpentinites of the belt exhibit a closely-spaced well-developed S-C fabric. At micro-scale, they exhibit decussate, feathery and veined textures. They have a modal composition (visually determined) of serpentine (98-100%) and chrome spinel (0-2%). They generally exhibit a strong "vein texture" defined by non-aligned fine-grained fibrous antigorite which is strongly cross-cut by chrysotile veinlets.

The antigorite matrix occurs as non-aligned, relatively fine-grained (<0.05-0.2mm), subhedral elongate prismatic fibrous grains. These grains generally exhibit moderate undulose extinction and occur in the form of plumose aggregates.

The chrysotile veinlets occur as strongly cross-cutting, generally discontinuous (2-8mm) sigmoidal-shaped veinlets which have variable widths along their length (<0.1-1mm). They are generally of two distinct orientations perpendicular to each other. The earlier generation of these veinlets occurs as narrower veinlets and the chrysotile fibres within these veinlets are generally oriented parallel to the veinlet walls. The later generation of veinlets cross-cuts the earlier generation (which are also commonly micro-faulted) and the chrysotile fibres in the later generation of veinlets are generally oriented at 60° to the veinlet walls. The chrysotile within both veinlet generations exhibits moderate undulose extinction.

Chrome spinel is of rare occurrence as relatively large (0.2-0.5mm), subhedral equant-shaped grains which are moderately fractured and have both fracture- and rim-related replacement by fine-grained secondary magnetite.

Magnetite occurs in the following forms:

i) as relatively large (0.1-0.5mm), subhedral equant-shaped randomly distributed aggregates of very fine-grained (<0.05mm) magnetite.
ii) as discontinuous veinlets composed of fine-grained (<0.05mm) magnetite, which appear to define former olivine subgrain boundaries.
iii) as rim- and fracture-related replacement of the chrome spinel grains.
iv) as linear aggregates of fine-grained (<0.05mm) magnetite enclosed within the chrysotile veinlets.

Nodular serpentinites

At meso-scale, these serpentinites appear to consist of rounded clasts of massive serpentinite within a matrix of schistose serpentinite. At micro-scale, they exhibit porphyroclastic, decussate, veined and mesh textures. They have a modal composition (visually determined) of serpentine (85-86%), chrome spinel (1-2%), magnesite (10-13%) and rare hornblende (0-1%), along with cross-cutting veinlets of tremolite and secondary magnetite. Texturally, these rocks can be subdivided into two main parts:

Nodular clasts: consist of relatively large (with common maximum dimensions of 0.3 to 30mm), generally moderately rounded ovoid to sub-prismatic nodules. These nodules are generally composed of abundant fine-grained secondary magnetite (up to 50 modal% of the nodule) along with aggregates of ovoid-shaped magnesite (which are pseudomorphous after former olivine grains) and fracture-fill of chrysotile and tremolite. The nodules are commonly embayed by the matrix.

Matrix: consists of mesh-textured serpentine which is strongly cross-cut by relatively continuous sinuous veinlets of chrysotile and discontinuous veinlets of tremolite. The mesh-textured serpentine consists of two parts:

a) generally subrounded equant to elongate ovoid-shaped structureless cores (with common maximum dimensions of 0.1 to 0.5mm) which exhibit moderate undulose extinction.
b) narrow (with maximum widths of <0.05mm) rims which completely surround the above cores and consist of fibrous chrysotile grains which are generally oriented perpendicular to the rim walls and also exhibit moderate undulose extinction.

Chrome spinel is of minor occurrence as relatively large (0.1-1.5mm) generally subhedral, equant to prismatic grains which are commonly fractured (with the one dominant fracture orientation perpendicular to the long axis of these grains) and embayed by the matrix. These grains are moderately rim- and fracture-replaced by fine-grained (<0.05mm) equant-shaped magnetite. They are of far more common occurrence within the matrix. Hornblende is of very rare occurrence as moderately large (0.5-1mm) pale green euhedral short prismatic grains which have sharp grain boundaries and exhibit weak undulose extinction. They may be pseudomorphic after former diopside grains.

Talc-carbonate rocks

The talc-carbonate rocks of the Gundagai Serpentinite Belt can be further subdivided into talc and/or magnesite rich meta-ultramafic rocks, talc-carbonate rocks and talc schists.

The talc and/or magnesite rich meta-ultramafic rocks can themselves be further subdivided into the following:

Metapyroxenites

These rocks have a modal composition (visually determined) of tremolite (40%), actinolite (20%), magnesite (20%) and talc (20%), along with secondary magnetite. They generally exhibit a decussate texture defined by large patches of talc pseudomorphs after olivine, tremolite/actinolite pseudomorphs after pyroxenes, and cross-cutting patches of magnesite and tremolite/actinolite.

Talc generally occurs as relatively large (up to 10mm) pseudomorphs after former highly fractured, magnetite-veined olivine grains. These grains are strongly embayed by the matrix tremolite/actinolite/magnesite and are also overprinted by these grains. The original olivine grains were subhedral, moderately rounded and ovoid in shape. The magnetite veinlets within these grains are of two dominant orientations perpendicular to each other. The magnetite veinlets are composed of fine-grained (<0.05mm) equant-shaped magnetite.

Tremolite/actinolite occurs as colourless to pale green grains of the following forms:

i) as complete replacements of former diopside grains. The original diopside occurred as relatively small (1-2mm) subhedral equant to subprismatic grains. They are now composed of pseudomorphous elongate prismatic fibrous tremolite/actinolite grains and magnesite.
ii) as cross-cutting subhedral prismatic angular grains (0.2-1mm) which cross-cut the talc grains. These gains commonly consist of a pale green core and a colourless more fibrous rim.

Magnesite occurs as non-descript, very fine-grained (<<0.05mm) equant-shaped grains which occur in the form of granular aggregates throughout these rocks, and cross-cut and contain inclusions of the other phases present.

Metaserpentinites

The metaserpentinites have a modal composition (visually determined) of serpentine (40-65%), chrome spinel (0-3%), talc (0-40%), magnesite (17-39%) and Mg-chlorite (0-20%), along with secondary magnetite. They generally exhibit a pseudoporphyritic decussate texture defined by relatively large patches of talc and/or magnesite which strongly overprint a matrix of non-aligned fibrous antigorite and equant grains of chrome spinel.

Antigorite occurs as non-aligned, relatively fine-grained (<0.05-0.2mm) elongate prismatic grains. They commonly occur in the form of plumose aggregates and are overprinted by the other phases present. They generally exhibit moderate undulose extinction.

Chrysotile veinlets are of minor occurrence as generally continuous (1-20mm), strongly sigmoidal-shaped veinlets of variable width (<0.05-0.5mm). The chrysotile within these veinlets occurs as plumose aggregates composed of fibrous elongate prismatic grains which are generally oriented subperpendicular to the veinlet walls and exhibit moderate to strong undulose extinction.

Magnesite occurs in the following forms:

i) intimately associated with the talc grains, as "cores" within patches of talc.
ii) as randomly distributed, relatively large (1-4mm) single, subhedral subrounded equant to prismatic grains or, aggregates of these grains. These grains overprint both the antigorite and

chrysotile (which they commonly contain inclusions of) but are themselves rimmed by the chlorite grains.

Talc occurs as colourless, very fine-grained (<0.05mm) needle-like grains throughout the metaserpentinites. It appears to have preferentially replaced former pyroxene grains whose shape are retained, along with cleavage-parallel aggregates of fine-grained (<0.05mm) magnetite.

Chrome spinel generally occurs as subhedral equant to subprismatic, relatively large grains (0.5-1.75mm) which are in places, rimmed by talc. They are strongly fractured, with one dominant fracture orientation parallel to the long axis of the grains. They are cross-cut by all the other phases present and are commonly rimmed by fine-grained (<0.05mm) secondary magnetite.

Chlorite is of minor occurrence as non-pleochroic pale green subhedral angular platy grains (0.1-1.5mm) which overprint all of the other phases present. They exhibit weak undulose extinction and commonly rim the magnesite grains and contain inclusions of them.

Magnetite occurs in the following forms:
i) as linear aggregates of equant-shaped fine-grained (<0.05mm) magnetite which helps to define former grain boundaries in former pyroxene grains.
ii) as highly discontinuous veinlets of equant-shaped fine-grained (<0.05mm) magnetite which help to define former olivine subgrain boundaries.
iii) as relatively large (0.2-1.5mm) anhedral to subhedral, equant to subprismatic grains. Many of these grains are strongly embayed by the matrix and most likely represent magnetite pseudomorphs after former chrome spinel grains.
iv) as moderately continuous (2-8mm), generally narrow (<0.1mm) commonly sigmoidal-shaped veinlets which occur within the chrysotile veinlets. These veinlets are composed of very fine-grained equant-shaped magnetite grains.

The talc-carbonate rocks can be further subdivided into the following:

Massive talc-carbonate rocks
These rocks have a modal composition (visually determined) of chrome spinel (1-2%), talc (30-60%) and magnesite (40-70%), along with secondary magnetite. They generally exhibit a porphyroblastic texture defined by relatively large strongly interlocking mosaic grains of magnesite which strongly overprint a fine-grained matrix of talc grains.

Chrome spinel is of minor occurrence as relatively large (0.4-1.8mm) commonly subhedral, equant to prismatic grains. They are strongly fractured and moderately brecciated with fracture- and breccia-fill by talc. The fractures are of two main orientations, one parallel to the long axis of these grains, and the other perpendicular to the long axis of these grains. They have fracture- and rim-related replacement by secondary fine-grained magnetite and are wrapped-around by the talc grains. Although many of them are strongly brecciated, they have undergone only minor shear displacement and the fragments can be easily rematched.

Talc occurs as non-aligned, relatively fine-grained (<0.1-0.5mm) subhedral platy subprismatic angular grains. They exhibit strong undulose extinction and are cross-cut and overprinted by the magnesite grains. Magnesite occurs as relatively large (0.5-1mm), equant-shaped subhedral grains

which have highly sutured grain boundaries between each other and commonly contain inclusions of both talc and magnetite.

Magnetite appears to be preferentially distributed in discrete bands. Within these bands, the magnetite occurs as discontinuous linear aggregates of very fine-grained (<0.05mm) equant-shaped grains which appear to define former olivine grain boundaries. These veinlets are overprinted by both the talc and magnesite grains.

Schistose talc-carbonate rocks

These rocks have a modal composition (visually determined) of talc (60-70%) and magnesite (30-40%), along with secondary magnetite and weathering-produced goethite. They exhibit a well-developed S-C fabric defined by either:

a) zones of strongly aligned elongate talc grains
b) opaque-rich and opaque-poor zones
c) magnesite-rich and magnesite-poor zones

Talc occurs as strongly aligned (with the long axis of these grains oriented parallel to the main foliation within the rock), extremely fine-grained (<<0.05mm) elongate prismatic grains. They are commonly strongly bent (up to 60°) and are cross-cut by the magnesite grains. Magnesite generally occurs as non-descript patches and veinlets (with the patches having a maximum dimension of 4mm). The veinlets are relatively continuous (up to at least 35mm), sigmoidal in shape and variable in width (0.3-1.5mm). Both the patches and veinlets are composed of anhedral equant-shaped grains which are replacements after former patches of talc. Opaques occur as relatively large (0.2-1mm) commonly highly fractured and brecciated, subhedral equant-shaped grains.

Talc schists

The talc schists have a modal composition (visually determined) of serpentine (0-2%), chrome spinel (0-3%), talc (95-98%) and tremolite (0-3%), along with secondary magnetite. They generally exhibit a schistose texture defined by strongly aligned grains of fibrous talc.

Serpentine is of minor occurrence as relatively small (<0.05-0.2mm), generally elongate prismatic fibrous grains which exhibit moderate undulose extinction and occur as randomly distributed patches within the talc matrix which are embayed and overprinted by the talc grains.

Chrome spinel occurs as relatively large (0.2-1.3mm), subhedral equant to prismatic grains. They are highly fractured (with one dominant fracture orientation perpendicular to the long axis of the grains) and brecciated, with fracture- and breccia-fill by talc. Some of the grains appear to have been rotated (45-60°) during the formation of the prominent schistosity and have well-developed grains of talc which wrap-around these grains.

Talc occurs as strongly aligned, very fine to fine-grained (<<0.05-0.2mm), generally elongate prismatic needle-like grains. The two differing grain-sizes (i.e. <<0.05 and 0.1-0.2mm) are preferentially distributed with the coarser-grained talc forming less continuous and wider bands which appear to overprint the finer-grained talc. These coarser-grained bands are commonly sigmoidal in shape, are relatively continuous (1-20mm) and have variable widths (0.5-4mm). As these grains approach kink bands within the talc schists, they become strongly bent (up to 60°) within the kink planes.

Tremolite is of minor occurrence as subhedral, generally elongate prismatic grains. They are commonly bent (up to 30°) and fractured (with fracture-fill by the matrix talc). They appear to be preferentially distributed into discrete bands, and, as these bands merge into the kink bands, the tremolite grains become strongly bent (up to 60°) into the kink planes.

The kink bands are defined by narrow (up to 1mm) areas within the talc schists where the constituent phases are strongly bent into this plane of kinking. These bands are oriented approximately perpendicular to the main orientation of the grains (i.e. the dominant schistosity) and are relatively closely-spaced (1-2mm).

Chlorite rocks
The chlorite rocks of the Gundagai Serpentinite Belt can be further subdivided into the following two types:

Massive chlorite rocks
These rocks have a modal composition (visually determined) of Mg-chlorite (95-100%) and clinozoisite (0-5%), along with secondary magnetite. They generally exhibit a pseudoporphyritic decussate texture defined by porphyroblasts of opaque minerals in a non-aligned fine-grained matrix of chlorite.

Chlorite occurs in three main forms:
i) as extremely fine-grained (<<0.05mm), non-aligned pale green grains which occur in the form of plumose aggregates and exhibit strong undulose extinction.
ii) as colourless, more coarser-grained (0.1-0.5mm) strongly interlocking plumose aggregates of grains which exhibit strong radial undulose extinction and occur in the form of continuous veinlets (up to 16mm). These veinlets have variable widths (0.5-1.5mm), commonly have finer-grained chlorite at their veinlet margins, and are cross-cut by the opaque grains.
iii) as colourless, coarse-grained (0.1-0.2mm) chlorite which occurs in the form of strongly aligned parallel continuous (1-4mm) veinlets which have variable widths (0.1-0.5mm). The chlorite fibres within these veinlets are generally oriented at 60-75° to the veinlet walls and occur as elongate prismatic grains.

Opaques cut-across the other phases present and occur in the following forms:
i) as highly angular, subhedral to euhedral, equant to subprismatic grains (<0.05-2mm) which have a strong platy habit and may be ilmenite.
ii) as relatively large (0.1-1mm), commonly moderately fractured (with one dominant fracture orientation perpendicular to the long axis of these grains) subhedral equant to subprismatic grains.

Clinozoisite is of minor occurrence as subhedral to euhedral, generally small (0.05-0.2mm) equant-shaped grains which have sharp grain boundaries, cross-cut the chlorite grains, but are themselves cross-cut by the opaque grains.

Schistose chlorite rocks
The schistose chlorite rocks have a modal composition (visually determined) of Mg-chlorite (100%), along with minor talc and opaque minerals. These rocks have a strong schistose (S-C

fabric) texture defined by strongly aligned chlorite grains, along with cross-cutting grains of opaque minerals.

Chlorite occurs in two main forms:
i) as relatively fine-grained (<<0.05mm) pale green, strongly aligned (defined by the parallel alignment of the long axis of these grains) elongate prismatic grains.
ii) as coarser-grained (0.1-0.5mm) pale green, moderately aligned (defined by the parallel alignment of the long axis of these grains), generally subprismatic to prismatic grains which cross-cut the finer-grained chlorite and occur in the form of platy grains which exhibit strong undulose extinction.

Opaques cross-cut both varieties of chlorite and occur in the following forms:
i) as subhedral to euhedral, equant-shaped grains of highly variable grain-size (<0.05-0.5mm).
ii) as very linear, narrow (<0.1mm) discontinuous (up to 1mm) rod-like aggregates which are composed of tiny (<0.05mm) equant-shaped grains. They cross-cut all the other phases present.

Talc veinlets are very discontinuous (up to 1.8mm) and help to define the schistosity within these rocks due to the parallel alignment of these veinlets, and the main foliation. These veinlets are of variable width (0.1-2mm) and are generally composed of weakly aligned, anhedral to subhedral, platy, equant to subprismatic grains of talc which exhibit weak undulose extinction.

Felsic plutonic rocks
Although these rocks vary widely in composition (which is primarily expressed by the differing modal proportions of quartz and amphibole), they all contain essentially the same mineral assemblage and textures. They can essentially be subdivided into the following two groups:
i) those felsic plutonic rocks which contain < 50 modal% quartz and > 10 modal% amphibole are here defined as *tonalites*. These rocks have a modal composition (visually determined) of albitic plagioclase (40-60%), quartz (25-50%), hornblende (2-5%), blue-green amphibole (5-8%), chlorite (0-5%) and epidote (0-<1%), along with rare accessory sulfides. They exhibit either a) a granoblastic texture defined by strongly interlocking grains of quartz and plagioclase (of highly variable grain-size) along with weakly aligned grains of hornblende and cross-cutting grains of fibrous Na-amphibole; or; b) an S-C fabric defined by well-aligned aggregates of hornblende and Na-amphibole and moderately aligned grains of relatively large altered plagioclase in a matrix of fine-grained granular plagioclase+quartz.

Plagioclase occurs in two main forms:
i) as non-aligned to moderately aligned (defined by the parallel alignment of the long axis of these grains) relatively large (0.5-3mm), subhedral equant to prismatic grains which are commonly altered to fine-grained mixtures of quartz+albite+epidote. They have highly sutured, embayed and diffuse grain boundaries with the surrounding, very fine-grained granular plagioclase+quartz matrix. Subgrain development is widespread and well-developed at these grain boundaries and consists of much finer-grained, equant polygonal-shaped grains. Although they have been quite strongly altered, in places, these grains still exhibit quite well-developed closely-spaced multiple twin lamellae which is commonly moderately bent (up to 50°). Micro-faulted grains (with lateral displacement between the fragments of 0.08mm and fracture-fill by the granular matrix) are also quite common. These grains exhibit moderate undulose extinction and commonly contain epidote cores.

ii) as non-aligned, relatively fine-grained (<<0.05-0.5mm), generally subhedral grains with well-developed triple-junction grain boundaries. They exhibit weak to well-developed, widely to closely spaced multiple twin lamellae and appear to lack compositional zoning. They occur as subgrains on the edges of the larger plagioclase grains and as an integral part of the granular matrix in which they are intimately associated with quartz.

Quartz occurs within the granular matrix as anhedral to subhedral, equant to prismatic grains of highly variable grain-size (<<0.05-0.5mm). They have strongly sutured grain boundaries, often with well-developed triple-junction grain boundaries, and exhibit weak to moderate undulose extinction. They are intimately associated with plagioclase within the granular matrix.

Hornblende occurs as relatively large (0.5-2mm), generally subhedral, subprismatic to prismatic grains which commonly exhibit simple twinning. They are moderately pleochroic (deep emerald green to pale tan brown) and strongly fringed by secondary fibrous Na-amphibole. They commonly exhibit strong undulose extinction and are weakly to moderately aligned (with two main orientations approximately perpendicular to each other). They are strongly embayed by the fine-grained granular matrix and are moderately bent (up to 30°) and micro-faulted. In places, they are almost completely replaced by the secondary fibrous Na-amphibole.

The amphibole occurs as quite strongly pleochroic (olive-green to deep blue-green), fine-grained (<<0.05-0.1mm), elongate prismatic grains which cross-cut the hornblende, plagioclase and quartz grains. They are often very fibrous and occur in the following forms:
i) as rim and partial to complete replacements of the hornblende.
ii) as plumose aggregates randomly distributed throughout these rocks.
iii) as continuous, strongly aligned veinlets.

Chlorite occurs as non-pleochroic pale green, non-descript secondary veinlets. The chlorite occurs in the form of plumose aggregates (up to 0.2mm) and replaces both the hornblende and Na-amphibole grains. Sulfides generally occur as euhedral, equant-shaped grains (0.2-0.5mm) which are far more prevalent within the chlorite veinlets and overprint all the other phases present.

ii) those felsic plutonic rocks which contain > 50 modal% quartz and < 5 modal% amphibole are here defined as *quartz-rich granitoids*. These rocks have a modal composition (visually determined) of albitic plagioclase (25-35%), quartz (60-70%) and Na-amphibole (5%), along with accessory zircon and apatite, and cross-cutting quartzofeldspathic veinlets. They generally exhibit a granoblastic cataclastic texture defined by relatively large non-aligned grains of plagioclase and vein-like aggregates of quartz in a fine-grained quartzofeldspathic matrix, along with cross-cutting intergranular linear aggregates of Na-amphibole and minor cross-cutting quartzofeldspathic veinlets.

Plagioclase occurs in two main forms:
i) as relatively large (0.5-1.8mm) subhedral, equant to prismatic grains which have well-developed subgrains at their grain boundaries, and in places, are almost completely replaced by these subgrains. They are largely altered to fine-grained mixtures of quartz+plagioclase though still retain their former shape and moderately-developed closely-spaced twin lamellae. These twin lamellae are often quite strongly bent (up to 45°), with these bent grains exhibiting strong undulose extinction, and micro-faulting. They have very ragged, strongly sutured grain

boundaries which are very diffuse as these grains are commonly strongly embayed by the fine-grained quartzofeldspathic matrix and have intense fine-grained subgrain development at these boundaries.

ii) as relatively fine-grained (<<0.05-0.3mm) generally subhedral equant-shaped, commonly polygonal grains which are intimately associated with the quartz grains and have well-developed triple-junction grain boundaries. They either completely lack multiple twin lamellae or have straight, widely-spaced multiple twin lamellae.

Quartz commonly occurs in the form of discontinuous (up to 2mm) non-aligned vein-like aggregates randomly distributed throughout these rocks. These aggregates consist of relatively fine-grained (0.1-0.5mm) anhedral to subhedral, equant to prismatic, commonly polygonal-shaped grains with well-developed triple-junction grain boundaries. They have strongly sutured grain boundaries and generally exhibit weak undulose extinction. Extremely fine-grained (<<0.05mm) quartz is confined to discrete narrow zones (these zones consisting entirely of extremely fine-grained quartz and plagioclase) which appear to be cataclasite zones.

Amphibole cross-cuts both the plagioclase and quartz grains and occurs as quite strongly pleochroic (olive-green to deep blue-green) elongate prismatic fibrous grains which generally occur in the form of vein-like intergranular aggregates. They are generally subhedral in shape and are fine-grained (<0.05-0.3mm). It also occurs in the form of randomly distributed and non-aligned plumose aggregates.

Quartzofeldspathic veinlets cross-cut all of the other phases present but do not contain any inclusions of the Na-amphibole grains. These veinlets are composed of relatively coarse-grained (0.3-3mm) generally subhedral, equant to subprismatic, strongly interlocking grains of quartz and untwinned feldspar with well-developed triple junction grain boundaries. The quartz grains within these veinlets exhibit moderate to strong undulose extinction. Finer-grained quartz and feldspar (0.1-0.2mm) commonly occur at the margins of these veinlets.

Other rock types

This group of rocks includes all of the other rock types that were found to be completely enclosed within the Gundagai Serpentinite Belt during the course of this study, and cannot be classified into any of the above groups. This group can be subdivided into the following rock types:

Metabasalts

The metabasalts of the Gundagai Serpentinite Belt are here defined as those metabasaltic rocks (i.e. extrusive igneous rocks of basaltic composition which have undergone low grade greenschist facies metamorphism) which occur completely enclosed within the boundaries of the belt. They have a modal composition (visually determined) of albitic plagioclase (60-65%), tremolite/actinolite (10-35%), epidote/clinozoisite (1-20%), quartz (0-5%) and secondary carbonate (0-4%), along with accessory opaques. They generally exhibit a porphyritic intergranular texture, along with minor glomeroporphyritic, decussate and feathery textures. The porphyritic intergranular texture is defined by relatively large phenocrysts of albitic plagioclase in a fine-grained matrix of albite, epidote and tremolite/actinolite.

Albitic plagioclase phenocrysts generally occur as relatively large (1-4mm), subhedral to euhedral, equant to prismatic grains which commonly occur in the form of strongly interlocking grain

aggregates. They either completely lack, or have well-developed compositional zoning. They all exhibit well-developed multiple twin lamellae and are commonly cross-cut and fringed by secondary amphiboles. Some are moderately bent (with bent twin lamellae up to 30°).

Tremolite/actinolite generally occurs as relatively fine-grained (<0.05-0.5mm) subhedral prismatic to elongate prismatic grains. They are often quite strongly bent (up to 45°) and exhibit strong undulose extinction. They cross-cut all the other phases present, with the exception of the epidote grains, and occur in the following forms:

i) as well-developed rims and fringes of very fibrous needle-like grains around the plagioclase phenocrysts.
ii) as randomly distributed grains which cross-cut the plagioclase grains.

Epidote/clinozoisite is confined to the groundmass where it occurs as relatively small (<0.05-0.4mm) anhedral to subhedral, equant to prismatic grains which exhibit weak undulose extinction. They commonly occur in the form of granular aggregates which cross-cut the other phases present.

Quartz occurs in the form of relatively fine-grained (up to 1mm) subhedral equant-shaped aggregates which are composed of very fine-grained (<0.05-0.1mm) equant to subprismatic grains which have strongly sutured grain boundaries. They commonly have triple junction grain boundaries and exhibit moderate undulose extinction. Plagioclase in the groundmass occur as non-descript, highly altered fine-grained aggregates which are cross-cut by both the tremolite/actinolite and epidote/clinozoisite grains. Carbonate occurs as moderate-sized (0.2-1.5mm) aggregates of strongly interlocking, generally equant-shaped grains which cross-cut all the other phases present and commonly contain inclusions of them.

Metagabbros

The metagabbros of the Gundagai Serpentinite Belt are here defined as those gabbroic rocks (i.e. intrusive igneous plutonic rocks of gabbroic composition which have undergone low grade metamorphism) which occur completely enclosed within the boundaries of the belt. They have a modal composition (visually determined) of albitic plagioclase (50%), hornblende (25-45%), quartz (0-3%), tremolite/actinolite (2-15%), epidote (0-8%) and clinozoisite (0-2%), along with accessory zircon. They generally exhibit a hypidiomorphic granular texture defined by strongly interlocking non-aligned grains of plagioclase, hornblende and quartz, with cross-cutting grains of tremolite/actinolite, epidote and clinozoisite.

Plagioclase occurs in two main forms:

i) as relatively large (0.6-2mm), generally subhedral, equant to prismatic grains which exhibit well-developed multiple twin lamellae and common surface alteration to clay minerals. They also exhibit weak to moderate compositional zoning and are strongly embayed by both the hornblende and finer-grained plagioclase and quartz grains. Subgrain development is common at the grain boundaries of these larger plagioclase grains and occurs in the form of fine-grained plagioclase and quartz. The twin lamellae are commonly moderately bent (up to 30°) and micro-faulted (with lateral displacements of <0.1mm).
ii) as relatively fine-grained (0.1-0.5mm) generally subhedral prismatic grains which are intimately associated with the quartz grains and are confined to the grain boundaries of the larger plagioclase grains. They generally exhibit only weakly-developed multiple twin lamellae, have

strongly sutured grain boundaries, and exhibit moderate undulose extinction. They are also generally fresh and unaltered.

Hornblende generally occurs as moderately pleochroic (olive-green to tan-brown) subhedral, subprismatic to prismatic grains of variable grain-size (0.25-1.5mm). They are commonly moderately bent (up to 60°), with these bent grains exhibiting strong undulose extinction. They commonly exhibit simple twinning and often impinge on each other. They have ragged grain boundaries and are commonly cross-cut by the epidote, clinozoisite and tremolite/actinolite. Most of the grains exhibit weak to moderate undulose extinction and many of them are rimmed and partially replaced by fibrous tremolite/actinolite. The hornblende commonly occurs in the form of grain aggregates and these cross-cut the larger plagioclase grains.

Tremolite/actinolite occurs as pale green subhedral strongly fibrous elongate prismatic grains which are commonly moderately bent (up to 30°) and occur in the following forms:

i) as cross-cutting plumose aggregates of tiny (<<0.05mm) strongly fibrous grains which themselves are cross-cut by epidote/clinozoisite.
ii) as partial fibrous replacements of hornblende.
iii) as narrow rims of fibrous grains around the hornblende grains.

Epidote/clinozoisite occurs as anhedral to subhedral, equant to prismatic grains (0.1-0.5mm) which cross-cut the other phases present. They commonly occur in the form of interlocking aggregates and generally exhibit moderate undulose extinction.

Amphibole rocks

The amphibole rocks of the Gundagai Serpentinite Belt are here defined as those meta-mafic and meta-ultramafic rocks which are dominantly composed of fibrous secondary amphibole minerals. They have a modal composition (visually determined) of hornblende (10-20%), tremolite/actinolite (80-87%) and epidote/clinozoisite (3-10%), along with cross-cutting quartzofeldspathic veinlets. They generally exhibit a decussate granoblastic texture defined by relatively large grains of strongly interlocking hornblende along with intensely cross-cutting and pseudomorphous fibrous secondary tremolite/actinolite, and cross-cutting quartzofeldspathic veinlets.

Hornblende occurs as relatively large (1-6mm), moderately pleochroic (pale to medium olive-green), subhedral, prismatic non-aligned grains which commonly exhibit simple twinning. In places, these grains are quite strongly bent (up to 30°), micro-faulted (with lateral displacements of 0.25mm) and fractured (with fracture-fill by highly fibrous secondary tremolite/actinolite). They are strongly cross-cut and partially to completely replaced by secondary tremolite/actinolite. They have ragged grain boundaries and are commonly rimmed by secondary tremolite/actinolite.

Tremolite/actinolite is of variable grain-size (<0.05-1mm) and occurs as non-pleochroic, colourless or pale green subhedral prismatic to elongate prismatic, often fibrous grains. They are non-aligned and commonly moderately bent (up to 30°). They occur in the following forms:

i) as narrow rims and fringes of highly fibrous grains around the hornblende grains.
ii) as partial to complete replacements of the hornblende.
iii) as non-aligned, widely distributed grains.

Epidote generally occurs as aggregates (0.4-1.5mm) of smaller (0.1-0.5mm) anhedral, equant to subprismatic grains which are strongly interlocking with each other. Quartzofeldspathic veinlets are generally discontinuous (up to 8mm) and narrow (up to 0.1mm). They are composed of strongly interlocking grains of quartz and untwinned feldspar and are of two parts:

i) relatively fine-grained (<0.05-0.2mm) equant to subprismatic strongly interlocking grains which have strongly sutured grain boundaries and occur on the veinlet walls adjacent to the host rock (i.e. chilled margin).

ii) much coarser-grained (0.5-1.5mm) equant to subprismatic grains which have strongly sutured grain boundaries and occur away from the veinlet walls. The larger quartz grains exhibit strong undulose extinction.

Vitric lithic ash fall tuff

This rock is very fine-grained and has a modal composition (visually determined) of quartzofeldspathic matrix (85%), devitrified altered pumice fragments (10%) and lithic fragments (5%), along with accessory sulfides. It exhibits a laminated texture defined by aligned fragments of pumice (or devitrified glass?) in a very fine-grained strongly laminated matrix.

Pumice fragments have well-developed bomb sags at their base and are generally elongate and lenticular in shape (0.5-16mm). Though they were once largely composed of glass, they have been completely devitrified and now consist of strongly interlocking fine-grained quartz. They have strongly sutured grain boundaries, are commonly polygonal in shape, and often occur in the form of ribbon-like aggregates. They exhibit strong undulose extinction and have minor subgrain development.

The quartzofeldspathic matrix is very fine-grained (<<0.05mm) and is largely composed of quartz and phengitic muscovite. Sulfide grains cross-cut the lamellae and have well-developed narrow pressure shadows of quartz either side of them. They have been completely replaced by secondary goethite. These grains are strongly euhedral and cubic in shape (0.2-0.5mm).

Hybrid felsic/mafic rocks

These rocks comprise two components:

a) quartz+plagioclase bands

b) chlorite+sulfide bands

The overall texture is thus defined by domains of plagioclase and quartz (PQ domains; with well-developed triple junction grain boundaries between the grains) which are separated from each other by domains of colourless chlorite and goethite pseudomorphs after former sulfide grains (CS domains). They have a modal composition (visually determined) of albitic plagioclase (30%), quartz (30%) and chlorite (40%), along with accessory sulfides.

Plagioclase generally occurs as anhedral, subrounded, strongly interlocking equant-shaped grains (up to 1mm). They exhibit strong undulose extinction and have well-developed multiple twin lamellae. They are strongly recrystallised and have well-developed triple junction grain boundaries. Quartz occurs as non-descript, usually fragmented grains which are moderately rounded and subhedral in shape. They are generally equant in shape and exhibit weak to moderate undulose extinction. They are strongly recrystallised and have well-developed triple junction grain boundaries.

Chlorite occurs as colourless, radiating masses of platy grains which are confined to discrete bands within these rocks. The S-C fabric within these rocks is defined by the parallel alignment of these chlorite grains which wrap-around both the plagioclase and quartz grains. Sulfides are completely replaced by secondary goethite and occur as well-rounded, equant-shaped, moderately large grains (up to 1.5mm) which are confined to the chlorite bands. They are strongly fractured, with fracture-fill by the chlorite grains.

APPENDIX 6PD

PETROGRAPHIC DESCRIPTIONS OF ROCK TYPES FROM THE TUMUT PONDS SERPENTINITE BELT AND ABUTTING UNITS

Tumut Ponds Group and O'Hares Beds

G.R. 143 545. The metabasaltic rocks on the eastern boundary of the Tumut Ponds Serpentinite Belt were looked at in this area during the course of the present study. They were found to be of two distinct types:

Fine-grained massive granular-textured metabasalts

These metabasalts exhibit a granular pseudoporphyritic texture defined by relatively large aggregates of epidote-chlorite in a fine-grained matrix of non-aligned albitic plagioclase. They have a modal composition of albitic plagioclase (70%), epidote/clinozoisite (22%) and chlorite (8%), along with accessory opaques.

Plagioclase generally occurs as relatively fine-grained (<0.05-1mm) lath-like grains which comprise most of the matrix. They occur as subhedral, prismatic non-aligned grains which generally exhibit weakly developed multiple twin lamellae and compositional zoning. They have quite ragged grain boundaries and are cross-cut by both the epidote/clinozoisite and chlorite grains.

Epidote/clinozoisite occur as colourless to moderately pleochroic (pale to amber yellow) relatively fine-grained (<0.,05-0.5mm) subhedral, equant to subprismatic, strongly interlocking grains. They exhibit weak undulose extinction and have sharp grain boundaries. They occur as either randomly distributed grains interspersed throughout the rock or as relatively large grain aggregates, commonly associated with chlorite.

Chlorite occurs as non-descript, anhedral-shaped masses associated with epidote in the relatively large grain aggregates. These masses consist of extremely fine-grained (<<0.05mm) fibrous elongate prismatic grains which commonly contain euhedral epidote grains which appear to have nucleated from the walls of the masses inward.

Quench-textured metabasalts

These metabasalts exhibit a strong sub-ophitic quench texture defined by strongly interlocking grains of elongate prismatic plagioclase and subprismatic hypersthene along with cross-cutting grains of actinolite and chlorite. They also appear to consist of a relatively coarse-grained core surrounded by a finer-grained shell (i.e. a chilled margin) and therefore appear to be pillow basalts. They have a modal composition of albitic plagioclase (65%), hypersthene (5%), actinolite (25%) and chlorite (5%), along with accessory sulfides.

Plagioclase occurs as medium-grained (0.1-0.5mm) prismatic elongate lath-like subhedral to euhedral grains which are strongly interlocking with the hypersthene grains. They exhibit well-developed closely-spaced multiple twin lamellae and compositional zoning. They are cross-cut by the actinolite and chlorite grains and often contain hypersthene at their cores.

Hypersthene generally occurs as short prismatic euhedral grains which are weakly pleochroic (colourless to pale pink) and commonly partially to completely replaced by secondary actinolite. They commonly occur completely enclosed within the plagioclase grains and are commonly rimmed by highly fibrous actinolite. They are commonly fractured (with fracture-fill by both actinolite and chlorite) and generally exhibit moderate undulose extinction.

Actinolite occurs as moderately pleochroic (pale to dark blue-green), generally fine-grained (<0.05-0.3mm) subhedral prismatic non-oriented grains. These grains occur in the following different forms:

i) as narrow rims around the hypersthene grains.
ii) as partial to complete replacements of the hypersthene grains.
iii) as discontinuous intergranular veinlets throughout the rock.
iv) as randomly distributed aggregates throughout the rock.

Chlorite occurs as moderately pleochroic (pale to dark olive-green) non-descript fibrous masses which are intimately associated with the actinolite grains. Sulfides occur as subhedral, equant-shaped highly fractured and embayed grains (with fracture-fill by actinolite and chlorite).

The Tumut Ponds Serpentinite Belt

Metahornblende pyroxenite

XRD studies show that the metahornblende pyroxenite is largely composed of diopside and minor hornblende. This rock has a modal composition (visually determined) of diopside (70%), hornblende (20%) and tremolite (10%) and exhibits a cumulate sheared texture defined by strongly interlocking, highly fractured grains of altered diopside and hornblende, and fracture-fill of secondary tremolite.

Diopside occurs as relatively large (5-20mm) highly altered (partially replaced by fine-grained grossular?) generally equant-shaped subhedral grains which are cross-cut by the other phases present. They are highly fractured and brecciated in places (with fracture- and breccia-fill by tremolite). Subgrains are of common occurrence and most of the fractures appear to be along these subgrain boundaries. They appear to have been firstly replaced by hornblende and then later by tremolite, with both the hornblende and tremolite grains containing fragments of the diopside grains.

Hornblende occurs as quite strongly pleochroic (olive-green to tan-brown) moderately large (0.1-8mm) very platy elongate prismatic subhedral grains which commonly occur as intergranular space-filling between the highly fractured diopside grains. Many of these hornblende grains are partially replaced by secondary fibrous tremolite along their cleavage planes. They have firstly been replaced by weakly pleochroic (pale olive-green to pale blue-green) hornblende/actinolite and then further replaced by colourless, very fibrous fine-grained tremolite. In places, they are quite highly fractured (with fracture-fill by fine-grained tremolite) and generally exhibit moderate undulose extinction. They are also quite strongly bent (up to 45°) and micro-faulted (with lateral displacement up to 0.5mm).

Tremolite occurs as colourless, very fine-grained (<0.05mm) elongate prismatic fibrous grains which cross-cut all of the other phases present and generally occur in the form of cross-cutting veinlets. These veinlets are of two dominant orientations at 60° to each other.

Massive serpentinites

The massive serpentinites of the belt have a modal composition (visually determined) of chrome spinel (0-2%), serpentine (50-98%) and magnetite (accessory to 50%). They exhibit either:

i) a mesh texture defined by cores of non-descript lizardite which are surrounded by rims of fibrous chrysotile; or,
ii) a decussate feathery texture defined by patches of non-aligned feathery antigorite between which occur patches of abundant fine-grained magnetite.

All of the massive serpentinites are cross-cut by chrysotile veinlets.

Matrix serpentine is of two main forms:

a) as mesh-textured serpentine consisting of two parts:
i) cores of non-descript ovoid-shaped lizardite (0.1-0.5mm) which exhibit weak undulose extinction.
ii) narrow rims of fibrous chrysotile which completely surround the cores. The fibres within these rims are generally aligned perpendicular to the rim walls and exhibit moderate undulose extinction.
b) as non-aligned antigorite which occurs as fine-grained (<0.05-0.1mm) subhedral prismatic grains. These grains occur in the form of plumose aggregates and exhibit moderate undulose extinction.

Chrysotile veinlets are of minor occurrence and cross-cut the other phases present. These veinlets are of two main types:

a) as discontinuous (up to 2mm) narrow veinlets defined by the parallel alignment of chrysotile rims within the mesh-textured serpentine.
b) as more continuous (4-25mm) generally narrow (<0.05-0.4mm) highly sinuous veinlets which are of two dominant orientations perpendicular to each other.

Magnetite occurs in the following forms:

i) as randomly distributed, generally equant-shaped aggregates which commonly have tiny linear veinlets of magnetite trailing off them. These aggregates are composed of very fine-grained (<<0.05mm) equant-shaped grains which appear to represent magnetite pseudomorphs after former chrome spinel grains.

ii) as linear aggregates of very fine-grained (<<0.05mm) equant-shaped grains. In places, these veinlets are of a very consistent orientation and appear to define cleavage planes within former pyroxene grains (now completely replaced by fine-grained serpentine). They also occur as highly discontinuous veinlets of two main orientations perpendicular to each other.

Schistose serpentinites

The schistose serpentinites of the belt have a modal composition (visually determined) of chrome spinel (0-2%), serpentine (80-98%), tremolite (0-15%) and chlorite (0-5%), along with accessory secondary magnetite. They exhibit a schistose (S-C fabric) defined by the following:

i) regularly-spaced, well-aligned (defined by the parallel alignment of the long axis of the aggregates) boudins of non-oriented serpentine (in places associated with chrome spinel) which are surrounded by chrysotile veinlets parallel to the long axis of these boudins. These are regularly spaced and appear to define the C-surface.
ii) well-aligned linear aggregates of fine-grained magnetite which are surrounded by parallel chrysotile veinlets and are of two main orientations at approximately 45° to each other. The less

continuous aggregates (which appear to define the S-surfaces) merge into the more continuous aggregates (which appear to define the C-surfaces).

iii) well-aligned, less continuous chrysotile veinlets which are oriented at an angle of approximately 45° to the more continuous veinlets into which they merge. These veinlets appear to define the S-surfaces.

iv) strongly aligned sinuous veinlets of chlorite.

Chrome spinel is of rare occurrence as relatively large (1mm) highly fractured and brecciated grains which are commonly rimmed and replaced by fine-grained magnetite. These grains commonly occur within the serpentine boudins.

Serpentine occurs in three main forms:

i) as non-aligned relatively fine-grained (<0.05-0.1mm) subhedral fibrous grains which occur in the form of boudins between the S-C fabric chrysotile. These grains occur in the form of plumose aggregates and exhibit quite strong undulose extinction. They act as a "matrix" within the schistose serpentinites and are generally overprinted by the other phases present (with the exception of the serpentine pseudomorphs after orthopyroxene grains which are commonly embayed by this matrix serpentine).

ii) as randomly distributed, equant to subprismatic, subhedral grains which consist of parallel-aligned serpentine grains (whereas the serpentine in the surrounding matrix is non-aligned). These grains exhibit extreme undulose extinction and appear to be pseudomorphs after former orthopyroxene grains. They are strongly embayed by the matrix serpentine and cross-cut by the chrysotile veinlets.

iii) as strongly aligned, highly fibrous elongate veinlets which cross-cut and wrap-around the other phases present (with the exception of the tremolite grains). These veinlets are of two main orientations perpendicular to each other, are generally narrow (<0.05-0.3mm) and continuous (>20mm). In the earlier generation of these veinlets, the chrysotile fibres are oriented perpendicular to the veinlet walls whereas in the later generation of these veinlets, the chrysotile fibres are oriented 30° to the veinlet walls. In all generations, the chrysotile fibres exhibit moderate undulose extinction.

Tremolite cross-cuts the other phases present and generally occurs as strongly cross-cutting aggregates of non-aligned plumose aggregates of fine-grained (<0.05mm) elongate fibrous prismatic grains. Mg-chlorite occurs as moderately aligned, sinuous narrow discontinuous veinlets which are composed of colourless fine-grained (<<0.05mm) elongate prismatic, moderately aligned fibrous grains which exhibit moderate undulose extinction. These veinlets are generally narrow (0.1mm) and up to 4mm in length.

Magnetite occurs as very fine-grained (<0.05mm) grains in the following forms:

i) as randomly distributed subhedral equant-shaped grains.

ii) as aggregates of the above grains.

iii) as linear aggregates (vein-like disseminations) of tiny subhedral grains.

Talc-carbonate rocks

The talc-carbonate rocks of the belt have a modal composition (visually determined) of serpentine approx .(20%), talc (50%) and magnesite (30%), along with abundant secondary magnetite. They

exhibit a domainal granoblastic texture defined by large patches of talc and/or magnesite which strongly overprint the serpentine and magnetite grains.

Serpentine occurs as non-aligned, plumose aggregates which form the "matrix" to these rocks. The plumose aggregates consist of relatively fine-grained (<0.05-0.2mm) subhedral, elongate prismatic fibrous grains which generally exhibit strong undulose extinction and are cross-cut by the other phases. Talc occurs as extremely fine-grained (<<0.05mm) non-descript fibrous "mats" which strongly overprint the "matrix" serpentine (inclusions of which it commonly contains0 but itself is overprinted by the magnesite grains.

Magnesite occurs as discontinuous veinlets and patches throughout the rock and appears to overprint all of the other phases present. The patches commonly exhibit a colloidal texture defined by strongly interlocking and zoned (radial zoning) relatively even-grained polygonal-mosaic grains. The magnesite itself is non-descript, relatively coarse-grained (0.5mm), and commonly contains inclusions of the other phases present. Magnetite is of common occurrence as euhedral equant-shaped grains (<0.05mm) or aggregates of these grains (0.1-0.75mm). In places, these grains are strongly concentrated in narrow (1mm) linear zones which define magnetite-rich bands in these rocks.

Gabbros

The gabbros of the belt have a modal composition (visually determined) of diopside (45%), albitic plagioclase (40%), orthopyroxene (5%), clinozoisite (3%), chlorite (2%) and quartz (<1%), along with rare accessory opaques. They exhibit a pseudoporphyritic texture defined by relatively large, strongly kinked and bent pyroxene grains in a matrix of fine-grained completely saussuritised plagioclase.

Diopside occurs as relatively large (up to 4mm), subhedral to euhedral, generally elongate prismatic grains which exhibit well-developed diallage parting and contain "herringbone structure" exsolution lamellae of orthopyroxene. These grains have undergone quite intense brittle-ductile deformation with strongly bent (up to 45°) grains which exhibit extreme undulose extinction, and in places, quite strongly fractured and brecciated grains (with fracture- and breccia-fill by chlorite). These grains are strongly embayed by the saussuritised plagioclase matrix. In general, they appear to be moderately aligned (with this alignment being defined by the parallel alignment of the long axis of these grains).

Orthopyroxene occurs as moderate-sized (up to 2mm) subhedral, equant-shaped grains which exhibit extreme undulose extinction and are strongly embayed by the saussuritised plagioclase.

Plagioclase occurs as very fine-grained (<<0.05mm) completely saussuritised grains which occur as post-cumulus space-filling throughout the rock. Due to the intensity of this saussuritisation, no original features of the plagioclase grains have been retained.

Cross-cutting veinlets composed of either a mixture of epidote/clinozoisite/quartz/chlorite or chlorite occur throughout the gabbros.

Rodingites

The rodingites of the belt have a modal composition (visually determined) of diopside (0-10%), grossular/hydrogrossular (55-85%), epidote/zoisite (0-35%) and chlorite (0-15%), along with accessory magnetite. They exhibit a well-developed granoblastic texture defined by strongly interlocking grains of the constituent phases.

Diopside occurs as relatively large (0.1-2mm) subhedral, generally equant to subprismatic, subrounded grains. They are either randomly distributed throughout the rodingites or occur as diopside-dominant sub-layers consisting of strongly interlocking parallel-aligned grains (defined by the parallel alignment of the long axis of these grains). The diopside grains are commonly fractured (with fracture-fill by grossular/hydrogrossular) and bent (up to 45°) and exhibit moderate to extreme undulose extinction. They have well-developed closely-spaced diallage parting and in places, are quite strongly embayed by the grossular/hydrogrossular matrix suggesting that they are relict primary magmatic grains.

Grossular/hydrogrossular occurs as subisotropic to isotropic, non-distinct, generally fine-grained (<0.05-1mm) anhedral-shaped grains. They commonly embay the diopside grains but are themselves cross-cut by the epidote/zoisite and chlorite grains.
Epidote/zoisite occurs as colourless, fine-grained (<0.05-0.3mm) subhedral prismatic grains which strongly overprint both the diopside and grossular/hydrogrossular grains. They commonly occur in the form of non-aligned, randomly distributed, stellate aggregates which exhibit weak to moderate undulose extinction. In places, they are commonly rimmed by very fine-grained (<<0.05mm) emerald-green plumose aggregates of fibrous chlorite.

Chlorite occurs as randomly distributed, generally ovoid-shaped (0.1-0.5mm) patches. These patches consist of very fine-grained (<0.05mm) non-aligned fibrous elongate prismatic grains. Aggregates of both grossular/hydrogrossular and magnetite commonly occur within these patches.

Metabasalts

The metabasalts of the belt can be subdivided into two main types:

quench-textured metabasalts

These rocks have a modal composition (visually determined) of albitic plagioclase (30%), actinolite (55%), epidote (10%) and chlorite (5%), along with accessory sulphides and sphene. They exhibit a well-developed sub-ophitic quench texture defined by non-aligned grains of elongate prismatic plagioclase and actinolite, along with cross-cutting veinlets of actinolite and chlorite.

Plagioclase occurs as medium-grained (0.5-1mm), elongate prismatic euhedral grains. They commonly exhibit closely-spaced multiple twin lamellae but lack compositional zoning. They are strongly cross-cut and embayed by the other phases present.

Actinolite occurs as very fine-grained (<0.05-0.6mm), moderately pleochroic (pale to dark olive green) generally subhedral prismatic grains. These grains commonly exhibit simple twinning and are moderately bent (up to 45°) with these bent grains exhibiting extreme undulose extinction. They cross-cut all the other phases present and occur as randomly distributed aggregates throughout these basalts.

Epidote occurs as small (<0.1mm) subhedral, equant-shaped pleochroic (pale to amber yellow) grains which are randomly distributed throughout these basalts. Chlorite occurs as yellow/green non-descript plumose aggregates.

Opaques occur as rare relatively large (0.1-1mm) euhedral, equant-shaped grains. They are strongly fractured and brecciated (with fracture- and breccia-fill by epidote and actinolite) and are highly embayed by the matrix.

Meta-andesitic tuffs

These rocks have a modal composition (visually determined) of albitic plagioclase (40%), actinolite (50%), quartz (5%), epidote/clinozoisite (3%) and chlorite (2%), along with accessory sulfides. They exhibit a domainal texture defined by actinolite-rich and actinolite-poor zones. In discrete zones within these rocks, the plagioclase grains are strongly aligned (defined by the parallel alignment of the long axis of these grains) defining a magmatic flow texture.

Plagioclase occurs as moderately large (0.1-2.5mm) subhedral to euhedral, heavily saussuritised prismatic grains. They generally exhibit strong undulose extinction, lack any multiple twin lamellae or compositional zoning, and have very diffuse grain boundaries.

Actinolite occurs as strongly pleochroic (olive-green to intense blue-green) relatively fine-grained (<0.05-0.5mm) non-aligned subhedral prismatic grains. It generally occurs as intergranular veinlets between the saussuritised plagioclase. Within these veinlets, the actinolite is intimately associated with both epidote and chlorite.

Epidote/clinozoisite occurs as moderately pleochroic (pale to amber yellow) non-descript tiny (<0.01mm) grains which are intimately associated with the actinolite and chlorite grains in the actinolite-dominant veinlets. Chlorite occurs as a replacement of the actinolite within the actinolite-dominant veinlets (with the chlorite occurring within the centre of these veinlets) and is more common where quartz is a component of these veinlets. It also occurs as randomly distributed, strongly pleochroic green aggregates. Quartz occurs as tiny (<0.01mm) subhedral, strongly recrystallised grains within the actinolite-dominant veinlets and as randomly distributed aggregates.

APPENDIX 7PD

PETROGRAPHIC DESCRIPTIONS OF ROCK TYPES FROM THE OTHER SERPENTINITE BELTS AND ABUTTING UNITS

The Wagga Group

G.R. 692 310. Highly foliated recrystallised micaceous quartzites near the western contact with the Eurongilly Serpentinite Belt. These quartzites have a modal composition of recrystallised quartz (90%), muscovite (5-7%) and biotite altering to chlorite (3-5%), along with accessory magnetite and zircon. They exhibit a strong domainal texture defined by mica-rich (M-domains) and quartz-rich (Q-domains) zones.

Both the muscovite and biotite grains within these quartzites overprint the quartz grains and are strongly aligned. The quartz grains are strongly recrystallised with well-developed triple junction grain boundaries. The foliations within these rocks are defined by both the distribution and preferred alignment of the mica grains.

The Eurongilly Serpentinite Belt

G.R. 692 310 (Junee 1: 25 000 sheet)

Meta-olivine pyroxene hornblendites

These rocks have a modal composition (visually determined) of hornblende (30%), diopside (15%), olivine (7%), magnesite/calcite (30%), serpentine (10%), talc (5%) and chlorite (3%), along with abundant accessory magnetite. They have a sheared granoblastic texture defined by strongly interlocking fractured grains of hornblende, diopside and olivine, with fracture-fill of serpentine, magnesite/calcite and chlorite.

Meta-pyroxene hornblende peridotites

These rocks have a modal composition (visually determined) of olivine (25%), hornblende (20%), diopside (10%), chrome spinel (3%), magnesite (32%), chlorite (5%), talc (3%) and actinolite (2%), along with abundant accessory magnetite. They exhibit a hypidiomorphic granular texture defined by strongly interlocking highly fractured grains of olivine, diopside and hornblende, with fracture-fill and replacement grains of magnesite, chlorite and actinolite.

Carbonate-rich metaserpentinites

These rocks have a modal composition (visually determined) of orthopyroxene (0-1%), serpentine (7-30%), magnesite/calcite (7-55%), quartz (0-5%), chlorite (5-15%) and talc (0-75%), along with abundant accessory magnetite. They exhibit a number of different textures:

a) a well-developed linear domainal texture defined by alternating carbonate-dominant (C-domains), chlorite-dominant (Ch-domains) and serpentine-dominant (S-domains) zones along with cross-cutting veinlets and patches of quartz. These domains are of a very strong linear nature and define schistosity planes within these rocks.

b) a granoblastic veined texture which is defined by either:

i) aggregates of talc which strongly overprint a matrix of non-aligned serpentine, serpentine pseudomorphs after orthopyroxene, chlorite, and cross-cutting discontinuous carbonate veinlets.

ii) cross-cutting veinlets of carbonate, quartz and goethite which strongly overprint a matrix of non-aligned serpentine and chrome spinel.

G.R. 688 332 (Junee 1: 25 000 sheet)

Massive serpentinites

These serpentinites have a modal composition (visually determined) of serpentine (90%) and secondary weathering-produced goethite (10%), along with abundant accessory magnetite. They exhibit a strong decussate feathery texture defined by non-aligned fibrous aggregates of serpentine which cross-cut each other.

Schistose serpentinites

These serpentinites have a modal composition (visually determined) of serpentine (90%), Mg-chlorite (5%) and secondary weathering-produced goethite (5%), along with abundant accessory magnetite. They exhibit a well-developed S-C fabric defined by well-aligned parallel aggregates of fine-grained serpentine which wrap-around relatively large grains of magnetite.

The Darbalara Serpentinite Belt

XRD studies were made on serpentinite samples of the Darbalara Serpentinite Belt at G.R. 098 240 (Gundagai 1: 25 000 sheet). These studies reveal that the serpentinite is largely composed of antigorite and chrysotile, along with possible minor lizardite. A body of meta-hornblendite occurs associated with a body of massive serpentinite at G.R. 108 231 (Gundagai 1: 25 000 sheet). This meta-hornblendite had a modal composition (visually determined) of hornblende (95%) and clinoclinozoisite (5%) (both determined by XRD methods), along with rare cross-cutting veinlets of chlorite. This rock displays a lepidoblastic decussate texture defined by non-aligned decussate grains of hornblende along with cross-cutting aggregates of clinoclinozoisite and rare chlorite.

The Western Wambidgee Serpentinite Melange

Clinopyroxenites

The clinopyroxenites exhibit well-developed cumulus textures (particularly post-cumulus space-filling and postcumulus overgrowth) defined by strongly interlocking grains of relatively large strongly bent and fractured grains of clinopyroxene and orthopyroxene along with fracture-fill of relatively fine-grained serpentine and talc. They have a modal composition (visually determined) of clinopyroxene (60-90%), orthopyroxene (5-15%), fresh olivine (up to 1%), serpentine (5-15%), talc (1-15%), and tremolite (up to 5%), along with abundant accessory magnetite. Strongly sheared varieties of the clinopyroxenites are very common and exhibit a well-developed sheared (S-C fabric) defined by fractured fragments of randomly distributed clinopyroxene and orthopyroxene grains in a finer-grained matrix of aligned fibrous talc, serpentine, chlorite and tremolite grains. These sheared varieties have a modal composition (visually determined) of clinopyroxene (20-80%), orthopyroxene (5-10%), serpentine (5-30%), tremolite (up to 5%), talc (up to 35%) and chlorite (up to 5%), along with abundant secondary magnetite. The abundance of the secondary minerals (i.e. talc, serpentine, chlorite and tremolite) increases substantially with the intensity of shearing.

Lherzolites

The lherzolites are of rare occurrence and are intimately intermixed with the clinopyroxenites. They generally exhibit a granoblastic postcumulus overgrowth texture defined by relatively large, strongly interlocking granoblastic grains of olivine, clinopyroxene and orthopyroxene, along with cross-cutting shear bands of talc and serpentine, and cataclasite zones consisting of finer-grained fragments of olivine, clinopyroxene and orthopyroxene in a finer-grained matrix of talc and serpentine. They have a modal composition (visually determined) of fresh olivine (65%),

clinopyroxene (15%), orthopyroxene (15%), serpentine (4%) and talc (up to 1%), along with abundant accessory magnetite.

Pyroxenites
One outcrop (G.R. 990 337; Coolac 1: 50 000 sheet) of an unusual pyroxenite was found to occur within this unit. It has a sheared granoblastic texture defined by patches of strongly interlocking equant-shaped pyroxene grains interspersed with zones of fracture-fill chlorite (determined by XRD methods). The pyroxene grains are strongly pleochroic (pale to dark orange-brown) and XRD investigations reveal that it is the mineral ferroan Fassaite, an Fe-Al diopside or augite (Nickel & Nichols 1991) which is restricted to forming in quartz-free environments (Deer, Howie & Zussmann 1985).

Serpentinites
Both relatively massive and sheared varieties occur and XRD investigations reveal that the dominant serpentine group minerals within these serpentinites are Al-rich lizardite 1T and chrysotile. These serpentinites can be subdivided into pseudoharzburgitic and schistose types:
Pseudoharzburgitic serpentinites: exhibit a pseudoporphyritic decussate mesh texture defined by relatively large serpentine pseudomorphs after orthopyroxene grains and porphyroblastic grains of magnesite in a fine-grained matrix of non-aligned serpentine grains. They have a modal composition (visually determined) of serpentine pseudomorphs after orthopyroxene (15%), matrix serpentine (70%) and magnesite (15%), along with abundant accessory secondary magnetite.

Schistose serpentinites: exhibit a well-developed schistose decussate feathery texture defined by non-aligned matrix serpentine which is cross-cut by aligned chrysotile veinlets. They consist only of serpentine, along with abundant accessory secondary magnetite.

Talc schists
The talc schists exhibit a well-developed schistose decussate texture defined by strongly aligned prismatic elongate fibrous talc grains enveloping much larger strongly fractured, equant-shaped grains of chrome spinel. They have a modal composition (visually determined) of talc (98%) and chrome spinel (2%), along with abundant accessory secondary magnetite.

Gabbros
Most of the gabbros are quite strongly sheared, metamorphosed and altered and can be further subdivided into hornblende-clinopyroxene gabbros and completely altered gabbros.

Hornblende-diopside gabbros: generally exhibit an allotriomorphic granular texture defined by strongly interlocking grains of saussuritised plagioclase, hornblende and diopside, along with cross-cutting grains and aggregates of tremolite, chlorite and epidote. They have a modal composition (visually determined) of hornblende (15-20%), diopside (when present, up to 30%), albitic plagioclase (up to 50%), chlorite (up to 5%), tremolite/actinolite (3-25%), quartz (up to 3%), epidote (<1%) and carbonate (<1%), along with common accessory opaques and apatite.

Completely altered gabbros: generally exhibit a cataclastic texture which is defined by either:
i) large zones of non-aligned fine-grained (with maximum dimensions of 0.5mm) equant-shaped subrounded grains in a very fine-grained (with maximum dimensions of <<0.05mm) matrix.

ii) strongly interlocking granoblastic grains of saussuritised plagioclase separated by zones of intergranular tremolite.
Both types have a modal composition (visually determined) of albitic plagioclase (50%), saussuritised plagioclase (up to 30%), tremolite/actinolite (10%), clinozoisite (up to 5%), epidote (up to 5%), carbonate (up to 3%) and chlorite (up to 2%), along with rare accessory opaques.

Plagiogranite
The one plagiogranite found to date, is strongly sheared in places and generally exhibits an allotriomorphic granular sheared texture defined by zones of strongly cross-cutting fine-grained quartz+plagioclase in a matrix of much coarser-grained strongly interlocking quartz+plagioclase, along with overprinting plumose aggregates of tremolite/actinolite. This plagiogranite body has a modal composition (visually determined) of quartz (40-54%), albitic plagioclase (40-45%), alkali feldspar (up to 3%), tremolite/actinolite (2-5%), chlorite (up to 5%), epidote (<1%) and clinozoisite (up to 2%), along with accessory apatite and opaques.

Metabasaltic rocks
The metabasaltic rocks which occur as discrete lenses with the Western Wambidgee Serpentinite Melange exhibit a porphyritic intergranular texture defined by relatively large phenocrysts of albitic plagioclase, and quartz- and chlorite-filled amygdules in a fine-grained groundmass of albite laths and epidote. They have a modal composition (visually determined) of albitic plagioclase phenocrysts (5%), albite groundmass (82%), epidote (3%), quartz-filled amygdules (5%) and chlorite-filled amygdules (5%), along with accessory opaques and apatite.
The metabasaltic rocks which occur as enclaves completely enclosed within the plagiogranite body exhibit a decussate feathery texture defined by non-aligned fine-grained interlocking grains of actinolite, chlorite, albite and tremolite, along with discontinuous cross-cutting narrow veinlets of albite+epidote. They have a modal composition (visually determined) of actinolite (40-70%), albite (45-50%), chlorite (10%), quartz (up to 5%) and tremolite (<1%), along with accessory apatite.

Dacitic tuffs
The tuffs are generally fine-grained, and in places, may be flow-banded and well-laminated. They generally exhibit a well-developed porphyritic banded texture defined by strongly aligned, generally parallel bands of albite, along with randomly distributed phenocrysts of plagioclase and opaques within an extremely fine-grained non-descript felsic groundmass. They have a modal composition (visually determined) of albite phenocrysts (up to 30%), quartz (up to 10%), clinozoisite (up to 2%), chlorite (up to 3%), albite bands (up to 5%), white phengitic mica (up to 5%), and a fine-grained matrix (up to 95%), along with accessory opaques.

Quartzites
The quartzites exhibit a well-developed granoblastic domainal texture defined by patches of relatively coarse-grained quartz within a matrix of relatively fine-grained quartz. They are almost completely composed of quartz, along with very minor chlorite and accessory opaques.

Exotic rock types
Unusual zoisite-dominant rocks occur near the western margin of the Western Wambidgee Serpentinite Melange and exhibit a granoblastic texture. They have a modal composition (determined by XRD methods and visually) of zoisite (50-90%), chlorite (up to 40%), actinolite (up to 10%) and carbonate (up to 8%), along with rare accessory ilmenite.

APPENDIX 10UPBR

U/Pb SHRIMP RESULTS

PRISE
Precise Radiogenic Isotope Services

Research School of Earth Sciences
The Australian National University
Canberra ACT 0200 Australia

Telephone: IDD 616 STD 06 249 5507
Facsimile: 616 / 06 249 4835
Email: Prise.Fanning@anu.edu.au
Prise.Armstrong@anu.edu.au

9 February 1996

Department of Applied Geology
University of Technology, Sydney
PO Box 123
Broadway NSW 2007

for the attention of:
A/Professor B. J Franklin
Mr I.T. Graham

Report A95-130

SHRIMP U-Pb zircon dating of plagiogranites from the Coolac Serpentinite Belt

C.M. Fanning
Principal Research Scientist

SHRIMP U-Pb zircon dating of plagiogranites from the Coolac Serpentinite Belt, NSW.

1. INTRODUCTION

This report formalises SHRIMP U-Pb analyses of zircons from plagiogranites from the Coolac Serpentinite Belt. The work is for, and in collaboration with, Associate Professor B.J. Franklin and Mr I.T. Graham from the Department of Applied Geology, University of Technology, Sydney.

Initially a request was received by letter from Mr Graham (dated 14 November 1994) for SHRIMP work on a mineral separate labelled sample 238. The mineral separate did not contain sufficient zircon for analysis, and further sample and residues from the initial separation were forwarded to the Research School of Earth Sciences for processing.

A second request, dated 7 February 1995 was received from Mr Graham for SHRIMP analyses of zircons for samples 20, 169, 189 and BF91/33f. A package was received containing mineral concentrates understood to have been prepared at CSIRO, North Ryde.

2. PROCEDURES

Apart from sample 238, the zircons have been hand picked from the mineral concentrates as received. Grains from all 5 samples have been mounted in epoxy together with a chip of the RSES standard zircon SL13, sectioned approximately in half and polished. The mount, Z2138 has been analysed using SHRIMP II on 27 March 1995 and SHRIMP I on 27 September 1995. The analyses consist of 6 scans through the mass range. The SHRIMP data has been reduced in a manner similar to that described by Compston *et al* (1992) and Williams and Claesson (1987), with augmented uncertainties for the isotope ratios using software of Dr T.R. Ireland (RSES). The observed coefficient of variation in the Pb/U ratio measured for the SL13 standard was 2.37% and 2.36% respectively. The Pb/U ratios have been normalised relative to a value of 0.09279 for the $^{206}Pb/^{238}U$ ratio of this standard, that is equivalent to an age of 572 Ma for SL13. Uncertainties given for individual analyses (ratios and ages) are at the one sigma level, however all uncertainties in calculated weighted mean ages are as 95% confidence limits.

3. RESULTS

The U-Pb results are presented in Tables 1 to 5 and Figures 1 to 8. Preliminary results from the first analytical session have been given to Mr Graham and a compilation of the two days results faxed and sent by electronic mail to UTS on 4 October 1995.

3.1 Sample 238

Despite carrying out two mineral separations for this sample only a small number of zircon grains were separated. They are mostly euhedral clear, elongate grains with pyramidal terminations (grains 1, 2 and 8), or are fragments of such grains (grain 4). Some are clearly zoned; others are complex comprising structurally distinct, inherited and/or metamict central components with clear rims (grains 6, 7 and 9). Grains 3 and 5 are more equant in shape and have multifaceted terminations.

Fifteen areas have been analysed on 9 grains, Table 1 and Figures 1 and 2. On a Tera and Wasserburg concordia of the measured $^{207}Pb/^{206}Pb$ versus $^{238}U/^{206}Pb$ ratios there is a main group of analyses with similar $^{238}U/^{206}Pb$ ratios, and ^{207}Pb corrected $^{206}Pb/^{238}U$ ages of c.400 Ma (Table 1 and Fig.1). Analysis 3.1 plots well to the right of this group and the area analysed is interpreted as having lost radiogenic Pb.

Analyses 1.2, 5.1 and 9.2 yield $^{206}Pb/^{238}U$ ages that are significantly older than c.400 Ma. Analysis 1.2 is near the centre of grain 1 and has a ^{207}Pb corrected $^{206}Pb/^{238}U$ age of c.524 Ma. The tip has a $^{206}Pb/^{238}U$ age that is within uncertainty of the c.400 Ma group. Grain 1 is an optically simple ?magmatic zircon and cathodoluminescence images will be made to ascertain whether there is a "hidden" inherited component.

Grain 5 is a more equant multifaceted grain. The morphology is consistent with having formed at a deep crustal level and it is interpreted as an inherited grain with respect to this zircon population. The area analysed is near one tip and has a $^{206}Pb/^{238}U$ age of c.640 Ma.

Grain 9 has a structurally distinct centre with a zoned overgrowth. Analysis 9.2 of the centre has a $^{206}Pb/^{238}U$ age of c.900 Ma with a ^{204}Pb corrected $^{207}Pb/^{206}Pb$ age of c.1320 Ma. Analysis 9.1 of the zoned rim has a $^{206}Pb/^{238}U$ age of c.400 Ma. It must be noted that despite a range in ages for individual areas analysed, the Th and U contents and Th/U ratios are relatively similar and are not characteristic of a particular age paragenesis. This true for the other zircons analysed from sample 238.

The remaining 11 analyses have similar $^{206}Pb/^{238}U$ ratios, however a weighted mean of the $^{206}Pb/^{238}U$ ages has excess scatter about a mean of c.402 Ma (χ^2 = 2.48). The excess scatter is attributable to analysis 7.1 which is near the pyramidal tip of slender grain with an inherited centre. Analysis 7.1 has a $^{206}Pb/^{238}U$ age of c.430 Ma (Table 1 and Fig.2). A second analysis near the other end of this grain, also of a pyramidal tip, has a $^{206}Pb/^{238}U$ age of c.395 Ma (analysis 7.2). If analysis 7.1 is excluded then a weighted mean of the 10 analyses has no excess scatter giving an age of 400 ± 8 Ma. On the basis of the current data this is interpreted as the magmatic crystallisation of zircon in this sample (Fig.2).

3.2 Sample 20

The mineral concentrate received in Canberra had a small yield of zircons. Many of the grains are slender clear fragments of zircon, some with pyramidal terminations and some zoned from centre to rim (grains 1, 2, 3 - twinned crystal, 4, 5 and 7). Others are less clear, more strongly zoned and may have complex internal structures (grains 6, 8, 9 and 10).

Ten areas have been analysed, Table 2 and Figure 3. The analyses are notably near to concordant and all 10 have similar $^{238}U/^{206}Pb$ ratios (Fig.3) even though there is a considerable range in Th and U contents and Th/U ratios (Table 2). A weighted mean of the ^{207}Pb corrected $^{206}Pb/^{238}U$ ages has no excess scatter at 412 ± 8 Ma. On the Tera-Wasserburg plot it appears that it may be possible to divide the points into two arbitrary subgroups, one with a weighted mean age of 427 ± 15 Ma and a second at 402 ± 13 Ma. However, the two morphological types outlined above are present in both sub-groups, thus on the basis of morphology and U-Th chemistry the subdivision is not as clear as on the Tera-Wasserburg plot. From the current analyses, the age of the simple magmatic zircon and other types that may be more complex is given by the weighted mean $^{206}Pb/^{238}U$ age of 412 ± 8 Ma.

3.3 Sample 169 PLAG 6

Only 8 zircons grains were hand picked from the mineral concentrate provided for sample 169 PLAG 6. Three grains are very clear, sub- to anhedral fragments of zircon (grains 1, 2 and 6). Grains 3, 7 and 8 are relatively small, zoned prismatic zircon. Grain 4 is a larger zoned fragment whilst grain 5 is a small zoned elongate zircon fragment which has a sub-round shape.

Nine analyses have been made on the 8 grains (Table 3 and Figures 4 and 5). Analysis 5.1 of the sub-round zoned grain is near concordia with a ^{207}Pb corrected $^{206}Pb/^{238}U$ age of c.1630 Ma and a ^{204}Pb corrected $^{207}Pb/^{206}Pb$ age of c.1655 Ma (Table 3 and Fig.4). The single analysis of grain 3 is significantly enriched in U and Th, c.2825 ppm and c.5060 ppm respectively. Analysis 3.1 has a $^{206}Pb/^{238}U$ age of c.500 Ma and may be considered to be an inherited component together with grain 5.

Three of the areas analysed have similar $^{206}Pb/^{238}U$ ages of c.460 Ma (analyses 4.1, 7.1 and 8.1; Table 3 and Fig.5). Two of the areas are enriched in Th and U with contents greater than 3900 ppm and 3000 ppm respectively. The third area is more normal in its Th-U chemistry with c.550 ppm U and c.140 ppm Th. A weighted mean of the $^{206}Pb/^{238}U$ ages for these three analyses has no excess scatter at 461 ± 27 Ma. This may also be interpreted as an inherited component in sample 169 PLAG 6.

Analyses of very clear, sub- to anhedral fragments of zircon (analyses 1.1, 2.1, 6.1 and 6.2) are near concordia at about 400 Ma. The Th and U contents range from c.30 to 430 ppm and c.350 to c.900 ppm respectively. A weighted mean of the $^{206}Pb/^{238}U$ ages has no excess scatter at 401 ± 14 Ma. It is possible that this is the magmatic age for sample 169 PLAG 6. However as only 8 zircons were separated, and of those only 3 give an age of c.400 Ma, the geological significance rests heavily with the concordance of the 401 ± 14 Ma result with the magmatic ages for other plagiogranite samples analysed in this study.

3.4 Sample 189

The zircons from sample 189 are notably coarser grained than the other 4 samples analysed in this study. Many are zoned elongate zircons that are cracked or have metamict centres. Some have pyramidal terminations and are slender in shape whilst a few are relatively clear fragments of zircon. More equant, zoned blocky grains are also present.

Twelve grains have been analysed, Table 4 and Figure 6. Two of the areas analysed have $^{206}Pb/^{238}U$ ages that are significantly younger than the others (analyses 2.1 and 7.1, Fig.6). Grain 7 is a zoned slender prism with pyramidal termination. Analysis 7.1 near the tip is significantly enriched in U at c.2440 ppm and also has a high Th content of c.620 ppm. The area analysed has a $^{206}Pb/^{238}U$ age of c.330 Ma and it is possible that the high U and Th have resulted in loss of radiogenic Pb. Analysis 2.1 is of a small zoned fragment of zircon with U and Th contents similar to other zircons analysed from this sample. It also has a $^{206}Pb/^{238}U$ age of c.330 Ma, though the proposed radiogenic Pb loss does not equate with the relatively lower Th and U contents of this area. Both these analyses are discordant (Fig.6) and it is proposed that they have indeed lost radiogenic Pb. Despite the coincidence of the $^{206}Pb/^{238}U$ ages, no geological significance is placed on this c.330 Ma age for the present.

The remaining 10 analyses have similar $^{238}U/^{206}Pb$ ratios and are near concordia at about c.400 Ma (Fig.6). A weighted mean of the $^{206}Pb/^{238}U$ ages has excess scatter around an age of c.405 Ma ($\chi^2 = 2.5$). Most of the scatter is attributable to two slightly older analyses, 5.1 and 8.1 which have $^{206}Pb/^{238}U$ ages of about 432 Ma and 437 Ma respectively (Table 4 and Fig.6). Analysis 4.1 records a slightly younger $^{206}Pb/^{238}U$ age of c.382 Ma. The areas analysed are not distinctly different from others in this group, and so on morphological grounds these analyses are not anomalous when examined in the transmitted light photomicrographs.

A weighted mean for seven analyses (1.1, 3.1, 6.1, 9.1, 10.1, 11.1 and 12.1) has no excess scatter giving an age of 404 ± 7 Ma. If analysis 4.1 is included the 8 analyses have a weighted mean $^{206}Pb/^{238}U$ age of 401 ± 8 Ma. Clearly the zircon in this sample crystallised at just over 400 Ma and for the present, the best estimate is 404 ± 7 Ma.

3.5 Sample BF 91/33f

In previous communications, this sample had been labelled 9V338. However in hind sight it is now understood that the markings on the vial are 91/33f.

The zircons from this sample are dominantly zoned elongate grains with pyramidal terminations or are fragments of such grains. Some are more prismatic in character and some are needle-like in shape. Simple, clear, more equant to elongate grains are also present.

Fourteen grains have been analysed (Table 5 and Figure 7). The analyses have similar $^{238}U/^{206}Pb$ ratios and are near concordia at about c.400 Ma. A weighted mean of the $^{206}Pb/^{238}U$ ages has excess scatter around an age of c.406 Ma (χ^2 = 2.64). Three of the areas have slightly older $^{206}Pb/^{238}U$ ages, analyses 6.1, 7.1 and 10.1, and a weighted mean of the $^{206}Pb/^{238}U$ age for these three gives 432 ± 20 Ma. The areas analysed are not distinctly different from other zircons in this sample, nor are the Th and U contents notably different. Nevertheless, as has been seen in other samples from this study there is a slightly older group of analyses at about 430 Ma.

A weighted mean for the remaining 11 analyses has no excess scatter giving an age of 399 ± 7 Ma. This is considered to give the crystallisation age for the zoned magmatic zircon.

4. SUMMARY

A summary tabulation of the SHRIMP U-Pb zircon results for samples of plagiogranite from the Coolac Serpentinite Belt is as follows:

Sample	U-Pb zircon Age	Comments
238	400 ± 8 Ma	magmatic age, inheritance at c.430 Ma, c.640 Ma and c.1320 Ma
20	412 ± 8 Ma	magmatic crystallisation age (?arbitrary c.430 Ma group)
169 PLAG 6	401 ± 14 Ma 461 ± 27 Ma	magmatic crystallisation age inherited zircon component, other inheritance at c.500 Ma and c.1655 Ma
189	404 ± 7 Ma	magmatic crystallisation age some radiogenic Pb loss and inheritance at c.430 Ma
BF91/33f	399 ± 7 Ma 432 ± 20 Ma	magmatic crystallisation age ?inherited zircon component,

It is clear that all five samples record a dominant c.400 Ma magmatic crystallisation event even though only a few grains have been separated from several of the samples. Figure 8 is a composite plot of the c.400-430 Ma analyses. There are some 48 analyses shown on this Figure and a weighted mean for all 48 has excess scatter with a χ^2 of 2.06. It must be noted that this mean includes 10 analyses which appear to be slightly older, say around c.430 Ma. If these 10 analyses are excluded, the weighted mean of the $^{206}Pb/^{238}U$ ages for the remaining 38 analyses has no excess scatter at 401.3 ± 3.4 Ma. Given the paucity of

grains from some samples, this combined mean may have more significance than using the individual sample ages listed above.

A weighted mean for the 10 analyses excluded in the above grand mean has no excess scatter at 431 ± 8 Ma. This may record a slightly older zircon crystallisation event either in the source of the plagiogranites or it could be a crustal contaminant in the magma. The latter is more likely given that older inheritance is also recorded in some samples.

There is no doubt that zircon crystallised in these 5 plagiogranites within analytical uncertainty of 400 Ma. This is significantly older than that for plagiogranites from the New England Orogen (Aitchison and Ireland, 1995), though is within uncertainty of ages predicted for granites in the Lachlan Fold Belt (I. Williams, pers comm. 1995).

5. REFERENCES

Aitchison, J.C. and Ireland, T.R., 1995. Age profile of ophiolitic rocks across the late Palaeozoic New England Fold Orogen, New South Wales: implications for tectonic models. *Australian Journal of Earth Sciences* **42**, 11-23.

Compston W., Williams I. S, Kirschvink J. L., Zhang Z. & Ma G. 1992. Zircon U-Pb ages for the Early Cambrian time-scale. *Journal of the Geological Society, London* **149**, 171-184.

Williams, I.S. and Claesson, S., 1987. Isotopic evidence for the Precambrian provenance and Caledonian metamorphism of high grade paragneisses from the Seve Nappes, Scandinavian Caledonides. II. Ion microprobe zircon U-Th-Pb. *Contributions to Mineralogy & Petrology* **97**, 205-217.

Table 1. Summary of SHRIMP U-Pb data for zircons from sample 238.

Grain .spot	U (ppm)	Th (ppm)	Th/U	Pb* (ppm)	$^{204}Pb/^{206}Pb$	$^{206}Pb/^{238}U$	±	Age (Ma) $^{206}Pb/^{238}U$	±
1.1	490	79	0.16	28	0.002030	0.0612	0.0016	382.9	9.5
1.2	267	123	0.46	24	0.000186	0.0847	0.0023	524.2	13.4
2.1	198	177	0.89	15	-	0.0661	0.0017	412.4	10.6
2.2	133	135	1.02	9	0.000233	0.0607	0.0018	379.8	10.8
3.1	315	26	0.08	9	0.000447	0.0301	0.0008	191.3	5.2
4.1	447	142	0.32	28	0.000401	0.0649	0.0017	405.6	10.3
5.1	315	48	0.15	30	0.000010	0.1047	0.0027	641.8	15.5
6.1	407	88	0.22	26	0.000147	0.0667	0.0018	416.5	10.7
6.2	198	66	0.33	12	0.000859	0.0596	0.0023	372.9	13.7
7.1	459	230	0.50	31	0.000517	0.0694	0.0018	432.2	10.8
7.2	482	162	0.34	29	0.000915	0.0633	0.0017	395.3	10.2
8.1	320	118	0.37	20	0.000153	0.0642	0.0017	401.3	10.5
8.2	158	113	0.71	11	0.001148	0.0646	0.0019	403.5	11.7
9.1	633	180	0.28	38	0.004871	0.0672	0.0018	419.5	10.7
9.2	335	100	0.30	46	0.001117	0.1499	0.0043	900.2	23.9

Note :
1. - signifies no ^{204}Pb detected.
2. Uncertainties given at the one sigma level.
3. Correction for common Pb made on the basis of extrapolation to concordia along a mixing line with common Pb, following Tera & Wasserburg (1972), as outlined in Compston et al (1992).

Table 2. Summary of SHRIMP U-Pb data for zircons from sample 20.

Grain .spot	U (ppm)	Th (ppm)	Th/U	Pb* (ppm)	$^{204}Pb/^{206}Pb$	$^{206}Pb/^{238}U$	±	Age (Ma) $^{206}Pb/^{238}U$	±
1.1	386	12	0.03	24	0.000456	0.0685	0.0032	427.2	19.6
2.1	428	10	0.02	25	0.000010	0.0638	0.0016	398.7	9.9
3.1	167	2	0.01	10	0.000334	0.0686	0.0023	427.4	13.8
4.1	259	6	0.02	15	0.001142	0.0635	0.0017	396.7	10.4
5.1	349	4	0.01	20	0.000444	0.0637	0.0017	397.8	10.2
6.1	1371	67	0.05	86	0.000682	0.0687	0.0017	428.3	10.3
7.1	1042	56	0.05	64	0.000464	0.0667	0.0017	416.1	10.1
8.1	5287	206	0.04	326	0.000100	0.0675	0.0020	421.1	11.9
9.1	1752	69	0.04	102	0.000494	0.0640	0.0030	399.9	18.5
10.1	1053	791	0.75	81	0.000350	0.0693	0.0024	431.9	14.6

Note : 1. Uncertainties given at the one sigma level.
2. Correction for common Pb made on the basis of extrapolation to concordia along a mixing line with common Pb, following Tera & Wasserburg (1972), as outlined in Compston et al (1992).

Table 3. Summary of SHRIMP U-Pb data for zircons from sample 169 PLAG 6.

Grain .spot	U (ppm)	Th (ppm)	Th/U	Pb* (ppm)	$^{204}Pb/^{206}Pb$	$^{206}Pb/^{238}U$	±	Age (Ma) $^{206}Pb/^{238}U$	±
1.1	455	185	0.41	30	0.000049	0.0653	0.0018	408.0	10.9
2.1	903	435	0.48	59	0.000025	0.0634	0.0016	396.4	9.6
3.1	2825	5061	1.79	315	0.000546	0.0805	0.0019	499.4	11.6
4.1	553	352	0.64	44	0.000079	0.0751	0.0019	467.1	11.5
5.1	575	143	0.25	168	0.000047	0.2874	0.0070	1629	35
6.1	353	34	0.09	21	0.000214	0.0627	0.0017	391.7	10.2
6.2	470	42	0.09	29	0.000818	0.0661	0.0019	412.5	11.4
7.1	3060	3906	1.28	276	0.000334	0.0721	0.0026	448.8	15.9
8.1	3809	4719	1.24	344	0.000055	0.0740	0.0035	460.4	21.2

Note : 1. Uncertainties given at the one sigma level.
2. Correction for common Pb made on the basis of extrapolation to concordia along a mixing line with common Pb, following Tera & Wasserburg (1972), as outlined in Compston et al (1992).

Table 4. Summary of SHRIMP U-Pb data for zircons from sample 189.

Grain .spot	U (ppm)	Th (ppm)	Th/U	Pb* (ppm)	$^{204}Pb/^{206}Pb$	$^{206}Pb/^{238}U$	±	Age (Ma) $^{206}Pb/^{238}U$	±
1.1	310	27	0.09	18	0.000183	0.0632	0.0016	394.9	9.9
2.1	200	17	0.09	10	0.001266	0.0519	0.0014	326.4	8.8
3.1	453	55	0.12	27	0.000165	0.0631	0.0016	394.7	10.0
4.1	602	96	0.16	35	0.000066	0.0611	0.0016	382.1	9.4
5.1	778	120	0.15	51	0.000305	0.0693	0.0018	431.9	10.6
6.1	163	13	0.08	10	0.000287	0.0636	0.0017	397.5	10.6
7.1	2444	622	0.25	123	0.000576	0.0523	0.0013	328.5	7.9
8.1	435	34	0.08	28	0.000221	0.0701	0.0020	437.0	12.1
9.1	974	147	0.15	61	0.000157	0.0661	0.0017	412.6	10.3
10.1	969	111	0.11	59	0.000122	0.0654	0.0019	408.3	11.7
11.1	1004	155	0.15	62	0.000066	0.0656	0.0017	409.4	10.1
12.1	673	85	0.13	42	0.000627	0.0660	0.0017	411.8	10.2

Note : 1. Uncertainties given at the one sigma level.
2. Correction for common Pb made on the basis of extrapolation to concordia along a mixing line with common Pb, following Tera & Wasserburg (1972), as outlined in Compston et al (1992).

Table 5. Summary of SHRIMP U-Pb data for zircons from sample BF 91/33f.

Grain .spot	U (ppm)	Th (ppm)	Th/U	Pb* (ppm)	$^{204}Pb/^{206}Pb$	$^{206}Pb/^{238}U$	±	Age (Ma) $^{206}Pb/^{238}U$	±
1.1	710	162	0.23	42	0.000536	0.0622	0.0016	389.2	9.5
2.1	653	378	0.58	42	0.000010	0.0615	0.0016	384.5	9.8
3.1	411	230	0.56	29	0.000175	0.0661	0.0017	412.7	10.3
4.1	754	428	0.57	51	0.000118	0.0637	0.0016	397.8	9.9
5.1	545	288	0.53	38	0.000093	0.0661	0.0017	412.9	10.1
6.1	576	320	0.56	42	0.000097	0.0691	0.0017	430.7	10.5
7.1	471	233	0.50	34	0.000127	0.0689	0.0017	429.4	10.4
8.1	974	595	0.61	66	0.000007	0.0632	0.0016	395.1	9.4
9.1	772	554	0.72	52	0.000236	0.0628	0.0016	392.7	9.7
10.1	410	189	0.46	30	0.000024	0.0699	0.0019	435.3	11.5
11.1	499	259	0.52	34	0.000551	0.0653	0.0018	407.7	11.1
12.1	376	179	0.48	23	0.000382	0.0603	0.0024	377.5	14.6
13.1	832	547	0.66	59	0.000115	0.0655	0.0017	409.1	10.2
14.1	186	65	0.35	12	0.000941	0.0664	0.0021	414.5	12.6

Note : 1. Uncertainties given at the one sigma level.
2. Correction for common Pb made on the basis of extrapolation to concordia along a mixing line with common Pb, following Tera & Wasserburg (1972), as outlined in Compston et al (1992).

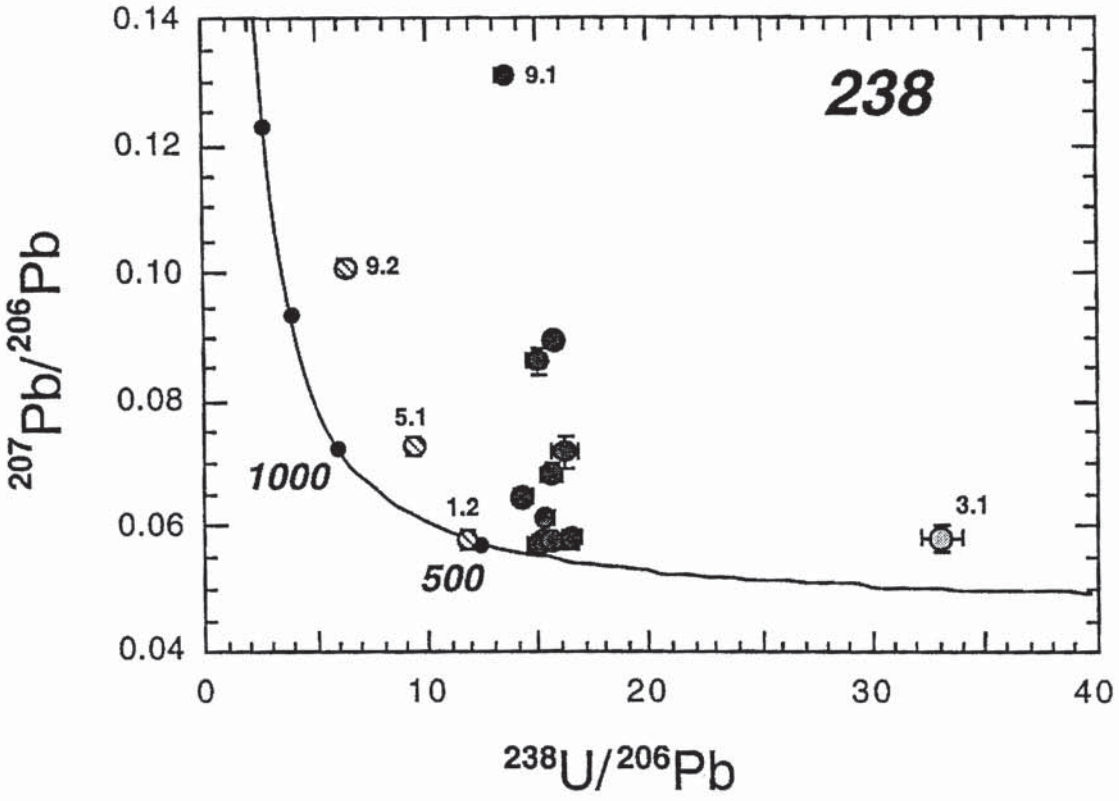

Figure 1. Tera-Wasserburg concordia plot of all SHRIMP zircon analyses for sample 238. Analyses plotted, uncorrected for common Pb, with one sigma error bars.

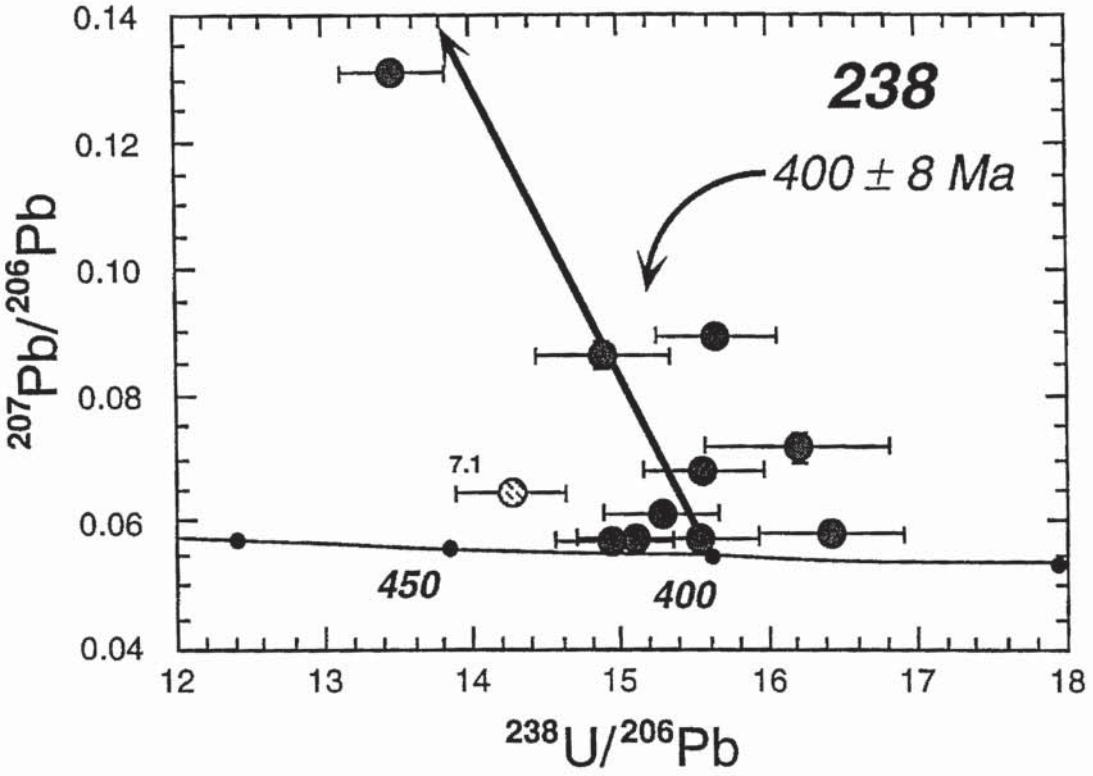

Figure 2. Enlarged Tera-Wasserburg concordia plot for SHRIMP analyses of zircons from sample 238. Analyses plotted, uncorrected for common Pb, with one sigma error bars. A mixing line is shown for reference between the 400 Ma radiogenic end member and to common Pb. Shaded analyses used for the weighted mean age calculation shown.

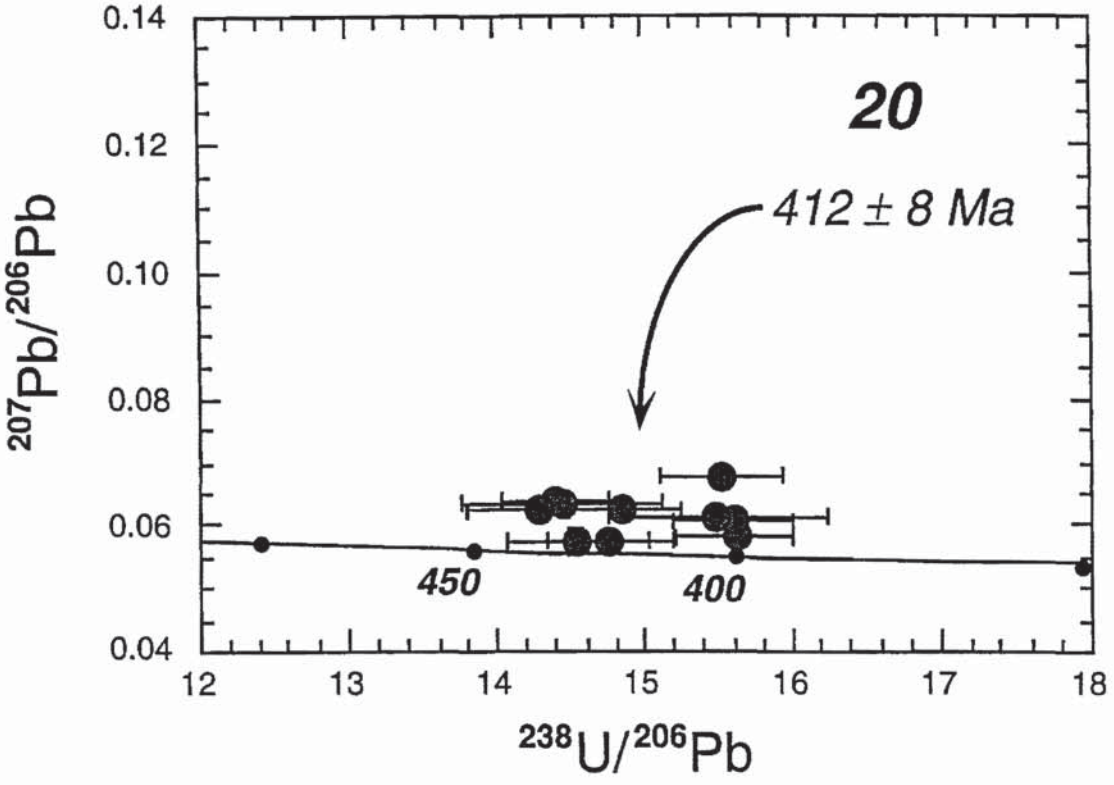

Figure 3. Tera-Wasserburg concordia plot for SHRIMP analyses of zircons from sample 20. Analyses plotted, uncorrected for common Pb, with one sigma error bars. All analyses used for the weighted mean age calculation shown.

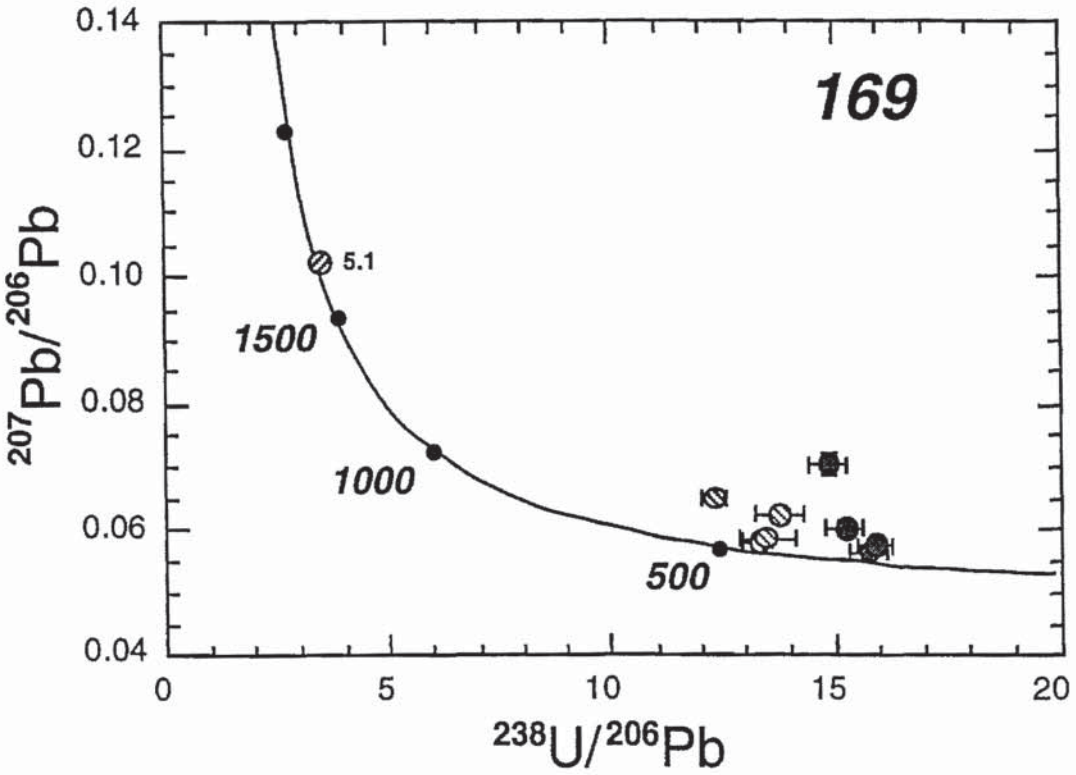

Figure 4. Tera-Wasserburg concordia plot of all SHRIMP zircon analyses for sample 169. Analyses plotted, uncorrected for common Pb, with one sigma error bars. Analysis 5.1 is near concordia with a ^{204}Pb corrected $^{207}Pb/^{206}Pb$ age of c.1655 Ma.

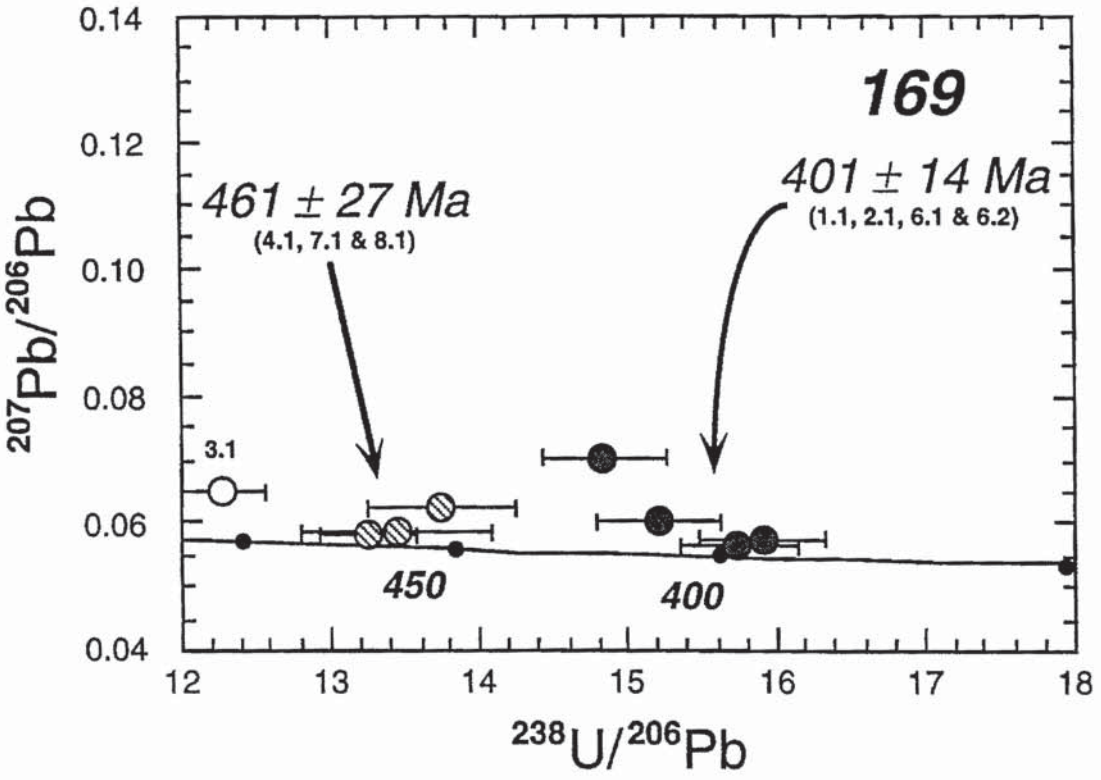

Figure 5. Enlarged Tera-Wasserburg concordia plot for SHRIMP analyses of zircons from sample 169. Analyses plotted, uncorrected for common Pb, with one sigma error bars. Analyses used for the weighted mean age calculations shown are shaded (c.400 Ma) or striped (c.460 Ma).

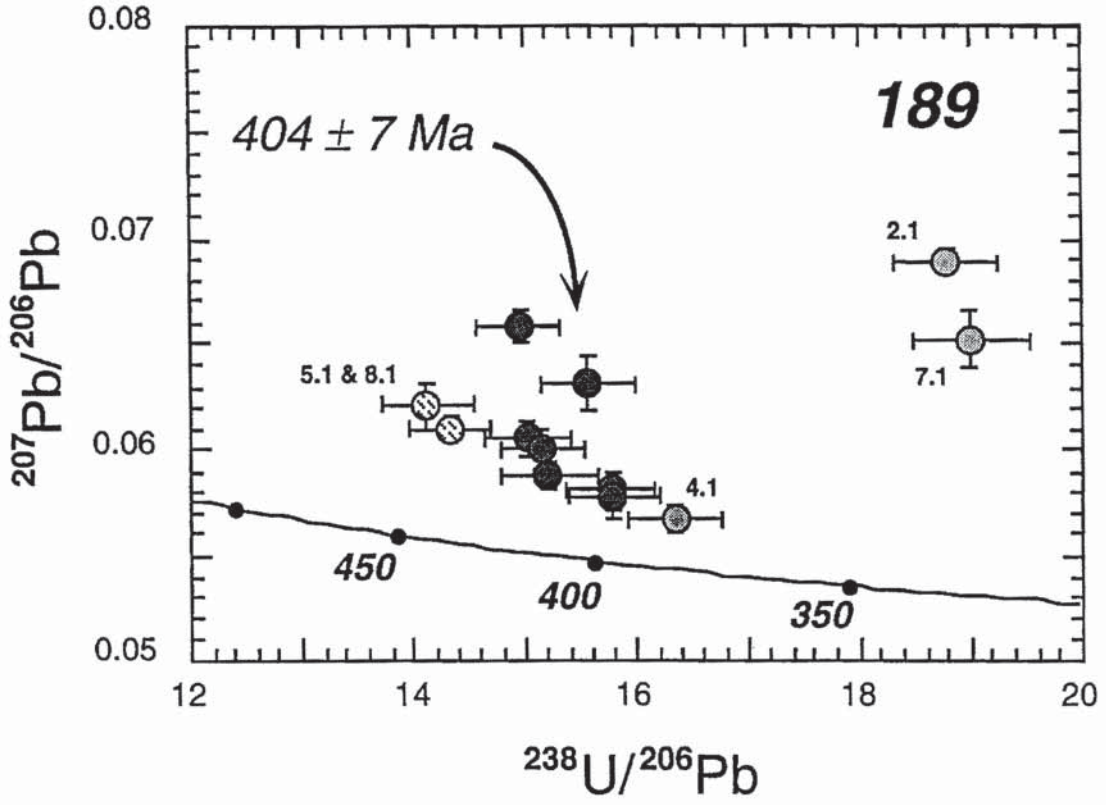

Figure 6. Tera-Wasserburg concordia plot for SHRIMP analyses of zircons from sample 189. Analyses plotted, uncorrected for common Pb, with one sigma error bars. Shaded analyses used for the weighted mean age calculation shown.

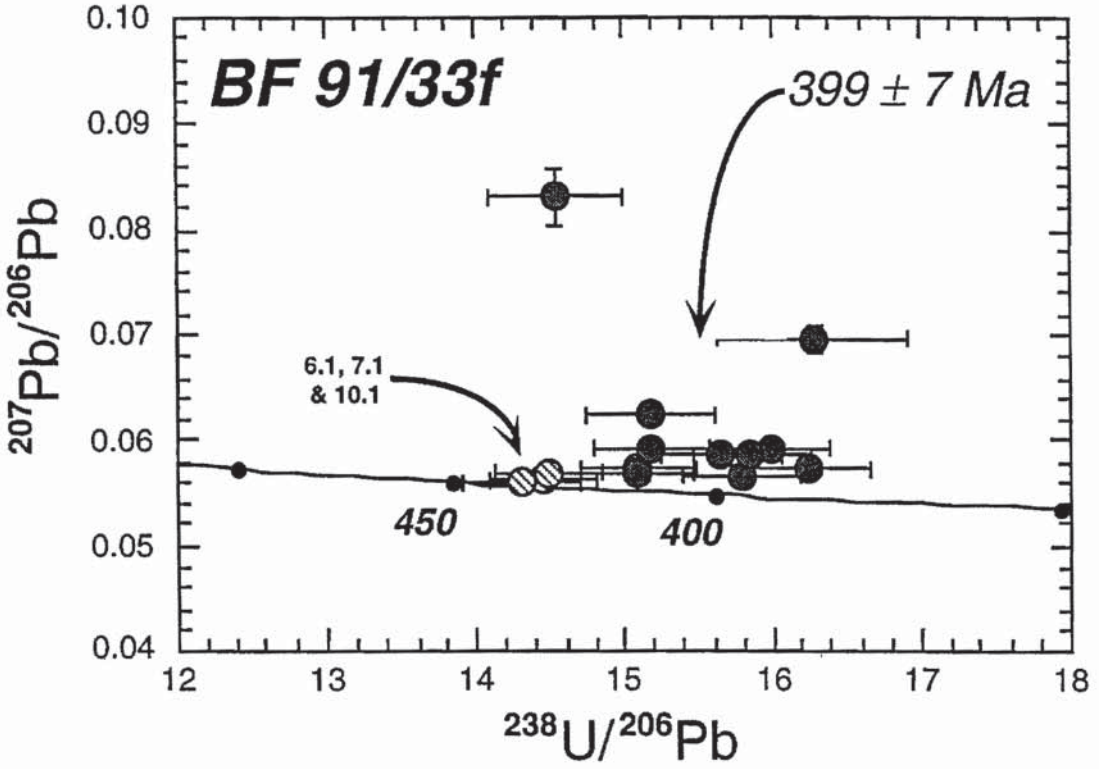

Figure 7. Tera-Wasserburg concordia plot for SHRIMP analyses of zircons from sample BF 91/33f. Analyses plotted, uncorrected for common Pb, with one sigma error bars. Shaded analyses used for the weighted mean age calculation shown.

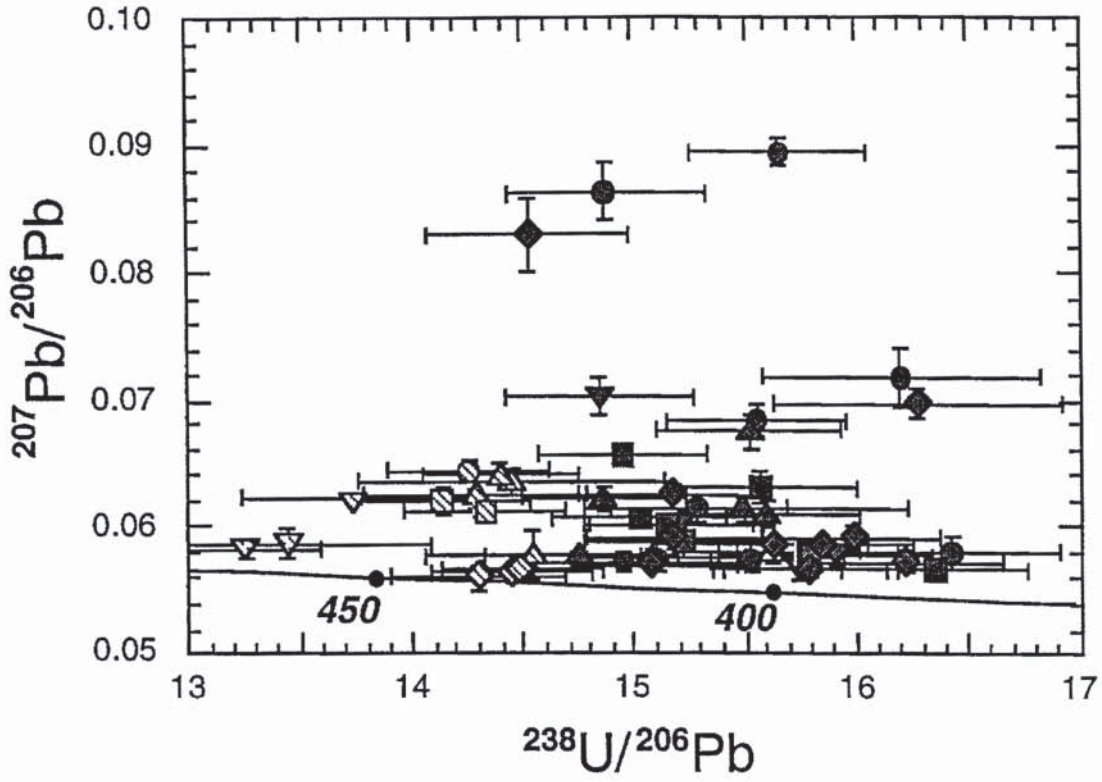

Figure 8. Composite Tera-Wasserburg concordia plot for SHRIMP analyses of zircons from samples 238 (circles), 20 (triangles), 169 PLAG 6 (inverted triangles), 189 (squares) and BF 91/33f (diamonds). Analyses plotted, uncorrected for common Pb, with one sigma error bars. A weighted mean of the ^{207}Pb corrected $^{206}Pb/^{238}U$ ages for 38 analyses gives a pooled age of 401.3 ± 3.4 Ma (shaded symbols). Some 10 analyses are older at 431 ± 8 Ma (striped symbols).

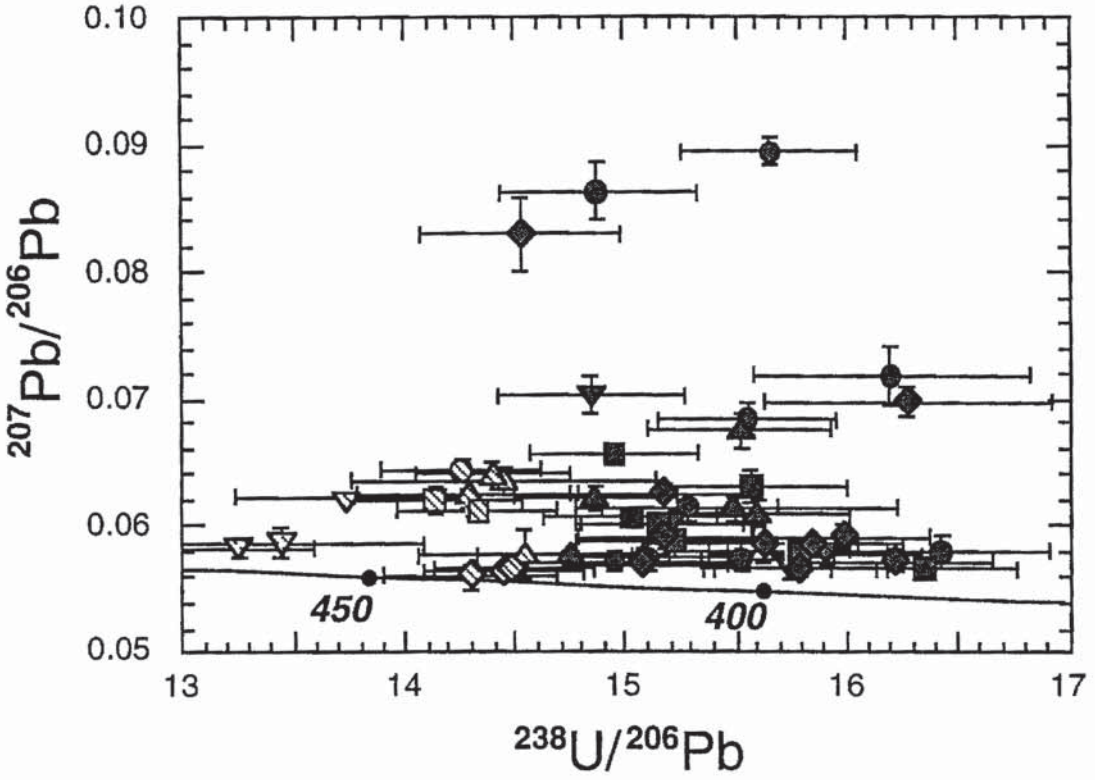

Figure 8. Composite Tera-Wasserburg concordia plot for SHRIMP analyses of zircons from samples 238 (circles), 20 (triangles), 169 PLAG 6 (inverted triangles), 189 (squares) and BF 91/33f (diamonds). Analyses plotted, uncorrected for common Pb, with one sigma error bars. A weighted mean of the ^{207}Pb corrected $^{206}Pb/^{238}U$ ages for 38 analyses gives a pooled age of 401.3 ± 3.4 Ma (shaded symbols). Some 10 analyses are older at 431 ± 8 Ma (striped symbols).

APPENDIX PUB

PUBLICATIONS

The following articles have been removed due to copyright restrictions. They are still available in the hardcopy version of this thesis held at UTS library (city campus)

Source, Transport and Deposition of Metals, Pagel & Leroy (eds) © 1991 Balkema, Rotterdam. ISBN 90 5410 020 6

PGE remobilization, Coolac Serpentinite, Australia

Jan T. Graham, Brian Marshall & Brenda J. Franklin
Department of Applied Geology, University of Technology, Sydney, Broadway, NSW, Australia

IAGOD

Commission on Ore Deposits in Mafic and Ultramafic Rocks

6th International Platinum Symposium

PROGRAMME and ABSTRACTS

Editor: Stephen J. Barnes

July 8th-11th 1991

Perth, Western Australia

Australian Journal of Earth Sciences (1992) 39, 365–371

Remobilization of PGE in podiform chromitite in the Coolac Serpentinite Belt, Southeastern Australia

B. J. FRANKLIN,[1] B. MARSHALL,[1] I. T. GRAHAM[1] AND J. McANDREW[2]

[1]*Department of Applied Geology, University of Technology, Sydney, PO Box 123, Broadway NSW 2007, Australia.*

[2]*CSIRO, Division of Exploration Geoscience, PO Box 136, North Ryde, NSW 2113, Australia.*

IAVCEI
CANBERRA 1993

ABSTRACTS

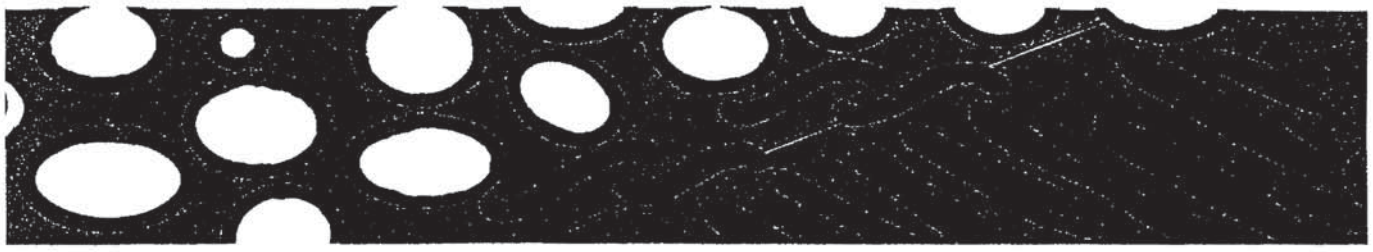

GENERAL ASSEMBLY
SEPTEMBER 1993 - CANBERRA AUSTRALIA

ANCIENT VOLCANISM & MODERN ANALOGUES

Current Research in Geology Applied to Ore Deposits. Fenoll Hach-Alí, Torres-Ruiz & Gervilla (eds) (1993). ISBN 84-338-1772-8

TEXTURES OF PODIFORM CHROMITITE, SOUTHEASTERN AUSTRALIA

ournal and Proceedings, Royal Society of New South Wales, Vol. 128, 79-88, 1995
SSN 0035-9173/95/020079-10 $4.00/1

THE OCCURRENCE AND ORIGIN OF WELL-CRYSTALLISED UVAROVITE GARNET FROM THE PODIFORM CHROMITITE DEPOSITS OF SOUTH-EASTERN NEW SOUTH WALES.

Ian T Graham and David M Colchester

Mineralogy and Petrology (1996) 57: 129–150

Mineralogy and Petrology

Chemistry and mineralogy of podiform chromitite deposits, southern NSW, Australia: a guide to their origin and evolution

I. T. Graham, B. J. Franklin, and **B. Marshall**

University of Technology, Sydney, Australia

With 4 Figures

Received February 3, 1995
accepted July 24, 1995

GEOLOGICAL SOCIETY OF AUSTRALIA, ABSTRACTS No. 41
13th Australian Geological Convention, Canberra, February 1996

AGE AND TECTONIC SIGNIFICANCE OF OPHIOLITIC ROCKS FROM THE TUMUT-GUNDAGAI REGION OF NSW

Ian T.Graham[1], Brenda J.Franklin[1], Brian Marshall[1], Evan C.Leitch[1] and Mark Fanning[2]
[1]Department of Applied Geology, UTS, PO Box 123 Broadway, NSW 2007
[2]PRISE, Research School of Earth Sciences, ANU, Canberra, ACT 0200

Tectonic significance of 400 Ma zircon ages for ophiolitic rocks from the Lachlan fold belt, eastern Australia

I. T. Graham
B. J. Franklin
B. Marshall
E. C. Leitch
Department of Applied Geology, University of Technology, Sydney, P.O. Box 123, Broadway, Sydney, NSW 2007, Australia

M. Fanning
Research School of Earth Sciences, Australian National University, Canberra, ACT 2601, Australia

GEOLOGICAL SOCIETY OF AUSTRALIA, ABSTRACTS No. 49
14th Australian Geological Convention, Townsville, July 1998

U/Pb AND Nd/Sm GEOCHRONOLOGY OF OPHIOLITIC ROCKS FROM THE TUMUT SERPENTINITE PROVINCE, SOUTHERN NSW

Ian T.Graham, Brenda J. Franklin, Brian Marshall and Graziella Caprarelli
Department of Applied Geology, UTS, PO Box 123 Broadway, NSW 2007